OCTOBER 1976

analytical chemistry

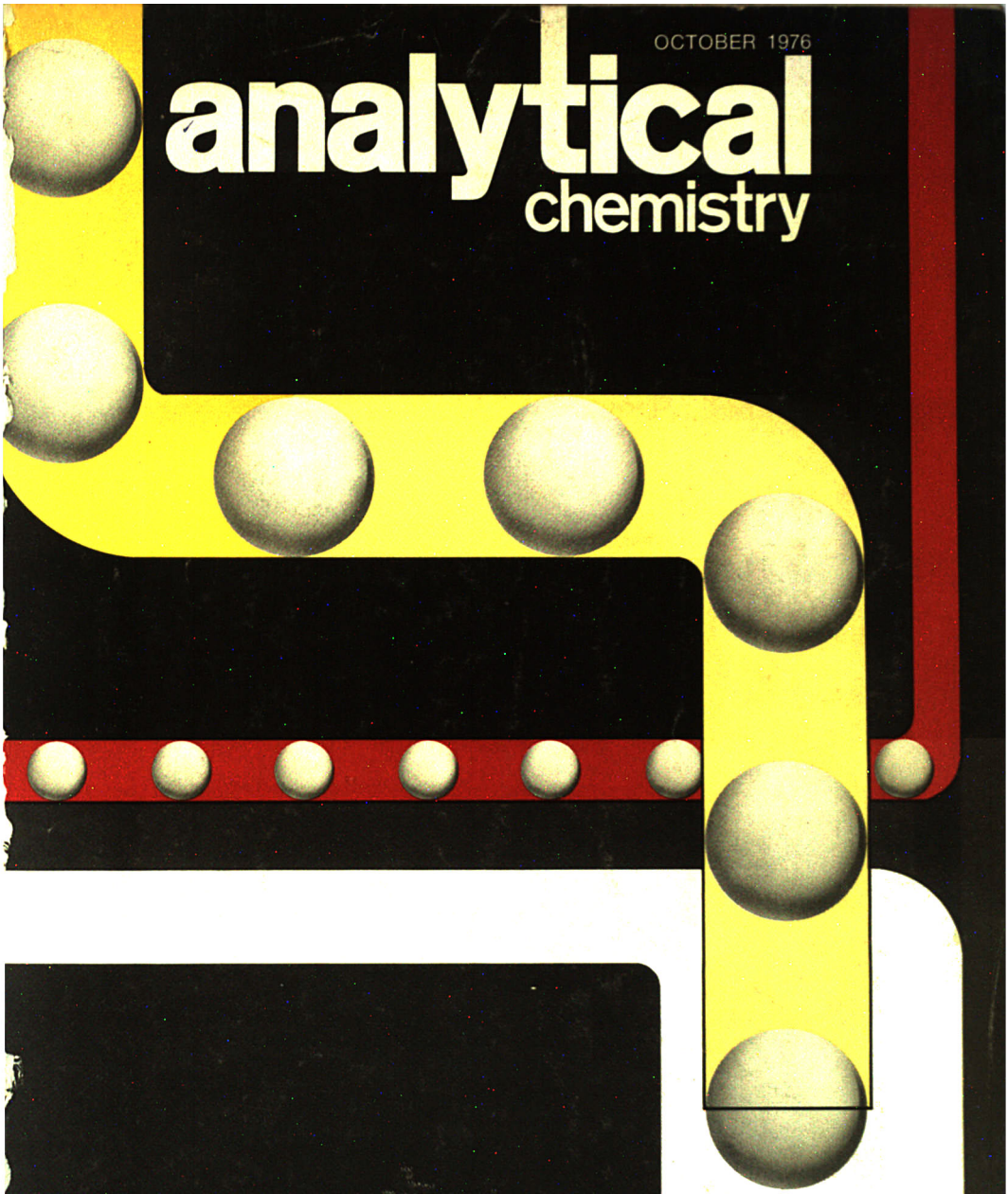

CONTINUOUS FLOW SYSTEMS

Model 3010 Trace Metals Analyzer. Measures up to 200 micro or macro samples daily at 90 seconds or less per sample using a rapid exchange reagent. Cost per sample: about one-third that of conventional methods. Excellent accuracy and precision at the nanogram level. **Circle No. 41**

Model 4000 ZnP Hematofluorometer. Determines the amount of zinc protoporphrin in whole blood without sample preparation. Principle approved by the Center for Disease Control of HEW for lead intoxication and/or iron deficiency anemia. **Circle No. 42**

Model 3040 Programmable Potential Coulometer. For electro-chemical analyses, measuring chemical levels or changes in solutions, selection and detection of complex compounds, process control, and similar applications. Pushbutton programmable. Available with flow cells, trap cells, and other sensors. **Circle No. 45**

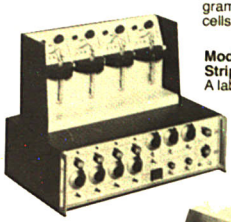

Model 2014 Multiple Anodic Stripping Analyzer. A laboratory instrument that will perform quantitative or qualitative analyses on trace metals in numerous matrices without destroying the sample. Available with extender units to handle up to 12 discrete samples simultaneously, and with a variety of equipment options for routine analysis or basic research. **Circle No. 46**

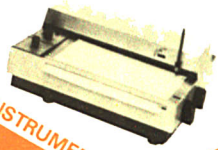

ANALYTICAL INSTRUMENTS

ANALYTICAL INSTRUMENTS

Look at this trace metals complex

...and for halides, chemicals, and other substances and solutions, too.

ESA is a multi-faceted company with capabilities in such diverse areas as industrial hygiene, clinical laboratories and health care centers, industrial processes, environmental technology, and quality control. We operate one of the largest private blood lead screening laboratories in the world, provide the food industry with instruments for measuring and monitoring trace metals in food products and containers, test air filters, and analyze water and soil for lead, tin, cadmium, copper, arsenic, mercury, bismuth, thallium and other heavy, precious, or toxic metals in a variety of matrices. Look us over—then tell us your requirements.

Model 2011 Single Cell Anodic Stripping Voltammeter. A portable, single cell version of the Model 2014 that will operate on line power or from a 12-volt storage battery and inverter. **Circle No. 43**

ANALYTICAL INSTRUMENTS

RESEARCH AND DEVELOPMENT

The R&D Laboratory consists of both in-house and consulting groups for development of hardware, and for analytical projects ranging from emission surveys from power plants and smelters to the effectiveness of existing techniques for controlling the environment. **Telephone or letterhead request only, please.**

SERVICE LABORATORIES

Screening Laboratories for screening of children and industrial personnel for blood and urine lead, erythrocyte protoporphrin, and hematology testing.... determining the presence and amount of lead, cadmium, copper, mercury, arsenic, tin, bismuth, and thallium in various matrices....or for intermediate or massive repetitive analyses of other trace elements in solids and aqueous solutions. **Circle No. 44**

SYSTEM ACCESSORIES

Sampling Kits for obtaining, handling, shipping, and storing blood or other biologicals. **Circle No. 47**

Fast Exchange Reagents that obsolete preparative chemistry for lead in food, water, blood, urine....and other trace substances in different matrices. **Circle No. 48**

Flow Cells and Sensors for continuous or batch measurement and monitoring of chemical and industrial processes, capturing and eliminating undesirable ingredients, and other uses. **Circle No. 49**

esa

ENVIRONMENTAL SCIENCES ASSOCIATES, INC.
175 Bedford Street, Burlington, MA 01803 — Telex: 94-9367

How about an "Instant Replay"

this time undistorted

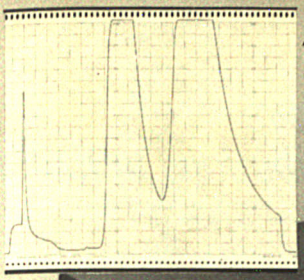

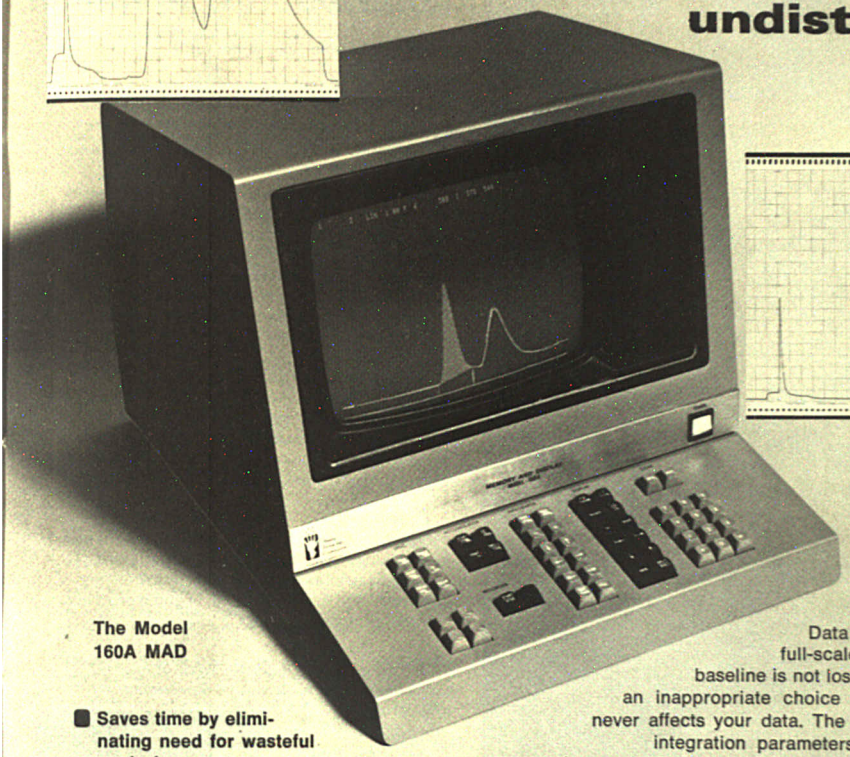

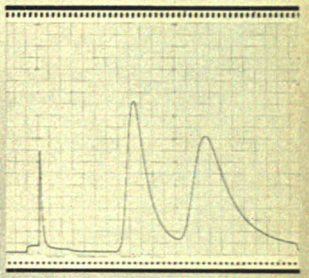

The Model 160A MAD

- **Saves time by eliminating need for wasteful analysis re-runs**
- **Reduces work by eliminating pre-run predictions and manual post-run calculations**
- **Saves paper by permitting chart recordings to be made after data display parameters are properly set**
- **Increases usefulness of most analytical instruments: GC, LC, TLC, MS, IR, UV/Vis, X-ray fluorescence, etc.**

Data that exceeds display full-scale or recedes into the baseline is not lost in the Model - 160A; an inappropriate choice of attenuator setting never affects your data. The choice of display or integration parameters and all other data-processing decisions need only be made after the data has been acquired, when such decisions are easy to make.

- **Computes important parameters such as peak areas, heights, and retention times**
- **Transfers full-range data into permanent storage when used with the Model - 170 Diskfile accessory**
- **Resolves smallest data structure regardless of background signal amplitude.**

PRICE: $9850, FOB Pasadena, California

For further information write or call: Marketing Department

Analog Technology Corporation

3410 E. Foothill Boulevard, Pasadena, California 91107 (213) 449-8440 TWX: 910-588-376

CIRCLE 1 ON READER SERVICE CARD

We have contributions to make.

Our contributions take three forms.

First—Tools. Our Whatman brands of column packing media for analysis of biochemical/biomedical compounds are the most complete in the world. Many, indeed most, of these are unique and uniquely useful.

Recently developed among these media are two new microparticulate bonded ion exchangers—the first such materials anywhere commercially available. At a stroke they advance the art considerably. Partisil™-10 SAX is a strong anion exchanger, Partisil™-10 SCX a strong cation exchanger. They are extraordinary.

Second—Data. We are about to publish "The Analysis of Nucleic Acid Constituents," to be followed shortly by publication of successive volumes on analyses of other biologically important classes of compounds. This is but one of a number of relevant Whatman publications.

Third—Support. We maintain an Advanced Technology Center where, among other activities, methodologies optimizing HPLC separations of biochemical/biomedical substances are developed and published in an on-going program. One of our many services.

Those interested in receiving (free of charge) the "Analysis of Nucleic Acid Constituents" and/or in receiving other data re Whatman brand HPLC products, methods and the like, or in technical discussion with our Center personnel are invited to write or phone.

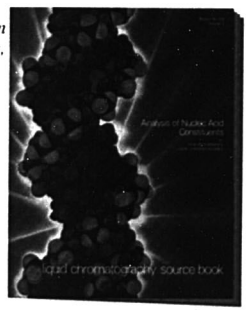

Whatman Inc.
9 Bridewell Place,
Clifton, N.J. 07014
Tel. (201) 777-4825
Telex 133426.

Whatman

CIRCLE 229 ON READER SERVICE CARD

Volume 48, No. 12, October 1976

ANCHAM
48(12) 897A–1018A/1657–1832 (1976)
ISSN 0003-2700

Published monthly with review issue added in April and Laboratory Guide in August by the American Chemical Society, from 20th and Northampton Sts., Easton, Pa. 18042. Executive and Editorial headquarters, American Chemical Society, 1155 16th St., N.W., Washington, D.C. 20036 (202) 872-4600. Second class postage paid at Washington, D.C., and at additional mailing offices.

1976 Subscription rates—including surface postage

	1 yr	2 yr	3 yr
MEMBERS:			
Domestic	$ 9.00	$16.00	$22.00
PUAS	15.75	29.50	42.25
Canada, Foreign	16.75	31.50	45.25
NONMEMBERS:			
Domestic	12.00	21.00	29.00
Canada	19.75	36.50	52.25
PUAS	21.75	41.00	60.25
Foreign	22.75	43.00	63.25

Airmail and air freight rates are available from Membership & Subscription Services, ACS, P.O. 3337, Columbus, Ohio 43210, (614) 421-7230.

New and renewal subscriptions should be sent with payment to the Office of the Controller at the ACS Washington address.

Subscription service inquiries and changes of address (include both old and new addresses with ZIP code and *recent mailing label*) should be directed to the ACS Columbus address noted above. Please allow six weeks for change of address to become effective.

Claims for missing numbers will not be allowed if loss was due to failure of notice of change of address to be received in the specified time; if claim is dated (a) North America: more than 90 days beyond issue date, (b) all other more than one year beyond issue date, or if the reason given is "missing from files".

Microfiche subscriptions, one year only, are available at the same rates but are mailed first class domestic and airmail foreign. Direct all inquiries and payments to Business Operations, Books and Journals Division, at the Washington address or call (202) 872-4444.

	Write or call
Single issues, current year, $2.50 except review issue, $4.00	Special Issues Sales American Chemical Society 1155 16th St., N.W. Washington, D.C. 20036
Back issues and volumes	
Microfilm editions from Vol. 1 to present	202-872-4364

Advertising Management: Centcom, Ltd., 50 West State St., Westport, Conn. 06880 (203) 226-7131

analytical chemistry

CONTENTS

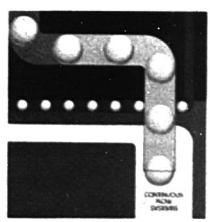

Our cover art is based on the REPORT and illustrates continuous-flow segmented by air bubbles

Briefs

* Corresponding author.

pH today
tomorrow the works

For $895 you can have a meter that will handle today's pH measurements — and tomorrow the gamut of analyses possible with ORION specific ion and gas-sensing electrodes.

The Model 701A meets or surpasses the specifications of other 4½-digit meters selling for over $1000. It gives pH readings precise to 0.001 over the entire pH range, and millivolt readings precise to 0.1 mv.

The Model 701A has a big, bright LED display and the latest in high reliability circuitry. It's so reliable, we dare to give it our "no lemon" guarantee. If it quits within one year of purchase, we'll replace it with a brand new one. Immediately.

If you'd like us to demonstrate the 701A in your laboratory, call our toll-free numbers: (800) 225-1480 (except Mass.) in the U.S.A., or (800) 363-9270 in Canada.

ORION electrodes for — ammonia — bromide — calcium — cadmium — carbon dioxide — chloride — chlorine — copper — cyanide — fluoride — fluoroborate — hydrogen sulfide — iodide — lead — nitrate — nitrogen oxide — perchlorate — potassium — silver — sodium — sulfide — sulfur dioxide — thiocyanate — water hardness

ORION RESEARCH

380 Putnam Avenue, Cambridge, Massachusetts 02139 U.S.A.

CIRCLE 157 ON READER SERVICE CARD

Briefs

Automated Composite Analysis of Major Sinter Components 1701

After fusion with sodium carbonate and sodium peroxide in a vitreous carbon crucible, acidifying gives a clear solution for use in the AutoAnalyzer for determination of components: Al_2O_3 (0.4 to 1.5%); SiO_2 (3 to 12%); CaO (5 to 14%); MgO (2 to 10%); and total iron (50 to 66%).

Om P. Bhargava* and W. Grant Hines, Chemical and Metallurgical Laboratories, The Steel Company of Canada, Limited, Wilcox Street, Hamilton, Ontario, Canada, L8N 3T1

Anal. Chem., 48 (1976)

Determination of Total Estrogens in Urine with 3-Methyl-2-benzothiazolinone Hydrazone 1704

Alternative colorimetric method (used manually or with an AutoAnalyzer) gives a correlation coefficient of 0.96 with the fluorometric method and a coefficient of 0.94 with the gas chromatographic method.

Hugh Y. Yee* and Bobette Jackson, The Department of Pathology, Hutzel Hospital, 432 East Hancock, Detroit, Mich. 48201

Anal. Chem., 48 (1976)

Gas Liquid Chromatographic Determination of Therapeutic and Toxic Levels of Amitriptyline in Human Serum with a Nitrogen-Sensitive Detector 1708

An accurate, sensitive, and specific method requiring no derivitization uses protriptyline as internal standard. The limit of detection is 1 ng/ml with a relative standard deviation of 4% at the 300 ng/ml level.

John Vasiliades* and Kerry C. Bush, Department of Pathology, The University of Alabama in Birmingham, Birmingham, Ala. 35233

Anal. Chem., 48 (1976)

Intercalibration of Gas Chromatographic Analyses for Hydrocarbons in Tissues and Extracts of Marine Organisms 1711

A program of measurements by three laboratories is described. Results were $(\bar{x} - \hat{x}/\hat{x})$ and $s/\bar{x}$ of 0.09, 0.06; 0.50, 0.26; and 0.69, 0.34 for three different petroleum hydrocarbon mixtures spiked to cod liver oil: and $\bar{x} \pm x$ of 37.7 ± 4.6 μg/g for estimate of petroleum in tuna meal.

John W. Farrington,* John M. Teal, Gilbert C. Medeiros, Kathryn A. Burns, and E. Arthur Robinson, Jr., Woods Hole Oceanographic Institution, Woods Hole, Mass. 02543, and **James G. Quinn and Terry L. Wade,** Graduate School of Oceanography, University of Rhode Island, Kingston, R.I. 02881

Anal. Chem., 48 (1976)

Gas Chromatographic Separation of Lower Aliphatic Amines 1716

A complete gas chromatographic separation of a mixture of 8 primary (as their Schiff bases), 3 secondary, and 2 tertiary amines uses a Tenax-GC column in programmed temperature gas chromatography.

Yasuyuki Hoshika, Aichi Environmental Research Center, 7-6, Tsuji-machi, Kita-ku, Nagoya-shi, Aichi, Japan

Anal. Chem., 48 (1976)

Coupled Gas Chromatography–Atomic Absorption Spectrometry for the Nanogram Determination of Chromium 1717

Introducing gas chromatographic effluent directly into the burner head of an atomic absorption spectrometer gives a specific, relatively interference-free detection system for volatile chromium chelates.

Wayne R. Wolf, Nutrient Composition Laboratory, Nutrition Institute, Agricultural Research Service, U.S. Department of Agriculture, Beltsville, Md. 20705

Anal. Chem., 48 (1976)

Optimization of Gas Chromatographic Analysis of Complex Mixtures of Unknown Composition 1720

Method can be used in GLC or GSC with any type of column. Analysis of an industrial still residues sample of 10 major and 33 minor unknown components illustrates the method.

R. J. Laub and J. H. Purnell,* Department of Chemistry, University College of Swansea, Swansea, Wales SA2 8PP

Anal. Chem., 48 (1976)

High-Pressure Liquid–Liquid Partition Chromatography of Metal Chelates of Tetradentate β-Ketoamines 1725

Separation of Co^{II}, Ni^{II}, Cu^{II} is achieved with reversed phase technique. The dependence of the uv detector response on the amount of metal in aqueous solutions is reported for Ni and Cu.

Enrico Gaetani and Carlo F. Laureri, Istituto di Chimica Farmaceutica e Tossicologica, Universita di Parma, 43100 Parma, Italy, and **Alessandro Mangia* and Giovanni Parolari,** Istituto di Chimica Generate ed Inorganic, Universita di Parma, 43100 Parma, Italy

Anal. Chem., 48 (1976)

Liquid Chromatography of Aromatic Hydrocarbons on Ion-Exchange Resins 1728

A 4% crosslinked cation-exchange resin carrying iron(III) or calcium ions is an effective stationary phase for chromatography of polycyclic aromatic hydrocarbons and their chlorinated derivatives.

David M. Ordemann and Harold F. Walton,* Department of Chemistry, University of Colorado, Boulder, Colo. 80309

Anal. Chem., 48 (1976)

Determination of Anhydrotetracyclines in Tetracycline by High-Pressure Liquid Chromatography 1731

The epimeric anhydrotetracyclines ATC and EATC are determined quantitatively at low levels in tetracycline samples (RSD < 1.5%). An anhydrotetracyclines standard is described and analysis of other tetracyclines is discussed.

Richard F. Lindauer,* David M. Cohen,* and Kevin P. Munnelly,* Pfizer Inc., Quality Control Division, Brooklyn, N.Y. 11206

Anal. Chem., 48 (1976)

Separation and Quantitation of Diazonium Salts as Heptanesulfonate Ion Pairs by High Pressure Liquid Chromatography 1734

An octadecyl reverse phase column is used to separate and quantitate several diazonium salts in typical reprographic formulations. Standard deviation is 0.2%.

Edward Fitzgerald, GAF Corporation, 25 Ozalid Road, Johnson City, N.Y. 13790

Anal. Chem., 48 (1976)

Matheson has

189 Flowmeters

Specialty Gas Handling equipment is our business. Matheson has engineered 189 different flowmeters, all of which feature accuracy, precision, quality and durability. When you buy from Matheson, our experience and technology allow you to measure the flow of over 130 different gases.

Electronic Mass Flow Controllers And Flowmeters

These electronic units sense the mass flow of gas by measuring the differential cooling between two points. They are dependent on heat capacity and provide accurate readings regardless of temperature and pressure changes in the gas stream. All meter circuitry is solid state. The long list of units includes over 30 linear models ideal for use with integrators, totalizers and computer data reduction equipment.

Mass flow controllers incorporate a valve controlled by the flow transducer to reduce or increase flow to maintain a constant stream.

CIRCLE 175 ON READER SERVICE CARD

150mm Flowmeter Units, 7600 Series

Matheson's most versatile rotameter series. Can be panel or bench mounted with the valve on the outlet or inlet. Accuracy of 3% and 5% of full scale depending upon the rate of flow. The series offers a wide selection of flowmeter tubes with ranges from 0.0084 SCFH to 104 SCFH. Floats of glass, stainless steel, and tantalum. Accessories of brass, stainless steel, and Monel. Available with various needle valves including Matheson's new PC metering valve. Typical calibration curves for many gases available. 24 basic models to choose from.

CIRCLE 179 ON READER SERVICE CARD

The Gas Proportioner

A 2-component mixture with component accuracy to ±5% can be made with this unit. Most simply it consists of 2-150mm tubes, a mixing tube, valves (we recommend high accuracy valves) and is compensated for back pressure by outlet valves. A high sensitivity regulator (Matheson's No. 8) is a necessary accessory. You specify the mixture you need — Matheson does the rest.

CIRCLE 176 ON READER SERVICE CARD

Acrylic Purge Meters, 7260 Series

These have an accuracy of 10% full scale. They are low-priced units for use with noncorrosive gases. Direct reading scales indicate maximum flows from 0.01 to 50 SCFH of air. This series can by easily panel mounted. The acrylic body is protected by an aluminum frame. Pressure is rated at 100 psig, temperature to 150°F. Four standard ranges available.

CIRCLE 180 ON READER SERVICE CARD

150mm Four Tube Flowmeter Units, 7400 Series

Four tube units can produce 3 and 4 component gas mixtures, or permit metering of 4 separate streams of gases by changing the configurations. You can specify 3 tube mixers and a mixing tube to produce a homogeneous mixture of 3 gases. Or, 4 tubes and one discharge port to produce a 4 component mixture. Four tubes and 4 outlets permit the monitoring of 4 separate streams. Specifications are the same as those for the 150mm Series. Two models available in brass and 316 stainless steel.

CIRCLE 177 ON READER SERVICE CARD

65mm Flowmeter Units, 7200 Series

This glass flowmeter is accurate to 5% of full scale. It possesses a single float and is calibrated to read directly in SCFH of air (the series range is 0.2 to 45 max SCFH air). Correction factors for many gases are available. Fittings are of aluminum and stainless steel. Pressure to 200 psig; temperature to 250°F. Five standard ranges are available.

CIRCLE 181 ON READER SERVICE CARD

Flowmeter Calibration Services

Calibration of *all* Matheson flowmeters can be provided for virtually any gas and pressure. An actual flowmeter calibration can increase accuracy of your flow measurements. The gases shown are a partial listing of some past calibrations. Air, argon, 1,3-butadiene, butane, carbon dioxide, carbon monoxide, cyclopropane, dimethyl ether, ethane, ethylene, helium, hydrogen, isobutane, isobutylene, methane, methyl acetylene, nitrogen, nitrous oxide, oxygen, propane, propylene, refrigerants, sulfur hexafluoride and vinyl chloride.

CIRCLE 178 ON READER SERVICE CARD

Matheson®
Lyndhurst, N.J. 07071

East Rutherford, N.J. 07073
Morrow, Georgia 30260
Gloucester, Massachusetts 01930
Joliet, Illinois 60430
La Porte, Texas 77571

Cucamonga, California 91730
Newark, California 94560
Whitby, Ontario, Canada L1N 5R9
Edmonton, Alberta, Canada T5B 4K6
B 2431 Oevel, Belgium

Briefs

Analysis of Solid Materials by Laser Probe Mass Spectrometry 1735

Three lasers are used as ion sources for the analysis of solid materials by mass spectrometry. The results indicate that they are comparable with the conventional rf spark.

R. A. Bingham, AEI Scientific Apparatus Ltd., Barton Dock Road, Urmston, Manchester, England, and **P. L. Salter,*** Department of Applied Physics, University of Hull, Hull, Yorkshire, England *Anal. Chem., 48 (1976)*

Concentration Instabilities in Liquid Chromatography 1741

Methods to stabilize systems include using larger mixers, a circuit designed to use the limited frequency response of the column, a constant pressure valve, and pressure derivative feedback on the liquid flow rates.

John C. Helmer, Varian Instrument Division, Palo Alto, Calif. 94303 *Anal. Chem., 48 (1976)*

Liquid Chromatographic Identification of Oils by Separation of the Methanol Extractable Fraction 1747

Liquid chromatography fingerprints oils. Using peak-height ratios of eluting bands, oil spill suspects are first screened and then compared to the spill chromatogram statistically for objectively "matching" oils.

W. A. Saner,* G. E. Fitzgerald, and J. P. Welsh, U.S. Coast Guard Research and Development Center, Avery Point, Groton, Conn. 06340 *Anal. Chem., 48 (1976)*

Determination of the Specific Surface of Absorbents by the Dynamic Adsorption Method 1754

These studies show that the partial pressure of benzene diluted by H_2 flowing through an unsaturated adsorption column decreases exponentially with increasing column length. Approximate equations describing the adsorption course are derived.

Henryk Golka and Boguslawa Jezowska-Trzebiatowska,* Institute of Chemistry, University of Wroclaw, Wroclaw, Poland *Anal. Chem., 48 (1976)*

Correlation between Electron Capture Response and Chemical Structure for Alkyl Halides 1760

The dissociative electron capture reaction for alkyl halides is measured with an electron capture detector. The reaction mechanism and the relationship between molecular structure and activation energy are discussed.

Tsugio Kojima* and Yasukazu Tanaka, Department of Industrial Chemistry, Faculty of Engineering, Kyoto University, Yosida, Kyoto, Japan, and **Masaru Satouchi,** Department of Industrial Chemistry, Shiga Prefectural Junior College, Hikone, Shiga, Japan *Anal. Chem., 48 (1976)*

Comparison of Positive Ions Formed in Nickel-63 and Corona Discharge Ion Sources Using Nitrogen, Argon, Isobutane, Ammonia, and Nitric Oxide as Reagents in Atmospheric Pressure Ionization Mass Spectrometry 1763

The formation of N^+, N_2^+, N_4^+, and Ar^+ ions in a corona discharge source at atmospheric pressure is described. The formation and reactions of $t\text{-}C_4H_9^+$, NO^+, and NH_4^+ ions with organic compounds are compared for ^{63}Ni and corona discharge sources.

I. Dzidic, D. I. Carroll, R. N. Stillwell, and E. C. Horning,* Institute for Lipid Research, Baylor College of Medicine, Houston, Texas 77025 *Anal. Chem., 48 (1976)*

Large-Scale Mass Spectral Analysis by Simplex Pattern Recognition 1768

Prediction performance of weight vectors representing 11 functional group categories are examined using a test set of over 1900 mass spectra. Simplex-derived vectors are superior for linearly inseparable data.

T. Fai Lam, Charles L. Wilkins,* Thomas R. Brunner, Leonard J. Soltzberg, and Steven L. Kaberline, Department of Chemistry, University of Nebraska-Lincoln, Lincoln, Neb. 68588 *Anal. Chem., 48 (1976)*

Comparison of Continuum Models in Quantitative Diffuse Reflectance Spectrometry 1775

The failure of the Kubelka–Munk and other simple reflectance theories is due to the assumption of isotropic scatter. Reflectance data can be quantitatively interpreted using more general phase factors.

Harry G. Hecht, Department of Chemistry, South Dakota State University, Brookings, S.D. 57006 *Anal. Chem., 48 (1976)*

Determination of Ammonia by Mercury-Sensitized Luminescence 1780

Mercury-sensitized luminescence combined with chromatographic separation is used to determine ammonia in both nitrogen and air. The sensitivity for ammonia is 0.5 pg in N_2 and 3.0 pg in air.

William Ho* and A. B. Harker, Science Center, Rockwell International, Thousand Oaks, Calif. 91360 *Anal. Chem., 48 (1976)*

Determination of *p*-Aminobenzoic Acid by Room Temperature Solid Surface Phosphorescence 1784

The phenomenon of room temperature phosphorescence of molecules adsorbed on sodium acetate is discussed. A sensitive method for the phosphorimetric determination of *p*-aminobenzoic acid in vitamin tablets is described.

R. M. A. von Wandruszka and R. J. Hurtubise,* Department of Chemistry, University of Wyoming, Laramie, Wyo. 82071 *Anal. Chem., 48 (1976)*

Determination of Tin by Gas Phase Atomization and Atomic Absorption Spectrometry 1788

A hydride generation–atomic absorption procedure is outlined for the determination of tin in different matrices with an accuracy of 97% and precision of 6% RSD.

Prem N. Vijan* and Chris Y. Chan, Air Quality Laboratory, Ministry of the Environment (Ontario), Toronto, Ontario, Canada *Anal. Chem., 48 (1976)*

Briefs

Studies on the Mechanism of Atom Formation in Graphite Furnace Atomic Absorption Spectrometry 1792

The mechanism of atomization of a number of elements in a Perkin-Elmer HGA 2100 atomizer proceeds by three major pathways: thermal dissociation of the oxide or halide, and carbon reduction of the oxide followed by atomization of the free metal.

R. E. Sturgeon, C. L. Chakrabarti,* and C. H. Langford, Metal Ions Group, Department of Chemistry, Carleton University, Colonel By Drive, Ottawa, Ontario, Canada K1S 5B6

Anal. Chem., 48 (1976)

Correspondence

Sulfate Formed by Interaction of Sulfur Dioxide with Filters and Aerosol Deposits 1808

William R. Pierson,* Robert H. Hammerle, and Wanda W. Brachaczek, Ford Motor Company, Research Staff, P.O. Box 2053, Dearborn, Mich. 48121 *Anal. Chem., 48 (1976)*

Modified Buffer for Use with Fluoride-Selective Electrodes 1811

J. Bagg, Department of Industrial Science, University of Melbourne, Parkville, Victoria 3052, Australia

Anal. Chem., 48 (1976)

Chromatographic Analysis of Gaseous Products from Pyrolysis of Organic Wastes with a Single Column 1812

Peter T. Brodowski, Norma B. Wilson, and William J. Scott,* Resource Recovery Systems Division, Barber-Colman Company, Irvine, Calif. 92714 *Anal. Chem., 48 (1976)*

Free Energy Correlations with Solvatochromic Red Shifts for Indicators in Aprotic Solvents 1814

Orland W. Kolling, Chemistry Department, Southwestern College, Winfield, Kansas 67156 *Anal. Chem., 48 (1976)*

Application of a Vidicon Tube as a Multiwavelength Detector for Liquid Chromatography 1815

Alan McDowell and Harry L. Pardue,* Department of Chemistry, Purdue University, West Lafayette, Ind. 47907

Anal. Chem., 48 (1976)

Aids for Analytical Chemists

Determination of Low Concentrations of Hydrogen Chloride in Moist Air 1818

R. R. Bailey, P. E. Field, and J. P. Wightman,* Department of Chemistry, Virginia Polytechnic Institute and State University, Blacksburg, Va. 24061 *Anal. Chem., 48 (1976)*

Determination of Methacrylic Acid by Coulometric Titration 1820

D. H. Grant* and V. A. McPhee, Department of Chemistry, Mount Allison University, Sackville, N.B., Canada EOA 3C0

Anal. Chem., 48 (1976)

Performance Test for Direct Reading Balance 1821

Don H. Anderson* and N. B. Woodall, Eastman Kodak Company, Kodak Park Division, Industrial Laboratory, Building 34, Rochester, N.Y. 14650 *Anal. Chem., 48 (1976)*

Sniffer to Determine the Odor of Gas Chromatographic Effluents 1821

T. E. Acree,* R. M. Butts, R. R. Nelson, and C. Y. Lee, Department of Food Science and Technology, Cornell University, New York State Agricultural Experiment Station, Geneva, N.Y. 14456

Anal. Chem., 48 (1976)

Modification of Graphite Furnace Power Supply to Allow Interruption of Analytical Cycle 1822

E. W. Cooper* and J. V. Dunckley, Electronic Engineering Department, Dunedin Hospital, Dunedin, New Zealand

Anal. Chem., 48 (1976)

External Reference Signal in X-ray Energy Spectrometry 1823

P. J. Van Espen and F. C. Adams,* Department of Chemistry, University of Antwerp (U.I.A.), B2610 Wilrijk, Belgium

Anal. Chem., 48 (1976)

Dual Column Operation for Gas Chromatograph—Mass Spectrometer 1826

Leo Kazyak, Division of Biochemistry, Walter Reed Army Institute of Research, Washington, D.C. 20012

Anal. Chem., 48 (1976)

Gas Chromatograph—Mass Spectrometer with Dual Electron Impact/High Pressure Ion Source 1829

Ragnar Ryhage, Laboratory for Mass Spectrometry, Karolinska Institute, S-104 01 Stockholm 60, Sweden

Anal. Chem., 48 (1976)

Self-Positioning Anti-Vortex Plug for Nuclear Magnetic Resonance Sample Tubes 1832

LeRoy F. Johnson, Nicolet Technology Corporation, Mountain View, Calif. 94041 *Anal. Chem., 48 (1976)*

Correction. Kinetically Assisted Equilibrium Based Repetitive Determination of Iron(II) with Ferrozine in Flow-Through Systems 1832

V. V. S. Eswara Dutt, A. Eskander-Hanna, and H. A. Mottola

The perfect balance.

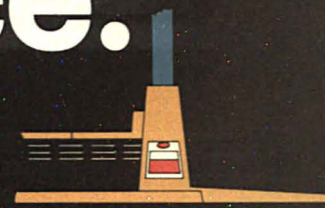

The perfect balance between price and speed, with the accuracy necessary to make speed count... in schools, hospitals, industrial labs:

The Ohaus Cent-O-Gram 311's four-tiered beams have notched and windowed poises for foolproof reading.

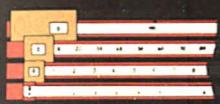

On the comparable Ohaus Dial-O-Gram 310, two beams and poises are replaced by a precision engraved dial and vernier. This dial incorporates a spring that applies torque to the beam at its fulcrum, the torque being equal to the weight indicated on the dial.

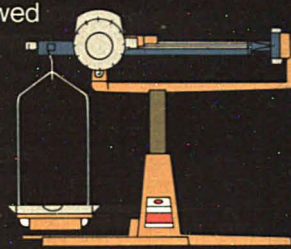

Another of the many features that make these scales invaluable in the laboratory is a self-storing platform for quick and easy specific gravity measurements.

For our illustrated 32-page catalog, write: Ohaus Scale Corporation, 29 Hanover Road, Florham Park, N.J. 07932.

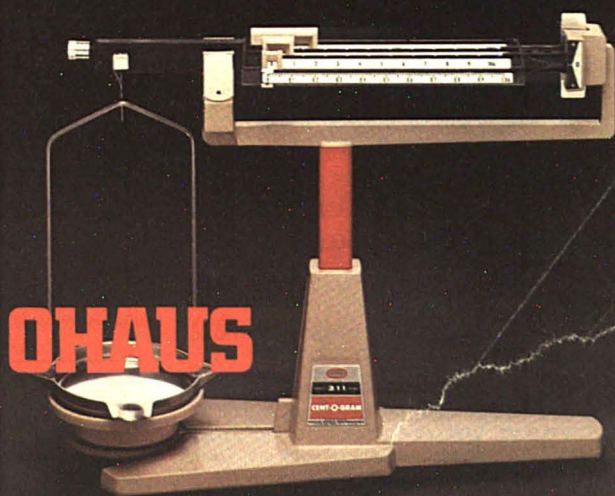

Measuring up since 1907

CIRCLE 159 ON READER SERVICE CARD

THE TALL METERS

ORIGINATED BY CORNING

Tall to look you straight in the eye.

Tall to take up half as much bench space as short meters.

Tall with a swift, steady side-arm to ease and speed your work.

A new generation of pH meters from a wedding of bio-engineering and solid state of the art electronics. Digital display on top where your eyes are. Controls down the side where your hands are. Flexing side-arms to take electrodes where the work is. It's more like communicating than reading.

I-C chips. One, easy-to-replace circuit board. Cool, energy-saving Light Emitting Diode display. U/L and CSA listings.

THREE YEAR WARRANTY

THAT'S HOW RELIABLE THE TALL ONES ARE.

Corning Glass Works warrants pH meters Model 125 and Model 130 to be free from defects in material and workmanship when used under normal laboratory conditions for a period of three (3) years.

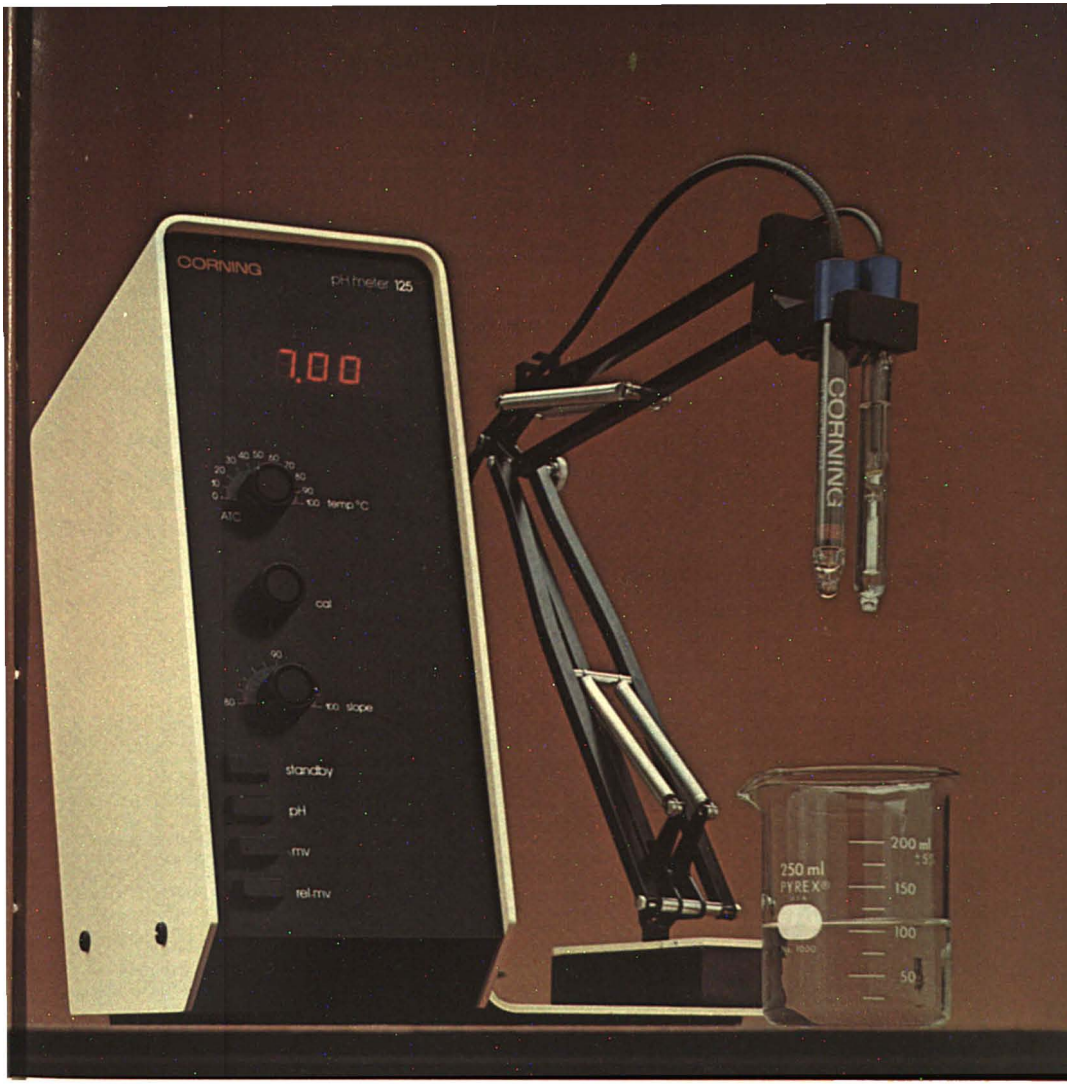

Even the back is all up front. Everything orderly and easy to get at.

The tall meters are ambidextrous. You decide whether they function left-handed or right.

Corning tall meters are lean . . . and that includes their price. Even with a general purpose pH and a reference electrode thrown in, they actually cost less than comparable short meters.

They can be used with ion selective electrodes, too.

Both Corning originals are at your dealer now. Ask for a demonstration. The Model 130 is a 3 decimal unit with fine tuning. $895. suggested list price. The Model 125 has all the critical features with a 2 decimal display. $595. suggested list price.

CORNING™
pHware

CIRCLE 34 ON READER SERVICE CARD

Third Annual Meeting

FACSS

November 14–19, 1976
Philadelphia, Pa.

In Philadelphia the seven sponsoring groups that make up the Federation of Analytical Chemistry and Spectroscopy Societies (FACSS) combine with the XIX Colloquium Spectroscopicum Internationale and 6th International Conference on Atomic Spectroscopy to present a 4½ day program of 400 technical papers.

Approximately 20% of the papers are from outside the U.S. with the largest numbers from Canada, England, Germany, France, and Russia. Special award symposia include the Lippincott Award, Benedetti-Pichler, and Anachem. R. C. Lord, winner of the Lippincott Medal, will discuss strategy and tactics in the Raman spectroscopy of biomolecules, Tuesday morning, Nov. 16. Wednesday morning, the Anachem Award lecture by winner John M. Vandenbelt will cover standards in analytical instrumentation. Thursday morning, T. S. Ma, Benedetti-Pichler award recipient, will describe the objectives and implications of microchemistry. In addition to sessions on chromatography, spectroscopy, and electrochemistry, special sessions will cover museum science, computers, biochemical and pharmaceutical applications of NMR, thermal methods, excitation sources in spectroscopy, air and water quality, NMR instrumentation and quantitation, image detectors in spectroscopy, teaching analytical chemistry, trace elements and reference standards, clinical problems, x-ray diffraction, furnace atomic absorption, spectroscopy of surfaces, environmental aspects of GC, process control analyzers, particle characterization, atomic fluorescence, polymer analysis, ion probe and SIMS, and detection of chemical species.

Short courses, workshops, and technical films form part of the scientific program. The Society for Applied Spectroscopy will present courses on modern emission spectroscopy and Fourier transform spectroscopy: IR and NMR. For details, see the August issue, page 764 A. The American Chemical Society has five short courses scheduled (see this issue, page 970 A). There will also be workshops on ion-selective electrodes, energy-dispersive x-ray analysis, and use of powder diffraction file.

Because of the many guests from outside the U.S. and the many attractions of the Bicentennial City, an extensive cultural, educational, and social program has been planned. There will be stimulating and interesting activities throughout the week beginning Sunday evening at the Philadelphia Sheraton with a talk by Whitfield J. Bell, Jr., about Ben Franklin and his cronies and continuing through Friday afternoon when the Philadelphia Orchestra will be in concert at the Academy of Music. Included are city tours, walking tours, museum visits, and visits to research establishments. An instrument exposition will accompany the meeting. Exhibitors and their products are listed on the following pages. Further information concerning the exhibits may be obtained from Edward Ruffing, Scherago Associates, 11 W. 42nd St., New York, N.Y. 10036.

All of the technical activities will take place in the Civic Center or nearby hotels. Housing forms and information are available by writing to the FACSS Housing Bureau, Philadelphia Convention Bureau, 1617 John F. Kennedy Blvd., Suite 1420, Philadelphia, Pa. 19103.

Preregistration fees are $30 or if a member of a national or international sponsoring group, $25. To qualify for preregistration, completed forms must be received by October 30. Forms and further information may be obtained from Theodore C. Rains, Analytical Chemistry Division, National Bureau of Standards, Washington, D.C. 20234.

The complete technical program for the 3rd FACSS meeting is given on the following pages of ANALYTICAL CHEMISTRY.

1976 Meeting Officers


Brame


Dunlop


Ferrari


Robinson

Cochairmen

Arrangements: *Edward G. Brame, Jr.*, Du Pont

Program: *Edward C. Dunlop*, Du Pont

Cochairmen-Elect

Arrangements: *Mitch Kapron, James A. Burns, Jr.*, Ethyl Corp.

Program: *Jeanette G. Grasselli*, Standard Oil Co. (Ohio)

Program Committee

Chairman: *E. C. Dunlop*, Federation of Analytical Chemistry and Spectroscopy Societies

Cochairman: *K. F. J. Heinrich*, XIX Colloquium Spectroscopicum Internationale

Cochairman: *S. R. Koirtyohann*, VI International Conference of Atomic Spectroscopy

Treasurer: *Louis Brancone*, Lederle Laboratories

Budget: *Paul Lublin*, GTE Laboratories

Publicity: *Hal Ferrari*, Lederle Laboratories

Registration: *Ted Rains*, National Bureau of Standards

Arrangements: *Doug Robinson*, Pennwalt Corp.

Exposition: *James Devlin*, Du Pont Marshall Laboratories

Employment: *David Nash*, Bell Telephone Laboratories

Message Center: *Alex Presioso*, Laboratory Data Control

Student Awards: *Leonard Klein*, FMC Corp.

Workshops: *James Lindsay*, U.S. Geological Survey

Cultural, Educational, & Social: *Anne Donnell*

Hospitality: *Richard Knauer*, Armco Steel

Housing: *George Davis*, Delare Assoc.

Publications: *Galen Ewing*, Seton Hall University

Monday Morning, Nov. 15

Analytical Chemistry in Museum Science

E. C. Dunlop, *Presider*, Du Pont

9:00 Opening Remarks. E. C. Dunlop

9:05 Welcome by General Chairman. E. G. Brame

9:10 Welcome by Philadelphia Officials

9:15 Identification of Art Objects by X-ray Fluorescence Spectroscopy. V. Hanson, Winterthur Museum

10:15 Curational-Scientific Appraisal of Selected Pewter Objects. J. H. Carlson, D. Fennimore, Winterthur Museum

10:45 Standard Reference Materials for Analysis of Glasses. I. L. Barnes, NBS

11:15 Surface Studies of Ancient Gold Coins and Modern Copies by X-ray Fluorescence, SEM, and Auger Spectroscopy. L. J. Cline Love, L. Soto, Seton Hall U; B. Reagar, Bell Labs; J. V. Noble, Museum of the City of New York

Computers in Analytical Chemistry

P. Jurs, *Presider*, Penn State U

10:00 Design Philosophy of Portable On-Line Infrared Computer System. A. Savitsky, Perkin-Elmer

10:30 Computerized Pattern Recognition as Viable Tool in Laboratory Automation. S. P. Perone, Purdue U

11:00 Time-Shared Pattern Recognition in Laboratory Medicine Using APL. J. C. MacDonald, Fairfield U

11:20 Use of Microcomputer-Controlled IR Spectrometer for Automatic Identification of Organic Compounds. W. L. Truett, Wilks Scientific Corp.

11:40 Quantitative Electron Spin Resonance Measurements Using Programmable Desk Calculator. A. J. Dupuis III, D. C. Warren, Houston Baptist U

12:10 Design and Application of Programmable Calculator-Controlled Instrument for Potentiometric Analysis. J. M. Baldwin, H. R. Deveraux, Allied Chemical Corp.

NMR Biochemical and Pharmaceutical Applications

R. Cox, *Presider*, U of Georgia

10:00 Recent Advances in ^{3}H NMR. L. Altman, SUNY

10:30 Recent Advances and Applications of ^{2}H NMR. J. Whidby, Philip Morris

11:00 Spectroscopic Study of Sodium Solvation Sodium—23 Nuclear Magnetic Resonance Studies in Nonaqueous Solvents. J. H. Ambrus, U.S. Naval Surface Weapons Center; D. N. Kender, Ciba-Geigy

11:20 Quantitative Analysis of Degradation Products in Ophthalmic Formulations of Pilocarpine Hydrochloride. G. A. Neville, Health and Welfare Canada; F. B. Hasan, I. C. P. Smith, National Research Council of Canada

11:40 Compositional Analysis of Sucrose Polyether Polyols by ^{13}C and ^{1}H NMR. C. H. Ke, G. P. Cunningham, P. E. Pierce, PPG Industries

Thermal Methods of Analysis

J. Jordan, *Presider*, Penn State U

10:00 Recent Developments in Thermal Analysis. W. W. Wendlandt, U of Houston

10:30 Approach to Comprehension of Phenomena in Nonflame Atomic Absorption Spectroscopy by Thermogravimetry, Combined Electron Microscope–Micro-Probe, and Oscilloscopy. J. Sire, Laboratoire Regional des Ponts and Chaussees, France; I. A. Voinovitch, Laboratoire Central des Ponts and Chaussees, France

10:50 Thermometric Detection of Biochemical Reactions. N. D. Jespersen, U of Texas

11:20 Improved Subambient Operation of Differential Scanning Calorimeter (DSC). K. F. Baker, P. S. Gill, Du Pont

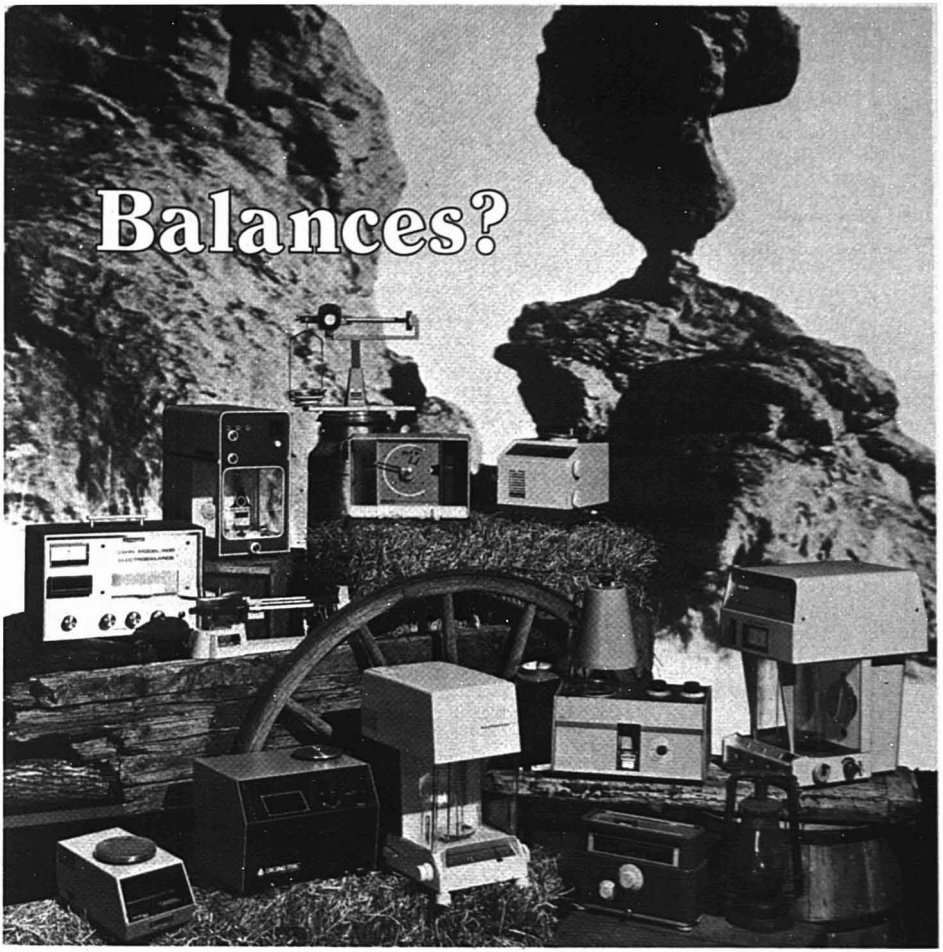

..we have the right model for you -- whatever your weighing need!

Shown are just twelve of the one-hundred-two-plus balances we stock. Balances by such outstanding makers as Ainsworth, Biolar, Cahn, Digimetric, Ohaus, Sartorius, Sauter, Torsion and Voland. We supply balances covering the spectrum of laboratory weighing from a particle to a mass; balances for every purpose from routine work to a host of highly specialized needs: analytical balances, animal balances, air pollution balances, assembly-line balances, digital balances, electrobalances, direct-reading balances, micro balances, macro balances, moisture balances, student balances, research balances.

Literature pertaining to your particular balance requirements will be sent on request.

SGA

SCIENTIFIC

BLOOMFIELD, N. J. 07003

Laboratory apparatus • instruments chemicals • glassware

Branches: Boston, Mass./Elk Grove Village, Ill./Fullerton, Calif./New Haven, Conn./Philadelphia, Pa./Silver Spring, Md./Syracuse, N.Y.

CIRCLE 190 ON READER SERVICE CARD

11:40 Thermogravimetric Determination of Stability of Metal-Protein Complexes. S. Gorinstein, Hebrew U of Jerusalem, Israel

Excitation Sources for Spectroscopy

R. Barnes, *Presider*, U of Massachusetts

10:00 Excitation Conditions and Interferences in Inductively Coupled Plasma. L. de Galan, Technische Hogeschool, The Netherlands

10:40 Studies of Interferences with ICP Used in OES. M. H. Abdallah, J. M. Mermet, J. Robin, C. Trassy, Institut National de Sciences, France

11:00 Inductively Coupled Plasma–Atomic Emission Spectroscopy—Spatially Resolved Radial Excitation Temperatures and Electron Number Distributions Experienced by Analyte Species. D. J. Kalnicky, V. A. Fassel, R. N. Kniseley, Iowa State U

11:20 Computer Simulation of Inductively Coupled Plasma Discharge. S. Chandra, R. M. Barnes, U of Massachusetts

11:40 Experimental Temperature and Velocity Profiles in Inductively Coupled Plasma Discharge. J. Genna, R. M. Barnes, U of Massachusetts

12:00 Induction-Coupled Plasma Emission from a Different Angle. F. E. Lichte, S. R. Koirtyohann, U of Missouri

Air and Water Quality

H. E. Allen, *Presider*, Illinois Institute of Technology

10:00 Environmental Chemistry: Validity of Data Obtained. J. L. Monkman, Environmental Protection Service, Canada

10:30 Contribution of Atmospheric Transported Materials to Chemical Budget of Aquatic Systems. F. C. Elder, Canada Centre for Inland Waters

10:50 Determination of Water Quality by Means of Remotely Sensed and Locally Acquired Optical Data. R. P. Bukata, J. E. Bruton, J. H. Jerome, Canada Centre for Inland Waters

11:10 Wastewater Monitoring Program by City of New York. S. L. Kirschner, City of New York Environmental Protection Administration

11:30 Improved Method for Quantitative Measurement of Adenosine Triphosphate in Lake Waters, Activated Sludge Systems, and Sediments. B. K. Afghan, J. F. Ryan, R. S. Tobin, Canada Centre for Inland Waters

Monday Afternoon

Computers in Analytical Chemistry

P. Jurs, *Presider*, Penn State U

2:00 Visual Information Interpretation—A Low-Cost Color Display System. T. L. Isenhour, J. deHasetn, G. T. Rosmussen, W. S. Woodward, U of North Carolina

2:30 Computer-Assisted Analytical Data Analysis. P. C. Jurs, Penn State U

3:00 General Electronic Data Processing Technique for Atomic Absorption Spectroscopy. G. E. Harrison, A. M. Yoakum, P. L. Stewart, Stewart Labs

3:35 Some Observations on Use of Echelle "Computer-Aided Direct Reader" for Multielement Atomic Spectroscopy. W. G. Cox, Naval Underwater Systems Center

3:55 New Transducers for Computer Interfacing of Flame Spectrometer. T. W. Hunter, G. M. Hieftje, Indiana U

4:15 Simulation in Spectrochemical Analysis and Atomic Absorption Spectroscopy. Ya. D. Raikhbaum, K. F. Popoff, A. I. Kuznetsova, E. S. Kostukova, Siberian Department of the Academy of Sciences, USSR

4:35 Microcomputer-Controlled Monochromator Accessory Module for Dual-Wavelength Spectrochemical Measurements. J. D. Defreese, H. V. Malmstadt, U of Illinois

4:55 Double-Scanning Technique for Measuring Statistical Distribution of Impurity Molecules. T. Tamm, J. Kikas, Estonian Academy of Sciences, USSR

NMR Instrumentation and Quantitation

D. Leyden, *Presider*, U of Denver

2:00 Recent Advances in Fourier Transform NMR. T. Farrar, National Science Foundation

2:30 Quantitative Measurements Using ^{13}C Fourier Transform NMR. J. Shoolery, Varian

3:00 Quantitative Aspects of Studies of Polymers by High-Resolution NMR. F. Bovey, Bell Labs

3:45 Recent Developments in Solid-State NMR—Are Many Photons Better Than One? A. Pines, U of California

4:15 Optimization of NMR Tuning. M. R. Willcott, S. N. Deming, U of Houston

4:35 Optimized GC–IR–NMR Techniques. K. L. Gallaher, J. G. Grasselli, Standard Oil Co. (Ohio)

4:55 ^{13}C NMR of Fluorinated Compounds Using Wideband ^{19}F Decoupling. D. W. Ovenall, J. J. Chang, Du Pont

Molecular Spectroscopy

A. H. Hardin, *Presider*, Canadian Centre for Mineral and Energy Technology

2:00 Infrared Spectroscopy of Mixtures. T. Hirschfeld, Block Engineering

2:20 Fourier Infrared Spectroscopy of Transients. A. W. Mantz, Digilab

2:40 Detection Limits in FT–IR Spectroscopy. T. Hirschfeld, Block Engineering

3:00 Weird Apodizations in FT–IR. T. Hirschfeld, Block Engineering

3:35 Limitation of Quantitative FT–IR. R. Julian, Nicolet Instrument Corp.

3:55 Sensitivity Comparisons of FT–IR Techniques. D. Mattson, Nicolet Instrument Corp.

4:15 Infrared and Raman Spectra of Vanadium Phosphate Crystals and Glasses. R. A. Condrate, Sr., R. N. Bhargava, Alfred U

4:35 Application of Infrared to Kinetic Analysis. S. G. Linsley, Wilks Scientific Corp.

4:55 Liquid-Phase Isotopic Shift in Benzyl Halides. R. Julian, Nicolet Instrument Corp.

Image Detectors in Analytical Spectroscopy

H. L. Pardue, *Presider*, Purdue U

2:00 Rapid Scanning Fluorescence Spectroscopy in Analytical Chemistry. G. D. Christian, U of Washington

2:30 Time-Resolved Resonance Raman Spectroscopy. W. H. Woodruff, Syracuse U

3:00 Instrumentation for Spectroscopy in Ultraviolet and Visible Regions Using Computerized TV Readout System. D. L. Wood, Bell Labs

3:45 Sensitivity of Silicon Vidicon Detectors Used for Atomic Spectrochemical Analysis. N. G. Howell, G. H. Morrison, Cornell U

4:05 Linear Silicon Photodiode Arrays with Parallel Data Output as Radiation Detectors in Optical Emission Spectrometry. H. Bubert, W. D. Hagenah, K. Laqua, Institut fur Spektrochemie und Angewandte Spektroskopie, Germany

4:25 Microprocessor-Controlled Photodiode Array Spectrometer. D. Lovse, H. V. Malmstadt, U of Illinois

4:45 Design of Versatile Multielement Spectrometer for Atomic Spectroscopy Using Image Dissector. J. S. Garden, K. M. Aldous, New York State Department of Health

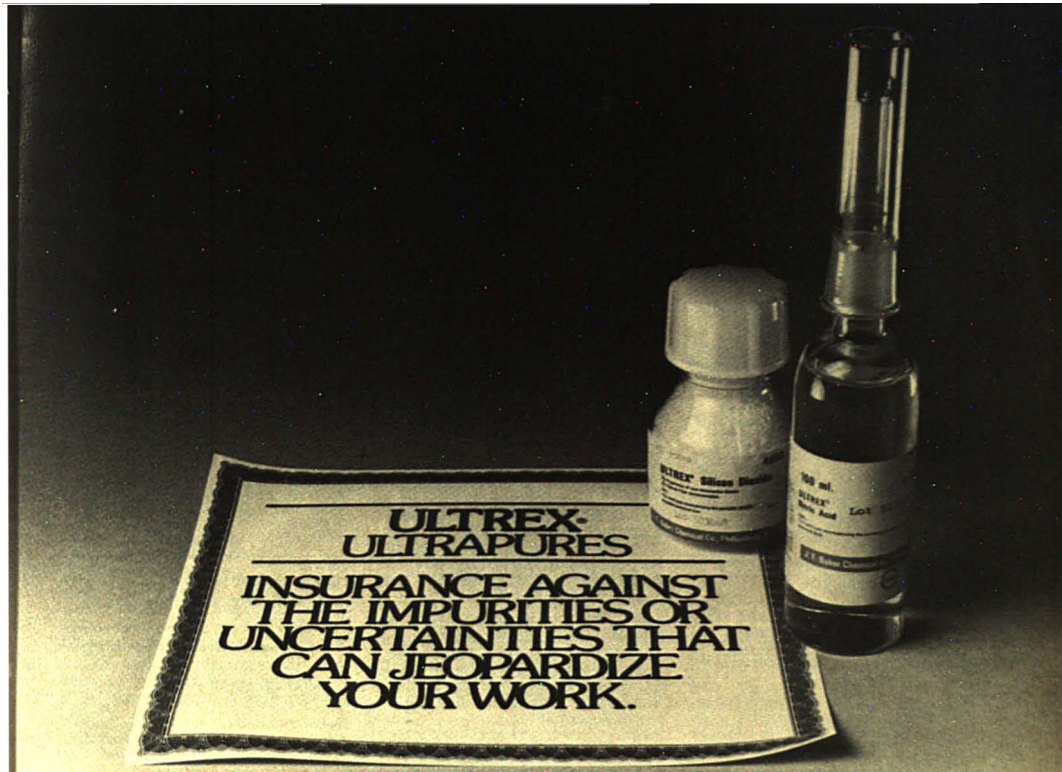

The ULTREX concept

1. To provide the purest products available for the most demanding endeavors.
2. To provide maximum product definition.

In other words: to provide insurance against the impurities or uncertainties that can jeopardize your work.

The ULTREX line

Nearly 100 of the finest ultrapure reagents and chemicals available anywhere in the world. Every product is accompanied by a detailed Certificate of Analysis of the actual lot supplied. Take the ULTREX Nitric Acid label, for example: HNO_3 assay, residue after ignition, specific gravity, non-metallic impurities (6), metallic impurities (23), plus a note re measurement techniques. In terms of spectrochemically detectable impurities, ULTREX products are typically 99.995 to 99.9999 pure. And the extremely low content of *all* impurities (often at the parts per billion level) satisfies the most rigid use requirements.

A note to those now considering ultrapures

Ultrapures are not inexpensive. But where appropriate, they can be your best investment. Whenever your requirements for purity and product definition are stringent, ULTREX products can indeed insure against loss of time, effort, and other expenses. Consider ULTREX when you just can't afford to gamble with impurities or uncertainties.

A note to those who do their own purification

ULTREX products are made with the latest in advanced equipment in Baker's brand new Class-100 clean room installation in Winchester, Va. The ULTREX analysis, an extensive proof of purity, is performed by Ph.D. analytical chemists in Baker's research laboratories. The actual lot analysis for a typical ULTREX product takes three days, while nearly 40 manhours are required for products such as sodium chloride. When the analysis is complete Baker's Director of Research verifies the work and signs the certificate. This certificate is supplied with each package of that ULTREX product. Consider letting us supply your needs. We may well save you time. We *know* we'll save you time.

For more information

See pages 145 to 180 in our Catalogs

750/760 or write for our 36 page ULTREX brochure. And if you find that we now don't supply an ultrapure you need, let's talk.

Finally, there's Super Service

If your Baker distributor is out of stock on ultrapures that you need *now*, he can call a Baker Super Service Center and, if he calls by 3:30 p.m. our time, your order will go out directly to you in most cases on the very next business day. That's Baker Super Service.

J. T. Baker: "use-matched" products and... Super Service.

J.T.Baker® CHEMICALS

J. T. Baker Chemical Company
Phillipsburg, New Jersey 08865
201/859-5411

Teaching Analytical Chemistry Objectives, Performance, and Evaluation

W. H. Harris, *Presider*, U of Alberta

2:00 Teaching Analytical Chemistry—Objectives, Performance, and Evaluation. H. Diehl, Iowa State U

2:30 Real World Needs and Expectations from Teaching of Analytical Chemistry. J. Grasselli, Standard Oil Co. (Ohio)

3:00 Teaching Analysis as Symbiosis. R. Ramette, Carleton Coll

3:45 College Graduate to Analytical Chemist—How Does It Happen? H. Pardue, Purdue U

4:15 Modular Microprocessor System for Both Teaching and Analytical Automation. J. Avery, D. Lovse, H. V. Malmstadt, U of Illinois

4:45 Evaluation—Why and How? B. Kratochvil, W. E. Harris, U of Alberta, Canada

Trace Element Analyses and Reference Standards

G. A. Uriano, *Presider, NBS*

2:00 Concept of Accuracy in Chemical Analytics. H. Kaiser, Dortmund, West Germany

2:30 Application of Poly(dithiocarbamate) Chelating Ion-Exchange Resins to Trace Analysis. D. Hackett, S. Siggia, U of Massachusetts

2:50 Determination of Ultratraces of Elements in $SiCl_4$ by Flameless Atomic Absorption Spectrometry. T. Y. Kometani, Bell Labs

3:10 Optimized Calibration Procedure for Spectrochemical Analysis. D. G. Mitchell, W. N. Mills, M. Zdeb, New York State Department of Health

3:45 Direct Determination of Trace Elements in Water by Graphite Furnace Atomization—AAS. T. C. Rains, I. L. Barnes, M. S. Epstein, NBS

4:05 Total Solution Technique for Preparing Spectrochemical Standards. H. C. Whitehead, ERDA

Excitation Sources for Spectroscopy

R. Barnes, *Presider*, U of Massachusetts

2:00 Aspects of Inductively Coupled Plasma Spectroscopy. S. Greenfield, Albright and Wilson Ltd., England

2:40 Improved Ultrasonic Nebulization Facility for Ultratrace Multielement Analysis. Evaluation and Comparison with Pneumatic Nebulization in Inductively Coupled Plasma–Atomic Emission Spectrometry. K. W. Olson, W. J. Haas, Jr., V. A. Fassel, Iowa State U

3:00 Evaluation of Proposed Solutions to Stray Light/Background Problem in Ultratrace Analysis by Atomic Emission Spectrometry. V. A. Fassel, W. J. Haas, Jr., J. M. Katzenberger, R. N. Kniseley, G. F. Larson, R. K. Winge, Iowa State U

3:35 Reduction of Stray Light in Inductively Coupled Plasma Emission Spectrometry. C. C. Wohlers, Fisher Scientific

3:55 Trace Level Multielement Analysis by Atomic Emission Spectrometry. Applications of Simultaneous Multielement Wavelength Profiling Facility for Diagnosis of Stray Light and Spectral Line Interference Effects. W. J. Haas, Jr., R. K. Winge, V. A. Fassel, R. N. Kniseley, Iowa State U

4:15 Accuracy of Determination by Induction-Coupled Plasma in Complex Biologic Matrices; Some Important Factors. R. L. Dahlquist, R. D. Irons, J. W. Knoll, U of Rochester

4:35 Trace Elemental Analysis in Environmental and Biological Samples Using Inductively Coupled Argon Plasma–Optical Emission Spectrometry. A. F. Ward, H. R. Sobel, Fisher Scientific

4:55 Preservation of Accuracy in Determination of Trace Elements in Complex Matrices Using Inductively Coupled Argon Plasma–Optical Emission Spectrometry. A. F. Ward, R. L. Crawford, H. R. Sobel, Fisher Scientific

5:15 New Lines of Sulfur Provided by AR–H_2S ICP. J. Jarosz, J. M. Mermet, Institut National des Sciences, France

Air and Water Quality

I. H. Suffet, *Presider*, Drexel U

2:00 Identification and Measurement of Trace Organics in Water: An Overview. W. T. Donaldson, Environmental Research Lab

2:30 Application of Direct Head Gas Analysis for Determination of Chloroform in Drinking Water. S. L. Friant, Academy of Natural Science; I. H. Suffet, Drexel U

2:50 Microcoulometric Method for Determination of Total Organic-Bound Chlorine in Drinking Water. W. H. Glaze, G. R. Peyton, J. E. Henderson IV, R. Rawley, North Texas State U

3:10 Low-Molecular-Weight Aromatic Hydrocarbons in Drinking Water. R. D. Smillie, T. Sakuma, W. K. Duholke, Ontario Ministry of the Environment, Canada

3:45 Recovery and Identification of Trace Quantities of Phenolic Compounds from Natural Waters. G. T. Hunt, W. H. Clement, S. D. Faust, Rutgers, The State U

4:05 On the Beach—Infrared Spectroscopy in the Real World. C. W. Brown, W. P. Lee, P. F. Lynch, M. Ahmadjian, U of Rhode Island

4:25 Measurement of Organics in Some Treated and Untreated Water Supplies of Southern Ontario. F. P. Cappelli, J. Lawrence, P. D. Goulden, Canada Centre for Inland Waters

Tuesday Morning, Nov. 16

Lippincott Medal Symposia: Medal Ceremony

J. E. Katon, *Presider*, Miami U

9:00 Welcoming Remarks. E. G. Brame

9:05 Presentation of 1976 Lippincott Medal. By J. E. Katon, President, Society for Applied Spectroscopy, to R. C. Lord, MIT

9:15 Lippincott Medal Address: Strategy and Tactics in Raman Spectroscopy of Biomolecules. R. C. Lord

Lippincott Medal Symposia: Ellis R. Lippincott Memorial Symposium

R. J. Jakobsen, *Presider*, Battelle-Columbus Lab

10:15 Legends of Ellis R. Lippincott. W. G. Fateley, Kansas State U

10:40 Some Research in the Footsteps of Lord and Lippincott. F. A. Miller, U of Pittsburgh

11:10 Recent Advances in C–H Stretching Frequencies. L. J. Bellamy, Ministry of Technology, England

11:40 Recent Advances in Application of Analytical Techniques to Study of Hydrocarbons in Marine Environment. D. W. Mayo, Bowdoin Coll

Excitation Sources for Spectroscopy

R. Barnes, *Presider*, U of Massachusetts

10:00 Plasmatrons for Spectral Analysis. Z. Zheenbaev, V. S. Engelsht, K. Urmanbetov, Academy of Sciences of Kirgizskaja, USSR

10:20 Study of Processes in Emission Spectral Analysis. A. V. Karykin, USSR Academy of Sciences

10:40 Diagnostics of Analytical Plasmas–Flames and DC Arcs at Atmospheric Pressures by Moving Double-Floating Probes. R. Avni, U. Carmi, I. Inspector, Nuclear Research Centre, Negev, Israel

11:00 Luminosity and Radiometry Measurements of Pyrotechnic Flames. T. A. Doris, W. J. Puchalski, Frankford Arsenal; P. N. Keliher, Villanova U

11:20 Concerning the Use of DC Argon Plasma as Excitation Source

in Emission Spectroscopy. M. D. Sands, Raytheon Co.; W. G. Cox, Naval Underwater Systems Center

11:40 Analysis of Phosphorus by Plasma Emission Spectroscopy—Some Practical Applications. E. Griffin, Texas Instruments

12:00 Emission Spectroscopical Investigations on Methane Pyrolysis in AC Arc. H. Nickel, G. Heinrich, M. Mazurkiewicz, Kernforschungsanlage Julich GmbH, Germany

Analytical Chemistry for Clinical Laboratories

G. N. Bowers, Jr., *Presider*, Hartford Hospital

10:00 Overview of Cellular Respiration. R. Poynton, U of Connecticut

10:30 Instrumentation Developments on Automated System for Clinical Analyses. M. McCracken, H. V. Malmstadt, U of Illinois

10:50 Clinical/Analytical Applications of New Automated Analyzer System. D. Krottinger, H. V. Malmstadt, U of Illinois

11:10 Nicotinamide Adenine Dinucleotides—Metabolic and Analytical Considerations. L. W. Bond, St. Vincent Hospital

11:40 Analyzing Drugs and Their Metabolites by HPLC. J. Strimaitis, D. Wittmer, G. Hawk, Waters Associates

12:00 New Procedure for Extracting Drugs. S. A. Ibrahim, New York U

Recent Trends in Mass Spectrometry

F. H. Field, *Presider*, Rockefeller U

10:00 Chemical Ionization Mass Spectrometry Ten Years Later. M. S. B. Munson, U of Delaware

10:40 Mass Spectrometer as GC Detector. C. C. Fenselau, Johns Hopkins U

11:20 Sequencing Biopolymers by Mass Spectrometry. D. V. Bowen, Rockefeller U

X-ray Diffraction

R. J. Fredericks, *Presider*, Ethicon

10:00 Applications of X-ray Diffractometry. D. Smith, Pennsylvania State U

10:30 Special Problems in Powder Diffractometry. B. Post, Polytechnic Institute of New York

11:00 Unusual Applications of X-ray Diffraction. R. Jenkins, Philips Electronic Instruments

11:20 Automation Procedures in Powder Diffraction. C. Hubbard, NBS

11:40 Multicomponent Mixtures—Is X-ray Diffraction Adequate? A. W. Hounslow, J. B. Krause, R. K. Corbett, Colorado School of Mines Research Institute

12:00 High-Precision Computer-Controlled X-ray Diffractometer. J. A. Keenan, P. F. Cox, H. F. Schaake, Texas Instruments

Air and Water Quality

B. K. Afghan, *Presider*, Canada Centre for Inland Waters

10:00 Analytical Process for Air and Water Quality Studies. P. W. West, Louisiana State U

10:30 Analytical Evaluation of Multistage Air Sampling Device for Mercury. M. L. Bolyard, J. C. Haartz, National Institute for Occupational Safety and Health

10:50 Analysis of Air and Water with X-ray Spectrometry. R. Plesch, Siemens AG, W. Germany

11:10 Anodic Stripping Voltammetry of Atmospheric Samples. M. D. Ryan, D. D. Siemer, Marquette U

11:30 Quantitative Analysis of Atmospheric Pollutants Using Microcomputer-Controlled Single-Beam Infrared Spectrometer. R. J. Syrjala, Wilks Scientific Corp.

Trace Element Analyses and Reference Standards

P. D. LaFleur, *Presider*, NBS

10:10 Use of Reference Materials in Improving Accuracy of Trace Elemental Analyses. G. A. Uriano, R. E. Michaelis, I. L. Barnes, NBS

10:40 Preparation and Analysis of Some Environmental Standards. K. Fuwa, U of Tokyo, Japan

11:10 Botanical Standard Reference Materials. J. R. Moody, NBS

11:30 Primary and Transfer Standards for Transmittance Accuracy in Spectrophotometry. R. Mavrodineanu, R. W. Burke, K. D. Mielenz, NBS

11:50 ERDA's Role in National Standards and Measurement Assurance Program for Safeguarding Nuclear Materials. J. A. Goleb, ERDA

Tuesday Afternoon

Lippincott Medal Symposia: Raman Spectroscopy

Arranged by Raman Technical Group

J. E. Griffiths, *Presider*, Bell Labs

2:00 Coherent Anti-Stokes Raman Spectroscopy of Gases. J. W. Nibler, J. R. McDonald, W. M. Shaub, A. B. Harvey, Naval Research Lab

2:30 Use of Techniques Developed in Integrated Optics for Exciting the Raman Effect. R. Dupeyrat, U of Paris, France

3:00 Advances in Laser Raman Techniques. M. Delhaye, U of Lille, France

3:45 Microanalysis by Raman Spectroscopy. G. J. Rosasco, NBS

4:15 Laser Excitation Matrix Isolation Spectroscopy. W.L.S. Andrews, U of Virginia

4:45 Vibrational Spectroscopy as Tool for Studying Phase Diagrams. B. J. Bulkin, K. Krishnan, Polytechnic Institute of New York; N. Yellin, NIH

5:05 Raman Spectroscopy of Adriamycin. K. W.Hillig II, M. D. Morris, U of Michigan

Excitation Sources for Spectroscopy

R. Barnes, *Presider*, U of Massachusetts

2:00 High-Intensity Continuum Radiation from Exploding Wires. R. D. Sacks, P. L. Thomas, U of Michigan

2:20 Time- and Spatially-Resolved Spectra of Exploding Al Foils. R. D. Sacks, C. S. Ling, U of Michigan

2:40 Preliminary Studies of Exploding-Film Excitation for Atomic Emission Determination of Selected Trace Metals. R. D. Sacks, D. V. Duchane, U of Michigan

3:00 Liquid Layer Spark Sampling Technique. R. Coraor, R. M. Barnes, U of Massachusetts

3:35 Characterization of Atmospheric Pressure Glow Discharge. L. R. Layman, Pacific Lutheran U

3:55 Diagnostics of Argon Microwave Plasma Under Flow Conditions by Symmetrical Double-Floating Probes. A. Inspector, U. Carmi, R. Avni, Nuclear Research Centre, Negev, Israel

4:15 Spectroscopic Investigation of Low-Pressure Oxygen Plasma Discharge. R. J. Winslow, R. M. Barnes, U of Massachusetts

4:35 Width of Spectral Lines Excited in Grimm-Type Glow Discharge Source and Use of This Lamp with Resonance Detection for Emission Spectrochemical Analysis. C. D. West, Occidental Coll; L.R.P. Butler, H.G.C. Human, CSIR, S. Africa

4:55 Spatially Resolved Radiation Patterns in N_2O–C_2H_2 Flame. R. D. Sacks, B. Joshi, U of Michigan

5:15 Interferometric Atomic Line Profile Measurements of Plasma Sources. G. F. Kirkbright, S. L. Castleden, Imperial Coll, UK

The Search for What and How Much ends with Spectronic®

Spectrophotometers

At the heart of qualitative and quantitative analysis are the questions WHAT and HOW MUCH. Spectronic® Spectrophotometers aid your search for answers to those questions.

Each model in the Spectronic family was built to help meet the different needs of different labs at different times. Select the performance you need at a price that's right.

Spectronic mini 20

Conduct field analyses with this HAND-HELD unit that has a 20nm spectral slit width. Use all kinds of cuvettes. Complete with rechargeable battery.

Find out what made Spectronic 20 the MOST POPULAR ever made. More than 100,000 have been bought.

Spectronic 20

Select from an unsurpassed variety of sampling capabilities. Eliminate cuvette matching with micro flow-thru cell and process more than 300 SAMPLES PER HOUR. Also get direct concentration readout plus best meter readability anywhere. (16 inches of linear absorbance).

Spectronic 88

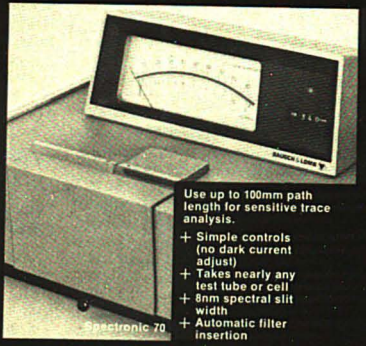

Spectronic 70

Use up to 100mm path length for sensitive trace analysis.

+ Simple controls (no dark current adjust)
+ Takes nearly any test tube or cell
+ 8nm spectral slit width
+ Automatic filter insertion

CIRCLE 23 ON READER SERVICE CARD

Expand selected segments of the standard curve with TWO CONCENTRATION MODES. Use modular quick-change sampling systems, including micro-flow-thru, to process more than 300 samples per hour. Inserts filters automatically. All this, plus built-in UV power supply.

Stability you need for LC MONITORING. Special push button to verify instrument setup and check reagent quality and standard curve reproducibility. Don't overlook the high-resolution 2nm spectral slit width.

Step into the UV region the solid state way and get the WIDEST WAVELENGTH RANGE (200-1000nm). Simple to use color-coded controls and digital readout. FOR QC: Push a button and verify instrument setup, and check reagent quality and standard curve reproducibility.

Digital readout provides stable and accurate readings of KINETIC REACTIONS or small changes in concentration. Pick your own decimal position. Check out electronic calibration yourself.

AUTOMATE. Expand Spectronic Spectrophotometers to automated systems with data printer, sampler for unattended operations, diluter-pipetter for sample/reagent dispensing. Lets you identify samples, consume less reagents, all automatically.

DOUBLE BEAM TOO. Five spectral slit widths to .25nm. Reflectance and high scanning speed modules. Couple to recorder for data display. Flow-thru accessories available.

The Spectronic series delivers quality in quantity. End your search for what and how much with Spectronic Spectrophotometers.

BAUSCH & LOMB
ANALYTICAL SYSTEMS DIVISION
CIRCLE 23 ON READER SERVICE CARD

For full details, write Bausch & Lomb, Analytical Systems Division, 820 Linden Avenue, Rochester, New York 14625.

Help Me In My Search . . . 87

My application involves _____

_____

_____

Call for an appointment ☐ Send me literature On ☐ _____

_____

Name _____

Company _____ Title _____

Address _____

City _____ State _____ Zip _____

Phone _____

CLIP AND MAIL

Analytical Chemistry for Clinical Laboratories

George N. Bowers, Jr., *Presider*, Hartford Hospital

2:00 Preparation and Characterization of High-Purity NADH. R. Schaffer, S. A. Margolis, NBS

2:30 Spectrophotometric Constants, LDH Inhibitors, and Purity of Commercially Available NADH. R. B. McComb, Hartford Hospital

3:00 TLC Classification of Antibiotics Exhibiting Antitumor Properties. H. J. Issaq, A. Aszalos, E. W. Barr, T. Wei, C. Meyer, NCI Frederick Cancer Research Center

3:35 Enzymatic Determination of Cholesterol Using Miniature Centrifugal Fast Analyzer. G. Wengert, H. V. Malmstadt, U of Illinois

3:55 Adaptation of Enzyme Immunoassay Techniques to Modified Miniature Centrifugal Analyzer. S. D. Brunk, H. V. Malmstadt, U of Illinois

4:15 Rapid Scanning Spectrometer for Analysis of Hemoglobins in Whole Blood. M. J. Milano, K.-Y. Kim, SUNY

4:35 Laser Excited Fluorescence Determinations of Clinical Samples on Miniature Centrifugal Analyzer. M. J. Simmons, H. V. Malmstadt, U of Illinois

4:55 Automated Multichannel Pipet and Miniature Centrifugal Analyzer System for Rapid Clinical Analyses. R. Gregory, H. V. Malmstadt, U of Illinois

Recent Trends in Mass Spectrometry

F. H. Field, *Presider*, Rockefeller U

2:00 ^{252}Cf–Plasma Desorption Mass Spectrometry—New Approach to High-Temperature Chemistry. R. D. MacFarlane, Texas A & M U

2:40 Structural Information from Collisional-Activation and Computer-Interpreted Mass Spectra. F. W. McLafferty, Cornell U

3:35 Modern Isotope Dilution Mass Spectrometry as Definitive Analytical Tool. L. J. Moore, T. J. Murphy, I. L. Barnes, NBS

3:55 Factor Analysis of Mass Spectra. R. W. Rozett, E. M. Petersen, Fordham U

4:15 Identification of *n*-Octylcyanide in In Situ Shale Oil. F. R. McDonald, F. A. Birkholz, ERDA

4:35 Characterization of Oil Shale and Shale Oil. S. Siggia, P. C. Uden, D. E. Henderson, A. Carpenter, Jr., F. P. DiSanzo, H. Hackett, U of Massachusetts

Air and Water Quality

J. L. Monkman, *Presider*, Environmental Protection Service, Canada

2:00 Complexation of Metals in Natural Waters. H. E. Allen, T. Brisbin, Illinois Institute of Technology; M. L. Crosser, Amoco Research Center

2:30 Graphite Filtration and Direct Atomic Absorption of Trace Metals in Air. D. D. Siemer, P. Koteel, H.-Y. Wei, Marquette U

2:50 Emission Spectrometric Determination of Atmospheric Particulates. R. K. Skogerboe, A. Sugimae, Colorado State U

3:10 Automated Microprocessor-Controlled Atomic Absorption Analysis of Natural Water for Arsenic and Selenium. R. W. Morrow, T. L. Futrell, T. T. Adams, Union Carbide

3:45 Determining Arsenic and Selenium by Atomic Absorption Spectroscopy—A Comparative Study. K. Brodie, B. Culver, Varian

4:05 Colorimetric Analysis of Ammonia in Water. R. L. Gross, F. W. Carson, American U

4:25 Application of New Type of Hydride Generator to Analysis of Selenium. E. E. Peck, Ralston Purina Co.

Trace Element Analyses and Reference Standards

I. L. Barnes, *Presider*, NBS

2:00 Candoluminescence Spectrophotometry: Recent Developments in Analytical Chemistry. R. Belcher, S. Karpel, K. P. Ranjitkar, M. Shahidullah, A. Townshend, U of Birmingham, UK

2:20 Determination of Traces of Rare Earth Metal Ions by Candoluminescence. R. Belcher, T.A.K. Nasser, A. Townshend, U of Birmingham, UK

2:40 Determination of Nitrogen-Containing Compounds by MECA. R. Belcher, S. L. Bogdanski, A. Calokerinos, A. Townshend, I. Z. Al-Zamil, U of Birmingham, UK

3:00 Determination of Some Drugs, Amino Acids, Proteins, and Other Compounds of Biochemical Interest by MECA. M. Q. Al-Abachi, R. Belcher, S. L. Bogdanski, A. Townshend, U of Birmingham, UK

3:35 Inorganic Ion Analysis by Laser Excitation of Precipitates. J. C. Wright, U of Wisconsin

3:55 Sub-Part-Per-Trillion Detection of Riboflavin by Laser-Induced Fluorescence. J. H. Richardson, B. W. Wallin, D. C. Johnson, L. W. Hrubesh, Lawrence Livermore Lab

4:15 Determination of Trace Metals by Chemiluminescent Oxidation of Gallic Acid. S. Stieg, T. A. Nieman, U of Illinois

4:35 Analytical Error: Observational, Manipulative, and Evaluative. W. E. Harris, U of Alberta, Canada

Furnace Atomic Absorption

C. L. Chakrabarti, *Presider*, Carleton U, Canada

2:00 Carbon Furnace Atomic Emission Spectrometry. J. M. Ottaway, R. C. Hutton, D. Littlejohn, F. Shaw, U of Strathclyde, Scotland

2:30 Sources and Structure of Background Light Losses in Graphite Furnace Atomizers for Atomic Absorption Spectrometry. J. Y. Marks, R. J. Spellman, R. Cone, Pratt and Whitney Aircraft

2:50 Limitations of Background Correction Systems for Use with Graphite Furnace Atomizers and Consequences of Background Correction Errors. J. Y. Marks, G. C. Welcher, Pratt and Whitney Aircraft

3:25 Evaluation of Interferences in Application of Wavelength Modulation Graphite Furnace Atomic Emission Spectrometry to Sample Analysis. M. S. Epstein, T. C. Rains, NBS; T. C. O'Haver, U of Maryland

3:45 Some Recent Studies with Electrothermal Atomizers Used in AAS. G. F. Kirkbright, M. J. Adams, R. D. Snook, Imperial Coll, UK

4:05 Flameless Atomic Absorption Theory Applied to Methods Development. R. H. Emmel, M. A. Bancroft, S. B. Smith, Jr., Instrumentation Lab

4:25 Capacitive Discharge Heating of Graphite Flameless Sample Cell. R. D. Sacks, W. Corey, U of Michigan

4:45 Automated Sample Introduction in Flameless AA with Graphite Tubes. M. Stoeppler, Nuclear Research Centre Juelich, Germany; B. Welz, Bodenseewerk Perkin-Elmer and Co. GmbH, Germany

Instrumentation

2:00 Automated DC Plasma—Echelle Spectrometer System for Trace Metal Analysis. C. D. Neefus, T. R. Gilbert, New England Aquarium

2:20 Performance of Multichannel Spectrochemical Analysis System for Use with Inductively Coupled Plasma Source. J. W. Kemp, A. E. Bernhard, C. J. Landry, Labtest Equipment Co.

2:40 Astigmatism and Ray Tracing Calculations for Spatially Resolved Images in Spark Discharges. C. Poirier, R. Coraor, R. M. Barnes, U of Massachusetts

3:00 Investigation of Influence on Droplet Size of Electric Field Applied During Pneumatic Nebulization. R. N. Savage, G. M. Hieftje, Indiana U

Varian Announces the CDS-111 Chromatography Data System... a better, easier way to quantitate your chromatograms

The CDS-111 is more than a powerful chromatography data system. It will automatically quantitate most chromatograms completely on its own. It will control an entire chromatography system—chromatograph, AutoSampler, valving, external events—in automatic closed-loop operation. It has large-computer power to store, for use on command, up to 9 (nine) complete method files each of which can be tailored to automatically control a complex analysis from start to finish. It will even link method files so that a single chromatogram can be automatically edited and calculated up to nine different ways. And the CDS-111 Chromatography Data System makes it all easy.

It automatically quantitates most chromatograms entirely on its own. You don't have to punch in sets of prerun instructions. The CDS-111 already knows what to do. All the critical measuring parameters are factory preset and the CDS-111 automatically updates the parameters throughout the run to accurately quantitate most types of chromatograms. For unusual, or complex analyses, you can easily override the presets and set whatever values you need.

It accurately measures the areas of all types of peaks, simple and complex. For accurate, precise measurement of all true peaks, the CDS-111 continuously filters the noise from the chromatographic signal and keeps the peak detection threshold-to-noise ratio constant throughout the analysis.

The CDS-111 automatically calculates the results according to any of 6 (six) different methods: internal standard, external standard, calibration factor, relative response factor, area % and normalized area %. Through powerful file linking, any combination of these methods can be automatically applied to the data from a single injection and the results automatically reported in more than one form, e.g., weight %, mole %, and volurne %.

The CDS-111 stores, for immediate use, up to 9 (nine) complete method files, each tailored to control a specific analysis. Files can be simple, using only their presets which will handle most analyses. Or they can be sophisticated, controlling the entire chromatographic process—the AutoSampler, the Model 3700 chromatograph, external devices, data acquisition, calculations and final report. You don't have to set up the CDS-111 every time you run a different sample. You can call up your stored file at the touch of a button.

The CDS-111 controls are simple. Four switches, a small keyboard and 6 (six) indicator lights give you complete control and you don't really need the keyboard at all unless you want to override the automatic settings, edit a report, or build or alter a method file.

The CDS-111 makes chromatography automation available to every lab. It interfaces simply with both gas and liquid chromatographs. Two different basic models are available, so you can choose a system that best meets your particular needs and budget.

For Full Information, circle Reader Service No. 222

To Have a Varian Representative Call, circle No. 223

varian

Varian Instrument Division
611 Hansen Way, Box D-070
Palo Alto, California 94303

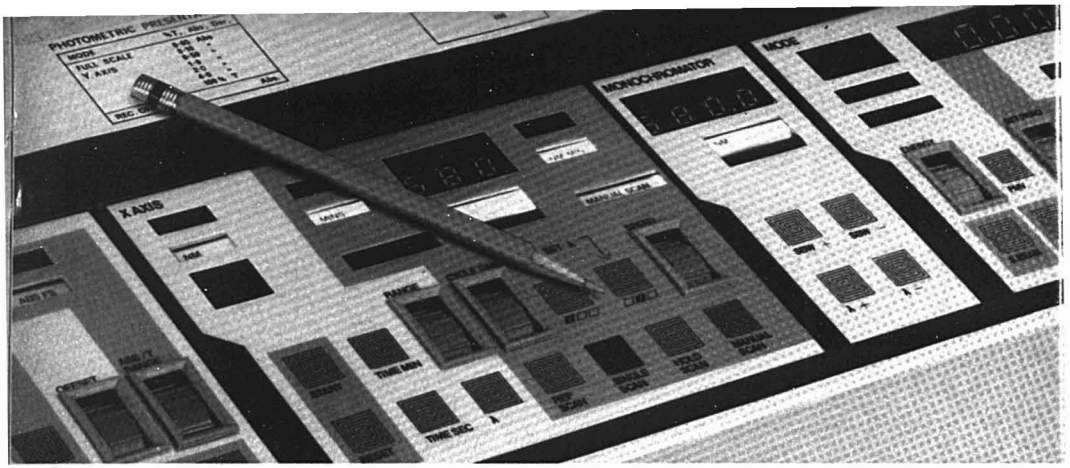

Does your spectrophotometer have these capabilities?

Compare all the standard, built-in features of SuperScan™ 3 against those of other UV-Vis spectrophotometers.

☐ Versatile wavelength programming console. Here's where you select starting wavelength and wavelength scan range. Just press SINGLE SCAN and the programmer automatically records spectra with maximum wavelength expansion on the convenient 20 x 40 cm chart paper. After each scan, SuperScan automatically returns monochromator and recorder pen to original position.

☐ Overlay spectra with ease — automatic repetitive scanning with a selectable cycle time of 0 to 20 minutes.

☐ Baseline correction with an automatically programmed memory. A single scan through the wavelength region of interest compensates for baseline deviations.

☐ Four-figure digital readout precisely indicates the wavelength isolated by the monochromator.

☐ Nothing's left to chance. Program for AUTO and the source change is made automatically at 350 nm.

☐ Superb readout capabilities. In addition to the absorbance mode, SuperScan provides % transmission, concentration and first derivative data.

Be sure you have full facts on SuperScan, the most capable spectrophotometer in the mid-price field. Write Varian Instrument Division, 611 Hansen Way, Box D-070, Palo Alto CA 94303.

Circle 247 for the complete data package.

Circle 248 if you'd like our technical representative to contact you.

Varian UV-Vis spectrophotometers for every need.

varian

3:35 Electronically Controlled Droplet Generator for Use with Micro-Samples. L. A. Powell, G. M. Hieftje, Indiana U

3:55 Influence of Wave Form on Refractor Plate Background Compensation in Emission Analysis. S. R. Koirtyohann, E. Hinderberger, F. E. Lichte, U of Missouri

4:15 Accuracy and Precision of Background Correction in Atomic Absorption Spectrophotometry. R. G. Schleicher, S. B. Smith, Instrumentation Lab

4:35 Peak Area vs. Peak Height in Flameless Atomic Absorption Measurements. H. J. Issaq, R. M. Young, E. W. Barr, NCI Frederick Cancer Research Center

Wednesday Morning, Nov. 17

Anachem Award

J. A. Howell, *Presider,* Western Michigan U

9:00 Introduction of Awardee. Reminiscence of a Well-Spent Youth. S. Fusari, Parke, Davis and Co.

9:15 Anachem Award Lecture. Standards in Analytical Instrumentation. J. M. Vandenbelt, Parke, Davis and Co.

10:15 Problem Solving in Pharmaceutical Analysis. J. Holcomb, Parke, Davis and Co.

10:35 Characteristics of Equilibrium Reaction of Some Pyrazolo Diavetinones in Aqueous Solutions. W. H. Hong, C. Johnston, D. Szulczewski, Parke, Davis and Co.

10:55 Development of Stability-Indicating Assay for Guana Benz Acetate. C. Shearer, Parke, Davis and Co.

11:15 Photo Excitation State of First Primary Band of Benzene. L. Doub, J. M. Vandenbelt, Parke, Davis and Co.

Lippincott Medal Symposia: IR and Far IR Studies Using FT Techniques

Arranged by the Fourier Transform Spectroscopy Group

J. W. Brasch, *Presider,* Naval Surface Weapons Center

10:00 Determination of Barriers to Internal Rotation of Asymmetric Rotors and Conformational Analysis by FT Spectroscopy. J. Durig, U of South Carolina

10:30 Spectroscopy Studies of Ionic Solids and Gases. W. Risen, Brown U

11:00 FT–IR and Resonance Raman Spectra of Metastable Species in Irradiated Solids. J. Bates, ORNL

11:30 Preliminary Experiments on Infrared Frequencies and Intensities as Function of Density. J. W. Brasch, Naval Surface Weapons Center; R. J. Jakobsen, Battelle-Columbus Lab

Spectroscopy of Surfaces

D. M. Hercules, *Presider,* U of Pittsburgh

10:00 Quantitative Analysis and Electronic Structure Characterization of Surface Absorbed Species by Photoelectron Spectroscopy. C. R. Brundle, IBM

10:35 Surface Analysis by High-Performance Ion Scattering Spectroscopy. G. R. Sparrow, 3M Co.

11:10 Surface Spectroscopy of Polymers: Application of XPS, UPS, and SIMS. W. M. Riggs, Physical Electronics Industries

11:30 Study of Oxide Film Formation by SIMS. G. J. Scilla, V. L. Wrick, G. H. Morrison, Cornell U

11:50 Performances of Cold Cathode Windowless Tube for Thin Oxide Film Studies. M. Romand, G. Bouyssoux, R. Bador, U Claude Bernard, France; B. Grubis, Compagnie Generale de Radiologie, France

12:10 Characterizing Cosmetic Effects and Skin Morphology by Scanning Electron Microscopy. C. A. Garber, C. T. Nitingale, Structure Probe

Environmental Aspects of Gas Chromatography

G. R. Umbreit, *Presider,* Greenwood Labs

10:20 Determination of Trace Amounts of Nonvolatile Organic Contaminants in Water. J. S. Fritz, Iowa State U

10:50 Gas Chromatographic Determination of Volatile Organic Contaminants in Water at Trace Levels. C. D. McAuliffe, Chevron Oil Field Research Co.

11:20 Procedure for Analysis of Nonionic Chlorinated Pesticides in Lipid of Poultry, Swine, Beef, Soybeans, and Corn Prepared for Gas Chromatography Analysis by Gel Permeation Chromatography. L. D. Johnson, G. L. Brookhart, R. H. Waltz, Analytical Biochemistry Labs

11:40 GLC Determination of Pirimicarb and Its Carbamate Metabolites as Applied to Field Trials for Potatoes. S. J. Jankowski, ICI United States

Process Control Analyzers

J. W. Loveland, *Presider,* Suntech

10:15 Process On-Line Sulfur-in-Oil Analyzer. G. R. Johnson, Y. Takeuchi, M. Kyono, Yokogawa Corp. of America; J. W. Loveland, Suntech

10:40 New Instrument for Continuous Measurement of Sulfur Dioxide. J. W. Butler, A. D. Colvin, Ford Motor Co.

11:00 Personal Monitoring Device for Vinyl Chloride Utilizing Permeation Technique for Sampling. P. W. West, L. H. Nelms, K. D. Reiszner, Louisiana State U

11:20 Process Control Using On-Line Ion Chromatography. T. S. Stevens, W. R. Albe, Dow Chemical Co.

11:40 Immobilized Enzyme-Based Flowing-Stream Penicillin Analyzer. Applications to Measurement of Penicillin in Fermentation Broths. J. F. Rusling, G. J. Papariello, G. H. Luttrell, L. F. Cullen, Wyeth Labs

Furnace Atomic Absorption

C. L. Chakrabarti, *Presider,* Carleton U, Canada

10:00 Electrothermal Atomization—The Way Toward Absolute Methods of Atomic Absorption Analysis. B. V. L'vov, Leningrad Polytechnic Institute, USSR

10:40 Dynamics of Atom Formation in Graphite Furnace Atomic Absorption Spectroscopy. R. E. Sturgeon, C. L. Chakrabarti, C. H. Langford, Carleton U, Canada

10:20 Application of Carbon Furnace Atomic Emission Spectrometry to Determination of Minor Constituents of Steels. J. M. Ottaway, F. Shaw, D. Littlejohn, U of Strathclyde, UK

11:40 Performance of AS-1 Auto Sampler with HGA-2100 Graphite Furnace. A. R. Knott, W. B. Barnett, S. DeNuzzo, Perkin-Elmer

Wednesday Afternoon

Anachem Award: Absorption Spectroscopy

J. A. Howell, *Presider,* Western Michigan U

2:00 Ultraviolet Determination of Steroid Halcinonide: Differential Reduction with Sodium Borohydride Solution Activated by 1,2-Propanediol. J. Kirschbaum, Squibb Institute for Medical Research

2:20 Organophosphorus Esters as Donors and Solvents in Studies of Charge-Transfer Phenomena Involving Iodine and Iodide. T. J. Novak, E. J. Poziomek, W. A. Mosher, R. A. Mackay, contribution from Edgewood Arsenal, U of Delaware, and Drexel U

2:40 Spectrophotometric Studies of Microgram Quantities of Halides of Berkelium, Californium, and Einsteinium. J. P. Young, R. G. Haire, R. L. Fellows, J. R. Peterson, ORNL and U of Tennessee

3:00 Effect of Carbontetrachloride on Equilibria of Inorganic Nu-

trients in Soils During Displacement Procedure of Soil Solution. A. Mubarak, J. Amend, R. Woodriff, Montana State U

3:35 Chemical Analysis of High-Purity Alumina. B. B. Elrod, J. B. Ezell, Jr., Reynolds Metal Co.

3:55 Use of Long Path Cell with Multilayer Dielectric Coatings to Increase Selectivity of Absorption Gas Analysis. N. K. Sukhodrev, A. M. Livshits, S. I. Sagitov, Academy of Sciences, USSR

4:15 Medium-Speed, Accurate, Spectrophotometric Method for Determination of Protein in Rice by Biuret Reaction. F. C. Strong III, U Estadual de Campinas, Brazil; P. Theis-Maimone, U Central de Venezuela

Lippincott Medal Symposia: Environmental Monitoring by Vibrational Spectroscopy

Arranged by the Coblentz Society

P. R. Griffiths, *Presider,* Ohio U

2:00 Infrared Absorption Spectroscopy of Atmospheric Contaminants Using Grating Spectrometers. J. Diaz-Fueda, H. J. Sloane, R. J. Obremski, Beckman Instruments

2:30 On-Site Analysis of Pollutants Near OSHA Limits Using Infrared Analyzers. P. A. Wilks, Wilks Scientific Corp.

3:00 Recent Developments in Use of Tunable Semiconductor Lasers for Molecular Pollutant Detection. E. D. Hinkley, R. T. Ku, MIT

3:45 Emissions Monitoring by Infrared Emission Spectroscopy. W. F. Herget, EPA

4:15 State-of-the-Art in Remote Raman Spectroscopy. T. Hirschfeld, Block Engineering

Physical Chemistry of Gas Chromatographic Process

R. L. Grob, *Presider,* Villanova U

2:00 New Insights Through High-Precision Measurements. L. B. Rogers, U of Georgia

2:50 Physical Chemical Measurements by Gas Chromatography: A Physical Chemist's View. J. F. Wojcik, Villanova U

3:40 Accuracy and Precision of Physical Measurements by Gas Chromatography. M. A. Kaiser, U of Georgia

4:05 Selective Transition Metal Salt-Modified Stationary Phases in Gas-Solid Chromatography. E. F. Barry, N.H.C. Cooke, J. B. Cox, U of Lowell

4:30 Thermodynamic Studies of Interactions at Catalytic Surfaces by Gas-Solid Chromatography. R. L. Grob, M. J. O'Brien, Villanova U

X-ray Spectrochemical Analysis

K.F.J. Heinrich, *Presider,* NBS

2:00 Present State-of-the-Art of X-ray Spectrochemical Analysis. J. Gilfrich, Naval Research Lab

2:30 X-ray Fluorescence Quantitative Analysis: Concerning Relationships Between Equivalent Wavelength and Effective Influence Coefficients. R. Vie Le Sage, U Paris, France; R. Tertian, Rhone-Poulenc Industries, France

2:50 Evaluation and Application of Automatic Fusion Technique to Major-Element XRF Analysis of Silicate Rocks. B. P. Fabbi, H. N. Elsheimer, U.S. Geological Survey

3:10 Nondestructive Determination of Phosphorus Impurities in Thin Anodic Film by X-ray Fluorescence Analysis. R. Bador, M. Romand, G. Bouyssoux, U Claude Bernard, France

3:45 X-ray Emission Analysis of Microsamples by Electron, X-ray, and Proton Bombardment. D. N. Breiter, NBS

4:05 Simple Energy-Dispersive X-ray Fluorescence Method for Determination of Twenty-Eight Trace and Two Major Elements in Geochemical Specimens. R. D. Giauque, R. B. Garrett, L. Y. Goda, Lawrence Berkeley Lab

4:25 Data Reduction Procedure for Monochromatic X-ray Fluorescence with Si(Li) Detector. R. L. Myklebust, C. E. Fiori, D. N. Breiter, K.F.J. Heinrich, NBS

4:45 Multielement Analysis of Geological Material Using Pressed Powders and Energy-Dispersive X-ray Fluorescence Analysis. J. A. Cooper, B. D. Wheeler, D. M. Bartell, Ortec

Characterization of Particles

W. C. McCrone, *Presider,* W. C. McCrone Associates

2:00 Choice of Analytical Method for Particle Analysis. J. Gavrilovic, W. C. McCrone Associates

2:30 Manipulation of Small Single Particles. A. Peetsob, W. C. McCrone Associates

2:50 Evaluation of Polarizing Microscope for Characterization of Urban Dust Samples. R. Bradway, GCA/Precision Scientific

3:05 Chemical Identification of Airborne Particulates by Laser Raman Spectroscopy. E. Etz, G. Rosasco, NBS

3:40 Glass Standards for Microanalysis of Particles. R. B. Marinenko, K.F.J. Heinrich, C. E. Fiori, M. M. Darr, D. H. Blackburn, D. E. Newbury, J. A. Small, NBS

Molecular Fluorescence and Phosphorescence

L. Cline Love, *Presider,* Seton Hall U

2:00 Use of High Repetition Rate Pulsed Lasers in Time-Resolved Fluorimetry. F. E. Lytle, Purdue U

2:30 Recent Developments in Room Temperature Phosphorimetry. T. Vo Dinh, E. L. Yen, J. D. Winefordner, U of Florida

2:50 Spectrofluorometric Determination of Substituted Tetrahydrocarbazoles by Methylene Blue Sensitized Photolytic Reaction. J.A.F. de Silva, N. Strojny, F. Rubio, J. C. Meyer, B. A. Koechlin, Hoffmann-LaRoche

3:10 Benzopyrene Fluorescence Studies in Liposome Membrane Systems. K. P. Li, T. Vo Dinh, J. D. Winefordner, U of Florida

3:45 Automated Dye Laser Spectrofluorometer for Obtaining Corrected Excitation and Emission Spectra. M. F. Bryant, H. V. Malmstadt, U of Illinois

4:05 Direct Determination of Uranium in Water and Ores by Laser and X-ray Excited Optical Luminescence Techniques. A. P. D'Silva, V. A. Fassel, M. Isles, Iowa State U

4:25 Electronic Excitation Energy Transfer from Tb^{3+} to SM^{3+} in $POCl_3$: $SnCl_4$. P. Tokousbalides, J. Chrysochoos, U of Toledo

Instrumentation

2:00 Analytical Optoacoustic Spectrometry for Solid Samples. G. F. Kirkbright, Imperial Coll, UK

2:20 Theory of Wavelength Modulation Spectrometry. T. C. O'Haver, U of Maryland

2:40 Correlation of Measurements of Absorbance by Spectrophotometers Having Different Spectral Bandwidths. F. C. Strong III, U Estadual de Campinas, Brazil

3:00 Improved UV/Visible Multichannel Spectrophotometer. J. Avery, H. V. Malmstadt, U of Illinois

3:35 Microcomputer-Controlled Infrared Analyzer. W. B. Telfair, A. C. Gilby, D. T. Thompson, Wilks Scientific

3:55 Design and Evaluation of Novel Fluorometric Flow Cell. R. M. Smith, K. W. Jackson, New York State Department of Health

4:15 Glass Transition Pressures of Fluids from Bandwidths and Frequencies of Fluorescence Spectrum of Ruby. J. L. Lauer, M. E. Peterkin, Sun Oil Co.

General Spectroscopy

B. Scribner, *Presider,* NBS

2:00 Application of Atomic Emis-

Varian Announces the 3700... Not just a great gas chromatograph, the greatest gas chromatograph

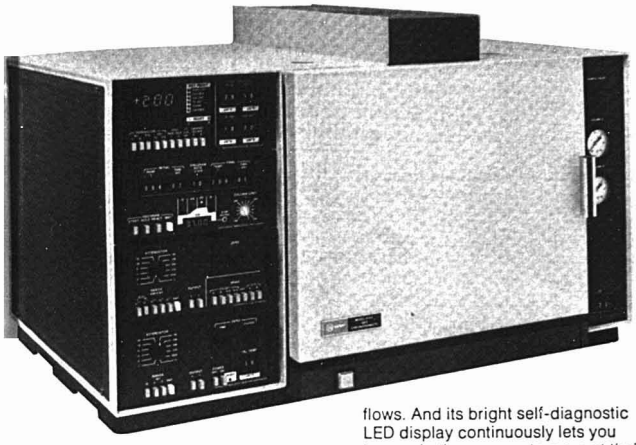

This is the chromatograph that all the others have been leading up to. It's the one that chromatographers made for chromatographers. In a single instrument the 3700 brings together all the major chromatographic breakthroughs plus new applications-oriented design concepts in every component: new injectors, new detectors, new column oven, new programmers, new flow controllers, new electronics and new automation. The result: pushbutton simplicity combined with more capability to handle applications than ever before.

Modular flexibility. The 3700 is modular so you can easily choose a chromatograph for your specific application. You can begin at low cost with a basic dual-column unit and add capability as you need it. Or, you can start right now with the world's most powerful and versatile GC system.

Here are some of the 3700's new performance features:

New ESP* monitor continuously checks 3700 operating parameters for you — injectors, column oven, detectors, flows. And its bright self-diagnostic LED display continuously lets you know whether parameters are at their settings.

*Electro Sensor Panel

New digital controls let you set all chromatographic conditions in a few seconds. And there's no resettability error.

Extra-large, 1350 cubic inch, column oven with removable door gives you more room to install columns.

New Automatic Linear Temperature Programmer (ALTP). So good it will even operate the oven at 12°C above room temperature without cryogenic cooling, giving you increased resolution of low boiling components.

New non-contaminating flame ionization detector reduces down time and obtains detection over a wide range of sample concentrations.

Universal ionization detector bases let you interchange FID and ECD detectors yourself in minutes.

New flame-out indicator light and automatic reignite provide extra FID safety protection and help assure trouble-free automatic operation.

New pulsed ^{63}Ni electron capture detector has a linear dynamic range better than 10^4 and an MDQ better than 0.1 pg of lindane.

New differential electrometer will handle both FID and ECD.

New highest sensitivity thermal conductivity detector has a built-in amplifier that can amplify the bridge output signal to the recorder up to 10 times — greatly increasing capability to record and measure trace amounts.

New flow control convenience because all pneumatics are arranged in a large compartment planned for operator access.

New carrier gas flow stability and reproducibility because all critical flow control elements are isolated in an independently heated and thermostatted oven within the pneumatics compartment. This minimizes the effect of laboratory temperature changes and improves the precision and reproducibility of the data.

New flow control automation. New dual Automatic Flow Controller lets you dial-in carrier gas flow rates.

New versatile injector system has universal bases and quickly interchangeable injector bodies.

New cool injector septum holder reduces septum bleed. It also seals without compressing the septum so there's no danger of cutting off the gas flow and you don't bend needles on compressed septa.

New applications automation capabilities. The 3700 combines with the AutoSampler and CDS-111 Chromatography Data System to provide complete GC automation.

For full information, Circle Reader Service No. 220

To have a Varian Representative call, Circle No. 221

varian

Varian Instrument Division
611 Hansen Way, Box D-070
Palo Alto, California 94303

sion and Absorption Flame Spectrometry for Trace Detection. E. D. Prudnikov, A. Zhdanov, Leningrad State U, USSR

2:20 Emission Spectra in Vacuum Ultraviolet for Highly Ionized Fluorine. E. J. Knystautas, R. Drouin, Laval U, Canada

2:40 Inhomogeneous Distribution in Vibronic Spectra of Impurity Molecules in Solids. K. K. Rebane, Estonian SSR Academy of Sciences, USSR

3:00 Spectroscopy and Luminescence of Crystals and Molecules. L. A. Rebane, Academy of Sciences, USSR

3:35 Fourth Period Elements Spectra Isoelectronic with ScI, NaI, and OI. A. N. Ryabtsev, Academy of Sciences, USSR

3:55 Spectral and Luminescent Evidence of Charge Transfer in Rare Earth Activated Crystals. P. P. Feofilov, Academy of Sciences, USSR

4:15 Atomic Spectrometry Study of Absorption Isotherms of Niobium, Zirconium, and Titanium on Glass. D. S. Azambuja, CIENTEC, Brazil; Y. P. Dick, U Federal do Rio G. do Sul, Brazil

4:35 Physical Limitations of Intensity of Resonance Line Sources. H. Falk, Academy of Sciences of the GDR, Germany

Thursday Morning, Nov. 18

Benedetti-Pichler Award

P. N. Keliher, *Presider*, Villanova U

9:00 Introduction of Benedetti-Pichler Award Recipient

9:05 Microchemistry: Its Objectives and Implications. T. S. Ma, City U of New York

10:00 Some Innovations in Sample Combustion Equipment. H. J. Francis, Jr., Pennwalt Corp.

10:30 New Directions in Atomic Spectrometry Using Micro Samples. R. F. Browner, Georgia Institute of Technology

11:10 Micro Atomic Absorptiometric Method for Determination of Serum Iron and Its Incorporation into Combined Lead Poisoning/Anemia Testing Procedure. K. W. Jackson, T. D. Fuller, K. M. Aldous, New York State Department of Health

11:30 UV Absorption Spectra of Some Anions. W. Szafranski, M. Szyper, P. Zuman, Clarkson College of Technology

Furnace Atomic Absorption

C. L. Chakrabarti, *Presider*, Carleton U, Canada

10:00 Some Theoretical and Practical Observations on Graphite Furnace Atomic Absorption Spectrometry. L. de Galan, Technische Hogeschool, The Netherlands

10:30 Atomic Absorption Studies of Spatial Distributions Above Electrically Heated Filament Atomizer. D. N. Baxter, E. H. Pals, E. R. Johnson, S. R. Crouch, Michigan State U

10:50 Improvements and Uses of Constant Temperature Atomic Absorption Furnaces. R. Woodriff, J. R. Amend, Montana State U

11:10 Spectroscopic Fluorine Analysis. L. Hageman, R. Woodriff, Montana State U

11:30 Flameless Atomic Absorption Measurements of Metals in Electrical Insulating Fluids. T. J. Gedemer, McGraw-Edison Power Systems Division

11:50 Advantages and Limitations of Pyrolytic Graphite-Coated Furnace Sampling Tubes in Atomic Absorption Spectroscopy. D. C. Manning, F. J. Fernandez, G. E. Peterson, Perkin-Elmer

New Developments in Atomic Fluorescence

J. D. Winefordner, *Presider*, U of Florida

10:00 Some New Applications of Nondispersive Flame Fluorescence. P. L. Larkins, CSIRO, Australia

10:30 Arc-in-Flame Atom Reservoir for Atomic Fluorescence Spectroscopy—Minimization of Vaporization Interferences. S. Martin, H. V. Malmstadt, U of Illinois

10:50 Recent Applications of Tunable Dye Lasers to Flame Spectrometry. B. Smith, S. Weeks, J. D. Winefordner, U of Florida

11:10 Microprocessor-Controlled Dye Laser for Multielement Atomic Fluorescence Analysis. J. Perry, H. V. Malmstadt, U of Illinois

11:30 Automated Atomic Fluorescence and Emission Spectroanalytical System. H. V. Malmstadt, S. Martin, U of Illinois

11:50 Laser Atomic Absorption and Fluorescence Spectrometry. E. H. Piepmeier, J. W. Hosch, Oregon State U

Liquid Chromatography

D. Gere, *Presider*, Hewlett-Packard

10:00 Recent Advances in Development of Amperometric Detectors for Liquid Chromatography. P. T. Kissinger, W. P. King, L. A. Pachla, Purdue U

10:30 Practical Considerations in Use of HPLC Columns. R. Majors, Varian

11:00 Solvent Elimination Techniques for On-Line LC–IR. D. Kuehl, P. R. Griffiths, Ohio U

11:20 Analysis of Some Nitrogenous Compounds of Pharmaceutical Interest by High-Speed Liquid Chromatography. R. G. Achari, E. E. Theimer, Cooper Labs

11:40 High-Pressure Chromatographic Analysis of Steroidal Carboxylic Acids. R. Farhi, C. Monder, Hospital for Joint Diseases and Medical Center, New York

Polymer Analysis

T. K. Wu, *Presider*, Du Pont

10:00 End Group Characterization of Synthetic Polypeptides. H. J. Harwood, U of Akron

10:30 Spectroscopic Determination of Butadiene Rubber in Acrylonitrile/Methylacrylate/Butadiene Resins. P. L. Wancheck, J. R. Mooney, Standard Oil Co. (Ohio)

10:50 Determination of Composition and Molecular Weight of Polyester Urethanes. F. W. Yeager, J. W. Becker, Du Pont

11:10 Spectroscopic Analysis of Polyesters and Related Monomers. J. Young, J. R. Mooney, Standard Oil Co. (Ohio)

11:30 New Dynamic Mechanical Analysis System for Physical Properties Characterization. R. L. Blaine, L. Woo, Du Pont

11:50 Separation of Poly(ethylene terephthalate) Oligomers by HPLC and TLC. W. R. Hudgins, K. Theurer, T. Mariani, Allied Chemical Corp.

Ion-Selective Electrodes

R. R. Durst, *Presider*, NBS

10:00 Ideal and Nonideal Responses of Ion-Selective Electrodes. R. P. Buck, U of North Carolina

10:40 Bio-Selective Membrane Electrodes. G. A. Rechnitz, SUNY

11:25 Study of CuS/Ag_2S–Membrane Ion-Selective Electrodes. W. E. Van Der Linden, G. J. Heijne, U of Amsterdam, The Netherlands

11:50 Automated Ion-Selective Electrode Analysis. J. W. Ross, Jr., Orion Research

Ion Probe Analysis and Sims

D. E. Newbury, *Presider*, NBS

10:00 Ion Microscope Imaging. G. H. Morrison, Cornell U

10:40 Static Techniques of SIMS and Its Relation to Dynamic SIMS—A Review. A. Benninghoven, U of Munster, Germany

More liquid chromatography solutions from Varian

1. An analytical system that will solve almost any LC problem... Model 8520 LC with the new Varichrom UV-Vis detector.

This is the most capable liquid chromatography system available today. The 8520 Liquid Chromatograph is designed for both analytical and preparative work. The new Varichrom is a nearly universal detector covering the entire UV-Vis range from below 200 nm to 700 nm. This extended wavelength range lets you optimize for most organics and permits monitoring many new compound classes such as lipids, mono-olefins and carbohydrates.

The chromatograph's superior syringe pump provides precisely controlled pulseless flow and low noise so you can detect and measure the smallest quantities.

Varichrom and the 8520 couple directly in a configuration that eliminates dead volume and preserves peak resolution. For full details on this capable combination, shown below, circle *Reader Service No. 243.*

2. A new Automatic LC that will increase sample throughput, improve reproducibility, and calculate and report analysis results.

Varian's new Automatic LC System handles up to 60 samples unattended. It is completely automatic from injection through separation, calculations and final report.

The system's Model 8500 positive displacement pump with Autorefill provides the pulseless, repeatable flow required for good accuracy, reproducibility, detectability and high efficiency. The reliable 8050 AutoSampler obtains reproducibility with a coefficient of variation less than 1%. The third system component, the CDS-111 Chromatography Data System, gives you full computer power to calculate the results from a single sample by any or all six methods including internal standard, external standard, normalization and response factors. Nine completely different method files can be stored for use as dictated by the AutoSampler. The CDS-111 permits closed loop operation of all three system components. For full information on the new Automatic LC, above, circle *Reader Service No. 244.*

To have a Varian representative call you, circle *Reader Service No. 245.*

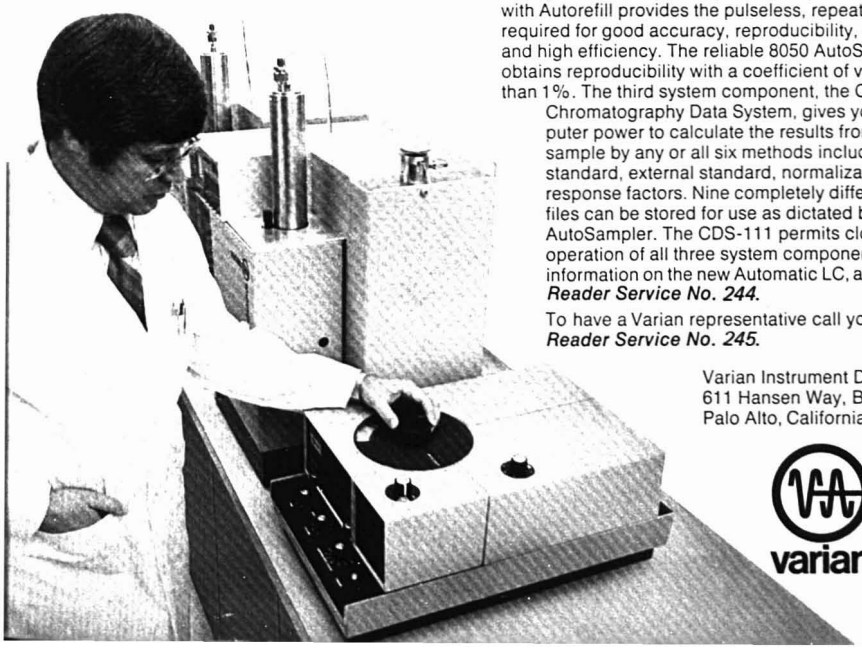

Varian Instrument Division
611 Hansen Way, Box D-070
Palo Alto, California 94303

varian

11:20 Present Status of SIMS and AES in Japan. Y. Sakaki, Dr. Tojta, Toyoto Technical Coll, Japan

11:40 Combined AES and SIMS Studies. S. Komiya, ULVAC Corp., Japan

Thursday Afternoon

Furnace Atomic Absorption

C. L. Chakrabarti, *Presider*, Carleton U, Canada

2:00 Interference Effects in Furnace Atomization. J. P. Matousek, U of N.S.W., Australia

2:30 Mechanism of Interferences in Carbon Furnace Atomic Absorption Spectrometry. R. C. Hutton, J. M. Ottaway, T. Platt, U of Strathclyde, UK

2:50 Optimization of Heater Tube Length in Atomic Absorption Furnace Spectroscopy. M. Marinkovic, R. Woodriff, Montana State U

3:25 Advantages of Direct Measurement and Control of Temperature in Furnace Atomic Absorption. B. Welz, G. Siess, K. Rogasch, E. Wiedeking, Bodenseewerk Perkin-Elmer and Co., GmbH, W. Germany

3:45 Pressurized Atomization in Graphite Furnace Atomic Absorption Spectroscopy. R. E. Sturgeon, C. L. Chakrabarti, P. C. Bertels, Carleton U, Canada

New Developments in Atomic Fluorescence

J. D. Winefordner, *Presider*, U of Florida

2:00 Application of Flame Resonance Spectrometer to Analysis of Biological and Environmental Samples. J. C. Van Loon, B. Radziuk, U of Toronto, Canada

2:20 Continuum Source Atomic Fluorescence Spectrometry at Wavelengths Below 200 nm. F. W. Plankey, E. M. Heithmar, U of Pittsburgh

2:40 Fluorescence Correlation Spectroscopy. J. M. Ramsey, G. M. Hieftje, Indiana U

3:00 Automatic Background Corrected Atomic Fluorescence Spectroscopy. B. R. Bartschmid, VPI&SU

3:35 Performance of Image Dissector Multielement Spectrometer for Atomic Absorption and Atomic Fluorescence. K. M. Aldous, J. S. Garden, New York State Department of Health

3:55 Determination of Metals in Metalloenzymes by Atomic Fluorescence Spectrometry. C. Veillon, Harvard Medical School

4:15 Measurement and Prediction of Laser-Excited Atomic Fluorescence Saturation Power Densities in Analytical Flame. D. R. Olivares, U de Los Andes, Venezuela; G. M. Hieftje, Indiana U

Liquid Chromatography

D. Gere, *Presider*, Hewlett-Packard

2:00 Therapeutic Monitoring—Applications Using LC. D. T. Stafford, U of Tennessee

2:30 HPLC Applied to Cereal and Grain Analysis. D. Wetzel, Kansas State U

3:00 High-Speed Steric Exclusion Chromatography of Small Molecules with Columns of Porous Silica Microspheres. J. J. Kirklan, P. E. Antle, Du Pont

3:35 Separation of Optical Brighteners by Liquid-Solid Chromatography. D. Kirkpatrick, Consumer Product Safety Commission

3:55 Concentration and/or Separation of Organics with Cross-linked Polyvinylpyrrolidone. T. Mourey, S. Siggia, U of Massachusetts

4:15 Characteristics of Size Exclusion Chromatography with Small Particle Silica Supports. S. D. Abbott, Du Pont

4:35 In Situ Modification of LC Packings. R. K. Gilpin, McNeil Labs

Polymer Analysis

T. K. Wu, *Presider*, Du Pont

2:00 Studies of Polymer Structure and Interactions by Inverse Gas Chromatography. J. Guillet, U of Toronto, Canada

2:30 Physical Aspects of Polymer Analysis. H. W. Siesler, Bayer AG, W. Germany

2:50 Estimation of Polyethylene Morphology by Nitric Acid Etching and Gel Permeation Chromatography. R. C. Ferguson, H. J. Stoklosa, W. W. Yau, H. H. Hoehn, R. R. Hebert, Du Pont

3:10 Preparative GPC of Low-Molecular-Weight Compounds for Subsequent Qualitative Analysis. R. A. Shoemaker, Armstrong Cork Co.

3:45 Raman and Infrared Spectroscopic Studies on State of Order in Isotactic Poly(1-alkylethylenes). K. Holland-Moritz, U of Koln, Germany

4:05 Polymers Containing Benzene Rings: Characteristics of Absorption Spectra in Far Infrared. W. Frank, U of Ulm, Germany

4:25 Characterization of Polymers via Pyrolysis—IR Assisted by Adjunct Substances. W. L. Truett, Wilks Scientific Corp.

4:45 Analysis of Automotive Paints by Pyrolysis Gas Chromatography. E. J. Levy, Chemical Data Systems

Electrochemistry

B. K. Afghan, *Presider*, Canada Centre for Inland Waters

2:00 Electrochemical and Chemical Reactivity of Some Unsaturated Aldehydes. L. Spritzer, P. Zuman, Clarkson College of Technology

2:20 Electrooxidation of Heterocyclic Aldehydes. K. Bratin, P. Zuman, Clarkson College of Technology

2:40 Differential Pulse Polarographic Determination of Acrolein in Water Samples. L. H. Howe III, Tennessee Valley Authority

3:20 Determination of CO in Tobacco Smoke Using Electrochemical Transducer. R. F. Browner, Georgia Tech; G. K. Copeland, P. B. Stockwell, Lab of Govt. Chemist, England; I. Bergman, Safety in Mines Research Establishment, England

3:35 Electrochemical Data and Solvatochromic Effects. M. Szyper, P. Zuman, Clarkson College of Technology

3:55 High-Precision Gravimetric Coulometry Using Silver-Perchloric Acid Coulometer: Titration of Arsenious Oxide with Electrogenerated Iodine. C. M. Newton, Bell Labs

Gas Chromatography

James Fritz, *Presider*, Iowa State U

2:00 New Capabilities in Infrared Identification of Gas Chromatograph Peaks. D. Wall, R. Lansil, G. Ferla, A. W. Mantz, Digilab

2:20 Data Manipulation Techniques for GC–IR. P. Coffey, Nicolet Instrument Corp.

2:40 DC Plasma Emission Gas Chromatographic Detector. R. J. Lloyd, W. G. Elliott, R. M. Barnes, P. C. Uden, U of Massachusetts

3:00 Microwave-Excited Emission Detector for Gas Chromatography. S. R. Goode, D. C. Otto, J. Horvath, U of South Carolina

3:35 Quantitation of Sub-Parts-per-Million Levels of Aromatic Amines by Absorption Technique with Flame Ionization Gas Chromatography. B. E. Bowen, Du Pont

3:55 Use of Gas-Liquid Chromatography for Separation of Monomethylguanine–TMS Derivatives. G. M. Muschik, W. B. Manning, W. L. Zielinski, Jr., NCI Frederick Cancer Research Center

4:15 Analyses for Chloroprene by Gas Chromatography. V. R. McCathern, R. F. Willis, D. A. McCrea, Du Pont

4:35 Evaluation of Porous Polymers for Gas Analysis by Gas Chromatography. B. Thompson, Varian

Now, even the most complex analysis has a simple solution...the new Varian mat-44 Quadrupole GC/MS System.

You'll be amazed at just how fast and easy such a sophisticated instrument can be to operate.

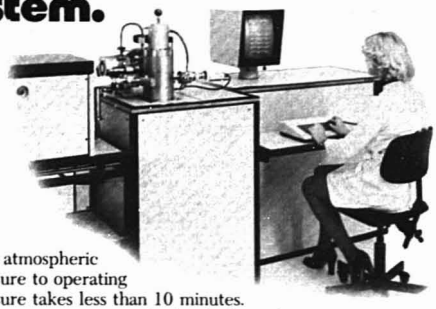

Complete Microprocessor Control. The new mat-44 is the first fully microprocessor-controlled quadrupole GC/MS System. Operation is via simple keyboard instructions and all programs for operation, optimization and self-diagnosis are stored on diskettes.

Quantitative GC/MS may be automatically performed with the basic mat-44 system. The GC takes both packed and capillary columns and is linked to the ion source either directly or via a jet separator.

Continuous Real Time Display. A large TV monitor displays in real time all important operating parameters as well as spectra, chromatograms, and mass chromatograms. The display may be hard-copied via a hard copy unit or oscillographic recorder. Alternatively, it may be videotaped for storage and later replay.

New Quadrupole Geometry. Varian's unique hyperbolic quadrupole analyzer provides excellent resolution and sensitivity which is maintained throughout its mass range (up to 1200).

Combined EI/CI Source. The mat-44 uses the well-proven Varian combined EI/CI ion source. Change of optimized ionization mode takes only 6-8 seconds.

Unique Turbomolecular Pumping. This pumping system requires no cryo-baffles or isolation valves. Turnaround from atmospheric pressure to operating pressure takes less than 10 minutes. The pumps contain no fluids which results in very clean instrument background. The mat-44 contains a built-in water recirculator and needs only an electrical supply for operation.

New SS 200 Data System. This new system can *simultaneously* acquire and process data. Together with the mat-44's TV display monitor the user can acquire data, monitor the progress of the run and simultaneously process data via the system's advanced interactive display. These features give the mat-44 GC/MS/DS exceptional capabilities. A 4.8M-word dual disc and alphanumeric/graphic display terminal are standard hardware features.

Never before has GC/MS analysis been so easy . . . you have to see it to appreciate it. Call or write today for a demonstration and complete specifications.

VARIAN mat MASS SPECTROMETRY,
25 Route 22, Springfield, NJ 07081
Telephone (201) 467-3660

CIRCLE 219 ON READER SERVICE CARD

varian

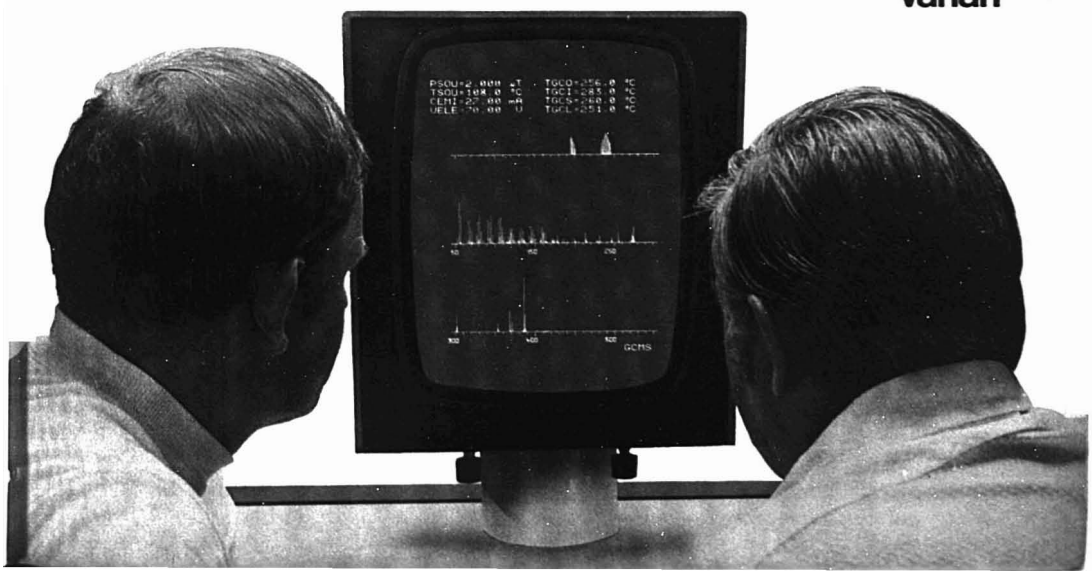

4:55 Determination of Morphine by Electron Capture Gas-Liquid Chromatography. G. Nicolau, G. Van Lear, American Cyanamid Co.

New Developments in Atomic Absorption

S. R. Koirtyohann, *Presider*, U of Missouri

2:00 Atomic Absorption Spectrophotometry Using Zeeman Effect. H. Koizumi, K. Yasuda, Hitachi Ltd., Japan

2:20 Alleviation of Spectral Interferences in Atomic Absorption Spectrometry. A. T. Zander, T. C. O'Haver, U of Maryland; P. N. Keliher, Villanova U

2:40 Theoretical Investigations of Spectral Overlaps in Atomic Absorption Spectroscopy. R. J. Lovett, M. L. Parsons, Arizona State U

3:00 Recent Advances in Spectroscopy of Highly Ionized Atoms. S. L. Mandelshtam, Academy of Sciences, USSR

3:35 Evaluation of Role(s) of Aerosol Transport Phenomena in Flame and Plasma Spectrometry. R. K. Skogerboe, S. J. Freeland, Colorado State U

3:55 Matrix Effects in Determination of Ruthenium by Atomic Absorption Spectroscopy. C. M. Young, Allied Chemical

4:15 Enhancement of Atomic Absorption Sensitivity for Chromium, Cobalt, Molybdenum, and Zinc by Means of Solvent Extraction. B. E. McClellan, T. W. Lassiter, Murray State U

4:35 Matrix Study on Determination of Sodium and Potassium by Atomic Absorption Spectroscopy. M. J. Miller, GTE Sylvania

4:55 Evaluation of Helium–Oxygen–Acetylene Flame as Atom Source for Atomic Spectrometry. K. A. Saturday, G. M. Hieftje, Indiana U

Ion Probe Analysis and SIMS: Quantitation

K.F.J. Heinrich, *Presider*, NBS

2:00 Secondary Ion Emission Models and Mass Spectrometry of Alloys. J. Schroeer, Illinois State U

2:20 Theory of Ion Sputtering. H. Prival, EG and G

2:40 Local Thermal Equilibrium Analysis of Secondary Ion Mass Spectra from Multielement Glasses. D. E. Newbury, R. L. Myklebust, K.F.J. Heinrich, NBS

3:00 Evaluation of Simplified Local Thermal Equilibrium Model for SIMS Analysis. D. S. Simons, General Electric Co.; C. A. Evans, Jr., U of Illinois

3:35 Ion Implanted Silicon and Silicon Dioxide Standards for Empirical Quantitation of Ion Microprobe Microanalyzer. R. D. Dobrott, G. B. Larrabee, A. Keenan, Texas Instruments

Ion Probe Analysis and SIMS: Instrumentation

J. Schroeer, *Presider*, Illinois State U

3:55 Wittmaack, Gesellschaft fur Strahlen-und Umweltforschung mbH, Germany

4:15 Complete Computer-Based Automation System for Quadrupole SIMS Instrument. J. R. Hinthorne, R. L. Conrad, R. D. Fralick, J. K. Finster, Applied Research Labs

4:35 Secondary Ion Quadrupole Mass Spectrometry (SIQMS). C. W. Magee, W. L. Harrington, R. E. Honig, RCA

4:55 Sputtered Neutral Mass Spectroscopy (SNMS) as Tool for Chemical Surface Analysis and Depth Profiling. H. Oechsner, Technischen U Clausthal, W. Germany

Friday Morning, Nov. 19

Modern Voltammetric Techniques

M. S. Spritzer, *Presider*, Villanova U

9:00 Voltammetric Measurement of Rapid Chemical Kinetics. P. J. Elving, U of Michigan

9:30 Software Approaches to Improving Voltammetric Measurements. J. Flato, Princeton Applied Research Corp.

10:15 Assay of Some Organic Compounds by Controlled Potential Coulometry. O. B. Mathre, Du Pont

10:35 Mercaptan Analysis of Phase-Selective Cathodic Stripping Voltammetry. W. M. Moore, Standard Oil Co. (Ohio)

10:55 Lead Dioxide-Catalyst Electrode Sensitive to Hydrogen Peroxide. K. G. Schick, V. Magearu, C. O. Huber, U of Wisconsin

11:15 Electrochemical Reduction of Cinoxacin. E. C. Rickard, A. Dinner, Eli Lilly and Co.

Liquid Chromatography

D. Gere, *Presider*, Hewlett-Packard

9:00 Preparative LC on New Large Bore Column. F. M. Rabel, A. G. Caputo, E. T. Butts, Whatman, Inc.

9:20 Use of Reduced Pathlength Sample Cells in Infrared Detectors for Chromatographs. C. W. Salisbury, Wilks Scientific Corp.

9:40 Novel High-Performance Liquid Chromatographic Method for Separation of Oligomers. A. F. Poile, J. S. Stoveken, R. W. Yost, Perkin-Elmer

10:15 High-Pressure Liquid Chromatographic Analysis of Fatty Acids in Edible Oils and Shortenings. W. C. Kossa, P.T.S. Pei, S. Ramachandran, R. S. Henly, Applied Science Labs

10:35 Parameters in Analysis of Isocyanates by High-Performance Liquid Chromatography. T. R. Ryan, C. Y. Ko, C. R. Hastings Vogt, U of Missouri

10:55 Some Considerations in Performing Quantitative Analysis with Gradient Elution in High-Pressure Liquid Chromatography. S. Abbott, R. Stevenson, J. Berg, B. Suits, Varian

11:15 Some Typical Applications in Fluorescence Detection in High-Performance Liquid Chromatography. E. Johnson, R. E. Majors, Varian

New Developments in Atomic Absorption

S. R. Koirtyohann, *Presider*, U of Missouri

9:00 Newly Devised LCAAS System and Its Applications to Biochemistry. M. Umebayashi, K. Kitagishi, Mie U, Japan

9:20 Determination of Lead in Biological Materials Using Microsampling Cup Atomic Absorption Spectrometry with Air–Acetylene and Nitrous Oxide Acetylene Flames. D. G. Mitchell, W. N. Mills, New York State Department of Health

9:40 Organic Functional Group Analysis by Atomic Absorption Spectrophotometry. P. R. D'Alonzo, S. Siggia, U of Massachusetts

10:15 Characterization of Selective Spectral Line Modulation Technique for Continuum Source Atomic Absorption Spectrometry. R. L. Cochran, G. M. Hieftje, Indiana U

10:35 Atomic Absorption Spectrometry Using Discrete Microvolume Nebulization. Application to Clinical and Metallurgical Analysis. J. E. Cantle, Instrumentation Laboratory (UK) Ltd., England

10:55 Determination of Factors Which Govern Atomization Efficiency in Atomic Spectrometry. G. J. Bastiaans, Georgetown U

11:15 Factors Influencing Atomic Absorption from Line Source. S. R. Goode, R. A. Goode, U of South Carolina

11:35 Influence of Particle Vaporization and Atomic Diffusion on

Distribution of Atoms in Analytical Flames. C. B. Boss, G. M. Hieftje, Indiana U

Ion Probe Analysis and SIMS

G. Morrison, *Presider*, Cornell U

9:00 **SIMS Multielement Depth Profiling of Solids.** R. D. Fralick, R. L. Conrad, J. R. Hinthorne, Applied Research Labs

9:20 **Some Measurements on Self-Diffusion of Oxygen in Al^2O^3.** D. J. Reed, A. J. Garratt-Reed, MIT

9:40 **Depth Profile Analysis of Surface of Alloy Steel Sputtered by O^{2+} Ion in IMMA Analysis.** T. Shiraiwa, N. Fujino, J. Murayama, N. Usuki, Sumitomo Metal Industries, Ltd., Japan

10:15 **Analysis of Hydrogen and/or Deuterium in Some Exothermic Metals by SIMS.** M. Someno, M. Kobayashi, H. Saito, Tokyo Institute of Technology, Japan

10:35 **SIMS Spectra of Amino Acids.** A. Benninghoven, U of Munster, Germany

10:55 **Secondary Ion Microanalysis of Biological Specimens.** A. J. Tousimis, Tousimis Research Corp.

11:15 **Identification of Sputtered Ion Species Using Precise Mass Measurement Techniques.** P. Williams, D. S. Simons, C. A. Evans, Jr., U of Illinois

Detection of Chemical Species

J. C. Von Loon, *Presider*, U of Canada

9:00 **Metal Specific GC Detectors Using AAS.** J. W. Robinson, Louisiana State U

9:30 **Flame Spectroscopic Methods of Detection for High-Speed Liquid Chromatography.** S. E. Manahan, D. R. Jones, D. Coppenaal, U of Missouri

10:15 **Element- and Speciation-Specific Techniques for Organometallic Compounds.** Y. K. Chau, P.T.S.. Wong, Canada Centre for Inland Waters

10:45 **Nondispersive Atomic Fluorescence Spectroscopy—Multielement, Metal Specific, Detector for Chromatography.** J. C. Van Loon, B. Radziuk, U of Toronto, Canada

11:05 **Determination of Element Speciation with Plasma Spectrometry.** S. Hanamura, I. L. Barnes, NBS

11:25 **Thermal Vaporization into Flameless, Flame, and RF Plasma Cells for Inorganic Speciation.** M. D. Silvester, D. J. Koop, Barringer Research Limited, Canada

11:45 **Graphite Furnace Atomic Absorption Spectrophotometer as Detector in Speciation of Trace Metals in Aquatic Environment.** R. D. Guy, C. L. Chakrabarti, Carleton U, Canada

Hewlett-Packard stands GC/MS technology on its ear.

Four major breakthroughs yield the first high performance GC/MS system that fits on your lab bench, the 5992A.

Here's what this revolutionary new GC/MS system offers you:

Quadrupole Analyzer Inside Diffusion Pump. An innovative pump design that reduces the 5992A's size, adds to its efficiency and reliability.

There's less volume to evacuate, so the system pumps down faster—the entire vacuum sequence is automated, by the way.

There are fewer parts; hence, fewer chances for leaks. For example, there's only one vacuum flange in the entire system. And it doesn't even use bolts!

Result: Rapid performance you can count on, from a system that occupies about half the space of its smallest counterpart.

Hyperbolic Quadrupole. GC/MS designers have long known that hyperbolic rods approached theoretical perfection. But how to create the technology? We found the answer.

Result: Excellent sensitivity and resolution; sharp consistent peak shapes.

Automatic Tuning. You no longer have to manually adjust the various voltages that control the ion optics of the MS. Just load the AUTOTUNE program, and the 5992A optimizes itself.

Result: Spectra of consistent quality and high sensitivity, no matter who's minding the system.

Incidentally, you can override this program any time, but it's not likely that you'll ever have to.

Calculator Control. The reason the 5992A has no knobs. You talk to it via Hewlett-Packard's powerful desktop programmable calculator, the HP 9825A.

The HP 9825A gives you speed, power and capacity (16K memory) that approach minicomputers, but it's much easier to operate.

Result: Normalized data. The HP 9825A performs your data manipulations. Also, you can do selected ion monitoring.

Incidentally, you can use the calculator separately from the GC/MS; you can even use it to solve independent problems while the GC/MS is working.

Unmatched Price: Performance. The bottom line result of the technological advances outlined above: the reason your organization should equip you with a 5992A.

It can solve your problems faster, more accurately and with less fuss than GC/MS systems that cost considerably more.

We'd like to prove it to you, with specific examples. Just call your local HP office, or write us at 1601 California Ave., Palo Alto, CA 94304

Delivery. We are currently shipping, and will try to deliver your 5992A within 60 days after you order it, tested and ready to go to work.

P.S.: Need chemical ionization capability or added flexibility? Consider our 5980A series GC/MS family.

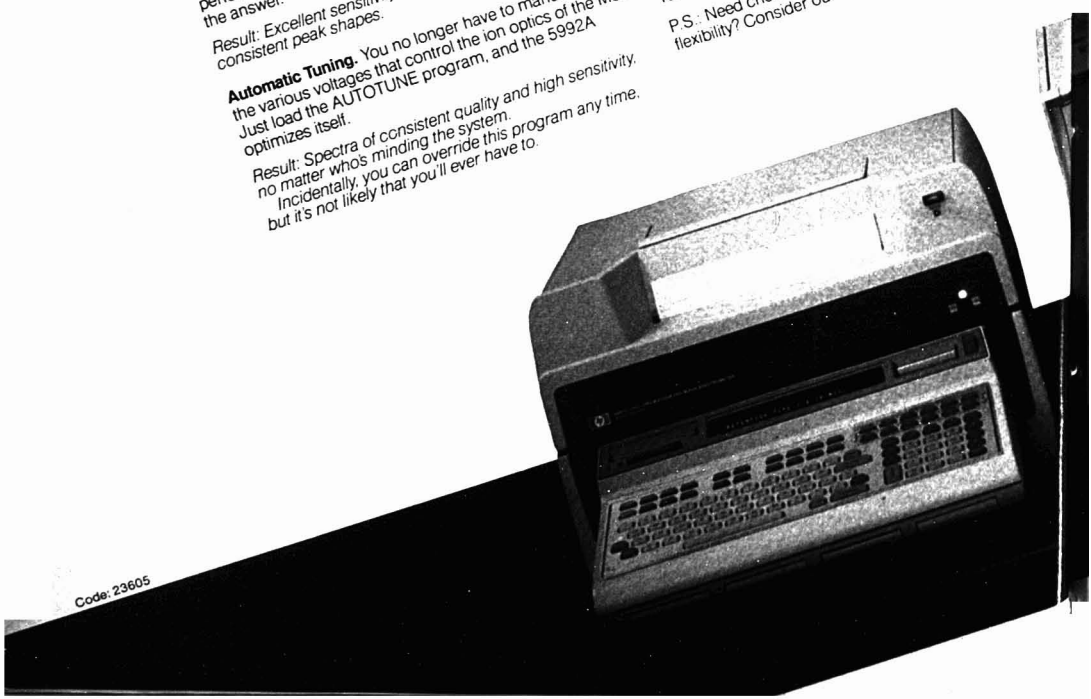

Code: 23605

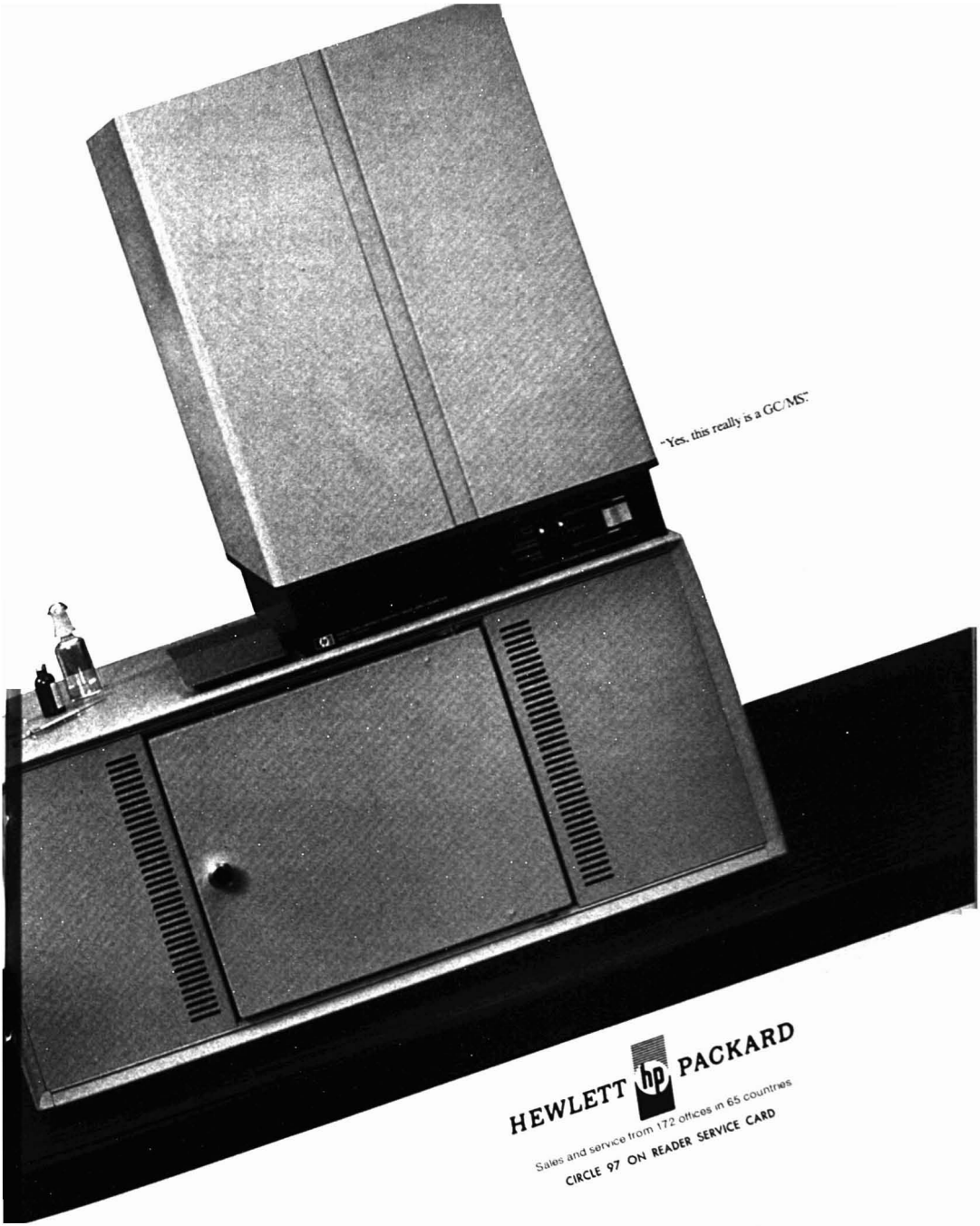

HEWLETT hp PACKARD

Sales and service from 172 offices in 65 countries

CIRCLE 97 ON READER SERVICE CARD

Exposition

The Exposition at the 3rd FACSS Meeting will be held in the Civic Center, Philadelphia, Pa., Nov. 15 to 18, 1976

Exhibit Hours

Monday, Nov. 15: 10:30 a.m. to 5:00 p.m.
Tuesday, Nov. 16: 9:30 a.m. to 5:00 p.m.
Wednesday, Nov. 17: 9:30 a.m. to 6:00 p.m.
Thursday, Nov. 18: 9:30 a.m. to 2:00 p.m.

Altex Scientific, Inc.
1450 Sixth St., Berkeley, Calif. 94710. Chemically inert fittings & valves, motorized valves, glass LC columns, prepacked HPLC columns, HPLC sample injection valves and accessories, gradient programmer, solvent HPLC metering pumps, fixed and variable UV–VIS LC detectors, liquid chromatographs.

American Society for Testing & Materials
1916 Race St., Philadelphia, Pa. 19103. Publications dealing with liquid, gel, and gas chromatography; air and water pollution; metallurgical analysis; paint and plastics testing; forensic sciences; mass spectral data; x-ray emission data; free catalogs.

Angstrom, Inc.
P.O. Box 248, Belleville, Mich. 48111. Automatic fusion device, laboratory disc mill, particle size classifier, spectrochemical supplies and accessories.

Applied Research Laboratories
P.O. Box 129, Sunland, Calif. 91040. Inductively coupled RF plasma quantometer (ICPQ) for simultaneous multielement analysis of solutions and solid metal samples.

Applied Science Laboratories, Inc.
P.O. Box 440, State College, Pa. 16801. Complete line of products for gas, liquid, and thin-layer chromatography; radiochemicals; reagents; drug standards; biochemicals.

August Sauter of America
80 Fifth Ave., New York, N.Y. 10011. Electrons and mechanical weighing equipment; weighing systems for laboratory, industrial, and medical applications; portable weighing equipment.

B/R Glass, Inc.
P.O. Box 7, Pasadena, Md. 21122. Spinning band and analytical distillation columns, solvent recovery stills, micro distillation columns, vacuum sublimation apparatus.

Beckman Instruments, Inc.
Rte. 22 at Summit Rd., Mountainside, N.J. 07091. 4260 high-performance IR, acculab IV routine IR, acta M IV, 25 dissolution system, pH meters, O_2 analyzers, KF-4B titrator, balances, instrument supplies.

Buck Scientific, Inc.
Princes Pino Rd., W. Norwalk, Conn. 06850. Used scientific instruments, assay for scientific instruments, Westinghouse hollow cathode lamps, linear recorders, salt crystals for IR, service for P&E and Hilger Watts instruments.

Carle Instruments, Inc.
1141 E. Ash, Fullerton, Calif. 92631. Analytical gas chromatographs featuring automated series-S and series-R factory engineered for specific application, low-cost Basic gas chromatographs and complete line of Carle valves and valve automation accessories for all GC applications.

Chemical Data Systems, Inc.
RD 2, P.O.B. 74, Oxford, Pa. 19363. Model 820WP water pollution analysis system, Model 820D controlled atmosphere pyrolysis system, Model 800 reaction systems, Model 1200 elemental analyzer & peak identifier, Model 700 bacteria identification system, Model 120 pyroprobe solids pyrolyzer with programmable option, Model 200 multichannel temperature controller.

Columbia Scientific Industries
P.O. Box 9908, Austin, Tex. 78766. Supergrators: computing integrators for chromatography, mass spec data systems, portable x-ray analyzers, ozone and NO/NO_x analyzers.

CRC Press
18901 Cranwood Pkwy., Cleveland, Ohio 44118. Second edition of "Atlas of Spectral Data & Physical Constants for Organic Compounds", with IR, UV, HNMR, mass spectra, Raman (R), and carbon 13 (^{13}CNMR) for over 21 000 compounds; "Handbook of Spectroscopy"; "Handbook of Chromatography"; "Critical Reviews in Analytical Chemistry"; "Diffuse Reflectance Spectroscopy in Environmental Problem Solving"; "Mass Spectrometry of Pesticides & Pollutants"; "Handbook of Tables of Functions for Applied Optics"; and many more.

Digilab, Inc.
237 Putnam Ave., Cambridge, Mass. 02139. Standard line of instrumentation together with some of its newest innovations in the field of Fourier IR spectroscopy.

Digital Equipment Corp.
146 Main St., Maynard, Mass. 01754. Interactive laboratory computer system designed to interface with gas chromatographs and other analytical instruments, special laboratory applications software packages which acquire, analyze, and process laboratory data.

Drummond Scientific Co.
500 Parkway, Broomall, Pa. 19008. Complete line of positive displacement precision microliter pipetting aids, six new fixed-volume microdispensers plus dialamatic and standard 1–5-μl microdispensers, finest hardheld ML pipetting device, the Pipet-Aid.

Du Pont Instruments
1007 Market St., Wilmington, Del. 19898. CA-848 system consisting of high-performance liquid chromatograph, flow controller, and automatic sampler designed for unattended overnight operation.

Hanson Research Corp.
19727 Bahama St., Northridge, Calif. 91324. "Dissograph" automated dissolution system: pharmaceutical test equipment and apparatus for dissolution, disintegration, and timed release testing; data & instruments for monitoring vibration during pharmaceutical testing.

Harrick Scientific Corp.
Croton Dam Rd., P.O.B. 867, Ossining, N.Y. 10562. Complete line of IR–VIS–UV spectrometer attachments and accessories for internal reflection spectroscopy, fluorescence, external reflection and transmission; beam condensers for microsampling; precision demountable liquid cells; optical windows and precision optical elements; plasma cleaner for ashing and ultraclean surfaces; rapid scan spectrometer (1000 spectra/s) for UV–VIS–NIR; double-beam goniometer.

Hewlett-Packard
1501 Page Mill Rd., Palo Alto, Calif. 94304.

Heyden & Son Ltd.
Spectrum House, Alderton Crescent, London, NW4 3XX, England. Books on spectroscopy covering monographs, data products, proceedings, introductions, pro-

grammed texts and audiovisual aids; journals covering organic mass spectrometry, biomedical mass spectrometry, x-ray spectrometry; fire and materials and interdisciplinary science reviews; *European Spectroscopy News*.

IBM Instrument Systems
1000 Westchester Ave., White Plains, N.Y. 10604. Laboratory and production measurement devices.

Instrumentation Laboratory
113 Hartwell Ave., Lexington, Mass. 02173. Modern atomic absorption equipment including Model 351 251 with Tektronix 31 programmable calculator, new version of flameless atomizer and new accessories.

J.Y. Optical Systems
173 Essex Ave., Metuchen, N.J. 08840. Raman and CD spectrometers, high-resolution monochromators, preparative liquid chromatograph, holographic and ruled diffraction gratings.

Johns-Manville
Greenwood Plaza, Denver, Colo. 80217. Variety of supports and adsorbents for use in both gas and liquid chromatography.

Joint Committee on Powder Diffraction Standards
1601 Park Lane, Swarthmore, Pa. 19081. Powder Diffraction File featuring data cards, microfiche, search manuals, data books and data base tapes.

Labconco Corp.
8811 Prospect Ave., Kansas City, Mo. 64132. Bench top freeze dryer or freeze dryer 3, controlled atmosphere glove box, glassware washer, fume hood and base cabinet, cart freeze dry accessories.

Labindustries
1802 Second St., Berkeley, Calif. 94710. All-glass repetitive Repipet reagent dispensers and diluters in sizes 0.5–100 ml; Repipet Jr. plastic dispensers for noncaustic reagents; Labindustries' micropipettor, micropipets; Repipet sampling system transfer pipets; Karl Fischer aquametry apparatus for water determinations; Labquake test-tube shakers and rotators.

Marcel Dekker, Inc.
270 Madison Ave., New York, N.Y. 10016. Books and journals.

Mettler Instrument Corp.
P.O. Box 100, Princeton, N.J. 08540. Analytical & top-loading balances, thermal analysis instruments, titrators, density meters, nitrogen analyzers.

Nicolet Instrument Corp.
5225 Verona Rd., Madison, Wis. 53711. NIC-7199 FT–IR system with complete software package and full range of options and accessories performs automatic ratio recording with better than 0.07 cm^{-1} resolution throughout 4000–400 cm^{-1} spectral range; NIC-1180 data system for FT–NMR, laser Raman, EPR, and FT–IR spectroscopy features complete application software package.

Nissei Sangyo Instrument Co.
2672 Bayshore Frontage, Mt. View, Calif. 94043.

Perkin-Elmer Corp.
Main Ave., Norwalk, Conn. 06856. IR, atomic absorption UV–VIS, and fluorescence spectrophotometers; NMR spectrometer; gas and liquid chromatographs; autobalances, thermal and elemental analyzers; polarimeters.

Plasma-Therm, Inc.
Rte. 73, Kresson, N.J. 08053. Fully automated operational inductively coupled plasma (ICP) source for use with emission spectrometers for simultaneous and single-element analysis; new low-cost ICP source for use with AA spectrometers.

Plenum Publishing
227 W. 17th St., New York, N.Y. 10011. Books and journals in areas of analytical chemistry and spectroscopy.

Precision Gas Products, Inc.
681 Mill St., Rahway, N.J. 07065. Ultra-high-purity carrier and reference gases; PGP-2 carbon monoxide monitor; Big Shot disposable calibration gases; "Gas Analysis News", a new technical newsletter; leak detection apparatus and other gas handling equipment.

Princeton Applied Research Corp.
P.O. Box 2565, Princeton, N.J. 08540. Microprocessor-based polarographic analyzer for high-speed, high-sensitivity analyses of metals, ions, and organics; automated cell sequences system for automated high-volume analyses using differential pulse voltammetry; corrosion measurement systems for evaluation of materials for passivation characteristics, pitting tendencies, corrosion rates, and many other corrosion experiments.

Princeton Gamma Tech
P.O. Box 641, Princeton, N.J. 08540. PGT-500 x-ray spectrochemical analyzer for rapid, nondestructive analysis of up to 82 elements; Model 100 chemical analyzer: bench-top series; PGT-1000 multichannel x-ray analyzer for quantitative or qualitative column applications.

Prochem/Isotopes
47 Meadowbrook Place, Maplewood, N.J. 07040. Compounds labeled with carbon-12, carbon-13, oxygen 17, oxygen 18, and nitrogen-15; also multiply labeled compounds.

Sadtler Research Laboratories, Inc.
3316 Spring Garden St., Philadelphia, Pa. 19104. CIRA 101 chromatographic infrared analyzer; new inexpensive GC/IR technique; Sadtler standard & commercial reference spectra (IR, NMR, UV, Raman, fluorescence, DTA, C-13 NMR, IR vapor phase); audiovisual programs (chemistry, math, lab skills); technical books; educational courses in spectroscopy & chromatography; analytical services.

Schoeffel Instrument Corp.
24 Booker St., Westwood, N.J. 07675. Liquid chromatography: new continuously variable fluorescence and absorption detectors; UV–VIS spectrophotometer with unique conversion feature for microliter and standard size cells. Thin-layer chromatography: SD-3000 monochromatic, double-beam chromatogram scanner for TLC and TLE; accessories include computing integrator, printout, and recorder interfacing. Light and light measurement products: generation, dispersion, and detection of light including xenon and mercury-xenon compact arc illumination systems and accessories for lamps up to 6500 W; grating and quartz prism monochromators; photodetection systems including photomultiplier photometers and photodetector housing, both standard and thermocooled, for side-on and end-on tubes. Other analytical instruments: RRS-1000 research grade corrected spectra ratio spectrophotometer/fluorometer, microspectrofluorometers, and turbidimeters.

Schott, Jenaer Glaswerk Schott & Gen., Inc.
11 E. 26th St., New York, N.Y. 10010. Automatic viscosity measuring system for Ubbelohde-type capillary viscometers: up to 10 samples can be measured automatically according to test program selected, and results are printed out by seven-digit printer; pH glass electrodes for industrial application.

Scientific Information Resource
5116 Woodlawn Ave., Chicago, Ill. 60615. Catalogs and brochures of a number of companies' products and services.

Siemens Corp.
186 Wood Ave. S., Iselin, N.J. 08830. SRS, K805 generator, measuring panel.

Spectrametrics, Inc.
204 Andover St., Andover, Mass. 01810. Spectraspan plasma spectrometers for trace level analysis utilize argon plasma excitation source, echelle grating spectrometer, and microcomputer readout & control; systems available for qualitative & quantitative analysis; sequential & multielement modes.

Spectrex Corp.
3594 Haven Ave., Redwood City, Calif. 94063. Vreeland spectroscope for rapid elemental analysis, particle counter for particle sizing in liquids (1–100 μm), electronic pumps for 0–15 lpm flow.

Spex Industries, Inc.
3880 Park Ave., Metuchen, N.J. 08840. High-aperture, high-resolution scanning spectrometers and monochromators; vidicon detection systems; corrected spectrofluorometer; laser Raman spectroscopy equipment and computer systems; Chromalytics thermal chromatograph and concentrator.

Supelco, Inc.
Supelco Park, Bellefonte, Pa. 16823. Gas chromatographic column packings, supports, custom-made and stocked glass columns; Hamilton, precision sampling, and SGE syringes; educational materials for GC thin-layer chromatography, lipids, carbohydrates, amino acids, and reagents.

Arthur H. Thomas Co.
Vine St. at Third, Philadelphia, Pa. 19105. Thomas peak detector system; new Big Dipper; Mettler balances; Thomas printers; Hitachi single-, double-, and dual-wavelength spectrophotometers; new atomic absorption spectrophotometers.

Tracor, Inc.
6500 Tracor Lane, Austin, Tex. 78721. 560 GC, 550 GC, variable UV detector, 6960 LC, detectors for GC and LC recorders, Tracor analytical processor.

Varian
611 Hansen Way, Palo Alto, Calif. 94303. New gas and liquid chromatographs with autosampler, new mass spectrometer.

Waters Associates, Inc.
Maple St., Milford, Mass. 01757. Complete line of high-performance liquid chromatography instrumentation and accessories including solvent delivery systems, injectors, detectors, programmers, GC and LC packings, packed columns.

John Wiley & Sons, Inc.
605 Third Ave., New York, N.Y. 10016. Professional reference books and college textbooks in analytical chemistry and spectroscopy and related areas from Wiley-Interscience, Wiley College Division, and Halsted Press.

Wilks Scientific Corp.
140 Water St., S. Norwalk, Conn. 06856. Complete line of portable & stationary ambient air analyzers, IR quantitative analysis systems for repetitive measurements of liquids, complete line of IR accessories for all commercial spectrophotometers.

Wilmad Glass Co., Inc.
U.S. Rte. 40 & Oak Rd., Buena, N.J. 08310. Tubes, cells, and accessories; recording charts; deuterated solvents; microliter syringes; precision dispensers and diluters; special pH probe for NMR sample tubes.

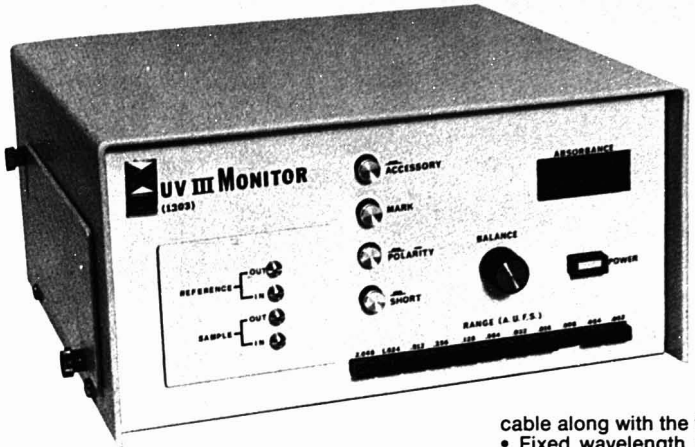

Laboratory Data Control, now has the LDC Model 1203 UV Monitor III. Ultraviolet absorbance measurements can be made over a wide choice of fixed wavelengths. Featuring a totally removable cell and easily varied wavelengths. Standard 254 nm cell is therefore replaced with a choice of 214 (planned), 280, 350, 410, 440, 510, or 550 nm wavelengths. Cell volume is only 10 μl with standard 10 mm pathlength. The cell is temperature compensated to minimize the effect of refractive index changes on the solvent. The optical assembly and electronic controls are contained in one unit thereby eliminating interconnecting cable along with the following features:

A "New Era" UV Monitor for HPLC

- Fixed wavelength measurements over eight choices of wavelength.
- Ten sensitivity ranges from 0.002 to 2.048 Å.
- Digital display of differential absorbance.
- Switch selectable time constant delay.
- Flow cell design is dual flow, totally removable and temperature compensated.

For complete technical details on the UV III Monitor or other high quality equipment for HPLC, contact Laboratory Data Control today.

The Chromatography Connection

LDC is the ideal source for HPLC systems which can be custom tailored to your specific laboratory requirements. The setup illustrated shows the new UV III Monitor, together with a CONSTAMETRIC IIG constant flow metering pump (with control module); a CONSTAMETRIC I constant flow metering pump; a Chromatography Accessory Module; a Model 1601 Gradient Master; a Model L Computing Integrator (also available in the Model E configuration), and a Model 3402 Recorder. Full details on the system and its potential benefits for you are immediately available from LDC.

LDC's Modular HPLC System

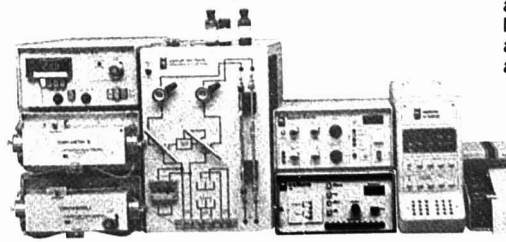

LABORATORY DATA CONTROL
DIVISION OF MILTON ROY CO.
P.O. BOX 10235 • RIVIERA BEACH, FLA. 33404
305-844-5241 • TELEX 513479

CIRCLE 131 ON READER SERVICE CARD


Jarrell-Ash
INPUT
OUTPUT
WAVELENGTH
H.C. CURRENT
AVG. PERIOD
SLIT SIZE
COMPUTER CONTROLLED
READOUT MODE
ANALYTICAL MODE
COMPUTER STATUS
BURNER
OXIDANT
FUEL

Fisher Jarrell-Ash: No.1 in computer-controlled AA instrumentation.

Model 850, the world's only microcomputer-controlled atomic absorption instrument is the first completely digital and fully integrated AA system ever. None of the so-called AA leaders (No.'s 1, 2 or 3)* can match Model 850.

Unparalleled convenience and outstanding analytical performance make Model 850 a new leader. While other AA instrument manufacturers are trying to make-do with computer-interfaced systems or add-on calculators, Model 850 is here, a certain forerunner of the next generation of AA instruments — years ahead of all the rest.

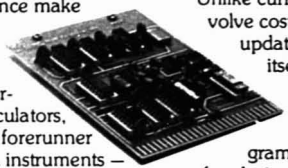

Keyboard Conversation

You "talk" to our "intelligent" 850 by keyboard. A simple coded language enables set-up in just a few minutes. The 850 micro processor is the control center for the instrument. It will turn on the hollow cathode, set operating current, slit width, wavelength, and averaging period — simple as 1, 2, 3. It automatically recalibrates itself; reads wavelength you specify; and "locks on" the most intense absorption line in that spectral area. AA operation has never been simpler or quicker.

Analytical Excellence

The essentially all-digital Model 850 is a generation ahead of AA units with analog limitations. Using Auto-Zero, Auto-Calibration, and Auto-Curve Correct as examples, the Model 850 **computer-calculates** the constants for these functions — accurate to six significant figures. Analog devices, by contrast, rely on mathematical approximations which, at best, are half as accurate. Clearly, the electronic precision of the 850 outperforms all the rest.

The Interaction Secret

What causes electronic "drift" in today's AA instruments? It's an analog answer — you see, all AA's have interacting gain and auto-zero functions. When they are set and then held by analog memories the inevitable drift occurs with time.

With Model 850, gain and auto-zero functions become stored digits — numbers that cannot change with time. Result, drift is gone — for zero, for gain, for concentration, for scale expansion — gone for good.

Anti-obsolescence

Unlike current instruments which involve costly hardware changes to update, Model 850 can improve itself with the addition of new software (pre-programmed silicon chips), which incorporate new programs and capabilities. Our way of replacing chips costs hundreds. The other way of "junking" entire instruments or adding modules, motors, amplifiers etcetera costs thousands. The long range economy and foresight of the 850 makes a lot of sense.

Redefining Convenience

For the ultimate convenience, Model 850 introduces an automatic programmer. This accessory lets you pre-program routine analyses for total automation. Once you program the tape (it's quite simple), just insert it, and push one button. Model 850 does the rest. Unequalled AA convenience, unavailable anywhere else.

Footnote

Model 850 is the first computer-controlled AA instrument. For this accomplishment, we are proud. However, it's not a totally new phenomenon for us. Four years ago, the Fisher Jarrell-Ash Division introduced the first computer-controlled direct-reading spectrometer. Today, it's unquestionably the No. 1 direct reader in the world. Our envious Model 850 AA engineers won't rest until they're No. 1 in AA. We think they're on the way.

For complete information on the **new No. 1 AA** instrument, Model 850, write for free bulletin.

Fisher Scientific Company

*Ranking pertains to total AA units sold.

CIRCLE 80 ON READER SERVICE CARD

Introducing the Antlia™ pneumatic hand pump system.

Applies needed pressure to membrane filtration problems.

Give your filtration problems a shot in the membrane with the new Antlia pneumatic hand pump system. It's designed to provide needed pressure for fluids with high viscosity. Fluids with large concentrations of particles. And for filtering through membranes with pore sizes as small as 0.01 μm.

Insert a new membrane, glass, or paper filter in either its 25mm or 47mm thread-on holder, and the Antlia pump instantly adapts to a new application. Sterile filtration, clarification. On-the-spot testing of membrane performance. And a host of others.

A pump within a pump makes it all possible. The Antlia unit consists of two concentric polycarbonate cylinders. The outer cylinder holds up to 50ml of solution. The inner one functions like a bicycle pump. Sliding on silicone O-rings, it exerts air pressures as high as 115+ psi. Safety valves relieve over-pressurization. Components are stable at temperatures up to 130°C, can be autoclaved, and are chemically resistant.

An accessory three-way valve permits filtration of large volumes by allowing the user to draw fluids up into the cylinder and discharge them through the filter without having to disassemble the unit each time.

Selectron® membranes, as well as S&S glass and paper filters for the Antlia system, come in diameters of 25 and 47mm. And in a wide range of pore sizes.

For details, send for our new Instructional Bulletin, S-4, 'The Antlia Pneumatic Hand Pump System.' We'll also send you our complete catalog of materials and equipment for separation science.

SCHLEICHER & SCHUELL

Keene, New Hampshire 03431
Schleicher and Schuell GmbH, D-3354, Dassel, West Germany
Schleicher & Schuell AG, 8714 Feldbach ZH, Switzerland

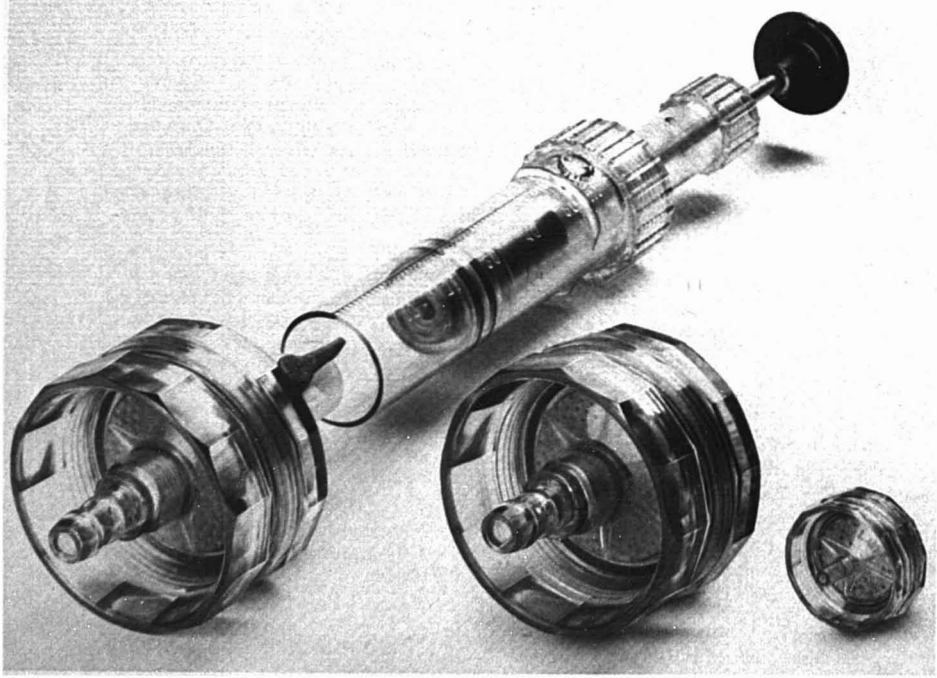

CIRCLE 193 ON READER SERVICE CARD

Lloyd Snyder, Jacob Levine, Robert Stoy, and Aldo Conetta

Technicon Instruments Corp.
Tarrytown, N.Y. 10591

Automated Chemical Analysis:

In the late 1950's, medical facilities in the United States came under increased demand for their services. The availability of medical insurance from both the federal and private sectors of the economy gave large segments of the public access to better care. As the physician became overloaded with additional patients, he turned to the laboratory to speed up and enhance the diagnostic process. In addition, specialized tests involving the quantitation of serum enzymes, electrolytes, protein fractions, and circulating hormones moved from the research laboratory to routine testing. As a result, the clinical chemistry laboratory became a major user of analytical methods and equipment, and in 1976 about 100 million samples will be assayed in domestic clinical laboratories.

Equipment designed for the clinical laboratory has to meet several major requirements. It must be rugged with minimum downtime, produce reliable data which are comparable with reference methods used to establish clinical guidelines, and be relatively simple to operate and cost effective. Designing these features into instrumentation has been a major challenge to chemists and engineers during the last 20 years. The lessons learned in the clinical laboratory should be of interest to other analytical chemists faced with the problem of producing large volumes of precise and accurate data. In fact, many of the approaches first used in the clinical laboratory have now been adapted to automated, routine testing in other industries.

Almost all large hospital laboratories presently rely on sophisticated, automated clinical analyzers. This equipment utilizes a variety of detection techniques (e.g., colorimetry, flame photometry, electrochemistry), can simultaneously assay as many as 20 constituents in as little as 0.5 ml of serum, and can furnish up to 3000 separate assays per hour. Automated analyzers can be classified into one of three categories: continuous-flow (CF), discrete, and centrifugal. While this article will focus mainly on CF analyzers, other types of instrumentation will be described briefly for purposes of comparison.

Continuous-Flow Systems

Continuous-flow analysis was invented by Leonard Skeggs, a Cleveland biochemist with joint academic and hospital affiliations. This technique was introduced commercially in 1957 by the Technicon Corp., and these AutoAnalyzer CF systems became the first widely used automated

Update on Continuous-Flow Approach

equipment for clinical and other analyses. These systems were modular in design and were used mainly for large-volume individual tests, e.g., glucose and urea nitrogen in serum. CF analysis is carried out with a series of connected components: a sampler, a multichannel peristaltic pump, one or more mixing/reaction coils, a dialyzer (sometimes), and a recording colorimeter or other detector. A typical CF flow diagram is shown in Figure 1. Samples and intersample wash fluid are intermittently aspirated at the sampler; the resulting stream is segmented by air bubbles and combined with a diluent A from the pump, passed through a mixing coil, and then enters the dialyzer. Dialyzable analyte diffuses through the dialyzer membrane into a second segmented stream B, is combined with a reagent C, passes through a thermostated reaction coil where a chromogenic reaction takes place, and is finally fed to a colorimeter. In this way it is possible for a series of separate steps in an analytical procedure to be carried out in a controlled, reproducible, and fully automatic fashion: precise dilution of sample, quantitative addition of one or more reagents, sample cleanup by dialysis, reaction of sample for a given time at some chosen temperature, and measurement of the final absorbance of reacted sample.

Although the original AutoAnalyzer system was capable of being switched from one test to another simply by changing assay manifolds (that part of the system between pump and detector), it was often dedicated to the batch analysis of only one or two serum components. This perpetuated the traditional mode of clinical laboratory organization, where individual tests were performed in separate work stations. A major change in approach was the development in the mid-1960's of multichannel biochemical analyzers, where up to 12 separate assays could be simultaneously carried out on a single sample at sampling rates up to 60/h (*1*). This quickly led to a major reorganization within many large clinical laboratories, with the bulk of the workload now being handled by a single analytical unit: a Technicon SMA 12/60 system and later the 18/60 (12 or 18 assay-channels, running at 60 samples/h). An important side effect was the widespread acceptance of the concept of profiling, where all patients upon admission to a hospital are tested for a standard 12 (or more) serum parameters (*2*). These trends in the use of CF analysis in the clinical laboratory culminated

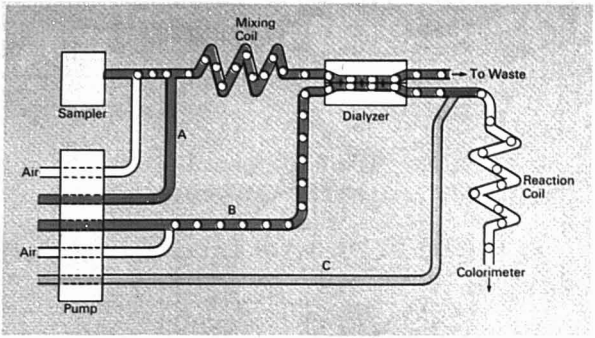

Figure 1. Example of continuous-flow analysis scheme
A, B: diluents; C: reagent stream

in 1972 with the introduction of the Technicon SMAC biochemical analyzer (*3*), which allows the simultaneous assay for 20 serum parameters on each sample at rates of 150 samples/h.

Discrete Analyzers

These systems are designed to simulate the same operations used in manual procedures. Pneumatic or motor-driven syringes are used to meter reagents and sample into test tubes or "discrete" reaction vessels placed in a conveyor belt or reaction wheel. The combined sample–reagent mixture is agitated mechanically and passed through a water bath for temperature control. Additional reagents can be added prior to readout at a cuvette station. Many of these designs include a "laundry system" to wash the reaction vessels and recycle them back into the analytical train. The Hycel Mark X and Super Seventeen, the Coulter Chemistry System, the Ortho Basic, the Du Pont ACA, and the American Monitor KDA systems are currently available instruments built on this approach. These instruments are generally capable of carrying out a variety of different tests on the same system.

Discrete analyzers offer the opportunity for automated adaptation of existing techniques by direct duplication of established manual methods. They also have a potential advantage, in the case of multichannel analyzers, in that reagents are used only for those tests requested on the sample. This assay selectivity is not possible with CF analyzers. One disadvantage of discrete analyzers is their mechanical complexity, particularly when compared with the simple flow of liquid in CF systems. This means that the design of discrete analyzers for mechanical reliability is much more demanding.

Centrifugal Analyzers

Both CF and discrete analyzers are limited by the fact that samples enter the detector serially, so that each sample spends a certain fixed time in the detector. In many kinetic assays (as for serum enzymes), it is desirable to monitor the assay over an extended period of time. With only a single detector in the analytical system (for each assay channel), as is normally the case for CF and discrete analyzers, throughput rates are inversely proportional to assay "look-time" (the time each sample spends in the detector). Therefore, a compromise is normally required: either look-times must be short, or throughput rates must be small. An alternative approach, the centrifugal or GEMSAEC analyzer, was developed by Norman Anderson (*4*) in the late 1960's at the Oak Ridge National Laboratory. Centrifugal analyzers effectively multiplex the detector by rotating a tray of samples past a single detector station. In this way the look-time can be increased, and sampling rate is not sacrificed because several samples are being monitored during a single extended look-time.

Centrifugal analyzers also provide for the controlled addition of reagents to sample by centrifugal action, in place of the mechanically demanding syringe operations of discrete analyzers. The main disadvantage of centrifugal analyzers is their batch mode of operation, which requires reloading trays with both reagents and samples for each group of samples analyzed. This also precludes running individual samples for different tests at the same time.

Fundamental Aspects of Continuous-Flow Analysis

The shape of the signal produced by the flow-through detector in CF analysis is fundamental to a basic understanding of this technique. The quality of this signal is influenced by the following key variables: sample dispersion, mixing, and flow stability. Over the past several years the effects of these variables in CF analysis have been studied in detail both at Technicon and elsewhere. As a result, we now have a good understanding of both the potential and limitations of CF analysis, and how such assays can be optimized for accuracy, precision, and maximum analysis rates.

Sample Dispersion. The potential rate-limiting effect of dispersion is illustrated in Figure 2a, where analyte concentration vs. time is shown at the beginning (sampler) and the end (detector) of CF analysis. The beginning curve is a rectangular input function, corresponding to the successive aspiration of samples and analyte-free wash fluid. The heights of these sample curves reflect the analyte concentrations in each sample. At the end of CF analysis, we see some rounding of the initial input curves, due to axial dispersion of analyte molecules along the flowing stream. The extent of this dispersion depends upon the experi-

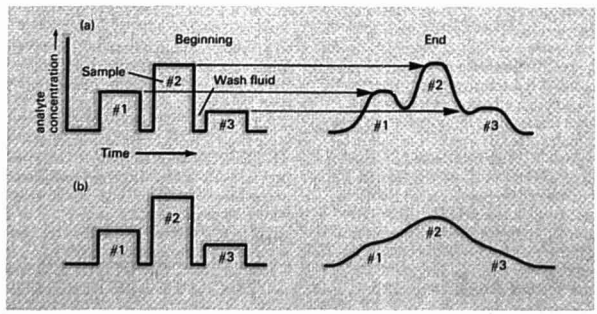

Figure 2. Effect of dispersion during continuous-flow analysis on sample concentration curve shape
(a) Acceptable dispersion; analyte and analyte-chromogen concentrations plotted on molar basis; (b) unacceptable dispersion

{ENGINEER / PHYSICIST / CHEMIST} + PATENT AGENT = NEW HORIZONS

INCREASE YOUR INCOME — MULTIPLY YOUR OPTIONS — PROTECT YOUR OWN INVENTIONS
PRACTICE PATENT LAW [*WITHOUT BEING A LAWYER*] AS A PATENT AGENT

Patents protect and make money for new technology. Scientific and engineering knowledge is the entering argument for effective patent protection. Although not widely known, engineers and physical scientists need not go to law school to be licensed as Patent Agents to represent clients before the U.S. Patent Office in the writing and obtaining of patents. The Supreme Court has held that Patent Agents may practice patent law from anywhere in the United States under the protection of the federal supremacy clause of the United States Constitution.

But to become a Patent Agent you must pass the one day, six hour examination in patent law currently given each March and September in all major cities throughout the United States by the U.S. Patent Office. Even lawyer-engineers who aspire to patent specialization are required to pass this examination.

Now, for the first time in the 186 year history of our patent system, you can rapidly learn patent law so thoroughly as to pass the licensure exam and also practice professionally, either as a full time pursuit or as a part-time supplement to your regular technological activities. Most importantly you can study at home, in your spare time and at your pace. No need to spend $10,000 and three years on law school. No need to give up your job or change your routine in the process. To the contrary, the more technological experience you have, the more valuable you will be as a Patent Agent and the more effective you will be in securing patents for your own inventions. There is no downside risk. At the very least patent know-how enhances every technically trained person's value to his employer or to his own business.

PATENT PREPARATION & PROSECUTION PRACTICE, which has just been published, is the answer. It is a 6-volume self-training treatise of over 1200 pages in 25 chapters filled with text, hypotheticals, forms and practical instruction. A seventh 200-page companion volume of questions and answers is included that covers the material of the six volumes. This is NOT a correspondence course. But it IS a complete self-contained training program all in your hands at one time. It is designed to give step-by-step, incremental self-instruction to engineers and physical scientists who have absolutely no prior legal knowledge at all. At each point in the Treatise every concept needed to understand the exposition has either already been explained or is explained then and there.

PATENT PREPARATION & PROSECUTION PRACTICE is the ultimate for learning to be a patent practitioner. It distills 24 years of practice and 12 years of teaching by Dr. Irving Kayton who is Professor of Law and Director of the Patent Law Program at The George Washington University in Washington, D.C. Professor Kayton spent eight years designing the Treatise and two years editing and coauthoring it with six coauthors who are partners in leading patent law firms throughout the United States.

Professor Kayton is the only full-time law professor in the United States who spends the major part of this time teaching patent practice. He has trained more patent lawyers and agents than any person alive. The Treatise is the fruition of all his experience; it is what he uses now to teach both lawyers and engineers to become patent practitioners. Neither it nor anything like it is available anywhere else. You too may have it as a tool for building an enriched career, a versatile future and to get out of the lab or a narrow technical pursuit if you so wish. Assiduous step-by-step study of the Treatise can give mastery of its contents to anyone intelligent enough to have earned a degree in engineering or one of the physical sciences. Mastery of its contents guarantees passing the Patent Agent's examination.

Any U.S. citizen with a degree in any field of engineering or one of the physical sciences may apply to take the Patent Agent's Examination by writing to: Clerk of the Committee on Enrollment, U.S. Patent Office, Washington, D.C. 20231.

Below are excerpts from unsolicited letters to Professor Kayton. The courses mentioned (and much more) are now incorporated in PATENT PREPARATION & PROSECUTION PRACTICE.

I received notification that I made a passing grade on both the morning and afternoon sections of the Patent Bar Examination. Prior to your course, I had no exposure to patent law except for a few random articles in newspapers and magazines, that I read occasionally. At least 99% of my success with the examination is therefore attributable to your course. Hugh P. Nicholson, Huntsville, Alabama.

I was successful in my assault upon the Patent Bar Examination. Inasmuch as I had little or no experience as a Patent Agent-Trainee prior to taking the exam, I feel your course was instrumental in pulling together the information . . . on the substantive Law of Patents and Patent Procedure. Booker T. Hogan, Jr., Hughes Aircraft, Los Angeles, California.

Thank you. I attained a passing grade on the examination for registration to practice before the U.S. Patent Office. This couldn't have been accomplished by me if it were not for the Patent Bar Course administered under your direction. Being such a novice, as I truly am, in the Patent Law art, failure in this exam would have been certain but for your course. Edward S. Sherman, Union Carbide, Chicago, Illinois.

Research, development and invention have increased radically over the past ten years. New products are keyed to new technology. Demand for competent patent practitioners has grown by leaps and bounds. But there has been virtually no increase in the rate of supply. The result has been skyrocketing salaries and hourly fees for those licensed to practice patent law. You can share in it, because you are needed; but what will it cost? Only the price of PATENT PREPARATION & PROSECUTION PRACTICE under the options set forth below and diligent, serious study at home, in your spare time. It surely is a reasonable investment for the potential return in satisfaction, professional versatility, security and material well-being. **Were you to secure only one patent for yourself or a client, the price of the Treatise would be recaptured three to twenty times over.**

First Option: Purchase Volumes 1, 2, 3 and 7 (Questions and Answers) for $250.00 with a 15-day inspection, money-back guarantee. If for any reason you do not wish to keep the Treatise, return it during the inspection period for a prompt, full and courteous refund. If you keep it, Volumes 4, 5 and 6 may then be purchased for $200 (this price is guaranteed for six months after your original purchase). But Volumes 4, 5 and 6 will be sold only to purchasers of record of the first part of the Treatise. Postage, handling and insurance are free. Under this option, the total price will be $450.00.

Second Option: Purchase the entire Treatise, Volumes 1 - 7, at one time for $375.00; postage, handling and insurance also free. A saving of $75.00 over the first option. Sorry, no return privileges at this reduced price. Of the hundreds of sets of the Treatise already sold, fewer than 2% have been returned for any reason.

These options and prices are restricted to the continental limits of the United States and may not be available after October 29, 1976. District of Columbia residents add 5% sales tax.

To order the Treatise, BankAmericard, Master Charge and American Express credit card buyers may simply CALL TOLL-FREE (800) 424-9771; or mail your check or money order (or request for more information) to:

Patent Resources Institute, Inc.
Treatise Purchase Dept.
2011 Eye Street, N.W.—Suite 800
Washington, D.C. 20006

mental conditions used in a particular CF analysis and is markedly reduced by the segmenting air bubbles which serve as physical barriers to dispersion. In the example of Figure 2a, dispersion is not excessive, and the "flat" for each sample curve still reflects the true (nondispersed) analyte concentration of that sample. The observed detector output will mirror this final concentration-time plot, and the height of the "flat" above baseline is proportional to analyte concentration. Comparison of the "flat" height of an unknown to the response of a reference sample (standard) makes it possible to convert the analog signal to concentration.

The effect of excessive dispersion can be seen in Figure 2b. Sample carryover or interaction occurs, so that one sample overlaps the "flat" region of an adjacent sample, ths altering its apparent concentration. The "flat" time for each sample is also reduced by excessive dispersion. This effect can be countered by increasing the intersample wash time at the expense of sampling time (so as to keep sampling rate constant). However, this approach further reduces "flat" time and eventually results in sample maxima that are not at steady state. The heights of nonsteady-state peaks are still proportional to sample concentration and can therefore be used for analysis. However, relative peak heights are now strongly dependent upon dispersion within the system and (unlike steady-state measurements) can change with time. Therefore, use of nonsteady-state output is generally avoided where maximum precision is desired.

Another possibility is to increase the length of sampling time until steady state (a "flat") is achieved. This results in increased sample and reagent consumption plus decreased throughput rate: analysis rate and the consumption (per assay) of sample and reagent are inversely related in CF analysis.

The main contribution to sample dispersion in well-designed CF systems arises from the flow of the sample slug through the CF network. The physical basis of this dispersion process is illustrated in Figure 3. Assume that a marker-dye (or sample) is injected into segment #0 of Figure 3. Because the flowing stream normally wets the inside walls of the CF tubing, a thin film of liquid phase is laid down by each moving segment. The film from segment #0 will then be overtaken and mixed into segment #1, allowing dye to move from #0 to #1. Subsequently, the dye built up within segment #1 can in the same way be transferred to #2, and so on. Thus, in time the dye originally contained only in segment #0 will have become dispersed over many following segments.

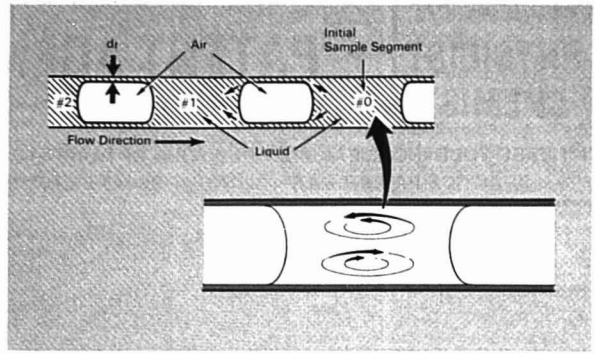

Figure 3. (a) Sample dispersion during segmented flow through open tube with marker-dye sample injected into segment #0. Film of liquid phase (d_f = film thickness) from segment #0 will be overtaken and mixed into segment #1, allowing dye to move from #0 to #1; dye built up within segment #1 can also be transferred to #2. Dye will become dispersed over many following segments. (b) Bolus circulation within moving liquid segment occurs naturally in any segmented-flow system

CF dispersion is conceptually similar to certain other processes of interest to analytical chemists (countercurrent distribution, chromatography, etc.), and a general mathematical model based on the above description has been known for about 10 years (*5*). More recently (*6, 7*), this model has been expanded to allow the prediction of dispersion as a function of experimental conditions. The amount of dispersion expressed as the variance σ_t^2 of the sample curve, as in Figure 2a (end), can be related to tube inside diameter d_t, liquid flow rate F_1, bubble segmentation rate n, liquid viscosity η and surface tension γ, time t in the flow network, and a sample mass transfer coefficient $D_{u,25}$. Dispersion is mainly a function of F_1, d_t, n, η, and t, with dispersion being less for smaller values of t, d_t, and η. The variation of dispersion with F_1 and n, holding other variables constant (d_t = 1 mm, t = 500 s), is illustrated in Figure 4. Optimum values of n and F_1 exist for a given set of conditions, so as to yield the lowest possible dispersion (value of σ_t). For normal CF analysis with "flats", sample plus wash time should equal about 8 σ_t. Figure 4 therefore suggests possible analysis rates of 250 samples/h, which is approached by state-of-the-art CF analyzers (SMAC). Further reduction in dispersion is possible if the residence time of samples (so-called "dwell-time") in the CF system can be reduced below 500 s, and if tubing i.d. is reduced below 1 mm. Ultimate sampling rates of about 600/h can then be predicted for CF analysis, but this is well beyond the capabilities of presently available systems.

Mixing. Mixing of sample and diluent is required in all CF systems, and usually several such mixing operations take place as successive reagent additions are made. Complete mixing must occur in each liquid segment (as though each segment were a microcuvette), and the penalty for failing to mix completely is a "noisy" detector output, which is in fact indicative of unmixed solution. Mixing in continuous-flow takes advantage of the natural fluid motions that occur within a

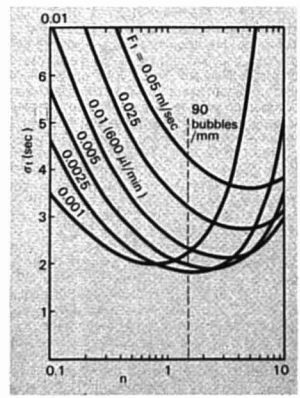

Figure 4. Dependence of sample dispersion on liquid flow rate F_1 and segmentation frequency n

Other conditions representative of SMAC analyzer: t = 500 s; temperature, 25°; d_t = 1 mm; 170 mol wt sample with surfactant-water as liquid

The pollution you want is the pollution you get.

Pollution standards that aren't standard can give you a lot of trouble.

So to save you a lot of trouble (and us lost business), we do a lot of things to make sure you get the exact pollution mixture you want.

We use the best calibration equipment there is. And the calibration techniques we use are based on those specified in the preparation of Standard Reference Materials supplied by the National Bureau of Standards. Not everybody does that.

The gas we put in the cylinder is accurate to within fractional parts per million when you get it. And to make sure it stays that way as you use it—for years and not just weeks—we developed Spectra-Seal™ aluminum cylinders. They eliminate chemical reactions between gas mixtures and the cylinder walls, so that changes in concentration (if they occur at all) are less than one part per million.

For specifics, call or write Hank Grieco, Airco Industrial Gases, 575 Mountain Avenue, Murray Hill, New Jersey 07974. (201) 464-8100.

He'll tell you how to get exactly what you want.

AIRCO
Industrial Gases

CIRCLE 4 ON READER SERVICE CARD

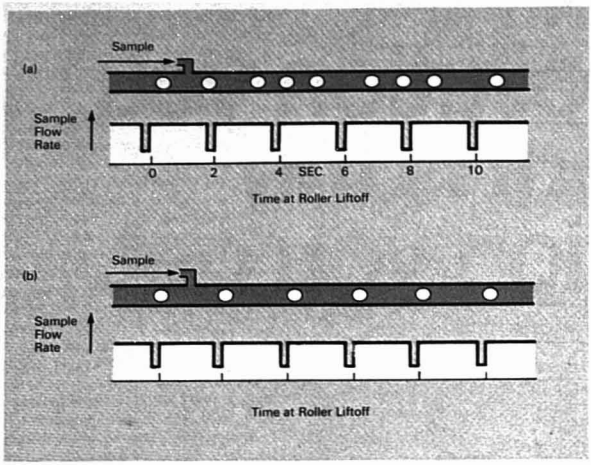

Figure 5. Sample proportioning as function of air bubble injection
(a) Air segmentation with no air-bar
(b) Air segmentation with air-bar timed at roller liftoff

short segment of liquid enclosed at each end by the gas-liquid interface. The pattern of fluid motion, so-called bolus flow, occurs naturally in any segmented-flow system, e.g., the microcirculation, where slugs of plasma are separated by red blood cells in the narrow capillaries. This bolus circulation within a moving liquid segment is illustrated in the blowup of segment #0 in Figure 3. An important advantage of mixing in continuous-flow is that no external means (stirrers, vibrators, vortex mixers) are necessary. Only a sufficient length of tubing (and time) is required.

Bolus mixing achieves rapid longitudinal exchange of fluid when the liquid segment is short, since the intrasegmental fluid elements make about one circuit of the slug for each 1.5 segment lengths traversed by the slug. The rate-limiting mixing process occurs in the radial direction across the fluid streamlines, and most improvements in CF mixing come about by enhancement of this radial mass transfer. In straight lengths of tubing, radial mass transfer occurs mainly by molecular diffusion, which is slow in liquids. This can be overcome by creating convective radial mixing simply by substituting a helical coil for the straight tube. Helical coils also permit a more compact physical arrangement of the final manifold.

Studies of mixing efficiency show that both liquid physical properties and tube geometry are important in determining the total time required for complete mixing. Liquid viscosity, density, and flow rate all affect mixing, with viscosity being most significant. Those systems which pump solid suspensions (hematology instruments assaying whole blood) are also affected by the concentration of suspended solids. Tube internal diameter, helix coil diameter, and segment length are other major parameters. For example, short segments mix in less time than long segments, but short segments imply a large number of air-liquid interfaces within the manifold and an unacceptable increase in pressure drop across the system (discussion of ref. 8). Dispersion also increases as liquid segments become very small, as seen in Figure 4 (small segments mean large n values).

Flow Stability. A stable liquid-air stream in a CF manifold is one in which the proportions of sample to reagents are constant for all segments, from one sampling cycle to the next. If proportioning varies during this period, analysis precision is adversely affected. Variation in proportioning appears as a "noisy" detector output, fluctuating about a mean corresponding to the steady-state "flat". Several events can occur to create an incorrectly proportioned stream: varying liquid or air flow rates, intersample air compression, a short sample, sample-probe or manifold-tube blockage, etc.

Proportioning of sample and reagents is a problem of dispenser precision in discrete analyzers and of constant pump delivery rates in CF systems. If constant-delivery, pulseless pumps were cheaply available and were not affected by back pressure, precisely proportioned segments in CF systems would be easily achieved. However, the low-cost, multichannel peristaltic pumps presently used in CF systems exhibit flow pulsation as a result of roller liftoff from the platen. Many schemes have been proposed and verified to reduce or eliminate pump pulsations. However, a more elegant and economical solution to this problem is simply to synchronize the pulsations of all sample and reagent streams by injecting air bubbles in phase with roller liftoff. An illustration of unsynchronized (random) air bubble injection is shown at the top of Figure 5. The resultant sample/diluent stream will be incorrectly proportioned, because roller liftoff (shown by the pulse in sample flow rate) affects some segments and not others. The illustration at the bottom of Figure 5 shows a correctly proportioned stream, where roller liftoff occurs in phase with the injection of an air bubble. Proper proportioning in this fashion is most easily achieved with a so-called air-bar, a mechanical pinch-valve that opens and closes an air-line in phase with roller liftoff.

Flow stability is also affected by many other variables, whose impact can be blunted in well-designed CF systems. Surging of the more-or-less smooth fluid flow coming from the pump can be caused by the sudden injection of air bubbles, by changes in temperature along the flow network (as in high-temperature reaction baths), and by the use of liquids that do not wet the tubing walls. Discussion of how these problems are handled in practice is beyond the scope of the present article.

New Technology and Applications

Particle Monitoring. Sophisticated techniques for differentiating and counting the particles in mixtures such as whole blood have been adapted to CF technology. The recently marketed Technicon Hemalog D automated leukocyte differential analyzer represents a completely new approach to the routine clinical measurement of white cell differentials (9). This instrument aspirates whole blood samples, reduces cell concentrations by dilution, adds specific cytochemical stains that selectively color different cell types, and analyzes the number of each cell type in a special sheath flow cell via scatter and absorbance measurements at different wavelengths. Ten thousand cells per sample are measured in this fashion at rates of 60 samples/h.

The approach used in the Hemalog D system requires maximum utilization of CF technology, particularly in minimizing sample dispersion for maximum analysis rates. The sample

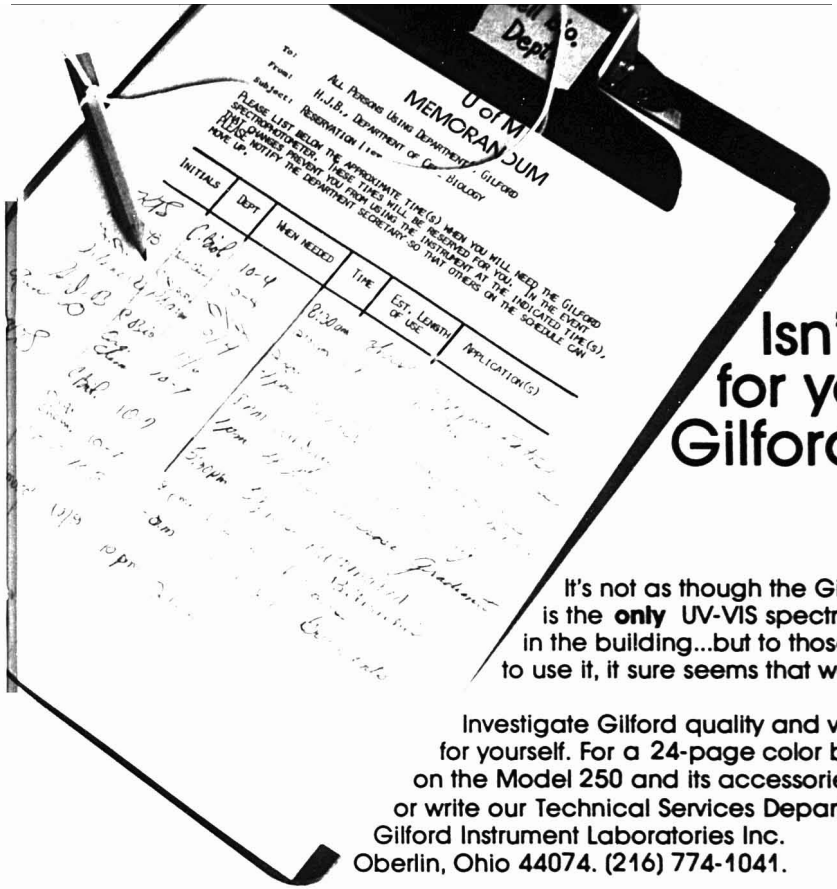

Isn't it time for your **own** Gilford?

It's not as though the Gilford Model 250 is the **only** UV-VIS spectrophotometer in the building...but to those waiting to use it, it sure seems that way.

Investigate Gilford quality and versatility for yourself. For a 24-page color brochure on the Model 250 and its accessories, call or write our Technical Services Department 7-10-1.
Gilford Instrument Laboratories Inc.
Oberlin, Ohio 44074. (216) 774-1041.

The Gilford Model 250:

All the spectrophotometer you will ever need.

gilford INSTRUMENT
Oberlin, Ohio 44074
Paris (Malakoff), France
Dusseldorf, W. Germany
Teddington, Middx., England
(216) 774-1041 Cable: GILLABS

CIRCLE 87 ON READER SERVICE CARD

dispersion theory reviewed earlier must be modified to account for the behavior of the particulate samples involved; cells do not move as readily as liquid through the film between air bubble and tube wall. The presentation of individual cells to the optical system for counting and classification is achieved by a sheath flow cell (Figure 6). The sample stream is introduced at the center of a coaxial sheath stream, so that the sheath separates the cells from the walls of the flow cell. The cross section of the flow cell is then reduced to allow contraction of the sample-stream diameter to 50 μm. In this way sample dispersion and flow cell clogging are minimized, and cells are presented sequentially one-by-one to the optical system resulting in negligible coincidence error.

It has been shown that 10 000 cell counts via CF analysis provide more precise estimates of the true white blood cell (WBC) distribution than are possible by 100 cell counts (as provided by manual or automated pattern recognition assays). Since the imprecision (standard deviation) from counting statistics is proportional to $1/\sqrt{n}$, where n is the number of total cells counted per sample, the Hemalog D provides 10 times better precision than is obtainable from 100 cell counts. This, in turn, means that small (clinically significant) shifts in WBC counts can now be easily detected and monitored for the first time.

Kinetic Assays. CF analysis does not directly provide the opportunity to follow an assay reaction as a function of time. Since the determination of enzymes in serum is of major interest in clinical analysis, much attention has been given to this fundamental limitation. Initially, CF enzyme assays were simply carried out as single-point measurements: sample and reagents were mixed and incubated for a fixed time, and a product of the enzyme reaction was measured in the usual way. These single-point enzyme assays became widely accepted in the clinical laboratory, because no alternative originally existed for handling large numbers of samples.

Objections to single-point assays were raised in some cases: endogenous interferences, competing (nonspecific) enzyme reactions, and occasional gross errors due to lag phases, substrate depletion, etc. Many of these objections can be overcome by running parallel blank assays for each CF test (with an essential reactant eliminated in the blank channel) or by reagent optimization. However, true kinetic (multipoint) assays for enzymes on CF systems only became possible with the minimization of sample dispersion to the point where multiple flow cells (detector stations) could be used in a single assay channel. The reaction mixture could then be incubated between flow cells, so that each flow cell reading corresponded to a different reaction time. In this way three-point kinetic assays for the transaminase enzymes AST and ALT are routinely provided by the SMAC analyzer (*3*). A key feature of such assays is the use of bubble-through flow cells, with electronic correction of the detector signal for the air bubbles passing through the flow cell.

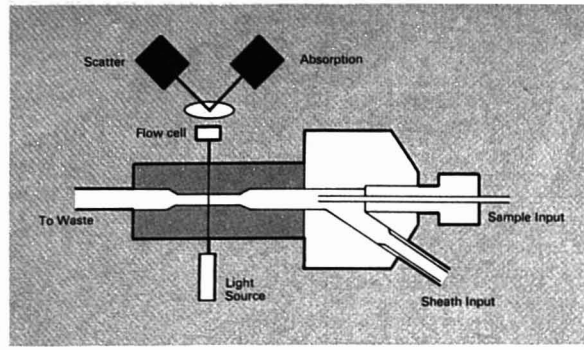

Figure 6. Particle counting and classification in sheath flow cell
Sample stream introduced at center of coaxial sheath stream so that sheath separates cell from walls of flow cell

The multiple flow cell approach in CF analysis might be extended to more than three-point assay, but this is problematical. Alternative CF approaches have, however, been proposed and verified. One approach, the AutoZyme enzyme rate analyzer, was introduced in 1969 (*10*), based upon varying reagent and sample pumping rates during the sampling cycle. In this way the reaction mixture is made to flow at varying rates through the incubation bath, so that solution arriving at the detector spends varying times in the bath, meaning a variation in reaction time from one end of the sample flat to the other. The detector output for each sample is then equivalent to a plot of product concentration vs. reaction time, i.e., a true kinetic analysis.

A more recent type of kinetic CF analysis is based on flow reversal (*11*). A valve arrangement provides for the introduction of a particular sample/reaction mixture into a thermostated reaction coil until the particular sample mixture fills the entire coil. The activation of the valve provides for reversal of flow, so that the first segment entering the coil is the last segment to leave the coil. Now each segment spends a varying time in the bath, and the detector output is similar to that provided by the AutoZyme system. These and other techniques allow true kinetic assays to be carried out in CF analysis.

Detectors and Reagents for CF Analysis. The detector–reagent combination in a reaction-analysis system aims at achieving an appropriate selectivity and sensitivity in the assay. There exists a vast general literature on this subject (*12*) which applies to CF analysis as well. Until recently, narrow band-pass UV–VIS photometers were used almost exclusively in CF analysis, augmented occasionally by fluorometers for special applications (especially those requiring increased sensitivity or specificity). More recently, a variable-wavelength spectrophotometer detector has been designed specifically for CF analysis. An early departure from simple optical detectors was required in assays of the alkali metals, where no good colorimetric reactions exist. Flame emission photometers were introduced to CF analysis in the mid-1960's for analysis of Na and K in serum. These devices were superseded in 1972 by flow-through ion-selective electrodes (ISE's) (*3*). While the main application of the latter detectors is still for assays such as K^+, Na^+, F^-, NH_3, and pH, extension of ISE's in CF analysis can be expected for such electrolytes as Cl^-, Ca^{++}, phosphate, and bicarbonate. Even more exciting is the possibility of coupling certain easily determined (electrochemically) ions as I^-, Ag^+, H^+, NH_4^+, NAD^+, etc., plus gases such as O_2, CO_2, and NH_3 to a broad range of biochemical assays, as summarized in Table I. The attraction of such general purpose electrodes as CF detectors stems from several factors such as new types of specificity, ability to handle turbid solutions, and equipment simplicity.

While the main emphasis in CF de-

Mettler is instrumental in getting accurate lab results fast.

METTLER/PAAR DIGITAL DENSITY METERS

Measure density or specific gravity of liquids or gases without time-consuming, tedious procedures. Mettler density meters will do it in seconds, even with unskilled technicians. No need to determine weight, volume or temperature. Therefore, you eliminate a major source of errors. Measure in range of 0 to 4 g/cm³, from −10°C to +60°C. Available in three models.

CIRCLE 237 ON READER SERVICE CARD

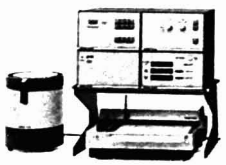

CALORIMETRIC THERMAL ANALYZER

Features calorimetric reproducibility of ±0.5% and 0.016 millicalories per second per inch sensitivity. Covers range from −170°C to +550°C with temperature measurement precision of ±0.1°C. Noise level is less than ±1 microcalorie per second. Modular design makes expansion of system convenient.

CIRCLE 238 ON READER SERVICE CARD

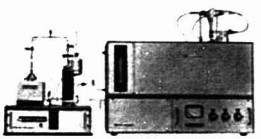

METTLER/HERAEUS NITROGEN ANALYZER

Gives rapid results in determining nitrogen and protein content. Operator able to perform 50 to 60 analyses per day. No calibration or standardization needed. Avoids the lengthy Kjeldahl method. Complies with EPA and OSHA regulations. Cuts operating/sampling costs 25% to 75%. Increases plant productivity and profitability.

CIRCLE 239 ON READER SERVICE CARD

MELTING/SOFTENING POINT DETERMINATIONS

Mettler FP series of modular instruments determines exact melting ranges using polarized light thermal microscopy. Provides extremely fast response over the -20°C to +300°C range. Thermal events are digitally displayed. Replaces old ASTM method and Wiley melting point method.

CIRCLE 240 ON READER SERVICE CARD

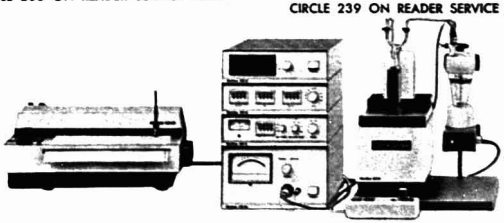

AUTOMATIC TITRATION SYSTEM

All the automatic titration capability you need is in this system. Fixed end point titration, titration curve or first derivative recording, pH stat recording, manual fixed increment titration and manual titration.

Easy to operate. Simple programming controls. Meets all potentiometric needs for aqueous and nonaqueous titrations as well as specific ion applications.

CIRCLE 241 ON READER SERVICE CARD

Mettler®

Mettler Instrument Corporation • Box 100 • Princeton, NJ 08540

Table I. Electrometric Methods Adaptable to CF Analysis

Analyte	Enzyme or substrate	Measurement method[a]	Species monitored
Glucose	Glucose oxidase	A	O_2, H_2O_2 (I^- via ISE)
Urea	Urease	P	NH_4^+, HCO_3^-, $NH_{3(g)}$, $CO_{2(g)}$
Creatinine	Creatininase	P	NH_4^+, $NH_{3(g)}$
Uric acid	Uricase	A (P)	O_2, H_2O_2 (I^- via ISE)
Cholesterol	(Cholesterol oxidase) (cholesterol hydrolase)	A (P)	O_2, H_2O_2 (I^- via ISE)
Lactatic acid	Lactic dehydrogenase	A	NAD^+/NADH
Inorganic phosphorus	Alkaline phosphatase	A	O_2, H_2O_2
Lactate dehydrogenase	Lactic acid	A	NAD^+/NADH
Glutamic-pyruvic transaminase	Lactic dehydrogenase	A	NAD^+/NADH
Creatine phosphokinase	Hexakinase, glucose-6-phosphate dehydrogenase	A (P)	O_2, H_2O_2 (I^-) $NADP^+$/NADPH
Cholineesterase	Acetylcholine	P	H^+
Alkaline phosphatase	Phenyl phosphate polyphenoloxidase	A	O_{2+}
Proteins		P	Ag^+
Lipase	Triglyceride	P (P)	H^+

[a] A = amperometric methods with Pt, glassy carbon electrodes as transducers. P = potentiometric methods with ISE's as transducers.

tectors is increased sensitivity and/or specificity, some assays benefit from a reduction in sensitivity, e.g., assays for a major component in a sample, such as total P in a fertilizer or phosphate rock. For this kind of application, thermometric detectors have been found useful. These are simply thermostated thermistor systems which measure change in solution temperature as a result of a chemical reaction; this temperature increment is then directly relatable to the concentration of the analyte undergoing reaction.

Nephelometric detectors have been used in CF immunoassays for serum proteins since 1970. The immune-precipitin reaction is followed via the scattering which results from the presence of a precipitate.

The reagents used in CF analysis are usually the same reagents used in manual reaction assays. One objection that has been raised against CF analysis in this respect is "wasteful consumption of reagents". Because of the continuous flow of reagents through the system both during startup and actual sampling, it is argued that the usage of reagents per assay must exceed that in well-designed manual or alternative automated systems. Actually, reagent consumption per assay can be quite low in CF analysis, e.g., 200 μl total reagent per assay for state-of-the-art equipment. With further reduction in tube diameter and increase in sampling rate (as discussed earlier), the ultimate reagent consumption per assay could be reduced further.

However, there are more important factors to consider in this regard. First, the increased reagent usage in CF analysis (where that is indeed the case) is repaid by the availability of function monitoring as discussed below; the ability to monitor a series of reaction segments for each assay (or sample) allows a considerable increase in the reliability of that assay. Second, there is increasing concern, not with the volumetric consumption of total reagent, but with the cost of expensive reagents that are used once per assay and then discarded. In some cases, particularly highly specific enzyme reagents that have recently become popular, the cost of these reagents may preclude their widespread application in this fashion. CF analysis, on the other hand, is uniquely suited to reusable reagents such as bound enzymes (*13*). Expensive enzymes or other reusable reagents can be physically or chemically bound to the inside of the tubing used in CF analysis, so that the consumption per assay of such reagents is decreased by two or three orders of magnitude, with a great decrease in cost per assay. For example, as many as 30 000 glucose assays have been carried out with a single glucose oxidase-coated tube (*13*). Equally important, such bound enzymes often have other important advantages such as greater stability and convenience in handling and makeup and less variability in the effective reagent concentration over a series of assays. In some cases, for example, creatinase used in the assay for serum creatinine, the decomposition of this reagent on standing yields a product of the assay reaction (ammonia), thereby complicating its use for this purpose. However, with bound enzymes any such complication is completely avoided, since such decomposition products are washed from the tube continuously during normal use and simply become part of an independently established reagent baseline absorbance. Finally, many additional possibilities exist for such immobilized reagents in CF analysis, quite apart from enzymes which have been the main example in the past.

Curve Monitoring and Analysis. With present discrete and centrifugal analyzers, it is difficult to flag certain kinds of assay error: malfunction in reagent or sample dispense, insufficient sample or reagent available for a given test, and incomplete mixing of sample and reagents. The reason such errors may go undetected is that dispensing and mixing are usually completed prior to arrival of sample/reagent mixture at the detector. Such errors are then buried within the observed detector signal. In CF analysis quite a different situation prevails. Customarily, the curve "flat" will include several liquid segments, each of which may be regarded as a separate (repeat) assay of the same sample, since each segment should contain the same sample/reagent mixture. We can then examine each CF sample curve for constant response over the normal "flat" region (function monitoring), which is equivalent to repetitive assay of the same sample. When the proportions of sample and reagents in any segment change, due to errors of the above kind, this is apparent as a departure from curve flatness. Such assays can then be flagged as questionable and rerun.

Other possible errors such as carryover from a high-concentration sample to a following low-concentration sample are also apparent by inspection of the sample curve, and again suspect results can be flagged and rerun. In the SMA analyzers, curve monitoring in this fashion is done by analog means with operator inspection of the analog signal. SMAC, with its dedicated computer, achieves the same result automatically and digitally, allowing more precise limits to be set on possible assay errors. The tedium and operator error associated with human monitoring of an analog signal are likewise eliminated.

With more sophisticated approaches to curve monitoring and analysis, it has become possible to utilize the nonflat portion of the sample curve to further improve assay reliability and precision. Thus, on the SMAC system, most of the curve is inspected by the computer and compared with the pat-

Precision balances and weighing systems by SAUTER.

Precision Balance, Type KM 200/KM 1000

Electronic Precision Balance, Type K 1200

Electronic Precision Balance, Type R 300/R 3000

Electronic Precision Balance, Type RS 25

Precision Balance, Type SM 1600

Precision Balance, Type MPR

Precision Balance, Type L 1/L 10

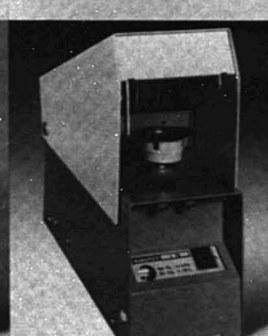

Analytical Balance, Type 404/13

SAUTER balances have earned a reputation for ease of operation, economy and practical technology. No wonder SAUTER balances are the choice in research and development laboratories, in industry and scientific institutions, just about everywhere.

SAUTER precision toploading balances have weighing ranges from 160 g to 10 kg and more. Resolutions from 1 mg to 1 g.

SAUTER analytical balances are available with weighing ranges of 100 and 200 g. Resolution of 0.01 mg or 0.1 mg.

Electronic precision balances are available with weighing ranges of 120 g, 300 g, 1200 g, 3000 g, 12 kg, 25 kg and 120 kg. The K 1200, for example, combines two weighing ranges in one balance, touch a button and you can switch to a capacity ten times greater – from 120 g and a readability of 0.01 g to 1200 g and a readability of 0.1 g.

Shown here is but a small sample of the complete SAUTER line, affording high accuracy in weighing ranges from a few grams up to a ton.

Please write and let us help solve your particular balance problems.

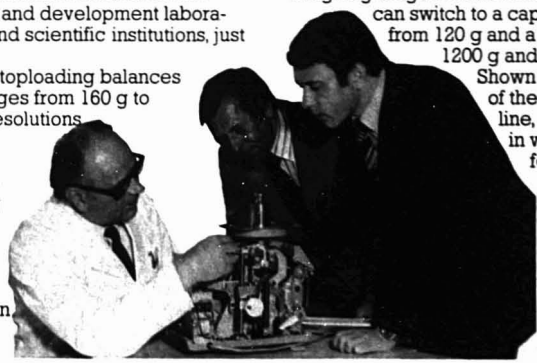

SAUTER

August Sauter of America, Inc.
80 Fifth Avenue, New York N.Y. 10011
Tel. (212) 685 6659, Telex 421790

August Sauter s.r.l.
70 Via Carlo Farini, 20159 Milano
Tel. 60 60 80, 60 38 53

August Sauter GmbH
Waagen und Systeme
Postfach 250, D-7470 Albstadt 1
Tel. (0 74 31) 5 10 56, Telex 07 63 851

tern expected for "normal" curves. When curve quality does not meet preselected criteria, the computer flags such assays for rerunning. At the same time the computer interprets curve abnormalities in terms of specific machine malfunctions and alerts the operator to the need for corrective action. As a result of these quality control operations by the computer, SMAC provides precise and reliable data in the routine clinical laboratory (*14*).

Another interesting approach, pioneered by Walker (*15*), is the use of curve regeneration or deconvolution. Knowing the theoretical shape of a normal CF sample curve, it is possible by analog or digital means to process overlapping and/or nonsteady-state curves so as to restore the original sample curves prior to dispersion. This then allows for increased accuracy and precision as well as higher sampling rates.

Research and Industrial Applications. The major application of CF analysis has so far been in the clinical laboratory. There the relatively small number of separate assays that require high-speed, dedicated analyzers has restricted the instrumental approaches so far offered commercially. However, there is a vast literature (*16*) which explores the application of CF analysis to a wide variety of research and industrial problems and which describes the automation of virtually every operation previously used in manual analysis. Here, we will attempt to point out the major nonclinical areas where CF analysis is being applied, and focus on some of the more widely used techniques and special modules.

CF analysis in the nonclinical world is divided mainly among environmental, pharmaceutical, food and agriculture, both for laboratory and process monitoring applications. The diverse nature of the samples encountered, as well as the specific methodologies dictated by regulatory bodies in many cases, requires that CF methods be quite versatile: solid samples which cannot be aspirated directly into a conventional CF system may be involved, liquid samples may have to be concentrated by large factors to increase sensitivity to suitable levels, multiple separation steps may be required to provide the requisite analysis specificity, and acid or base digestion at high temperatures may be involved, etc.

The Technicon Solidprep Sampler II module for handling solid samples provides for fully automated, serial access of solid samples to a high-speed blender. There the sample can be contacted with a variety of solvents including corrosive chemicals such as concentrated acids. After a programmable stirring and dissolution period, supernatant is sampled into a connected CF system for completion of the analysis. Such samples as drug

Table II. Examples of Assays Requiring On-Line Separation in CF Analysis

Separation step	Analyte
Filtration	Any solid-sample component
Flash distillation	HF, HCN, phenol, amines
Solvent extraction	Thiamine, chlorpheniramine maleate, α-keto steroids
Ion-exchange	Sulfate, calcium pantothenate
Gas diffusion	CO_2, SO_2, thiols, HCN
Sparing	NH_3, amines
Dialysis	Ascorbic acid, niacinamide

In Radiometer pH Meters...

Carefully Matched and Tested Components
Greater accuracy — proven reliability — consistently dependable results.

Ultra-Stable Amplifier
Virtually drift-free long-term stability.

Precise Tolerance Resistors
Wire wound resistors at critical points for accuracy.

Advanced Circuit Design
Dependable state-of-the-art components and integrated circuits.

High Impedance Input Design
Matches modern high impedance electrodes.

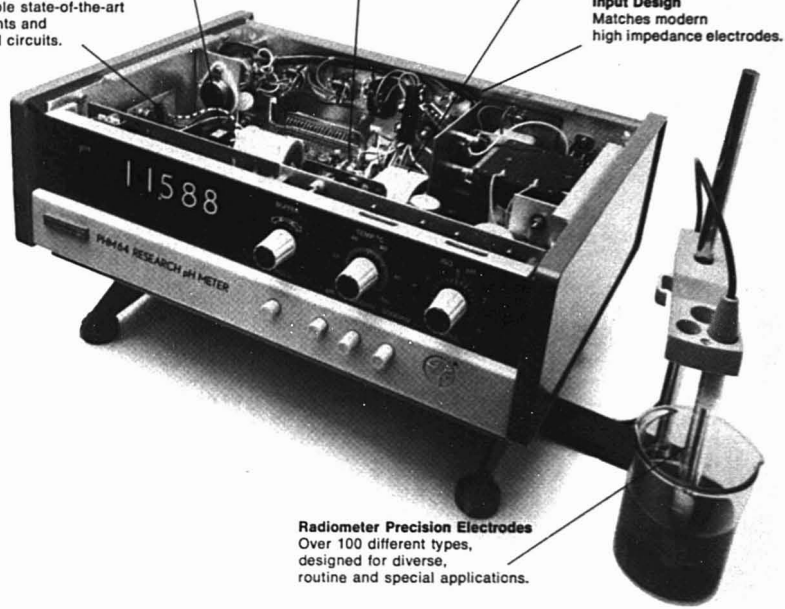

Radiometer Precision Electrodes
Over 100 different types, designed for diverse, routine and special applications.

It's the "Guts" that Count!

Looking for superior performance in a pH meter? — Look inside a Radiometer. You'll see fine components, superbly assembled and thoroughly tested in their application. You will also see why *stability*, *accuracy* and *dependability* have been a traditional part of Radiometer pH meters and electrodes for almost 40 years.

There's a digital or analog model to match your application — research or routine, in-lab or on-site. Our new pH meter catalog is yours for the asking. Request it now and you will also receive the Radiometer Electrode Catalog, listing over 100 electrodes for thousands of applications.

Call your London Company Representative or contact us today . . .

THE LONDON COMPANY
811 Sharon Drive • Cleveland, Ohio 44145
Telephone (216) 871-8900

Radiometer . . . Masters of pH measurement since 1937.

CIRCLE 129 ON READER SERVICE CARD

tablets and powders have been successfully analyzed in this fashion.

Many liquid or solid samples require further separation during CF analysis, and such techniques as filtration, flash distillation, solvent extraction, ion-exchange, gas diffuion, sparging, and dialysis can be used more or less routinely and in fully automated form (Table II).

CF allows multiple separation techniques to be used in conjunction with the same methodology. For example, the analysis of phenol in water and wastewater may require filtration to remove particulate matter, distillation to separate the phenol from the sample matrix, reaction with 4-aminoantipyrine and alkaline ferricyanide, and solvent extraction of the complex with isobutanol. The final absorbance is then measured at 480 nm. CF analysis has also been used to analyze column effluents from liquid chromatography, and this application is compatible with the very efficient columns now in common use (*7*).

Future Applications. New adaptations of continuous-flow to automated analysis will depend on the successful matching of the advantages of this technique to previously nonautomated procedures. For example, radioimmunoassay (RIA) is becoming quite popular for the determination of trace levels (picogram/ml and lower) of certain compounds in serum and other physiologic fluids. However, present manual methods suffer from a variety of problems: imprecision, a need for frequent restandardization, long incubation times, and (especially) unstable radiolabeled reagents. Many of these limitations can be overcome through the use of appropriate CF techniques.

Many analytical procedures rely on reagents with short shelf life and which are best made from scratch each day. Continuous-flow can be applied to the on-line synthesis of such reagents [for RIA (*17*)], thus reducing the inconvenience of such reagents and improving the quality of the assay through use of immediately prepared reagents. Costs for such reagents can also be markedly reduced as a result of making just the amount of reagent required.

The screening of biological particles such as bacteria and fungae can certainly be expanded by making use of technology pioneered in the development of the Hemalog D system. The automation of sample preparation for such commonly used techniques as liquid and gas chromatography is now a necessity for many laboratories since this step often takes much longer than the actual chromatographic analysis (*18*). Many other examples of the possible application of CF analysis to present problems can readily be cited.

References

(1) L. J. Skeggs, *Anal. Chem.*, **38**, 31A (May 1966).
(2) E.V.D. Muehl and P. L. Wolf, in "Practical Clinical Enzymology", P. L. Wolf, Ed., Chap. 22, Wiley-Interscience, New York, N.Y., 1973.
(3) "Advances in Automated Analysis", 1972 Technicon Int. Cong., Vol. 1, pp 1–47, Mediad Inc., Tarrytown, N.Y., 1973.
(4) C. A. Burtis, W. F. Johnson, J. C. Mallin, J. B. Overton, T. O. Tiffany, and M. B. Watsky, *Clin. Chem.*, **19**, 895 (1973).
(5) R. Thiers, A. Reed, and K. Delander, *ibid.*, **17**, 43 (1971).
(6) L. R. Snyder and H. J. Adler, *Anal. Chem.*, **48**, 1017, 1022 (1976).
(7) L. R. Snyder, *J. Chromatogr.*, **125**, in press (1976).
(8) C. Horvath, B. A. Solomon, and J. M. Engasser, *Ind. Eng. Chem. Fundam.*, **12**, 431 (1973).
(9) H. P. Mansberg, A. M. Saunders, and W. Groner, *J. Histochem. Cytochem.*, **22**, 711 (1974).
(10) S. Morgenstern et al., "Advances in Automated Analysis", Vol 1, p 85, Therman Assoc., Miami, Fla., 1971.
(11) D. A. Burns, U.S. Patent 3,876,374 (April 8, 1975).
(12) M. Pesex and J. Bartos, "Colorimetric and Fluorimetric Analysis of Organic Compounds and Drugs", Marcel Dekker, New York, N.Y., 1974.
(13) L. P. Leon, S. Narayanan, R. Dellenbach, and C. Horvath, *Clin. Chem.*, **22**, 1017 (1976).
(14) J. O. Westgard, R. N. Carey, D. N. Feldbruegge, and L. M. Jenkins, *ibid.*, p 489.
(15) W.H.C. Walker, *Clin. Chim. Acta*, **32**, 305 (1971).
(16) Technicon Bibliography 1967–75, Technicon Corp., Tarrytown, N.Y., 1975.
(17) L. R. Snyder, U.S. Patent 3,954,411 (May 4, 1976).
(18) D. A. Burns, L. R. Snyder, and H. J. Adler, "Advances in Automated Analysis", 1972 Technicon Int. Cong., Vol 6, p 23, Mediad Inc., Tarrytown, N.Y.

Snyder

Levine

Stoy

Conetta

Lloyd Snyder is vice president and director of the Clinical Chemistry Department at Technicon. He graduated with BS and PhD degrees in chemistry from the University of California at Berkeley, and prior to 1971 was a senior research associate at the Union Oil Co. Research Center in California. Dr. Snyder is a past member of the ANALYTICAL CHEMISTRY Advisory Board and is well known for his work in liquid chromatography and petroleum analysis. He received the 1970 American Chemical Society Award in Petroleum Chemistry and the 1976 Stephen Dal Nogare Award for contributions to chromatographic science. His current research interests include high-pressure liquid chromatography and new approaches to automated clinical analysis.

Jacob Levine is manager of scientific relations in the Clinical Marketing Division at Technicon. He works closely with the Clinical Methods Department in the planning and field evaluation of new products and maintains technical liaison with customers in the field. Prior to his present responsibilities, Mr. Levine spent eight years in the Clinical Chemistry Department as research chemist and group leader, working mainly on lipid and enzyme assays for SMA 12/60 and related systems. Active in the American Association for Clinical Chemistry, he is currently program chairman for its New York Metropolitan Section. He graduated from CCNY in 1957 with a BS degree in chemistry.

Robert Stoy is senior scientist in the Hematology Advanced Development Group, responsible for development of new fluid delivery systems. He received his BS and PhD from Georgia Tech in the field of gas dynamics, an area in which he taught at the University of Connecticut prior to joining Technicon. His research in industry and as a faculty member includes work in computational fluid dynamics and in the dynamics of blood flow in capillaries. Dr. Stoy is an active member of both the American Physical Society and the American Institute of Aeronautics and Astronautics.

Aldo Conetta is manager of applications for Technicon Industrial Systems. His responsibilities include the development of new automated analytical methods covering all aspects of the industrial market area. In addition, he maintains technical liaison with field evaluation systems and with field representatives developing new techniques and procedures. He has authored and coauthored a number of technical articles. Mr. Conetta received his BA and MS degrees from New York University.

3 things you need for reliable spectrophotometry.

(And 2 of them are free!)

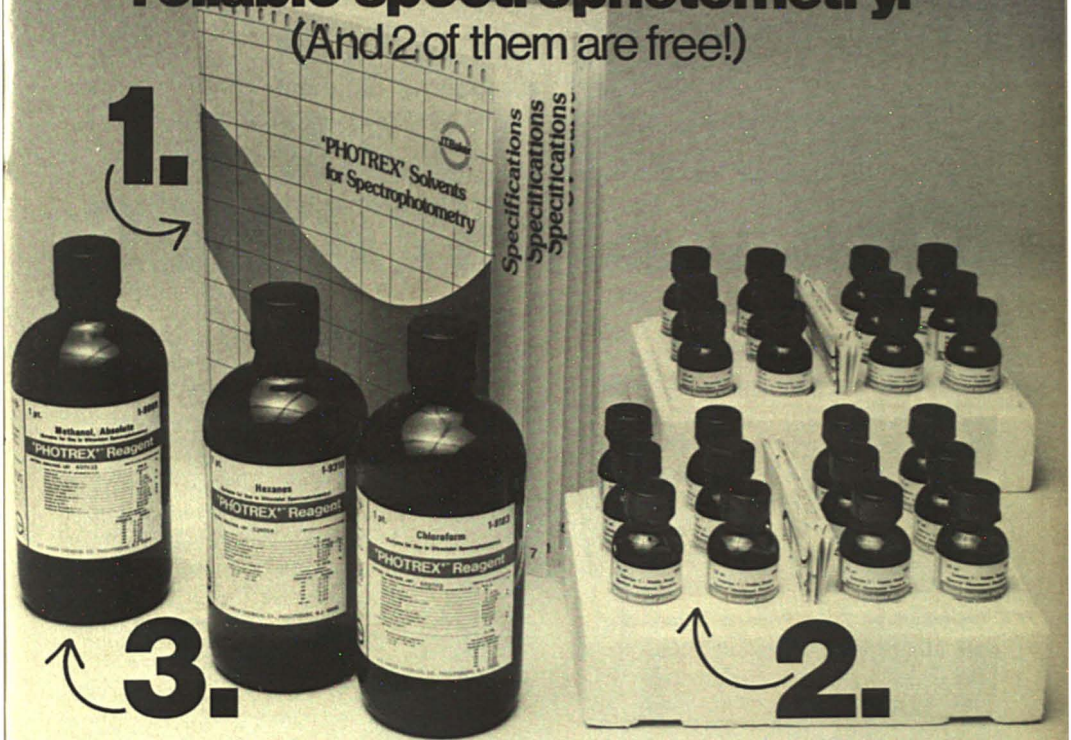

1. Solvent Selection Manual (free)
This is an invaluable guide for selecting the appropriate solvents for spectrophotometric methods. Provides information on solvent properties, UV curves, wave length/wave number conversion, impurity level specifications, etc. Write to Dept. TPM, address below.

2. Spectrophotometer Standards Kit (free*)
Standards for checking spectrophotometer performance are essential to provide assurance of reliability. Baker has developed UV and visible range spectrophotometric standards kits for simple and precise assessment of instrument linearity of response and sensitivity. Either kit is available free with the purchase of PHOTREX solvents. Send this ad (or a photocopy) with a proof of case purchase to Dept. TPM, address below. Please specify kit desired: UV range kit (#4844), visible range kit (4845). *(Both* free with minimum 2 case purchase.)

These kits are described in the solvent manual above and on p. 284 of the J. T. Baker Catalogs 750/760.

*This is a limited time offer subject to termination.

3. PHOTREX™ Spectrophotometric Solvents.
35 unsurpassed spectrophotometric solvents with detailed definition by UV absorbances and GC assay. Extra precaution: adherence to specs is always checked *after* final packaging lest some contaminant be introduced after manufacture. The result of all this: absolutely clean curves.

The assurance of quality is always on the 'Baker Analyzed' product label itself: every label carries the actual lot analysis showing the GC assay, trace impurity analysis, and lot absorbance values at key wavelengths in the UV region. The "windows" in the IR region are also provided.

And at least as important: the PHOTREX solvents are available in stock. *Consistently* available.

All of these solvents are described in the above solvents manual and are available from the J. T. Baker distributors listed in our Catalogs 750/760. (If you need help, please call 201/859-5411.)

Finally, there's Super Service
If your Baker distributor is ever out of stock on a PHOTREX spectrophotometric solvent that you need *now*, he can call a Baker Super Service Center and, if he calls us by 3:30 p.m. our time, your order will go out directly to you in most cases on the very next business day. That's Baker Super Service.

J. T. Baker: "use-matched" products and...Super Service.

J.T.Baker
CHEMICALS

J. T. Baker Chemical Company
Phillipsburg, New Jersey 08865
201/859-5411

CIRCLE 26 ON READER SERVICE CARD

YOU HAVE NEVER SEEN A SMALLER SYRINGE.

That needle in the foreground is really a small precision syringe. The tiny tungsten wire behind it fits in the needle and discharges the complete sample. The total capacity of this Hamilton syringe is one microliter... and it's all contained in that needle. With any degree of skill, you can repeatably inject samples to ±1%.

It's called our 7001 Syringe. There are other members of the 7000 Series with 2 µl and 5 µl capacities. Your sample never reaches the glass barrel. The barrel is used simply as a volume indicator.

All the 7000's will take a Hamilton plunger guide or Chaney Adaptor to make injections easier and strengthen the plunger against bending.

There's a Teflon seal in the hub that can be finger tightened to compensate for wear and to prevent leakage. You simply tighten the knurled hub to make the adjustment for a leak-tight seal.

Every 7000 Series syringe is tested for accuracy by injecting a series of samples into a GC. When you purchase a Hamilton 7000 Syringe, you have our guarantee that it will deliver the capacity with reproducibility to ±1%.

If you need to inject samples smaller than 1 µl, this is your syringe. Five models, three capacities, selling for $35.00. For literature, write to John Nadolny. Hamilton Co., P.O. Box 10030, Reno, Nevada 89510.

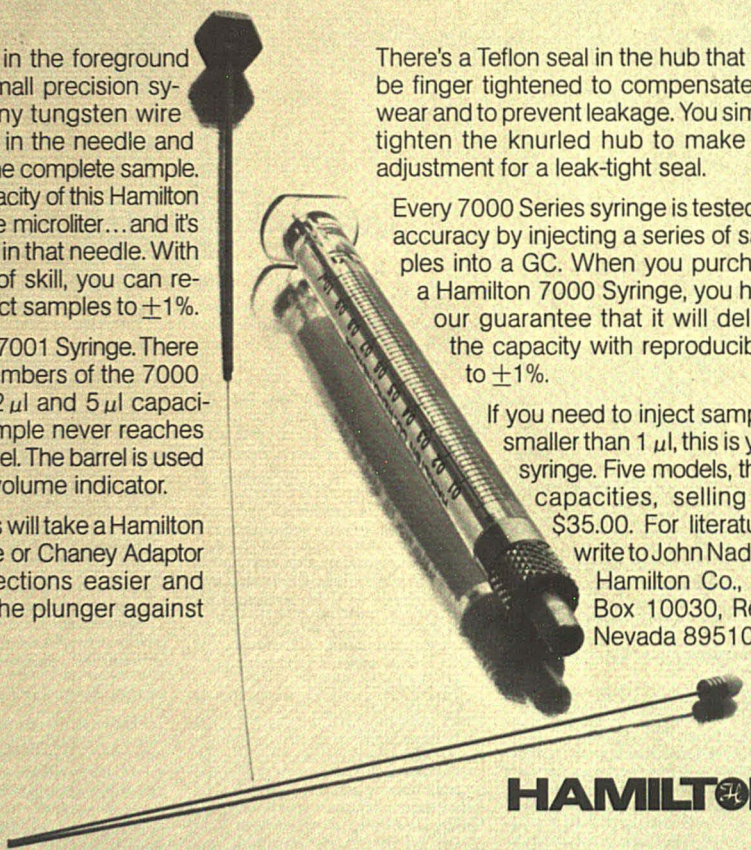

HAMILTON

CIRCLE 99 ON READER SERVICE CARD

American Chemical Society 1977 Award Winners

George G. Guilbault and Raymond P. W. Scott win the ACS Awards in Analytical Chemistry and Chromatography

The winners of 1977 ACS awards were announced at the 172nd ACS National Meeting held in San Francisco, August 29–September 3. These awards will be presented at the 1977 ACS Spring Meeting in New Orleans. Among the 21 people named to receive awards are two analytical chemists of distinction. They are George G. Guilbault of the University of New Orleans for the analytical chemistry award and Raymond P. W. Scott of Hoffman-La Roche Inc., Nutley, N.J., for the chromatography award. The analytical chemistry award, which has been sponsored by Fisher Scientific Co. since 1947, consists of a $2000 honorarium and an etching. Supelco Inc., is the sponsor of the chromatography award, which was established in 1959 and initially sponsored by Lab-Line Instruments. The award consists of $2000 and a certificate.

George G. Guilbault, 39, has been a professor of chemistry at Louisiana State University in New Orleans, La., since 1966. Prior to that he worked as a research chemist for five years with the Department of Defense, serving as a section chief, Physical and Biochemical Methods Section, Research Labs, Edgewood Arsenal, Md. He received his BS degree in chemistry from Loyola University in New Orleans in 1958 and the MS and PhD degrees in analytical chemistry from Princeton University in 1960 and 1961, respectively.

Professor Guilbault's outstanding contributions to analytical chemistry include, among other things, his pioneering work on enzyme electrodes and on a solid surface fluorescence monitoring system, both used in solving analytical problems in the clinical chemistry laboratory. He was the first to develop stable useful enzyme electrodes. These electrodes, as simple in operation as pH electrodes, are used for the determinations of clinically important substances such as urea (test for renal function), phenylalanine (test for phenylketonurea), glucose (test for diabetes), creatinine, and others. These electrodes are now marketed by Radiometer, Owens-Illinois, Leeds and Northrup, Yellowsprings Instrument Co., and others.

He also developed a new concept in fluorescence instrumentation for the analysis of clinically important substances, i.e., enzymes such as alkaline phosphatase, LDH, GOT, GPT, GGTP, α-HBD, lipase, and cholinesterase; and substrates such as urea, glucose, uric acid, creatinine, phenylalanine, phosphate ion, and others. A commercial instrument based on the unique features of his concept will soon be available.

George G. Guilbault

Raymond P. W. Scott

Professor Guilbault has authored over 200 papers, 30 review articles, and six books. He has presented more than 200 invited lectures in the U.S. and abroad and has organized or chaired over 20 national and international meetings. His further contribution to the field of analytical chemistry includes his founding and editorship of an international journal, *Analytical Letters.*

He has had a total of 12 PhD and MS students and 45 postdoctoral fellows, all now serving analytical chemistry in various positions. Recently, he was appointed to serve on the National Research Council-National Academy of Sciences.

Raymond P. W. Scott, 52, a native of England, held several key research chemist positions both in industry and government in the United Kingdom before he moved to the United States in 1969 to assume his present position as Manager of the Physical Chemistry Division at Hoffman-La Roche. He received his BS and DSc degrees from the University of London in 1946 and 1956, respectively.

For the past 20 years, Dr. Scott has been working in the field of gas and liquid chromatography, concentrating particularly on apparatus and techniques. Among his many contributions to the field is his landmark paper entitled "A New Detector for Vapour Phase Partition Chromatography" presented at the first international meeting on the subject in 1956. At that meeting he was the first to report on a flame thermocouple detector, the forerunner of what is now known as the flame ionization detector. As early as 1958 he was able to separate all the isomeric heptanes and 13 of the octane isomers on a 100-ft-long packed column, operating at pressures of 200 psi and providing efficiencies of over 40 000 theoretical plates. This is still recognized as the highest efficiency

thus far obtained from a packed gas chromatographic column.

In 1962 Dr. Scott developed and patented the wire transport detector for use in liquid chromatography. From the late 1960's until the present, he has confined his work to the development of liquid chromatography. He has improved the original wire transport detector and introduced the technique of incremental gradient elution. This technique allows the rapid separation of any complex mixture of compounds which exhibit a wide polarity range. He has also designed and developed suitable apparatus and a rational series of solvents to be used with the system. In 1974 at the International Symposium on Chromatography, Dr. Scott reported the first effective LC/MS system that would provide electron impact spectra of eluted solvents. This apparatus utilized a quadrupole mass spectrometer fitted with novel interfaces, which he devised, to permit a moving wire to pass through the source of the mass spectrometer without affecting its performance.

Dr. Scott edited the 1960 Gas Chromatographic Discussion Group Symposia Proceedings and played an important part in organizing the meeting. He has authored more than 70 technical papers and written on several topics for a number of textbooks.

Undergraduate Awardees Receive ANALYTICAL CHEMISTRY

The Division of Analytical Chemistry of the American Chemical Society has awarded 15-month subscriptions to ANALYTICAL CHEMISTRY to 407 chemistry students at U.S. colleges and universities in honor of the students' outstanding scholastic records. The recipients were named by the chemistry departments at their respective institutions. Fifteen-month subscriptions will begin with this issue, except in cases where the student is already a subscriber. In these cases, subscriptions will be extended 15 months. In addition, student winners will receive the Analytical Division Newsletters throughout the year. These awards, given by the Division for the past several years, are designed to recognize excellent scholarship and encourage the recipients' interest in chemistry in general and analytical chemistry in particular.

Geraldine M. Huitink, associate professor of chemistry at Indiana University in South Bend, is in charge of this project for the Analytical Division.

Symposium on High-Performance Mass Spectrometry

November 3–5

A symposium entitled "Chemical Applications of High-Performance Mass Spectrometry" will be held at the University of Nebraska-Lincoln, November 3–5, 1976. This meeting is jointly sponsored by the University of Nebraska-Lincoln, the National Science Foundation, AEI Scientific, and INCOS Corp. A total of 18 plenary lectures will be presented by leading scientists in research areas which make use of high-performance mass spectrometers. Further information may be obtained from M. L. Gross, Department of Chemistry, University of Nebraska, Lincoln, Neb. 68588. The

Because we thought most GC syringes were old-fashioned:

Pressure-Lok® Microsyringes for Chromatography

We felt there was a need for a better GC syringe, something that would contribute to the quality of chromatography and take the state of the art that much further into the future.

The result was our line of Pressure Lok® Microsyringes—sturdy, smooth-working instruments designed to improve sample injection precision by eliminating the old problems of plunger blow-by and plunger freeze-up.

Pressure Lok® Microsyringes are built from barrels of fine, chemically-resistant, borosilicate glass. Each piece of raw glass is calibrated and before delivery, each lot of finished syringes is rechecked with a microbalance. Plungers are precisely-fitted stainless steel shafts tipped with durable Teflon*.

Wear becomes infinitesimal and plunger freezing is practically unknown. Smooth septum penetration is accomplished by hollow-ground, polished needles, either fixed or removable, designed to minimize plugging. Syringe capacities from one to 100 ul.

We must have had the right idea. Because more and more laboratories are adopting the Pressure Lok® Microsyringe line as the new standard for GC sample injection. We'd like to tell you about it. Please write for details.

PRECISION SAMPLING CORPORATION
Post Office Box 15119
Baton Rouge, Louisiana 70815
Telephone 504-927-1128

*Reg. DuPont trademark

CIRCLE 165 ON READER SERVICE CARD

program consisting of five technical sessions is scheduled as follows:

Wednesday, Nov. 3

Chemical Ionization
Biochemical-Biomedical Applications

Thursday, Nov. 4

Environmental and Petroleum Chemistry
Computer Applications
Metastable Ion Applications and Ion Structures

Movie for Users of Analytical X-ray Equipment

"The Double-Edged Sword" is a 16-mm documentary color film on x-ray hazards produced by Durrin Film under contract with the National Bureau of Standards and the Food and Drug Administration's Bureau of Radiological Health. The title of the film denotes the serious nature of x-ray hazards. Reenactment of accidents, first-hand accounts of accident victims, and photographs from medical records are used to demonstrate the potential for serious injury from analytical x-rays if safety procedures are not followed. Equipment manufacturers, university professors, state and federal officials, radiation safety officers, and laboratory managers discuss all phases of the safety problem.

The 23-min film is available for free loan through Association-Sterling Films, 1815 North Fort Myer Drive, #107, Arlington, Va. 22209, and can be purchased from the National Audiovisual Center, Washington, D.C. 20409. In addition, color video cassettes of the film are available for free loan from the Training Resources Center, Bureau of Radiological Health.

Nobel Hall of Science

The National Science Foundation has awarded a $75,000 grant to Chicago's Museum of Science and Industry to develop a "Nobel Hall of Science" honoring American scientists who have received the prize. The NSF grant is being supplemented by grants from the Chicago Community Trust, Swedish Government, Nobel Foundation, Chicago's Swedish community, and others. The exhibit will contain information about the 104 Americans who have received the Nobel Prize in three scientific categories—chemistry, physics, and medicine. In addition, it will contain exhibit units explaining many of their basic discoveries and how the new knowledge was applied in society.

Analytical Chemistry at Work

Drug Testing at the Olympics

Six athletes were found to have used banned drugs at the Olympic Games in Montreal this summer. These athletes used amphetamine, fencamfamine, phenylpropanolamine, and anabolic steroids. The latter drugs, newly tested for this year, are found by using more sensitive and time-consuming methods than are needed with the more common stimulating drugs. Three athletes were identified as using the anabolic steroids, and testing is still proceeding at this writing.

Michael Bertrand, codirector with Robert Dugal of the analytical group at the National Institute for Scientific Research (NSIR), part of the University of Quebec, presented a paper at the Fall ACS Meeting in San Francisco describing the overall analytical scheme for the Olympic drug testing. All urine samples underwent an organized computerized procedure. This consisted of a relatively crude, but simple extraction procedure followed by a gas chromatographic screening technique which used a Perkin-Elmer nitrogen detector. Since well over

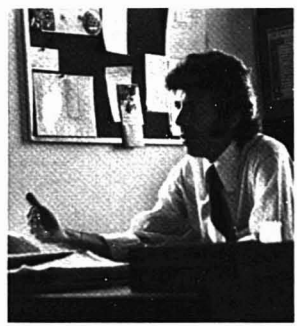

Robert Dugal, pharmacologist, codirector of the analytical unit charged with drug testing at the Montreal Olympics

99.9% of the likely banned drugs do contain nitrogen, this procedure eliminated the mass of nondrug-containing samples before the final step which involved the use of gas chromatography/mass spectrometry for definite identification in suspicious cases.

Anabolic steroids are taken because of their muscle-building ability. These

(*Continued on page 966 A*)

TWO WAYS TO BUY TOP-OF-THE-LINE ATOMIC ABSORPTION

THE 603 WAY

Everything you could possibly want in atomic absorption is built into our top-of-the-line Model 603. Features you couldn't get before and still can't find anywhere else. The 603 puts all the latest advances in AA literally at your fingertips. With pushbutton ease, you enjoy state-of-the-art versatility, performance, convenience and speed.

From arsenic at 194 nm to cesium at 852 nm, no other instrument can match the complete performance capabilities of the 603. The 603's double-beam optical system and high-resolution, dual-grating monochromator are the standard against which all other AA instruments must be compared.

THE 460 WAY

If our 603 has more than you need, you'll find *all* you need in the lower-priced Model 460. In anyone else's line, it would be at the top. The 460 differs from the 603 primarily in its optical system. The 460's double-beam optical system also uses high quality, coated front-surfaced optics and a wide-range detector. Its monochromator, however, uses a single large (64x64 mm), finely ruled (1800 lines/mm) grating to provide high energy and performance and broad wavelength coverage at a moderate cost.

EITHER WAY, YOU'RE AHEAD

Both the 603 and 460 share these advanced features:

Plain-talk, no-code microcomputers. The 603 and 460 are controlled by a microcomputer that talks your language. You don't need computer expertise. No complicated codes. The microcomputer even catches mistakes. And the optional RS-232-C interface lets you expand the instruments' capabilities with a wide variety of data handling and data logging systems.

Pushbutton simplicity. Whether you're calibrating with up to three standards, setting integration time from 0.2 to 60 seconds or setting expansion from 0.01 to 100X, all you do is push the buttons. The microcomputer does the rest – automatically, quickly, and accurately.

Unmatched versatility. The 603 and 460 let you select atomic absorption or flame emission, continuous or integrated readings, peak height or integrated peak area measurements. Both are designed for flame and flameless sampling. And both are compatible with the largest product line of light sources, sampling devices and other key accessories available from any manufacturer.

Proven reliability. The 603 and 460 are designed to provide the reliability you need in analytical instrumentation – from their high-energy optical systems to the proven performance of the nebulizer and laminar-flow burner system; from the safety features of their gas controls to the proven reliability of their solid-state microcomputer electronics.

PLUS COMPLETE BACKUP

With the 603 and 460, you also get all the unexcelled backup that comes from the world leader in atomic absorption. Technical assistance in using your instrument to its full abilities. Product specialists located throughout the world to help you with your analytical problems. Factory trained service personnel close by to keep your instrument's performance at its peak. Plus our AA "Cookbook," the Atomic Absorption Newsletter, and a wide variety of other technical materials to keep you current in atomic spectroscopy.

If you need help in deciding between the 603 and 460, your nearest Perkin-Elmer representative can make your task easier. Just ask for details or a demonstration. Write Perkin-Elmer Corporation, Main Avenue, Norwalk, CT 06856. Or phone (203) 762-1000.

PERKIN-ELMER

CIRCLE 161 ON READER SERVICE CARD

Custom Built SHAKERS

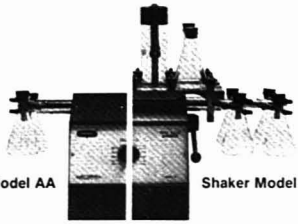

Shaker Model AA — Shaker Model BT

- Gentle Swish to Violent Swirl • Replicable Operation
- Handles Flasks, Beakers, Separatory Funnels, and Fleakers

Burrell Shakers perform any action from a slight tilt, gentle agitation to a pitched, violent swirl. All at a constant speed for as long as necessary. Results can be replicated by simply duplicating the initial angle and speed settings. Exclusive Build-Up design permits short or long side arms, the top platform and separatory clamps to be easily added or removed. Burrell Wrist-Action™ Shakers . . . can we custom build one for you?

BURRELL **BURRELL** CORPORATION
2223 Fifth Avenue, Pittsburgh, PA 15219
412/471-2527
QUALITY INSTRUMENTS FOR SCIENTISTS AND ENGINEERS

CIRCLE 30 ON READER SERVICE CARD

VERSATILE DESICCANT

DRIERITE is a low-cost, all-purpose anhydrous calcium sulfate used in desiccators, U-tubes, drying columns, drying tubes and large drying cabinets to dry air and gases. DRIERITE is also ideal for drying organic liquids in either the liquid or vapor phase.

The moisture remaining in a gas after drying with DRIERITE amounts to only 0.005 mg per liter.

DRIERITE is available in two forms—Regular or Indicating—from all leading Laboratory Supply Dealers.

REGULAR DRIERITE is constant in volume, inert except toward water, insoluble in organic liquids and refrigerants, non-disintegrating non-wetting, non-poisonous, non-corrosive, repeatedly regenerative, and non-channeling.

INDICATING DRIERITE has all of the properties of Regular DRIERITE, but is impregnated with C.P. cobalt chloride and, hence, makes a clearly visible change from blue when dry to pink when exhausted.

W. A. HAMMOND DRIERITE CO.
Xenia, Ohio 45385

SOLIDS-LIQUIDS-GASES-SOLIDS-LIQUIDS-GASES-SOLIDS
DRIERITE ®

CIRCLE 101 ON READER SERVICE CARD

The Bath People

FORMA

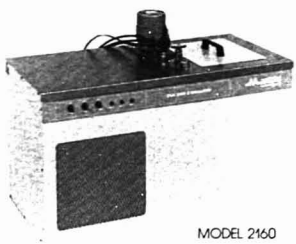

MODEL 2160

A bath and a circulator. Refrigerated and heated. −30° C to + 100° C, ± 0.02° C. A large 9.7 gallon liquid capacity for temperature stability. Solid-state controls for dependability. Our literature has the details.

Forma Scientific
BOX 649 • MARIETTA, OHIO 45750 • AREA CODE 614/373-4763
TELEX 24-5294 • TOLL FREE IN-WATS SERVICE 800-848-9730 AREAS 1, 2 & 3

CIRCLE 76 ON READER SERVICE CARD

NEW

Pharmacia Peristaltic Pump P-3

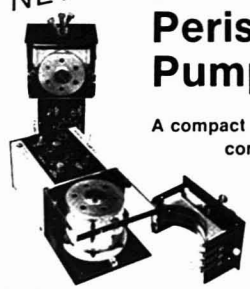

A compact pump electronically controlled for constant liquid flows in chromatography and gradient formation

You can

- obtain three different flow rates at the same time through the three individually tensioned pumping channels
- change tubes in seconds with the snap-in cassette
- forget about pulsation thanks to the large driven rollers
- rely on a constant motor speed, electronically compensated for load and temperature
- use any flow rate between 0.6 and 400 ml/h per channel with the same gear box
- reverse the flow instantly
- push for maximum flow and clear pump lines rapidly

For free descriptive literature, write or call:

Pharmacia Fine Chemicals
Division of Pharmacia, Inc
Piscataway, New Jersey 08854
Phone (201) 469-1222

Pharmacia Fine Chemicals

CIRCLE 170 ON READER SERVICE CARD

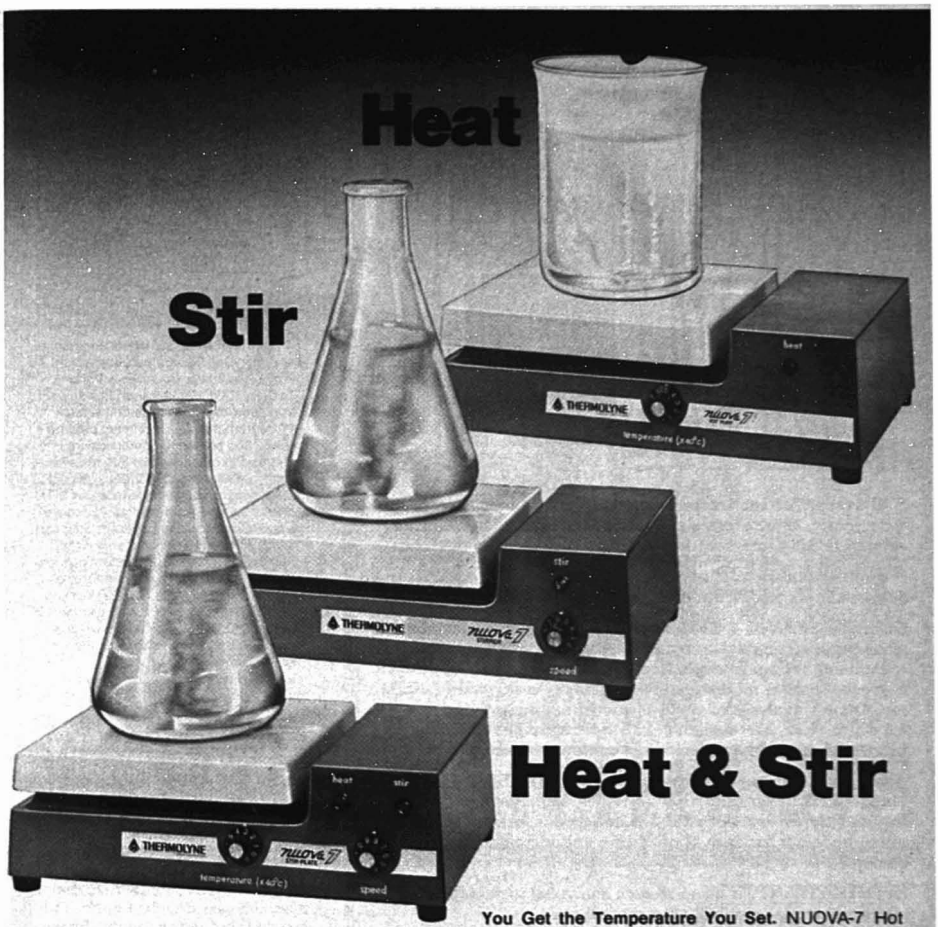

Heat & Stir

When you invest in heating and stirring apparatus, get the best.

Our NUOVA-7 Series Hot Plates, Stirrers and Stir Plates have many dramatically different features . . . attractive, low profile design . . . side mounted controls and stirring motors . . . all vital working parts securely protected from spill damage . . . fast heat-up . . . solid state speed control assures constant stirring . . . 7" square unbreakable, Nucerite®-coated top plates.

You Get the Temperature You Set. NUOVA-7 Hot Plates and Stir Plates heat up fast . . . 371°C in 8 minutes. Positive, no-drift temperature controls hold surface temperatures to within ±3°C. A demand-type thermostatic control rapidly responds to any change in surface area temperature.

You Get the Stirring Speed You Set. Right away with no time lag or readjusting. NUOVA-7 Stirrers and Stir Plates have a superior solid state stirring speed control that responds automatically to each setting from 60 to 1200 RPM.

Attractive, Whisper-Quiet and Very Efficient. The NUOVA-7 low profile units are the design of tomorrow available today through your laboratory dealer.

Write Thermolyne, ask for Catalog No. 600.

THERMOLYNE
SYBRON CORPORATION
2555 KERPER BOULEVARD, DUBUQUE, IOWA 52001

CIRCLE 203 ON READER SERVICE CARD

A plant chemist at the Monticello Nuclear Generating Plant, a part of the Northern States Power Co., uses a Varian Tectron 1200 atomic absorption spectrophotometer to analyze condensate taken from the plant's primary process water. The presence of magnesium is checked to monitor leaks into the system from the mineral-rich Mississippi River water through tiny condenser tube cracks into the plant's primary process water. Corrosion and system fouling can occur if mineral levels become high. Samples of 15 l. are passed through ion-exchange columns to remove magnesium from the sample. The magnesium is eluted from the resin with hydrochloric acid and tested along with known concentrations of magnesium with the AA instrument

synthetic steroids resemble the male sex hormone, testosterone, and affect much the same organs. They are, however, very dangerous with serious side effects including, among others, premature aging, cancer of the bladder, possible sterility in men, and feminizing in women. They are difficult to detect and to measure partly because they are used differently from the more common stimulant drugs. They may be taken intermittently, for instance, and stopped before competition. Detecting these drugs presents a real challenge to the analytical chemist. Of the three persons who were found to have taken these drugs, two were men in the weight lifting competition, and one was a woman. Testing continues on 300 samples.

Other tests used included headspace gas chromatography for alcohol and atomic absorption for metals.

Clinical Chemistry Automation in Saudi Arabia

The July–August 1976 issue of *Du Pont Magazine* relates the "adventures" of Debora Krakowski, senior technical specialist in Du Pont's Automatic Analysis Division, in providing on-site support for the installation and operation of the company's Auto-

STRAY LIGHT 10^{-14}

RESOLUTION $0.2\ cm^{-1}$

HIGH PERFORMANCE LASER RAMAN SPECTROMETER HG.2S

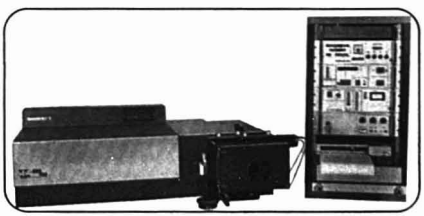

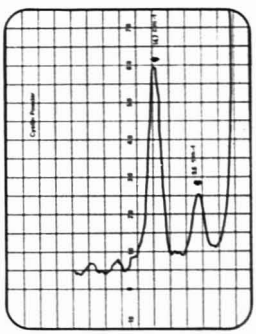

Introducing a new generation Raman monochromator with concave holographic gratings

Jobin-Yvon
- First in holographic gratings
- Most experienced in monochromator production

- U.V. and I.R. capabilities available
- Accessible Sample Compartment
- Versatile Data Acquisition System

JOBIN YVON
Division
d'INSTRUMENTS S.A.
16-18, rue du Canal
91160 LONGJUMEAU
FRANCE
Tel. 909.34.93

JOBIN YVON
DIVISION d'INSTRUMENTS S.A.

CIRCLE 117 ON READER SERVICE CARD

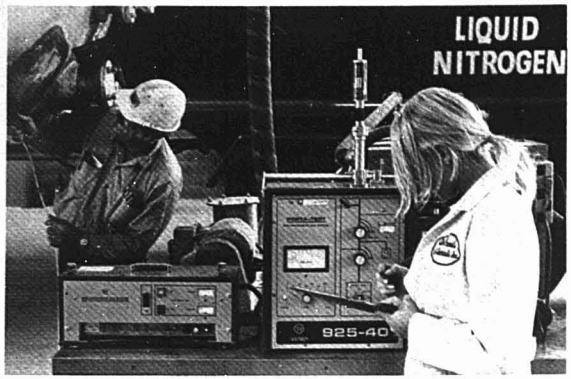

Technicians for Air Products and Chemicals, Inc., check one of the company's cryogenic liquid trailers for leaks with a Varian 925-40 Porta Test, a portable mass spectrometer capable of finding leaks as small as 10^{-10} cc/s. The tanks used by the Industrial Gas Division of Air Products range in size from 50 to 30 000 gal and are used to store a variety of liquid gases from argon to xenon. Before the use of portable mass spectrometers for leak detection, most outfits were forced to use the old-fashioned soap test. Mass spectrometry testing for leaks is more accurate, less time-consuming, and more economical than other methods based on human observation

matic Clinical Analyzers (aca's) in Saudi Arabia. Whittaker Corp., Los Angeles, with a contract to manage the staffing and operation of three military hospitals in Saudi Arabia, also supplied instrumentation and equipment. Aca's were installed in hospitals in Jeddah, Takub, and Khasmis Mushayt. An aca was also installed by the Hospital Corporation of America in the 300-bed King Faisal Specialist Hospital and Research Center in the Saudi Arabian capital city of Riyadh. Debby Krakowski found the experience a challenge because of the language barrier and because few of the Middle Eastern technologists had had experience with highly automated clinical systems. Language and electromechanical problems were eased by the presence of Du Pont's Lebanese-born Ali El-Ali, aca technical representative in the Middle East, and Walt Cummings, a customer service representative from the U.S. Du Pont's flexible aca is capable of performing 30 different analyses on samples of blood, urine, or spinal fluid. It can be easily modified for new tests or to meet changing laboratory needs.

The modern hospital facilities provide a startling contrast with the rural remoteness of both Khamis Mushayt and Tabuk. However, according to Debby Krakowski, Riyadh is a very modern city, and the King Faisal Hospital is one of the best equipped she has seen.

Call for Papers

4th SAC Conference of the Analytical Division of the Chemical Society

Birmingham University, England. July 17–22. Papers are invited on all aspects of analytical chemistry for this conference organized by the Analytical Division of the Chemical Society and sponsored by the International Union of Pure and Applied Chemistry. The topics of analytical chemistry to be covered are: instrumentation in analysis; atomic spectroscopy; chromatography and other separation methods; nuclear and radiochemical analysis; thermal analysis; microchemical techniques and analytical microscopy; electroanalysis, including ion-selective electrodes; analysis in the life sciences; analysis in industry; pollution and environment control analysis; forensic analysis; and newer techniques. Submit abstracts (up to 200 words) before November 30 to A. Townshend, Chemistry Department, The University, P.O. Box 363, Birmingham B15 2TT, England.

New York Microscopical Society's Dialogues in Microscopy '77 Meeting

Statler Hilton Hotel, New York City. May 14–19, 1977. Contributing papers are solicited on all aspects of microscopy including fluorescence, microspectrophotometry, microrefractometry, qualitative measurements, interference microscopy, scanning transmission electron microscopy, contrast enhancement, microholography, and staining and sample preparation for TEM, SEM, and optical microscopy. Prospective authors should submit abstracts, not later than November 15, to John A. Reffner, Program Chairman, NYMS Dialogues '77, Institute of Materials Science, University of Connecticut, Storrs, Conn. 06268.

Meetings

The following meetings are newly listed in ANALYTICAL CHEMISTRY. *The 1976 and 1977 meetings listed earlier appear in the September issue*

- **151st National Meeting of the Electrochemical Society.** May 8–13, 1977. Philadelphia. *Contact: The Electrochemical Society, Inc., P.O. Box 2071, Princeton, N.J. 08540*
- **5th International Conference on Thermal Analysis.** Aug. 1–6, 1977. Kyoto, Japan. *Contact: The Secretariat, ICTA V, c/o Society of Calorimetry and Thermal Analysis, Japan, Daiichi Kanamori Bldg., 1-5-31 Yushima, Bunkyo-ku, Tokyo 113, Japan*
- **International Solvent Extraction Conference, ISEC 77.** Sept. 9–16, 1977. Toronto, Ontario. Sponsored by the Canadian Institute of Mining and Metallurgy, the Canadian Society for Chemical Engineering, and the Society for Chemical Industry. The program includes analytical sessions. *Contact: M.H.I. Baird, Secretary, ISEC 1977, Chemical Engineering Dept., McMaster U., Hamilton, Ont. L8S 4L7, Canada*
- **7th International Vacuum Congress and 3rd International Conference on Solid Surfaces.** Sept. 12–16, 1977. Vienna, Austria. *Contact: NancyHammond, Executive Secretary, American Vacuum Society, 335 East 45th St., New York, N.Y. 10017*

Short Courses

ACS Courses. For more information, contact: Department of Educational Activities, American Chemical Society, 1155 16th St., N.W., Washington, D.C. 20036. 202-872-4508

HPLC Apparatus Workshop
New York City. Oct. 7–8. David H. Freeman. $155, ACS members; $190, nonmembers

OVERWHELMING PERFORMANCE

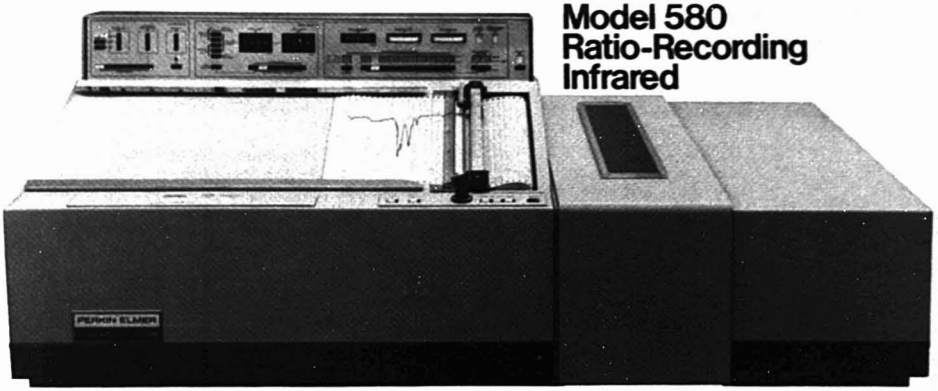

The Model 580 IR. No other medium-priced infrared gives you ratio recording – the biggest exclusive of all. No other infrared approaches its accuracy, speed and simplicity.

Qualitate and quantitate. With ratio recording – unlike optical null instruments – the system is still "live" at 0% transmission. Result: extreme ordinate accuracy – repeatability better than 0.2% T. You can qualitate *and* quantitate even at lowest transmission levels.

Integrated scan modes. No more trade-off judgments involving noise, resolution, and scan time. Simply press the button for one, and the Model 580 optimizes the others. You can't get a bad spectrum. Resolution of 0.4 cm^{-1}. You also get 30 scan modes plus a high-speed survey scan that records a full range spectrum from 4000 cm^{-1} to 180 cm^{-1} in two minutes.

Automatic wavenumber corrector. For abscissa accuracy, this unique feature keeps the 580 calibrated at all scan speeds. All you do is initiate the scan and the automatic wavenumber corrector applies the appropriate correction for each scan mode.

Computer compatible. Its RS-232-C accessory interfaces with any minicomputer. You can average spectra, subtract one spectrum from another, reformat spectra – all automatically without re-analyzing. Under computer control, the panel controls won't function, so the operator can't accidentally interfere.

All the software, too. Perkin-Elmer is the only manufacturer who supplies a complete infrared software package. It would take two years to develop it yourself. Another big exclusive.

Get more out of your sample in less time than ever before possible. Learn what the Model 580 can do. For more information and a demonstration, contact your Perkin-Elmer representative or write Perkin-Elmer Corporation, Main Avenue, Norwalk, CT 06856.

Perkin-Elmer also offers the industry's largest line of infrared accessories. Ask for our Accessories Catalog L-396.

PERKIN-ELMER

CIRCLE 174 ON READER SERVICE CARD

News

Intermediate Chromatographic Systems: Maintenance and Troubleshooting
Chicago (given in conjunction with ASTM Meeting). Oct. 15–16. John Q. Walker, Minor T. Jackson, Jr., and M.P.T. Bradley. $155, ACS members; $190, nonmembers

Solving Problems with Modern Liquid Chromatography
Washington, D.C. (given in conjunction with AOAC Meeting). Oct. 16–17. J. J. Kirkland and Lloyd R. Snyder. $155, ACS members; $190, nonmembers. Page 824 A, Sept.

Laboratory Safety—Recognition and Management of Hazards
Washington, D.C. Oct. 28–30. Norman Steere and Maurice Golden. $190, ACS members; $230, nonmembers

Recent Developments in Thermal Analysis
Philadelphia (given in conjunction with FACSS Meeting). Nov. 13–14. Wesley W. Wendlandt and Ilya Sarasohn. $145, ACS members; $170, nonmembers

Laboratory Automation: Micro-, Mini-, or Midicomputers?
Philadelphia (given in conjunction with FACSS Meeting). Nov. 13–14. Raymond E. Dessy and the Chemistry Dept. Instrument Design and Automation Research Group from VPI&SU. $145, ACS members; $170, nonmembers

Column Selection in Gas Chromatography
Philadelphia (given in conjunction with FACSS meeting). Nov. 13–14. Harold M. McNair and Walter R. Supina. $120, ACS members; $145, nonmembers

Automated Analysis
Philadelphia (given in conjunction with FACSS Meeting). Nov. 13–14. Hans Veening and Carl Burtis. $145, ACS members; $170, nonmembers

Modern Liquid Chromatography
Philadelphia (given in conjunction with FACSS Meeting). Nov. 19–21. Lloyd R. Snyder and J. J. Kirkland. $160, ACS members; $195, nonmembers

Thin-Layer Chromatography
Chicago. Dec. 2–3. Victor Rodwell and Donald McNamara. $145, ACS members; $170, nonmembers

Microprocessors and Minicomputers: Interfacing and Applications
Blacksburg, Va. Dec. 5–10. Raymond Dessy and the Chemistry Dept. Instrument Design and Automation Research Group from VPI. $355, ACS members; $395, nonmembers

Scanning Electron Microscopy
Mohonk Mountain Resort in New Paltz, N.Y. Oct. 18–22. *Contact:* Angelos V. Patsis, Chairman, Department of Chemistry, State University of New York at New Paltz, New Paltz, N.Y. 12561. 914-257-2175

Identification of Small Particles
Chicago. Oct. 18–22. $550 (includes Particle Atlas Two). *Contact:* McCrone Research Institute, 2820 S. Michigan Ave., Chicago, Ill. 60616. 312-842-7105

X-ray Photoelectron Spectroscopy (ESCA)
Chicago. Oct. 25–29. $400. *Contact:* McCrone Research Institute, 2820 S. Michigan Ave., Chicago, Ill. 60616. 312-842-7105

Microscopy for Polymer Scientists
Chicago. Nov. 1–5. $400. *Contact:* McCrone Research Institute, 2820 S. Michigan Ave., Chicago, Ill. 60616. 312-842-7105

For Your Information

The 1976 edition of **Technical Books and Monographs** just published by the Energy Research and Development Administration contains a bibliography of energy-related books and monographs sponsored by the ERDA and by the organizations brought together to form ERDA. This edition provides for most publications a brief descriptive statement, lists or descriptions of the contents, and availability. The more than 500 publications are grouped under 13 subject categories: general reference, biology and medicine, chemistry, computers, energy, engineering and instrumentation, environment, health physics, isotope separation, metallurgy, physics, reactors, and vacuum technology. The catalog is available as TID-4582-R11 without charge from ERDA Technical Information Center, P.O. Box 62, Oak Ridge, Tenn. 37830.

Walter C. McCrone Associates, Inc. (2820 South Michigan Ave., Chicago, Ill. 60616), has announced the formation of an autonomous subsidiary, **McCrone Accessories and Components,** to market microscope accessories and related products. The new subsidiary will handle products manufactured by approximately 60 companies in the U.S. and other countries, as well as those developed by McCrone Associates. The parent company is a microanalytical consulting firm headquartered in Chicago.

Utopia Instrument Co. (P.O. Box 863, Caton Farm Rd., Joliet, Ill. 60434) has been appointed exclusive distributor in the U.S., Canada, and Mexico by Knauer of Berlin, West Germany, for its complete line of vapor pressure, membrane and cryoscopic osmometers used for molecular weight measurements.

High chlorine content and corrosion rate in crude oil distillation tower, as well as tube blockage caused by corrosion inhibitor, present complex problem

Refinery Crisis Solved

S. A. Schmidt and V. F. Gaylor

The Standard Oil Co. (Ohio)
4440 Warrensville Center Road
Cleveland, Ohio 44128

It began with an innocent-sounding telephone call. "Please attend a Corporate Engineering meeting to discuss a refinery corrosion problem." That meeting was the beginning of a crash analytical effort that involved nearly all the R&D analytical groups.

The crisis occurred during the beginning of crude oil and energy shortages when our refineries had to operate with whatever crude oils the Purchasing Department could supply. And they had to *keep* operating to supply the gasoline-hungry public. But one of our refineries was in trouble. Abnormally high corrosion rates were being measured in the naphtha handling system just downstream from the crude oil distillation tower. High corrosion rates were accompanied by solids buildup in a crucial part of the system. Both problems were so alarming that shutdown of the crude oil distillation tower was a very real threat. As an additional complication, the light crude naphtha was reported to be high in total chlorine content (10–100 ppm), and some inorganic chlorine-containing compounds can easily damage postdistillation naphtha refining facilities. The refinery engineers were convinced that all of their troubles were chlorine derived!

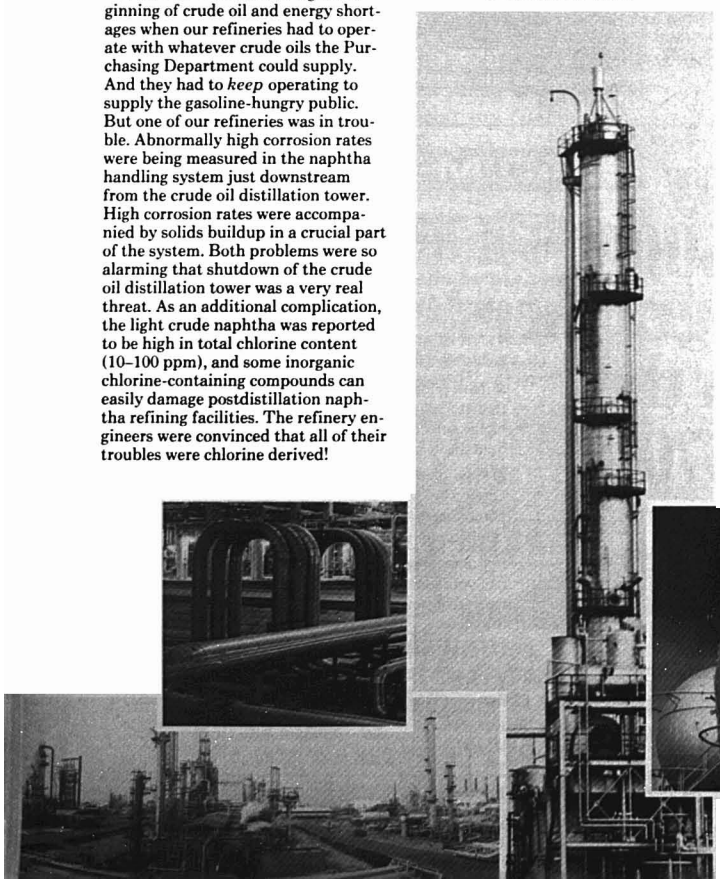

Diagnostic Plan

Figure 1 is a simplified schematic of the part of the refinery directly involved in this crisis. Crude oils delivered to refineries contain significant quantities of water and hydrolyzable chloride salts. Most of the water and salts are electrostatically removed in the desalter. Trace quantities of water and chloride salts are, however, present in the feed to the crude oil distillation tower and can generate HCl during distillation. An amine corrosion inhibitor is therefore injected into the light hydrocarbon overhead to neutralize the corrosive acid. The amine–HCl salt is subsequently removed in the water knockout tank in the water phase. The acid-free hydrocarbon stream is then fed to the naphtha splitter, where the crude naphtha is separated into light and heavy naphtha fractions.

The crisis centered around the naphtha splitter reboiler furnace. Tubes in the furnace were plugging (high-pressure readings), corrosion meters indicated a corrosion rate of $\frac{1}{16}$ in. per year, and crude naphtha from the splitter was reported to be high in total chlorine.

In cooperation with Corporate Engineering, we outlined possible reasons

for the three refinery problems (Figure 2) and planned the analytical approaches accordingly. Both chlorine- and sulfur-containing compounds can corrode refinery equipment. Therefore, our analyses included both types of compounds.

Was It Chlorine Corrosion?

The initial work listed in Table I seemed to eliminate chloride salts as the cause of corrosion. The desalter was working properly; we found no unusually high levels of Cl^- and no unusual metals in the desalted crude oil. Furthermore, no unusual levels of HCl were generated on distilling the crude oil in the lab. Acidity level of the undistilled crude oil was also normal.

Chlorinated hydrocarbons are sometimes used for secondary crude oil recovery from wells, and the presence of these materials could account for total chlorine found in the naphtha. But we could find no chlorinated hydrocarbons by polarography.

Was the total chlorine determination valid? That was a question asked early, and the answer turned out to be "No". The refinery lab was using a nonstandard, combustion/microcoulometric method (Dohrmann) for total chlorine. With the refinery's procedure, we confirmed apparent high concentrations of chlorine in the naphtha. But further experimentation showed that high levels of sulfur interfere with this chlorine method. After reducing total sulfur concentration by precipitating H_2S and RSH with Cd^{2+}, the apparent total chlorine concentration dropped to insignificant levels.

There was no "high chlorine" problem. It was analytical error—a false trail for diagnosing the corrosion problem and due to sulfur interference with the Dohrmann chlorine measurement.

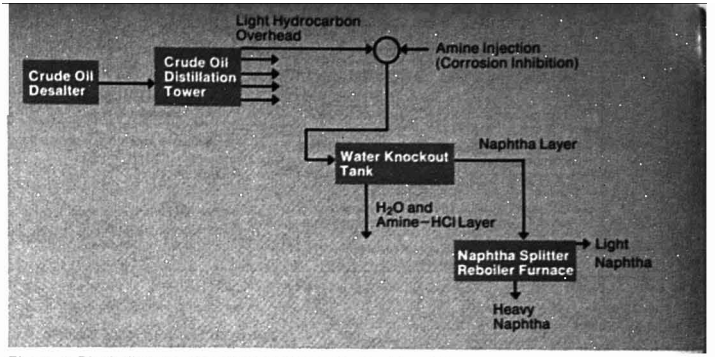

Figure 1. Block diagram of portion of refinery involved in crisis

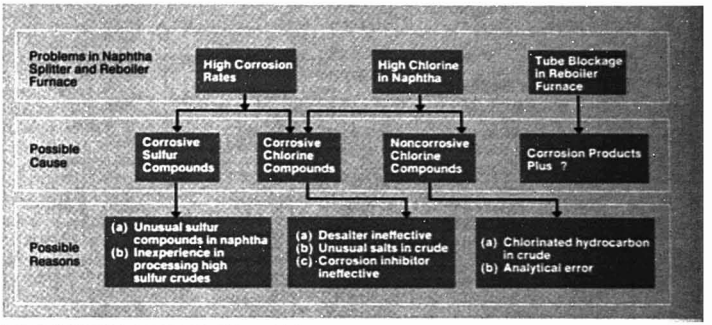

Figure 2. Possible causes of refinery crisis

Table I. Analysis of Desalted Crude and Crude Naphtha Streams for Chlorine- and Sulfur-Containing Compounds

Method	Results: Desalted crude	Results: Crude naphtha
	CHLORINE	
Titrimetry and selective ion electrode	Normal Cl^- levels. Desalter effective	
Emission spectrography	No unusual metal salts present	
Titrimetry and polarography	Normal acidity levels	No acidity detected
HCl evolution test	Normal HCl levels generated	
Polarography		No chlorinated hydrocarbon detected
Dohrmann microcoulometry on untreated samples		Apparent high total chlorine
Dohrmann microcoulometry after RSH and S^{2-} removal		Total chlorine insignificant
	SULFUR	
X-ray fluorescence spectroscopy	High total sulfur	High total sulfur
Titrimetry	High H_2S and RSH	High H_2S and RSH
Corrosive sulfur evolution test	High levels of corrosive sulfur generated on heating	No corrosive sulfur generated on heating. (No unusual sulfur compounds present)

Table II. Analysis of Corrosion Inhibitor

IR analysis	GC–MS analysis	Neutralized with HCl recovered salts	
Complex mixture of cyclic amines in aromatic solvent	Approx. equal amounts of five cyclic amines, C_8–C_{12} benzenes, and C_{10}–C_{14} naphthalenes	Partitioned between H_2O–HC	Heated 6 h at 250 °F
		>20% into HC phase	Brownish black tar, contained chlorine, water soluble

Was It Sulfur Corrosion?

There were high levels of corrosive sulfur compounds (H_2S and RSH) in the crude oil, and more were generated on heating (Table I). Therefore, the naphtha also contained high levels of corrosive sulfur compounds. We concluded that a major part of the corrosion problem was due to processing high sulfur crude oil.

What Was Blocking the Reboiler Tubes?

Buildup of corrosion products contributes to tube blockage in the reboiler furnace. However, the engineers were convinced that the pressure buildup rate far exceeded that expected from corrosion rate measurements. The corrosion inhibitor was the major remaining unknown in the whole system. Corporate Engineering had no prior experience with the inhibitor in use; it was not used in any other company refinery.

Table III. Analysis of Solids from Reboiler Tubes

Appearance	Black, soft spongy texture
Solubility	54% soluble in H_2O 4% soluble in CCl_4
Elemental analysis	31.9% carbon 5.1% hydrogen 9.5% nitrogen 16.0% chlorine 13.1% sulfur 6.6% iron 8.0% ash
Infrared analysis	Amines, amine salts, and amides. *Good spectral match with tars made by heating neutralized corrosion inhibitor*
X-ray diffraction analysis	FeS_2 present. (Elemental sulfur may also be present)

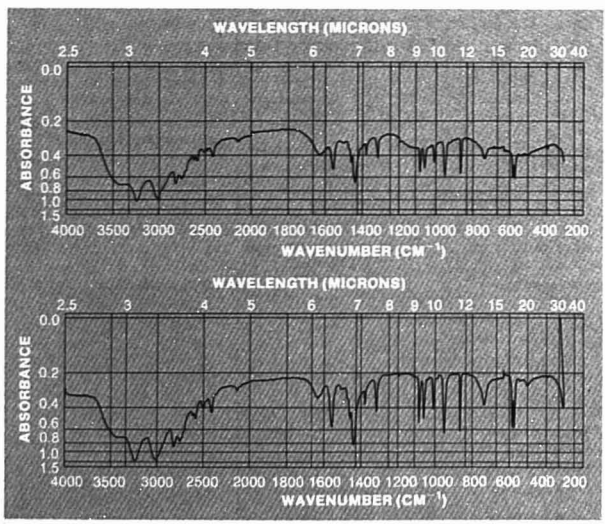

Figure 3. Infrared spectra of: upper: solids from naphtha reboiler furnace tubes; lower: tars formed on heating HCl salts of corrosion inhibitor

We characterized the inhibitor by the tests summarized in Table II. The inhibitor was a very complex mixture of cyclic amines and aromatic hydrocarbons. Partitioning of the inhibitor–HCl salts between water and hydrocarbon was unfavorable; this partitioning experiment suggested that all the amine salts were not removed in the water knockout tank (Figure 1). Some amine salts were carried into the furnace reboiler. And the thermal stability test (Table II) showed that the amine salts would indeed produce tars on heating in the tubes.

We concluded that tube blockage was caused by the corrosion inhibitor and recommended the refinery change to a company-proven inhibitor.

Epilogue

A brief shutdown of the naphtha splitter provided an ultimate test of our diagnoses. Refinery management concluded the partially plugged reboiler furnace had to be cleaned before switching to the recommended corrosion inhibitor. Engineers responsible for the cleaning job found voluminous quantities of a black, spongy solid in the furnace tubes and retrieved a representative sample for analysis. It was a most unusual "plant crud" sample (Table III) with an ash content of only 8% and a high water solubility of 54%! FeS_2 and maybe elemental sulfur were present, confirming our diagnosis of sulfur-caused corrosion. Large quantities of nitrogen and chlorine, as well as carbon and hydrogen, pointed to HCl salts of the corrosion inhibitor. This was nicely confirmed by infrared analysis which identified amines, amine salts, and amides. And the spectral match with laboratory prepared tars from the neutralized corrosion inhibitor was excellent (Figure 3).

Three Problems—Three Solutions

High chlorine problem: Analytical error

Corrosion problem: Corrosive sulfur compounds from crude oil

Furnace tube blockage: Caused by corrosion inhibitor

Acknowledgment

The authors are grateful to T. E. Andrews, N. R. Anthony, P. A. Budinger, L. M. Klimas, J. E. Sucher, M. S. Vigler, and R. Zuback whose analytical work helped us solve this problem, and to Gary Greeves, the engineer member of the troubleshooting team and an active participant in solving the problem.

INDEX TO ADVERTISERS IN THIS ISSUE

* *See ad in ACS Laboratory Guide*

** See ad in ACS Laboratory Guide*

Advertising Management for the American Chemical Society Publications

CENTCOM, LTD.

Thomas N. J. Koerwer, President: Clay S. Holden, Vice President: Benjamin W. Jones, Vice President; Robert L. Voepel, Vice President; C. Douglas Wallach, Vice President; 50 West State Street, Westport, Connecticut 08880 (Area Code 203) 226-7131

ADVERTISING SALES MANAGER
Thomas N. J. Koerwer

SALES REPRESENTATIVES

Chicago ... Eugene Eldridge, CENTCOM, LTD., 540 Frontage Rd., Northfield, Ill. 60093. 312-441-6383.

Cleveland ... Michael Hayes, CENTCOM, LTD., Suite 205, 18615 Detroit Ave., Lakewood, Ohio 44107. 216 228–8050.

Houston ... Michael Hayes, CENTCOM, LTD., 216-228-8050.

Denver ... Clay S. Holden, CENTCOM LTD., 213-776-0552.

Los Angeles 90045 ... Clay S. Holden, Robert E. LaPointe, CENTCOM, LTD., Airport Arcade Bldg., 8820 S. Sepulveda Blvd., Suite 215, 213-776-0552

New York 10017 ... Richard L. Going, CENTCOM LTD., 60 East 42nd St., 212-972-9660

Philadelphia ... CENTCOM LTD., 113 Essex Ave., Narberth, Pa. 19702. Telephone: 215-667-9666

San Francisco ... Clay S. Holden, CENTCOM, LTD., 213-776-0552

Westport 06880 ... Don Davis, CENTCOM, LTD., 50 West State Street, 203-226-7131.

Manchester, England ... Jill E. Loney, Technomedia Ltd., 216, Longhurst Lane, Mellor, Stockport, SK6 5PW, Telephone: 061-427-5660

Reading, England ... Malcolm Thiele, Technomedia Ltd., Wood Cottage, Shurlock Row, Reading, RG10 OOE. Telephone 073-581-302

Paris, France ... Patric B. Hale, Technomedia Ltd., 18 Rue Gounod, 92 Saint-Cloud, Paris. Telephone: 602-24-79

Tokyo, Japan ... Haruo Moribayashi, International Media Representatives Ltd., 1, Shibe-Kotohiracho, Minato-ku Tokyo. Telephone: 502-0656

PRODUCTION DEPARTMENT

Production Director
Joseph P. Stenza

Advertising Production Assistant
Alice M. Hansen

Analytical Chemistry — OCTOBER 1976 — Valid through FEBRUARY 1977

NEW PRODUCTS, CHEMICALS, LITERATURE: 401 402 403 404 405 406 407 408 409 410 411 412 413 414 415
416 417 418 419 420 421 422 423 424 425 426 427 428 429 430 431 432 433 434 435 436 437 438 439 440 441 442
443 444 445 446 447 448 449 450 451 452 453 454 455 456 457 458 459 460 461 462 463 464 465 466 467 468 469
470 471 472 473 474 475 476 477 478 479 480 481 482 483 484 485 486 487 488 489 490 491 492 493 494 495 496

ADVERTISED PRODUCTS: 1 2 3 4 5 6 7 8 9 10 11 12 13 14 15 16 17 18 19
20 21 22 23 24 25 26 27 28 29 30 31 32 33 34 35 36 37 38 39 40 41 42 43 44 45 46
47 48 49 50 51 52 53 54 55 56 57 58 59 60 61 62 63 64 65 66 67 68 69 70 71 72 73
74 75 76 77 78 79 80 81 82 83 84 85 86 87 88 89 90 91 92 93 94 95 96 97 98 99 100
101 102 103 104 105 106 107 108 109 110 111 112 113 114 115 116 117 118 119 120 121 122 123 124 125 126 127
128 129 130 131 132 133 134 135 136 137 138 139 140 141 142 143 144 145 146 147 148 149 150 151 152 153 154
155 156 157 158 159 160 161 162 163 164 165 166 167 168 169 170 171 172 173 174 175 176 177 178 179 180 181
182 183 184 185 186 187 188 189 190 191 192 193 194 195 196 197 198 199 200 201 202 203 204 205 206 207 208
209 210 211 212 213 214 215 216 217 218 219 220 221 222 223 224 225 226 227 228 229 230 231 232 233 234 235
236 237 238 239 240 241 242 243 244 245 246 247 248 249 250 251 252 253 254 255 256 257 258 259 260 261 262

PRODUCT CAPSULES: 301 302 303 304 305 306 307 308 309 310 311 312 313 314 315 316 317 318 319 320 321 322 323
324 325 326 327 328 329 330 331 332 333 334 335 336 337 338 339 340 341 342 343 344 345 346

Name_____ Position_____

Company_____

Street_____ City_____

State_____ Telephone_____

FIRST CLASS
Permit No. 25682
Philadelphia, Pa.
19101

BUSINESS REPLY CARD
No postage stamp necessary if mailed in the United States

POSTAGE WILL BE PAID BY

ANALYTICAL CHEMISTRY
P. O. Box #8660
Philadelphia, Pennsylvania 19101

PRODUCT CAPSULES

Scan this list for products of interest. Then, circle the indicated numbers on the adjacent reply card and selected literature from advertisers in the previous issue will be sent to you

No.	Product Capsules
301	Balances
302	Baths; Circulators
303	Biological Analyzers
304	Books; Periodicals; Catalogs
305	Centrifuge Equipment
306	Chemicals; Reagents; Gases
307	Chromatography, Gas
308	Chromatography, Liquid
309	Chromatography, Thin Layer
310	Computers; Calculators
311	Coolers; Freezers
312	Densitometers
313	Electrical Equip: Amplifiers; Power Supplies; Voltmeters; etc.
314	Electrochemical: pH Meters; Ion Meters; Titrators; Electrodes
315	Electrophoresis
316	Elemental Analyzers
317	Environmental Analyzers
318	Fourier Transform Data Systems
319	Furniture; Fume Hoods
320	Gas Chrom/Mass Spec Systems
321	Labware: Glass; Plastic; Metal
322	Lasers
323	Mechanical Equip: Presses; Mills; etc.
324	Microscopes
325	Mixers; Stirrers; Blenders; Shakers
326	Nuclear Instruments
327	Oscilloscopic Instruments
328	Ovens; Furnaces; Heaters
329	Photometers; Colorimeters
330	Pipets; Samplers; Dispensers
331	Pumps; Flowmeters
332	Recorders; Integrators
333	Services, Analytical; Consultants
334	Signal Averagers
335	Spectro, AA
336	Spectro, Fluorescence
337	Spectro, Infrared
338	Spectro, Mass
339	Spectro, NMR
340	Spectro, UV/Vis
341	Spectro, X-Ray
342	Stills; Demineralizers
343	Supplies: Lubricants; Detergents; etc.
344	Thermal Analyzers
345	Valves; Fittings; Tubing
346	Vacuum Equipment

New Report Available*

Carle's $5610 Answer to Complete Analysis of Refinery Gases

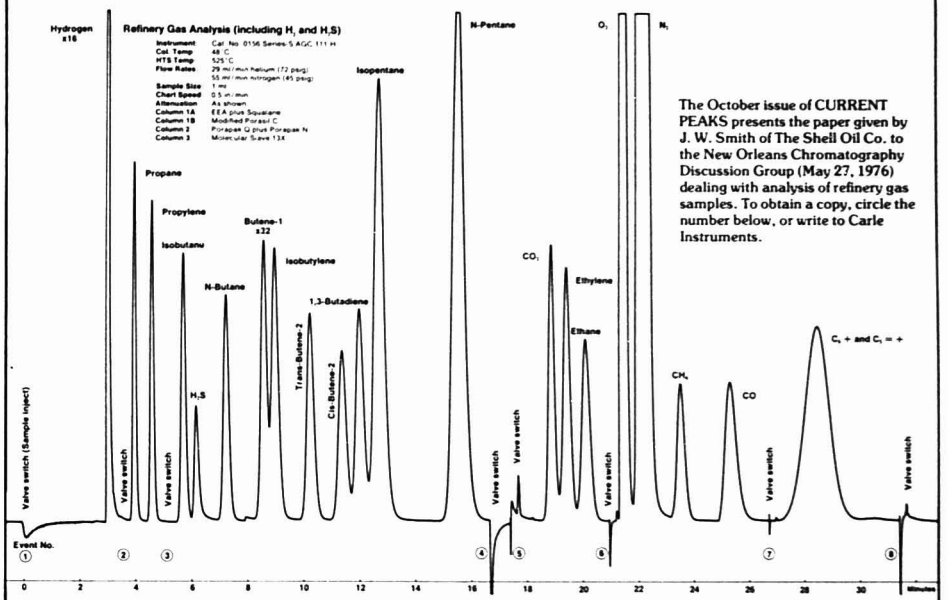

The October issue of CURRENT PEAKS presents the paper given by J. W. Smith of The Shell Oil Co. to the New Orleans Chromatography Discussion Group (May 27, 1976) dealing with analysis of refinery gas samples. To obtain a copy, circle the number below, or write to Carle Instruments.

One of 15 Optimum, Factory-Programmed Answers Available from Carle's Automated Series-S AGC

There are fourteen more hard gas analysis problems answered automatically by Carle's Series-S AGC's. Each dedicated instrument is factory programmed, completely tested and ready for immediate use. Each utilizes Carle's unique column sequencing techniques to produce fast, sensitive, complete analyses. Lower cost manual versions are also available.

Complete data on the above answer, plus information on all 15 Series-S AGC's and a listing of their manual equivalents will be sent to you on request.

CARLE
INSTRUMENTS, INC.

1141 East Ash Avenue · Fullerton, CA 92631 · 714-879-9900

CIRCLE 35 ON READER SERVICE CARD

New Products

This gradient system for high-performance liquid chromatography utilizes two advanced metering pumps with electronic pulse correction for precise flow rates to 10 ml/min at 10 000 psi. Two modes of operation permit constant flow for maximum chromatogram reproducibility or constant pressure where column or packing pressure limits override flow considerations. The solvent programmer can be used to program flow rate or gradient profiles up to 18 h. Operating mode selections include manual solvent scouting, up to a 60-min hold at final gradient concentration, and automatic column reequilibration. A UV–VIS detector with an 8-μl flow cell and wavelength selectability from 254 to 660 nm completes the system. Altex Scientific, Inc. **401**

IR Spectrometer

The Model 80 microcomputer-controlled infrared quantitative spectrometer is compact and versatile, accommodates a wide variety of sample-handling accessories, controls all instrument settings, and obtains extremely accurate quantitative data on solids, liquids, or gases. It features a 16-key system for entry of instrument settings and factors for data manipulation. Through signal averaging, 256 measurements are made at each wavelength over a 1–180-s interval. Up to 17 separate wavelengths can be measured in less than 2 min. Digital printout provides a permanent record and eliminates ambiguity of readings. Computer interface with RS 232C format communication link is available. Wilks Scientific Corp. **408**

Computing Integrator for GC and HPLC

Models L and E real-time chromatography data processors feature run parameters programmed by the operator, two separate run parameter program files, normalized peak reporting, two-channel input selector, optional post-run calculation routines standard, peak detection and baseline parameters programmable to suit changing run conditions, automatic noise level assessment, and six programmable external event signals. Model L also includes total area normalization. Model E includes total area normalization as well as response factors and internal and external normalization. Laboratory Data Control **409**

For more information on listed items, circle the appropriate numbers on one of our Readers' Service Cards

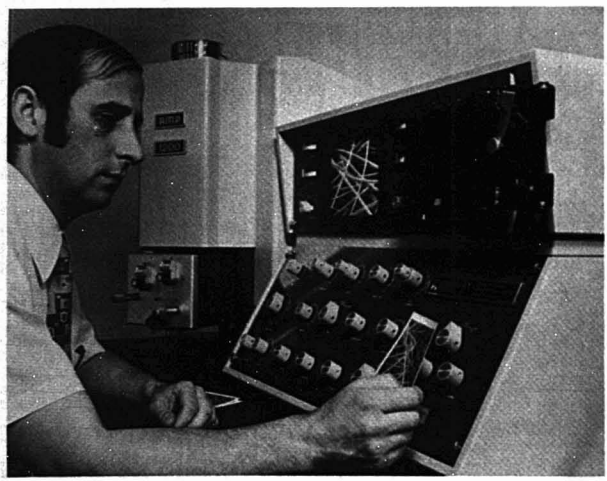

AMR 1200/01 scanning electron microscope is compact and provides 70 Å resolution. It incorporates Z-motion stage, autofocus control, externally selectable and alignable final apertures, high-resolution camera recording system, and gamma nonlinear amplification. It can be operated in the secondary electron, backscattered electron, line, spot, and cathodoluminescence modes. The AMR 1200/01 has a magnification range at normal working distances of 20X to 300 000X with capability to go down to 5X. Priced under $29,000. AMR Corp. **402**

Stirred-Slurry Column Packer

Model 705 enables the chromatographer to easily and reproducibly pack HPLC columns using microparticle materials. The technique is simple and fast and takes about 30 min for a 4 mm i.d. X 25 cm column packed with 10-μm silica gel. The pumping system of any high-pressure liquid chromatograph is readily adapted to pressurize the column packer and provide flow to move the slurry into the column. $320. Micromeritics Instrument Corp. **415**

Ionization Gauge Controls

Ratiomatic 842 and Ratiomatic 843 eliminate the need to hold the emission current constant, offer complete gauge tube protection from pressure bursts, and can be used with standard sized ion gauge cable lengths up to 100 ft. Both controls can also be supplied with set-point protection for the gauge tube or vacuum system components. The controls measure pressures from 10^{-3} to 10^{-8} torr. Varian Vacuum Division **416**

Three new sorbents for Reversed Phase Chromatography:

Now, for the first time, a series of organosilane derivatized sorbents with varying hydrocarbon lengths, RP-2, RP-8 or RP-18, is available for reversed phase chromatography. They've just been introduced by the world's leader in chromatography--E. Merck, Darmstadt, Germany.

- For the HPLC user, these new packings can mean optimized efficiency. Obtain "Chromatographic Flexibility in Reversed Phase Chromatography" by selecting the RP packing which best fits your sample/solvent parameters.
- For the thin layer and column chromatographer, these sorbents are available on pre-coated TLC plates and for columns; they represent the introduction of reversed phase chromatography in your disciplines. They are especially suitable when negligible polarity differences exist between components being separated.
- Reversed Phase pre-coated TLC plates are also ideal tools for the chromatographer to evaluate sample/solvent combinations prior to High Speed Liquid Chromatography.

No chromatographer is up to date unless he has information on these important new products. EM Laboratories' chromatography catalog has the facts you need. Send for your copy today by circling the reader service number indicated below. You'll see why RP-2, RP-8 and RP-18 deserve "Best of Show" honors in Reversed Phase Chromatography.

EM Laboratories, Inc.
associate of
E. Merck, Darmstadt, Germany
500 Executive Boulevard
Elmsford, N.Y. 10523
(914) 592-4660

Pure Consistency...

◆ laboratory reagents and indicator strips ◆ sorbents, plates and columns for chromatography
◆ biochemical specialties ◆ instrumentation chemicals

CIRCLE 64 ON READER SERVICE CARD

The idea

A simple way to monitor the rate of slow reactions involving the hydrogen ion.

In a nutshell, we stabilize the pH of the reaction mixture by adding an appropriate titrant at such a rate that hydrogen ion released or used up is immediately consumed or replaced. By plotting the volume of titrant used against time, we derive a curve which directly reflects the reaction rate.

To obtain meaningful curves it is essential to control the temperature of the reaction mixture and, as well, to agitate it vigorously to prevent the formation of concentration gradients.

We put all of these functions—pH control, volume-time recording, temperature control and mixing—into an instrumentation package: our Thermostatic Recording pH-Stat, which is portrayed schematically in the accompanying diagram.

The pH-Stat involves a lot of things we know a good deal about, e.g. laboratory strip chart recorders, motor driven burets, pH meters and thermistor thermometer circuits, and we have used our experience to put together an instrument which allows you a great deal of latitude in selecting the parameters for a high precision study of reaction rates.

Sensitivity of the pH control system is 0.005 pH and any pH from 0 to 14, preselected to 0.01, is held to ±0.01 pH. Temperature of reaction mixtures up to 100 ml in volume can be regulated to ±0.05°C over the range, 20° to 50°C (or ambient −15° to ambient +40°C with a special thermistor available to order). With the 2.5 ml buret supplied, full volume scale calibrations of 0.5 and 2.5 ml are available and three chart speeds, 1/60, 1/10 and 1 inch per minute are switch selected. Accuracy of volume recording is ±0.1% of buret capacity. Dimensions of chart paper grid, 250 mm x 36.6 meters.

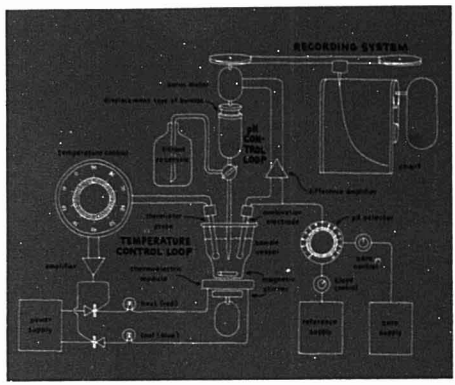

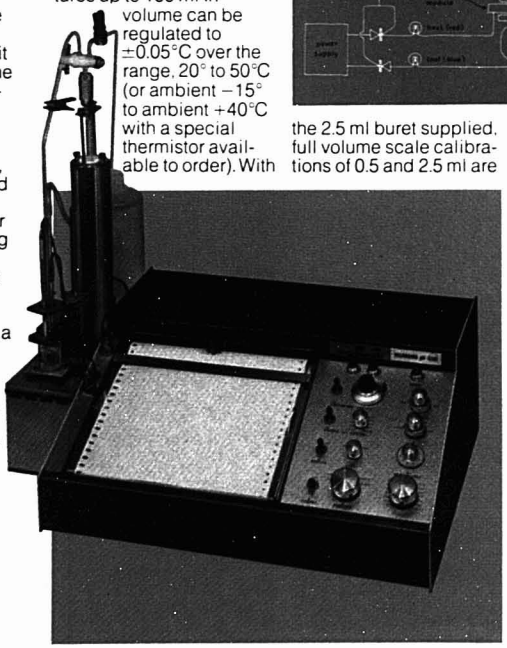

There is a lot more to say about our pH-Stat than space here allows. If you're interested, we have a new bulletin we'd like to send you. For your copy, phone, write or circle the reader service number.

S-30240 pH-STAT—Recording, Thermostatic, Sargent-Welch. Complete with all necessary operating supplies. For 115 volt 60 Hz A.C. **3500.00**

SARGENT-WELCH SCIENTIFIC COMPANY

7300 NORTH LINDER AVENUE • SKOKIE, ILLINOIS 60076 • (312) 677-0600

Anaheim/Birmingham/Chicago/Cincinnati/Cleveland/Dallas/Denver/Detroit/Springfield, N.J./Toronto/Montreal

CIRCLE 188 ON READER SERVICE CARD

Model 6970 liquid chromatograph features a precision, constant flow, dual-piston pumping system, a double-beam variable wavelength detector, and a stop flow injector. The complete system's performance is enhanced by inclusion of a completely automatic, digitally controlled solvent and flow programmer and a variable volume valve loop injector. The instrument features continuous digital readout of flow, pressure, wavelength, solvent composition, absorbance, and/or detector high voltage. Mechanical design is compact and modular permitting easy accessory accommodation and variable instrument configuration. Tracor, Inc. **403**

TM Cavity for EPR Spectrometers

Model E-238 transverse-mode sample cavity produces twice the signal strength from aqueous samples as conventional cavities. Several features include increased value of the H_1 field along the sample axis which effectively enlarges the active region of the cavity, considerably higher Q than standard cavities, and greater sample capacity in the active region of the cavity without high loss in Q. Comes in kit form which includes wave-guide and hardware for use with all E-line and E-line Century Series EPR spectrometers. Varian Instrument Division **412**

Programmable Precision Pulse Generator

Model 9010 features remote programming of the pulse amplitude from 0 to ±9.999 V with 1-mV resolution and a pulse DC mode which allows direct measurement of the pulse top with a digital voltmeter. Other features include variable rep rates from DC to 1 MHz, independently variable rise and fall times, adjustable pulse delay and width, single- or double-pulse mode, 50 ohm output impedance, and tail or flat top pulses with 0.01%/°C temp coefficient. $1520. Berkeley Nucleonics Corp. **413**

For more information on listed items, circle the appropriate numbers on one of our Readers' Service Cards

Corrected Spectra Unit

This new accessory is offered initially for use with Models MPF-4, MPF-44, MPF-44A, 512, and 512A fluorescence spectrophotometers. The unit makes it possible to easily generate accurate excitation and/or emission spectra automatically. During the "calibration" mode the operator scans the spectrophotometer in a prescribed way. For subsequent wavelength scans, in either corrected excitation or corrected emission modes, the information stored in memory during the calibration mode scan is recalled and used to automatically correct spectral data. Perkin-Elmer Corp. **410**

Two-Pen X-Y1, Y2 Recorder

Model VP-6432A provides a sensitive calibrated range of 200 μV/cm. Sensitivity can be adjusted in 15 steps to 10 V/cm, and a variable control continuously increases sensitivity up to 2.5 times. Two pen capability makes this instrument suitable for plotting three parameters simultaneously. Writing speed is greater than 500 mm/s for three axes, allowing accurate recordings of fast-changing input signals. Standard features also include a large recording area, a full-scale 100% zero shift, high linearity with use of a linear potentiometer, and a full-scale zero set. Soltec Corp. **411**

Microtrace Si(Li) x-ray analyzer system for electron column instruments features 148-eV detector resolution and a unique trace element capability called Bulk Mode which allows detection of medium Z elements in the 10 ppm range. The liquid nitrogen holding time is guaranteed 10 days, and remote-controlled motor-driven detector positioning is offered. Prices range from $15,000 for semiquantitative systems to $40,000 for computerized quantitative systems. Nuclear Semiconductor **404**

Model FP61 melting point instrument is highly compact and readable to 0.1 °C over a range of 0–300 °C. After insertion of the capillary in the furnace, the rest of the test is automatic. There are five selectable heating and cooling rates: 0.2, 1, 2, 3, and 10 °C/min. The heating process stops automatically as soon as the sample is melted. The final result is held on the display until either the instrument is turned off or another sample run is started. $2750. Mettler Instrument Corp. **405**

Ion Sensing Electrodes

Series IS-146 ion selective electrodes can be used to selectively measure such anions as chloride, sulfide, cyanide, iodide, and bromide. Cations which can be measured include silver, lead, copper, sodium, and potassium. The electrodes come in three different sizes including one model which is 10 in. long and ¼ in. in diameter and is designed for use in flasks or narrow test tubes. The sensing tips are specially formulated solid-state film deposited onto a metallic substrate giving high selectivity and fast response time. They can be used with all existing pH/millivolt meters. Lazar Research Laboratories, Inc. **414**

Chemicals

GC Packings

Spherocarb is a hard, nonfriable, spherically shaped carbon molecular sieve which is excellent packing for the separation of permanent gases, light hydrocarbons and traces of water in organics. Due to its high purity, it eliminates many of the adsorption problems associated with conventional as well as activated charcoal packings. Textured glass beads are also available as a new support. The beads are made from a specially formulated soda lime silica which materially reduces tailing. The textured exterior provides increased surface area for retention of the liquid phase on the support. Two forms are available, regular and DMCS coated. Analabs, Inc. **418**

infrared replacement windows

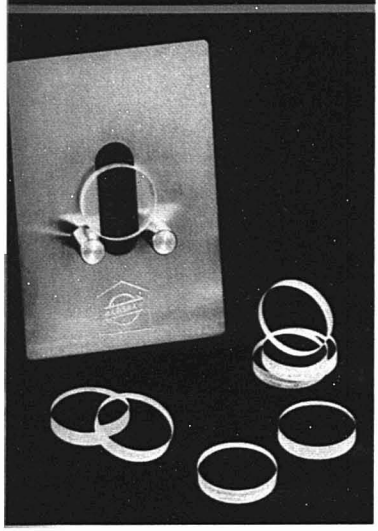

Harshaw IR windows provide optimum transmission at minimum cost.

GUARANTEED QUALITY

Precise IR measurements deserve the consistently high quality of Harshaw's IR windows. Harshaw carefully controls each manufacturing step, including purification, growth, fabrication and crystal polishing. The result is dependable Harshaw quality—at low prices.

PROMPT DELIVERY

IR windows for Perkin Elmer, Beckman, Wilkes and Barnes spectrophotometer accessories are available from stock. Call or write for more information about Harshaw's line of IR windows and accessories — (216) 248-7400

HARSHAW

The Harshaw Chemical Company
Crystal & Electronic Products Dept.
6801 Cochran Road, Solon, Ohio 44139
de Meern, Netherlands: Harshaw Chemie B.V.
Wermelskirchen, West Germany
Harshaw Chemie GmbH
A kewanee INDUSTRY

CIRCLE 98 ON READER SERVICE CARD

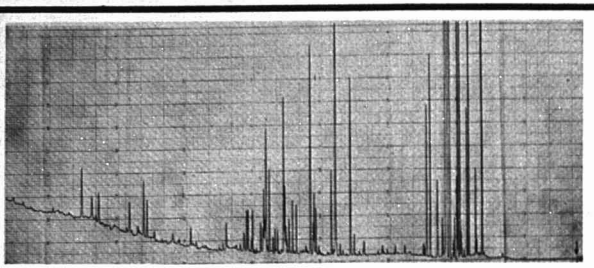

chromatogram

This excellent chromatogram shows the analysis of an Angelica Seed Oil sample on a 102 m long glass capillary column coated with Carbowax 20M liquid phase. Conditions: column temperature programmed from 70 to 240 °C at 2 °C/minute.

SUPERB HIGH-RESOLUTION GLASS CAPILLARY COLUMNS FOR GAS CHROMATOGRAPHY

These inert, magnificent high-resolution open tubular glass capillary columns prepared by the use of a unique and very advanced thin-film technology are available in lengths up to 100 meters. Because of the novel coating procedure, many stationary phases now can be used in the 240– 280+ °C temperature range. The high-efficiency columns can be readily installed in any modern gas chromatograph equipped with either a split-flow or splitless sample introduction system.

Columns 0.75 mm O.D. by 0.25 mm I.D. coated with the following eight phases are available from stock:

OV-101	Carbowax 20M
SE-30	FFAP
OV-17	SILAR 5 CP (Silicone ASI)
OV-275	SILAR 10C (APOLAR 10C)

Custom-made columns coated with other liquid phases are prepared upon request.

Each column is tested with a sample conforming to the characteristics of a particular liquid phase; orders for custom-testing with a special sample are also accepted.

Special discounts are available on three- and four-column packages consisting of columns of different polarity. These combinations represent the most reliable and economical way to introduce sophisticated high-resolution gas chromatography to your laboratory.

Write for brochure and price list.

QUADREX CORPORATION

Post Office Box 993
Darien, Connecticut 06820
Tel: (203) 655-0526

CIRCLE 186 ON READER SERVICE CARD

Manufacturers' Literature

Columns and Packings for HPLC. Describes Zorbax and Zipax packings, a new line of size exclusion columns, and a series of preparative columns. 12 pp. Du Pont Co. **421**

Flame Photometers. Features Models 430 and 450 digital readout instruments. Both have built-in capability for Na, K, and Li determinations. Corning Scientific Instruments **422**

Multipurpose GC Inlet System. System facilitates splitless injection on open tubular columns. Best suited to trace-component analysis and complements conventional sample splitting techniques. ANGC 4-76, 6 pp. Hewlett-Packard Co. **423**

Gas Chromatograph. Specifications and description of the GC-mini 1 are given. This very compact GC features a flame ionization detector and temperature programmer. 6 pp. Shimadzu Scientific Instruments, Inc. **424**

Scanning Electron Microscope. Describes the simple and compact Stereoscan 600 system in detail, along with all of its optional capabilities. 15 pp. Cambridge Instrument Co., Inc. **425**

Continuous Gas Monitors. Describes a series of new trace level analyzers with photoionization detection designed to meet requirements of continuous monitoring in process streams, stack gases, or ambient air. 6 pp. HNU Systems Inc. **426**

Programmable Calculator. Model 31 data acquisition and control system is featured as an OEM component for analytical systems in such areas as industrial, laboratory, and medical applications. 6 pp. Tektronix, Inc. **427**

Analytical Instrument Line. Features the complete line of products from the Instrument Group. Includes gas and liquid chromatographs; UV–VIS and AA spectrophotometers; NMR, EPR, and mass spectrometers; electromagnets; electrometers; and instrument data systems. 8 pp. Varian Instrument Group **428**

GC Valve Automation Accessories. Several new valve programmers and accessories for automating GC valves are presented. 6 pp. Carle Instruments, Inc. **429**

Spectrophotometer Cells. Reference chart includes over 180 cells including self-masking cells, quartz and optical glass cells, disposable cells, and flow cells. Markson Science Inc. **430**

Chromatography Newsletter. Describes four applications in the field of liquid chromatography. Vol. 4, No. 1. 13 pp. Perkin-Elmer Corp. **431**

Gas Analysis by GC. ANGC 3-76 gives details on an automated analyzer, which performs an entire analysis of gas extracted from electrical transformer oil with a single sample injection of only 0.5 ml. 5 pp. Hewlett-Packard Co. **432**

Light and Light Measurement Components. Features instruments for the generation and detection of light including monochromators, light sources, and photo detectors. 6 pp. Schoeffel Instrument Corp. **433**

Gas-Chrom Newsletter. May/June issue features articles on aflatoxin standards, *t*-butyldimethylchlorosilane/imidazole reagent kits, and the Kalrez HPLC septums. 8 pp. Applied Science Laboratories, Inc. **434**

Paired-Ion Chromatography. Describes a highly efficient method of separating and analyzing both ionic compounds and mixtures of ionized and nonionized material. 13 pp. Waters Associates **435**

Pollution Brochure. Features apparatus for analysis of environmental pollutants including glassware, pH meters and electrodes, conductivity meters, and water stills. 24 pp. Tudor Scientific Glass Co. **437**

Excitation Source. The HCD-unit, a hollow cathode-like excitation source designed for analyses of plane metallic samples and pellets of pressed powder samples, is described. 12 pp. Spectroscandia AB, SF-21660 Nagu, Finland

NMR Spectrometer. Describes the FX100 high-performance multinuclear 100-MHz FT–NMR spectrometer and the full line of accessories and extension kits. 24 pp. Jeol Analytical Instruments, Inc. **438**

For more information on listed items, circle the appropriate numbers on one of our Readers' Service Cards

Sulfuric Acid. Provides complete information on the various grades available along with handling suggestions and possible applications. 4 pp. J. T. Baker Chemical Co. **440**

Catalogs

Fume Hoods. Contains complete selection of standard, induced air, and specialized fume hoods with illustrations and detailed specifications. Duralab Equipment Corp. **443**

Laboratory Supply News. Thirty-sixth edition features many new and useful items including calculators, petroleum testing equipment, and an expanded section of Teflon goods. 64 pp. Laboratory Supplies Co., Inc. **451**

Plotter Chart Paper. Features full line of chart paper to fit Broomall, Calcamp, Houston, and Zeta plotters. 10 pp. Graphic Controls Corp. **452**

Thermometers. Catalog 760 lists the full line of thermometers and accessories available. Helpful technical usage data included. 33 pp. Brooklyn Thermometer Co., Inc. **453**

PHI® EQUIPMENT ANALYZES SURFACES . . . So Who Cares?

YOU SHOULD . . . if you're involved with problems in **CATALYSIS, CORROSION, EMBRITTLEMENT, ADHESION, or SEMICONDUCTOR PROCESSING.** In these fields success or failure is often determined by the composition of the top 25 Å of material. Standard analytical techniques can't analyze a layer that thin. And, if you have no way to study that critical surface layer, you're in trouble. That's where PHI equipment comes in. PHI has major product lines featuring ESCA, Auger and SIMS with a wide variety of accessories.

AUGER tells you what's on the surface and where it is.

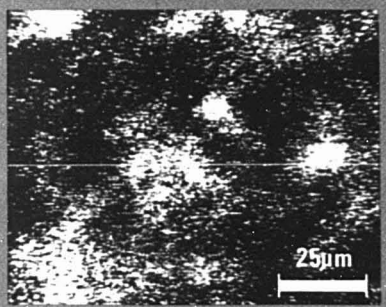

Auger Image showing distribution of nickel on surface of methanation catalyst.

ESCA can tell you the bonding state of what's there.

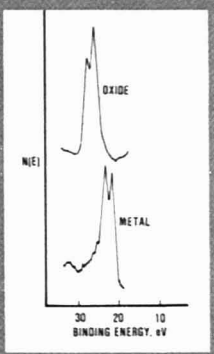

Tantalum 4f ESCA spectra from oxide and metal states.

SIMS can give you ultra sensitivity and isotope separation.

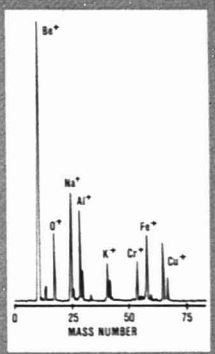

Positive SIMS spectrum showing surface contamination.

And that's just part of our capability.

SO . . . If you're being harassed by surface related problems, maybe you should find out more about PHI. For more details on equipment or analytical services . . .

Call PHI®

PHYSICAL ELECTRONICS INDUSTRIES, INC.
6509 Flying Cloud Drive Eden Prairie, Minnesota 55343
(612) 941-5540 Telex 29-0407

CIRCLE 162 ON READER SERVICE CARD

finnigan GC/MS and Data Systems

Finnigan—the No. 1 in GC/MS instrumentation—offers the most advanced, complete, and flexible GC/MS and data systems available today. Systems that meet every GC/MS analytical need. Systems that provide the best performance/price ratio.

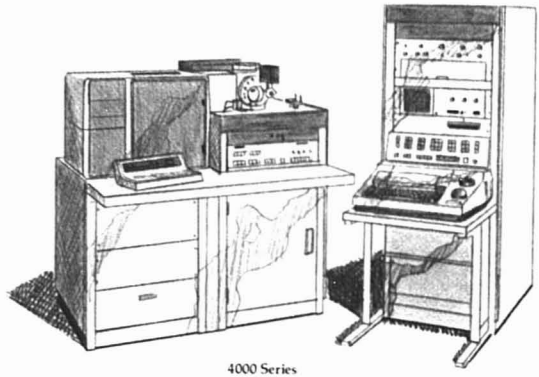

4000 Series

Finnigan 4000 Series GC/MS Systems

The highest performance available in a commercial GC/MS system. The 4000 is a highly flexible instrument, providing both EI and CI operation in the same unique source. Look for new developments to be introduced soon—LC/MS and Negative/ Positive Ion CI.

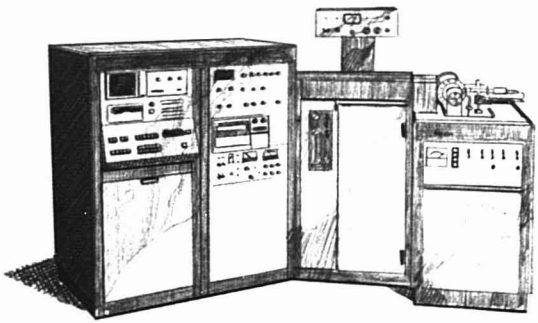

3000 Series

Finnigan 3000 Series GC/MS Systems

The No. 1 GC/MS systems world-wide, both in number of installations and in proven performance and reliability. The complete GC/MS system for operation in EI or CI. And at a price you can afford.

Finnigan/Incos Data Systems

The most advanced data systems on the market. Modular software, simultaneous acquisition and processing, simultaneous interfacing to magnetic or quadrupole systems, or both. Unique features, such as user Fortran programmable, diagnostics programs, isometric mapping, and many more not found in any other data system.

Finnigan 6000 Series Data Systems

From the top of the line Model 6110 to the new low-cost Model 6105, these are unique user-oriented systems with easy pushbutton operation. Ideally suited for total automation of your GC/MS system. Unsurpassed archival storage with low-cost magnetic tape cartridges.

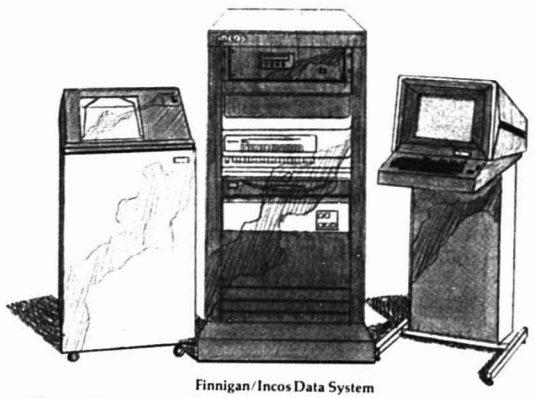

Finnigan/Incos Data System

For all your GC/MS needs, talk to the specialists—talk to Finnigan.

finnigan

845 W. Maude Ave.
Sunnyvale, CA 94086
Munich Basel Hemel Hempstead

CIRCLE 78 ON READER SERVICE CARD

A Guide for Young Professionals

Entering Industry: A Guide for Young Professionals. Fred W. Billmeyer, Jr., and Richard N. Kelley. xi + 281 pages. John Wiley & Sons, Inc., 605 Third Ave., New York, N.Y. 10016. 1975. $14.50

Reviewed by Kenneth W. Gardiner, Applied Science Program, University of California at Riverside, Riverside, Calif. 92502

This is a nicely organized and concise presentation of what can best be described as the "facts of life" relative to pursuing a professional career in industrial science or engineering. As such, the authors specifically direct their comments toward "young professionals"—an apparent initial limitation in appeal that is neatly dispelled by the following prefatory statement: "If you are still in the university, at any level from undergraduate through graduate, post doctoral, and young staff member, to the senior faculty member with a well-developed sense of responsibility to the students; if you have recently entered industry but haven't yet mastered all its ins and outs, learned all you ought to know about it, found your own place in it to your full and lasting satisfaction; or if you have done all these things but are still young in heart, retaining that important desire to find out what makes things work and how you fit into the picture, then you are *young* by our definition." The authors could have also included that rather sizable group of so-called career counselors now to be found as a student service at most universities!

Rather than trying to cover all types of industries that afford scientific and engineering career opportunities, Billmeyer and Kelley have wisely selected the chemical industry as a model, a most appropriate choice in view of their own professional training and experience. In this context, they thoroughly cover all aspects from entry level job applications to the characteristics, responsibilities, and rewards of top management. In effect, this small volume of just some 270 pages is a remarkably complete handbook of the whys and wherefores and the do's and don'ts of getting ahead professionally by really trying.

The subject matter is presented in 12 chapters, with four supportive appendixes. The first five chapters (110 pages) introduce the reader to the chemical industry. Chapters 1 and 2 are replete with facts and figures covering such things as the type, size, and distribution of chemical companies, amounts of money spent on technology, and salary and manpower usage information. Chapter 3 is devoted to the niceties of landing a job in such companies, while Chapter 4 covers the nowadays-all-important area of professional responsibilities. Appendixes I and II provide appropriate examples of guidelines for professional employment and the employment agreement in support of these chapters. Matters pertaining to advancement are dealt with in only 10 pages (Chapter 5), and if the book has a weakness, it is that this critically important aspect is given such short shrift.

Chapters 6–10 outline the workings of those functional departments in typical chemical companies that do afford career opportunities for scientists and engineers. Included are research and development, manufacturing, marketing, staff divisions, and patent functions. This is a most useful and complete treatment and provides a direct answer to that often asked question by students as to what they might do out in the real world.

Chapter 11 is a concise description of management and this reviewer, as a professor of management, was pleased to recognize the works of such familiar, traditional authorities as Maslow, McGregor, Herzberg, Koontz and O'Donnel, and Drucker used as direct quotes and references in this section.

In all, this is a very well-written book in which the authors have certainly achieved their intent. The use of some appropriate and popular media cartoons that have decorated more than one department bulletin board provides an added flair! This reviewer has no hesitancy in recommending it to all "young professionals".

Ion Exchange Chromatography. Harold F. Walton, Ed. xviii + 440 pages. Halsted Press, 605 Third Ave., New York, N.Y. 10016. 1976. $30

Reviewed by L. S. Ettre, The Perkin-Elmer Corp., Norwalk, Conn. 06856

This book is the first in a series representing collections of the most important papers of the development of an analytical technique.

The editor collected 48 papers starting with the 1939 paper of Samuelson on the potentialities of ion exchange in analytical chemistry and ending with the 1973 paper of Davankov et al. on the separation of racemates by means of ligand-exchange chromatography. The book is organized into 13 parts. After the paper by Samuelson which serves as an introduction, the papers are mainly grouped according to application. Thus, we have parts representing the key papers dealing with the analysis of rare-earth mixtures, transuranium elements, isotopes, metals, inorganic ions, nucleotides, amino acids, carbohydrates, and nonionic compounds; besides these, papers dealing with theoretical aspects, the use of mixed solvents, and

Books

inorganic and special exchangers are organized as separate parts.

Each part is introduced by the editor's comments giving the background and importance of the selected papers and their connection with other papers not included in the collection. The individual papers are reproduced in the original form. Papers published in a language other than English are reprinted in the original language followed by a good abbreviated translation. The reproduction is clear and well readable. The only problem is that each page has two page numbers: the page number of the book at the bottom and the original page number of the journal in the running head. This is confusing, and probably the latter should have been deleted.

In such a collection it is inevitable that the selection of the papers represents the editor's preference, and one can always debate whether paper X not included would be more important than paper Y which was included. It is true that the editor, in his introduction, always explains the reasoning for his selection and quotes other papers which the reader might look for. I personally found only two serious omissions: the *very first* paper of Samuelson [*Z. Anal. Chem.*, **116,** 328 (1939)] and the paper by M. Lederer [*Anal. Chim. Acta*, **12,** 142 (1955)] describing the first preparation and use of ion-exchange papers for paper chromatography. I also disagree with deletion of part of the paper of Spackman et al. describing the first recording apparatus for the analysis of amino acids.

As mentioned earlier, the reprints are primarily organized according to the application of the technique. Sometimes this is artificial and thus a number of papers which really deal with the technique itself and its improvements, and are using the application only as an example, are lost in the various parts. The best illustration for this shortcoming is represented by the two papers of Horvath and Lipsky and the paper of Kirkland which—as the editor correctly points out in his introduction—really represent the beginning of modern high-speed liquid chromatography. In these papers nucleotides are only the model substances the researchers happened to use to investigate the influence of operation parameters on the separation and column performance. In my opinion, these papers and some others should have been included in a special part dealing with the advancement of the technique.

This is an important book for everybody active in ion-exchange—and in fact, generally in liquid—chromatog-

raphy. Similar compendiums dealing with the other variants of chromatography would be most welcome.

Statistical Methods for Engineers and Scientists, Vol. 15. Robert M. Bethea, Benjamin S. Duran, and Thomas L. Boullion. xxi + 583 pages. Marcel Dekker, Inc., 270 Madison Ave., New York, N.Y. 10016. 1975. $25.50

Reviewed by David S. Chambers, Department of Statistics, University of Tennessee, Knoxville, Tenn. 37916

This book joins a growing number designed for the increasing market in undergraduate engineering and physical science. The content is similar to that of Walpole and Myers' "Probability and Statistics for Engineers and Scientists" and Freund and Miller's "Probability and Statistics for Engineers". The objective is to provide a basic course in methods. The topics are many and varied, extending from basic probability through regression and experimental design. The book makes no pretense to heavy involvement in the development of theory; it is intended as a source of methods useful to its readers, together with some explanation of the way to use these methods. The authors provide convenient instructions as to which topics should be omitted in the event only one semester is available; it is expected that the entire book will be covered in two quarters.

Many examples are included in the text material, and numerous problems at the end of each chapter have been selected from the literature in science and engineering, providing a decided "applied" flavor. Sources of these problems are frequently cited. A good introductory year of college mathematics should be sufficient preparation, and no previous statistics is assumed. There is an appendix on matrix algebra useful for the regression discussion.

The format is the usual one for Marcel Dekker. If one wishes a book to use in a pragmatic course in statistics, this text might well be considered. In the hands of a trained and experienced instructor, it can be the basis for a satisfactory methods course.

The book is in obvious need of more careful editing, and it is hoped that needed changes can be made through the use of an errata sheet and alterations in subsequent printings. On initial reading, errors ranging from misspelled words to confusing statements were noted on approximately 25 pages (about a 4% error rate). Some examples are cited. Page 123, line 5: "How-

TRY THIS AND ADD ANOTHER DIMENSION TO YOUR LAB

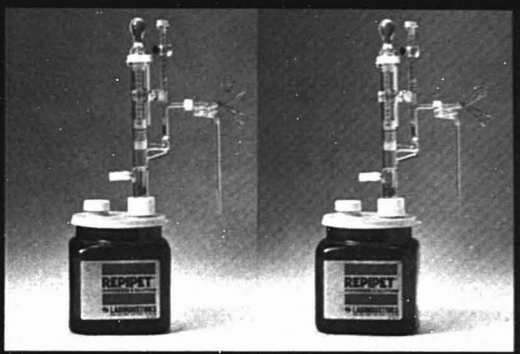

You can see the single-stroke REPIPET® dilutor above in 3-D without any aids whatsoever by following these directions.

It will take a minute the first time, but after you've seen it once, you will always see such pictures in 3-D, instantly. Hold the pictures directly in front of your eyes at your best reading distance. Look right through the pictures at an imaginary object about ten feet away. You'll see three pictures, the central one in 3-D. You may sharpen the focus by bringing the pictures closer or further away. (A few people cannot see the 3-D.)

Like the picture above, the time-saving and improved-precision potential of the REPIPET® dilutor may just take a minute to realize in the following and countless other applications: Clinical and industrial determinations, radioactive cocktails, scintillation counting, deproteinization, atomic absorption dilutions and wherever you add reagent to an aliquot.

You can make a complete dilution in 2 to 4 seconds, 1.5% accuracy, 0.5% precision. Just lift and press. So simple, it's difficult to make a mistake. Keep both hands free. Use the foot-operated model.

Low silhouette single stroke dilutors, $146, $158. Order from your local distributor. For specialized information and/or complete Labindustries catalog with price list contact Labindustries.

LABINDUSTRIES

1802 Second Street/Berkeley, California 94710/Phone (415) 843-0220

© L/I 8-76

CIRCLE 127 ON READER SERVICE CARD

ever, σ^2/n tends to zero as n tends to $\mu \ldots$". The use of $\sigma\sqrt{n}$ instead of $\sigma/\sqrt{n}$ in several places on the same page. The statement on page 181, line 9 that the hypothesis H_o is not rejected at the 99% significance level (the 1% level is intended). The insistence on the use of a *representative* sample (pages 2 and 94) when a random sample is meant.

On page 99 it is stated that data which fluctuate over a wide range will have a large variance (true) and that a large variance indicates data have a wide spread about the mean (true). The authors then state that if the *sample values* are very close together, the sample variance will be quite small (true). They then state that the latter case is highly desirable. The meaning is not clear. Is the advice to draw a sample so that the values are close together? If so, what about the principle of random sampling? Or does it refer to a compact population with a small variance? If so, sampling is not involved. Such offhand advice to the reader leads to reader difficulty. More careful writing will be beneficial.

It is obvious that the authors have vast experience in applying statistical methods to engineering and scientific data. Use of this text might well be considered by others equally experienced. Unfortunately, the reviewer has not had an opportunity to teach from the book, and that is the only way one can become totally aware of its strengths and weaknesses.

Chromatographic Analysis of the Environment. Robert L. Grob, Ed. x + 734 pages. Marcel Dekker, Inc., 270 Madison Ave., New York, N.Y. 10016. 1975. $49.50

Reviewed by Robert K. Stevens, Atmospheric Instrumentation Branch, U.S. Environmental Protection Agency, Research Triangle Park, N.C. 27711

This book with contributions from 19 scientists from academic, government, and industrial laboratories is highly recommended for individuals who are involved in measuring trace contaminants in our environment. The text is an up-to-date survey of gas, liquid, paper, thin-layer, and ion-exchange techniques for air, soil, water, and waste samples.

Despite the wide range of topics covered, the authors are largely successful in presenting a comprehensive review of chromatographic procedures related to environmental analysis.

This reviewer was particularly impressed with the section on air pollution by Robert S. Braman and the sec-

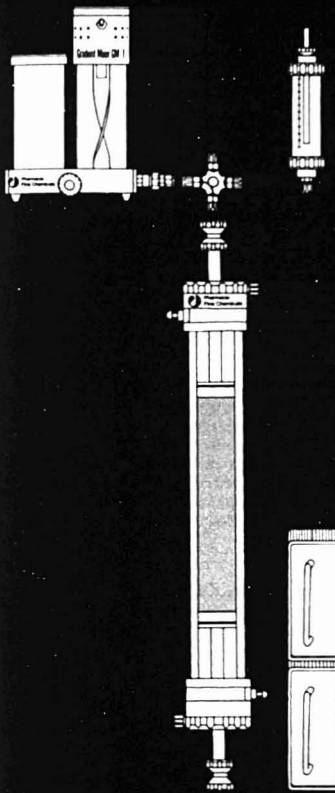

Modular components for liquid chromatography systems

Gradient Mixer GM-1
Valve LV-3
Reservoir R-9
Flow Adaptor A-26
Column K-26
UV Monitor
RI Monitor
Two Channel Recorder

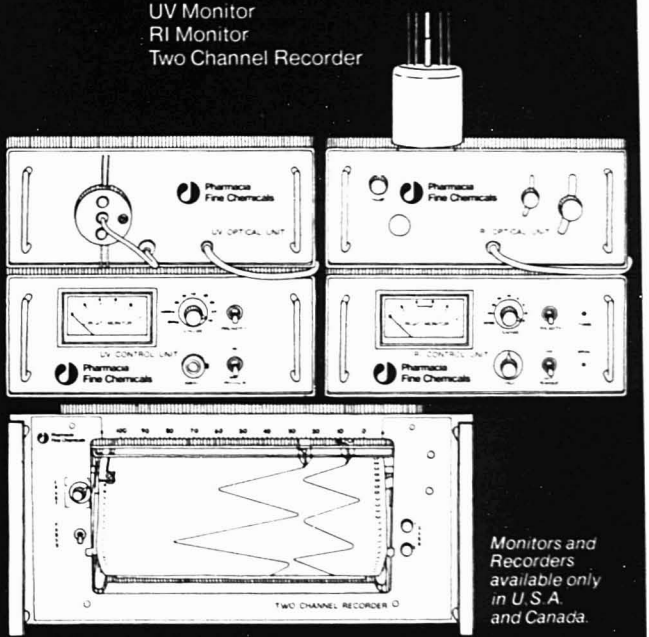

Monitors and Recorders available only in U.S.A. and Canada.

Pharmacia Fine Chemicals
Division of Pharmacia, Inc.
Piscataway, New Jersey 08854
Phone (201) 469-1222

Pharmacia Fine Chemicals

For additional information write or call PHARMACIA FINE CHEMICALS INC., Piscataway, New Jersey

CIRCLE 169 ON READER SERVICE CARD

tion on thin-layer chromatographic analysis in air pollution by Daniel F. Bender and W. C. Elbert. These sections contained considerable detail and discussion of GC and thin-layer methods for a variety of pollutants. The reviews contained enough detail of the original work to make it easy for the reader to select the best method for a particular analytical problem.

The chapters dealing with soil and waste analysis contained valuable information on the types of substances that generally occur in these media and the chromatographic methods that have been employed for their analysis.

There is some theoretical discussion; however, the emphasis is on the practical application of chromatographic principles to analytical problems. For example, several of the chapters provide valuable and detailed information on calibration of GC's which is often overlooked in some reviews.

Chapter 1 deals with the theory and practice of chromatography, is well organized, and is an excellent primer for beginning chromatographers.

Although the book is generally free from errors, the reviewer found to his dismay that his initials had been changed from R. K. to R. H. (Ref. 55, Chapter 2) and that O'Keeffe was misspelled in Ref. 55, Chapter 2.

New Books

An Introduction to Microcomputers, Vol. 1: Basic Concepts. xvii + 287 pages. Adam Osborne and Associates, Inc., 2950 Seventh St., Berkeley, Calif. 94710. Publication No. 2001. 1976. $7.50 (add 30¢ for surface mail and $2.50 for airmail)

Following a great success with the first edition published December 1975 (reviewed in ANALYTICAL CHEMISTRY by Raymond Dessy, 777 A, August), Osborne & Associates are now offering the first installment of the expanded second edition in two volumes. Volume 1 is approximately the equivalent of Chapters 1–6 of the first edition, but extensive sections have been added to cover two topics which were left out of the first edition—chips slice products and serial I/O. The aim of the book is to give the reader a thorough understanding of what microcomputers are and how they differ from other computer products from a user's point of view, and ultimately to enable the reader to develop the capability to select the right microcomputer for the particular application at hand. Since the book does not assume any prior contact with computers on the part of the reader, basic concepts are covered in considerable detail.

Emission Spectroscopy. Ramon M. Barnes, Ed. xii + 548 pages. Halsted Press, 605 Third Ave., New York, N.Y. 10016. 1976. $35

Compiled in this volume are reproductions of selected papers which have made landmark contributions to the development of emission spectroscopy over the last 100 years. The papers are arranged in a semichronological order, beginning with a description of the history and literature of spectrochemical analysis. The contributions between 1860 and 1930 are grouped in Part I. Part II concentrates on the growth of quantitative emission methods stimulated by developments in emulsion calibrations, spark sources, grating ruling and replication, multiplier phototubes, and techniques

for solids, solutions, and microsamples. Semiquantitative and universal methods, advances in continuous current discharges (arcs), and matrix effects highlight Part III. The applications of the time-resolution technique keynote Part IV, and the development of emission sources other than arcs and sparks is emphasized in Part V. Part VI surveys the present state-of-the-art.

Advances in Mass Spectrometry in Biochemistry and Medicine, Vol. 1. Alberto Frigerio and Neal Castagnoli, Eds. 586 pages. Halsted Press, 605 Third Ave., New York, N.Y. 10016. 1976. $40

This volume contains the proceedings of the 2nd International Symposium of Mass Spectrometry in Biochemistry and Medicine held June 1974 in Milan, Italy. The conference was sponsored by the Mario Negri Institute for Pharmacological Research to provide an opportunity for the continued exchange of information in the rapidly expanding application of mass spectrometry for the analysis of biologically active compounds. Fifty-one papers contributed by over 140 authors examine all aspects of mass spectrometry, gas chromatography–mass spectrometry, and gas chromatography–mass spectrometry–computer systems for the analysis of complex mixtures of biological origin.

Continuing Series

Residue Reviews, Vol. 60. Francis A. Gunther, Ed. vi + 160 pages. Springer-Verlag New York Inc., 175 Fifth Ave., New York, N.Y. 10010. 1976. $18.80

"Sumithion" is a trade name registered by Sumitomo Chemical Co., Ltd., of Japan for its proprietary formula *O,O*-dimethyl *O*-(3-methyl-4-nitrophenyl) phosphorothioate, an organophosphorus insecticide having a broad range of insecticidal effect and yet having low toxicity to mammals and fish to make its handling of less concern. Much of the information compiled in this volume on "Sumithion" comes from members of Sumitomo Co. engaged in the research and development of the compound. Five chapters written by 13 authors concentrate on discussions of different chemical aspects of the compound. The first two chapters review general chemistry and available analytical methods used to determine the compound when it is present in technical products and formulated materials. The next two chapters discuss formulation of "Sumithion" and its effect on biological systems. Finally, the last chapter describes the residue analysis. Also included in this 60th volume of the series are (as in volumes 10, 20, 30, 40, and 50) an abbreviated 10-volume table of subjects, a 10-volume author index, and 10-volume cumulative subject matter index.

Separation and Purification Methods, Vol. 4. Edmond S. Perry, Carel J. van Oss, and Eli Grushka, Eds. Marcel Dekker, Inc., 270 Madison Ave., New York, N.Y. 10016. 1976. $32.50

The separation and purification techniques reviewed in this volume are at least as diverse as they were in the previous three volumes. They range from modernized distillation methods to modern countercurrent distribution techniques, to name only a few. Seventeen authors of this volume are all new to the series. The extensive literature references provided

Books

at the end of each chapter include some as recent as 1975. The text is reproduced from author-furnished typewritten manuscript.

Encyclopedia of Electrochemistry of the Elements, Vol. VI. Allen J. Bard, Ed. xiv + 341 pages. Marcel Dekker, Inc., 270 Madison Ave., New York, N.Y. 10016. 1976. $64

The aim of the series is to provide a critical and comprehensive review of the electrochemical behavior of the elements and their compounds. The elements covered in each volume are grouped together according to the organizational scheme devised for the series. The elements reviewed in this volume by eight contributors include Al, In, Ir, Os, Pd, Pt, Rh, Ru, Sc, Y, and lanthanides. Each of the nine chapters is organized into five sections of introduction and standard potentials, voltammetric characteristics, kinetic parameters and double-layer properties, electrochemical studies, and applied electrochemistry. The book is a photo-offset copy of typewritten text.

Applied Spectroscopy Reviews, Vol. 10. Edward G. Brame, Jr., Ed. xv + 305 pages. Marcel Dekker, Inc., 270 Madison Ave., New York, N.Y. 10016. 1976. $32.50

Unlike its predecessors which reviewed primarily vibrational spectroscopy, this volume devotes more attention to emission spectroscopy. In addition to emission spectroscopy there is coverage in the fields of photoelectron, nuclear magnetic resonance, mass, fluorescence, and ultraviolet spectroscopy. The first review is by R. T. Bailey and F. R. Cruickshank on applications of infrared fluorescence. The second review on biomedical applications of selected ion monitoring is written by workers from the School of Medicine at Vanderbilt University, F. C. Falkner, B. J. Sweetman, and J. T. Watson. The next review by R. K. Harris and B. J. Kimber covers ^{29}Si NMR spectroscopy. The fourth review by G. K. Oertel and G. L. Epstein treats a broad area of study in the applications of spectroscopy to solar research. The next one by P. J. Slevin and W. W. Harrison on the hollow cathode discharge as a spectrochemical emission source describes the use of this emission source as well as its fundamental principles of operation. Finally, the last review by G. K. Schweitzer on elevated temperature vapor photoelectron spectroscopy covers a field that is undergoing a rapid rise in use. The book is reproduced from typewritten text.

Filter paper in Kent, England won't help your lab in Oklahoma City.

Our worthy competitor manufactures most of his filter paper in Kent, England. Which can leave the lab person here in a position of waiting for weeks for his ship to come in.

Schleicher & Schuell® filter papers are made in this country, so they're available to do the job when the job needs to be done.

But readily available supplies and prompt delivery aren't all you get when you buy from Schleicher & Schuell. S&S has been making quality papers for over a hundred years. We not only have more filter paper on hand, we have more different kinds on hand. Papers you can order by brand name, and by what you want to do with them—application; nature of the fluid being filtered; size, quantity and nature of the substance being retained; desired output; filtration method; and degree of precision required.

Yes, look for our name on the package. But also look for the exact type of paper you need. S&S has it—in stock.

Think about that the next time you're at sea over a filter paper order.

Contact your laboratory supply dealer for fast delivery from stock, or more information. Or send for our complete catalog, 'Products for Separation Science'.

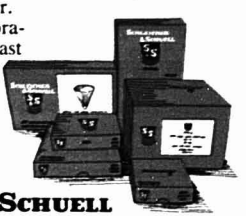

SCHLEICHER & SCHUELL

Keene, New Hampshire 03431

Schleicher & Schuell GmbH, D-3354, Dassel, West Germany

Schleicher & Schuell AG, 8714 Feldbach ZH, Switzerland

CIRCLE 195 ON READER SERVICE CARD

Analytical eXcellence with PGT X-ray fluorescent systems

The PGT-500 X-ray Spectrochemical Analyzer features:

- ☐ rapid, nondestructive X-ray fluorescence analysis
- ☐ simultaneous analysis of up to 82 elements—from sodium through uranium
- ☐ Si(Li) detector for high resolution analysis
- ☐ unique pulsed or constant current air-cooled X-ray tube
- ☐ functional keyboard commands and pushbutton controls for ease of operation
- ☐ qualitative and quantitative data processing equipment that is both automatic and user programmable
- ☐ automatic data acquisition, processing and storage
- ☐ mass storage capabilities
- ☐ 18-sample, drop-in carousel with automatic and manual sample sequencing
- ☐ minimal sample preparation for analysis of samples in liquid, powder or solid form
- ☐ detectability levels between parts-per-million and 100 percent
- ☐ nonfocusing X-ray optics
- ☐ automatic or manual operating modes
- ☐ modular and compact construction
- ☐ interfaces for peripheral equipment

PGT

PRINCETON GAMMA-TECH

Box 641 • Princeton, N.J. 08540 • Tel: 609 924-7310 • Cable PRINGAMTEC • Telex: 843486

CIRCLE 172 ON READER SERVICE CARD

Editors' Column

Microprocessors Impact Analytical Instrumentation

Since it seems highly likely that most new analytical instrumentation is going to be based in part on microprocessor technology, it behooves the analytical research community to have some understanding of the capabilities and limitations of this latest technology. The term *microprocessor* was coined to reflect its limited functions when compared with computers; thus, it represents something less than a microcomputer. (See "An Introduction to Microcomputers. Vol. I. Basic Concepts" by Adam Osborne, listed on page 996 A, this issue.) However, these distinctions between microprocessor and microcomputer have blurred with usage so that both terms are used to represent logic devices on chips.

Microcomputers are usually comprised of 1–5 or so chips with other support chips to control and interface. The key costs are associated with memory chips. Custom-designed chips now available normally contain 4–8 bits. Predictions are that perhaps in 5–8 years, most 16-bit processors will also be in chip form. Volume applications of microprocessors, however, are likely to be in 8-bit processors.

Will microprocessors replace minicomputers, and how do they differ? Microprocessors are three to five times slower than minicomputers, and, of course, minicomputers have much more capability. Microprocesors can readily be coded to do specific functions and will probably find use as support components to larger minicomputer systems. However, it appears that microprocessors will replace minicomputers only where the latter now represent overkill: too much function for the job at hand.

These devices vary so much one from another, and this state of flux and lack of standardization are apt to continue for some time. As is often the case, the software presents a problem, and getting people skilled in programming these devices is difficult.

Applications of these devices in consumer products such as TV games, automobiles, and appliances will be forthcoming. What is their role in analytical instrumentation? It has been suggested that their introduction will have revolutionary effects on instrumentation. Closer questioning and further examination of their likely uses, however, suggest that the effects will be evolutionary rather than revolutionary. Their incorporation into analytical instruments is spurred by their cost effectiveness, reliability, and ease with which they can be designed to do specific jobs. Instruments so designed will be easy to use, reliable, and less expensive. Designing for improved performance in individual instruments up to this point has added not only money, but complexity. Microprocessors can provide improved performance with greater simplicity and less cost. Although these results are highly desirable, they do not seem to be revolutionary.

Instruments with microprocessors have great sales appeal, so much so, that it might be tempting to use microprocessors in applications where hardwiring would be a better solution. At any rate, it seems certain at this time that analytical instruments under development will include microprocessors.

Data Validity

Information theory and complex statistical techniques are making their contributions to analytical chemistry research efforts. The computer learning techniques including pattern recognition have now reached the point where applications are reported. The very existence of computers with their ability to handle efficiently and well reams of data has tempted technological sophisticates to move in these directions. Also, the real complexity of some measurement problems would appear to be ideally suited to these treatments. However, is it not possible to use these methods past the point of their usefulness to try to extract more information from data than is really there? Detector signals can be improved by certain signal-to-noise enhancement methods and data manipulated readily via the computer, but there is still a limit to how much information is contained in the data. The analyst cannot lose sight of the fact that the validity of the data is still basically tied to the real sample, the real detector, and the actual measurement scheme with all the limitations and variables involved therein. Especially when the applications involve real situations with legal, economic, and social implications, the analyst must be certain that his data-handling methods have statistical validity and his conclusions are supported by the data collected.

Josephine Petruzzi

A NEW WINNER!

GILSON RACE TRACK FRACTIONATOR for liquid chromatography

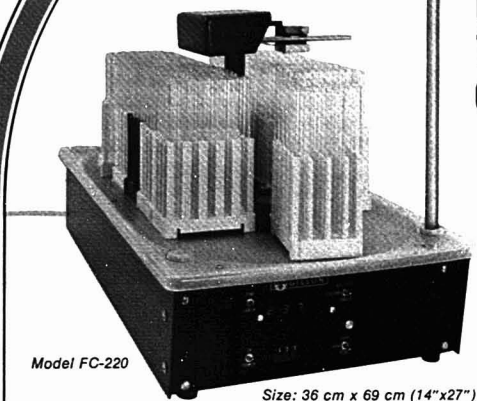

Model FC-220

Size: 36 cm x 69 cm (14"x27")
Weight: 13 Kg (28 lbs.)

- 220 test tubes (18 x 150 mm)
- Drop counting-time
- Control box can be removed for remote operation
- Shut-off for column effluent and pump
- Electronic digital counter
- Rugged construction prevents jamming of racks

The Gilson FC-220 RACE TRACK FRACTIONATOR is the newest addition to the Gilson Fraction Collector family. It contains eleven Polypropylene racks which move in a recirculating oval race track pattern. Each racks holds 20 glass test tubes (18 x 150 mm). Thus, 220 tubes can be collected during unattended operation or collection can be continued indefinitely, without interruption, by periodically removing filled test tube racks and adding empty racks.

A single-piece molded Polypropylene pan prevents spillage and foreign material from falling into the lower mechanism.

Multiple-column collection can be performed from 2 to 5 columns.

An accessory solenoid shut-off valve is available for stopping the column flow after the last tube is filled, to prevent drying of the column packing. It also stops column flow while changing from one test tube to the next.

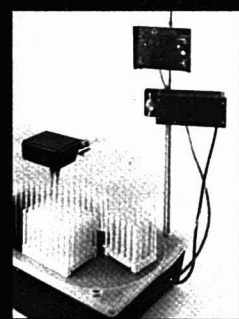

Model FC-220 with control box and shut-off valve mounted on mast

Call or write TODAY

GILSON MEDICAL ELECTRONICS, INC.

P.O. BOX 27, MIDDLETON, WISCONSIN 53562 • TELEPHONE 608/836-1551

EUROPEAN MANUFACTURING PLANT

Gilson Medical Electronics
69, rue Gambetta, 95-Villiers-le-Bel, FRANCE
Telephone 990-54-41

CIRCLE 88 ON READER SERVICE CARD

William L. Switzer
Department of Chemistry
North Carolina State University
Raleigh, N.C. 27607

Asynchronous Serial Computer Interfaces

In their REPORT in ANALYTICAL CHEMISTRY, Dessy and Titus (*1*) reviewed many problems associated with computer interfacing. They discussed trade-offs in selecting and/or designing an appropriate interface. Particularly noteworthy was their "TTL" principle which describes the trade-offs among *T*ime, *T*alent, and *L*ucre. The reason often given for designing an interface oneself is to save money. But building an interface from components is inexpensive if and only if the costs associated with time and talent can be neglected or at least amortized over a number of projects. A better reason may be that the experience gained in designing one's own interface can greatly simplify future interfacing problems.

With even minimal knowledge of the philosophies of digital data transmission, the scientist with some background in digital electronics can design in block diagram fashion a digital data link between his laboratory instrument and a computer or a teletypewriter. On considering his block diagram in more detail, he will likely become discouraged at the straightforward but extensive circuitry required. Designing such a circuit from small- and medium-scale integrated circuits is not practical for most novice circuit designers. Starting from large-scale integrated circuits or multicomponent circuits will still offer many design challenges. Herein lies the purpose of this article, to examine the problems and some solutions for designing an interface between the user's laboratory instrument and a computer or teletypewriter. This article deals with a very specific, but generally applicable, type of interface in which the user's parallel TTL (*T*ransistor *T*ransistor *L*ogic) output is transmitted in an asynchronous serial fashion.

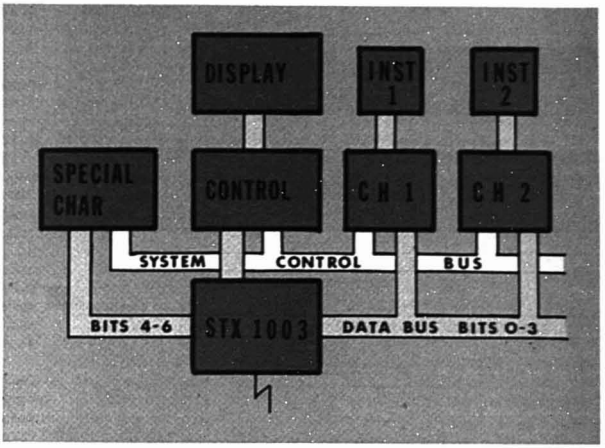

Figure 1. Multichannel asynchronous serial transmitter
Block diagram shows two instruments connected to two active channels

Data Codes

Before proceeding, let us review the concepts of a digital code and the two methods for transmitting that code: parallel and serial. (This subject is discussed extensively in ref. *1*). A digital code is a string of *bi*nary digit*s*, or bits. This string of bits, logic 0's and 1's, has a unique meaning to the interpreter. The three most popular codes are binary, *B*inary *C*oded *D*ecimal (BCD), and *A*merican *S*tandard *C*ode for *I*nformation *I*nterchange (ASCII).

In Table I the decimal number 15 is shown in each code. In each case there is a one-to-one relationship between the decimal number and its digital code. The binary code is simply the base 2 representation of the number which is 1111_2; this code requires the fewest bits for representing any number. The BCD representation for 15 is the base 2 representation of each decimal digit and is $0001_2\,0101_2$; this code is the easiest for converting between decimal and BCD. The ASCII representation precedes each BCD digit with the three bits 011_2 (for numeric data); thus, 15 is $0110001_2\,0110101_2$. The extended word length of the ASCII code allows one to represent as a string of bits, not only numeric characters, but also alphabetic and special characters.

These digital codes should not be confused with octyl (base 8) and hexadecimal (base 16) codes which are merely shorthand representations of the binary codes shown in Table I. Digital interfaces always involve only two "levels" of information, logic 0 and logic 1, *not* 8 or 16 as might be inferred from the use of these bases.

Parallel vs. Serial Transmission

If each bit of the digital code is simultaneously available, the code is presented in parallel. If each bit is sequentially available (one bit at a time) starting with the least significant bit, the code is presented serially. With serial data exchange, timing becomes especially important since each bit in the code must be transmitted and received during a finite time interval from the beginning of the transmission. Data exchange between transmitter and receiver is synchronized using digital timing techniques. Two

Table I. Digital Codes for Decimal Number 15

Code	Binary (base 2) representation	Octyl (base 8) representation	Hexadecimal (base 16) representation
Binary	1111_2	17_8	F_{16}
BCD	$0001_2 0101_2$	025_8	15_{16}
ASCII	$0110001_2 0110101_2$	$061_8 065_8$	$31_{16} 35_{16}$

methods are commonly employed: synchronous and asynchronous serial data exchange. Synchronous receivers and transmitters use a common clock, while asynchronous devices use separate clocks operated at the same frequency. Synchronous devices transmit each bit only during specified pulses of the clock, while asynchronous devices transmit data whenever it becomes available. For this reason asynchronous transmission is more suitable for interfacing both chemical instrumentation and devices such as keyboards, which produce data randomly with respect to any clock pulses. A more detailed comparison of the two methods of serial data exchange is discussed by Finkel (2), but further consideration here will be limited to asynchronous serial data exchange.

Consider the problem of transmitting 8 bits of digital data. In parallel transmission, 8 transmission lines plus a reference line (9 total) are required; in serial transmission, only 1 line plus a reference (2 total) are required. The main advantage of serial transmission is that it requires only a single pair of wires. When transmitting across a room, wiring 9 transmission lines and their associated connectors is practical, but when transmitting to a remote location, dual-line transmission is usually more practical. Even when transmitting short distances, if the data are transmitted to different receivers on different occasions, the scientist will quickly tire of wiring multipin connectors. Thus, considering the number of transmission lines, serial transmission is simpler.

Disregarding for the moment the obvious requirement of more complex electronics to "catch" data "on-the-fly", another obvious disadvantage of serial transmission is that data are transmitted more slowly. At first glance it should take eight times longer to transmit 8 bits serially than in parallel. The situation is actually somewhat worse. Consider the serial transmission mode used by a teletypewriter. In addition to a 7-bit ASCII character, a parity bit, a start bit (signaling the beginning of transmission), and two stop bits (a "rest" interval between transmissions) are required. Thus, a total of 11 bits is transmitted in order to transmit the 7-bit code. One loses about a factor of 10 in the transmission speed.

Returning to the illustration in Table I, one sees that the fastest way to transmit the number 15 requires transmitting the binary code in parallel. The slowest way requires transmitting the corresponding ASCII code in a serial fashion; this method requires 22 times longer (2 characters × 11 bits each), presuming the serial and parallel receivers accept bits at the same rate. Nevertheless, transmitting serial ASCII code has the advantage of being nearly universally accepted by teletypewriters (if transmitted at 110 baud) as well as nearly all computers. (The baud rate is the transmission rate; 110 baud means 110 bits/s, *but* these bits include the 7-bit code, the parity bit, the start bit, and two stop bits. Each character requires that 11 bits be transmitted; thus, one character is transmitted every 100 ms at 110 baud.) With many computers the baud rate may be greatly increased, thus increasing the transmission speed. Besides being compatible with computer hardware, serial ASCII is also compatible with most computer software. Many Basic and Fortran compilers can perform I/O directly in the ASCII code. Considering both hardware and software interfacing problems, serial ASCII data transmission is highly desirable despite its slowness and possible problems in generating the ASCII code.

Thus far, primarily data transmission has been discussed. The reverse operation, data reception, must also be considered. Herein the serially

Fireworks or Fireflies

Get your data on the fly

Spectra shown below were acquired from a living firefly (presently in retirement in rural New Jersey) and from a Bicentennial Fourth of July aerial display. The storage capacity and high sensitivity of the Optical Multichannel Analyzer (OMA®) enabled us to acquire a spectrum from George, the firefly, at his convenience. He was neither vivisected nor was he shocked. George prefers this kind of data acquisition, perhaps you will too.

A fireworks display such as the one shown here is beyond George's best efforts, but no difficulty at all for the OMA. The OMA was set up several hundred meters away and spectra were acquired for nearly every shot. Identical techniques can acquire spectra of explosions, flash lamps and other transient phenomena.

These spectra illustrate how the sensitivity and single shot capability of the OMA can simplify data acquisition for you. While fireflies may not be at the forefront of bioluminescence technology, other critters such as cancer cells are presently being analyzed in vivo with OMAs. Similarly, fireworks are not frequently optically analyzed, but many researchers need better spectra data acquisition techniques to avoid fireworks in the laboratory. For more information and specific applications advice about our OMA Systems, write or call.

Model 1208 Polychromator with Model 1205D Intensified Detector Head and Model 1205A OMA Console

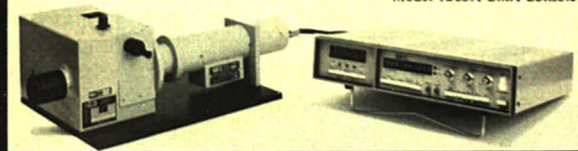

OMA spectrum of a single aerial burst

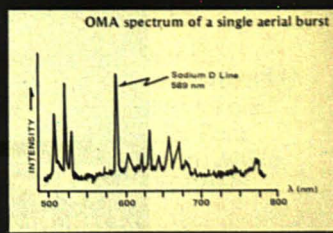

Single flash from firefly (photinus sp.)

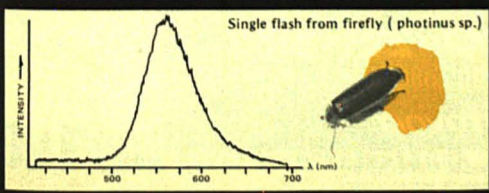

Princeton Applied Research Corporation

P. O. Box 2565 • Princeton, New Jersey 08540 • U.S.A.

Telephone: 609/452-2111 • Telex: 84-3409

CIRCLE 173 ON READER SERVICE CARD

transmitted string of bits must be received "on-the-fly" and converted to a parallel format. Any start and stop bits, which were added on transmitting, must be removed on receiving; also, the parity must be checked, and an appropriate error output set.

Universal Asynchronous Receiver/Transmitter—UAR/T

Although simple in principle, transmitting and receiving data serially require rather sophisticated electronics. The novice would be wise to avoid starting from basic TTL gates. However, a large-scale integrated circuit called a UAR/T (General Instrument Corp., 600 W. John St., Hicksville, N.Y. 11802) is available which sacrifices little in general applicability. In fact, it would be both time consuming and expensive for the novice to design such a versatile system from scratch.

The UAR/T consists of separate transmitter and receiver sections. The transmitter accepts bit-parallel input and produces bit-serial output; the receiver accepts bit-serial input and produces bit-parallel output. The transmitter and receiver may be operated independently of each other (full duplex) or in series (half duplex), meaning that whatever is transmitted is also received. The number of bits in the code can be selected (5–8 bits; ASCII is a 7-bit code). An optional parity bit may be added to the code when transmitting or deleted when receiving (an error flag is set if appropriate), and the parity may be selected even or odd. The UAR/T also adds the start bit and stop bit(s) (one or two stop bits may be selected) when transmitting and deletes them when receiving. The UAR/T also provides two status outputs, one indicating that the transmitter buffer is empty, the other indicating that the receiver buffer is full. The baud rate is determined by an external clock.

All inputs and outputs on the UAR/T are TTL compatible. Most modern devices, which are likely to be interfaced with the parallel inputs and outputs, will be TTL compatible. However, serial input and output devices are often not TTL compatible. The two most popular logic conventions are current loop and RS-232. Current loop, which is used by conventional teletypewriters and, hence computers with teletype interfaces, specifies that logic levels 0 and 1 are nominally 20 and 0 mA, respectively. RS-232, which is used by most modems, specifies that logic levels 0 and 1 are +5 to +15 and −5 to −15, respectively. (Modem is a device which codes and decodes logic 0 and 1 as two different frequencies. This is generally used for long distance data links.)

Converting between TTL logic levels and current loop or RS-232 and vice versa is quite easy. Larsen and Rony (*3*) give simple circuits for accomplishing this conversion. With TTL, current loop, or RS-232, interfacing can nearly always be accomplished.

For transmitting a single character serially, the UAR/T requires little more than connecting the parallel inputs and starting transmission, while receiving a single character requires little more than sampling the parallel outputs when the device indicates data are available. However, most scientists wish to transmit more than a single character. The UAR/T requires that each character (or word) be loaded in a word-serial, bit-parallel fashion. Building a transmitter/receiver from a UAR/T still requires considerable electronic design to load in this fashion. For many applications, such as transmitting data from a digital panel meter, the data are available in a word-parallel, bit-parallel fashion. The designer must therefore convert from this word-parallel format to a word-serial format. On command to

(*Continued on page 1010 A*)

Run repetitive LC analyses unattended with the Du Pont 848 System.

It's 1:00 a.m. The QC lab is dark—except for the lights on the Du Pont 848 High Performance Liquid Chromatography System. It's busy running the samples programmed the previous afternoon.

Day or night, the Du Pont 848 HPLC System offers you complete automation for repetitive analyses.

It runs up to 95 samples and performs duplicate or triplicate analyses, if needed, without operator attention.

The system can perform in all chromatographic modes of separation, including size exclusion (GPC). It incorporates true flow-feedback control, pulse-free delivery, wide flow rate range and high sensitivity detectors. The automatic sampler module in this system also is compatible with other liquid chromatographs.

Learn about the full capabilities of the 848 HPLC System by writing for our new brochure. Du Pont Instruments, Room 24026, Wilmington, DE 19898.

Du Pont Instruments

DU PONT

CIRCLE 59 ON READER SERVICE CARD

...announcing the

7th Technicon International Congress
December 13-15, 1976
The New York Hilton, New York City

"Advances in Automated Analysis and Information Systems"

Technicon Industrial Systems will assume a major role in the forthcoming 7th Technicon International Congress with symposia on automated analytical chemistry affecting virtually every area of interest.

Time and technology never stand still. Many advances in methodology, by themselves, may not appear to have major impact. Many small refinements in instrumentation may not appear noteworthy when singled out. Expanding legislation and its resultant regulatory impact play a distinct role in the needs of the analytical laboratory. Rising costs create a demand for more effective analytical procedures. And, of course, major instrumentation developments with their relevance to the laboratory, the economy, industry, food and agriculture, always stand out.

Only in a meeting having the magnitude of an international congress can these individual influences be focussed to form the complete picture. Technicon is proud to present this forum, where dedicated analytical scientists can receive and review the current state of the art from all directions. Over 75 papers will be presented, and more than 4,500 square feet will be devoted to exhibits displaying the latest automated analytical systems and instrumentation.

Major papers covering legislation, economic impact, technical developments in instrumentation and methodologies will be presented under 5 categories of Industrial Symposia:

1. Automated Instrumental Analysis and the Environment
2. Automated Instrumental Analysis and the Food Supply
3. Automated Instrumental Analysis and the Pharmaceutical Industry
4. Automated Instrumental Analysis for Animal Health and Herd Management
5. A Symposium on New Technology in Automated Analysis

Clinical Symposia: Worldwide leaders from Medicine, Academia and Health Care Delivery will present papers on developments in Clinical Pathology, Diagnostic Medicine and Regulatory Affairs. A Hospital Management Symposium on Computerized Hospital Services will also be held.

For a complete schedule and registration package on the Industrial (and Clinical) Symposia, write Department 254, Technicon Industrial Systems, Tarrytown, New York 10591 or telephone toll-free: 800-431-1974.

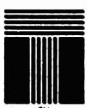

Technicon
Industrial Systems
Tomorrow's Technology Today

load his transmitter, the data must be saved, and the first character must be transferred to the parallel inputs on the UAR/T and transmitted. Then each successive character must be routed to the parallel inputs and transmitted when the previous transmission is complete. Although simple in principle, designing such a circuit can be quite time consuming.

*SER*ial *D*ata *EX*change—SERDEX

A device which more closely meets the usual laboratory requirement of transmitting word-parallel, bit-parallel data is the STX 1003 SERDEX (Analog Devices, P.O. Box 280, Norwood, Mass. 02062). This device, which was described by Larsen and Rony (*4*), retains many of the features of the UAR/T. It has separate transmitter and receiver sections and can be operated either full duplex or half duplex. The number of bits per word can be selected from 5 to 8; parity is optional and can be selected either even or odd. The start and either one or two stop bits are added to the code. The baud rate is determined by an external clock. The STX 1003 also provides switching circuitry for interfacing by current loop.

A companion component is the SCL 1006 clock module which provides the appropriate clock pulses for selecting baud rates from 110 Hz to 19.2 kHz. From a +5-V power supply, it also produces −15 V, which is required by the STX 1003. Thus, the SCL 1006 and STX 1003 may be operated from a single +5-V power supply.

Considering first the STX 1003 as a transmitter, one sees that the principal difference between the UAR/T and the SERDEX is the ability to load in full parallel, i.e., word-parallel, bit-parallel, up to 8 words each having 4 bits. This ability is sufficient to load up to 8 BCD or octyl characters in full parallel as provided by most digital output devices. Following a load command, the data are latched and then transmitted 4 bits of latched data per character. Transmission continues until a 1111_2 is detected; this character serves as a STOP character. Transmitting until a special character is detected simplifies the use of this device in some respects, but complicates its use in others.

The advantages and disadvantages arising from the STOP character will be discussed further below. But returning to the character makeup, one sees that each of the 4-bit words which were loaded in parallel is preceded by 1–4 bits depending on the number of bits of code selected and on whether parity is generated. (Preceded here means the bits are more significant; they are, in fact, transmitted last since the least significant bits are transmitted first.) The added bits may be loaded in a word-serial (not parallel), bit-parallel fashion. For most interfacing applications, which require transmitting numeric data only, loading the most significant bits in this fashion causes little difficulty. Consider the problem of transmitting an ASCII code for a BCD digit. As noted earlier, the ASCII code for numeric data is the BCD code preceded by 011_2. The three most significant bits are always the same and, hence, may be "hard-wired" to the appropriate logic level.

When attempting to transmit any data other than numeric data, problems arise requiring user-designed circuitry. Then one must somehow load the appropriate 3-bit prefix in a word-serial, bit-parallel fashion. One may either add three shift registers which allows him to load the entire 7-bit code in a word-parallel, bit-parallel fashion or attempt to generate the appropriate 3-bit prefix as each word is transmitted. Appropriate synchronization signals are provided to facilitate either approach. Adding shift registers is the most versatile approach for expanding the character set; however, this requires adding 24 (3 × 8) parallel input lines to the 32 (4 × 8) already required. Generating the 3-bit prefix "on-the-fly" is usually preferred if only a few nonnumeric characters are required.

The nonnumeric characters, which are frequently useful, are + and − signs, *C*arriage *R*eturn (CR) and *L*ine *F*eed (LF), comma, and space. The "SERDEX User's Guide" (*5*) is helpful in describing how to transmit a sign; the ASCII characters for + and − require a prefix of 001_2. This reference also describes a convenient manner for producing CR/LF which requires a prefix of 000_2. Lorimer and Bell (*6*) describe a system in which they sample and transmit a digital panel meter nine times before producing a CR/LF. With minor modifications this circuit could transmit any number of samples per line. In their circuit, each transmission is separated from the previous one by a comma, which requires a prefix of 010_2. With minor modification the comma could be changed to an ASCII space character, which requires the same prefix. Adding one or two nonnumeric characters to a numeric character set is relatively easy as long as they occur at exactly the same point in each transmission (preferably first or last).

Returning now to the use of a special character to stop transmission, one can see both advantages and disadvantages. As mentioned earlier, a 1111_2 serves as the STOP character. Depending on which of several 3-bit prefixes precede this, several characters in the ASCII set will terminate transmission. On the one hand, having even one character terminate transmission is a disadvantage since transmitting the entire ASCII character set is difficult, although not impossible, since one can inhibit detection of the STOP character. On the other hand, having more than one character stop transmission is an advantage, since the user can stop transmission with one of several characters which can be generated under different conditions. Depending on which STOP character is detected, the user's computer can tell which condition caused termination.

On examining the SERDEX more closely, the STOP character is really $X1X1111_2$ where X may be either 0 or 1. The STX 1003 changes this to a $X0X1111_2$, if detection of STOP has not been inhibited. The reason can be readily seen. Since the three most significant bits will usually be 011_2 for numeric data, the resulting ASCII character is nonprinting, if the STX 1003 changes these to 001_2. This means that with a teletypewriter the STOP character will be deleted from the printed output.

However, other problems with the STOP character can still arise, as Lorimer and Bell (*6*) point out. In transmitting to their computer, which is programmed in Fortran, the STOP character is illegal and causes an input error. These authors describe a method for deleting the STOP character by shorting the current loop outputs from the STX 1003 when STOP is detected.

Considering now the STX 1003 as a serial receiver, one finds very little difference between the SERDEX and the UAR/T. Both provide word-serial, bit-parallel output. However, the STX 1003 also decodes certain special characters providing an open-collector, pulsed output when anyone of these is detected. These special characters include: ?, *, %, !, ', =, and $. These characters generate useful output pulses for controlling the user's instrument.

Multichannel Data Transmission

As already discussed, the UAR/T requires little additional circuitry to transmit one ASCII character. Similarly, the STX 1003 requires little additional circuitry to transmit as many as eight ASCII characters as long as only numeric characters are allowed. But for transmitting more than one channel having as many as eight characters each, the user must design his own circuit. In our laboratory, we built such a multichannel transmitter. With this device, we wanted to transmit channel-parallel, word-parallel, bit-parallel data. Desiring to minimize the design effort, we chose the STX 1003 as the basis for this interface. Using

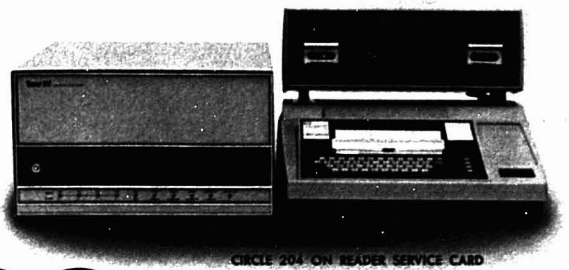

CIRCLE 204 ON READER SERVICE CARD

Tracor Chromatography

Tracor offers everything you need for high efficiency separations of complex materials. Our state-of-the-art-technology results in the latest system design—in GC, LC and analytical data processing.

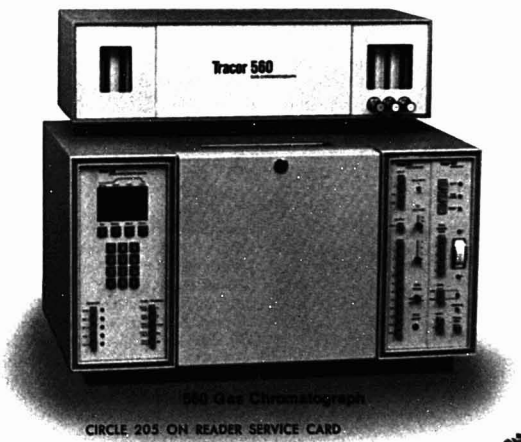

560 Gas Chromatograph

CIRCLE 205 ON READER SERVICE CARD

Our **812 TAP** (analytical processor) is supplied with software designed for the ultimate in accurate data retrieval and ease of operation. This means "plug-in" installation and uncomplicated operator/computer communication.

Our **560 GC**, controlled by a keyboard entry digital processor, is available with a wide range of Tracor patented detectors and other accessories. This means high precision, sensitivity and operator convenience.

Our **6970 LC** includes our new 970 variable wavelength detector equipped with the latest fiber optics and holographically ruled grating, and a constant flow pumping system. This means best reproducibility, wide detector spectral response and excellent quantitative performance.

6970 Liquid Chromatograph

CIRCLE 206 ON READER SERVICE CARD

Send for your free subscription to our periodical, "Retention Times."

CIRCLE 207 ON READER SERVICE CARD

Tracor Instruments Tracor, Inc 6500 Tracor Lane Austin, Texas 78721 Telephone 512 926-2800

Table II. Character Set

LF	0	0	0	0	1	0	1	0
CR	1	0	0	0	1	1	0	1
+	0	0	1	0	1	0	1	1
−	0	0	1	0	1	1	0	1
EOT	1	0	1	0	1	1	1	1
STOP	0	0	1	1	1	1	1	1
NUMERIC	X	0	1	1	X	X	X	X

the STX 1003 requires scanning each active channel to load and transmit data. The system is constructed so that the user's laboratory instrument communicates with a data acquisition computer, an IBM SYS/7 in our case. One may substitute a teletypewriter for the SYS/7, allowing the same instrument control from a keyboard. For obtaining a printout of data and for debugging computer-controlled data acquisition, this teletypewriter compatibility has proved valuable.

Figure 1, which shows a block diagram of the system, illustrates the complexity of a multichannel transmitter. The master control coordinates the interactions of all other components in the system. The special character generator and each channel are connected via a common control bus. The STX 1003 and display are connected via other lines. On receiving an inquiry, which is the ASCII character for "?", the STX 1003 produces a pulse which starts the sampling sequence. From each active channel, the master control waits for a return signal indicating valid data at the inputs.

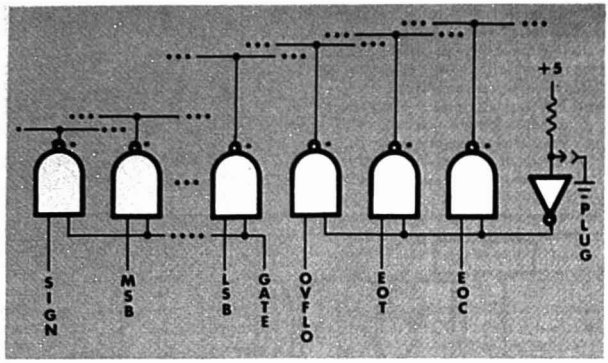

Figure 3. Data bus routes input data into STX 1003 parallel inputs and control indicators into appropriate control logic

One set of open-collector gates required for each channel. SIGN: HI for +; MSB → LSB: parallel input data; GATE: HI to route data onto bus; OVFLO: HI to signal overflow condition; EOT: HI to signal end of data acquisition sequence; EOC: HI to signal conversion complete; PLUG: activates channel when grounded by input connector

Only those channels connected are queried and transmitted. Each channel is routed sequentially onto a data bus. The system has been built with only two channels, but is expandable, and the control logic has been breadboarded with four channels. The control block also activates appropriate indicator lights on the display panel and accepts certain manual override inputs.

Table II shows the allowed character set, which consists of LF, CR, +, −, *E*nd *O*f *T*ransmission (EOT), STOP, and numeric data. The EOT character differs from the STOP in that it signals the SYS/7 to terminate a run. Note that we have taken advantage of having multiple STOP characters. Both EOT and STOP terminate transmission from the STX 1003, but STOP only indicates to the SYS/7 that transmission of each channel is complete, while EOT signals the end of a data acquisition sequence. Except for the +, −, and CR, the lowest order four bits are loaded from the data bus. The + and − signs are generated using circuitry suggested in the "SERDEX User's Guide" (*5*). The lowest order four bits for a CR are identical with those for the − sign and thus produced as if for a − sign. The special character generator, shown in Figure 2, produces the three most significant bits of the ASCII code excluding parity. By default, this circuit produces 011_2 for numeric data and STOP. But for CR and LF it produces 000_2 and for +, −, and EOT, 010_2. Parity is generated internally by the STX 1003. Figure 2 serves to illustrate how complicated the circuitry becomes to produce even this limited set of nonnumeric ASCII characters.

Figure 3 shows the data bus over which data and control logic from each channel are routed to the STX 1003. A channel is activated by grounding a single pin on the input connector. Overflow, end of transmission, and end of conversion are held HI if the channel is not active. These are the no overflow, no end of transmission, and conversion complete conditions. If a channel is activated, each control input must be held at the appropriate logic level by the input device. The sign and each bit are sequentially gated onto

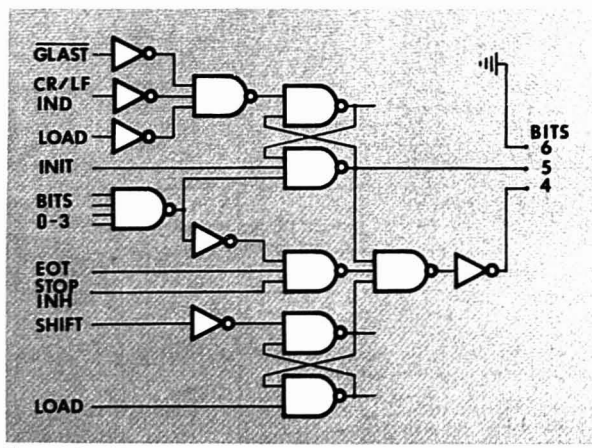

Figure 2. Special character generator

Generates bits 4, 5, and 6 of ASCII code. GLAST: LO when last active channel loaded; CR/LF IND: LO when CR/LF plug connected; LOAD (twice): LO to latch STX 1003 inputs for transmission; INIT: LO to initialize all counters and flip flops; bits 0 → 3: four least significant bits of ASCII code; EOT: HI to signal end of data acquisition sequence; STOP INH: LO to inhibit detection of STOP; SHIFT: positive edge advances STX 1003 to next latched character; bits 4 → 6: three most significant bits of ASCII code

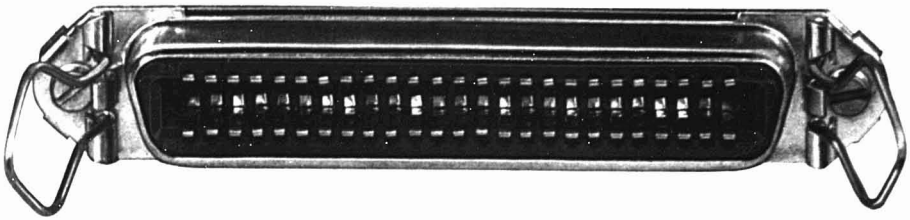

The Mettler Connection.

IT PUTS YOU IN TOUCH WITH THE DIGITAL WORLD.

The Mettler Connection is the BCD output that's built into most Mettler electronic balances. Suddenly you can do more than just weigh with your balance. BCD adds another dimension, giving you some very interesting connection possibilities.

Built-in parallel BCD. Mettler's PL, PS and PT series balances can be connected directly to printers, desk-top calculators, counting systems, digital comparators, weight converters, remote readouts. If you want to go all the way to your computer, that's easy too. Weighing results can be transmitted to another lab, another building, another city.

Some of the possibilities. For example, plug in the Mettler GA20 Calculating Printer and you have a printing balance. It prints out transferred weighing data, keyed-in values and calculation results automatically as well as operating as a four-function calculator. Or, attach the BCD output to our GC11 Weight-Count Converter. Now you have a system to count small parts or a system to convert grams to ounces, grains, pennyweights, etc. Connect the balance to a GC10 Digital Comparator. Here you have an ideal module when applications call for accurate dispensing of powders or liquids, or for simpler, more reliable checkweighing.

Reliable and easy to use...our hallmarks. Simple to use, these dependable Mettler top-loading balances are available with capacities from 320 g to 15 kg, with corresponding readabilities of 0.001 g and 0.1 g. They give reliable, reproducible results in 1.5 seconds. One touch bar control turns the unit on or off, sets zero or tares. And all our electronic balances are backed up by standard warranties plus a field force of 40 service technicians nationwide.

Get in touch... If you need a balance with multi-connection possibilities, call Mettler. If you don't need this capability and just want a balance that does superb weighing, call us anyway. Our balances range from the very basic to the very sophisticated—both mechanical and electronic. You just match one up to your requirements. Our phone is (609) 448-3000. If you prefer to write, we are: Mettler Instrument Corporation, Box 100, Princeton, NJ 08540.

Mettler

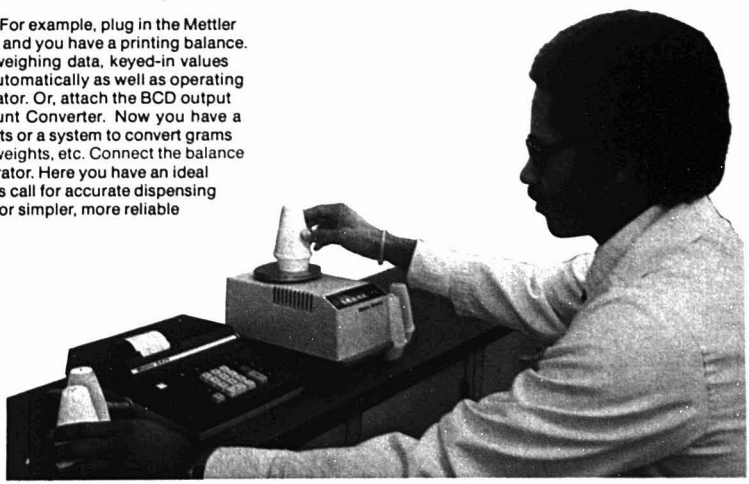

CIRCLE 142 ON READER SERVICE CARD

Table III. Channel Gate Truth Tables

	G1	G2	G3
ONE CHANNEL	1	0	0
TWO CHANNELS	1	0	0
	0	1	0
	1	0	0
THREE CHANNELS	1	0	0
	0	1	0
	0	0	1
	1	0	0

the data bus by the channel gate.

Table III shows the truth tables for the channel gates. These truth tables depend on the number of activated channels. If only one channel is connected, then channel one is always active and all other channels are inactive. If two or more channels were connected, then each would be gated onto the data bus and following transmission of the last channel, the gate configuration would return to its initial state. This gating sequence is accomplished through an expandable ring counter and a retriggerable RS flip flop, the channel scanner.

Figure 4 shows the expandable ring counter. The first channel requires one JK flip flop and two NAND gates; each other channel requires one JK flip flop and one open-collector NAND gate. Outputs G1 and G2 are the gate signals for channels 1 and 2, respectively. If only one channel is connected, G1 remains HI and G2 remains LO on the positive edge of a clock pulse produced by the *chan*nel *scan*ner (CHAN SCAN). If, however, a second channel is connected, G1 begins HI while G2 is LO, but on the first positive edge of CHAN SCAN, G2 goes HI and G1 goes LO. On the second positive edge G1 returns HI and G2 returns LO.

The channel scanner, which generates the clock pulse to advance the channel gates, must produce one pulse if only one channel is active, two if two are active, etc. Figure 5 shows the circuit which accomplishes this. It consists of two monostable multivibrators and one RS flip flop made from NAND gates. The RS flip flop, which is the channel scanner output, is initially set to HI. On an end of conversion (all conversion complete), monostable M1 clears the RS flip flop. This loads the STX 1003 and starts the transmission. The STX 1003 sends a shift pulse indicating transmission has begun; this resets the RS flip flop. If monostable M2 is activated, it again clears the RS flip flop on the positive edge of $\overline{\text{XMIT}}'$. (XMIT is an output from the STX 1003 which is HI during

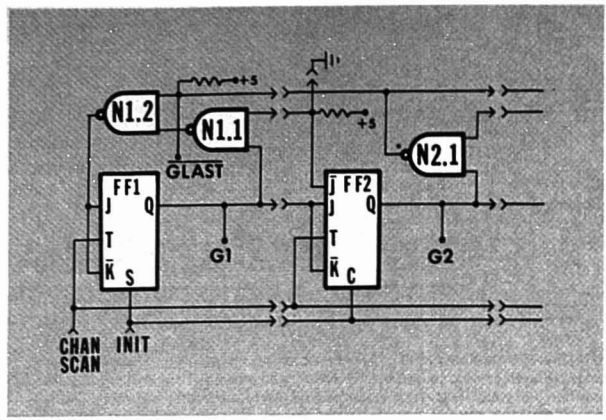

Figure 4. Expandable ring counter

Generates gating pulses for sequentially routing active channels onto data bus. CHAN SCAN: clock pulse which advances channel gate; INIT: LO to initialize all counters and flip flops; G1 and G2: HI to route data onto bus; GLAST: LO when last active channel gated onto bus

transmission. XMIT′ is generated with external circuitry and remains HI long enough for transmitting one additional ASCII character. $\overline{\text{XMIT}}'$ is the complement of XMIT′.) If only one channel is connected, G1, the gate pulse to channel 1, remains HI. This inhibits M2 from triggering on $\overline{\text{XMIT}}'$ and leaves CHAN SCAN HI. If, however, more than one channel is connected, G1 goes LO on the first positive edge activating M2 for a positive edge transition of $\overline{\text{XMIT}}'$. Monostable M2 clears the RS flip flop which loads the second channel and starts its transmission. Alternately, the channel gate will be advanced and transmission will begin until G1 again returns HI, indicating that all channels have been transmitted. M2 will again be inhibited until a new end of conversion is detected.

This data acquisition system has served our laboratory well. It ap-

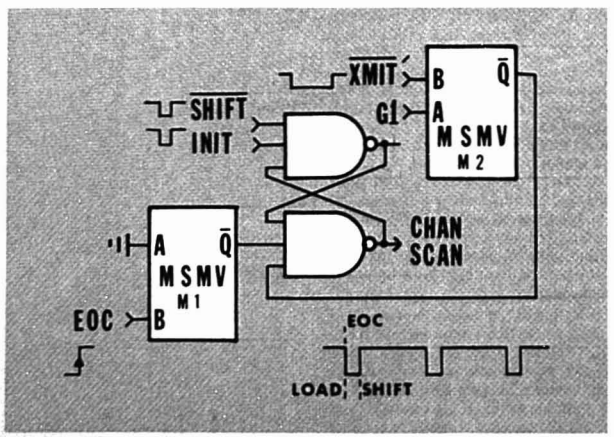

Figure 5. Channel scanner

Serves both to trigger STX 1003 for beginning transmission of each active channel and to advance channel gate for routing active channels onto data bus. EOC: positive edge signals all conversions complete; $\overline{\text{SHIFT}}$: negative edge advances STX 1003 to next latched character; INIT: LO to initialize all counters and flip flops; $\overline{\text{XMIT}}'$: positive edge signals STX 1003 available for reloading; G1: HI when first channel gated onto data bus; CHAN SCAN: negative edge loads STX 1003, positive edge advances channel gate

With An Incos MS Data System
You Can Do This And A Lot More

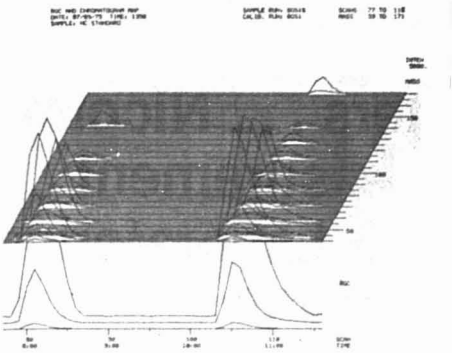

Reconstructed gas chromatogram and isometric chromatogram map. This useful, time-saving display format is unique to Incos data systems. Mass spectra or mass chromatograms may be displayed in a three-dimensional format either before or after data enhancement. The operator specifies a range of scan numbers and a mass range or list of individual mass regions. A fragmentation series or parent ion series can be displayed quickly in the isometric format and interpreted immediately.

Incos system hardware embodies the latest advances in solid-state microelectronics. The central processing unit is a NOVA 3, 16-bit-word minicomputer with 700 nsec cycle time. The dual-disk drive is a top-loading unit operating at 2400 rpm with an average access time of 50 msec. Data storage capacity is 1.25 million 16-bit words per disk, or a total of 2.5 million words. Capacity can be increased to 5 million words with the optional dual-density feature. The printer/plotter is a Versatec 800A 500-line-per-minute electrostatic printer/plotter with very high print quality. The keyboard graphic display terminal is a Tektronix 4010 with a 5.6" X 7.5" screen.

- Simultaneous data acquisition/processing
- Both high and low resolution mass spectrometer interfacing
- Both quadrupole and magnetic system control
- Simultaneous multiple instrument interfacing
- REmote DIagnostics
- User Fortran programmable
- Accurate mass assignment
- Automatic GC/MS data enhancement
- Instrument diagnostics
- Multi-parameter library searching

Combining state-of-the-art hardware, modular Fortran programming, and advanced design concepts, Incos data systems offer proven capabilities that greatly extend the power and versatility of **any** mass spectrometer. They also offer the most complete software package available, enabling you to obtain accurate data in the format best suited to your needs.

An Incos data system can process data as they are being acquired, process previously acquired data files while new data are being acquired, or run any Fortran program you wish while the system is acquiring data.

Incos data systems can be interfaced to any make or type of mass spectrometer—high or low resolution, magnetic or quadrupole. They can be interfaced with any desired combination of mass spectrometers, and can provide simultaneous operation of the MS systems. Additional display terminals at remote locations can also be accommodated.

In addition to several diagnostic programs that enable the operator to optimize overall performance parameters, the system has remote diagnostic capability. A modem enables the user to establish a direct telephone link between his data system and any Incos service center. This enables problems to be diagnosed quickly and service provided rapidly.

Send for the brochure describing the many features that make the Incos systems the most advanced and flexible MS data systems available. Incos data systems do so much more. Why settle for less? For your GC/MS data system needs—ask the specialists.

INCOS

Incos Corporation
A wholly owned subsidiary of Finnigan Corporation
1332 Sixth St.
Berkeley, CA 94710

CIRCLE 79 ON READER SERVICE CARD

From Signal Averagers to complete Fourier Transform Infrared Spectrometers . . . Nicolet is helping solve measurement problems in over 2000 Laboratories Around the World

For over ten years Nicolet Instrument Corporation products have been used to analyze scientific and engineering problems around the world. The continuous expansion of the Nicolet product line from one single line of signal averagers in 1965 to its present diversified product group has certainly enhanced the versatility of, and demand for, Nicolet instrumentation.

The **1070 signal averager** has, for over eight years, served many areas of scientific research in providing reliable signal averaging with post-averaging processing capability. Nicolet has incorporated many new technological advances into the 1070 over the years but the measurement capabilities have maintained a wide range of versatility over the years. Nicolet recently introduced an inexpensive, single input signal averager, the NIC-527, for applications which do not require the 1070's versatility.

CIRCLE 151 ON READER SERVICE CARD

The Nicolet 1090A EXPLORER **Digital Oscilloscope**, the other kind of oscilloscope, is in service testing hockey helmets for **shock absorption**, analyzing pulsed nmr signals in **liquid crystal research,** searching out leaks in nuclear reactor coolant systems, capturing **stress and strain data** in materials testing and making measurements in hundreds of other applications that require its accuracy, resolution, and ability to interface to other instruments for data recording or modification.

CIRCLE 152 ON READER SERVICE CARD

Nicolet data systems are in worldwide use for **nuclear magnetic resonance chemical analysis** determining the structural and motional characteristics of a wide range of chemical systems. Other applications of the new NIC-1180 data acquisition and processing system include **flash photolysis epr studies, ESCA and auger spectroscopy,** and **laser raman** investigations.

CIRCLE 153 ON READER SERVICE CARD

Fourier Transform NMR accessories, designed and manufactured by Nicolet Technology Corporation, are in use on instruments such as the XL-100, HR-220, T-60, R-12 and R-32. NTC has announced a new high resolution **Fourier Transform Ion Resonance Mass Spectrometer** which offers greatly improved resolution and sensitivity along with the ability to examine higher molecular weight compounds.

CIRCLE 154 ON READER SERVICE CARD

The first Nicolet **Fourier Transform Infrared Spectrometers,** which incorporate the NIC-1180, have been installed recently, and are already being employed for studies of chemical structure and dynamics. Worldwide this unit is in use in analytical chemistry laboratories taking advantage of the increased sensitivity and ease of operation offered by an FTIR system compared to conventional IR analytical techniques. The unique Nicolet FTIR software package makes this system even more versatile.

CIRCLE 155 ON READER SERVICE CARD

What about your signal processing requirements? If you have a signal averaging, data acquisition or spectroscopy-related measurement problem please phone or write to describe your needs.

5225 Verona Road
Madison, Wisconsin 53711
Telephone: 608/271-3333

proaches very closely the "ideal" computer interface with which the users can wire for each channel a single, parallel connector between his instrument(s) and this system and operate his instrument under control of the device linked serially with the STX 1003. Besides operating this interface with teletypewriter and IBM SYS/7, we have also operated it with an Altair 8800 microcomputer. We have used the interface both full duplex and half duplex. We also have a limited capability for selecting the baud rate through control logic.

Future Serial Computer Interfaces

But despite the versatility of the system built around the STX 1003, microprocessors will undoubtedly play an important role in future serial computer interfaces. With an 8-bit microprocessor and its clock, a parallel I/O port, and a serial I/O port, one could eliminate the need for almost any electronic design. Under program control, one could select and/or change baud rates, codes, numbers of channels transmitted, and formats. Designing microprocessor-controlled serial interfaces would be reduced to wiring a parallel input connector and to programming a PROM (*P*rogrammable *R*ead *O*nly *M*emory). Changing the interface tailored for one instrument to that for another would require changing PROM's. Standard, high-volume serial interfaces between commercially available instruments and commercially available computers would require the same microprocessor-based interface and a much cheaper, mass-produced ROM (*R*ead *O*nly *M*emory).

In summary, serial computer interfaces can be made quite generally applicable for interfacing many instruments having parallel I/O with computers and many hard-copy devices. Serial interfaces suffer only when required to handle extremely high data rates. Finally, one should not underestimate the power, simplicity, and convenience of a single pair of wires for a computer interface using serial data exchange techniques.

References

(1) R. E. Dessy and J. Titus, *Anal. Chem.*, **46**, 294A (1974).
(2) J. Finkel, "Computer-Aided Experimentation: Interfacing Minicomputers", Wiley, New York, N.Y., 1975.
(3) D. G. Larsen and P. R. Rony, "The Bugbook IIA", E & L Instruments, Inc., Derby, Conn., 1975.
(4) D. G. Larsen and P. R. Rony, *Am. Lab.*, **7**, 116 (1975).
(5) "SERDEX User's Guide", Analog Devices, P.O. Box 280, Norwood, Mass. 02062.
(6) D. H. Lorimer and A. T. Bell, *Ind. Eng. Chem. Fundam.*, **15**, 71 (1976).

BRUKER

Announcing the NEW WP-80

A LOW-COST, HIGH RESOLUTION FT NMR SYSTEM WITH INCREDIBLE PERFORMANCE

- 80 MHz operation for protons (20 MHz operation for ^{13}C)
- 10 mm variable temperature probe capability
- Fully multinuclear with pre-tuned plug-ins
- Quadrature phase detection
- Guaranteed S/N for ^{13}C 150:1 on ethylbenzene

Inquire about the other exciting features of this outstanding instrument.

BRUKER INSTRUMENTS, INC.

Manning Park
Billerica, Mass. 01821
Phone 617-272-7527

539 Beall Avenue
Rockville, Maryland 20850
Phone 301-762-4440

1548 Page Mill Road
Palo Alto, Calif. 94304
Phone 415-493-3173

5200 Dixie Road, Ste. 116
Mississauga, Ontario, Canada L4W1E4
Phone 415-625-2375

CIRCLE 29 ON READER SERVICE CARD

analytical chemistry

October 1976, Vol. 48, No. 12

Editor: **Herbert A. Laitinen**

EDITORIAL HEADQUARTERS
1155 Sixteenth St., N.W.
Washington, D.C. 20036
Phone: 202-872-4570 Teletype: 710-8220151

Managing Editor: Josephine M. Petruzzi
Associate Editor: Andrew A. Husovsky
Associate Editor, Easton: Elizabeth R. Rufe
Assistant Editors: Barbara Cassatt, Nancy J. Oddenino
Editorial Assistant: Deborah M. Cox
Production Manager: Leroy L. Corcoran
Associate Manager: Charlotte C. Sayre
Art Director: John V. Sinnett
Artist: Diane Reich

Advisory Board: Donald H. Anderson, Edward G. Brame, Jr., Richard P. Buck, Warren B. Crummett, Merle A. Evenson, Velmer Fassel, A. F. Findeis, Robert A. Hofstader, Marjorie G. Horning, Richard S. Juvet, Jr., Lynn L. Lewis, Harry B. Mark, Jr., Walter C. McCrone, Eugene A. Sawicki, W. D. Shults

Instrumentation Advisory Panel: Stanley R. Crouch, Nathan Gochman, Robert W. Hannah, Gary Horlick, James N. Little, Harold M. McNair, David Seligson, R. K. Skogerboe, Donald E. Smith

Contributing Editor: Claude A. Lucchesi
Department of Chemistry, Northwestern University, Evanston, Ill. 60201

Published by the
AMERICAN CHEMICAL SOCIETY
1155 16th Street, N.W.
Washington, D.C. 20036

Books and Journals Division
Director: D. H. Michael Bowen
Editorial: Charles R. Bertsch
Graphics and Production: Bacil Guiley
Research and Development: Seldon W. Terrant
Circulation Development: Marion Gurfein

Manuscript requirements are published in the December 1975 issue, Page 2525. Manuscripts for publication (4 copies) should be submitted to ANALYTICAL CHEMISTRY at the ACS Washington address.

Chemical Characterization

A modernized name for qualitative analysis is chemical characterization, a name that implies a more detailed identification than the classical detection of elements or compounds in a sample. Thus chemical characterization may involve the identification of the oxidation state, coordination state, crystalline form, distribution of impurities, surface structure, and many other types of information besides composition.

Even if we are dealing with composition, we can visualize many "nonclassical" situations arising, for example the identification of transient species or steady-state occurrence of activated species in the upper atmosphere or molecules in intergalactic space. What about identification of larger units than molecules in biological systems? It seems difficult to draw the line between macromolecular species, miceller units, membranes, organelles or cells, all of which have a characteristic chemical makeup. Somewhere along the line we begin to use functional descriptive names such as egg albumen or *E. coli* mitochondria that adequately characterize the material for the intended purpose.

We come to the nub of the matter when we recognize the problem-oriented nature of chemical characterization, or for that matter of analytical chemistry as a whole. Chemical characterization includes as much or as little detail as is necessary for the problem at hand. For some situations it is entirely adequate to report elemental composition in the classical way, but if the problem being tackled requires more detailed information, it is necessary to seek it. A good example is particulate matter in the atmosphere. A first-level characterization is simply to collect and weigh filterable particles in a known volume of air. A second level of sophistication involved a breakdown by particles size distribution. A third level is to examine the size fractions for elemental composition. A fourth level is to determine the nature of the individual particles (e.g., silica, rag weed pollen, lead halides, etc.). A fifth level is to characterize specific crystalline forms (e.g., various forms of asbestos). Each of these characterizations has a place appropriate to an environmental problem. It is the responsibility of the analytical chemist to choose the characterization method to yield the needed information efficiently, i.e., without wasted effort.

H. A. Laitinen

Long-Lived Potassium Ion Selective Polymer Membrane Electrode

Oliver H. LeBlanc, Jr.* and W. T. Grubb

General Electric Research and Development Center, Schenectady, N.Y. 12301

Long-lived potassium-selective electrodes were constructed from membranes incorporating potassium valinomycin tetraphenylborate salt in a polymeric matrix. The polymer was a block copolymer of poly(bisphenol-A carbonate) and poly(dimethylsiloxane) with sufficient cyanoethyl substitution in the latter to provide a dielectric constant of 5.2. Nearly ideal Nernstian response to K^+ from 10^{-5} to 10^{-1} N was observed over more than 3 years of exposure to neutral electrolytes.

Following the discovery by Mueller and Rudin (*1*) that the macrocyclic antibiotic Valinomycin induces specific K^+ ion conductance through lipid bilayer membranes, Stefanac and Simon (*2*), and many others since, employed Valinomycin as a neutral carrier to construct practical K^+ -ion-selective electrodes; see the review by Buck (*3*).

In 1970 (*4*), electrodes incorporating Valinomycin as the K^+ ion carrier were prepared in a special elastomeric polysiloxane poly(bisphenol-A carbonate) block copolymer matrix (*5*) prepared by the late Johannes F. Klebe of our laboratories. The use of this copolymer membrane in pH-sensing electrodes for in vivo biomedical applications has been described (*6*). Such block copolymers containing about 50% of each constituent polymer are actually heterogeneous, two-phase systems, the poly(siloxane) blocks comprising a continuous, amorphous phase through which molecular transport occurs rapidly, as in all silicones, while the poly(carbonate) blocks form a discontinuous, crystalline phase that cross-links the structure (*7, 8*). Because such cross-linking is destroyed by poly(carbonate) solvents, such as methylene chloride, these elastomers are solvent castable, a useful property.

If such copolymers contain only dimethylsiloxane moieties in the poly(siloxane) blocks, they do not perform well in ion-selective electrodes as matrices for ion-specific carriers. Presumably, their dielectric constants (2.5–3.0) are too low to permit significant ion unpairing or electrical charge injection at the aqueous/membrane interfaces (*9*). Adding ionic carriers of various sorts to them yielded membranes of very high electrical resistances and erratic transmembrane potentials between aqueous solutions containing the transportable ions. Accordingly, Klebe synthesized modified copolymer materials in which the poly(siloxane) blocks were a random sequence of dimethylsiloxane and cyanoethylmethylsiloxanes. Sufficient cyanoethyl groups to yield a dielectric constant between 4 and 13 gave copolymers which performed well in ion-selective electrodes. Klebe also achieved improved hydrolytic stability of these copolymers by employing a carbamate linkage, rather than the more customary aryl–oxy–silicon linkage between the poly(siloxane) and poly(carbonate) blocks. Synthetic procedures are described in detail in Ref. 4.

K^+ ion selective electrodes formed by simply incorporating neutral Valinomycin (Calbiochem, LaJolla, Calif.) into films of the above polymers showed some K^+ response, but resistances were so high ($\gtrsim 10^9\ \Omega$) that measurements of transmembrane potentials were exceedingly difficult. Using the salt formed between the K^+ : Valinomycin complex cation and the tetraphenylborate anion yielded much lower resistance membranes with good K^+-response characteristics.

EXPERIMENTAL

The electrodes were constructed using the poly(siloxane)–poly(bisphenol-A carbonate) block copolymer preparation specifically designated as example number 2 in Ref. 4. This contained 52% siloxane, with 2.2 dimethylsiloxanes per cyanoethylmethylsiloxane with a static dielectric constant of 5.2, and an intrinsic viscosity of 0.3 dl/g in chloroform at 25 °C.

The carrier salt was prepared from potassium tetraphenylborate precipitated from aqueous solutions of KCl and sodium tetraphenylborate. After careful washing and drying 3.3 mg (9.2 mmol) of this salt plus 12.2 mg (10.9 mmol) of Valinomycin were dissolved in 8 ml of methylene chloride in about 3 h. (Potassium tetraphenylborate is insoluble in methylene chloride, but the complex salt is soluble.) The complex salt formed more rapidly in the mutual solvent acetone, which was removed in vacuo before dissolving the salt in methylene chloride.

The complex salt in methylene chloride was added to methylene chloride solution of the block copolymer to obtain about 3% solids in solution consisting of 3.0 parts salt to 100 parts copolymer by weight. After filtering through a glass frit to remove any particles, the solvent was partially evaporated until there was about 7% solids solution. This solution was poured onto a glass plate, allowing it to spread freely, and allowed to dry overnight with a Petri dish cover to slow solvent evaporation. The resulting film, 60–90 μm in thickness, was peeled from the plate. It was tough, rubbery, colorless, and slightly cloudy, probably indicating that the complex salt was present slightly in excess of its solubility in the copolymer.

Small circular disks 6 mm in diameter, punched from this film with a stainless steel punch, were incorporated in two electrodes whose structure is shown in Figure 1. The electrode body was a 10-cm length of Pyrex tubing, 5.0-mm o.d. and 3.3-mm i.d., with ends ground flat. One end of the tube was coated with a small quantity of silicone rubber cement (RTV 108, General Electric, Waterford, N.Y.), the tube mounted in a micromanipulator, and the cement-coated end lowered into concentric contact with the slightly larger 6.0-mm diameter disk of the K^+ -sensitive film. The silicone rubber cement was allowed to cure overnight, forming the first of two seals between glass and film.

Making of the second seal was simplified by use of a shaped sleeve. This had been preformed from heat-shrinkable polyolefin tubing (Flexite PO-135, expanded i.d. 6.3 mm, recovered 3.2 mm, L. Frank Markel & Sons, Norristown, Pa.) by shrinking it onto a Teflon polymer rod machined to two diameters of 5.0 and 6.0 mm with a shoulder between. The Pyrex glass tube was held vertically with the membrane at the top, and the shaped sleeve positioned about half-way up the tube with its larger diameter facing upward. The annular space between the sleeve and the tube was filled by injecting more of the RTV-108 silicone from a syringe. The sleeve was then slid upwards until it touched the membrane. The outer edges of the membrane were gently pressed down to make good contact with the silicone rubber cement, which then was allowed to cure overnight.

Thus, two independent seals were formed sequentially, providing better assurance against pinhole leaks. The silicone rubber cement used to make these seals adheres extremely well to poly(siloxane) materials, and also to clean glass surfaces.

An internal reference element consisting of a chloride silver wire was sealed into a sized piece of the heat-shrinkable polyolefin tubing. A vent hole was provided in this to facilitate final assembly of the electrode, after it was filled with a reference electrolyte solution, by simply sliding the snugly-fitting polyolefin tubing onto the open end of the Pyrex glass tube.

The two electrodes constructed on November 11, 1970, have had slightly different histories. Electrode A was stored wet at room temperature, filled with and immersed in a solution of either 4 mM KCl

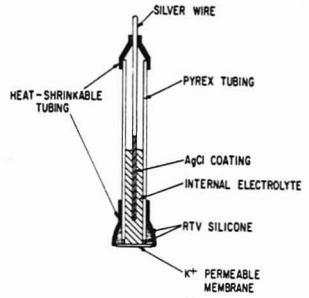

Figure 1. Construction of the electrodes.

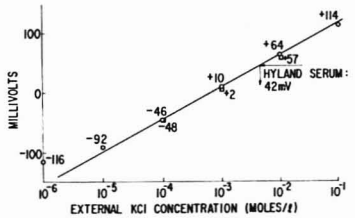

Figure 2. Electrode potential as a function of K^+ ion concentration

Internal electrolyte: 140 mM NaCl plus 4 mM KCl. Reference electrode: saturated calomel. External solution: (O) KCl alone; (□) KCl plus 140 mM NaCl. The K^+ ion concentration in Hyland serum was calculated by interpolation from the potentials measured in it, in 1 mM KCl plus 140 mM NaCl, and in 10 mM KCl plus 140 mM NaCl. Value found: 4.1 mN; Hyland assay: 4.3 mN

and 140 mM NaCl or 10 mM KCl and 150 mM NaCl. Electrode B was stored dry for approximately five months and in the same manner as Electrode A since then.

From time to time, the electrodes were briefly removed from storage for testing. The internal electrolyte solutions were renewed if necessary. Electrode potentials were conventionally measured against a reference electrode using high impedance electrometers or pH meters. Electrode resistances were measured by a variable frequency audio bridge with extrapolation to zero frequency or by measuring the electrode potentials as a function of imposed shunt load resistances. All data were obtained at room temperatures, 23 ± 2 °C.

RESULTS AND DISCUSSION

Static potential response of electrode A to variations in external K^+ ion concentrations is shown in Figure 2; the characteristics of electrode B were indistinguishable. The same response, repeatedly observed for both electrodes for a period of three years was nearly linear from 10^{-2} to 10^{-5} N $[K^+]$ and not exactly linear at higher concentrations because of the variation of activity coefficients. For example, the response was 56 ± 2 mV when the external solution was changed from 1 mM KCl to 10 mM KCl at 23 °C. This is Nernstian behavior considering the activity coefficient differences between these two solutions.

To determine if the electrodes are useful in the determination of $[K^+]$ in whole blood plasma, separated plasma, or serum, in which Na^+ is present (≈140 mN Na^+ vs. ≈4 mN K^+), potentials were determined in the presence and absence of 140–150 mM NaCl. As Figure 2 shows, the addition of NaCl generally *decreased* the electrode potential, as expected for activity coefficient effects, rather than *increasing* them, as would be expected for Na^+ ion interference. A test of reconstituted human blood serum (Hyland Clinical Control Serum, Hyland Division, of Travenol Laboratories, Los Angeles, Calif.) is shown in Figure 2. The agreement with the Hyland assay shows that these electrodes can be used to determine K^+ ions in plasma or serum.

Table I. Resistance as Function of Time Elapsed Since Beginning of Continuous Storage in 0.15 M NaCl, 0.01 M KCl

Date tested	Electrode A Time, days	Electrode A Resistance, MΩ	Electrode B Time, days	Electrode B Resistance, MΩ
11/25/70	14	22		
12/10/70	29	20		
1/20/71	70	27		
4/22/71	103	21		
5/11/72	547	35	384	22
11/13/72	733	35	570	17
5/17/72	917	30	754	18
11/19/73	1104	35	941	18
2/10/76	1917	29	1754	6

For three years after they were constructed, the response time of both electrodes was such that steady potentials were obtained in less than 1 min after changing the external solutions. This was probably limited by the time of mixing.

Electrical resistance was monitored as a sensitive measure of the stability of ion selective electrodes (probably more sensitive than the electrode potential itself). The resistance will undergo changes due to deteriorations in either the "liquid membrane" matrices or the carrier systems, or due to the development of pinhole leaks, long before any of these phenomena lead to detectable changes in electrode potential characteristics. The resistance data obtained on the present electrodes are listed in Table I. They demonstrate that the electrodes were surprisingly stable for 3 years, with detectable changes occurring at 5 years.

At 5 years of age, both electrodes had deteriorated, as judged by all criteria for evaluating their performance. The resistances had noticeably decreased. The potential response to changes in external $[K^+]$ was now sluggish, steady potentials being reached only after as long as 5–10 min. The static response was now low; the potential now changed only +50 mV for electrode A and +54 mV for electrode B when the external solution was changed from 1 mM KCl to 10 mM KCl.

The reason for this ultimate deterioration in performance is not certain, but all the observations would be consistent either with the development of Na^+ (or Cl^-) interference in the membrane proper or with the development of pinhole leaks around or in the membrane. The latter is considered more probable.

CONCLUSION

The long life of these electrodes is remarkable. Clearly, the poly(siloxane)–poly(bisphenol-A carbonate) block copolymer synthesized by Klebe is quite stable in contact with neutral aqueous solutions. The potassium Valinomycin tetraphenylborate complex salt remained active in the membrane during a 3-year period without dissolving into the aqueous solutions or hydrolytically decomposing. Similar long life behavior has also now been observed with ion-selective electrodes constructed using plasticized poly(vinyl chloride) as the "liquid membrane" material (*10–17*), which suggests that the phenomena may be general to electrodes constructed with noncrystalline polymer matrices. The electrodes of the present paper have utility in biomedical applications such as blood serum K^+ determinations.

The deterioration in transmembrane potential and response time properties and the accompanying decrease in electrical resistances at 5 years' life may indicate the onset of electrolytic shorting paths through or around the membranes. The use of

thicker membranes or even better adhesive or sealing procedure might yield electrodes with longer life.

Finally, the elastomeric copolymer applied in this work may be useful as a host matrix for other ion-selective carriers, providing improved stability and lifetime.

LITERATURE CITED

(1) P. Mueller and D. O. Rudin, *Biochem. Biophys. Res. Commun.*, **26**, 398 (1967).
(2) J. Stefanac and W. Simon, *Microchem. J.*, **12**, 125 (1967).
(3) R. P. Buck, *Anal. Chem.*, **46**, 28R (1974).
(4) J. F. Brown, O. H. LeBlanc, and W. T. Grubb, U.S. Patent 3,767,533 (October 23, 1973).
(5) H. A. Vaughan, *J. Polymer Sci., Part B*, **7**, 569 (1969).
(6) O. H. LeBlanc, J. F. Brown, J. F. Klebe, L. W. Niedrach, G. M. J. Slusarczuk, and W. H. Stoddard, *J. Appl. Physiol.*, **40**, 644 (1976).
(7) R. P. Kambour, *J. Polymer Sci., Part B*, **7**, 573 (1969).
(8) D. G. LeGrande, *J. Polymer Sci., Part B*, **7**, 579 (1969).
(9) R. M. Fuoss and C. A. Kraus, *J. Am. Chem. Soc.*, **57**, 1 (1935).
(10) G. J. Moody, R. B. Oke, and J. D. R. Thomas, *Analyst (London)*, **95**, 910 (1970).
(11) R. W. Cattrall and H. Freiser, *Anal. Chem.*, **43**, 1905 (1971).
(12) J. E. W. Davies, G. J. Moody, and J. D. R. Thomas, *Analyst (London)*, **97**, 87 (1972).
(13) H. James, G. D. Carmack, and H. Freiser, *Anal. Chem.*, **44**, 856 (1972).
(14) G. H. Griffiths, G. J. Moody, and J. D. R. Thomas, *Analyst (London)*, **97**, 420 (1972).
(15) J. Ruzicka, E. H. Hansen, and J. C. Tjell, *Anal. Chim. Acta*, **67**, 155 (1973).
(16) U. Fiedler and J. Ruzicka, *Anal. Chim. Acta*, **67**, 179 (1973).
(17) G. D. Carmack and H. Freiser, *Anal. Chem.*, **47**, 2249 (1975).

RECEIVED for review April 19, 1976. Accepted June 24, 1976.

Determination of Subnanogram Amounts of Fluoride with the Fluoride Electrode

Alan S. Hallsworth,* John A. Weatherell, and Dan Deutsch

Department of Oral Biology, Dental School, University of Leeds, Leeds LS1 3EU, England.

An extremely sensitive method of determining fluoride with the Orion electrode is described having an absolute detection limit of 10 pg (10^{-11} g) of F^-. One-microliter volumes of sample solution are confined as thin layers between the fluoride-ion sensing element of a standard Orion electrode and the flat sleeve-junction of a calomel reference electrode mounted immediately below it. One hundred picograms (10^{-10} g) of F^- have thus been determined with a precision (relative standard deviation) of 5%: the precision improving to 2.8% at the 1-ng level. Sample preparation procedures and a fluoride microdiffusion technique of great sensitivity and range (<1 ng to 100 ng F^-) are also described. These techniques, while developed primarily for the mineralized tissues, can be used to analyze many other fluoride-containing materials. Similar electrode assemblies, used to determine ultramicroamounts of chloride ion (1 ng) and hydrogen ion are discussed.

The Orion fluoride electrode (*1*) has been used to determine less than 100 pg of fluoride ion with reasonable accuracy and precision, this high sensitivity being achieved by using a minimum convenient sample volume of 1 μl. The fluoride electrode, *without modification*, is used with a separate reference electrode and a special ground-sleeve junction.

A fluoride diffusion technique of comparable sensitivity is used when the sample fluoride content is extremely low and must be concentrated into a small volume of solution to enable accurate measurements to be made, or when some of the fluoride is complexed by sample components.

These analytical methods have been in use for a number of years, being employed by the authors to measure fluoride concentrations in dental enamel, dentin, bone, and other biological materials. They can, however, be applied to a wide range of fluoride-containing materials. The principle upon which the electrode assembly is based has been similarly applied to the ultramicrodetermination of chloride and hydrogen ions and could, with little difficulty, be used in the electrode determination of many other ions.

EXPERIMENTAL

Apparatus. *Sample Preparation Block.* Solutions of samples soluble in 1 M perchloric acid are prepared in 50-μl capacity chambers or microtubes (2.5-mm diameter × 10 mm deep) drilled in a block of polypropylene (Figure 1). Before use, the sample block is cleaned by immersion in 10% Decon 90 at 80 °C for 60 min, rinsed with fluoride-free water and then immersed in 30% perchloric acid at 80 °C for about 20 min, care being taken to ensure that the acid completely fills each chamber. The block is rinsed at least 6 times with fluoride-free water and dried in vacuo over sodium hydroxide pellets.

Fluoride Microdiffusion Cells. Diffusion cells were made from polypropylene specimen-embedding capsules and push-fit polyethylene stoppers (Figure 2). The embedding capsules (8-mm diameter) may be obtained from TAAB Laboratories, Reading, England. The polyethylene stoppers (Reference 39/H/1001) are available from Johnsen & Jorgensen Ltd., London S.E.7, England. Prior to use, the capsules and stoppers are cleaned with laboratory detergent and 30% perchloric acid as described above.

Fluoride Electrode Assembly (Figure 3). This consists of an Orion fluoride electrode, models 96-09 or 94-09; a saturated calomel reference electrode, Radiometer types K100, K130, or K1301; and a specially-designed, ground-sleeve junction, made as described below.

The sleeve-junction is connected to the reference electrode by a salt-bridge, filled with saturated KCl solution from the reservoir. This solution also fills the reference electrode and the ground-sleeve junction (Figure 5). An expanded scale pH meter/millivoltmeter (Radiometer type PHM 26) readable to ±0.1 mV is used to measure electrode potential.

Ground-Sleeve Junction. This is made from a borosilicate $^{5}/_{13}$ joint (Quickfit CNB 5 cone and SRB 5 socket, Figure 4*a*). The small end of the glass cone is first sealed in an oxygen–gas flame and the fit of the cone in its socket is improved by lightly lapping them together with Aloxite optical grade (No. 40) powder and water. This operation determines the leak rate of the sleeve-junction, a very low rate (ca. 0.1 μl/h) being essential. The socket is then cut from the remainder (i.e., the shank) of the SRB 5 joint to make the sleeve. The cone and sleeve are mated and the smaller end of the joint ground flat and *exactly* perpendicular to its long axis with 400 grit silicon carbide powder and water. Both components (Figure 4*b*) are then chemically cleaned, rinsed thoroughly with water, and dried at 105 °C. *While still warm*, the small ends of the cone and sleeve are mounted in silicone rubber molds and coated separately with 2–3 mm of liquid epoxy resin (Araldite AY 103 resin + HY 956 hardener, 5:1 by wt) as shown in Figure 4*c*). This resin coating which prevents fluoride ion in the an-

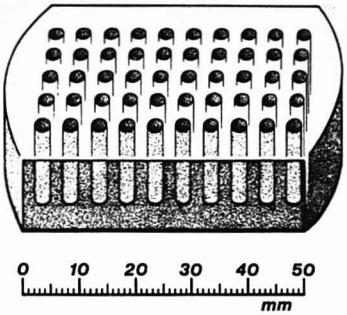

Figure 1. Polypropylene block used to prepare test solutions from samples soluble in 1 M perchloric acid. The curved ends of the block enable it to be centrifuged within the 250-ml bucket of a preparative centrifuge

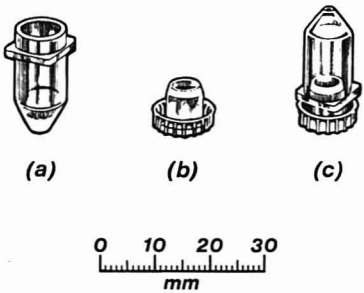

Figure 2. Microdiffusion cell used to separate 1–100 ng of fluoride

The cell (*c*) consists of an electron microscopy specimen-embedding capsule (*a*) and a push-fit polyethylene stopper (*b*)

alyte solution exchanging with ions in the glass, is cured at 105 °C for 16 h, ground to a uniform thickness of about 0.5 mm and polished with metal polish. A hole, 1 mm in diameter is drilled through the wall of the cone to connect its interior with the liquid junction which forms in the narrow annular space between cone and sleeve (Figure 4*d* and Figure 5).

Ground-Sleeve Junction—Determination of Leak Rate. Before commissioning the unit, check its leak rate by measuring the amount of Cl^- ion leaking from the sleeve. Connect the sleeve-junction to the reference electrode and fill with saturated KCl solution. Flush the junction with saturated KCl by opening the reservoir tap (Figure 3) and slightly loosening the glass sleeve. Reseat the sleeve firmly, close the tap, and remove all excess solution with paper tissue. Thoroughly rinse the working surfaces of both sleeve-junction and fluoride electrode with distilled water and dry with tissue. Pipet 10 μl of distilled water onto the sleeve-junction and lower the fluoride electrode to spread the water to the full diameter of the sleeve (cf. Figure 5). Readjust the position of the electrode from time to time to compensate for evaporation. After 1 h, absorb all the residual liquid onto a 20 mm × 10 mm strip of Whatman No. 50 filter paper (pre-extracted with water and dried at 105 °C). Dry the paper strip at 105 °C, add 1 ml of distilled water, and shake for 30 min at room temperature. Determine the chloride ion concentration of the aqueous extract with either a chloride electrode (Orion models 94-17, 96-17) or an automatic chloride titrator. Make serial dilutions of the saturated KCl solution and measure the chloride concentrations as indicated. Calculate the operational leak rate of the sleeve-junction from these data after carrying out 3 replicate determinations. A leak rate of 0.1–0.5 μl of saturated KCl per hour is about optimal.

Reagents and Standards. All chemicals used were of AnalaR, ACS, or equivalent grade. Solutions were made up in fluoride-free water, prepared by the single distillation of tap water (0.1 ppm F^-) in an all-glass still. The solutions were stored in polyethylene or polypropylene.

Perchloric Acid, 60%, Fluoride-Diffusion Grade. Heat 1-ml portions of 60% perchloric acid at 60 °C for at least 72 h in a microdiffu-

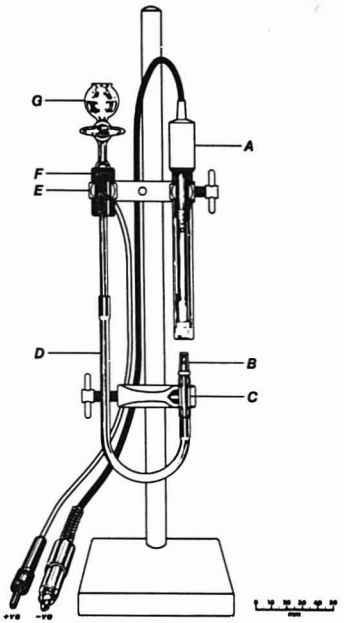

Figure 3. Fluoride electrode assembly

(A) Orion fluoride electrode; (B) ground-sleeve junction; (C) stainless steel holder with spring clips protected by plastic tubing; (D) Vinyl tubing filled with saturated KCl (E) electrode holder with polyethylene-coated spring clips; (F) saturated calomel reference electrode (Radiometer K100); (G) saturated KCl reservoir

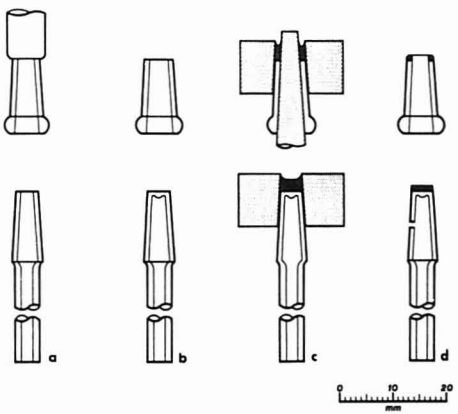

Figure 4. Stages in the construction of the ground-sleeve junction

The original $^{5}/_{13}$ cone-and-socket joint is shown in (*a*). In (*b*), the end of the cone has been flame-sealed and ground while the socket has been detached, lapped, and ground with the cone as described in the text. (*c*) illustrates the use of silicone rubber molds to coat and extend the ends of the sleeve-joint with epoxy resin. The two parts of the completed unit are shown in (*d*)

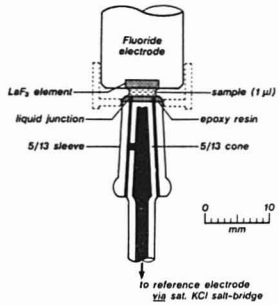

Figure 5. Detail of the fluoride electrode and sleeve-junction in use

For clarity, both the sample solution, normally a thin layer, and the annular space between the cone and sleeve have been greatly exaggerated in size. The polyethylene cap fitted on the sleeve-junction to reduce sample evaporation, is shown in broken outline. Clearances are just sufficient to permit the fluoride electrode to be raised or lowered with the cap in position

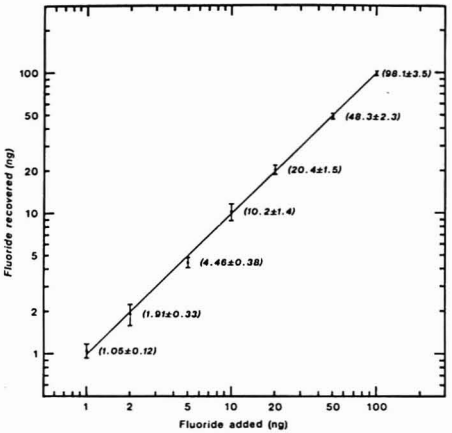

Figure 6. Fluoride microdiffusion

Regression curve obtained by plotting fluoride recoveries on a logarithmic scale vs. the fluoride microdiffused. The vertical bars represent the standard deviation at each level. The mean amounts of fluoride recovered and standard deviations are given in parentheses. The straight (regression) line represents the best fit through these points as determined by the least squares method

sion cell (*2*) and trap diffused fluoride in a thin layer of solid sodium hydroxide. Store the purified acid in the cell.

Perchloric Acid, 1 M.

Silver Sulfate, 0.12 M in Perchloric Acid, 60%. The solution should be freed from fluoride by a preliminary microdiffusion at 60 °C as described above.

Sodium Acetate Buffer, 1 M. Dissolve 20.7 g of sodium hydroxide in about 300 ml of fluoride-free water; add 30 g (28.7 ml) of glacial acetic acid and 1.05 g of citric acid with cooling and dilute the solution to 500 ml (520.5 g) by weight with fluoride-free water. This solution is about neutral. When mixed with M perchloric acid in the proportion 4:1 (v/v), the final pH of the solution is at 5.2–5.3.

Sodium Hydroxide, 0.1 M.

Sodium Fluoride Standard Solution (100 ppm F^-, pH 5.2). Dissolve 22.10 mg of sodium fluoride (Merck Suprapur, vacuum-dried) in a 4:1 v/v mixture of the 1 M sodium acetate buffer and 1 M perchloric acid (pH 5.2) and dilute to 100 ml with the same mixture.

Procedure. *Preparation of Sample Solutions. A. Perchloric acid-soluble samples.* Weigh the samples to ±0.1 μg, transfer them to separate chambers in the sample preparation block (Figure 1) and dissolve in 1 M perchloric acid (1 μl per 20 μg dental enamel, ashed dentin, or bone). Add 4 μl of 1 M sodium acetate buffer to each microliter of acid sample solution, hermetically seal the chambers with adhesive polyethylene tape, mix the solutions by gentle vibration and then centrifuge the block at low speed for about 30 s. The final pH of the buffered sample solutions should be 5.2 ± 0.1. For samples that contain excessively high concentrations of aluminum, ferric iron, or other fluoride-complexing ions (e.g., fossil enamel and bone), a citrate buffer such as that of McCann (*3*) may be required. When the fluoride concentrations of the samples are very low (e.g., fetal enamel), fluoride is separated and concentrated by microdiffusion at 60 °C from 60% perchloric acid solution as described below: the diffusates being redissolved in 1 M sodium acetate, 1 M perchloric acid buffer prior to analysis.

B. Perchloric-acid insoluble samples. The fluorine content of these materials must be converted quantitatively into soluble ionic fluoride by the appropriate sample preparation techniques (e.g., fusion with Na_2CO_3 or NaOH; combustion with oxygen in the Schöniger flask or Parr bomb) (*4*). Citrate may be added to sample solutions prepared from aluminum-containing minerals and other inorganic materials (*5–7*). A simple thermal ashing of biological and organic samples at 500–600 °C may suffice.

Separation of Fluoride by Microdiffusion. Remove the caps from clean TAAB capsules (Figure 2*a*) and evaporate 5 μl of 0.1 M NaOH to dryness in their pointed bases in vacuo over sodium hydroxide pellets. Weigh the sample to an accuracy of ±0.1 μg and transfer it to a polyethylene stopper (Figure 2*b*). Add 50 μl of 60% perchloric acid, fluoride-diffusion grade, to the sample and immediately fit the prepared TAAB capsule onto the stopper. Place the assembled cell (Figure 2*c*) in a closed container charged with sodium hydroxide pellets to ensure a fluoride-free atmosphere and allow the diffusion to proceed overnight (16 h) at 60 °C.

After diffusion, allow the cell to cool to room temperature in the closed container. Dissolve the fluoride-containing layer of alkali in 10 μl of a 4:1 v/v mixture of 1 M sodium acetate buffer and 1 M perchloric acid, pH 5.2. Mix the solution by gentle vibration and determine its fluoride concentration with the fluoride electrode assembly as described below. The diffusion of fluoride from samples of high chloride content may be incomplete owing to exhaustion of the alkali by the HCl simultaneously liberated. Such samples should be microdiffused from a 0.12 M solution of silver sulfate in 60% perchloric acid: a reagent devised by Hall (*8*).

Fluoride Determination. The fluoride concentrations of all solutions are determined with the fluoride electrode assembly shown in Figure 3. Place a 1-μl drop of sample solution upon the end of the ground-sleeve junction (B) and lower the fluoride electrode, confining the sample as a thin disk of liquid (Figure 5). Immediately raise the electrode 0.5 mm or so, and then lower it again with a slight twisting motion to recontact both sample and sleeve-junction. This operation results in an even distribution of the sample and tends to produce a more reliable electrode potential. Read the electrode potential to the nearest 0.1 mV after a further 1 min, raise the electrode, and remove the sample with paper tissue. Carry out at least 4 replicate determinations on each sample solution. Readings taken from the first and second 1-μl aliquots of the analyte solution tend to be inaccurate, the fluoride electrode taking rather longer than 1 min to reach equilibrium. The short equilibration period, however, reduces errors due to evaporation of the sample. The electrode potentials given by the third and subsequent aliquots will be progressively more consistent and reflect the fluoride concentration of the sample more accurately and are used when calculating the fluoride concentration of the sample. Sample consumption can be reduced, by fitting a polyethylene cap (an effective anti-evaporation cap is made from the base of a polyethylene vial, capacity 2.5 ml (Cat. No. XT 1530) available from Xlon Products Ltd., London, England) on the sleeve-junction (Figure 5) to minimize evaporation and enable readings to be obtained from a single 1-μl aliquot, 10 min or longer after its application. The sleeve-junction used must have an exceptionally low leak rate. Since the fluoride electrode has a "memory", solutions with the lowest fluoride concentrations should be analyzed first. Cross-contamination between samples of very different fluoride concentration may, however, be eliminated by rinsing the fluoride-sensing surface of the electrode and the ground-sleeve junction with water to a potential about 50 mV more positive than that given by the buffer blank. If the junction potential becomes unstable, because of dilution of the liquid junction with either water or sample, a fresh liquid junction should be prepared by opening the tap of the KCl reservoir (Figure 3) and slightly loosening the ground-glass sleeve. The sleeve is reseated firmly, the tap closed, and excess KCl solution removed with paper tissue.

Table I. Fluoride Ion Concentrations (ppm) and Their Precision of Measurement (± rel std dev %) as Determined in Replicate 1-μl Samples of Standard NaF Solution, pH 5.2[a]

F concentration of standard NaF solution (ppm) and F content of sample (ng)	Sample No.									
	1	2	3	4	5	6	7	8	9	10
0.050	0.018	0.027	0.033	0.041	0.047	0.049	0.051	0.050	0.050	0.050
	±30.71	±24.44	±20.98	±13.11	±10.77	±6.13	±6.45	±3.51	±1.64	±1.15
0.100	0.045	0.072	0.087	0.090	0.098	0.098	0.099	0.098	0.101	0.100
	±17.21	±12.84	±11.26	±4.32	±5.87	±4.89	±4.24	±3.30	±3.00	±2.26
0.200	0.089	0.150	0.176	0.186	0.192	0.199	0.201	0.200	0.200	0.200
	±5.64	±4.09	±5.27	±5.02	±3.26	±3.81	±3.69	±3.16	±2.96	±2.16
0.500	0.202	0.381	0.459	0.480	0.486	0.490	0.492	0.494	0.496	0.500
	±9.88	±3.48	±2.01	±1.52	±2.12	±2.12	±2.08	±2.14	±1.50	±0.88
1.000	0.473	0.763	0.875	0.910	0.961	0.969	0.977	0.992	0.992	1.000
	±8.37	±4.09	±2.67	±3.15	±2.47	±2.87	±2.67	±2.24	±1.96	±1.33
2.000	1.151	1.700	1.810	1.888	1.936	1.942	1.966	1.983	1.992	2.000
	±2.91	±2.80	±1.72	±1.49	±1.20	±1.24	±1.13	±1.36	±1.17	±1.57

[a] Each result in the table is derived from 10 electrode potential measurements as described in text.

Calculation of Results. The fluoride concentrations of all samples were determined by comparison with a standard curve of 0.1 ppm, 1.0 ppm, and 10 ppm F^- in 4:1 v/v 1 M sodium acetate–1 M perchloric acid buffer.

RESULTS

Precision and Percentage Recovery of Fluoride Diffusion. The microdiffusion procedure was checked over the range 1–100 ng F using standard solutions of NaF in water: replicate (12) portions, 1–10 μl in volume of each standard solution being microdiffused from 50 μl of 60% perchloric acid as described above. The fluoride contents of the diffused standards, *blank-corrected*, were plotted on a logarithmic scale (*y* axis) vs. the absolute amounts of fluoride added (*x* axis) to give the regression curve shown in Figure 6. The vertical bars through the points represent twice the standard deviation at each fluoride level. The straight line represents the best fit through these points as determined by the least squares method. The equation for the line is $y = 0.9883x^{0.9973}$ and the correlation of log *y* with log *x* is 0.9995. Fluoride recoveries varied between 89% and 105% with a mean diffusion blank of 1.26 ± 0.30 (std dev) ng F.

Precision and Absolute Detection Limit of Fluoride Analysis. Reproducibility measurements were carried out on standard solutions of NaF in 1 M sodium acetate–1 M perchloric acid buffer containing 0.05, 0.1, 0.2, 0.5, 1, and 2 ppm F. One-hundred electrode potential measurements were made on each standard solution. These measurements represented 10 "determinations", each "determination" consisting of the millivolt readings given after 60-s equilibration by 10 successive 1-μl aliquots of the standard solution. The results (Table I) show that the analysis tends to become more reproducible with both increase in the number of measurements made upon a standard solution and increase in its fluoride ion concentration. After 4–5 applications of standard solution, the precision of fluoride measurement at the 50 pg, 100 pg, and 1 ng levels was about 12%, 5%, and 2.8% (rel std dev), respectively. The effect of fluoride ion concentration on precision was still evident after 6 applications of standard but, with further 1-μl applications, rapidly declined into insignificance. Thereafter, the precision of measurement tended to be the same (±1–2%, rel std dev) at all fluoride concentrations: a feature characteristic of selective-ion electrodes when the electrode response is Nernstian (*7, 9*). The electrode potentials of all standards, measured after the fifth 1-μl application, were equivalent, in terms of fluoride concentration, to 93–98% of those given by the tenth application. In further tests (Table II), small sample particles (40–90 μg) were dissected from a compressed disk of bone ash of well-established fluoride content (1070 ppm, as determined by various conventional analytical procedures) and analyzed by the present method to yield a value of 1103 ± 40 ppm (std dev) or 3.7% (rel std dev). The *absolute detection limit* of the method was determined with standard solutions of NaF in 0.10 M sodium acetate–perchloric acid buffer, pH 5.2 containing 0 ppb F and 10 ppb F, respectively. Application of 1 μl of the 10-ppb F solution (i.e., 10 pg F^-) to an electrode assembly pre-equilibrated with the 0-ppb F solution caused a significant (3–4 mV) reduction in electrode potential.

Table II. Analysis of Sample Particles Dissected from a Compressed Pellet of Bone Ash of Known (1070 ppm) Fluoride Content

Sample Weight, μg	F concentration of sample solution analyzed, ppm	F concentration of sample, ppm	Mean result, ppm
39.0	1.68	1077	
44.7	1.92	1074	
47.8	2.05	1072	
50.2	2.29	1140	
54.9	2.52	1148	1103 ± 40 (std dev)
56.0	2.50	1116	(±3.7% rel std dev)
68.2	2.90	1063	
73.1	3.45	1180	
83.0	3.60	1084	
89.5	3.85	1075	

DISCUSSION

Fluoride ion in nanogram amounts or less is most reliably determined with the fluoride electrode at the maximum possible concentration or activity, i.e., in the *minimum volume of solution*. The high sensitivity of the present method resides entirely in the ability of the fluoride electrode assembly to handle microliter size sample volumes. The method is more sensitive than the hanging-drop fluoride electrode technique (*10*) which requires a minimum sample volume of about 5 μl, and almost ten times more sensitive than the procedure (*11*) using the combination fluoride electrode with confined

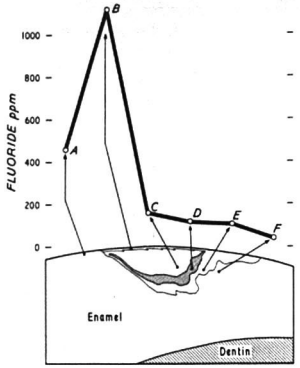

Figure 7. Fluoride uptake and distribution within an approximal carious lesion of enamel as determined by the present analytical methods

(*A*) Sound enamel surface; (*B*) carious enamel surface (surface zone); (*C*) body of lesion; (*D*) dark zone or positive zone; (*E*) primary translucent zone; (*F*) sound interior enamel used as control

spot-test paper (10-μl minimum sample volume). No modification (*12*) of the fluoride electrode itself or the construction of a special fluoride microelectrode (*13*) are necessary with the present technique. The reference electrode and sleeve-junction used however, must have a controlled, low leak rate consistent with the small volumes of analyte solution. The sleeve-junction provides stable junction potentials in spite of its low leak rate, and virtually no difficulty has been experienced with blockage or clogging.

Sample consumption is minimized and precision increased by using a polyethylene cap to reduce evaporation. This allows a much longer equilibration between sample and fluoride electrode. The procedure is, however, more time-consuming. Further marginal improvement in precision might result from the use of a silver/silver chloride reference electrode.

Linear null-point potentiometry (LNPP) (*14, 15*) is, in any case, the most precise way of determining fluoride with the electrode. The sleeve-junction used in the present method could easily be incorporated into the concentration cell employed by Durst and Taylor (*14*) and by Durst (*15*) to determine subnanogram amounts of fluoride by LNPP. This might improve the precision of fluoride measurement at the 100-pg level to about 1%, providing evaporation of the sample was controlled as described above.

The techniques described in this paper were first developed and then employed (*16–19*) to study the uptake and distribution of fluoride in mineralized tissues simply, quickly, and with reasonable accuracy and precision. The uptake of fluoride by dental enamel during carious attack is shown in Figure 7. Many other materials of biological origin, fluoride-containing minerals (hydroxyapatites, fluorapatites, microlites, etc.) have also been analyzed by these procedures.

Gas–liquid chromatography (GLC) is often used to determine fluoride in biological materials (*20, 21*). The current GLC technique (*20*) while having a better-than-1-ng sensitivity, is, however, less convenient than the present method and much less suitable for routine use by relatively unskilled operators. The fluoride microdiffusion technique is based upon the earlier and less sensitive procedures of Stuart (*2*), Rowley and Farrah (*22*) and Marshall and Wood (*23*). In all four methods, a thin layer of sodium hydroxide is used to trap diffused hydrogen fluoride. The present technique, however, like that of Stuart (*2*), has the advantage that all operations are carried out in the same container, thereby minimizing errors due to contamination and the nonquantitative transfer of solutions. The microdiffusion has a very low blank (see Results) and is as sensitive as an alternative separation procedure (*10*) using diphenylsilanediol as fluoride extractant.

The principle of the present method whereby the concentration of an ion in solution is measured by confining a drop of the solution between the flat, ion-sensing surface of an electrode and the flat surface of a ground-sleeve junction seems to be generally applicable. Similar electrode assemblies have been used by the authors to measure ultramicroamounts of hydrogen ion and chloride ion (unpublished work). The pH of 1 μl of solution was determined by replacing the fluoride electrode with a flat-membrane glass electrode. This technique, while much less sensitive than the nanoliter-scale pH determination of Pita (*24*) is convenient to use. For the chloride determination, it was necessary to replace the calomel reference electrode and the KCl salt-bridge with a chloride-free alternative—a mercurous sulfate electrode and saturated potassium sulfate salt-bridge was therefore used. The high and somewhat variable liquid junction potential normally associated with the mercurous sulfate electrode was eliminated by saturating the analyte solutions with K_2SO_4 prior to measurement. One nanogram of chloride ion (i.e., 1 μl of 1 ppm Cl^-) was thus determined with an Orion solid-state chloride electrode, a 10-fold increase in sensitivity over that previously obtainable with chloride electrodes.

LITERATURE CITED

(1) M. S. Frant and J. W. Ross, Jr., *Science*, **154**, 1553 (1966).
(2) J. L. Stuart, *Analyst (London)*, **95**, 1032 (1970).
(3) H. G. McCann, *Arch. Oral Biol.*, **13**, 475 (1968).
(4) "Analytical Methods Guide", 7th ed., Orion Research Inc., Cambridge, Mass., 1975, p 17.
(5) C. R. Edmond, *Anal. Chem.*, **41**, 1327 (1969).
(6) B. L. Ingram, *Anal. Chem.*, **42**, 1825 (1970).
(7) R. T. Oliver and A. G. Clayton, *Anal. Chim. Acta*, **51**, 409 (1970).
(8) R. J. Hall, *Analyst (London)*, **88**, 76 (1963).
(9) T. S. Light in "Ion-Selective Electrodes", R. A. Durst, Ed., National Bureau of Standards Special Publication 302, U.S. Government Printing Office, Washington, D.C., 1969.
(10) P. Venkateswarlu, *Anal. Chem.*, **46**, 878 (1974).
(11) Instruction sheet for combination fluoride electrode, model 96-09. Form IM96-09/866. Orion Research Inc., Cambridge, Mass., 1968.
(12) R. A. Durst and J. K. Taylor, *Anal. Chem.*, **39**, 1483 (1967).
(13) R. A. Durst, *Anal. Chem.*, **41**, 2089 (1969).
(14) R. A. Durst and J. K. Taylor, *Anal. Chem.*, **39**, 1374 (1967).
(15) R. A. Durst, *Anal. Chem.*, **40**, 931 (1968).
(16) J. A. Weatherell, C. Robinson, and A. S. Hallsworth, *Caries Res.* **6**, 312 (1972).
(17) J. A. Weatherell, A. S. Hallsworth, and C. Robinson, *Arch. Oral Biol.*, **18**, 1175 (1973).
(18) J. A. Weatherell, D. Deutsch, C. Robinson, and A. S. Hallsworth, *Nature, (London)*, **256**, 230 (1975).
(19) A. S. Hallsworth, J. A. Weatherell, and D. Deutsch, Proc. 22nd Meeting IADR, Brit. Div., Abstract 180; *J. Dent. Res.*, **53**, 1088 (1974).
(20) J. A. Fresen, F. H. Cox, and M. J. Witter, *Pharm. Weekblad.*, **103**, 909 (1968).
(21) O. Backer Dirks, J.M.P.A. Jongeling-Eijnhoven, T. D. Flissebaalje, and I. Gedalia, *Caries Res.*, **8**, 181 (1974).
(22) R. J. Rowley and G. H. Farrah, *Am. Ind. Hyg. Assoc. J.*, **23**, 314 (1962).
(23) B. S. Marshall and R. Wood, *Analyst (London)*, **94**, 493 (1969).
(24) J. C. Pita, *Anal. Chem.*, **41**, 273 (1969).

RECEIVED for review May 30, 1976. Accepted July 6, 1976. The authors thank the Medical Research Council of Great Britain for supporting this work (Grant No. 971/103/B).

Determination of Trace Elements in Zinc Plant Electrolyte by Differential Pulse Polarography and Anodic Stripping Voltammetry

Edwin S. Pilkington* and Christopher Weeks

CSIRO Division of Mineral Chemistry, P.O. Box 124, Port Melbourne, Vic. 3207, Australia

Alan M. Bond*

Department of Inorganic Chemistry, University of Melbourne, Parkville, Vic. 3052, Australia

Rapid determination of a number of trace elements in zinc sulfate electrolyte is essential for adequate plant process control. As a basis for an on-stream monitoring system, differential pulse polarography and differential pulse anodic stripping voltammetry at a hanging drop mercury electrode have been investigated, using conventional and computer-controlled instrumentation, for the determination of Cd, Cu, Pb, Sb, Co, Ni, Tl, and As. Cd and Cu were determined directly in the zinc sulfate solution down to 10 μg/l., and Sb to a similar low level after addition of concentrated hydrochloric acid. Pb, Co, Ni, Tl, and As were determined after addition of appropriate reagents in some cases; however, these determinations are generally better suited to higher concentration levels than for Cd, Cu, and Sb.

Successful operation of electrolytic zinc plants depends critically on the purity of the cell feed, both for product purity and for high current efficiency in the deposition stage (*1–4*); therefore, reliable analytical data are very important to the economics of the process. Over the years, reasonable process control has existed (*2, 5–9*) by virtue of manual sampling and rapid analysis for those impurity elements known to be most detrimental. Many elements can affect the efficiency of the process (*1–4, 8, 10–12*), particularly Fe, Ni, Co, Cu, Cd, Sb, As, Pb, Ag, Sn, Se, Ge, Te, Tl, and Cl at concentrations in the 10–1000 μg/l. range. Fortunately, it is not necessary to monitor all the significant elements with the same frequency. Normal processing technology involves three or four purification stages in which elements are removed in groups, and it therefore becomes possible to assess the purification at each stage by monitoring a relatively small number of elements.

For the present work it was established that determination of Cd, Cu, and Sb had the highest importance for achievement of rapid process control. Considerable importance attaches, also, to Co, Ni, Tl, Pb, and As, and these elements have therefore been included.

A typical composition of cell feed is given in Table I. This solution is the most significant and the most difficult to analyze, the various trace impurity elements being at their lowest concentrations. Monitoring of solutions at stages earlier in the purification system is a simple extension of techniques established for cell feed.

PRELIMINARY EVALUATION

The analytical problem of rapid determination of Cd, Cu, and Sb in concentrated zinc sulfate at levels in the range 10–1000 μg/l. is substantial. One possibility was to automate the existing manual spectrophotometric techniques (for Cu and Sb) and the dc polarographic technique (for Cd). Although this would increase the frequency of the data output for Cu and Sb, e.g., using discrete or continuous-flow analyzers, the operational time in these instances would make this approach unacceptable. This limitation does not apply, however, to Co, where the "fast chemistry" available in the Nitroso R Salt procedure can yield results in a continuous flow analyzer (Technicon) every 7 min. Other techniques were eliminated because of inadequate sensitivity at the extremely high concentration of zinc sulfate.

Modern polarographic ac and pulse techniques (*13*) are particularly suited for the rapid determination of low concentrations of selected elements in concentrated zinc sulfate solution. Zinc is reduced at more negative potentials than most of the elements to be determined in this case, and sulfate is inactive at the mercury electrode. Data published on fast sweep dc polarography (*14*), second harmonic and differential pulse anodic stripping voltammetry (*15*), and a range of anodic stripping techniques (*16*) indicate the possibilities for polarography with this electrolyte. The technique has, in fact, already been used for impurity determination in zinc plant solutions (*6, 7, 17*), but few data are available for the low levels present after the final purification stages.

EXPERIMENTAL

Instrumentation. For convenience, the three forms of instrumentation examined are described as conventional, semiautomated, and computerized.

Conventional. Either a PAR Electrochemistry System Model 170 or Polarographic Analyzer Model 174 was modified to perform a range of functions additional to those provided by the manufacturer (*18*).

Semiautomated. A combination of a PAR Polarographic Analyzer Model 174 and Automated Electroanalysis Controller Model 315 was used. All procedures except the readout were automatically controlled in these experiments.

Computerized. The polarographic instrumentation under computer control, essentially a differential pulse polarograph based on the design of Vassos and Osteryoung (*19*), was interfaced to a PDP8/E minicomputer with teleprinter output. The computer controls the degassing and the timing of all stages in anodic stripping voltammetry, initiates the potential sweep, and processes the i–E curve to generate the final print-out in units of concentration.

The system is currently being further developed to include automatic cell filling, rinsing, and draining under computer control, which will permit fully automated operation for on-stream industrial use. Further details of this are to be reported in a later paper.

Electrode Systems. A three-electrode system was used for all experiments with either a dropping or hanging drop mercury electrode (HDME) as the working electrode, platinum as the auxiliary electrode, and Ag/AgCl (1 M NaCl) or Hg/$HgSO_4$ (1 M H_2SO_4) as the reference electrode. For anodic stripping voltammetry, most experiments with conventional or semiautomated instrumentation used a Metrohm BM50-3 HDME. The computerized system used a PAR Model 314 Automated HDME. The HDME was selected in preference to a thin film mercury electrode essentially because linear response is obtained over a wider range of concentration without saturation or interference effects (*16*), and the automated version is ideal for on-stream work, allowing a fresh working electrode surface to be generated automatically for each analysis.

Reagents. Preliminary investigations were undertaken using re-

Table I. Typical Composition of Cell Feed

g/l.		mg/l.		μg/l.	
Zn	120	Ca	500	Fe	600
SO_4	210	Na	500	Ni	200
Mn	10	K	400	Cu	100
Mg	3	SiO_2	100	Cd	300
		Cl	150	Sb	30
		Co	10	Pb	100
				As	<50
				Tl	100
				Bi	1
				Se	<10
				Ge	3
				Sn	<200
				Ag	<20

Table II. Direct Determination of Cd in Zinc Sulfate Plant Electrolyte by DPASV Using Conventional and Computerized Instrumentation

Conventional, μg/l.	Computerized, μg/l.
10	20
70	70
110	100
240	280
270	270
170	180

Table III. Determination of Cu in Zinc Sulfate Plant Electrolyte by DPASV and Spectrophotometry

DPASV μg/l.	Spectrophotometry, μg/l.
<10	7
<10	8
<10	5
30	29
10	6
20	30

agent grade zinc sulfate solutions at a concentration of approximately 300 g/l. However, to obtain a blank and to prepare calibration curves, further purification was required. Reagent grade material prepared as a 4-l. batch of solution at 440 g/l. $ZnSO_4 \cdot 7H_2O$ in water was acidified to pH 2 and treated with 20 g of powdered reagent grade zinc dust while heating to 50–60 °C. After stirring continuously for 2 h, the solution was filtered into a Buchner flask which had been previously thoroughly washed with dilute sulfuric acid and rinsed. Usually four treatments were adequate to reduce the concentrations of Cd and Cu from around 200 μg/l. to less than 5 μg/l., Cu being the more difficult to remove. Concentrations of other elements were acceptably low.

All metal standards were prepared as sulfate solutions with the exception of Pb which was prepared as nitrate. All other chemicals were of analytical reagent grade.

Plant Samples. Plant samples were collected in clean polyethylene containers and acidified to approximately pH 2 with sulfuric acid.

Procedures. All solutions were deoxygenated for a minimum period of 3 min using argon or nitrogen. During each potential scan the inert gas was passed over the solution. Elements were determined on aliquots of 20–40 ml at ambient temperatures of 23 ± 2 °C. Other details are presented in the Results and Discussion section.

Alternative Methods for Cu and Sb Determinations. In view of the significance of Cu and Sb in this work, and as a check on the analytical data at concentrations down to 10 μg/l., separate values were obtained using validated spectrophotometric procedures. An outline of the procedures (*20, 21*) is as follows.

Copper. After acidification and destruction of organic matter, copper is extracted with ammonium 1-pyrrolidine carbodithioate into carbon tetrachloride. The solvent phase is wet ashed and the copper re-extracted for spectrophotometric determination.

Antimony. After conversion to Sb(III) and extraction in an iodide system by 4-methyl-2-pentanone (MIBK), antimony is stripped from the solvent phase. After removal of thallium and oxidation to Sb(V), the Rhodamine B Complex is determined spectrophotometrically.

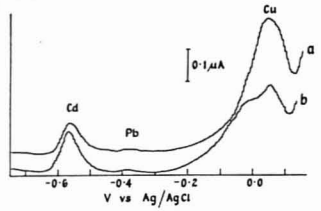

Figure 1. DPASV curves in plant zinc sulfate solution.

Deposition potential, −0.75 V vs. Ag/AgCl, with 2-min stirring and 30-s equilibration time. Pulse amplitude, 25 mV; duration between pulses, 0.5s; scan rate, 10 mV/s. (a) 20 μg/l. Cd, 30 μg/l. Cu; (b) 30 μg/l. Cd, 10 μg/l. Cu

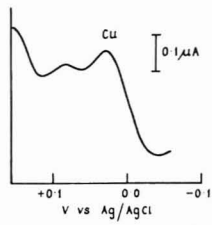

Figure 2. Differential pulse polarogram for 160 μg/l. Cu in plant zinc sulfate solution

Drop time, 2 s; pulse amplitude, −25 mV; scan rate, 1 mV/s

RESULTS AND DISCUSSION

Cadmium. At a DME cadmium gave extremely well defined reversible fundamental and second harmonic ac and pulse polarographic waves in zinc sulfate with an $E_{1/2}$ value of −0.58 V vs. Ag/AgCl. The calibration curves with ac and DPP methods were linear from the limit of detection ($\simeq 5 \times 10^{-7}$ M) to at least 10^{-3} M (50–100 000 μg/l.) with the response in plant electrolyte equally satisfactory as that for purified synthetic solution. Fast sweep polarographic methods (*22*) at a single mercury drop were also satisfactory and have the added advantage of shorter analysis time. For lower concentration levels encountered in cell feed, however, anodic stripping voltammetry is preferable. Figure 1 shows DPASV curves for samples of plant electrolyte (acidified to pH 2), including one sample with the lowest concentration encountered (20 μg/l.). As the matrix is essentially constant, the use of a calibration curve based on purified zinc sulfate was investigated rather than a standard addition technique. A linear response extending well into the polarographic range (>10^{-6} M) and passing through the origin was obtained. Results from standard addition agreed well with calibration curves with good reproducibility (<5%) several days apart. Where available, polarographic and DPASV data gave acceptable agreement, further validating the DPASV procedure. For the concentration range 10–500 μg/l., a deposition time of 2 min with stirring and 30 s without stirring, at a potential of −0.75 V vs. Ag/AgCl, was used. The scan rate was 10 mV/s, with a pulse amplitude of 25 mV, and duration between pulses of 0.5

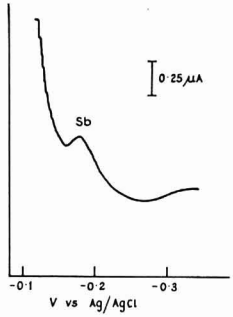

Figure 3. Differential pulse polarogram for 210 μg/l. Sb in plant zinc sulfate solution diluted 1:1 with concentrated HCl

Drop time, 5 s; pulse amplitude −25 mV; scan rate, 0.5 mV/s

s. Table II shows results obtained for cadmium using DPASV with both the conventional and computer-controlled systems. The results validate the latter and demonstrate the practicality of a fully automated method.

Copper. Copper in synthetic zinc sulfate gave well defined DPP curves, although a sloping baseline caused difficulties with ac techniques and the latter were not considered suitable. The $E_{1/2}$ value was about 0.03 V vs. Ag/AgCl. The detection limit was approximately 5×10^{-7} M, and calibration curves were linear over the range 5×10^{-7} M to 10^{-3} M (30–60 000 μg/l.). However, in plant solutions considerable interference from unidentified neighboring peaks was found. Figure 2 shows the difficulties experienced near the detection limit. The interfering species could be chloride ion and degradation products or organic additives.

In synthetic zinc sulfate DPASV curves for Cu were almost as well defined as for Cd, and linear, reproducible calibration curves were obtained. Although plant solutions still presented some difficulties from neighboring peaks, particularly at very low concentrations, Cu could be determined over a wide range of concentration simultaneously with Cd, under the same electrolysis conditions as described above. Figure 1b shows a typical curve at low Cu levels. The sloping baseline can be attributed in part to chloride (Table I).

Table III shows Cu determinations at low levels, compared with those obtained by a spectrophotometric method. Agreement is adequate for process control purposes in the present project, in which the lowest level of interest is 20 μg/l. Improved Cu determination below 20 μg/l. can be obtained by using longer plating periods or chemical treatment with oxidants. Alternatively, deliberate addition of hydrochloric acid can be used as discussed below.

Lead. Extremely well defined DPASV curves are obtained for Pb with a peak potential of −0.51 V vs. Ag/AgCl. Interference from Tl and Sn does, however, occur when these elements are present at comparable or higher concentrations. The acid chloride medium discussed below is equally suitable for Pb determinations and eliminates difficulties which may arise in preparing Pb standards in concentrated sulfate media.

Antimony. Antimony cannot be determined directly in zinc sulfate solution by polarography. However, a very suitable medium is obtained by using a 1:1 mixture of zinc electrolyte sample and concentrated hydrochloric acid (*17*). In this medium, a close-to-reversible three-electron reduction is observed with an $E_{1/2}$ value of −0.26 V vs. Ag/AgCl. Excellent waves were obtained by both the differential pulse and ac

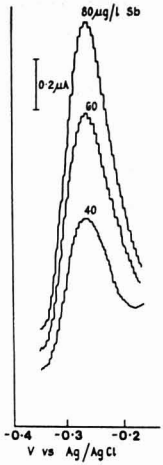

Figure 4. DPASV curves for Sb in plant zinc sulfate solution diluted 1:1 with concentrated HCl

Deposition potential, −0.35 V vs. Ag/AgCl with 2-min stirring and 30-s equilibration period. Pulse amplitude, 25 mV; duration between pulses, 0.5 s; scan rate, 5 mV/s

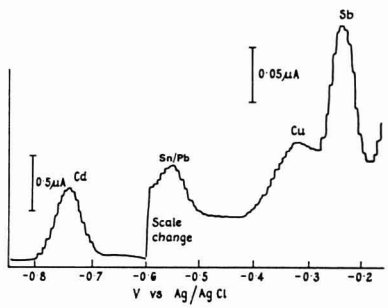

Figure 5. DPASV curves for Cd, Cu, and Sb in plant zinc sulfate solution diluted 1:1 with concentrated HCl

Deposition potential, −0.85 V vs. Ag/AgCl, with 3-min stirring and 30-s equilibration time. Pulse amplitude, 25 mV; duration between pulses, 0.6 s; scan rate, 7 mV/s. Approximately 400 μg/l. Cd, 100 μg/l. Cu, 80 μg/l. Sb

techniques. Linear calibration curves over the range 2×10^{-7} to 5×10^{-4} M (25–60 000 μg/l.) with respect to the original sample were obtained with DPP. Figure 3 shows a plant solution analysis for Sb near the detection limit, and for Sb levels in the above-mentioned range little difficulty was experienced. It should be noted, however, that the proximity of the Cu wave could cause difficulty if Cu was present at concentrations substantially higher than Sb.

With DPASV it is easy to obtain extremely well defined waves in synthetic zinc sulfate/HCl solution, and linear calibration curves are obtained. However, in plant solutions the deposition potential needs to be carefully chosen so as to avoid neighboring peaks. The best deposition potential found was −0.32 V vs. Ag/AgCl. Solutions were analyzed as soon as possible after addition of hydrochloric acid. Figure 4 shows typical curves for plant samples. Despite extremely high

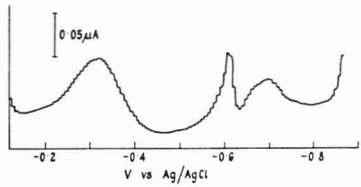

Figure 6. Differential pulse polarogram for 1.4 mg/l. of As in zinc sulfate solution diluted 1:1 with concentrated HCl

Drop time, 0.6 s; pulse amplitude, −25 mV; scan rate, 7 mV/s

sensitivity, the precision is not as high as for Cd and a precision of only ±10% was found. Comparison between standard additions and a calibration curve, however, gave good agreement.

Simultaneous Determination of Cd, Cu, Pb, and Sb. The 1:1 mixture of plant electrolyte and concentrated hydrochloric acid is a suitable medium for simultaneous determination of Cd, Cu, Pb, and Sb by DPASV. This method has advantages in simplicity and speed and eliminates any risk of precipitation of trace constituents which can occur at high pH. Further, the Cu peak is free from spurious interferences, and standard additions of Pb can be made. Sn, if present in concentrations comparable to Pb, will, however, interfere with the Pb determination. Using a three-electrode system and the DPP technique, we have not observed any loss of sensitivity for Sb at more negative plating potentials, as reported by Leclercq and Carlier (*17*).

Figure 5 shows a DPASV trace for a typical plant sample. In this medium the copper wave is a result of the Cu(0) → Cu(I) reaction, which yields a relatively broad Cu peak, causing some interference to the Sb peak. By using differential current values at appropriate potentials and applying mutual corrections calculated from the known peak shapes, it is possible to determine a corrected value for both peaks. Although tedious in conventional manual analysis, this procedure is relatively simple in a computer based system (*23*).

Cobalt. As the reduction step Co(II) + 2e → Co(0) occurs near that for Zn (*24*), it will be very difficult to determine Co by the direct use of the reduction step. However, provided Co(II) can be complexed, the possibility exists of using the oxidation wave Co(II) ⇌ Co(III) + e. Because most ligands forming complexes with Co also complex Zn, and the Zn is present in large excess, high concentrations of complexing reagent are likely to be required. In 0.1 M ethylenediamine/0.1 M KNO_3, the oxidation of Co(II) is reported to give a well defined wave (*24*) at −0.46 V vs. SCE and, accordingly, a method based on this complexing agent was investigated using DPP at −0.5 V vs. Ag/AgCl.

It was confirmed, however, that concentrations of at least 2 M ethylenediamine with dilution of the zinc electrolyte were required to achieve a determination level as low as 15 mg/l. Obviously, the alternative spectrophotometric technique is to be preferred.

Nickel. As with Co, complexation is required to permit the determination of Ni. The use of thiocyanate to produce fairly well defined waves is well documented (*24–26*), but, because of the presence of very high concentrations of Zn, higher than usual concentrations of thiocyanate were found to be essential. Addition of ammonia was also undertaken to shift the Zn to more negative potentials, enabling the Ni wave to be observed between those for Cd and Zn. Equal volumes of zinc electrolyte and 2 M NH_4SCN with the solution adjusted to approximately pH 8 with ammonia was found to provide a suitable medium for Ni determination by DPP, down to concentration levels at least as far as 1 mg/l. The peak potential for Ni was −0.83 V vs. Ag/AgCl in the medium used.

Attempts to determine Ni by DPASV were unsuccessful. Owing to the irreversible nature of the Ni(II)/Ni(0) process, stripping peaks occur at a more positive potential than the corresponding reduction peaks, so that overlapping with other waves (e.g. Cd, Pb, Tl) occurs.

Thallium. Thallium gives extremely well defined differential pulse polarograms and anodic stripping voltammograms in synthetic zinc sulfate. The peak potential under polarographic conditions was −0.47 V vs. Ag/AgCl using DPP. Overlap of the Tl wave with Cd occurs when Cd is in substantial excess (*18*), the typical plant situation (Table I). Under DPASV conditions the interference is overcome by using a deposition potential on the positive edge of the Cd stripping wave (−0.54 V vs. Ag/AgCl). However, the peak potential for Pb stripping at −0.41 V vs. Ag/AgCl prevents direct determination of Tl in the plant situation (*16*).

Temmerman and Verbeek (*27*) have shown that addition of EDTA leaves the potential of the Tl wave essentially unaltered, but shifts Cd and Pb to far more negative values, making this medium ideal for the stripping technique. Because of the high Zn concentration, a tenfold dilution of plant electrolyte with a 1.2 M ammonium EDTA solution was used. This dilution effectively raises the detection limit under polarographic conditions to approximately 10^{-5} M. Using DPASV, an electrolysis time of 10 min or more is necessary to achieve a sensitivity comparable with that for Cd or Cu.

Arsenic. The 1:1 mixture of zinc sulfate solution and concentrated hydrochloric acid is a suitable medium for polarographic determination of As. Three waves are observed similar to those reported by Myers and Osteryoung (*28*) for an HCl medium. Figure 6 is a differential pulse polarogram for 1.4 mg/l. of As(III) in a synthetic zinc sulfate electrolyte. Practical levels of As in cell feed are much lower, however, and interferences from other species in solution limit the value of this method. Attempts to determine As by DPASV in this medium were also unsuccessful.

ACKNOWLEDGMENT

We thank H. Blutstein, P. Smith, and W. Wilson for performing some of the experimental work, and G. C. Bratt for helpful comments.

LITERATURE CITED

(1) C. L. Mantell, "Electrochemical Engineering", 4th ed., McGraw-Hill, New York, 1960, p 210.
(2) G. T. Wever, *J. Metals*, **11**, 130 (1959).
(3) G. C. Bratt, *Electrochem. Technol.*, **2**, 323 (1964).
(4) V. L. Klimenko, *Sov. J. Non-Ferrous Metals*, **12** (11), 18 (1971).
(5) A. C. Jephson and R. E. Allen, *J. Metals*, **9**, 1381 (1957).
(6) B. S. Bruk and E. Ya. Ovcharenko, *Sov. J. Non-Ferrous Metals*, **12** (8), 18 (1971).
(7) L. S. Zaretskii, O. G. Vinogradov, and L. B. Babitskii, *Sov. J. Non-Ferrous Metals*, **13** (5), 30 (1972).
(8) A. R. Ault, J. H. Bain, D. J. Palmer, and J. B. Pullen, in "South Australia Conference 1975" (Australasian Institute of Mining and Metallurgy, Melbourne, 1975), p 225.
(9) D. H. Hart, J. H. McNicol, and J. D. Martin, in "South Australia Conference 1975" (Australasian Institute of Mining and Metallurgy, Melbourne, 1975), p 211.
(10) U. F. Turoshima and V. V. Stender, *J. Appl. Chem. USSR*, **28**, 151 (1955).
(11) H. H. Fukabayashi, T. J. O'Keefe, and W. C. Clinton, *U.S. Bur. Mines Rep.*, **RI 7966** (Rolla, Mo., 1974).
(12) G. Steinvelt and H. Holtan, Jr., *J. Electrochem. Soc.*, **107**, 247 (1960).
(13) J. B. Flato, *Anal. Chem.*, **44** (11), 75A (1972).
(14) T. M. Florence, *Proc. Roy. Aust. Chem. Inst.*, **39**, 211 (1972).
(15) H. Blutstein and A. M. Bond, *Anal. Chem.*, **46**, 1531 (1974).
(16) G. E. Batley and T. M. Florence, *J. Electroanal. Chem. Interfacial Electrochem.*, **55**, 23 (1974).
(17) M. Leclercq and S. Carlier, *Anal. Lett.*, **1**, 359 (1968).
(18) H. Blutstein and A. M. Bond, *Anal. Chem.*, **46**, 1754 (1974).
(19) B. H. Vassos and R. A. Osteryoung, *Chem. Instrum.*, **5**, 257 (1973–1974).
(20) E. S. Pilkington and P. R. Smith, unpublished work, CSIRO Melbourne (1975).

(21) E. S. Pilkington and W. Wilson, unpublished work, CSIRO Melbourne (1974).
(22) H. Blutstein and A. M. Bond, *Anal. Chem.*, **48**, 248 (1976).
(23) L. B. Sybrandt and S. P. Percne, *Anal. Chem.*, **44**, 2331 (1972).
(24) L. Meites, "Polarographic Techniques", 2nd ed., Wiley, New York, 1965, p 614.
(25) M. Pinta, "Detection and Determination of Trace Elements" (English translation, Israel Program for Scientific Translations, Jerusalem, 1966), Dunod, Paris, 1962.
(26) A. Lagrou and F. Verbeek, *J. Electroanal. Chem.*, **19**, 125 (1968).
(27) E. Temmerman and F. Verbeek, *J. Electroanal. Chem.*, **19**, 423 (1968).
(28) D. J. Myers and J. Osteryoung, *Anal. Chem.*, **45**, 267 (1973).

RECEIVED for review March 9, 1976. Accepted June 28, 1976. The work was supported in part by the Electrolytic Zinc Company of Australasia Limited.

Double Potassium Salt of Sulfosalicylic Acid in Acidimetry and pH Control

Richard A. Butler and Roger G. Bates*

Department of Chemistry, University of Florida, Gainesville, Fla. 32611

Upon partial neutralization of sulfosalicylic acid, a double potassium salt of the composition $KHSs{\cdot}K_2Ss{\cdot}H_2O$ can be prepared, where Ss represents the bivalent anion $^-OOC\text{-}C_6H_3(OH)SO_3^-$. The pK_2 for the carboxyl group has been found to be 2.85, with a variation of less than 0.01 unit in the range 15 to 45 °C. The double salt is a promising acidimetric standard, as the equivalent weight (550) is high and the pH change near the equivalence point in the titration with strong base is sharper than for the titration of potassium hydrogen phthalate. Solutions of this salt are also useful for acidity control near pH 2.8.

Sulfosalicylic acid ($2\text{-}HOC_6H_3\text{-}1\text{-}COOH\text{-}5\text{-}SO_3H$) is a triprotic acid. The sulfonic acid group is strong ($K > 0.1$), the carboxyl group is of moderate strength ($K \simeq 1.4 \times 10^{-3}$), and the phenol group is very weak ($K \simeq 4 \times 10^{-14}$ in salicylic acid (*1*)). In 1857, Mendius (*2*) reported that the primary and secondary potassium salts of sulfosalicylic acid crystallize as a 1:1 double salt.

This double potassium salt is of some analytical interest. It can be prepared in pure anhydrous form, is not appreciably hygroscopic, and has a very large equivalent weight (550.655). Hence, weighing errors may be relatively small. Furthermore, the strength of the second acid group, coupled with the essential inertness of the phenol group, permits the double salt to be titrated with high precision to the equivalence point for the carboxyl neutralization. This substance therefore shows promise as a standard for acidimetry. In addition, the double salt is a natural pH buffer, and solutions regulated at a pH near 2.8 can be prepared by weighing a single pure substance. In both acidimetry and pH control, this double salt appears to be superior to potassium hydrogen phthalate. We have now determined the second dissociation constant of sulfosalicylic acid, making clear these analytical applications.

SECOND DISSOCIATION CONSTANT OF SULFOSALICYLIC ACID

The dissociation constant K_2 of the carboxyl group was determined by emf measurements of the cell without liquid junction

$$Pd;H_2(g,1\ atm)|KHSs{\cdot}K_2Ss(m), KCl(m)|AgCl;Ag \quad (A)$$

where Ss represents the bivalent sulfosalicylate anion $^-OOCC_6H_3(OH)SO_3^-$ and m is molality. The techniques have been described in a number of earlier papers (*3*, *4*). If the activity-coefficient term is represented by the Debye-Hückel equation, each value of the emf E of cell A for solutions of known molality can be used to calculate a value for the "apparent" pK_2 (designated pK_2'), inasmuch as the standard emf $E°$ of the cell is known (*5*). The relationship is

$$pK_2' = \frac{(E - E°)F}{RT \ln 10} + \log \frac{m(m - m_H)}{m + m_H} + \frac{2AI^{1/2}}{1 + Ba\mathring{A}I^{1/2}} \quad (1)$$

In Equation 1, A and B are constants of the Debye-Hückel theory, å is the "ion-size parameter", and I is the ionic strength. The quantity pK_2' becomes equal to the thermodynamic value (pK_2) upon extrapolation to $I = 0$. The values of the ion-size parameter are chosen by trial to produce the best straight-line extrapolation. The ionic strength is given by

$$I = 5m + 2m_H \quad (2)$$

In view of the appreciable acidic dissociation of the carboxyl group of KHSs, estimates of the hydrogen ion molality (m_H) are needed to establish reliable values of the buffer ratio in Equation 1. In principle, m_H can be derived from the emf by the Nernst equation, provided that the activity coefficient of HCl in the buffer–chloride mixtures can be estimated with the required accuracy:

$$-\log m_H = \frac{(E - E°)F}{RT \ln 10} + \log m + 2 \log \gamma_{\pm}(HCl) \quad (3)$$

EXPERIMENTAL

The double salt $KHSs{\cdot}K_2Ss$ was prepared by combining sulfosalicylic acid of commercial grade with reagent-grade potassium carbonate in the proportions of 0.75 mol of bicarbonate to 1 mol of the acid. The product was recrystallized repeatedly until a sample, dried at 110 °C, assayed close to 100% by titration with strong alkali. The crystallization was effected by cooling an aqueous solution, saturated at about 70 °C, to 20 °C. In some instances, ethanol was added to the extent of about half the volume of the saturated aqueous solution to increase the yield of the double salt. The lot of salt used had been crystallized seven times. It was titrated with equally satisfactory results to the calculated equivalence point (pH 7.6 in 0.05 M solution) or to the first pink color of phenolphthalein. Two weight titrations of the final product gave 100.01 and 100.00%.

Recalculation of the analytical data given by Mendius (*2*) confirms that 1 mol of the double salt contains 2S and 3K and that the compound separates from aqueous solutions as a monohydrate. The water of hydration was easily lost, however, and, in our experience, the dried salt was not appreciably hygroscopic. The salt dissolves readily in water; at room temperature, a saturated solution is about 0.2 M.

Potassium chloride was purified by two crystallizations from water. The platinum bases for the hydrogen electrodes were coated with palladium black (*6*) after trial measurements with platinum black

Table I. Electromotive Force (E, in Volts) of the Cell: Pd; H_2 (g, 1 atm) |KHSs·K_2Ss (m_1), KCl (m_2) |AgCl; Ag from 10 to 50 °C

$m_1 = m_2$, mol kg^{-1}	10 °C	15 °C	20 °C	25 °C	30 °C	35 °C	40 °C	45 °C	50 °C
0.010 002	0.506 44	0.507 90	0.509 25	0.510 61	0.512 55	0.513 94	0.515 41	0.516 88	0.518 37
0.010 590	0.504 32	0.505 55	0.506 85	0.508 58	0.509 56	0.510 93	0.512 28	0.513 59	0.514 89
0.019 815	0.486 23	0.487 18	0.488 09	0.489 13	0.490 01	0.490 99	0.491 94	0.492 90	0.493 82
0.020 98	0.483 63	0.484 53	0.485 43	0.486 32	0.487 25	0.488 09	0.488 97	0.489 85	0.490 71
0.041 64	0.464 01	0.464 40	0.464 77	0.465 23	0.465 59	0.466 02	0.466 43	0.466 86	. . .
0.041 97	0.463 70	0.464 05	0.464 47	0.464 90	0.465 17	0.465 53	0.465 96	0.466 36	0.466 79
0.062 67	0.453 19	0.453 23	0.453 30	0.453 34	0.453 45	0.453 47	0.453 56	0.453 64	0.453 72
0.063 24	0.452 99	0.452 99	0.453 03	0.453 20	0.453 21	0.453 33	0.453 40	0.453 49	0.453 51
0.084 84[a]	0.445 70	0.445 46	0.445 26	0.445 10	0.444 94	0.444 76	0.444 59	0.444 41	0.444 22
0.106 60[a]	0.440 23	0.439 87	0.439 46	0.439 10	0.438 80	0.438 47	0.438 15	0.437 84	0.437 49

[a] Values of E are average results obtained for two different solutions of the same composition.

Table II. pK_2 for Sulfosalicylic Acid from 10 to 50 °C and Related Thermodynamic Constants

t, °C	pK_2	t, °C	pK_2
10	2.869	30	2.845
15	2.859	35	2.846
20	2.852	40	2.849
25	2.847	45	2.855
		50	2.862

ΔH° (25 °C) = 257 ± 55 cal mol^{-1}. ΔS° (25 °C) = −12.2 ± 0.2 cal K^{-1} mol^{-1}. ΔC_p° (25 °C) = −42 ± 7 cal K^{-1} mol^{-1}.

gave highly unstable values of the emf, presumably because of reduction of the aromatic ring.

The cells were immersed in a water thermostat controlled within 0.01 °C of each of the nine nominal temperatures. Temperatures were measured with a Hewlett-Packard quartz thermometer which had been compared with a calibrated platinum resistance thermometer. The emf was determined with a Hewlett-Packard digital voltmeter checked from time to time against laboratory standards consisting of two saturated standard cells maintained at a controlled temperature.

RESULTS

The observed values of the emf of cell A, corrected to a partial pressure of hydrogen of 1 atm, are listed in Table I. It has long been recognized that uncertainties in estimating the activity coefficient in Equation 3 and, hence, the molality of hydrogen ion, lead to appreciable errors in pK when the latter is less than 3 (*7*). For this reason, a close approximation to the activity coefficient of HCl in the buffer–chloride solutions was sought.

It was assumed that $\gamma_\pm$(HCl) in the solutions composed of potassium salts (chloride and sulfosalicylates) will be nearly the same as the "trace" activity coefficient $\gamma_\pm^{tr}$ of HCl in KCl solutions. From the values of α_{12} for HCl in HCl–KCl mixtures (*8*), one finds that the trace activity coefficient at 25 °C is 0.782 in 0.1 m KCl and 0.705 in 0.5 m KCl. These values and other intermediate values derived by interpolation of α_{12} are closely represented by

$$-\log \gamma_\pm^{tr} = \frac{AI^{1/2}}{1 + 4.1BI^{1/2}} - 0.065I \qquad (4)$$

which was used to obtain $\gamma_\pm$(HCl) for each of the cell solutions at 25 °C. The activity coefficient of HCl is not very sensitive to temperature changes. Hence, $\gamma_\pm$(HCl) at the other temperatures studied was obtained from the values at 25 °C with the use of the temperature coefficients found by Harned and Hamer (*9*) for the activity coefficient of HCl (0.01 m) in KCl solutions.

The values of m_H obtained by Equation 3 were used to calculate pK_2' by Equation 1. Visual examination as well as linear regression analysis dictated a choice of å = 6 Å as suitable for the evaluation of the intercept, pK_2. The standard deviation about regression varied from 0.002 at 25 °C to 0.006 at 15 °C. At a few of the temperatures, these deviations from linearity are larger than those normally expected in well-designed experiments of this type. They may indicate a slight residual tendency of the sulfosalicylate ions toward reduction at the palladium electrode. Nevertheless, it was clear from a comparison of data at 25 °C recorded at the beginning of the temperature series with those at the end that any irreversibility was of little consequence.

The values of pK_2 at the nine temperatures were fitted to a second-degree equation of the form proposed by Harned and Robinson (*10*) using the method of orthogonal polynomials described by Please (*11*). The result was as follows:

$$pK_2 = \frac{1420.41}{T} - 6.4925 + 0.015347T \qquad (5)$$

where T is the thermodynamic temperature in kelvins. The average deviation of the calculated values from the observed pK_2 was 0.002 unit. Table II lists the values derived from Equation 5, and at the foot of the table are found the standard changes in enthalpy, entropy, and heat capacity associated with the dissociation of the carboxyl group. These quantities are given in calories, where 1 cal = 4.184 J. The uncertainties assigned to the thermodynamic functions were calculated from the variance of pK_2 by the method of Please (*11*).

DISCUSSION

The double salt of monopotassium sulfosalicylate and dipotassium sulfosalicylate may prove useful as a standard for acidimetry. It can be prepared in pure form and, once dehydrated, shows little tendency to pick up moisture except from very humid atmospheres. Its equivalent weight (550.665) is high enough to minimize adventitious errors in weighing due to temperature fluctuations, absorption of moisture, and the like. When the double potassium salt is titrated with strong alkali, the pH rises sharply from near pH 4 through the equivalence point. If the concentration of Ss^{2-} at the equivalence point is 0.05 M, the pa_H calculated for $\gamma_{Ss} = 1$ is 7.77. If γ_{Ss} is given a more reasonable value of 0.5, the pa_H at the equivalence point is found to be 7.62. Accurate titrations can be performed with phenolphthalein as an end-point indicator. The pK_2 (2.85) is so low that the buffer capacity at the equivalence point is considerably smaller than is the case for titrations of potassium hydrogen phthalate (pK_2 = 5.4), and the feasibility of the titration is correspondingly greater.

The double salt is also useful for pH control. As can be seen in Table II, pK_2 is at a minimum near 30 °C. Consequently, the pH of solutions of this substance is almost unaffected by changes of temperature in the range 20 to 40 °C. Buffer solutions with pH somewhat below 3 are conveniently prepared

by a single weighing of a pure substance, and a buffer ratio very close to unity is assured.

The usefulness of some buffer substances such as potassium hydrogen tartrate and, to a lesser extent, potassium hydrogen phthalate is impaired by a tendency to support mold growth. Although molding in solutions of sulfosalicylates was not specifically investigated, it seems likely that the presence of a phenol group in the sulfosalicylate molecule may provide built-in mold inhibition.

LITERATURE CITED

(1) N. Konopik and O. Leberl, *Monatsh. Chem.*, **80**, 655 (1949).
(2) O. Mendius, *Ann. Chem.*, **103**, 39 (1857).
(3) G. D. Pinching and R. G. Bates, *J. Res. Nat. Bur. Stand.*, **40**, 405 (1948).
(4) G. D. Pinching and R. G. Bates, *J. Res. Nat. Bur. Stand.*, **45**, 322 (1950).
(5) R. G. Bates and V. E. Bower, *J. Res. Nat. Bur. Stand.*, **53**, 283 (1954).
(6) H. T. S. Britton, "Hydrogen Ions", 4th ed., Vol. I., Van Nostrand, Princeton, N.J., 1956, Chap. 3.
(7) R. G. Bates, *J. Res. Nat. Bur. Stand.*, **47**, 127 (1951).
(8) H. S. Harned and B. B. Owen, "The Physical Chemistry of Electrolytic Solutions", 3d ed., Reinhold Publishing Corp., New York, N.Y., 1958, p 608.
(9) H. S. Harned and W. J. Hamer, *J. Am. Chem. Soc.*, **55**, 2194 (1933).
(10) H. S. Harned and R. A. Robinson, *Trans. Faraday Soc.*, **36**, 973 (1940).
(11) N. W. Please, *Biochem. J.*, **56**, 196 (1954).

RECEIVED for review April 28, 1976. Accepted June 24, 1976. This work was supported in part by the National Science Foundation under Grant CHE73-05019 A02.

Semiintegral Electroanalysis: The Shape of Irreversible Neopolarograms

Masashi Goto[1] and Keith B. Oldham*

Trent University, Peterborough, Ontario, Canada

The equation of the m vs. E curve during the totally irreversible reduction of an electroactive species is derived: it resembles an irreversible polarogram at a stationary electrode, but is less asymmetric. The effects of ramp-rate and of initial potential are evaluated, and the relationship to linear scan voltammetry is explored. Neopolarograms have been determined experimentally, using the IO_3^- and Ni^{2+} electroreductions, and correlation between theory and experiment is sought by comparing transfer coefficient values determined from various features of the neopolarograms.

When an electrode in contact with a solution containing a reducible species is polarized by a potential E that becomes progressively and linearly more negative, the curve which results from displaying the semiintegral m of the faradaic current vs. $-E$ is termed a neopolarogram. If the electrode reaction is reversible, the shape of the neopolarogram is identical to that of a classical reversible polarogram (*1–3*). The usual equation describing this shape

$$E = E_{1/2} + \frac{RT}{NF} \ln\left(\frac{m_c - m}{m}\right) \tag{1}$$

may be rephrased as

$$m = \frac{m_c}{2} - \frac{m_c}{2} \tanh\left(\frac{NF}{2RT}[E - E_{1/2}]\right) \tag{2}$$

where m is the semiintegral (*4*), $d^{-1/2}\,i/dt^{-1/2}$, of the faradaic current i, m_c is an abbreviation for the constant

$$NAFC\sqrt{D} \equiv m_c \tag{3}$$

and other symbols have the significance commonly accorded them in electroanalytical chemistry. Note that the shape of a reversible neopolarogram depends on neither the initial potential E_0 nor the ramp-rate v, the two constants that jointly determine how the potential

$$E = E_0 - vt \tag{4}$$

changes with time.

[1] Present address, Department of Applied Chemistry, Faculty of Engineering, Nagoya University, Chikusa-ku, Nagoya, Japan.

Conditions wherein the electrochemical reduction

$$Ox + Ne^- \xrightarrow{k(E)} Rd \tag{5}$$

is totally irreversible or quasi-reversible have also been considered (*1, 2*). One of the major advantages of the semiintegral method, that has been exploited by Saveant and coworkers (*5*), is its ability to analyze electrochemical kinetics without preassuming any particular dependence of the heterogeneous rate constant $k(E)$ upon potential. For the present purpose, however, it will be assumed that the rate of reduction is governed by a volmerian,

$$k(E) = k_s \exp\left(\frac{-\alpha nF}{RT}[E - E_s]\right) \tag{6}$$

dependence on potential. If the rate-determining step of the electroreduction mechanism is an initial transfer of n electrons, then α is the transfer coefficient of that step. The shape of such irreversible neopolarograms is not independent either of E_0 or of v, so that it is impossible to write an equation of the form $m = f(E)$ in which the function f is independent of the starting potential and the ramp-rate. However, it is possible to derive an expression of the form $f(m,i,E) = 0$, relating potential to both the faradaic current and its semiintegral, and in which neither E_0 or v appears. Such a relationship (*1, 2*) is

$$E = E_s + \frac{RT}{\alpha nF} \ln\left(\frac{k_s[m_c - m]}{i\sqrt{D}}\right) \tag{7}$$

and has been verified experimentally. Though it certainly holds when the potential varies with time according to the linear relation 4, the validity of Equation 7 is not restricted to any particular temporal dependence of potential (*6*).

Equation 7 cannot be said to describe the shape of an irreversible neopolarogram; what it does is to provide an interrelationship between the shape of a neopolarogram and the shape of a linear-potential-scan voltammogram. The object of the present study is to produce and test an equation that, in fact, does describe the shape of an irreversible neopolarogram by giving the value of m as an explicit function, $m = f(E,E_0,v)$, of the variable E and the constants E_0 and v.

If E_0 is sufficiently positive, then its precise value is irrelevant. We shall see that, in this circumstance, the equation that relates m and E is

Table I. Values of m/m_c as a Function of the Parameter ξ (an Undimensionalized Potential, Defined in Equation 8b), Giving the Shape of an Irreversible Neopolarogram That Starts at a Sufficiently Positive Potential

ξ	m/m_c	ξ	m/m_c
$-\infty$	0	+0.4000	0.67678
−7.0000	0.00091	+0.6000	0.72955
−6.0000	0.00249	+0.6829	0.75000
−5.0000	0.00671	+0.7802*	0.77277
−4.0000	0.01810	+0.8000	0.77725
−3.0000	0.04810	+1.0000	0.81909
−2.0000	0.12333	+1.2000	0.85476
−1.8000	0.14768	+1.4000	0.88445
−1.6000	0.17612	+1.6000	0.90867
−1.4000	0.20904	+1.8000	0.92811
−1.2000	0.24672	+1.9346	0.9389
−1.1837	0.25000	+2.0000	0.94361
−1.0000	0.28930	+2.1292	0.9517
−0.8000	0.33669	+2.5185	0.9699
−0.6000	0.38850	+3.2969	0.9880
−0.4000	0.44401	+4.0000	(0.99483)
−0.2072	0.50000	+5.0000	(0.99830)
−0.2000	0.50212	+6.0000	(0.99943)
−0.0000	0.56140	+7.0000	(0.99981)
+0.2000	0.62020	$+\infty$	1

m/m_c values given to only four decimal places were derived from data in Ref. (*10*), while parenthesized values are from Expression 18. The asterisked entry corresponds to the peak of a linear scan voltammogram.

$$1 - \frac{m}{m_c} = \sum_{j=0}^{\infty} (-\exp\xi)^j/\sqrt{(j!)} \qquad (8a)$$

where ξ is the abbreviation

$$\frac{\alpha nF}{RT}[E_s - E] + \frac{1}{2}\ln\left(\frac{k_s^2 RT}{\alpha nFvD}\right) \equiv \xi \qquad (8b)$$

The derivation of Equation 8, and of the more complex relationship that covers cases in which E_0 is not indefinitely positive, is accomplished in the next section. This is followed by an experimental section which attempts to verify the theoretical predictions using the reductions of iodate and nickel ions at a mercury electrode.

THEORETICAL

On recognition that the current i is the temporal semiderivative, $i = d^{1/2}m/dt^{1/2}$, of m, Equation 7 may be recast as

$$\frac{\sqrt{D}}{k_s}\frac{d^{1/2}m}{dt^{1/2}} = [m_c - m]\exp\left(\frac{\alpha nF}{RT}[E_s - E_0 + vt]\right) \qquad (9)$$

after incorporation of relationship 4. This so-called semidifferential equation (*7*) contains m and t as the only variables. Simplification to

$$\frac{d^{1/2}\mu}{d\tau^{1/2}} = \gamma(1 - \mu)\exp\tau \qquad (10)$$

follows from the definitions

$$\frac{m}{m_c} \equiv \mu \qquad (11)$$

and

$$\frac{\alpha nFvt}{RT} \equiv \tau \qquad (12)$$

of two undimensionalized variables to play the roles of m and t, and of one dimensionless constant,

$$k_s\left(\frac{RT}{\alpha nFvD}\right)^{1/2}\exp\left(\frac{\alpha nF}{RT}[E_s - E_0]\right) \equiv \gamma \qquad (13)$$

whose value decreases as E_0 becomes more positive. Our approach to solving Equation 10 will be to first consider its solution in the $\gamma \to 0$ limit (as appropriate to neopolarograms which start at an arbitrarily large positive potential), before going on to a more general solution.

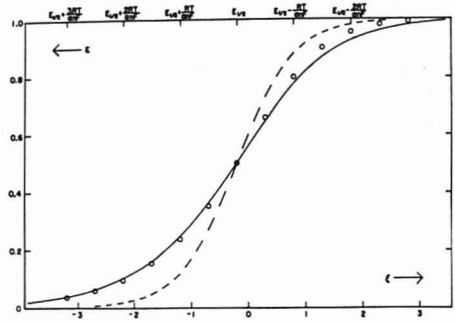

Figure 1. Comparison of the shape of an irreversible neopolarogram (full line) with a reversible (neo)polarogram (dashed line) and an irreversible polarogram (unconnected points)

The three curves, which are given by the expressions $1 - \Sigma(j!)^{-1/2}(-\exp\xi)^j$ where $\xi + 0.2072 = \alpha nF[E_{1/2} - E]/RT$; $\frac{1}{2} - \frac{1}{2}\tanh(NF[E - E_{1/2}]/RT)$; and $\sqrt{\pi}\lambda\exp(\lambda^2)\mathrm{erfc}\lambda$ where $\lambda = 0.433\exp(\alpha nF[E_{1/2} - E]/RT)$; have been scaled by assuming $\alpha n = N/2$ and by adjusting the half-wave potentials to coincide

Initial Potential Indefinitely Positive. Definitions 8b, 12 and 13 imply $\xi = \tau + \ln\gamma$, an identity which converts Equation 10 to

$$\frac{d^{1/2}\mu}{[d(\xi - \ln\gamma)]^{1/2}} = (1 - \mu)\exp\xi \qquad (14)$$

This becomes

$$\frac{d^{1/2}\mu}{[d(\xi + \infty)]^{1/2}} = (1 - \mu)\exp\xi \qquad (15)$$

in the $\gamma \to 0$ limit. Notice that ξ is simply a suitably undimensionalized potential. The $d^{1/2}/[d(\xi + \infty)]^{1/2}$ operator, corresponding to a lower limit of $-\infty$, is an instance of the Weyl differintegration operator (*7*), a class to which the rule

$$\frac{d^q\exp(\nu x)}{[d(x + \infty)]^q} = \nu^q\exp(\nu x),\ \nu > 0,\ \text{all } q \qquad (16)$$

applies. This simple rule permits immediate recognition of

$$\mu = -\sum_{j=1}^{\infty}(-)^j\frac{\exp(j\xi)}{\sqrt{(j!)}} \qquad (17)$$

as a solution to Equation 15. From here it is just a matter of changes of variable to generate the final result, Equation 8.

Table I contains accurate numerical data corresponding to Equation 17 and Figure 1 includes a graph of μ vs. ξ; that is, it shows the shape of an irreversible neopolarogram. For comparison, the shapes of a reversible neopolarogram (Equation 1 or 2) and of an irreversible polarogram at a stationary electrode (*8*) are also included in this diagram. (By the phrase "polarogram at a stationary electrode" we mean the i vs. $-E$ curve produced by a series of potential step experiments in which the current is measured after a constant time interval. The applied potential is changed slightly between experiments.) The three curves have been "fitted" at the half-wave point. As expected, the irreversible neopolarogram is decidedly less steep than the reversible curve. The irreversible neopolarogram is an asymmetric curve, its point of inflection lying somewhat negative of its half-wave potential. The asymmetry is mild enough to escape casual notice, how-

Table II. Comparison of Polarographic Features. D' **Is the Diffusion Coefficient of the Reduction Product**

Feature	Reversible neopolarogram or polarogram	Irreversible neopolarogram	Irreversible stationary electrode polarogram
$E_{1/2}$	$E_s + \frac{RT}{NF} \ln \sqrt{\frac{D'}{D}}$	$E_s + \frac{RT}{\alpha nF} \ln\left(1.23 k_s \sqrt{\frac{RT}{\alpha nFv}}\right)$	$E_s + \frac{RT}{\alpha nF} \ln\left(2.31 k_s \sqrt{\frac{t}{D}}\right)$
$E_{1/4} - E_{1/2}$	$1.099 \frac{RT}{NF}$	$0.977 \frac{RT}{\alpha nF}$	$0.940 \frac{RT}{\alpha nF}$
$E_{1/2} - E_{3/4}$	$1.099 \frac{RT}{NF}$	$0.890 \frac{RT}{\alpha nF}$	$0.809 \frac{RT}{\alpha nF}$
Slope at $E_{1/2}$	$-\frac{NF}{4RT}$	$-0.295 \frac{\alpha nF}{RT}$	$-0.313 \frac{\alpha nF}{RT}$
Maximum slope	$-\frac{NF}{4RT}$	$-0.297 \frac{\alpha nF}{RT}$	$-0.320 \frac{\alpha nF}{RT}$
Height of maximum slope (inflection point)	0.500	0.545	0.576
Potential of maximum slope	$E_{1/2}$	$E_{1/2} - 0.151 \frac{RT}{\alpha nF}$	$E_{1/2} - 0.241 \frac{RT}{\alpha nF}$
"Log plot" slope	$\frac{NF}{2.303\,RT}$	$\frac{1.178\,\alpha nF}{2.303\,RT}$ at $E_{1/2}$	$\frac{1.279\,\alpha nF}{2.303\,RT}$ at $E_{1/2}$

ever, and is certainly not as great as that of a classical stationary electrode irreversible polarogram. Features of the three curves are compared in Table II.

Early entries in Table I were calculated by using Equation 17. For ξ values in excess of about 2.0, the retention of sufficient computational precision makes this straightforward approach unrewarding. The parenthesized values listed in the tabulation for large ξ were calculated from the asymptotic expression

$$1 - \mu \sim \frac{\exp(-\xi)}{\sqrt{(\pi\xi)}} \tag{18}$$

Dependence on Ramp-Rate. We have established that, for irreversible neopolarograms which start at arbitrarily positive potentials, μ is a function of ξ only. It follows, therefore, that the change with v of any point on the neopolarographic wave (e.g., the half-wave potential, $E_{1/2}$, corresponding to $\mu = \frac{1}{2}$) is that required to maintain a constant value of ξ. Then by differentiating

$$\frac{\alpha nF}{RT}[E_s - E_\mu] + \frac{1}{2} \ln\left(\frac{k_s^2 RT}{\alpha nFvD}\right) = \xi_\mu = \text{constant} \tag{19}$$

to yield

$$-\frac{\alpha nF}{RT} dE_\mu - \frac{d \ln v}{2} = 0 \tag{20}$$

we find that

$$\frac{\Delta E_\mu}{\Delta \log v} = \frac{-2.303RT}{2\alpha nF} \tag{21}$$

In words, Equation 21 states that a tenfold increase in ramp-rate will shift the potential corresponding to any particular height up the wave ($E_{1/2}$,$E_{1/4}$,etc.) cathodically by $29.6/\alpha n$ mV at 298 K. Note that changing the ramp-rate merely shifts the entire wave along the potential axis, the shape of the wave remaining unaltered. This is in contrast to linear-potential-scan voltammetry, wherein changes in v also affect the height of the response.

Solution for Arbitrary Initial Potential. An exact solution of Equation 14, namely

$$\mu = -\sum_{n=1}^{\infty} (-\gamma)^n s_n(\tau) \tag{22}$$

is possible in terms of functions $s_n(\ )$ that are repeated semiintegrals of the exponential function. The recurrence

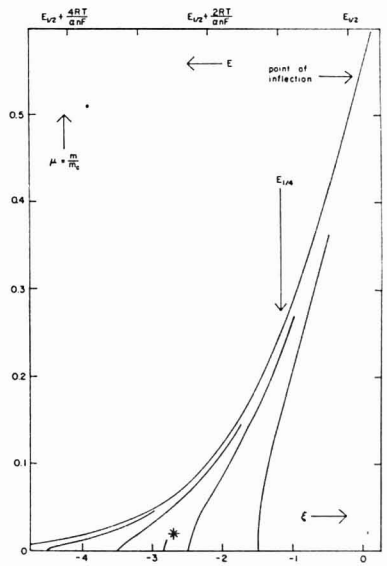

Figure 2. The upper curve is the foot of an irreversible neopolarogram that started at an indefinitely large positive potential

The four incomplete curves show the effect (from left to right) of making E_0 increasingly less positive. The fragment marked with an asterisk shows the start of the neopolarogram for which μ acquires the value 0.4900 at $E_{1/2}$

$$\frac{d^{-1/2}}{dx^{-1/2}}[\exp(x) s_{n-1}(x)] = s_n(x) \tag{23}$$

defines all these functions, $s_0(\ )$ being unity. Via polynomial approximations to these functions (9), tabular values of $s_n(\tau)$ were prepared and these enabled Figure 2 to be constructed. This diagram compares the theoretical shapes of the feet of neopolarograms that commence at various potentials. Note that the late-starting neopolarographic curves are initially vertical but that they soon veer to follow a course almost

Table III. Values of μ at $E_{1/2}$ for Various Initial Potentials

$\frac{\alpha nF}{RT}[E_0 - E_{1/2}]$	γ	μ at $E_{1/2}$
1.000	0.2990	0.4267
1.500	0.1814	0.4617
2.000	0.1100	0.4792
2.500	0.0667	0.4885
2.622	0.0591	0.4900
3.000	0.0405	0.4935
3.500	0.0246	0.4963
4.000	0.0149	0.4979
4.500	0.0090	0.4988
5.000	0.0053	0.4993
∞	0	0.5000

parallel to, but slowly converging with, the neopolarogram that started at an indefinitely positive potential.

Some time after the commencement of a neopolarogram, τ becomes large enough that an asymptotic summation (*9*) may be employed to replace that in Equation 22. Introduction of this simplification leads eventually to the result

$$\mu \sim \mu_\infty - \frac{1-\mu_\infty}{\sqrt{\pi\tau}} \int_0^\gamma \sum_{j=0}^{\infty} \frac{(-\exp u)^j}{\sqrt{(j!)}}\, du \qquad (24)$$

where μ_∞ is the value that μ would have had if E_0 had been infinite. The integrand in result 24 is the same function that appears in the expression (Equation 17) for μ_∞ itself. Values of the integral were calculated and were, in fact, used as an aid in the construction of Figure 2. Though its restriction to large τ must not be overlooked, Equation 24 tends to be more useful than Equation 22. The former correctly predicts that μ is invariably less than μ_∞, but that these two values converge as γ approaches zero or as τ approaches infinity.

Choice of Initial Potential. Though irreversible neopolarograms are simplest when the initial potential is very positive, in practice one must choose E_0 such that no electrooxidations occur. In this subsection, the effect upon the neopolarographic half-wave potential of starting the ramp at a less-than-infinitely positive potential will be evaluated. It will be demonstrated that, provided that the initial potential is at least $67.4/\alpha n$ mV more positive than $E_{1/2}$, effects are confined to the foot of the wave.

Making use of Table II and of Equations 12 and 13, one may demonstrate that at the true neopolarographic half-wave potential ($E_{1/2}$, corresponding to $\mu_\infty = \frac{1}{2}$), τ acquires the value $-\ln(1.23\ \gamma)$. Substitution of this value into Equation 24 gives

$$\frac{1}{2} - \frac{1}{\sqrt{-4\pi \ln(1.23\ \gamma)}} \int_0^\gamma \sum_{j=0}^{\infty} \frac{(-\exp u)^j}{\sqrt{(j!)}}\, du \qquad (25)$$

as the expression for μ at $E_{1/2}$. Values of this expression, which is a function of γ alone, are to be found in Table III.

From Table III, it is seen that γ must not exceed 0.0591 to ensure that μ lies between 0.4900 and 0.5000 at $E_{1/2}$. At T = 298 K, this corresponds to the inequality

$$\alpha n[E_0 - E_{1/2}] \geq 2.622 \frac{RT}{F} = 67.4 \text{ mV} \qquad (26)$$

Of course, the foot of the irreversible neopolarogram that just satisfies this inequality will be considerably distorted (the start of this neopolarogram is shown by the asterisk in Figure 2), but, in the vicinity of $E_{1/2}$ and at more negative potentials, the curve lies within experimental error of the ideal neopolarogram.

Relation to Linear Scan Voltammetry. Obviously, since a neopolarogram is the semiintegral of a linear-potential-scan voltammogram, the known shapes (*10*) of the latter curves could have been used to predict neopolarographic behavior. This method has not been followed here, because to have done so would have obscured the fundamentality of the semiintegral approach.

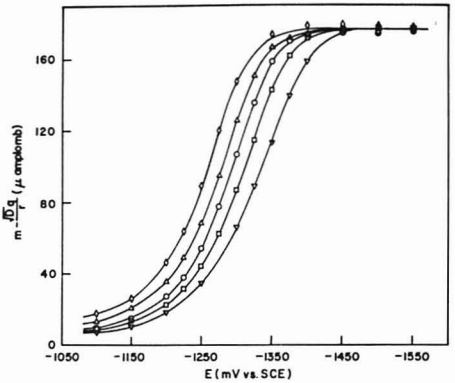

Figure 3. Neopolarograms for iodate reduction

Solution: 2.00 mM KIO_3 in 100 mM KNO_3; electrode area: 46.8 mm^2; initial potential: −800 mV vs. SCE; ramp-rates ($mV\ s^{-1}$): ◇ 20.5, △ 50.3, ○ 102, □ 205, and ▽ 509

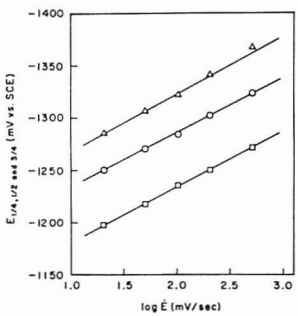

Figure 4. Dependence of the characteristic potentials (□ $E_{1/4}$, ○ $E_{1/2}$, and △ $E_{3/4}$) on the logarithm of the ramp-rate. Conditions as in Figure 3

As Reinmuth (*11*), in a different terminology, stressed: the linear relationship of m to the surface concentrations of electroactive species lends to m a basic significance that i does not share. In evidence of this, the shape of a reversible linear-potential-scan voltammogram (*10–12*) is described by the unfamiliar infinite sum

$$i = -m_c \left(\frac{NFv}{RT}\right)^{1/2} \sum_{j=1}^{\infty} (-)^j \exp\left(\frac{-jNF}{RT}[E_0 - vt - E_{1/2}]\right) \sqrt{j} \qquad (27)$$

whereas m is expressed by Equation 2, in terms of a single elementary transcendental function. From a mathematical viewpoint, the neopolarogram is far the simpler curve and consequently it is appropriate to regard the linear scan voltammogram as derived from it by semidifferentiation. That Equation 27 is indeed the semiderivative of Equation 2 follows immediately from the identity

Table IV. Summary of αn Results

Method	αn for reduction of IO_3^-	αn for reduction of Ni^{2+}
$E_{1/4}$ vs. log v slope	0.55	0.47
$E_{1/2}$ vs. log v slope	0.56	0.46
$E_{3/4}$ vs. log v slope	0.53	0.45
$E_{1/4} - E_{1/2}$ separation	0.47–0.50	0.53–0.54
$E_{1/4} - E_{3/4}$ separation	0.53–0.55	0.55–0.57
$E_{1/2} - E_{3/4}$ separation	0.58–0.69	0.58–0.61
Slope at v = 20.5 mV s^{-1}	0.52	0.57
Slope at v = 50.3 mV s^{-1}	0.51	0.61
Slope at v = 102 mV s^{-1}	0.48	0.59
Slope at v = 205 mV s^{-1}	0.48	0.53
Slope at v = 509 mV s^{-1}	(0.43)	(0.49)
Mean:	0.53 ± 0.04	0.54 ± 0.04
log $(m_c - m)/i$ vs. E slope	0.50	0.52

$$1 - \tanh\frac{x}{2} \equiv 2\sum_{j=0}^{\infty}(-)^j \exp(jx) \qquad (28)$$

and the Weyl rule, Equation 16.

For irreversible electroreductions, Equation 8, describing the neopolarographic wave shape, is not actually significantly simpler than its semiderivative,

$$i = -m_c\left(\frac{\alpha nFv}{RT}\right)^{1/2}\sum_{j=1}^{\infty}\frac{(-)^j}{\sqrt{(j-1)!}} \times \exp\left(\frac{-j\alpha nF}{RT}\left[E_0 - vt - E_s + \frac{RT}{2\alpha nF}\ln\frac{\alpha nFvD}{k_s^2RT}\right]\right) \qquad (29)$$

which governs the shape of a totally irreversible linear scan voltammogram (*10, 13*). Nevertheless, the neopolarogram has two simplifying features—near-symmetry and ramp-rate independence—not enjoyed by the voltammogram. As well, the attainment of a constant value m_c represents a decided advantage for neopolarography, especially where analytical applications are sought.

Because of Equation 7, there is a simple relationship between numerical values of i and m at each potential. This relationship was used to convert the tabular current data of Nicholson and Shain (*10*): some of these results are included in Table I to supplement the $\xi > 2$ range. Note that the cited data were not prepared using Equation 29 (which suffers the same limitations as Equation 8 at the more cathodic potentials) but by a numerical integration scheme.

EXPERIMENTAL

The apparatus and technique are unchanged from those described in previous articles of this series (*2, 4, 14*). A hanging mercury drop electrode was employed; in all cases the drop was "second hand" (*2*). Reagent grade chemicals were used without further purification. A supporting electrolyte of 0.10 M KNO_3 was used throughout. Two electroreducible species were examined: the iodate ion as 2.00 mM KIO_3 and the nickel(II) ion as 4.00 mM $Ni(NO_3)_2$. Both these ions have been extensively studied and their reduction at a mercury electrode is well known to be irreversible. Because a rather large initial current was observed in the case of the IO_3^- reduction, the working electrode was regularly maintained at the initial potential for about 45 s to eliminate such currents prior to the recording of the neopolarogram.

Analog semiintegration was employed, using a ladder network in the feedback loop of the Princeton Applied Research Model 170's integrator, as previously described (*15*). (Please note a typographical error in Figure 10 of this article; the resistor shown as 830 kΩ should have read 8300 kΩ.) The m values so measured were corrected for electrode sphericity (*1, 12*) by subtraction of the $qD^{1/2}/r$ term ($q = \int i\,dt$, r = drop radius).

RESULTS AND DISCUSSION

Experimental neopolarograms for iodate reduction are shown in Figure 3 for a variety of ramp-rates, v. Figure 4, derived from Figure 3, shows how the quarter-wave, half-wave, and three-quarters-wave potentials depend on ramp-rate. As predicted in Equation 21, each characteristic potential is seen to depend logarithmically on v. The equation was applied to the slopes of the Figure 4 lines, the αn values listed in Table IV being thereby calculated.

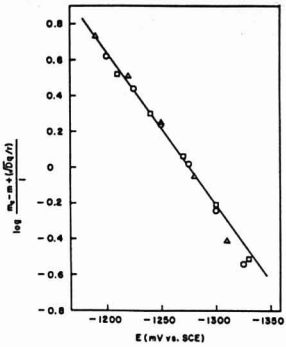

Figure 5. Plot based on Equation 7 for iodate reduction. Conditions as in Figure 3

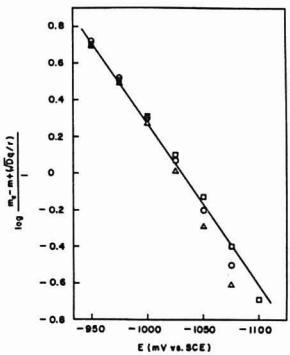

Figure 6. Plot based on Equation 7 for nickel reduction

Solution: 4.00 mM $Ni(NO_3)_2$ in 100 mM KNO_3; electrode area: 87.3 mm^2; initial potential: −650 mV vs. SCE; ramp-rates: as in Figure 3

Values of αn may be calculated, not only from the slopes of the lines in Figure 4, but also from the displacement of these lines from each other. This is evident from the predictions in Table II, which show that

$$\alpha n = \frac{25.1\text{mV}}{E_{1/4} - E_{1/2}} = \frac{48.0\text{mV}}{E_{1/4} - E_{3/4}} = \frac{22.9\text{mV}}{E_{1/2} - E_{3/4}} \qquad (30)$$

at 298 K. The αn values calculated from these relations are also displayed in Table IV; ranges of αn are reported because the lines in Figure 4 are not quite parallel. For iodate electroreduction, data determined from relations in Equation 30 demonstrate rather poor self-consistency; this reflects the fact, evident in Figure 3, that the iodate neopolarogram is slightly less symmetrical than theory predicts.

Yet another way of determining αn from the neopolarograms uses their slopes. According to Table II, the irreversible neopolarographic wave has a maximum slope almost equal to its slope at $E_{1/2}$, both these slopes being given within experimental precision by

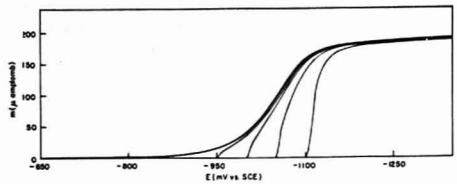

Figure 7. Neopolarograms for nickel(II) reduction with various initial potentials

Ramp-rate: 102 mV s^{-1}; other conditions: as in Figure 6

$$\frac{1}{m_c}\frac{dm}{dE} = \text{slope} = \frac{-\alpha n}{86.8\text{mV}} \qquad (31)$$

at 298 K. Using this equation and the curves shown in Figure 3, αn values were calculated for each ramp-rate, the results again being collected in Table IV. Apart from the datum obtained from the 509 mV/s ramp-rate (where pen response may have been a complicating factor), the values agree well and give an αn average value of 0.50.

Table IV permits an intercomparison of αn values determined for iodate reduction by all three neopolarographic methods. Though the agreement is less than might have been hoped, the scatter averages only 0.04 and confirms that theory and experiment are in broad agreement. Possible causes of the discrepancies include: imperfect correction for sphericity, interference from nonfaradaic and other background effects, and neglect of the role of the double-layer structure (*1*) on the kinetics of IO_3^- reduction.

Essentially similar results were obtained for Ni^{2+} reduction. Values of αn were calculated by the same method used for IO_3^- and the data are likewise assembled into Table IV. The agreement between αn values determined by the various methods is no better than in the iodate case, but it is interesting to note that the results for the two electroreducible species do not parallel each other. This suggests that divergencies arise from idiosyncrasies of the individual systems, rather than reflecting any general inadequacy of the theory.

Finally, a method of determining αn was employed that does not hinge on the theory presented in this article. This method uses Equation 7 and consists of plotting log $(m_c - m)/i$ vs. E. Figures 5 and 6 show these plots for iodate and nickel ion reductions respectively. From the slopes of the lines shown in these diagrams, which, it should be noted, embrace several ramp-rates, the αn values reported as the final items in Table IV were calculated. Agreement with the other tabulated values is good.

Figure 7 shows neopolarograms for the reduction of Ni^{2+} for a variety of initial potentials. We have not attempted to correlate these curves quantitatively with theory, but the qualitative agreement with Figure 2 is evident.

ACKNOWLEDGMENT

The computational assistance provided by Penny Dalrymple-Alford and Chummer Farina is gratefully acknowledged.

LITERATURE CITED

(1) J. C. Imbeaux and J. M. Saveant, *J. Electroanal. Chem.*, **44**, 169 (1973).
(2) M. Goto and K. B. Oldham, *Anal. Chem.*, **45**, 2043 (1973).
(3) P. E. Whitson, H. W. VandenBorn, and D. H. Evans, *Anal. Chem.*, **45**, 1298 (1973).
(4) M. Grenness and K. B. Oldham, *Anal. Chem.*, **44**, 1121 (1972).
(5) J. M. Saveant and D. Tessier, *J. Electroanal. Chem.*, **65**, 57 (1975).
(6) K. B. Oldham and J. Spanier, *J. Electroanal. Chem.*, **26**, 331 (1970).
(7) K. B. Oldham and J. Spanier, "The Fractional Calculus", Academic Press, New York, 1974.
(8) P. Delahay and J. E. Strassner, *J. Am. Chem. Soc.*, **73**, 5219 (1951).
(9) K. B. Oldham, unpublished work, details available on request.
(10) R. S. Nicholson and I. Shain, *Anal. Chem.*, **36**, 706 (1964).
(11) W. H. Reinmuth, *Anal. Chem.*, **34**, 1446 (1962).
(12) A. Sevcik, *Collect. Czech. Chem. Commun.*, **13**, 349 (1948).
(13) W. H. Reinmuth, *Anal. Chem.*, **33**, 1793 (1961).
(14) M. Goto and K. B. Oldham, *Anal. Chem.*, **46**, 1522 (1974).
(15) K. B. Oldham, *Anal. Chem.*, **45**, 39 (1973).

RECEIVED for review February 11, 1974. Resubmitted March 16, 1976. Accepted May 10, 1976. The financial support of the National Research Council of Canada is gratefully acknowledged.

Optical Pathlength Considerations in Transmission Spectroelectrochemical Measurements

F. R. Shu[1] and G. S. Wilson*

Chemistry Department, University of Arizona, Tucson, Ariz. 85721

A transmission spectroelectrochemical cell is described in which the optical path length can be varied to enable consideration of its effect on electrochemical characteristics such as cell time constant. The utility of the short pathlength cell was demonstrated in the measurement of the second order homogeneous electron transfer rate constant for the reaction of horse heart cytochrome *c* and hexaammineruthenium(II).

In the course of investigating electron transfer reactions involving fast kinetics via transmission spectroelectrochemical techniques, it is necessary to measure the absorbance changes corresponding to chemical reactions taking place at the electrode surface or in the diffusion layer of the working electrode. Under these conditions, the diffusion layer constitutes only a small fraction of the total optical path length. Thus, it is necessary to measure a small difference between two large numbers if the original reactant absorbs appreciably. Clearly, greater sensitivity can be achieved by reducing the total path length. Such an approach might lead to the use of optically transparent thin-layer electrodes (OTTLE). These have been used to considerable advantage for both chemical and biochemical applications (*1–4*), especially where final spectral

[1] Present address, Smith Kline Instruments, Inc. 880 W. Maude Ave., Sunnyvale, Calif. 94086

measurements are made under null current conditions. Unfortunately, thin-layer cells often exhibit large resistive effects which lead to poor potentiostatic control of the working electrode and nonuniform current density across the electrode surface (*5, 6*). In some applications (*7*), it is also desired to measure small ($<10^{-4}$) absorbance changes in short times (<50 ms). It is necessary in such cases to perform multiple experiments (ensemble averaging) and this, in turn, requires that the reaction layer be "refilled" after each experiment. We have shown that this can be conveniently accomplished by stirring the solution (*7*).

In this report, a variety of electrochemical experiments have been performed to demonstrate the conditions under which reliable spectral observations can be made in a short path length cell without interfering with the electrochemistry.

EXPERIMENTAL

Apparatus. The spectroelectrochemical cell was similar to that of Hawkridge and Kuwana (*8*) except that the body was constructed of Kel-F rather than Lucite because of superior chemical resistivity. The optical path is defined on one side by an optically transparent tin oxide electrode and on the other by an approximately 1.5-cm light pipe (⅛-in. diameter image conduit, American Optical Co.) with its optically flat ends oriented parallel to the electrode. The light pipe was permanently mounted by drilling a 0.32-cm hole in the rear of the cell block and cementing in place. The light pipe was positioned above the center of the cell cavity so that a small stirring bar could freely rotate at the bottom of the cell.

A piece of Pt wire sealed into the cell block served as the counter electrode. The wire was coiled around the light pipe near the indicating electrode end so that product generated there would not interfere with observations at the indicating electrode. The reference electrode (Ag/AgCl) was constructed as described previously (*8*) except that a luggin capillary constructed of polyethylene was used to orient the reference electrode probe immediately adjacent to the end of the light pipe. This modification improved the cell response significantly.

The indicating electrode was constructed with a 1.5 × 2 cm square of Sb-doped tin oxide (20 ohms/square) glass. The square was then painted with silver conductive paint so as to define a masked circular window slightly larger than the end of the light pipe. A thin layer of silicone rubber (Dow-Corning Silicone Rubber Sealer) was then applied to the electrode to mask that portion of the conducting paint which would otherwise come in contact with the solution.

The electrochemical instrumentation included a Princeton Applied Research Model 173 Potentiostat and Exact Model 126 signal generator. A double beam spectrophotometer was constructed using a 100-watt tungsten quartz iodine light source (Sylvania 6.6A/T2 1/2 Q/CL) Jarrell-Ash Model 82-410 (0.25 meter) monochromator, matched 1P28A photomultiplier tubes, Burr-Brown (Tucson, Ariz.) Model 3402A amplifiers as current-voltage transducers, and an OEI (Tucson, Ariz.) Model 2534 high speed log ratio converter. From this apparatus, an absorbance readout of 1.0 V/absorbance unit was obtained. All experiments were run under the control of a Hewlett-Packard 2100 minicomputer using a data acquisition system described previously (*7, 9*).

Reagents. All chemicals used in the present study were reagent grade unless otherwise specified and were used without further purification. Cytochrome *c* (Sigma Type VI) was prepared in 0.2 M phosphate buffer, pH 6.45, and was used to calibrate the optical path length of the cell. Methyl viologen was obtained from K and K Laboratories. Hexaammineruthenium(III) chloride was purchased from Strem Chemicals, Inc.

RESULTS AND DISCUSSION

Evaluation of Cell Spectral Characteristics (Static). Spectroelectrochemical cells with light paths of 0.021, 0.065, and 0.097 cm, respectively, were constructed for evaluation. The spectrum of reduced cytochrome *c* was measured from 400 to 600 nm and, in each case, was found to agree with that reported previously (*10*). Agreement was also observed for Beer's law as measured by the difference in molar absorptivity of the bands at 550 and 535 nm, respectively. Thus, it can be concluded that the use of a light pipe has no apparent effect on the quality of spectral measurements in the visible region.

Table I. Electrochemical Evaluation of Cell Characteristics

Optical path length cm	Estimated[a]	
	R (ohms)	*RC* (ms)
0.021	80	0.22
0.065	50	0.12
0.097	44	0.10

[a] Estimated from Equation 1 using solution blank, ΔE = 0.4 V, Elect. area ≈ 0.27 cm².

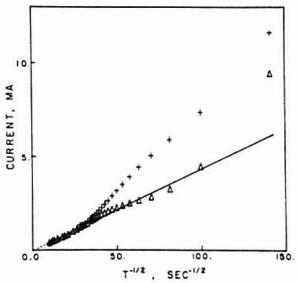

Figure 1. Current–time curve for potentiostatic reduction of methyl viologen

Uncorrected current (++); current corrected using Equation 11, Reference 11 (ΔΔ). R = 44 ohms, RC = 0.14 ms. Concn MV^{2+} = 10^{-3} M. Potential step −0.45 to −0.8 V vs. Ag/AgCl electrode. Results averaged from 7 experiments

The photometric broad band noise (0.001 A.U. P–P) of the system was not appreciably affected by the presence of the light pipe.

Evaluation of Cell Electrochemical Characteristics. The time constant of the electrochemical cell was evaluated using the recently described method of Perone and co-workers (*11*) in which it is assumed that the charging current is given by

$$i_{ch} = \frac{\Delta E}{R} e^{-t/RC} \quad (1)$$

where ΔE is the size of the potential step; R, the total uncompensated resistance; and C, the capacitance of the electrode double layer. The cell constant was determined from a potential step of 0.4 V in a solution containing only the phosphate buffer. The current was measured over the time interval $0 < t < 0.5$ ms. The values obtained are shown in Table I. It will be noted that influence of the light pipe on the resistance begins to become pronounced below a path length of 0.065 cm. If current–time data are to be utilized in the potential-step experiment, particularly at concentrations of 10^{-4} M or less, correction for charging current is absolutely essential. Unfortunately, the blank solution does not take into account the effects on the cell time constant resulting from the addition of the electroactive species. To deal with this difficulty, Perone and co-workers (*12*) have recently proposed a theoretical model which permits the estimation of the charging current in the presence of a faradaic component. Figure 1 shows that it is possible to obtain linear Cottrell behavior to within less than two cell time constants by subtracting the charging current using the correction procedure (*11*). A similar correction procedure has been developed which does not depend on the mechanism of the associated chemical reaction (*13*). Virtually identical results are obtained. From the Cottrell slope, a diffusion coefficient of 7.9×10^{-6} cm²/s can be calculated for methyl viologen (MV^{2+}) in its reduction

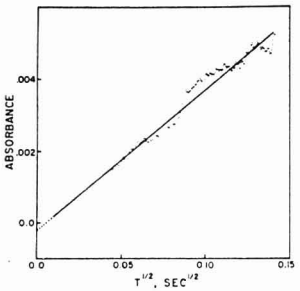

Figure 2. Absorbance–time curve for potentiostatic reduction of methyl viologen

Conditions same as Figure 1. Monitor wavelength 602 nm. Results averaged from 35 experiments

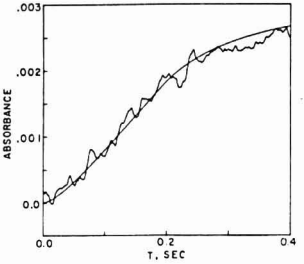

Figure 3. Absorbance–time curve for the reaction of $Ru(NH_3)_6^{2+}$–Cyt.^{III}c

Reaction condition: $Ru(NH_3)_6^{3+}$ = Cyt.^{III}c = 1×10^{-4} M; 0.2 M acetate buffer, pH 3.48. The potential was stepped from 0.2 V to −0.5 V (vs. Ag/AgCl) and back (τ = 0.2 s). Absorbance monitored at 550 nm. Results averaged from 7 steps. Solid line = rate constant 6×10^4 M^{-1} s^{-1}

to the free radical ($MV^{\cdot+}$). This value compares favorably with a value of $7.5 \pm 0.5 \times 10^{-6}$ cm^2/s obtained from the potential step chronoabsorptometry experiments to be described subsequently. As Perone has pointed out (*11*), the correct Cottrell slope is not obtained until rather long times (in our case greater than 0.5 ms) where the corrected data converge.

Cyclic Voltammetry. The cyclic voltammetric behavior of methyl viologen is very similar to that reported by Steckhan and Kuwana (*14*). The cathodic peak current (i_{pc}) varied linearly with scan rate over the range 0.039–16 V/s. The peak current ratio (i_{pc}/i_{pa}) was essentially unity over the scan range studied. The peak separation (ΔE_p) where $\Delta E_p = E_{pc} - E_{pa}$ increases with scan rate (v) as noted previously (*14*) and this is attributed to the inherent resistance of the tin oxide film. If a plot of peak separation vs. $\sqrt{v}$ is extrapolated to zero scan rate, ΔE_p values in the range of 0.045–0.053 V are obtained. It is possible that in addition to the resistive properties of the film, the behavior also is influenced to some extent by the presence of the light pipe, especially at low scan rates. Over the range studied, the peak separation does not depend on path length. A zero peak separation would be expected for the limiting case of a true thin-layer cell (*15*).

Potential Step Chronoabsorptometry. The absorbance–time response to a potential step is shown in Figure 2. The least-square fit follows the Cottrell equation for times greater than one time constant. It should be noted that these data are uncorrected for charging current; however its effect is apparent at short times. If the region between the y-intercept and the first data point (100 μs) is expanded, it can be shown that the absorbance–time curve (Figure 2) will pass through the origin. Thus, a lag time is produced during which current flow occurs but no product is produced. Data appear to be usable without correction after 1–2 time constants. Thus, it is still easier, in this case, to achieve linear Cottrell behavior with absorbance monitoring in this system than with current measurements. The very high molar absorptivity of $MV^{\cdot+}$ at the monitoring wavelength contributes significantly to this conclusion. After application of a potential step, the diffusion layer will move out into solution eventually reaching the end of the light pipe. At this point, the condition of semiinfinite linear diffusion no longer applies. For the 0.021-cm cell, deviation occurs at about 250 ms. This is considerably sooner than would be expected since the diffusion layer thickness should equal the optical path length after about 60 s. Undoubtedly, the diffusion layer is distorted by the irregular current flux resulting from the cell geometry. At times less than 100 ms, no difficulties are encountered.

The thin layer cell has been used to measure the second-order rate constant of the reaction between iron(III) cytochrome *c* and hexaammineruthenium(II):

$$Ru(NH_3)_6^{3+} + e \rightarrow Ru(NH_3)_6^{2+} \quad (2)$$

$$Ru(NH_3)_6^{2+} + Cyt^{III}c \rightleftharpoons Ru(NH_3)_6^{3+} + Cyt^{II}c \quad (3)$$

The reaction was monitored at 550 nm using a cell with a light path of 0.1 cm. As was expected, at least a sevenfold reduction in background absorbance was observed. Between 30 and 50 experiments were required to obtain a S/N ratio of 6 as compared to about 100 in the absence of the light pipe. Conditions can be further improved by signal conditioning with a 2-pole Butterworth filter (f_0 = 100 Hz) where only 7 to 15 cycles of signal averaging were required to achieve a smooth experimental curve (S/N = 6). A representative example of the experimental results is demonstrated together with a digital simulation curve in Figure 3. This result is in good agreement with the data reported in the literature (*16*).

CONCLUSION

The above described cell is well suited to experiments in which the diffusion layer is kept thin with respect to the optical path length. Because of the resistive properties of the tin oxide film, correct electrode potentials cannot be maintained (even in the absence of a light pipe) and these effects are apparently accentuated by the light pipe. Use of a more highly conducting thin film would aid this difficulty. The cell, however, will function most effectively under conditions where the current–time response is less strongly dependent on potential control, i.e., a potential step to the diffusion plateau.

ACKNOWLEDGMENT

We thank S. P. Perone for helpful discussions concerning this work and for providing preprints of the work cited.

LITERATURE CITED

(1) W. R. Heineman, J. N. Burnett, and R. W. Murray, *Anal. Chem.*, **40**, 1970 (1968).
(2) G. Peychal-Heiling and G. S. Wilson, *Anal. Chem.*, **43**, 545 (1971).
(3) J. G. Lanese and G. S. Wilson, *J. Electrochem. Soc.*, **119**, 1039 (1972).
(4) W. R. Heineman, B. J. Norris, and J. F. Goelz, *Anal. Chem.*, **47**, 79 (1975).
(5) I. B. Goldberg, A. J. Bard, and S. W. Feldberg, *J. Phys. Chem.*, **76**, 2550 (1972).
(6) I. B. Goldberg and A. J. Bard, *J. Electroanal Chem.*, **38**, 313 (1972).
(7) M. D. Ryan and G. S. Wilson, *Anal. Chem.*, **47**, 885 (1975).

(8) F. M. Hawkridge and T. Kuwana, *Anal. Chem.*, **45**, 1021 (1973).
(9) L. Ramaley and G. S. Wilson, *Anal. Chem.*, **42**, 606 (1970).
(10) D. Keilin and E. C. Slater, *Br. Med. Bull.*, **9**, 89 (1953).
(11) K. F. Dahnke, S. S. Fratoni, Jr., and S. P. Perone, *Anal. Chem.*, **48**, 296 (1976).
(12) S. S. Fratoni, Jr., and S. P. Perone, *Anal. Chem.*, **48**, 287 (1976).
(13) S. S. Fratoni, Jr., and S. P. Perone, *J. Electrochem. Soc.*, in press.
(14) E. Steckhan and T. Kuwana, *Ber. Bunsenges. Phys. Chem.*, **78**, 253 (1974).
(15) A. T. Hubbard and F. C. Anson in "Electroanalytical Chemistry", Vol. 4, A. J. Bard, Ed., Marcel Dekker, New York, 1970.
(16) R. X. Ewall and L. E. Bennett, *J. Am. Chem. Soc.*, **96**, 940 (1974).

RECEIVED for review December 3, 1975. Accepted June 21, 1976. This work was supported by National Science Foundation Grant MPS-73-08683 and by the Office of Naval Research.

Rotating Ring-Disk Enzyme Electrode for Surface Catalysis Studies

F. R. Shu[1] and G. S. Wilson*

Department of Chemistry, University of Arizona, Tucson, Ariz. 85721

A rotating ring-disk enzyme electrode (RRDEE) has been developed and evaluated. The enzyme, glucose oxidase, is immobilized at the surface of a carbon paste electrode. The progress of the enzymatic reaction was monitored at either the ring or disk. By varying the electrode rotation speed, the rates of substrate mass transport and catalytic reaction can be distinguished. The theory describing the electrode response has been developed and is in good agreement with experiment. The kinetic parameters of the immobilized enzyme have been determined along with the properties of the modified electrode surface. Performance as a selective sensor is discussed.

In recent years, there has been considerable interest in applying immobilized enzymes for specific assays. Among these applications, the so-called enzyme electrode is quite unique because it combines the enzyme specificity with the sensitivity and convenience of electroanalytical techniques in a compact form to facilitate analysis. The enzyme electrode is usually prepared by attaching an immobilized enzyme layer to an electrochemical sensor so that changes occurring as a result of the enzyme reaction can be monitored either potentiometrically or amperometrically (*1–3*). Regardless of the electrode sensor type, enzyme electrodes to date have been operated in a stationary manner. The mass transport of substrate to the catalytic layer is therefore controlled mainly by solution stirring and the diffusion rate inside the immobilized enzyme matrix (*4*). Neither of these processes is very effective in bringing the product of the enzyme reaction to the electrode surface. A recent model study of the theoretical aspects of amperometric enzyme electrodes by Mell and Maloy has shown that the sensitivity of a stationary enzyme electrode is determined by the proper balance of the catalysis rate of the enzyme on one hand and the diffusion rate of the substrate on the other (*4*). Since both processes are inherent properties of a particular system, it becomes apparent that there is very little one can do to improve the efficiency or the sensitivity, in practice, of a stationary enzyme electrode. Furthermore, as pointed out by these authors, the lack of a well defined boundary condition to describe the mass transport represents another difficulty in predicting the steady-state current of a stationary enzyme electrode. This, in turn, limits the potential of using a stationary enzyme electrode to evaluate the kinetic parameters of reactions at immobilized biosurfaces or other catalytic surfaces.

A rotating electrode provides several attractive advantages over its stationary counterpart. First, the rate of transport of a species from the bulk of the solution to an electrode can be controlled by varying the rotation speed of the electrode. The hydrodynamics of a rotating disk electrode is well defined (*5*). Therefore, it is possible to make mass transport competitive with the enzyme catalysis rate. As a result, the sensitivity of a particular enzyme electrode could be significantly improved. Second, because of the convective nature of the electrode, one would expect that a rotating enzyme electrode should give much faster response than a stationary electrode. This, of course, would shorten the analysis time. The third advantage of a rotating enzyme electrode is its potential as a tool for investigating the kinetics of surface catalytic reactions. Since the boundary conditions of a rotating disk electrode are well defined, a reliable mathematical model can be derived to predict its behavior. We have carried out a study to develop a rotating disk enzyme electrode and to investigate the theoretical aspects of its performance.

The system we selected to study is the glucose–glucose oxidase reaction:

$$\text{Glucose} + O_2 \xrightarrow{\text{glucose oxidase}} \text{Gluconic acid} + H_2O_2 \quad (1)$$

The formation of H_2O_2 is coupled with a fast indicator reaction:

$$H_2O_2 + 2H^+ + 2I^- \xrightarrow{\text{molybdate}} I_2 + 2H_2O \quad (2)$$

The amperometric detection of the formation of I_2 serves to measure the overall extent of the reaction (*4, 6*).

In addition to the theoretical studies, we also present some preliminary investigations of enzyme electrode performance.

EXPERIMENTAL

Instrumentation. The four-electrode potentiostat used in the present study was similar to that described by Shabrang and Bruckenstein (*7*). The rotating ring-disk electrode, Model DT-6, was purchased from Pine Instrument Co., Grove City, Pa. The disk part of the electrode was a 0.5-cm deep cavity with a diameter of 0.764 cm according to the manufacturer's specifications. Therefore, the calculated area of the disk electrode was 0.46 cm^2 when the cavity was filled with carbon paste. The width of the platinum ring electrode was 0.024 cm. It was separated from the disk electrode by a 0.016-cm wide epoxy gap. The collection efficiency of the DT-6 electrode was 0.18 as calculated from theory (*8*). A heavy gauge platinum wire counter

[1] Present address, Smith Kline Instruments, 880 W. Maude Ave., Sunnyvale, Calif. 94086.

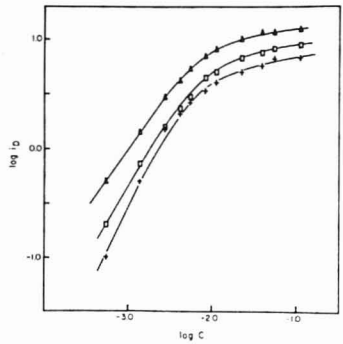

Figure 1. Experimental steady-state disk current ($i_D(\mu A)$) as a function of glucose concentration (M) at various electrode rotation speeds: 400 rpm (△), 900 rpm (□), and 1600 rpm (+)

electrode and a Ag/AgCl reference electrode ($E^{o\prime}$ = 0.200 V) were also used.

A Pine Instruments Model PIR rotator was used to control electrode rotation speed.

Preparation of Glucose Oxidase Electrode. The carbon paste used was prepared in the usual manner from 5 g of graphite powder (No. 38, Fisher Scientific Co.) and 3 ml of Nujol, except that 10 mg of *n*-octadecylamine (technical grade, Aldrich) was also added. The thoroughly mixed carbon paste was packed firmly into the disk cavity of the DT-6 electrode. The surface of the electrode was then polished with a piece of weighing paper. After the ring and the gap were wiped clean, the electrode was allowed to rotate in a 12.5% glutaraldehyde solution for 10–15 min, followed by washing in a cold 0.2 M phosphate buffer (pH 6.5) for 1 min. The rotating electrode was dipped into a bovine serum albumin solution (0.1 g/ml). (BSA, Fraction V 96–99%, Sigma Co.) The reaction was allowed to proceed for 2–3 min. Again the electrode was washed in a cold phosphate buffer for a minute after the BSA treatment. The electrode was then removed from the rotator and was positioned with the electrode surface facing up. A glucose oxidase solution prepared by dissolving 0.3 g of the enzyme (Glucose oxidase, Type II, 15000 units/g, Sigma Co.) in a 5% glutaraldehyde solution (buffered with phosphate at pH 6.5) was applied to the surface of the disk electrode. After standing at room temperature for 5 min, the excess enzyme solution was discarded and the ring and the gap of the electrode were carefully cleaned. The electrode was finally allowed to spin in a cold phosphate buffer at 2500 rpm for 5 min to remove physically entrapped or weakly bonded enzyme. This ensured reproducibility in subsequent measurements. The electrode was soaked in a phosphate buffer and stored at 5 °C overnight before use.

Solutions and Reagents. Unless otherwise mentioned, all chemicals used were reagent grade. The stock solution of 0.1 M glucose was allowed to mutarotate at room temperature for at least 24 h before using. All glucose testing solutions were prepared in a KI–buffer–catalyst solution, pH 6.1, as described previously (*4, 6*). The I_3^- solution employed to measure the effective electrode area was prepared according to Reference 9.

Procedure. The enzyme electrode was allowed to rotate in 20–30 ml of sample solution for about 20–30 s before stepping the potential of the indicator electrode to −0.2 V vs. the Ag/AgCl reference. This potential corresponded to a diffusion limited current for iodine reduction. The current transient resulting from potential application was then recorded to find the steady-state current. Measurements were repeated periodically to check for loss of enzyme activity.

BASIC PROPERTIES OF THE ENZYME ELECTRODE

The response of the rotating enzyme disk electrode prepared in this study is usually very rapid. At 400 rpm, steady-state current response can be reached in less than 50 s. Increasing the rotation speed can further reduce the response time. The steady-state disk currents at 400, 900, and 1600 rpm are plotted vs. glucose concentration in Figure 1. At 400 rpm, the calibration curve has a linear range from 10 mg/dl to 75 mg/dl. Comparing this observation with the data obtained by Guilbault and Lubrano (*2*), it is noticed that the detection limit of our electrode when it is rotated at 400 rpm is about twofold more sensitive. However, the upper limit of the linear range of a rotating enzyme electrode is much smaller than that of a stationary enzyme electrode. As the rotation speed of the enzyme electrode is increased, the magnitude of the steady-state current response becomes smaller. This is also accompanied by a reduction in the linear range of the calibration curve (Figure 1). An immediate conclusion reached from this observation is that the catalysis rate of the immobilized glucose oxidase cannot keep up with the pace of mass transport as the rotation speed of the electrode is increased. In order to understand the relation of these two important factors and to predict the optimal conditions for operating a rotating disk enzyme electrode (RDEE), the theoretical aspects of this electrode were explored in more detail.

DIGITAL SIMULATION

Digital simulation techniques have proved to be very useful in analyzing electrochemical boundary value problems (*10–14*). In our model, the electrode surface is defined as $X = 0$ in the simulation distance scale. The enzyme layer is assumed to extend into solution from this point to a point (*LEN*). The presence of this layer is further assumed not to interfere with diffusion to or from the electrode surface. If a thin enzyme layer is attached to the electrode surface, we must assume that the concentration of the enzyme is uniform in each volume element within the enzyme layer.

It has been shown that the solution velocity under a rotating disk can be expressed by:

$$V_x = -0.51\omega^{3/2}\nu^{-1/2}X^2 \tag{3}$$

where ω is the rotation speed of the disk expressed in rad/s, ν is the kinematic viscosity of the solution ($\nu = 0.01$ cm^2/s for water), and X represents the distance from the surface of the disk (*5*). This equation is valid only when X is much smaller than the hydrodynamic layer which is a function of ω. In order to simplify computation, it is assumed that the thickness of the immobilized enzyme layer is much thinner than the minimum hydrodynamic layer associated with the maximum rotation speed employed in the present study. In addition, it is also assumed that the enzyme layer attached does not affect the flow pattern near the electrode surface. Convective diffusion occurring within the enzyme layer is assumed to occur in the same manner. This last assumption is reasonable if the enzyme layer is thin.

The simulation time unit is given by

$$\Delta t = t_k/LT \tag{4}$$

where t_k is the convection time constant as defined by Prater and Bard (*13, 14*):

$$t_k = (0.51)^{-2/3}\omega^{-1}\nu^{1/3}D^{-1/3} \tag{5}$$

where D is the diffusion coefficient. In the program, the substrate and the product are assumed to have the same value of D. The definition of t_k greatly simplifies the mathematical treatment of the convective mass transport (*13*). By adjusting the value of LT, the desired accuracy of simulation can be obtained. The simulation distance, ΔX can be derived from Δt:

$$\Delta X = (D\Delta t/DM)^{1/2} \tag{6}$$

where DM is the diffusion coefficient in simulation units. Usually the ratio of D/DM has the value of 10^{-4}. The dimensionless enzyme layer thickness in simulation can now be related to the true enzyme layer thickness, d, by Equation 7:

$$LEN = d/\Delta X \quad (7)$$

The mass transport processes, i.e. convection and diffusion, are treated according to a previously described algorithm (*10, 13*).

For the enzyme electrode, it is convenient to express the concentrations of all species relative to the bulk substrate concentration, C. Thus, the true concentration of the substrate in a given volume element, J, can be expressed as:

$$[S] = C \cdot UUA(J) \quad (8)$$

Likewise, the concentration of the product:

$$[P] = C \cdot UUB(J) \quad (9)$$

The terms $UUA(J)$ and $UUB(J)$ are fractional concentrations of the substrate and the product, respectively. The fractional concentration of the substrate is defined initially as 1 while the fractional concentration of the product is zero. To calculate the perturbation of [S] and [P] as a result of the catalytic reaction, Michaelis–Menten kinetic theory is assumed:

$$E + S \underset{k_2}{\overset{k_1}{\rightleftharpoons}} ES \xrightarrow{k_3} P \quad (10)$$

where E is the enzyme and ES the enzyme-substrate complex. The rate of formation of the product is

$$d[P]/dt = k_3 C_E/(K_m/[S] + 1) \quad (11)$$

where K_m is the Michaelis–Menten constant. C_E is the analytical concentration of the active enzyme in the enzyme layer, i.e., the sum of free enzyme and enzyme substrate complex. Transforming Equation 11 to finite difference representation, one obtains:

$$C \cdot \Delta UUB(J)/\Delta t = k_3 C_E/(K_m/(C \cdot UUA(J)) + 1) \quad (12)$$

Substituting Equation 4 into Equation 12 and rearranging the expression that describes the effects of the enzyme catalysis results in:

$$DEL = \Delta UUB(J) = -\Delta UUA(J)$$
$$= (k_3 C_E/K_m) \cdot (t_k/LT) \cdot UUA(J)/(1 + (C/K_m) \cdot UUA(J)) \quad (13)$$

Equation 13 clearly indicates that the extent of the perturbation by the enzyme catalysis is dependent upon the substrate concentration as represented by C/K_m. Thus, the dependence of the current on concentration can be calculated by varying C/K_m. Another important feature of Equation 13 is that it compares the catalytic rate with convective mass transport implicitly. The parameter that compares these two processes can be extracted from Equation 13 and defined separately:

$$V = k_3 C_E t_k/K_m \quad (14)$$

Since t_k is a time constant associated with convection, the velocity parameter, V, actually reflects the amount of product that is allowed to form in a given time under a given convective condition. For example, a smaller t_k and V would result if the rotation speed of the electrode is increased. Thus, the assignment of V and C/K_m permits the combined effects of enzyme kinetics, convection, and concentration on current to be evaluated.

Under the diffusion limited condition, the concentration of the reaction product is zero at the electrode surface. Thus, the flux of the catalysis product is given by

$$ZZ = 2 \cdot DM \cdot UUB(1) \quad (15)$$

The current can then be expressed in terms of ZZ:

$$i(t) = nFAC \cdot ZZ \cdot \Delta X/\Delta t \quad (16)$$

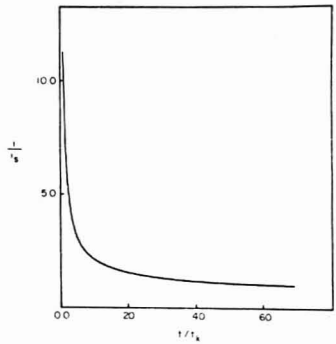

Figure 2. Simulated current transient at rotating disk electrode time (s) after application of potential, t. Steady-state current, i_s. Other parameters $LT = 300$, $DM = 0.45$, $\omega = 400$ rpm, $V = 0.2266$, and $C/K_m = 1$ are defined in text

where n, F, and A have their usual electrochemical significance. Substituting Equations 4 and 7 into Equation 16 and rearranging, we get

$$i(t) \cdot t_k/nFACd = ZZ \cdot LT/LEN \quad (17)$$

If we multiply both sides of Equation 17 by $(C/K_m) \cdot (1/V)$, we have:

$$i(t)/nFAdk_3 C_E = ZZ \cdot LT \cdot CKM/(LEN \cdot V) \quad (18)$$

where CKM stands for C/K_m. Inspection of this expression shows that the current is now rendered dimensionless by dividing by $nFAdk_3 C_E$. It also becomes calculable by simulation. Equation 18 allows straightforward correlation of digital simulation results with true current. The left-hand side of Equation 18 compares the current observed with the maximum catalysis rate, $k_3 C_E$.

Finally, the initialization of the simulation time scale should be mentioned. Since the three processes, electron transfer, enzyme catalysis, and mass transport can hardly occur simultaneously, a steady-state distribution of [S] and [P] has to be calculated prior to the calculation of current. Once the steady-state concentration distribution is reached, the calculation of simulated current can begin. In order to save computing time, the steady-state conditions for concentration and current are assumed to be reached when the variation between iterations of concentration or current is less than 0.01%. This approach is not only convenient but also parallels the manner in which the experiment is performed.

FORTRAN IV calculations were carried out with a DEC-10 time-sharing system at the University of Arizona.

In principle, the larger LT is, the closer the simulation will approximate the physical system. However, a practical concern in digital simulation is the computing time. With $LT = 300$, the steady-state calculation requires ~800 iterations for concentration distribution and ~210 iterations for the current. Most of our calculations were done with $LT = 300$. Since t_k varies with rotation speed, LEN also varies with respect to ω for a given enzyme layer thickness, d. Therefore, values of LEN at various rotation speeds are calculated prior to use of the program.

A typical simulated enzyme electrode current transient is shown in Figure 2. The results of our simulation indicate that the steady-state current can be reached in a time interval less than t_k regardless of the value of V.

Some simulated calibration curves are shown in Figures 3*a*

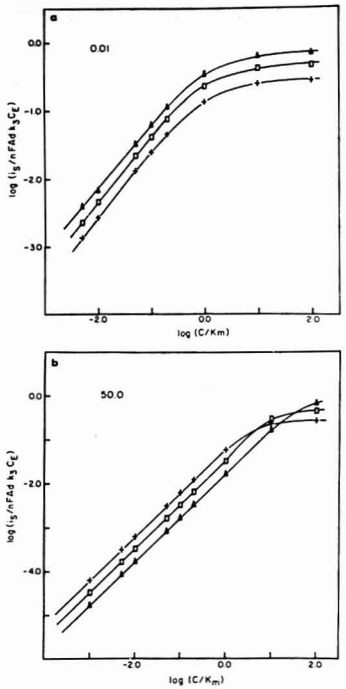

Figure 3. Simulated calibration curves for different kinetic conditions

(*a*) $k_3C_E/K_m = 0.01$; (*b*) $k_3C_E/K_m = 50.0$. Electrode rotation speeds: 100 rpm (△), 400 rpm (□), 1600 rpm (+)

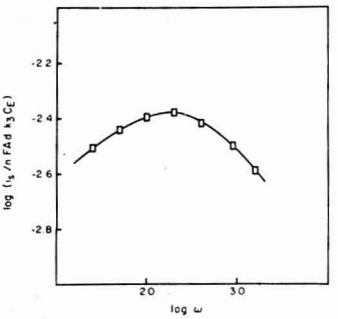

Figure 4. Effect of ω on simulated current. Parameters used: $k_3C_E/K_m = 1$. $C/K_m = 0.01$

and 3*b*. In these plots, the ordinate, i_s, stands for the steady-state current. It will be noted that the dependence of current on rotation speed reflects the relative effects of diffusion and catalysis. When the catalysis rate is slow, e.g., $k_3C_E/K_m = 0.01$, the current becomes smaller and the linear range of the calibration curve becomes narrower as the rotation speed of the electrode is increased. On the other hand, when the enzyme catalysis rate is very fast, e.g., $k_3C_E/K_m = 50.$, an increase in

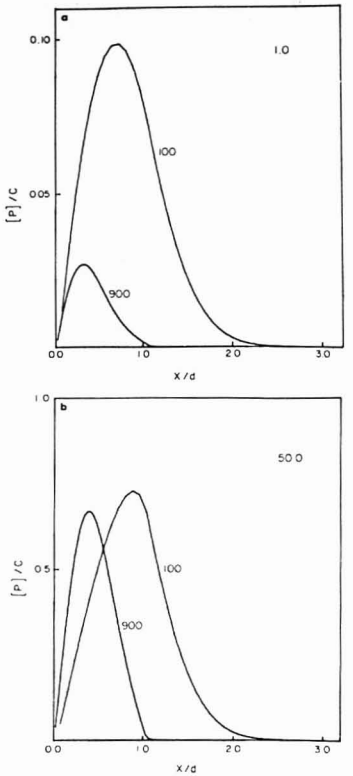

Figure 5. Concentration profile for enzyme electrode

(*a*) $k_3C_E/K_m = 1.0$; (*b*) $k_3C_E/K_m = 50.0$. Calculation made at 100 and 900 rpm as indicated

current sensitivity can be achieved by raising the rotation speed of the electrode although the upper linear limit of the calibration curve remains the same. These conclusions are consistent with the experimental results of Figure 1. A more thorough study of the sensitivity of the electrode indicates that the current passes a maximum at a characteristic rotation speed as shown in Figure 4. The position of this maximum is dependent upon the value of k_3C_E/K_m. Operating at this maximum where possible certainly improves the sensitivity of the electrode.

This behavior is understood in terms of the concentration profiles shown in Figures 5*a* and 5*b*. Regardless of enzyme catalysis rate, increasing the rotation speed of the electrode has the effect of reducing the residence time of the substrate in the enzyme layer, thus allowing less product to accumulate. However, the convective mass transport is more important than diffusion at higher rotation speeds. As a result, the concentration profile maximum is shifted toward the electrode, as the rotation speed is raised. The flux at $X = 0$ is increased leading to higher currents. If the enzyme catalysis rate is extremely fast, the peak of $[P]/C$ will be raised by a factor of about six even at higher rotation speeds (Figure 5*b*). Much of the product formed within the enzyme layer is lost into the bulk solution via diffusion at slow rotation speeds.

To obtain an empirical expression for the steady-state

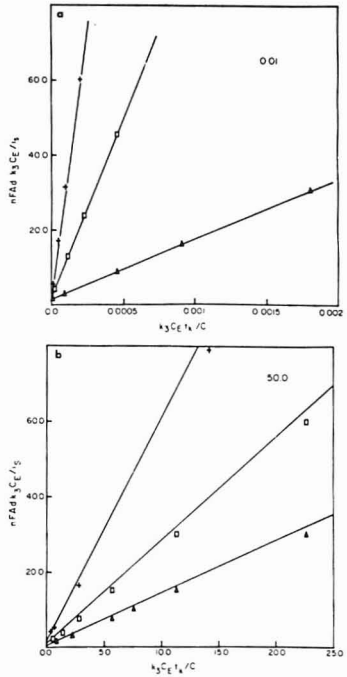

Figure 6. Lineweaver–Burk plots of simulated current

(*a*) $k_3C_E/K_m = 0.01$; (*b*) $k_3C_E/K_m = 50.0$. Electrode rotation speeds: 100 rpm (△), 400 rpm (□), and 1600 rpm (+)

current of a rotating disk enzyme electrode, we have treated our data in a manner similar to Mell and Maloy (*4*). The Lineweaver–Burk (*16*) plots of the simulated variables are shown in Figures 6*a* and 6*b*. The ordinate is the reciprocal of the value calculated from Equation 18 at the steady-state and the abscissa is the reciprocal of $V{\cdot}K_m/C$ ($= k_3C_Et_k/C$). If a line is drawn to connect the point of $C/K_m = \infty$ and the point of $C/K_m = 0.001$, all points will fall on the line provided that V is small ($V \leq 0.1$), i.e., the enzyme catalysis rate is slow with respect to convective diffusion (Figure 6*a*). In other words, a linear Lineweaver–Burk plot will result if the current is controlled by the catalysis rate. On the other hand, the points will show a negative deviation from the line if V is large, e.g., $V \geq 10$ (Figure 6*b*). This would be the case where the mass transport is the limiting process. The general equation that describes these lines may be written:

$$\frac{nFAdk_3C_E}{i_s} = m\frac{k_3C_Et_k}{C} + b \qquad (19)$$

where m is the slope and b is the intercept. From our calculations, it is found that b is solely a function of the rotation speed and the substrate diffusion coefficient. Some typical values of b are given in Table I.

The relation between m and V is not so straightforward. Figure 7 shows the plots of log m vs. log V when the catalysis rate is extremely fast with respect to convective mass transport, e.g., $V \geq 10$. Under this condition, the current becomes mass transport limited. From Figure 7, it is noticed that the slope of the line connecting the points of equal k_3C_E/K_m is exactly −0.5. Since t_k is inversely proportional to ω, the slope

Table I. Variation of Convection Coefficient, b, with Convection Parameters

	b	
ω	($DM = 0.45$)	($DM = 0.06$)
25	1.14	1.37
50	1.25	1.73
100	1.46	2.13
400	2.16	3.50
900	2.87	5.06
1600	3.65	6.50

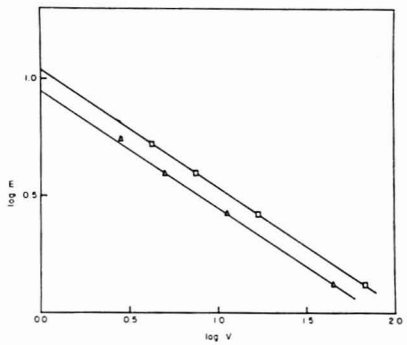

Figure 7. Relation of m and V (see text) under mass transport limiting conditions. Kinetic parameter (k_3C_E/K_m): 50.0 (△), 75.0 (□)

suggests that the current will be proportional to $\omega^{1/2}$. By extrapolating to log $V = 0$, it is found that the intercept of the lines in Figure 7 is 1.22 $(k_3C_Ed^2/K_mD)^{1/2}$. Therefore, the general equation that describes these lines can be expressed by:

$$m = 1.22(d^2/Dt_k)^{1/2} \qquad (20)$$

This equation is valid as long as the rotation speed of the electrode is kept low so that the condition of $V > 10$ is satisfied. Substituting Equation 20 into Equation 19 we obtain:

$$nFADk_3C_E/i_s = 1.22(d^2/Dt_k)^{1/2}(k_3C_Et_k/C) + b \qquad (21)$$

When the concentration of the substrate is sufficiently low so that b is insignificant compared to the first term, the steady-state current becomes:

$$i_s = 0.65nFAD^{2/3}\nu^{-1/6}\omega^{1/2}C \qquad (22)$$

This is virtually identical to the Levich equation for steady-state current of a rotating disk electrode (*5*). Thus, it is clear that the rotating disk enzyme electrode (RDEE) behaves like an ordinary rotating disk electrode under mass transport limiting conditions. The good agreement of Equation 22 with the Levich equation also confirms the validity of our model.

When the enzyme catalysis rate is slow with respect to convective diffusion, e.g., $V < 0.1$, the relation of log m with log V is demonstrated in Figure 8. If a straight line is drawn to connect the points of equal rotation speed, the slope of these lines reflects the effects of the enzyme catalysis on m. Again, extrapolation of these lines to log $V = 0$ leads to the equation:

$$m = \frac{b}{V} \qquad (23)$$

Thus, under catalysis controlled conditions, we have:

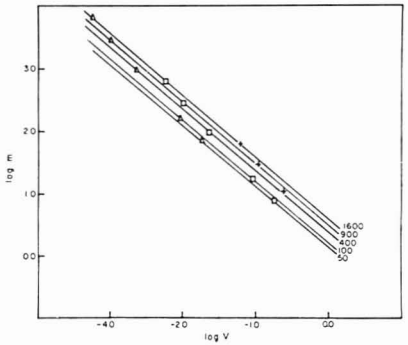

Figure 8. Relation of m and V under catalysis-controlled conditions. Kinetic parameter (k_3C_E/K_m): 0.01 (△), 0.1 (□), 1.0 (+). Rotation speeds indicated next to each curve

$$nFAdk_3C_E/i_s = (b/V)(k_3C_Et_k/C) + b = b(K_m/C + 1) \quad (24)$$

Rearranging Equation 24 gives:

$$\frac{nFAdk_3C_E}{bi_s} = \frac{K_m}{C} + 1 \quad (24a)$$

or

$$\frac{i_{max}}{i_s} = \frac{K_m}{C} + 1 \quad (24b)$$

Equation 24b allows us to plot the experimental i_{max}/i_s vs. $1/C$ to determine K_m. In dilute solutions when K_m/C is much greater than 1, Equation 24 can be simplified to:

$$i_s = nFAdk_3C_EC/(b \cdot K_m)$$

Thus a linear calibration curve is predicted. Assuming $D = 0.45 \times 10^{-4}$ and $\omega = 50$ rpm, the steady-state current response would be:

$$i_s = 0.80nFAdk_3C_EC/K_m \quad (26)$$

Comparing this with Equation 22 of Reference *4*, it can be concluded that the sensitivity of a rotating disk enzyme electrode will be at least 60% greater than its stationary counterpart.

Under either mass transport controlled or catalysis controlled conditions, the steady-state current approaches a limit when the substrate concentration is very high. From Equation 21 or Equation 24, the maximum current for a rotating disk enzyme electrode is:

$$i_{max} = \frac{1}{b}nFAdk_3C_E \quad (26)$$

The parameter b varies with the rotation speed and the diffusion coefficient.

RESULTS AND DISCUSSION

Proper immobilization of the enzyme on the electrode surface is critical to obtaining correct and reproducible results. In order to hold the enzyme at the surface of the electrode, it is found that the presence of a small amount of amine in the carbon paste is essential. If the concentration is increased by 10-fold over the designated amount, the disk current is greatly suppressed. This behavior is not unexpected since the amine is a surfactant. In comparing the cyclic voltammogram of the oxidation of I^- obtained with a pure carbon paste electrode and that obtained with an electrode containing amine, we found that there is no significant change in E_p and i_p at the amine level suggested. After glucose oxidase is attached to the electrode, both the anodic and cathodic peaks are broadened considerably. Nevertheless, a diffusion limited current for iodine reduction is still obtained at −0.2 volts vs. Ag/AgCl. At this point, the disk currents measured for a series of I_3^- solutions are exactly the same for both the pure carbon paste electrode and the glucose oxidase electrode (no substrate present). Based on the Levich equation (*5*), the effective electrode area calculated from the disk current is 0.21 cm^2 for both electrodes. This value is less than 50% of the projected electrode area based on its geometry. This finding suggests that less than 50% of graphite is in contact with the solution at the electrode surface. It also suggests that attachment of the enzyme to the electrode does not interfere with diffusion-controlled I_3^- reduction.

The chemistry involved in the enzyme immobilization procedure may be outlined as follows:

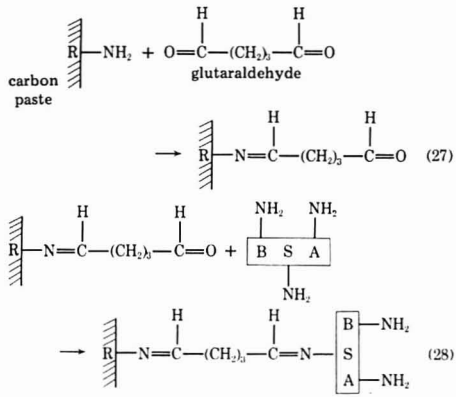

When the glucose oxidase–glutaraldehyde solution is introduced, the reactions outlined above are repeated with glucose oxidase replacing BSA. The BSA is assumed to provide additional enzyme coupling sites without blocking the electrode surface. The enzyme immobilized following this procedure has good thermal stability and excellent mechanical strength, i.e., it can survive stirring at high rotation speeds without losing noticeable activity. If it is stored at 4 °C while not in use, the electrode gives reproducible current response for a period longer than 6 days. We have observed an activity decrease of only 15% after one month of regular use. The enzyme electrode shows very similar pH behavior to that reported in Reference *6*. Above pH 7.2, the current response drops sharply. Further details of electrode performance, particularly for analytical applications, will be presented shortly in a separate paper.

A comparison of Figures 1 and 3 indicates that the electrode behavior predicted from the simulation model is qualitatively consistent with experiment. To correlate the experimental results with the digital simulation, we first compare the ratio of i_{max} at various rotation speeds with that calculated from the theory. The value of i_{max} can be obtained by extrapolating the plot of the reciprocal of the current vs. the reciprocal of the concentration. Since Equation 26 predicts that i_{max} is not affected by the process which controls the current, the ratio of i_{max} of a given electrode at various rotation speeds should agree with the corresponding ratio of $1/b$ (according to Equation 26). The values of b calculated with the reported diffusion coefficient of glucose (*15*) are shown in Table I. The

Table II. Evaluation of Enzyme Kinetic Parameters

Rotation speed, rpm	Ratio of i_{max}		Plot of Eq. 24b		$dk_3C_E \times 10^{10}$ (mol · cm^{-2} s^{-1})
	Exptl	Theor	K_m (M)	Intercept	
400	1.00	1.00	0.0077	0.94	1.13
900	0.74	0.69	0.0095	0.99	1.21
1600	0.57	0.54	0.0091	1.01	1.20

ratios of i_{max} are compared with the ratios of $1/b$ in Table II. Obviously, the agreement is excellent. The behavior of the calibration curves in Figure 1 as well as the linear plot of the reciprocal of current vs. the reciprocal of concentration suggest that the measured currents under experimental conditions are controlled by the enzyme catalysis rate. Therefore, Equation 24b should be used. A typical plot of i_{max}/i_s vs. $1/C$ is shown in Figure 9. Again, remarkable agreement with theory is observed. The values of the Michaelis–Menten constant, K_m, and the intercepts obtained from these plots are also included in Table II. It is noteworthy that the K_m values reported in Table II are not only self-consistent but also in excellent agreement with the reported values (*17, 18*).

According to Equation 26, the maximum catalysis rate of the enzyme, i.e., k_3C_E, can be determined from i_{max}. Unfortunately, we are unable to determine the thickness of the enzyme layer at the electrode surface. Therefore, only the combined term, dk_3C_E, is calculated for each rotation speed using Equation 26. These values are also given in Table II. We have established that the behavior of our enzyme electrode follows the pattern of catalysis controlled current behavior, $V \leq 0.1$. Based on this assumption, the maximum possible value of k_3C_E of the immobilized enzyme is 0.002 M^{-1} s^{-1} as calculated from Equation 14. The concentration of the glucose oxidase solution used to prepare the electrode is 0.3 g/ml. Based on the specific activity of the soluble enzyme, k_3C_E should be about 0.075 M s^{-1} assuming all of the added enzyme is attached and active. Based on these assumptions, about 3% at most of the original enzyme activity is retained after the enzyme is immobilized. We do not know at present how much of the original enzyme is actually attached so this value represents a lower limit. Taking 1.2×10^{-10} mol·cm^{-2} s^{-1} as the value of dk_3C_E, the minimum thickness of the immobilized enzyme thin layer would be 6×10^{-5} cm.

Although k_3C_E cannot be determined without knowing d, it is still possible to estimate this parameter using theory. This can be done by lowering the rotation speed of the electrode to a state where the enzyme catalysis competes with the mass transport effectively, i.e., a condition where both processes have comparable contributions to the steady-state current. Under this condition, matching the experimental results expressed in a proper form with the curve obtained from digital simulation would allow one to determine the k_3C_E value. For instance, if the plot of i_s/i_{max} vs. C/K_m obtained from an experiment matches with the plot calculated from the theory for a given V, then one should be able to determine k_3C_E from V by using known values of t_k and K_m. Further studies on this question are presently under way.

Finally, we would like to point out that the behavior of the ring current (with an enzyme disk) is very similar to that of the enzyme disk electrode. The ring current (no potential applied to the disk) due to the catalysis of glucose oxidase can be measured at a variety of glucose concentrations. If this current is plotted against the disk current measured in a separate set of experiments a linear relationship is observed. The slope of the plot does not change with rotation speed. Thus, the ring current is simply tracking the reaction at the disk as expected. It is also interesting to note that the slope of such a plot is 0.40 as compared to a collection efficiency 0.18

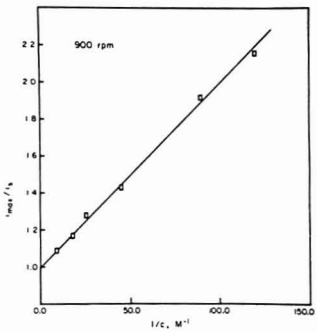

Figure 9. Determination of K_m (see also Table II)

calculated from electrode geometry. Both calculation and experiment give the value of 0.18 if collection efficiency is evaluated in the conventional way as a carbon paste RRDE. If the disk and ring currents are measured simultaneously with the enzyme electrode, i.e., potential applied to both the ring and disk, the slope obtained is 0.30. This indicates that only 25% of the total flux of I_2 that originally reaches the ring is lost to the disk if the disk is also at the reduction potential of I_2. We feel that this observation may be attributable to the fact that the iodine formed outside the disk electrode electrolytic diffusion layer could reach the ring electrode. It may be possible to estimate the thickness of the enzyme at the disk by comparing the ring and disk currents. This possibility is currently under investigation.

CONCLUSION

It has been shown that an enzyme can be attached to an electrode to produce a stable catalytic surface. Moreover, with the aid of a relatively simple model, it is possible to measure the rate of the catalytic reaction and to extract pertinent kinetic parameters. Although only a small portion of the attached enzyme is apparently active, it gives kinetic behavior very similar to the soluble protein. The structure of the attached enzyme is not known, but it behaves like a thin layer of about 1–50 microns. Attachment of the enzyme does not appear to interfere either with electron transfer at the disk or with hydrodynamic flow to the ring.

The ring-disk technique should also prove valuable for the study of kinetics of surface-catalyzed reactions including nonbiological reactions if reacting species can be monitored electrochemically. We have recently demonstrated the advantage of attaching the enzyme to one electrode and monitoring at another. The technique provides a convenient method for separating mass transport and kinetic control of surface catalyzed reactions by well defined variation of hydrodynamic conditions. Mass transport can always be made sufficiently rapid by increasing the rotation speed such that the observed currents will depend only on the catalysis rate.

LITERATURE CITED

(1) G. G. Guilbault and J. G. Montalvo, *J. Am. Chem. Soc.*, **91**, 2164 (1969).
(2) G. G. Guilbault and G. J. Lubrano, *Anal. Chim. Acta*, **64**, 439 (1973).
(3) G. D. Christian, "Advances in Biomedical Engineering and Medical Physics", Vol. 4, John Wiley and Sons, New York, 1971.
(4) L. D. Meli and J. T. Maloy, *Anal. Chem.*, **47**, 299 (1975).
(5) V. G. Levich, "Physicochemical Hydrodynamics", Prentice-Hall, Englewood Cliffs, N.J., 1962, pp 60–72.
(6) H. V. Malmstadt and H. L. Pardue, *Anal. Chem.*, **33**, 1040 (1961).
(7) M. Shabrang and S. Bruckenstein, *J. Electrochem. Soc.*, **122**, 1305 (1975).
(8) W. J. Albery and M. L. Hitchman, "Ring-Disk Electrodes", Oxford University Press, London, 1971, p 22.
(9) R. B. Fischer and D. G. Peters, "Quantitative Chemical Analysis", W. B. Saunders, Philadelphia, Pa., 1968, p 680.
(10) S. W. Feldberg in "Electroanalytical Chemistry", Vol. 3, A. J. Bard, Ed., Marcel Dekker, New York, 1969, Chapter 4.
(11) C. Y. Li and G. S. Wilson, *Anal. Chem.*, **45**, 2370 (1973).
(12) I. Ruzic and S. W. Feldberg, *J. Electroanal. Chem. Interfacial Electrochem.*, **50**, 153 (1974).
(13) K. B. Prater and A. J. Bard, *J. Electrochem Soc.*, **117**, 207 (1970).
(14) K. B. Prater in "Computers in Chemistry and Instrumentation", Vol. 2, J. S. Mattson, H. B. Mark, Jr., and H. C. MacDonald, Jr., Ed., Marcel Dekker, New York, 1972.
(15) R. C. Weast, "CRC Handbook of Chemistry and Physics", The Chemical Rubber Company, Cleveland Ohio, 1968.
(16) H. R. Mahler and E. H. Cordes, "Biological Chemistry", Harper and Row, New York, 1966, Chapter 6.
(17) H. H. Weetall, *Anal. Chem.*, **46**, 602A (1974).
(18) G. L. Smith, M.S. Thesis, University of Arizona, Tucson, Ariz., 1975.

RECEIVED for review April 7, 1976. Accepted June 24, 1976. This investigation was supported in part by National Science Foundation Grant MPS7308683.

Fully Automated Stopped-Flow Studies with a Hierarchical Computer Controlled System

Glen E. Mieling, Richard W. Taylor,[1] Larry G. Hargis,[2] James English, and Harry L. Pardue*

Department of Chemistry, Purdue University, West Lafayette, Ind. 47907

The development and evaluation of a fully automated, computer controlled stopped-flow spectrophotometer is described. A microcomputer controls several operations including the preparation of reagents from up to five different solutions and one diluent, the drawing of measured volumes of the reagent and sample into a sampling unit, and stopped-flow mixing of the reagent and sample. A minicomputer controls the operation of the microcomputer, performs data acquisition and processing operations, and makes decisions relative to the acceptability of acquired data. Quantitative data are presented to demonstrate the performance characteristics of individual components as well as the total system. Results reported include mole ratio and continuous variation plots for complexed metal ions, and a partial simplex study of the Ti(IV)–H_2O_2 complex in the presence of EDTA.

Several recent papers have described computer controlled instrumentation for equilibrium and kinetic studies (*1–4*). Because the computer is involved in a closed loop configuration with the reagent preparation and measurement hardware, some of these systems are applicable to both routine applications involving repetitive operations and nonroutine applications requiring predetermined or computer originated changes in experimental conditions based upon results of current experiments (*1*). One common feature among these systems is the fact that the minicomputer must handle all of the instrumental control functions in addition to data acquisition, storage, processing, and display and decision making operations. One objective of this work was to evaluate the capabilities of a microcomputer used in a hierarchical arrangement with a minicomputer to relieve the latter of some of the time-consuming control functions encountered with slow systems which require constant or frequent attention.

This report describes the design and performance characteristics of a completely automated stopped-flow instrument system which uses a microcomputer for control and a minicomputer for data acquisition and processing. Also, the paper describes a reagent preparation system which is more flexible and which is less subject to mechanical problems than syringe based systems described earlier (*1*). Quantitative data which illustrate the reliability of the system and which demonstrate its applicability to equilibrium and kinetic studies are included in the report. Data show that the system should be particularly useful for measurement and process optimization studies which have been gaining popularity in recent years (*5*).

INSTRUMENTATION

The automated stopped-flow instrument consists of a hierarchical computer system, a reagent preparation unit, a sampling unit, a Sturtevant-type stopped-flow mixing system and a stabilized photometer. Figure 1 represents the interactions among the minicomputer (Model 2100A, Hewlett-Packard Company, Palo Alto, Calif. 94304), the microcomputer (Model 8008, Intel Corporation, Santa Clara, Calif. 95051) and the other components of the stopped-flow system. Operator communication with the system is via the minicomputer which handles several other functions including scheduling and initiation of experiments, acquisition, processing, and display of data, as well as decision-making processes associated with any set of experiments. The microcomputer is dedicated to controlling the reagent preparation and stopped-flow mixing system and to monitoring the status of selected hardware components. Data transfer between the minicomputer and its several peripherals, including the microcomputer, is under priority interrupt control. Intercomputer data transfers are made via a 16-bit duplex register card in the minicomputer and a buffered 8-bit input multiplexer and a 16-bit latched output from the microcomputer.

The minicomputer interface includes a 12-bit, eight channel analog-to-digital converter (ADC) (Model AN 5200 Analogic Company, Waltham, Mass. 02154) and a general purpose interface which features a programmable clock, buffered input/output data lines, and expandable logic. Since this interface is similar to others used routinely on many laboratory computer systems (*6*), it is not discussed further here, but details can be supplied to interested readers.

The microcomputer used in this work was an Intel 8008 with 3072 words of random access memory (RAM) and 512 words

[1] Present address, Department of Chemistry, University of Oklahoma, Norman, Okla. 73069.
[2] Present address, Department of Chemistry, University of New Orleans, New Orleans, La. 70122.

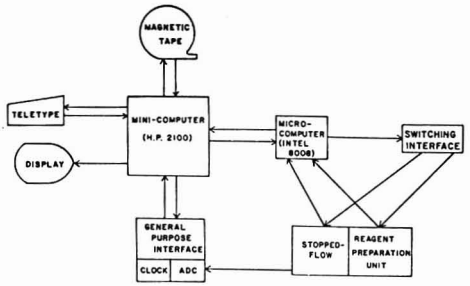

Figure 1. Block diagram of computer controlled stopped-flow system

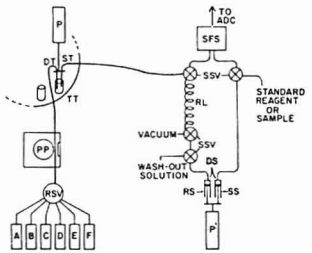

Figure 2. Schematic representation of automated stopped-flow system

A–F = Stock reagents and diluent, RSV = Reagent select valve, PP = Peristaltic pump, TT = turntable, DT,ST = Delivery and sampling tips, DS = Drive syringe, RS = reagent syringe, SS = sample syringe, SSV = Sampling system valves, RL = Reagent loop, SFS = Stopped-flow spectrophotometer, P, P′ = Pneumatic pistons

of programmable read only memory (PROM). The computer has eight 8-bit input ports and sixteen 8-bit output ports. Five input ports are used; one for the Teletype keyboard, one for status signals from instrument components such as valves, one as a flag buffer, one to accept data from the minicomputer, and one to read the front-panel switch register. Five output ports are used; two each for 16-bit word transfers to the minicomputer and instrument components, and one for output to the Teletype. More complete details of this system can be supplied upon request.

The microcomputer is interfaced to the instrument components represented in Figure 2 via a switching interface which contains optically isolated, zero crossing, solid state power relays (Model D 1202, Crydom Controls Division of International Rectifier, El Segundo, Calif. 90245). These relays supply power to electrically activated pneumatic solenoids which control the reagent delivery and pickup tips, the reagent select valve, the sampling unit valves, and the drive syringe piston, and to relays which control the reagent turntable and peristaltic pump. The switching interface includes a manual override switch so that all operations can be controlled by the operator.

Stopped Flow System. Figure 2 is a schematic representation of the reagent preparation, sampling, and mixing systems. Reagent delivery and sampling tips are raised from and lowered into the receiving vials by a pneumatic cylinder (Model 318-1009-024, ARO Corp., Bryan, Ohio 43506). Up to five reagents and one diluent are placed in their respective stock containers labeled A–F. The reagent select valve (Model R6031V6A, Chromatronix Inc., Berkeley, Calif. 94710) connects each reagent successively to the peristaltic pump (PP) (Compu-pet 100, General Electronics, Morris Plains, N.J. 07950) so that the desired amount of reagent can be pumped through the reagent line to the receiving vial on the turntable (Model 272, Fraction Collector, Instrumentation Specialties Co., Lincoln, Neb. 68501). The last position of the reagent select valve is reserved for the diluent which is used to wash all other reagents into the receiving vial and to adjust the volume to the desired final value. The reagents are thoroughly mixed in the receiving vial by a small magnetic stirring bar. The sampling system, described in detail in a previous paper (*3*), takes equal aliquots of both the prepared reagent and the sample and injects them through the mixing block into the observation cell. A microswitch senses the stopping point of the syringe drive mechanism and provides a trigger pulse to initiate data acquisition. Transmittance changes are monitored with the stabilized photometer described earlier. (*7*).

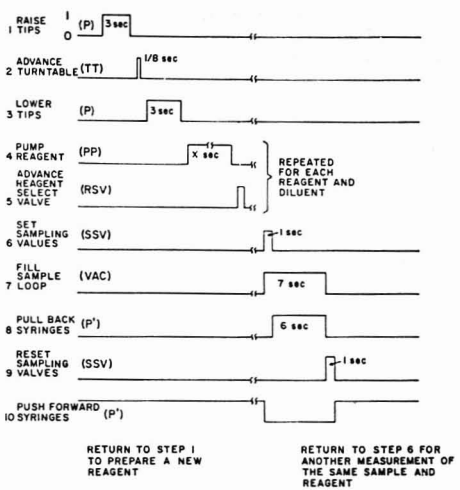

Figure 3. Timing sequence for reagent preparation and stopped-flow mixing

Figure 3 represents the electrical timing sequence for each step involved in the preparation and stopped-flow mixing of a reagent with a standard reagent or sample. The capital letters in parentheses associated with each step identify the device(s) in each step which is(are) activated by the 0 to 1 signal transition in that step. Steps 1 and 3 correspond to air pressure being applied via electrically operated valves to different ports of the pneumatic cylinder, P, so that the piston moves in opposite directions to raise and lower delivery and sample tips. Steps 8 and 10 correspond to similar operations on the pneumatic cylinder, P′, so that the drive syringe plungers are pulled back in step 8 and forced forward in step 10. The $\frac{1}{8}$-s duration pulse in step 2 initiates turntable motion, but the turntable requires about 1 s to change from one position to the next. It should be noted that the system cycles through steps 4 and 5 until all stock reagents and diluent (A–F in Figure 2) have been delivered. At the end of this sequence, the sampling valves are set in step 6 so that the prepared reagent can be drawn into the reagent loop, washout solution can be drawn into the reagent syringe (RS), and the standard reagent or sample can be drawn into the sample syringe (SS). The 7-s period used in step 7 to flush and fill the reagent loop was determined experimentally, and could be different for different valves, different tubing, and different vacuum levels.

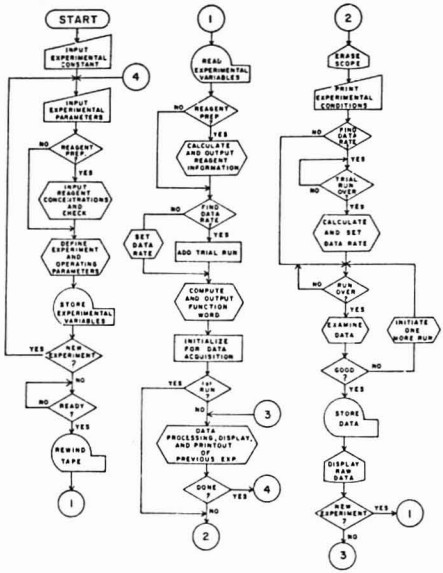

Figure 4. Flow-chart of minicomputer background program

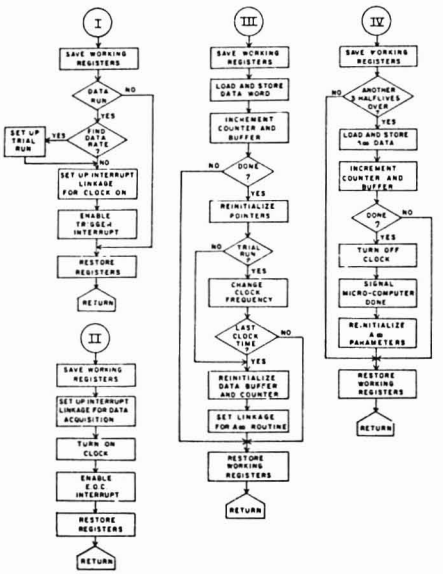

Figure 5. Flow-chart of minicomputer foreground program

(I) Subroutine to service microcomputer interrupt. (II) Subroutine to service stopped-flow trigger interrupt. (III and IV) Subroutine to service E.O.C. interrupts

The 6-s pull-back time for the drive syringes in step 8 was used to avoid degassing reagents being drawn into the syringe barrels. After the reagent loop and syringe barrels are filled with appropriate solutions, the sampling valves are reset in step 9 so that the prepared reagent in the reagent loop and sample in the sample syringe can be mixed in the mixing cell and monitored when the drive syringe plungers are forced forward in step 10.

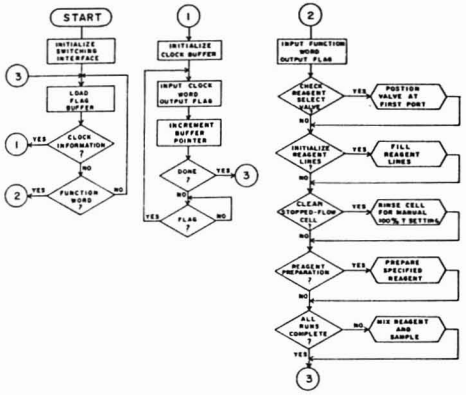

Figure 6. Flow-chart of microcomputer programs

This timing diagram will be helpful in discussing some of the software described in the next sections.

Software. Figures 4–6 represent flow charts of the mini- and microcomputer programs from which the reader can obtain an overview of the capabilities of the system. Each figure is discussed briefly below.

Minicomputer Background Program. Figure 4 represents the minicomputer background program which handles the organizational and bookkeeping functions. Some of the most important aspects of these routines are discussed here. Prior to the initiation of any set of experiments, the operator enters all pertinent information into the minicomputer via a Teletype dialog. The first column represents the operations involved in entering experimental information into the computer.

If one or more reagents are to be prepared by the system, the desired concentration data are entered into the computer which checks these entries, informs the operator if any requested conditions will exceed specified limits, and requests appropriate new values. When the concentration data for an experiment are accepted, then the type of experiment (equilibrium or kinetic) is specified and the computer requests several operating parameters. For example, for equilibrium experiments, the operator must specify the time from mixing until the start of data acquisition, while for kinetic experiments, the operator must specify whether pseudo-zero or first-order kinetics are expected, he must specify data rates or instruct the computer to calculate appropriate data rates from preliminary experiments, and he must specify a "rejection coefficient" which is used to detect anomalies in response curves caused by bubbles in the light path or other unexpected difficulties. For each experiment to be run, the operator must specify the total number of runs, which of these runs (if any) are for washout and which are to be ensemble averaged as valid data. All experimental parameters are stored on magnetic tape (Model 344, Dicom Industries, Sunnyvale, Calif. 94086) and the process is repeated for each experiment to be carried out.

A typical dialog for kinetic experiments involving two reagents prepared and processed by the system is included in Table I. The dialog appears to be straightforward and is not discussed further here.

Table I. Computer–Operator Dialog for Reagent Preparation and Stopped-Flow Kinetic Run [a]

Experimental constants [b]	Experimental parameters	
Calibration slope and intercept? 0.1156, −0.073	Initialization? 1 [c]	Initialization? 0 [c]
Stock concentrations?	Reagent preparation? 1	Reagent preparation? 1
0.1	Identification Code FESCN1	Identification Code FESCN2
0.2	Solution volume (ml) 30	Solution volume (ml) 30
0.3	Input concentration set	Input concentration set
0.4	0.01	0.02
0.5	0.02	0.03
Dead time (s) 0.012	0.03	0.04
Date 1/1/76	0.04	0.05
	0.05	0.06
	Type of experiment 1 [d]	Type of experiment 1 [d]
	Rejection coefficient 0.1	Rejection coefficient 0.1
	# of duplicate runs? 3	# of duplicate runs? 3
	# of ensemble averages? 3	# of ensemble averages? 3
	First data run? 2	First data run? 2
	Data rate? 0.001	Data rate? 0.002
	New experiment? 1	New Experiment? 0
		Ready? 1

[a] Underlined characters indicate operator input. [b] This table illustrates in detail the input dialog sequence shown in column 1 of Figure 4. [c] 1 = yes, 0 = no. [d] 0 = pseudo-zero order kinetics, 1 = pseudo-first-order kinetics, 2 = equilibrium measurement.

The second column in Figure 4 represents the major functions performed by the background program to prepare the mini- and microcomputers for each experiment. When the parameters for all experiments have been recorded, the minicomputer reads information for the first experiment from magnetic tape into core memory. If the system has been instructed to prepare a reagent, then concentration values are translated into 8-bit codes (which represent the time the peristaltic pump will deliver each reagent (A–F in Figure 2) into the receiving vial) and transferred to the microcomputer. If the system has been instructed to find a data rate which will take a fixed number of data points for a specified extent of the reaction, then the program adds one trial run to the number of data runs requested initially. Otherwise, a data rate defined by the operator is used and, in either case, the number of stopped-flow runs required for that experiment is translated into an 8-bit code and transferred to the microcomputer. Other information related to data acquisition, data processing, and display is retained in the minicomputer. After data buffers, data rate, clock, etc. are initialized and the stopped-flow trigger (microswitch) interrupt is enabled, then accepted data from the previous experiment (if any) are processed, displayed, etc., while the microcomputer begins the next reagent preparation or stopped-flow sequence of a new experiment.

The third column in Figure 4 represents the major steps in executing a single experiment. After the display oscilloscope is erased, and the conditions for the experiment being run are printed out, the data taken by the foreground program, either at a data rate specified in the initial dialog, or at a data rate obtained from a trial run, are examined. A derivative routine (*8*) analyzes the data for any anomalous changes in slope which would indicate bubble formation and requests new runs for bad data sets. When a data set is accepted, it is stored on magnetic tape and displayed on the oscilloscope. If no additional experiments were requested, then the data processing routines are implemented. A linear least-squares routine calculates a zero-order rate constant or estimates values of a first-order rate constant, k_1, initial absorbance, A_0, and final absorbance, A_∞, which are then used by a nonlinear regression routine (*9*) to obtain better estimates of these parameters via a fit to an exponential relation between absorbance, A_t, and time. The operator can request a display of residuals from the regression analysis. Computed results are stored on magnetic tape and are printed out via Teletype. The background program can also branch from the end of the third column to point 1 in the second column if a new experiment was requested.

Minicomputer Foreground Programs. The foreground programs are collections of subroutines written in assembly language. Typical functions of these subroutines are to output commands and data words to peripheral devices, set up transfer linkages to interrupt signals, and to service interrupt requests. The HP 2100A minicomputer interrupt system is a hardware feature in which each input/output channel has a specified memory location (or trap cell) associated with it. When an interrupt occurs on a given I/O channel, it causes the computer to interrupt what it is doing and execute an instruction in the associated trap cell which transfers control to a subroutine which services interrupts expected on that particular channel. It is the responsibility of the subroutine to save information the computer will need when it returns to the activity with which it was involved when the interrupt occurred.

Figure 5 represents four subroutines which make up most of the foreground programs. The primary functions of the first subroutine are to set up the interrupt linkage and enable the interrupt so that the hardware clock can be started when the trigger interrupt from the stopped-flow mixer is received. However, since the process of initialization or clean-up will produce several interrupt signals, the system must be able to differentiate between those results from initialization or clean-up operations and those corresponding to actual runs. A code word transferred from the micro- to the minicomputer permits the latter to differentiate between these operations, and to make the decision whether to implement or skip the major functions in the first subroutine. When the proper code word is received, the second subroutine is enabled so that the data rate clock is turned on by the next service request from the stopped-flow instrument (microswitch closure).

Each clock pulse triggers an ADC conversion and each end-of-conversion (EOC) pulse is serviced by the third subroutine. When an EOC interrupt is received, this subroutine stores the datum, increments the data counter and storage buffers, and decides whether all 250 data points have been collected. If more points are needed, then the computer returns to background operations until the next interrupt occurs. If all data have been collected, then the subroutine resets

pointers, buffers, and counters in preparation for the next run and sets the linkage for the A_∞ subroutine before returning to the main program. Another function performed by this subroutine is to generate an exponentially changing clock rate used to select the appropriate data rate from a trial run.

The fourth subroutine is designed to obtain an experimental estimate of A_∞ after approximately six halflives of a first-order reaction have elapsed. This subroutine is entered and exited without any action a specified number of times (usually 250 interrupts) while the reaction approaches completion. When the specified number of counts is exceeded, then the subroutine proceeds to collect and store data until another specified number (usually 30) of points are acquired. When all the A_∞ data are collected, then the subroutine proceeds to turn off the clock, inform the microcomputer that it can proceed with the next operation, and reinitialize the A_∞ data buffers, counters, etc.

Microcomputer Programs. Figure 6 represents flow charts of the more important functions of the microcomputer programs. At the start of the program, the microcomputer latches a control word at the input to the switching interface so that all the pneumatic solenoids and valves are in their initial states and the peristaltic pump and turntable are turned off. The microcomputer then enters a wait loop which interrogates a flag buffer illustrated in column 1. One flag signals waiting reagent information while the other flag indicates the arrival of a function word from the minicomputer. The reagent information, consisting of six pairs of digital numbers used along with the software clock to dispense appropriate amounts of reagents and diluent via the peristaltic pump, is loaded into the microcomputer as represented in column 2. The function word activates a service routine (in the third column) which decodes the word bit-by-bit to call subroutines which perform different operations on the instrument system. These operations include initializing reagent lines and reagent and sample valves, preparation of the reagent, and execution of the stopped-flow mixing operation. These routines utilize the external sensing capabilities of the microcomputer to detect the positions of the reagent select valve and stopped-flow drive syringes via microswitches. The stopped-flow service routine performs automatically all of the functions described earlier (*3*) for the washout, sampling, and mixing system. These operations appear to be sufficiently straightforward that they do not merit additional discussion.

SYSTEM EVALUATION

The various components of the instrumental system were evaluated individually and as an integrated unit. In addition, several different types of experiments were run in the completely automated mode to illustrate the capabilities of the system. The following section presents a description of the experiments and discusses the results obtained.

Reagents. All solutions were prepared in distilled deionized water. Those solutions for which reagent grade materials were not available or not adequate for intended purposes (NaOH vs. HCl titer, Ti(IV), H_2O_2, Zn(II), and zincon) were purified and/or standardized by conventional procedures (*10*).

Component Evaluation. *Peristaltic Pump.* To evaluate a calibration factor (volume vs. time) and the long time performance characteristics of the peristaltic pump, thermostated water (25.0 ± 0.1 °C) was pumped for different time periods into tared weighing bottles and weighed.

The relative standard deviation of replicate delivery volumes varies from about 1% at 1 ml to about 0.9% at 6 ml and 0.5% at 11 ml. Plots of volume delivered vs. pumping time were linear as expected. For an operating sequence in which the delivery tip was not immersed in the solution, the least squares slope and intercept had values of 0.115 ± 0.003 ml/s and −0.04 ± 0.02 ml, respectively, with a correlation coefficient of 0.9998. For a sequence in which the delivery tip was immersed in the solution, the slope and intercept values were 0.1156 ± 0.0001 and −0.073 ± 0.008 ml, respectively, and the correlation coefficient was 0.9995. The negative intercept probably results from starting inertia of the drive motor and the response time (~8 ms) at the zero crossing relay which activates the motor. We were unable to detect any significant carry-over due to liquid adhering to the delivery tip when it is immersed in the solution during delivery, and all subsequent experiments were performed in this fashion.

Initial studies of the long-term reproducibility of the delivery system were quite unsatisfactory. The problem was eventually traced to temperature variations at the pump head caused by the heat from a transformer mounted directly under it and the virtual absence of any ventilation in the case. This problem was solved by mounting the motor head assembly panel on a 2-inch high Plexiglas housing with ventilation holes and a small fan mounted to one side to move ambient air through the case. With this arrangement, repeated measurements (five per set) taken at one-week intervals over a four-week period gave a calibration value of 0.1417 ± 0.0002 ml/s demonstrating excellent long term reproducibility. We have found it necessary to lubricate the tubing in the rotor head assembly daily to avoid frequent replacement. The different calibration values noted above result from different varieties of tubing used with the pump.

Other experiments in which HCl delivered by the pumping system was titrated with carbonate free NaOH of known titer showed that the dead volume from the 6-port valve to the delivery tip was 1.35 ml and that 2.25 ml of water was required to deliver 99.5% of the solution in the line. Thus, in all subsequent experiments at least 2.25 ml of diluent was used to wash reagents from the line into the receiving vial.

Reagent Preparation System. Volumes of HCl and $K_3Fe(CN)_6$ solutions entered via Teletype were delivered under computer control to receiving vials. Volumes of HCl delivered were determined by NaOH titration and amounts of $K_3Fe(CN)_6$ were determined from absorbance measurements on a Cary Model 16 spectrophotometer. A least squares fit of observed vs. expected volume of HCl gave a slope of 0.996 ± 0.003 with an intercept of 0.0188 ± 0.0213 and a correlation coefficient of 0.9999. A Beer's law plot of the $K_3Fe(CN)_6$ data yielded a molar absorptivity value of 1071 ± 2 mol^{-1} cm^{-1} which is in good agreement with the literature value of 1060 mol^{-1} cm^{-1} (*11*). The correlation coefficient for these data was 0.9999.

Sampler, Stopped-Flow Mixer, and Detector. The dead-time of the stopped-flow mixing system, including the sample loop and valves, was determined by the extrapolation method (*12*) using the Fe(III)–SCN^- reaction to be 12 ± 3 ms. The path length of the observation cell was determined to be 3.009 ± 0.015 mm using a $K_3Fe(CN)_6$ solution which had been standardized on a Cary 16 spectrophotometer.

Because the mixed solution is in contact with a solution of the reagent and solvent used to force the reagent from the reagent loop, it is desirable to know the extent to which these solutions may mix. To evaluate this, the observation cell was thoroughly flushed with water and a single sample of $K_3Fe(CN)_6$ was injected. Absorbance measurements were taken periodically over a 2-h interval. The maximum deviation from the average was 0.0005 *A* during this period and there was no sign of a systematic drift in either direction.

One of the major goals of the design of the sampling system was to minimize carry-over from one sample or reagent to another so that either basic studies or routine analyses can be carried out efficiently under computer control. To evaluate the extent of carry-over, the cell was first thoroughly flushed and filled with either pure water or a $K_3Fe(CN)_6$ solution. Then the absorbance was measured for repeated injections

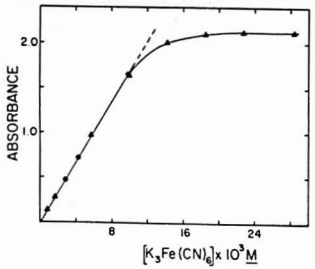

Figure 7. Absorbance vs. concentration for potassium ferricyanide solutions and measured by the automated stopped-flow system

λ = 420 nm, b = 0.30 cm, ϵ_{calcd} = 1070 ± 5 mol^{-1} cm^{-1}

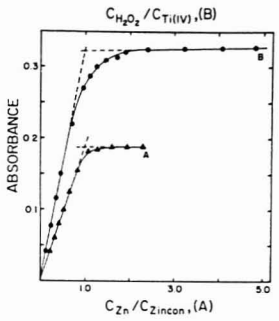

Figure 8. Mole-ratio data obtained by the automated system

Curve A. Zn(II) added to 9.77 × 10^{-5} mol/l. Zincon, pH 9, λ = 620 nm, mole ratio at intersection = 1.01. Curve B. Ti(IV) added to 1.33 × 10^{-2} mol/l. H_2O_2, $[H^+]$ = 0.056 M, λ = 410 nm, mole ratio at intersection = 1.02

of either $K_3Fe(CN)_6$ or pure water. The fraction, f, of the initial sample in the cell carried over to subsequent samples was calculated as follows (*13*). For $K_3Fe(CN)_6$ injected into a cell filled initially with water, the carry-over is computed as

$$f = 1 - \frac{A_o}{A_e} \quad (1)$$

and for water injected into a cell filled initially with $K_3Fe(CN)_6$, the carry-over is computed as

$$f = \frac{A_o}{A_p} \quad (2)$$

where A_o and A_e are the observed and expected (assuming no carry-over) absorbances and A_p is the absorbance of the previous sample. The carry-over was essentially the same (within ±2 SD) for both types of experiments. It varies from about 1.3% for one injection to a negligible value after five injections. Unless stated otherwise, all results reported from this point on are based upon two or more injections so that the carry-over should be less than about 0.6% (~16 μl).

To evaluate the performance of the sampling, mixing, and spectrometer systems operating as a unit, several dilutions of a $K_3Fe(CN)_6$ solution were prepared manually and placed in vials on the sample turntable in a sequence going from low to high to low concentration in a serial fashion. Each solution was sampled and measured five times with the absorbance for each sample being the average of 100 points taken at 25-ms intervals. Each solution was also measured on a Cary Model 16 spectrophotometer for comparison purposes.

The average molar absorptivity values of 1071 ± 8 and 1067 ± 8 for the increasing and decreasing concentration series, respectively, agree very well with the values of 1068 ± 7 obtained for the increasing concentration series with the Cary 16 and 1060 reported in the literature (*11*). Regression of the decreasing concentration series data as the dependent variable against the increasing concentration series data gave a slope of 0.9960 ± 0.0025 and an intercept of 0.0005 ± 0.0004. Thus, no significance is attached to the slight apparent differences between the two data sets.

Results reported to this point present a reasonably complete indication of how the individual components contribute to the performance characteristics of the system. We now turn our attention to the performance of the total system operated under computer control.

Total System Performance. Several types of experiments, including serial dilutions of stock reagents, mole ratio and continuous variation studies of metal–ion complexes, an elementary simplex optimization study, and a kinetic study were carried out to evaluate the hardware–software performance and to demonstrate some potential applications of this system.

Serial Dilutions. This series of experiments consisted of the computer controlled preparation and measurement of several solutions of $K_3Fe(CN)_6$ in a low to high to low concentration sequence. The absorbance of each solution was also measured on the Cary 16 for comparison purposes. Results for the computer controlled experiments are presented in Figure 7. Excellent linearity is observed for the absorbance range between 0 and 1.7. The nonlinearity above an absorbance of 1.7 results primarily from the stray light inherent in the monochromator used in this work (*3, 14*). The molar absorptivity value of 1070 ± 5 computed from the linear portion of the plot is in good agreement with the value of 1065 ± 4 computed from the Cary 16 data which exhibited good linearity over the total range of concentrations prepared by the system in these experiments. The relative standard deviation for all of the results of the computer controlled experiments was 0.87%.

Mole Ratio Experiments. In these experiments, the system was used to prepare a series of solutions containing the same concentration of Zincon indicator at pH 9 but different Zn(II)–perchlorate concentrations. Absorbances of these solutions were measured on the automated stopped-flow system and the Cary 16. Results obtained on the stopped-flow system are presented in Figure 8. The intersection of the extrapolated linear segments of the plot for the automated experiments is at 4.67 ml compared to a value of 4.65 ml for the Cary 16 data. The intersection corresponds to a mole ratio (C_{Zn}/C_{Zincon}) of 1.01. The mean relative standard deviation for all points is 1.2%.

Similar experiments were performed by preparing solutions containing a constant concentration of Ti(IV) and variable amounts of H_2O_2 in 0.05 M HCl. Results of these experiments presented in Figure 8 exhibit an intersection of the extrapolated straight line segments at a mole ratio of 1.02 compared to an expected value of 1.00. The mean relative standard deviation of all measurements is 0.86%.

Continuous Variation Experiments. A series of solutions containing a constant total concentration of Ti(IV) plus H_2O_2 was prepared by entering only the total concentration and the desired Ti(IV) concentration for each solution via Teletype. The computer calculated the required H_2O_2 concentration, controlled the preparation of solutions and measurement of absorbances, and reported the results presented in Figure 9. The extrapolated linear portions of the plots intersect at a ratio ($C_{Ti}/(C_{Ti} + C_{H_2O_2})$) of 0.508 compared to the expected value of 0.500. The mean relative standard deviation for all points is 0.91%.

Table II. Comparison of Kinetic Data Determined for Solutions Prepared Manually and Automatically

[Fe(III)] (Mol/l.) × 10^3	k_{obsd}[a] (s^{-1})		Rel std dev., %			
			Each run[b]		Among runs[a]	
	Man.	Auto.	Man.	Auto.	Man.	Auto.
5.0	2.41	2.40	0.3	0.4	0.8	1.2
7.5	2.96	2.92	0.2	0.3	1.4	1.4
10.0	3.45	3.44	0.2	0.3	0.7	2.0
12.5	3.99	4.00	0.2	0.3	0.6	2.0
15.0	4.52	4.51	0.2	0.3	0.8	1.0
17.5	5.09	5.08	0.2	0.2	0.9	1.9
20.0	5.59	5.52	0.3	0.3	0.7	1.0
22.5	6.10	6.14	0.2	0.4	1.3	0.1
Av	–	–	0.2	0.3	0.9	1.3

[a] Values quoted are averages of k_{obsd} and standard deviations for four duplicate runs of a given solution. [b] Values quoted represent standard deviations obtained from the least squares fit of $-\ln(A_\infty - A)$ vs. time data.

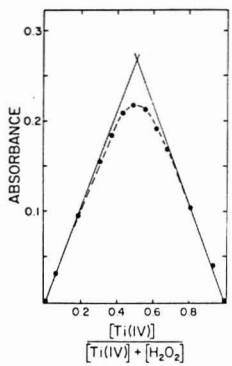

Figure 9. Continuous variation data obtained by the automated system for Ti(IV)–H_2O_2

$[H^+]$ = 0.056 M, λ = 410 nm, peak occurs at 0.508

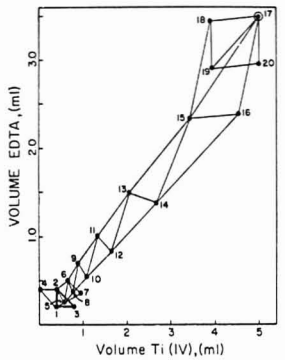

Figure 10. Two factor simplex experiment performed automatically on the Ti(IV)–EDTA–H_2O_2 reaction

pH 4.02, λ = 410 nm, $C_{H_2O_2}$ = 6.64 × 10^{-3} mol/l., $C_{Ti(IV)}$ = 4.83 × 10^{-2} mol/l., C_{EDTA} = 1.10 × 10^{-3} mol/l.

Simplex Design. The main purposes of this portion of the study were to demonstrate the capabilities of the system to design and execute experiments representing a wide range of conditions and to test software designed for simplex optimization studies (*5, 15*). The reaction of H_2O_2 with Ti(IV) in the presence of EDTA was chosen as a model system for this study (*16*). The responses to be optimized were the absorbance level and color stability as functions of Ti(IV) and EDTA concentrations. From the simplex point of view, the response was the product of absorbance times a stability parameter ($R = A \times s$). If absorbance measurements made at 1 and 10 min after solution preparation differed by more than 3%, then the stability factor was set to zero indicating an unsuitable response; otherwise the stability factor was set equal to unity.

A stock solution with the desired H_2O_2 concentration was placed on the sample side of the stopped-flow sampling system and the Ti(IV)–EDTA solutions were prepared automatically in reagent vials on the reagent turntable. The only inputs to the computer were the stock solution concentrations, boundary conditions, the delay time between readings, and initial simplex coordinates. The absorbance readings for the second of two runs from each solution were used in the simplex algorithms. The simplex procedure was terminated when the absorbance reading changed by 1% or less for five consecutive experiments.

Results of these computer generated experiments are represented in Figure 10. The numbers represent the order in which different experiments were conducted. The simplex appears to have moved along a ridge toward a plateau-like region. Actually, the movement was restricted by somewhat arbitrary constraints placed on the maximum amounts of Ti(IV) and EDTA solutions which could be used. As indicated earlier, the goal was not to optimize this chemical system, but rather to illustrate the capabilities of this instrument system for this type study which has been discussed in detail by other authors (*5, 15*).

Kinetic Studies. Data presented above and in earlier reports (*3, 7*) suggest that this automated system should be well suited for fast kinetic studies. The Fe(III)–SCN^- system was selected as a model reaction to test the capabilities of the integrated system. Solutions containing 0.20 M $HClO_4$ and variable amounts of Fe(III) and $NaClO_4$ (to maintain a constant ionic strength of 0.5) were prepared from stock solutions both manually and automatically. These solutions were then drawn into the reagent loop (see Figure 2) and mixed with an equal volume of 2 × 10^{-4} M KSCN in 0.20 M $HClO_4$ and 0.30 M $NaClO_4$ from the sample syringe. Kinetic plots of absorbance and $-\ln(A_\infty - A)$ vs. time were similar to those reported earlier (7). Values of the apparent first-order rate constant, k_{obsd}, obtained as the least squares slopes of $-\ln(A_\infty - A)$ vs. t plots are presented in Table II.

The regression equations for manually and automatically prepared reagents are $k_{obsd} = (212 \pm 1)\,[Fe^{3+}] + 1.35 \pm 0.02$ and $k_{obsd} = (213 \pm 2)\,[Fe^{3+}] + 1.33 \pm 0.03$, respectively. The correlation coefficients for the two data sets were 0.99991 and 0.99976. Students' t and F tests suggest that there are no

statistical differences between the average values of rate constants or the standard deviations for the two sets of experiments.

More complete data will be reported on this and other systems in the future.

LITERATURE CITED

(1) S. N. Deming and H. L. Pardue, *Anal. Chem.*, **43**, 192 (1971).
(2) E. C. Toren, R. N. Carey, G. S. Cembrowski, and J. A. Schirmer, *Clin. Chem. (Winston-Salem, N.C.)*, **19**, 1114, 1122 (1973).
(3) D. Sanderson, J. A. Bittikofer, and H. L. Pardue, *Anal. Chem.*, **44**, 1934 (1972).
(4) K. R. O'Keefe and H. V. Malmstadt, *Anal. Chem.*, **47**, 707 (1975).
(5) S. N. Deming and S. L. Morgan, *Anal. Chem.*, **45**, 278A (1973).
(6) J. E. Davis and E. D. Schmidlin, *Chem. Instrum.*, **4**, 169 (1973).
(7) B. G. Willis, J. A. Bittikofer, H. L. Pardue, and D. W. Margerum, *Anal. Chem.*, **42**, 1340 (1970).
(8) A. Savitsky and M. J. E. Golay, *Anal. Chem.*, **36**, 1627 (1964).
(9) P. R. Bevington, "Data Reduction and Error Analysis for the Physical Sciences", McGraw-Hill, New York, 1969, Chap. 11.
(10) A. I. Vogel, "Quantitative Inorganic Analysis", 3rd ed., J. Wiley and Sons, New York, 1961.
(11) I. M. Kolthoff, E. B. Sandell, E. J. Mcehan, and S. Bruckenstein, "Quantitative Chemical Analysis", 4th ed., The Macmillan Company, London, 1969, p 982.
(12) J. E. Stewart, Durrum Application Notes No. 4, "Flow Deadtime in Stopped-Flow Measurements".
(13) R. E. Thiers, A. H. Reed, and K. Delander, *Clin. Chem. (Winston-Salem, N.C.)*, **17**, 42 (1971).
(14) H. L. Pardue, A. McDowell, D. Fast, and M. J. Milano, *Clin. Chem. (Winston-Salem, N.C.)*, **21**, 1192 (1975).
(15) J. A. Nelder and R. Mead, *Computer J.*, **7**, 308 (1965).
(16) Anders Ringbom, "Complexation in Analytical Chemistry", Interscience, New York, 1969, pp 128–139, 287–289.

RECEIVED for review January 9, 1976. Accepted July 9, 1976. This work was supported in part by Grant No. MPS 75-15500 from the National Science Foundation and in part by Grant No. GM 13326-10 from the NIH–USPHS.

Linearizing the Calibration Curve in Determination of Sulfate by the Methylthymol Blue Method

George Colovos, Martha R. Panesar, and Edward P. Parry*

Air Monitoring Center, Rockwell International, 2421A West Hillcrest Drive, Newbury Park, Calif. 91320

The linearization of the calibration curve of the automated methylthymol blue (MTB) procedure for the determination of sulfates is described. This is accomplished by altering the barium-to-MTB molar ratio of the barium–MTB reagent used. Because of the low purity of the commercial dye, barium-to-MTB molar ratios of 0.9:1 or lower are usually needed for obtaining linear calibration curves. A linear relation between absorbance and sulfate concentration with a correlation coefficient of 0.9995 or better is obtained. The relative standard deviation among replicates, in the range of 0 to 100 μg/ml, is 1.4 to 0.4%. The sensitivity for this range is 4 μg/ml SO_4^{2-}.

Routine determination of sulfate in a large number of water and air samples is usually performed by a variety of automated wet chemical methods. The automated methylthymol blue method developed by Lazrus et al. (*1*) is gradually displacing all the other methods, and currently most of the Federal and State water and air pollution agencies have adopted this method for the determination of sulfates.

The method involves displacement of methylthymol blue (MTB) from a barium–MTB complex by sulfate and colorimetric measurement of the freed MTB in highly basic solution.

$$Ba^{2+} + MTB^{6-} \rightleftharpoons BaMTB^{4-} \quad (1)$$

$$BaMTB^{4-} + SO_4^{2-} \rightleftharpoons BaSO_4 + MTB^{6-} \quad (2)$$

The absorption maximum of the barium–MTB complex is at 610 nm and that of the free MTB is at 460 nm. Therefore, the free MTB can be measured at 460 nm without major interference from the barium–MTB complex. As Equation 2 shows, the concentration of MTB is directly related to the concentration of sulfate, which permits determination of the sulfate by measuring the concentration of the displaced MTB.

One of the most unwanted characteristics of this method has been the nonlinear relationship between the output of the instrument (absorbance) and the sulfate concentration. The plot of absorbance vs. concentration appears to be a parabolic function which becomes linear above a certain concentration of sulfate. Thus, in most cases, a calibration curve may be assumed as consisting of two linear portions of different slopes. The first linear portion corresponds to low sulfate concentrations (about one fifth of the total range), and the second to higher sulfate concentrations. The slope of the first linear portion of the calibration curve is lower by at least a factor of two from the slope of the second portion. Currently, two different approaches are used for the utilization of the nonlinear calibration curves for determination of sulfates. In the first approach, the output signals corresponding to each point of the calibration curve are linearized electronically with respect to the standard sulfate concentration, and thus the entire range can be utilized. In the second approach, only the linear portion of the calibration curve corresponding to higher sulfate concentrations is used for the analysis of samples. Both approaches have several disadvantages. For the electronic linearization, additional equipment and some extra effort to set the calibration are required. In the other approach, the sensitivity of the method is reduced by more than 20% and, therefore, low sulfate samples cannot be analyzed unless a larger or more concentrated sample is used.

In our laboratory, the MTB method is used extensively for determination of sulfate in environmental samples. To avoid all the disadvantages which arise from the nonlinear calibration curves, we investigated the chemistry involved in this system with the hope of linearizing the calibration curves by modifying the original analytical procedure.

In this paper, we wish to report the results of our research which enabled us to obtain linear response with respect to sulfates without any electronic linearization of the resulting signals.

EXPERIMENTAL

Instruments and Apparatus. A Technicon AutoAnalyzer II connected to an Automatic Sampler IV was used throughout this study. The flow diagram used in the present study was similar to the one recommended by Technicon for sulfate analysis in waste water (*2*). In this, the sample containing sulfate in the range of 4 to 100 μg/ml

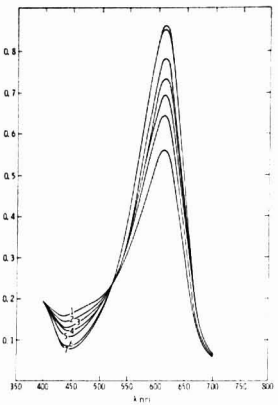

Figure 1. Absorption spectra of the barium-methylthymol blue complexes at various barium-to-MTB molar ratios

$[Ba^{2+}]/[MTB]$ for spectra 1, 2, 3, 4, 5, 6, and 7 was equal to 0.89, 1.07, 1.25, 1.43, 1.78, 2.32, and 2.94, respectively. pH = 12

is first diluted (1:9.7) with water, then passed through a cation exchange column to remove all the interfering cations, and finally reacted with a reagent containing barium ion and MTB (pH ~2.4) in a 20-turn mixing coil followed by addition of the appropriate amount of 0.18 N NaOH in a second 20-turn mixing coil to bring the pH to about 12. The absorbance of the resulting solution is monitored continuously in the colorimeter at 460 nm. Other, more sensitive, concentration ranges can be established by changing the sample dilution. Samples containing sulfate in the range of 0.5 to 10 μg/ml can be analyzed by eliminating the dilution and passing the sample directly into the ion-exchange column.

Reagents. Methylthymol blue (J. T. Baker, Baker grade) was used without further purification. The rest of the chemicals were reagent grade and were used without any further purification.

All the reagent solutions were prepared as described in the Technicon procedure (*2*) except the methylthymol blue reagent solutions, which were prepared in the following manner: a 6.796×10^{-3} M Ba^{2+} solution was prepared by dissolving 1.6601 g of $BaCl_2$ and diluting to 1 l. with distilled water. A methylthymol blue solution of the same molarity was prepared by dissolving 0.5193 g of MTB in 100 ml of distilled water. These two solutions were used for the preparation of the Ba–MTB reagent with varying barium-to-MTB molar ratios by adding: 12.4 ml aliquots of the $BaCl_2$ solution to each of several 250-ml volumetric flasks, then adding volumes of the MTB solution ranging from 9.0 ml (for $[Ba^{2+}]/[MTB] = 1.39$) to 16.0 ml (for $[Ba^{2+}]/[MTB] = 0.78$). Two ml of 1 N HCl, the appropriate amount of distilled water to bring the volume to 50 ml, and a small amount (1.5 ml) of wetting agent (Brij-35) were then added, and finally the solution were diluted to 250 ml with ethanol. The solutions were refrigerated overnight before they were used in the AutoAnalyzer II with the usual flow arrangement for the 4–100 μg/ml sulfate range.

The nominal $[Ba^{2+}]/[MTB]$ ratio of each reagent can be calculated from the volumes of the respective solutions used to prepare the particular reagent. Reagents of barium-to-MTB molar ratios above 1.39 or below 0.78 may also be prepared using a similar procedure.

Procedure. Nine-point calibration curves covering the operating range of 4 to 100 μg/ml SO_4^{2-} (4, 8, 12, 16, 20, 40, 60, 80, and 100 μg/ml, respectively) were run with each methylthymol blue reagent solution of varying barium-to-dye molar ratios. The instrumental parameters were kept constant throughout all these runs and they were as follows: standard calibration adjustment at 4.0, wash-to-sample ratio 1:3 and 30 samples/h sampling rate. The baseline was adjusted as necessary. After each reagent was run with the nine standards, the heights of the obtained peaks were measured and corrected for the baseline. The standard curve parameters (*3*) of slope (b) and intercept (a) were calculated from the known sulfate concentrations and the heights of the resulting peaks by using the linear least squares equation. The standard error of estimate

$$Sy = \sqrt{(\Sigma Y^2 - a\Sigma Y + b\Sigma YX)/n} \quad (3)$$

and the coefficient of correlation,

$$r = \frac{(\eta \Sigma XY - \Sigma X \Sigma Y)}{\sqrt{[n\Sigma X^2 - (\Sigma X)^2][n\Sigma Y^2 - (\Sigma Y)^2]}} \quad (4)$$

were calculated also for each set of data. Using the standard error and the coefficient of correlation as criteria, an optimum $[Ba^{2+}]/[MTB]$ ratio can be selected for the preparation of MTB reagent suitable for routine use. Using the selected $[Ba^{2+}]/[MTB]$ ratio, the weight of MTB dye for 1 l. of reagent can be calculated. This weight corresponds to the particular lot of commercial MTB and it can be used thereafter each time Ba–MTB reagent is prepared from the same lot of MTB dye. For each new lot of MTB, a linearity study should be performed to establish the optimum barium-to-MTB ratio.

Spectrophotometric Determination of the Purity of the Dye. The purity of the commercial dye can be estimated spectrophotometrically by measuring the absorbance of solutions of known concentrations and using the known molar absorptivity of MTB at that wavelength. The molar absorptivity at 435 nm for aqueous MTB solutions of pH 1.8 to 5.4 has been measured by Yoshino et al. (*4*). The reported value is 1.89 l. mol^{-1} cm^{-1}. An MTB solution was prepared by dissolving 0.1947 g MTB in 50 ml 0.001 N HCl, which gives a calculated concentration of 5×10^{-3} M. This MTB solution was diluted 1:100 with 0.001 N HCl and the absorbance at 435 nm was recorded with a Cary-14 spectrophotometer using a 1-cm cell. The purity was calculated from the relation:

$$\% \text{ purity} = 105.82\, A_{435\text{ nm}} \quad (5)$$

where $A_{435\text{ nm}}$ is the measured absorbance at 435 nm.

Spectrophotometric Investigation of the Formation of Binuclear Complexes. The change in the absorption spectra of solutions containing constant concentrations of MTB and varying amounts of barium was used to demonstrate the formation of binuclear complexes of barium with MTB. For this purpose 5.0 ml of a Ba–MTB reagent (3.8×10^{-5} M MTB) of known $[Ba^{2+}]/[MTB]$ ratio and appropriate amounts of $BaCl_2$ solution to yield the desired $[Ba^{2+}]/[MTB]$ ratio were added in 50-ml volumetric flasks followed by 3 ml of 0.18 N NaOH. Then the solutions were all diluted to the mark with distilled water and absorption spectra were recorded immediately with a Cary-14 spectrophotometer using a 1-cm cell.

RESULTS AND DISCUSSION

Methylthymol blue (MTB) is a derivative of thymol sulfonphthalein with two N,N'-di(carboxymethyl)aminomethyl groups attached to its 3,3′ position (*1*).

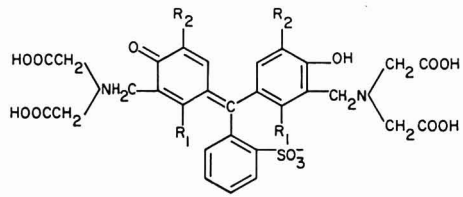

Because of these two groups, MTB behaves as a ligand capable of chelating with a metal atom at either one of the two end groups. However, because of the stereochemical hinderance of the bulky sulfonphthalein structure, the participation of both groups in the coordination sphere of a single metal ion is not feasible (*4*). Thus, the second group remains vacant and available for coordination with a second metal ion.

Formation of binuclear complexes of MTB with metal ions such as Co(II), Ni(II), Cu(II), and Zn(II) has been studied (*4–6*). It has been found that the absorption maximum of the binuclear complex is at the same wavelength (610 nm) as the 1:1 complex, but the molar absorptivity of the binuclear complex is significantly larger. The spectra of Figure 1 show the formation of the binuclear barium–MTB complex in alkaline solutions. It can easily be seen that the molar absorptivity at 610 nm increases as the barium-to-dye ratio increases up to about 2:1 indicating that the amount of barium in excess of that required for formation of the 1:1 complex forms further complexes. When the barium-to-dye ratio becomes higher

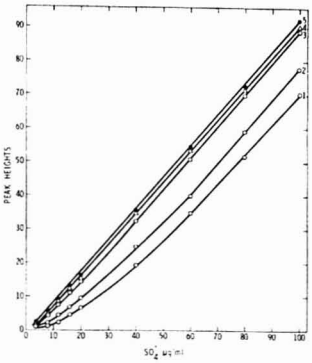

Figure 2. Change of the calibration curve with the barium-to-MTB ratio

$[Ba^{2+}]/[MTB]$ for curves 1, 2, 3, 4, and 5 was 1.39, 1.25, 1.00, 0.83, and 0.78, respectively

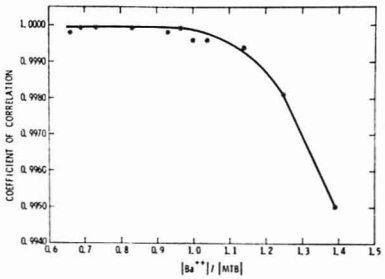

Figure 3. Change of the coefficient of linearity of the calibration curve with the barium-to-MTB molar ratio

than 2:1, the molar absorptivity does not increase further. It is, therefore, rather evident that MTB forms binuclear complexes with excess of barium ions.

Commercial methylthymol blue, as most dyes, is not 100% pure. In fact, the purity of MTB is even lower than many other dyes because the monosubstituted derivative of sulfonphthalein (semimethylthymol blue, SMTB), is produced along with MTB during preparation. SMTB can be separated from MTB by column chromatography (7).

As described in the previous section, the purity of MTB can be determined spectrophotometrically. This technique gives essentially a measure of the existing impurities which do not absorb at 435 nm. Impurities such as SMTB or unsubstituted sulfonphthalein which absorb at 435 nm cannot be determined. The amount of nonabsorbing impurities in commercial dye preparations has been shown to vary from lot to lot ranging from 10 to 50%.

This low purity of the MTB dye is the main reason for the nonlinear calibration curves. For example, the composition of the MTB reagent solution recommended by Lazrus et al. (*1*) and in the Technicon procedure (*2*) contains a barium-to-dye molar ratio equal to 1:1, but due to the low purity of the commercial dye, the actual ratio is usually considerably higher than that. Binuclear species are, therefore, formed along with the mononuclear complexes and the removal of small amounts of barium ions by the sulfate (at low sulfate concentration) results in the transformation of the binuclear to mononuclear complexes (Equation 6).

$$Ba_2MTB^{2-} + SO_4^{2-} \rightleftharpoons BaSO_4 + BaMTB^{4-} \qquad (6)$$

The molar absorptivity of the binuclear complex at 460 nm is lower than that of the mononuclear (Figure 1) and, therefore, under the above experimental conditions, the absorbance of the solutions will be increased only slightly with added sulfate. With higher sulfate additions, the 1:1 complex is converted to free MTB (Equation 2) resulting in a higher change in absorbance per mole of added sulfate.

The formation of binuclear complexes can be eliminated by changing the barium-to-dye molar ratio. Figure 2 shows the effect of the barium-to-dye molar ratio on experimentally obtained calibration curves. It can be seen that the deviation from the linearity increases as the barium-to-dye molar ratio becomes greater. This deviation from the linearity is shown better in Figure 3 where the coefficient of correlation of the calibration curve is plotted vs. the barium-to-MTB ratio.

Table I. Determination of Sulfate in Synthetic Solutions with the Modified MTB Procedure

SO_4^{2-} µg/ml			
Taken	Found[a]	Std dev	%
5.00	4.90	0.07	1.4
10.00	10.08	0.08	0.8
20.00	20.08	0.29	1.4
40.00	41.14	0.36	0.9
60.00	59.95	0.24	0.4
80.00	80.04	0.43	0.5
100.00	100.58	0.38	0.4

[a] Average of five runs.

These coefficients of correlation have been calculated from the 9-point calibration curves as described above, with five of these points located at the lower part of the calibration curve (4 to 20 µg/ml) where the curvature usually occurs. The coefficient of correlation approaches unity when sufficient excess of dye prevents the formation of binuclear species. Thus, by changing the concentration of MTB, the optimum barium-to-dye ratio can be established for any given lot of commercial dye preparation and then used thereafter for routine preparation of the reagent.

The spectrophotometrically determined purity of MTB correlates very well with the optimum barium-to-dye ratio established experimentally as it is described above. The commercially available dye usually contains inorganic salts as well as small amounts of SMTB and other organic compounds. However, the nonabsorbing species constitute the larger part of the commercial dye impurity and, therefore, the estimated spectrophotometrically purity of the dye can be used for establishing the barium-to-dye ratio required for the preparation of the MTB reagent. This is based on the assumptions, that 1) MTB forms mononuclear complexes when it is mixed with equimolar amounts of barium and 2) the concentration of organic impurities absorbing at 435 nm is very small. These two assumptions appear to be substantially supported by the experimental results. The value of the barium-to-dye molar ratio required for the preparation of the MTB reagent in most cases was found to be in the range of 0.8 to 0.9 which indicates dye purity of 80 to 90%. However, in some cases, commercially available dye preparation may be found to contain larger amounts of impurities. For example, a recent lot of dye was found to contain 51.3% absorbing species by the spectrophotometric method described above, and the linearity study yielded an optimum $[Ba^{2+}]/[MTB]$ molar ratio of 0.513. Therefore, the optimum barium-to-dye ratio might be defined using the spectrophotometrically de-

termined purity of the commercially available dye. However, the actual measurement of the correct barium-to-MTB ratio, by constructing calibration curves using various ratios, is preferred because of possible impact of the presence of absorbing impurities during the spectrophotometric determination.

Table I shows typical results obtained with the modified MTB procedure for determination of sulfate. For these, the instrument was calibrated independently with standard solutions, and slope and intercept of the calibration curve were determined by the linear least squares equation. The relative standard deviation for replicate standards was found to be between 0.4–1.4%. The sensitivity for this range (0 to 100 μg/ml) was found to be equal to about 4 μg/ml. Higher or lower sensitivities may be obtained by modifying the flow diagram of the Technicon AutoAnalyzer as described above. In our laboratory, we were able to obtain sensitivities of 0.5 μg/ml in a range up to 10 μg/ml by such modifications. Even with this sensitive range, the calibration curves remain linear when the MTB reagent is prepared using the weight of MTB dye calculated from the results of the linearity study.

Both the high (0–100 μg/ml) and low (0.5–10 μg/ml) ranges are used in our laboratory routinely for determination of sulfate, and the results obtained are always comparable to those described here.

LITERATURE CITED

(1) A. L. Lazrus, K. C. Hill, and J. P. Lodge, "Automation in Analytical Chemistry, Technicon Symposia, 1965", Mediad, 1966, pp 291–293.
(2) Technicon Industrial Method No. 118-71 W/tentative, Technicon Industrial Systems, Tarrytown, N.Y., 1972.
(3) T. Yamane, "Statistics, An Introductory Analysis", Harper and Row, New York, 1967, pp 340, 419–423.
(4) T. Yoshino, H. Imada, S. Murakami, and M. Kagewa, *Talanta*, **21**, 211 (1974).
(5) V. N. Tikonov, *Zh., Anal. Khim.*, **22**, 658 (1967).
(6) O. A. Tataev, S. A. Akhavedov, and B. A. Magomeclova, *Zh. Anal. Khim.* **25**, 1229 (1970).
(7) T. Yoshino, H. Imada, M. Kagewa, and K. Iwasa, *Talanta*, **16**, 151 (1969).

RECEIVED for review December 3, 1975. Accepted July 8, 1976.

Application of Thermal Analytical Methods in the Characterization of Carbonaceous Materials

Ralph T. Yang,* Meyer Steinberg, and Robert Smol

Department of Applied Science, Brookhaven National Laboratory, Upton, N.Y. 11973

Thermal analytical methods are applied to a study of the reactivities toward O_2 and CO_2 of three kinds of carbonaceous materials which give different rate expressions with respect to the fractional completion of the reaction. It is demonstrated that a pseudo-third-order reaction can give a bifurcated peak in the DTA curve and, therefore, the notion of the existence of two kinds of carbonaceous materials based on a bifurcated peak, as has often appeared in the literature, should be asserted with caution.

The thrust of developing more efficient energy systems from coal has renewed a great interest in the application of thermal analytical methods to the study of reactivities of carbonaceous materials toward gases. In the field of catalysis, meanwhile, the employment of differential thermal analysis (DTA) to examine the catalysts poisoned by carbonaceous materials deposited on the surface has attracted wide attention and application. More specifically, in the studies by Rode and Balandin (*1, 2*) on the nature of the carbonaceous deposits on chromia catalyst, the DTA curve produced by combustion of the deposits showed bifurcation, or two peaks, of the exothermic peak in some instances. The authors interpreted this as an indication of two types of carbonaceous materials on the surface. Thereafter, a bifurcated peak in the DTA curve has been quite commonly related to the notion of the existence of two kinds of carbonaceous materials (*3, 4*). Furthermore, it has been suggested that, by matching with a synthesized bifurcated DTA peak of a standard reference mixture consisting of two known carbonaceous materials, an unknown carbonaceous material could be analyzed quantitatively (*5*).

In this work, thermal analytical methods are used to study the reactivities of three widely different carbonaceous materials. The quantitative relationship between a single DTA curve and the kinetic parameters for a "first-order" heterogeneous reaction has been previously developed (*6*). The qualitative relationship between the general form of the rate expression and the shape of its corresponding DTA curve is examined in this study for two higher-order gas–carbon reactions. More importantly, it will be shown that a pseudo-third-order reaction can also produce a bifurcated peak in the DTA curve. Therefore, caution must be taken in relating such a peak to the existence of two kinds of carbonaceous materials.

KINETIC ANALYSES OF DTA CURVES

Extraction of kinetic information from DTA curves is, in general, limited to reactions with simple rate expressions (*6, 7*). For reactions with more complicated rate expressions, the approximate methods outlined by Kissinger (*8*) and by Yang and Steinberg (*6*) can also be applied; but the results would be lengthy and the mathematics tedious, and therefore such analyses would not be of practical interest.

In this section, it is not intended to extract the kinetic parameters from a DTA curve. Rather, the qualitative relationship between the rate expression and the general shape of the DTA curve is to be explored. More specifically, the possible number of peaks in a DTA curve will be predicted from the order of the reaction.

The rate of a heterogeneous reaction is expressed in the conventional fashion:

$$\text{Rate} = r = -\frac{1}{m}\frac{dm}{dt} \tag{1}$$

where m is the instantaneous mass of the reacting solid and t is the time.

The rate of a gas–carbon reaction at steady state, or at constant burnoff (x) is normally expressed as a function of the concentrations of the gases involved. However, in the DTA

measurements the gas concentrations are held constant, the rate is expressed in terms of x, and it can be shown that

$$-\frac{1}{m}\frac{dm}{dt} = \frac{1}{1-x}\frac{dx}{dt} \quad (2)$$

In this work, the order of a reaction will be expressed in terms of the following form:

$$\frac{dx}{dt} = r_0 e^{-E/RT}(1-x)^n \quad (3)$$

where n is the order, r_0 the frequency factor, E the activation energy, R the gas constant and T the absolute temperature.

Now we consider three general types of gas–solid reactions having individually the following characteristics: (1) the rate is independent of x; (2) the rate increases or decreases linearly with x and (3) a rate maximum or minimum exists in the curve of r with x. The corresponding general rate equations are:

$$\frac{dx}{dt} = r_1 e^{-E/RT}(1-x) \quad (4)$$

$$\frac{dx}{dt} = r_2 e^{-E/RT}(1-x)(x+l) \quad (5)$$

$$\frac{dx}{dt} = r_3 e^{-E/RT}(1-x)(x^2+px+n) \quad (6)$$

where l, p, and n are constants. According to Equation 3, Type 1 is first order and Types 2 and 3 are referred to as pseudo-second and pseudo-third-order reactions, respectively.

In DTA measurements, the temperature differential (ΔT) is recorded as a function of T. Assuming that the heat of reaction is detected instantaneously and that the thermal effect, either exothermic or endothermic, is dissipated to the flowing gas rapidly, ΔT is proportional to the mass rate, i.e., the total amount of mass being reacted per unit time, or to dx/dt

$$\Delta T = k(dx/dt) \quad (7)$$

The above assumptions are not unrealistic in the gas–carbon reactions in which diffusion is not the rate-controlling step and the reactions proceed uniformly throughout the sample.

By substituting the approximate expression for dx/dt for the three types of reactions in Equation 7, and setting $d(\Delta T)/dt = 0$, the following relations are obtained:

$$C_1\frac{E}{RT^2} = e^{-E/RT} \quad (8)$$

$$C_2\frac{E}{RT^2} = e^{-E/RT}(ax+b) \quad (9)$$

$$C_3\frac{E}{RT^2} = e^{-E/RT}(cx^2+dx+f) \quad (10)$$

where C_1, C_2, C_3 are positive constants and a, b, c, d, and f are constants that can be either positive or negative.

Equations 8–10 can be used to predict the peak temperatures of a DTA curve, provided that the functional form $x(T)$ is known. The $x(T)$ function can be approximated in a way similar to that outlined for a first-order reaction (*6*). However, it is of interest in this study to predict the number of peaks in the DTA curve based on the three general rate expressions as shown. For this purpose, Equations 8–10 are consequently solved graphically. It may be recalled that x increases from 0 to 1 with increasing T and assumes a fractional value which changes very slowly with T compared to the other two factors in the equations: $1/T^2$ and exp $(-E/RT)$. The equations are presented in graphical forms in Figure 1. The points of intersection of the curves representing the right-hand-side (RHS) and the left-hand-side (LHS) are the peak temperatures in a DTA curve. From Figure 1, it is clear that there is only one possible solution for Equation 8 or Equation 9, and

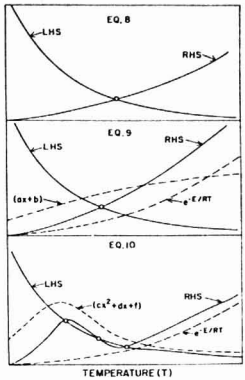

Figure 1. Number of solutions for Equations 8–10

there possibly exist three solutions for Equation 10. It is also possible that only one solution exists for Equation 10, depending on the constants in the equation. For the reaction with rate increasing monotonically with x, the characteristics of the graphical solution for Equation 9 in Figure 1 should also apply, and hence also only one solution would be expected. From this analysis, it can be seen that only one peak is possible in the first-order and pseudo-second-order reactions while two peaks, or a bifurcated peak, can occur for the pseudo-third-order reaction.

EXPERIMENTAL

A Mettler Differential Thermal Analyzer Model TA-1 was used to obtain the DTA curves. Reaction rates were measured gravimetrically (TG) and were expressed according to Equation 1.

The carbon samples used were: coke from Illinois No. 6 bituminous coal (coked at 1000 °C for about 20 h in flowing N_2); electrode graphite and a reactor-grade nuclear graphite. The nuclear graphite had less than 100 ppm ash content and more analyses have been given elsewhere (*6*). The coke gave the following analyses: ash content, 17%; SiO_2, 10%; Fe, 1.8%; Al_2O_3, 2.5%; and the balance of Ca, Mg, and Ti, etc. Analyses of the electrode graphite yielded: ash content, 2.7%; 1% Si; 0.1% B and Cu each; 0.03% Fe, Ni, Ag, and Ca each; 0.01% Mg, Al, Zn, and Mn each; and trace of Cr, Pb, and V. The elemental analyses were performed by emission spectroscopy.

Carbon dioxide was supplied by Matheson Gas Products Company and was of Coleman Instrument grade (99.99%). The gas was further purified of moisture and O_2 in a train of silica gel, $Mg(ClO_4)_2$ (both at room temperature) and copper turnings held at 500 °C. The DTA measurements involved dilution of the carbon sample in an inert material (Al_2O_3) which was also the reference. The dilution is necessary because of the high heat of reaction. Detailed procedures of the DTA and the rate measurements were given previously (*9*). It should be noted that a high gas flow rate was employed and that the thermocouples were placed at the center of the sample which was contained in a platinum sample holder. Under these conditions, the assumptions made for Equation 7 are not unrealistic.

RESULTS AND DISCUSSION

The temperature range and the other experimental conditions were chosen such that the overall reaction rates were dominated by the chemical rates. It has been demonstrated that the oxidation of carbons by air in the 500–600 °C range (*10*) and the oxidation of nuclear graphite by CO_2 at 1050 °C (*6*) are all in the chemical-controlled rate regime. In this regime, the rates of the diffusional steps are high compared to the chemical rates and the observed overall rates can be approximated as the chemical rates.

The following carbonaceous materials were used in this work, in the order of decreasing reactivities: coke, electrode

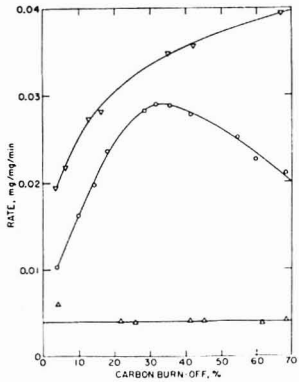

Figure 2. Dependence of oxidation rate of carbon on percentage burn-off

(Top) Coke in air at 525 °C. (Middle) Electrode graphite in air at 600 °C. (Bottom) Nuclear graphite in CO_2 at 1050 °C

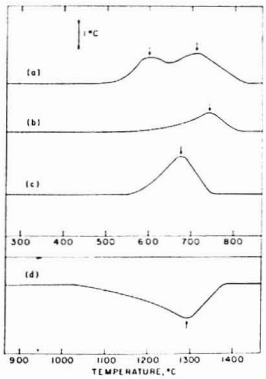

Figure 3. DTA curves

(a) Coke in air. (b) Coke (with 40% burn-off in air at 525 °C) in air. (c) Electrode graphite in air. (d) Nuclear graphite in CO_2

graphite, and nuclear graphite. Reaction rates were measured on the first two materials with air and on the nuclear graphite with CO_2. These three gas–solid reactions demonstrated the general behavior of the three types of reactions which were analyzed above. Some typical results are shown in Figure 2, at the specified temperatures. The reactions with nuclear graphite and with coke can be represented by rate expressions of the first- and pseudo-third-order types respectively. The rate with the electrode graphite does not increase linearly with burn-off, while it does increase monotonically. According to the preceding analysis, the reaction with the nuclear and the electrode graphites would give only one peak while the reaction with coke could give two peaks or a bifurcated peak in their corresponding DTA curves. Such predicted behavior was verified by the measured DTA curves, and they are shown in Figure 3. In this figure, three exotherms ($C + O_2$) and one endotherm ($C + CO_2$) are shown. An interesting feature in this figure is that the reaction with coke with 0% burn-off showed a bifurcated peak while the coke with 40% previous carbon burn-off showed a single peak. This is due to the fact that the

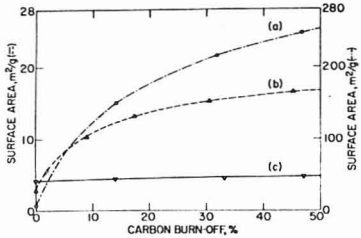

Figure 4. BET surface area (N_2, 77 K) vs. burn-off

(a) Coke. (b) Electrode graphite. (c) Nuclear graphite

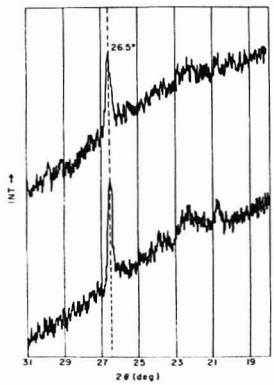

Figure 5. X-ray diffractograms of coke at (top) 0% burn-off and (bottom) 31.8% burn-off, copper $K\alpha$ radiation

rate of the reaction decreases monotonically after 40% burn-off, as shown in Figure 2. The reaction with the coke that has 40% burn-off can be categorized as a pseudo-second-order reaction and, hence, can produce only one peak in the DTA curve. Although it is not intended in this work to study the factors involved in determining the reactivities of the various carbonaceous materials, it is illustrative to study the specific rates, or the rates per unit reacting surface area. The total surface area of the materials was measured at various carbon burn-offs and the results are shown in Figure 4. From the data in Figures 2 and 4, the specific rates of the reactions with the two graphites were nearly constant with increasing burn-off. The specific rate of the coke was also nearly constant below about 30% carbon burn-off but decreased monotonically upon further increasing burn-off. The decrease may be due to two factors: (1) the increasing surface area of the mineral matters and (2) a possible decrease of the concentration of the active sites on the carbon surface which predominantly contribute to the rates (*11*, *12*).

To further examine the possibility of the existence of two kinds of carbons, x-ray diffraction patterns were obtained of the coke samples at various burn-offs. In Figure 5, the diffraction patterns of the coke at 0% and at 31.8% burn-off are shown. The peak at $2\theta = 26.5°$ is due to the (002) planes of the graphitic structure in the crystallites. No difference can be detected between the patterns and therefore it is unlikely that "two kinds of carbons" exist.

Based on the preceding kinetic analyses and the experimental results, one may conclude that a bifurcated peak, or two peaks, in the DTA curve does not provide a sufficient

condition for the existence of two kinds of carbonaceous materials. Furthermore, the same assertion should be valid in the application of DTA to the analyses of solid materials in general.

ACKNOWLEDGMENT

The authors acknowledge helpful discussions with G. Adler, C. R. Krishna, and D. J. Metz and a critical review by D. J. Metz. We also thank W. M. Reams for performing the x-ray diffraction analyses.

LITERATURE CITED

(1) T. V. Rode and A. A. Balandin, *J. Gen. Chem. USSR.* (*Engl. Transl.*), **28**, 2937 (1958).
(2) A. A. Balandin, *Proc. Second Int. Cong. Catal., Paris*, 1135–1157, (1960).
(3) T. Honda, T. Saito, and Y. Horiguchi, *J. Carbon* (*Jpn*), **72**, 14 (1973).
(4) J. W. Hall and H. F. Rase, *Ind. Eng. Chem., Process Des. Dev.*, **2**, 25 (1963).
(5) D. J. Swaine, "Thermal Analysis", R. F. Schwenker, Jr., and P. D. Garn, Ed., Academic Press, New York and London, 1969, Vol. 2, p 1377.
(6) R. T. Yang and M. Steinberg, *J. Phys. Chem.*, **80**, 965 (1976).
(7) C. B. Murphy, *Anal. Chem.*, **46**, 451 R (1974).
(8) H. E. Kissinger, *Anal. Chem.*, **29**, 1702 (1957).
(9) R. T. Yang and M. Steinberg, *Carbon*, **13**, 411 (1975).
(10) P. L. Walker, Jr., F. Rusinko, Jr., and L. G. Austin, *Adv. Catal.*, **11**, 133 (1959).
(11) N. R. Laine, F. J. Vastola, and P. L. Walker, Jr., *J. Phys. Chem.*, **67**, 2030 (1963).
(12) P. L. Walker, Jr., and E. J. Hippo, *Am. Chem. Soc., Div. Fuel Chem., Prepr.*, 45–51 (1975).

RECEIVED for review March 15, 1976. Accepted June 25, 1976. This work was performed under the auspices of the Office of Molecular Sciences, Division of Physical Research, U.S. Energy Research and Development Administration, Washington, D.C.

Determination of Aluminum in Bulk Iron Ore Samples by Neutron Activation Analysis

Mihai Borsaru* and Ralph J. Holmes

CSIRO Division of Mineral Physics, P.O. Box 124, Port Melbourne, Victoria 3207, Australia

Neutron activation analysis has been applied to the determination of aluminum in 25-kg iron ore samples at −6-mm particle size. By measuring the thermal and epithermal neutron fluxes reflected by the samples during irradiation, an accuracy of better than ±0.3% (95% confidence intervals) was achieved for alumina concentrations between 1 and 6%. Ore samples should be dried to <1% free moisture before analysis; if this is not possible, the free moisture content must be determined separately to obtain the alumina content on a dry weight basis.

The neutron activation technique is well established as a powerful tool for nondestructive analysis. Many published works (*1–6*) have dealt with the determination of ^{27}Al in different matrices, by employing either the thermal neutron reaction $^{27}Al(n,\gamma)^{28}Al$ or the fast neutron reaction $^{27}Al(n,p)^{27}Mg$. The samples analyzed were usually small, of such size that they would not significantly alter the neutron flux.

The present work deals with the use of neutron activation analysis for determination of aluminum in bulk samples of high grade Australian iron ore. The advantage of using large rather than small samples is that the tedious and time-consuming sample preparation process required to obtain a representative small sample is avoided. This is of particular interest to mining companies who require a quick answer for the percentage of a particular element in a given ore (without errors introduced by inadequate sampling techniques). Special care must be taken in using neutron activation for analysis of bulk samples, since either chemically bound water (usually referred to as loss-on-ignition for Australian iron ores) or free moisture will affect the available neutron flux and thereby introduce errors.

The development of this technique for "static" bulk analysis is a significant step towards development of methods for "on-stream" analysis of ore on a conveyor belt, which is potentially of great importance to the mining industry.

EXPERIMENTAL

The method is based upon the thermal neutron reaction $^{27}Al(n,\gamma)^{28}Al$ which has a cross section of 230 mb. The radioactive isotope ^{28}Al formed in this process has a half-life of 2.3 min and decays by emitting a γ ray of 1.78-MeV energy.

A ^{252}Cf neutron source with a neutron output of approximately 10^7 neutrons/s was used to irradiate the iron ore samples. This neutron source is suitable for exciting aluminum, since the average neutron energy is lower than that of (α,n) sources (e.g., Pu-Be), resulting in less interference from the fast neutron reaction $^{28}Si(n,p)^{28}Al$, as discussed later. The ^{252}Cf source was located at the bottom of a 10-cm diameter hole (9 cm deep) in a cylindrical polyethylene block to obtain a well thermalized neutron flux (7). The γ rays from the decay of the radioisotope ^{28}Al were detected with a 126 × 126 mm NaI(Tl) detector.

The bulk ore samples (≈ 25 kg) were irradiated from below in a rectangular wooden box (40 × 33 cm by 8 cm deep) for 6 min. A 9-cm thick paraffin block was placed on top of the sample container during irradiation to reflect some of the neutrons passing through the iron ore back into the sample, thus increasing the neutron flux in the ore. Two neutron detectors attached to the irradiation facility were located underneath the box to measure the thermal and epithermal neutron fluxes in the vicinity of the ore samples. The neutron detectors used were Texlium spectrometric detectors containing 4 atm ^3He and 2 atm Kr, and were shielded from the neutron source with cadmium sheet. The epithermal neutron detector was located in a cylindrical polyethylene tube covered with cadmium sheet so that only epithermal neutrons could enter the detector. These are thermalized in the polyethylene cylinder before reaching the neutron detector, to increase the counting efficiency. Samples were quickly transferred from the neutron source to the detector via a small railway track. The counting time was 5 min (live time).

RESULTS AND DISCUSSION

Measurements. Three independent sets of measurements under slightly different geometrical conditions were taken of 25 iron ore samples, each of approximately 25 kg in weight. Each sample was first crushed to −6-mm particle size and then dried to <1% free moisture before analysis. The chemical (bound) water in these samples varied from 0.3 to 6.6%. The neutron activation assays were obtained from an equation of the form:

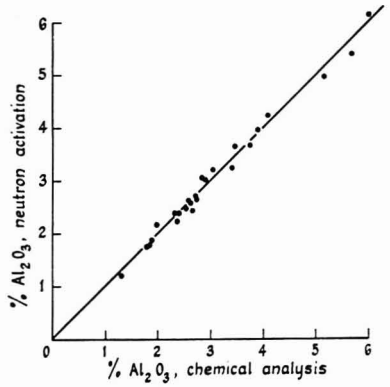

Figure 1. Comparisons of neutron activation assays for Al_2O_3 with chemical analyses

$$y = A + Bx + C\rho + Dw \quad (1)$$

where y is the neutron activation analysis assay, x is the number of γ-ray counts (thousands) in the 1.78-MeV aluminum peak after subtraction of background, ρ is the bulk density of the ore sample, w is the number of thermal neutrons, the number of epithermal neutrons or the ratio of thermal to epithermal neutrons, and A, B, C, D are constants determined by regression of the data against accurate chemical analyses.

Table I compares the overall accuracy of Al_2O_3 determinations (by activation analysis) at the 95% confidence level for various forms of the regression equation. It is clear from this table that the inclusion of neutrons improves the accuracy, the best results being achieved by employing the ratio between thermal and epithermal neutrons in the regression. This is not surprising, since any variation in the abundance of total water in the iron ore samples will cause the number of thermal and epithermal neutrons to vary in opposite directions, and hence the ratio is more sensitive to variations in total water. The regression equation for the third set of measurements, for example, was

$$y = 9.02 + 0.65x - 1.28\rho - 4.27w \quad (2)$$

where w is the ratio of thermal to epithermal neutrons. Comparisons of Al_2O_3 assays given by the above equation with chemical analyses are presented in Figure 1.

It should be mentioned that the figures for overall accuracy given in Table I include the chemical analysis error. From a statistical analysis of duplicate sampling and analysis data, the latter was estimated to be $\pm 0.12\%$ Al_2O_3 at the 95% confidence level. When this is taken into consideration, the estimated accuracy of $\pm 0.3\%$ Al_2O_3 (95% confidence intervals) for the activation method is improved to $\pm 0.27\%$ Al_2O_3.

Sources of Error and Limitations of the Present Method. Since the neutron output of the source used for the present measurements was only 10^7 neutrons/s, the statistical errors were quite large. This can easily be overcome by using a stronger neutron source. A further consequence of the low neutron output was the necessity to measure the natural γ-ray background to determine the net number of counts due to aluminum.

Inaccuracies in measuring the time interval between the end of the irradiation period and the commencement of counting also introduce errors. An automatic device would reduce this error to an acceptable level.

Table I. Accuracy ($\pm 2\sigma$) of Al_2O_3 Determinations, by Activation Analysis, for Various Forms of the Regression Equation

Run No.	w = ratio of thermal to epithermal neutrons	w = thermal neutrons only	w = epithermal neutrons only	w = 0 (No neutrons in regression equation)
1	0.25	0.27	0.31	0.32
2	0.28	0.31	0.34	0.34
3	0.30	0.31	0.35	0.37

As mentioned previously, the production of the radioisotope ^{28}Al from the reaction $^{28}Si(n,p)^{28}Al$ can interfere with the measurement. This reaction has an energy threshold of 3.8 MeV and a cross section of 100 mb for neutrons of 6-MeV energy. By irradiating pure quartz, it has been estimated that the contribution to the aluminum peak from ^{28}Si was less than 0.5% for SiO_2 concentrations up to 10%. In the samples used in this study, SiO_2 varied from 3 to 10%.

Other reactions which could interfere with the present measurements are the fast neutron reaction $^{56}Fe(n,p)^{56}Mn$ which has a threshold of 2.9 MeV, and the thermal neutron reaction $^{55}Mn(n,\gamma)^{56}Mn$. Both produce the radioisotope ^{56}Mn which has a half-life of 2.58h and decays by emitting γ rays of energy 0.847, 1.811, and 2.113 MeV. The resolution of the NaI(Tl) detector was insufficient to separate the 1.78-MeV γ ray due to ^{28}Al from the ^{56}Mn γ ray at 1.81 MeV.

The interference from the $^{56}Fe(n,p)^{56}Mn$ reaction was evaluated by irradiating pure Fe_2O_3. It was found that its contribution to the aluminum peak was less than 0.4%, which is much less than the statistical error.

The magnitude of the $^{55}Mn(n,\gamma)^{56}Mn$ interference was investigated using a high resolution intrinsic germanium solid state detector. At the Mn concentrations found in the samples used for this study (<0.05% Mn), no significant ^{56}Mn radiation (also due to ^{56}Fe, of course) was detected. This low level of Mn is typical of Australian iron ores of commercial significance presently being mined. However, precautions are necessary if the technique is applied to high Mn ores. It would then be necessary either to monitor Mn via the 0.847- or 2.113-MeV γ-ray line and apply corrections, or to take a second count of the sample after the ^{28}Al has decayed. In the present instance, only background radiation remained after the decay of ^{28}Al.

CONCLUSIONS

The present work demonstrates that neutron activation analysis can be applied to static bulk analysis of alumina in 25-kg iron ore samples. After correction for the influence of the sample on the thermal and epithermal neutron fluxes during irradiation, the accuracy is better than $\pm 0.3\%$ Al_2O_3 (95% confidence intervals) for alumina concentrations ranging from 1 to 6%.

The ore samples should be dried to 1% free moisture or less before irradiation; otherwise the free moisture content in the sample must be determined by an independent method and corrections applied to obtain alumina on a dry weight basis.

The total irradiation and counting time can be reduced to approximately 8 min by using a stronger ^{252}Cf source, e.g., $\approx 10^8$ neutrons/s.

ACKNOWLEDGMENT

The authors thank A. W. Wylie of the CSIRO Division of Mineral Physics for his helpful suggestions, and Hamersley Iron Pty Ltd for providing the assayed samples used in this work.

LITERATURE CITED

(1) D. De Soete, R. Gijbels, and J. Hoste, "Neutron Activation Analysis" (Vol. 34 of "Chemical Analysis", Monographs on Analytical Chemistry and Its Applications), Wiley-Interscience, London, 1972.
(2) J. Kuusi, *Nucl. Appl. Technol.*, **8**, 465 (1970).
(3) K. Mukai, K. Takano, and K. Takada, in "Nuclear Techniques in the Basic Metal Industries", IAEA, Helsinki, 1972, p 63.
(4) A. J. Lundan and O. P. Mattila, in "Nuclear Techniques in the Basic Metal Industries", IAEA, Helsinki, 1972, p 3.
(5) S. S. Gurna and A. S. Bhatnagar, *Indian J. Pure Appl. Phys.*, **11**, 805 (1973).
(6) L. Alaerts, J. P. Op De Beeck, and J. Hoste, *Anal. Chim. Acta*, **78**, 329 (1975).
(7) A. J. Cox, P. E. Francois, and R. P. Gatrell, *Int. J. Appl. Radiat. Isot.*, **19**, 541 (1968).

RECEIVED for review April 26, 1976. Accepted June 21, 1976.

Automated Composite Analysis of Major Sinter Components

Om P. Bhargava* and W. Grant Hines

Chemical and Metallurgical Laboratories, The Steel Company of Canada, Limited, Wilcox Street, Hamilton, Ontario, Canada, L8N 3T1

Automated systems were developed for the composite analysis of the major calcite sinter components: Al_2O_3 (0.4 to 1.5%); SiO_2 (3 to 12%); CaO (5 to 14%); MgO (2 to 10%); and total iron (50 to 66%) with a standard deviation of 0.03, 0.03, 0.1, 0.1, and 0.2, respectively. The sinter sample is fused in a vitreous carbon crucible with a mixed flux of sodium peroxide and sodium carbonate yielding a complete solution suitable for the analysis of the above-mentioned components in a single solution. The vitreous carbon crucibles are expensive but up to 18 fusions can be carried out per crucible. The simplification of sample dissolution and ease of operation justify the cost. Fusing iron ore or sinter sample in a zirconium crucible with sodium peroxide permits determination of the two key components—iron and silica—on the AutoAnalyzer. The zirconium crucible is almost indestructible. This application could prove useful at mine sites for monitoring and quality control during and after ore beneficiation.

Routine analysis of sinter—a recycled iron-bearing feed to blast furnaces—is carried out currently by x-ray fluorescence on a VXQ-72000. There is no back-up unit and traditional methods of chemical analysis (including our scheme for rapid analysis (*1*)) are slow and not available around the clock. The objective, therefore, was to devise an operationally simple alternative to cope with VXQ breakdown or provide an economical alternative at lower workloads.

AutoAnalyzer systems have been developed in our laboratory for determining acid soluble aluminum in steel, zinc, and galvanizing (*2*), and silicon (*3*) in steel and other matrices. Satisfactory performance of these methods around the clock in the routine control laboratory for several years has soundly established this technique.

AutoAnalyzer methods have also been developed for the successful determination of the major components of blast furnace slag, viz., CaO, SiO_2, MgO, and Al_2O_3 (*4*). Owing to the high concentration of iron in sinter as well as the appreciably different concentration range of the aforesaid components, the methods described there needed modification for application to sinter.

EXPERIMENTAL

Sinter Dissolution. *Fusion in Platinum Crucible.* Blast furnace slag responds to complete dissolution after sintering the sample with sodium peroxide at 380 °C in a platinum crucible for 20 min, in a muffle furnace. However this sintering technique was not successful for solubilizing the sinter, even after increasing the sintering time to an hour. Grinding the sinter sample down to 250 mesh and increasing the ratio of peroxide to sample still left some residue unattacked.

Kilsby (*5*) employed a 5:1 mixed flux (sodium carbonate–boric acid) for fusing the iron ore or sinters in a platinum crucible at 900 °C for 20 min in a muffle furnace. This approach was tried but proved unsuccessful leaving some unattacked sample. Increasing the fusion temperature from 900 to 1100 °C and the fusion time from 20 to 30 min did not help. Additionally, the flux was increased and a blast Meker burner was used, but still there was no improvement in dissolution. Alternative approaches were then explored.

Fusion in Zirconium Crucible. In our scheme (*3*) to determine silica in iron ore, sinter, and slag, it was demonstrated that iron ores and sinter are completely solubilized after fusion in a zirconium crucible. It was thought worthwhile to investigate whether this approach is compatible with the analysis of the other components, viz., Al_2O_3, MgO, CaO, and iron. Determination of silica had already been established. Determination of iron as an *o*-phenanthroline complex did not pose any problem.

After establishing the silica and iron systems on the AutoAnalyzer (fusion in zirconium crucible) efforts were directed towards investigating the use of this solution for determining magnesia. The solutions were run identically to the magnesium–Titan yellow system for blast furnace slags. However, the absorbance remained unchanged with increasing concentration of MgO in sinter samples. In our earlier study, we had established that iron interference is eliminated by incorporating the compensating solution. It became apparent that zirconium was the interfering species. This was confirmed by studying the effect of zirconium using synthetic solution. Zirconium greatly suppresses the absorbance of the magnesium–Titan yellow complex. Hence, an alternative solution was sought which was free from zirconium contamination.

Fusion in Iron Crucible. Fusion of sinter sample with sodium peroxide resulted in heavy erosion of the iron crucible contributing excessive and inconsistent amounts of iron to the solution. In spite of modifying the compensating solution to accommodate this increased and inconsistent excess of iron, the system did not work.

Bisulfate Fusion in Vycor Crucible. Fusion of sinter (0.100 g) in a Vycor (silica) crucible with potassium bisulfate (3 g $KHSO_4$ fused powder) was then tried. The fused melt was leached with 50 ml of 3.6 N HCl and filtered. The magnesium–Titan yellow complex was developed (manual operation) after establishing the optimum concentration of compensating solution used to mask the interfering elements. The system was then put on the AutoAnalyzer incorporating Titan yellow and sodium hydroxide into a single solution. This also eliminated the problem of occasional staining of the mixing coil. This system was suitable for determining MgO in the range 2 to 9%.

The next sinter component attempted was alumina. Prior knowledge of zirconium interference in aluminum determination precluded fusion in such a crucible. The solution used for magnesia determination (bisulfate fusion in Vycor crucible) was then investigated. On dissolving the sinter bisulfate fusion melt in 3.6 N HCl, a slight white residue was noticed. The solution was filtered. Recovery of alumina was somewhat low. Spectrographic examination of the residue showed evidence of aluminum. It was therefore concluded that bisulfate fusion of sinter is not suitable for alumina determination. Again an alternative solution was needed.

Fusion in Nickel Crucible. A method for determining alumina in sinter (*6*) etc. has been in use for 7 years and an automated version (AutoAnalyzer) for over 3 years. The sample is fused in a nickel cru-

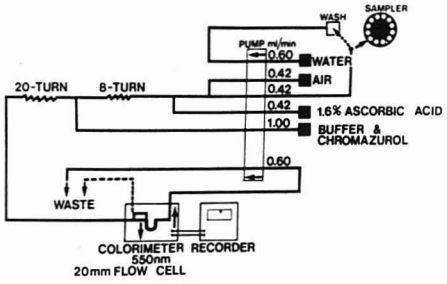

Figure 1. Alumina determination

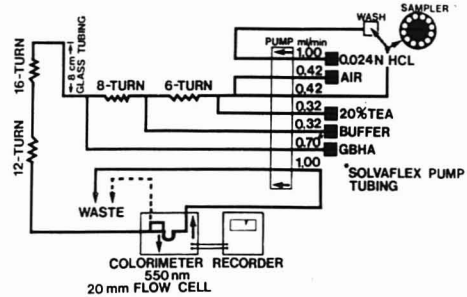

Figure 3. CaO determination

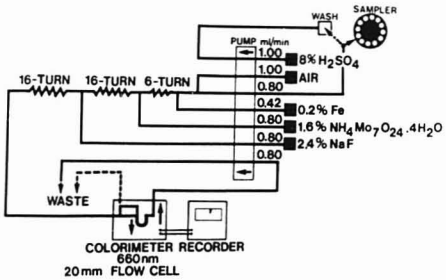

Figure 2. Silica determination

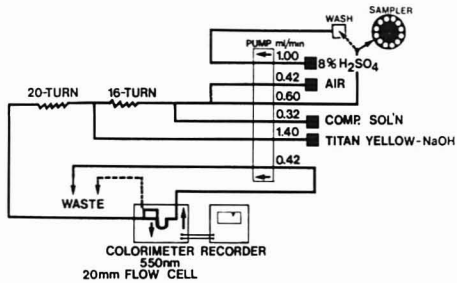

Figure 4. Magnesia determination

cible with sodium peroxide and solubilized with dilute HCl. After dilution, the colorimetry is carried out by treating the solution (aliquot) with ascorbic acid to reduce the ferric iron. The color complex of aluminum with Chromazurol is then developed in a solution buffered with sodium acetate at pH 5.3. Satisfactory precision and accuracy were obtained for this component.

The scheme is satisfactory for the simultaneous determination of silicon and iron fusing the sample in a zirconium crucible. However, separate fusions were required for magnesia (bisulfate in a Vycor crucible) and alumina (nickel crucible) to prevent the interference of zirconium in magnesia and alumina determinations and interference of nickel in iron, silica, and magnesia determinations. It is most desirable to have a single solution (for the analysis of all the major components in the sinter) which is free from interference.

Fusion in Vitreous Carbon Crucible. In the past, we had attempted to use the vitreous carbon crucible using both sintering at 380 °C with sodium peroxide as well as direct fusion on a Meker burner. Sintering was not adequate in decomposing the sinter while fusion eroded the crucible quite considerably. Sodium carbonate is incorporated in some fusion fluxes (using iron or nickel crucibles) to prevent a violent explosive reaction when decomposing some steelmaking reagents such as Calsibar and ferroalloys. It was thought worthwhile to incorporate sodium carbonate with sodium peroxide to fuse sinter samples in a vitreous carbon crucible. This modification completely solubilized the sinter in about 2-min fusion time. After acidifying the melt, a clear solution free from carbon specks and with no contaminants (such as zirconium, nickel, or iron) was obtained.

Apparatus. 1) A Technicon AutoAnalyzer II, comprising Sampler II, Proportioning Pump III, Colorimeter with a flow-through cell and interference filters (550 nm, 660 nm, and 520 nm) and two-pen chart recorder, was used in this study.

2) Vitreous carbon crucible, 20 ml. This crucible (Grade V25) "Le Carbonne—Lorraine" is available from Spectrex Ltd., 2245 St. Francois Rd., Dorval, P.Q.

Reagents. Reagents are grouped according to the component being determined.

Alumina. Ascorbic acid 1.6% w/v aqueous is used.

Combined buffer–Chromazurol solution is prepared by dissolving 54 g of sodium acetate trihydrate in 700 ml of water and filtering. Chromazurol–reagent (0.08 g) is dissolved in 200 ml of denatured (1 + 1) alcohol, filtered, combined with the filtered buffer solution, and diluted to a liter with water.

Silica. Iron 0.2% solution is made by dissolving high purity iron (1.00 g) in 80 ml of 8% v/v H_2SO_4. After the reaction is completed, 10 ml of 3% w/v freshly prepared ammonium persulfate are added, the solution is boiled for 2 min, and diluted to 500 ml.

Ammonium molybdate 1.6% w/v aqueous is used.

Sodium fluoride solution, 2.4% w/v aqueous, is stored in a polyethylene bottle.

Calcium Oxide. The wash solution is 0.024 N HCl.

Triethanolamine 20% v/v is used.

The buffer is prepared by dissolving 30 g of sodium hydroxide pellets in 600 ml of water, adding 10 g of Borax ($Na_2B_4O_7$·10 H_2O) and 5 g of potassium cyanide and diluting the solution to a liter with water.

Glyoxal bis(hydroxanil), GBHA, is made by dissolving 0.10 g of the reagent in 300 ml of denatured alcohol and then adding 200 ml of water. After mixing, this solution is stored in an amber colored glass-stoppered bottle.

Magnesia. The compensating solution is prepared as follows.

Dissolve 7.0 g EGTA (Ethylenebis(oxyethylenenitrolo)tetraacetic acid) in 15 ml of 10% w/v sodium hydroxide. The pH is adjusted to 7 with 2 N HCl. Sodium fluoride, 3 g, is then added and the contents are diluted to 500 ml with water. This follows the addition of 2.5 g of hydroxylamine hydrochloride and 0.225 g of aluminum chloride hexahydrate. After mixing, 70 ml of triethanolamine are added and the volume is made up to a liter with water. This solution is stored in a polyethylene bottle.

Titan yellow–sodium hydroxide solution is made as follows. Dissolve 60 g of sodium hydroxide in 600 ml of water and cool to room temperature. Into a 100-ml beaker, triturate 0.05 g of Titan yellow (also called Clayton yellow) in a minimum volume of water; then add 50 ml of water, mix to dissolve, and filter through a rapid filter into a 400-ml beaker. Wash the filter with about 200 ml of water. Add 100 ml of glycerol to the Titan yellow solution, mix, and add this solution to the sodium hydroxide solution. Dilute the combined solutions to 2 l. with water. Store in a polyethylene bottle.

Iron. Hydroxylamine hydrochloride solution, 1% w/v aqueous, is made fresh each day.

Sodium acetate trihydrate is 4% w/v.

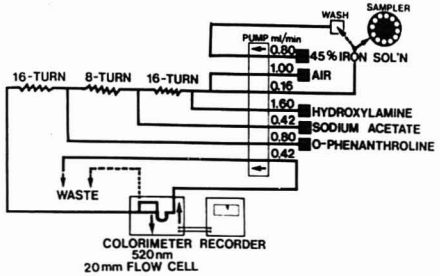

Figure 5. Iron determination

Table I. Alumina in Sinter

Sample identifications	n	% Al_2O_3 s	% Al_2O_3 $\bar{x}$	% Al_2O_3 Assigned or Cert.
April 25/71	7	0.027	0.51	0.45
March 18/69	7	0.022	0.68	0.60
May 28/69	7	0.035	0.73	0.70
June 20/64	7	0.029	0.91	0.91
Dec. 11/57	7	0.026	1.12	1.04
Nimba BCS Ore	4	0.026	1.05	1.08

Table II. Silica in Sinter

Sample identification	n	% SiO_2 s	% SiO_2 $\bar{x}$	% SiO_2 Assigned
April 25/71	5	0.023	4.25	4.20
May 28/69	5	0.033	5.06	5.10
March 18/69	5	0.014	5.20	5.20
Jan. 20/64	2	0.030	6.65	6.68
Dec. 11/57	5	0.030	11.43	11.38

O-Phenanthroline solution is prepared by dissolving 1 g of reagent in a liter of water containing 1 ml of HCl.

Wash solution (about 45% Fe) is prepared by treating an appropriate weight of iron ore or sinter sample (to provide the baseline) using the sample dissolution described below.

Procedure. *Sinter Dissolution.* Sinter (0.1000 g) is mixed with 0.5 g of sodium carbonate and 2 g of sodium peroxide in a vitreous carbon crucible and fused at low heat over a Meker burner for 2 min. The somewhat cooled melt is extracted with water followed by treatment with 25 ml of (3 + 2) HCl and boiled for 2–3 min. The solution is then transferred to a 1-l. volumetric flask containing 40 ml of 8% v/v sulfuric acid and about 500 ml of water and the contents are diluted to volume. This solution is then ready for the determination of Al_2O_3, SiO_2, CaO, MgO, and total iron on the AutoAnalyzer.

Internal reference sinter samples as well as NBS, BCS, and ISO reference standard iron ores and sinters are dissolved identically along with the unknown samples and run on the AutoAnalyzer to establish calibrations.

Alumina. The analytical system for determining alumina is assembled according to schematic flow diagram shown in Figure 1. The sample, air and ascorbic acid (1.6%) at 0.42 ml/min, each are mixed and passed through an 8-turn mixing coil. Buffer solution containing Chromazurol (0.08 g/l.) at 1.00 ml/min is added and passed through a 20-turn mixing coil. The absorbance of the Al–Chromazurol complex is recorded at 550 nm. Sample and wash/(water) cycles are 30 and 50 s, respectively.

Silica. The analytical system for SiO_2 is assembled according to the schematic flow diagram shown in Figure 2. The sample, iron solution (0.2%) and air at 0.80, 0.42, and 1.00 ml/min, respectively, pass through a 6-turn mixing coil followed by ammonium molybdate (1.6%) at 0.80 ml/min and mix through a 16-turn coil to form the silicomolybdate complex. Molybdenum blue is then formed by addition of NaF (2.4%) at 0.80 ml/min, and passage through a 16-turn coil to the colorimeter. Absorbance is measured at 660 nm. Sample and wash (8% H_2SO_4) cycles are 30 and 45 s, respectively.

Table III. Calcium Oxide in Sinter

Sample identification	n	% CaO s	% CaO $\bar{x}$	% CaO Assigned
Jan. 20/64	7	0.07	6.30	6.17
May 28/69	7	0.08	9.79	9.90
Dec. 11/57	7	0.13	10.95	10.90
March 18/69	7	0.12	11.18	11.26
April 25/71	7	0.08	12.90	12.83

Table IV. Magnesia in Sinter

Sample identification	n	% MgO s	% MgO $\bar{x}$	% MgO Assigned
Jan. 20/64	16	0.08	2.60	2.6
Dec. 11/57	16	0.15	4.42	4.3
April 25/71	16	0.05	5.71	5.7
May 28/69	16	0.08	7.04	7.4
March 18/69	16	0.12	8.06	8.1

Table V. Total Iron in Sinter

Sample identification	n	% Fe s	% Fe $\bar{x}$	% Fe Assigned
Dec. 11/57	4	0.07	50.0	50.2
March 18/69	3	0.11	52.1	52.2
May 28/69	3	0.22	54.1	53.7
April 25/71	3	0.19	54.1	53.9
Jan. 20/64	4	0.13	58.7	58.7

Calcium Oxide. The analytical system for CaO is assembled as shown in Figure 3. The sample, air, and triethanolamine at 0.42, 0.42, and 0.32 ml/min, respectively, pass through a 6-turn coil and meet buffer (NaOH 30 g/l., Borax 10 g/l., and KCN 5 g/l.) at 0.32 ml/min. After passing through an 8-turn coil, the stream meets glyoxal bis(hydroxanil) at 0.70 ml/min and traverses a 28-turn coil. The absorbance of the complex is then recorded at 550 nm. The sample and wash (0.024 HCl) cycles are 60 and 90 s, respectively.

Magnesia. The analytical system for MgO is assembled as shown in Figure 4. The sample, air, and compensating solution at 0.60, 0.42, and 0.32 ml/min, respectively, pass through a 16-turn coil and meet a Titan yellow–NaOH–glycerol solution at 1.40 ml/min. After passing through a 20-turn coil, the absorbance is recorded at 550 nm. The sample and wash (8% H_2SO_4) cycles are 50 and 60 s, respectively.

Iron. The analytical system for the determination of iron is shown in Figure 5. The sample, air, and hydroxylamine (1%) at 0.16, 1.00, and 1.6 ml/min, respectively, pass through a 16-turn mixing coil and meet sodium acetate at 0.42 ml/min. After traversing an 8-turn coil the stream meets *o*-phenanthroline and passes through a 16-turn coil to the colorimeter. The absorbance is measured at 520 nm. The sample and wash (45% Fe solution) cycles are 50 s each. The wash solution contains 45% Fe to establish the baseline and provide increased sensitivity in the range 50 to 66% Fe.

RESULTS AND DISCUSSION

As indicated earlier, the fusion of sinter samples in a vitreous carbon crucible with sodium peroxide incorporating sodium carbonate provided complete solution free from contaminants (interfering elements) such as zirconium, nickel, or iron from the respective crucibles. It was possible to analyze satisfactorily the components Al_2O_3, SiO_2, CaO, MgO, and total iron in sinter in a single solution on the AutoAnalyzer using the necessary reagents and the appropriately devised analytical schematics. The results are recorded in Tables I through V for alumina, silica, calcium oxide, magnesia, and total iron, respectively. The tables also show the standard deviation and comparison with the assigned values.

ACKNOWLEDGMENT

Acknowledgment is made to K. J. Alkerton and W. D. Lord for assistance in experimental work, and to The Steel Company of Canada, Ltd., for permission to publish.

LITERATURE CITED

(1) O. P. Bhargava and W. G. Hines, Paper presented at the 50th Annual Conference of the Chemical Institute of Canada, Toronto, June 1967.
(2) O. P. Bhargava, G. F. Pitt, J. F. Donovan, and W. G. Hines, Technicon International Congress 1970, New York, N.Y.; published in the *Congress Proceedings*.
(3) O. P. Bhargava, G. F. Pitt, and W. G. Hines, *Talanta*, **18**, 793 (1971).
(4) O. P. Bhargava, J. F. Donovan, and W. G. Hines, Paper presented at the 25th Pittsburgh Conference on Analytical Chemistry and Applied Spectroscopy, Cleveland, Ohio, March 1974.
(5) P. E. Kilsby, Technicon International Congress 1970, New York, N.Y.; published in the *Congress Proceedings*.
(6) O. P. Bhargava and W. G. Hines, *Anal. Chem.*, **40**, 413 (1968).

RECEIVED for review April 29, 1976. Accepted July 1, 1976. Paper presented at the Pittsburgh Conference on Analytical Chemistry and Applied Spectroscopy, Cleveland, Ohio, March 1976.

Determination of Total Estrogens in Urine with 3-Methyl-2-benzothiazolinone Hydrazone

Hugh Y. Yee* and Bobette Jackson

The Department of Pathology, Hutzel Hospital, 432 East Hancock, Detroit, Mich. 48201

An estrogen method has been developed that utilizes a colorimetric reaction consisting of the oxidative coupling of 3-methyl-2-benzothiazolinone hydrazone (MBTH) to the phenol portion of the steroid molecule. Colorimetric measurements are made at 530 nm manually or with an AutoAnalyzer at an analysis rate of 50 samples per hour. Comparison with a fluorometric method gave a correlation coefficient of 0.96 and with a gas chromatographic one, a coefficient of 0.94, so that the proposed method may be suitable as an alternative method for the determination of total estrogens in pregnancy urine samples.

The importance of assaying urinary estrogen concentrations to assess fetal growth and well being has been established and documented (*1*). To date, most procedures have not combined simplicity and specificity. Perhaps, the most rapid manual method for use is one that uses Amberlite XAD-2 resin to separate estrogens from urine, reaction with a Kober reagent, and a fluorometric measurement (*2*). A comparable colorimetric method has not been made available, as relatively longer times are needed (*3*).

We have investigated a procedure to assay urinary estrogens that uses either ethyl ether–ethanol extraction (*4*) or ammonium sulfate precipitation (*5*) of the steroids and reagents that are suitable for manual or automated quantification. Larger laboratories with a greater number of estrogen assays to perform would tend to use an automated procedure, and many excellent procedures are available (*6–9*). Most of the published procedures are carried out at an analysis rate of 15 to 40 samples per hour, and necessitate the use of a fluorometer. We have succeeded in extending the manual method reported here to a semiautomated estrogen method with an analysis rate of 50 samples per hour. The color reaction used in this procedure has been previously used for the determination of phenols in water supplies (*10, 11*).

EXPERIMENTAL

Apparatus. The manifold used for the automated procedure is shown in Figure 1. The AutoAnalyzer system (Technicon Corp., Tarrytown, N.Y.) consisted of sampler II, pump II, colorimeter, and recorder. Manual measurements were made with a Gilford Model 300-N spectrophotometer (Gilford Instruments Laboratory, Oberlin, Ohio). An International B-20 A high speed refrigerated centrifuge (Damon/IEC Division, Needham Heights, Mass.) was used to centrifuge the ammonium sulfate precipitates. Spectra were obtained with a Coleman Model 124 spectrophotometer (Coleman Instruments, Inc., Maywood, Ill.) with Model 165 recorder. Fluorometric measurements were made with an Aminco Model SPf 125 spectrofluorometer (American Instruments Co., Silver Spring, Md.). A Varian Aerograph Model 1440 chromatograph was used for the assay of estrogens by gas chromatography.

Reagents. *Isolation, Hydrolysis, and Purification.* Reagents used were 6 N H_2SO_4; 0.5 N H_2SO_4 in ethanol; 0.5 N H_2SO_4 in methanol; 1 N NaOH; 0.1 N NaOH; acetate buffer (2 mol/l.; pH 4.7); Glusulase, an enzyme mixture from Helix Pomatia containing approximately 200 000 units/ml of glucuronidase and 100 000 units/ml of sulfatase (Endo Laboratories, Garden City, N.Y.); 1 M K_2CO_3; $(NH_4)_2SO_4$; ethyl ether; methanol (aldehyde free); ethanol.

Manual Color Development. Use 0.2% w/v ceric ammonium sulfate (G. F. Smith, Columbus, Ohio) in 1.5% v/v H_2SO_4, store in an amber colored bottle; 0.15% w/v aqueous solution of 3-methyl-2-benzothiazolinone hydrochloride (MBTH) (Aldrich Chemical Co., Milwaukee, Wis.), keep refrigerated when not in use and discard after 2 weeks; 0.3% w/v EDTA (disodium salt); estriol standards 20 and 40 mg/l. in 25% v/v methanol or 100% methanol.

Automated Color Development. Wash water, add 0.1 ml Brij-35 (30% solution; Technicon Corp., Tarrytown, N.Y.) per liter; 0.2% w/v ceric ammonium sulfate in 2% v/v H_2SO_4, store in an amber colored bottle; 0.05% w/v MBTH in aqueous solution, keep refrigerated when not in use and no more than a 2-week supply; 0.3% w/v EDTA (disodium salt), add 0.1 ml Brij-35 per liter; stock estriol standard, 1 mg/ml in ethanol; dilute with 25% v/v ethanol to obtain standards of 5, 10, 20, 30, and 40 mg/l.

Procedure. *Isolation:* (*a*) *Ammonium Sulfate Precipitation.* In a 40-ml glass-stopper centrifuge tube containing 3.5 g $(NH_4)_2SO_4$, pipet 5 ml of urine from a 24-h collection, add 0.1 ml 6 N H_2SO_4, and mix the contents. Warm the contents of the tube in a 55 °C water bath for several minutes. Stopper the tube and vortex vigorously until the salt dissolves. Transfer the contents of the centrifuge tube to a *plastic* centrifuge tube. Centrifuge the tube in a high speed centrifuge at 17 000 rpm at 0–5 °C for 30 min. Remove the tube from the centrifuge and aspirate off the supernatant liquid, taking care not to remove any of the precipitate. Add 2 drops of 1 N NaOH and 1 ml of water. Vortex the contents. Add 3 ml of water and mix. Centrifuge for 5 min at 3000 rpm to pack any undissolved material. Transfer the purified urine extract to a clean 40-ml glass-stopper centrifuge tube.

Hydrolysis. Add 1 ml of acetate buffer and 0.5 ml of Glusulase. Mix and incubate the contents at 55 °C for 120 min.

Purification: (*a*) *Ammonium Sulfate Isolation.* Cool the tube containing the hydrolysate. Add 25 ml of ethyl ether and shake vigorously 3 times for 10-s intervals (release pressure after each 10-s shaking). After the layers have separated, aspirate off the lower phase. Wash the ether phase by shaking with 10 ml of 1 M K_2CO_3 and aspirating off the lower phase. Wash with 10 ml of water and aspirate off

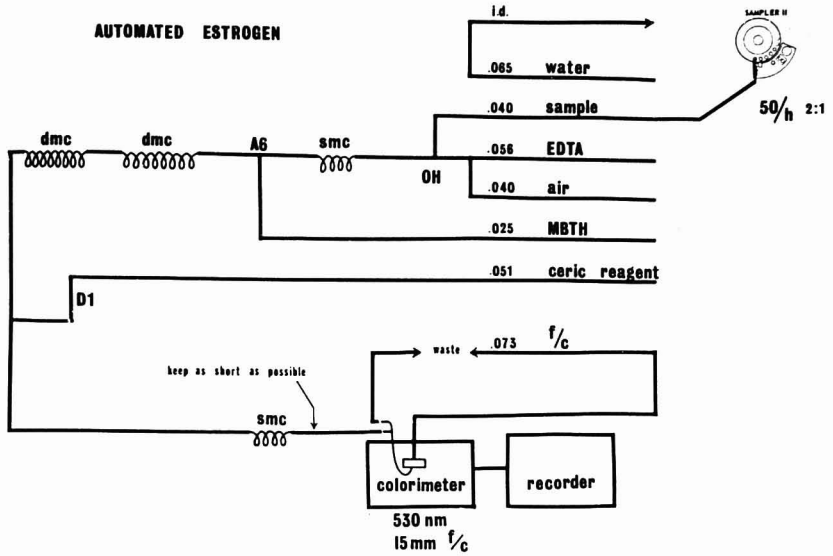

Figure 1. Manifold diagram for automated color development

the lower phase. Pipet a 10-ml aliquot of ether into a 40-ml conical test tube and evaporate the ether to dryness in a 55 °C bath. For automated color development, dissolve the sample residue in 0.5 ml of ethanol, making certain the sides of the tube are rinsed. Add 1.5 ml of water and mix well. For manual color development, substitute 2.0 ml of methanol. The solution is equivalent to 2 ml of urine.

Isolation: (b) Ether–Ethanol Extraction. In a 50-ml glass-stopper centrifuge tube containing 2.5 g $(NH_4)_2SO_4$, pipet 5 ml of urine, add 0.1 ml 6 N H_2SO_4, and mix the contents. Add 10 ml of ether–ethanol 3:1 v/v, and shake vigorously 3 times for 20-s intervals (release pressure after each 20-s shaking by carefully opening the stopper). Aspirate off the urine layer. Transfer the solvent to a clean 40-ml centrifuge tube and evaporate to dryness. Add 4 ml of water and mix.

Hydrolysis. Add 1 ml of acetate buffer and 0.5 ml of Glusulase. Mix and incubate the contents at 55 °C for 120 min.

Purification: (b) Ether–Ethanol Isolation. Extract the cooled hydrolysate with 25 ml of ether and shake vigorously 3 times for 10 s each (release pressure after shaking). Aspirate off and discard the aqueous phase. Wash the ether phase with 10 ml of 1 M K_2CO_3 followed by 10 ml of water. Pipet a 10-ml aliquot into a 15-ml conical test tube and evaporate the ether to dryness in a 55 °C bath. Redissolve the residue in 3 ml of ethyl ether. Add 1.6 ml of 0.1 NaOH and vortex. Aspirate off the ether phase. Transfer the alkaline phase to a clean test tube. Add 0.4 ml of 0.5 N H_2SO_4 in ethanol for automated color development or 0.5 N H_2SO_4 in methanol for manual development. Mix well.

Color Development and Measurement: Manual. Pipet 1 ml of the sample solution into a clean test tube. Pipet 1 ml of each standard, 20 and 40 mg/l., into separate tubes. For a reagent blank, use 1 ml of 25% v/v methanol or 100% methanol. Add 1 ml of 0.15% MBTH to all tubes and mix. Let stand 5 min. Add 1 ml of 0.2% ceric reagent, mix, and let stand 5 min. Measure the absorbance at 530 nm vs. the blank. Calculate the concentration of the sample from the standards. Multiply the concentration in mg/l. of the urine sample by the number of liters of the 24-h collection to obtain the mg/24 h. If the absorbance from a urine control is greater than anticipated, it may be necessary to prepare the estriol standards in a urine matrix.

Color Development, Measurement, and Calculations: Automated. Place the manifold on the pump (Figure 1), attach reagent lines, and pump reagents for at least 10 min to obtain a stable baseline. Place the 530-nm filters and the No. 1 aperture in position. Set baselines. If the 100% *T* baseline drift is pronounced, replace the sample line. Load the standards on the tray followed by three water wash cups, controls, water wash cup, and groups of six samples. Separate each group of samples with a water wash cup. Begin sampling at a rate of 50/h (2:1 sample wash; 48-s sample/24-s wash). After the highest concentration standard is recorded and the pen returns to or near 100% *T*, re-adjust the baseline if necessary. After all samples have been recorded, remove reagent lines and place them into water and pump water through the system for at least 20 min. Plot % *T* values of the standards vs. their respective concentrations using semilogarithmic graph paper. Read the concentrations of the samples directly from the plot. Multiply the concentration in mg/l. by the number of liters of the 24-h urine collection to obtain mg/24 h.

Table I. Recovery of Added Estriol[a]

Added	Calcd value	Found	Recovered	Recovery, %
0.0		5.8		
2.0	7.8	8.0	2.2	110.0
4.0	9.8	9.7	3.9	97.5
10.0	15.8	16.4	10.6	106.0
20.0	25.8	24.3	18.5	92.6

[a] Estriol was added to a urine containing 5.8 mg/l. of estrogen. All specimens were assayed in triplicate.

RESULTS AND DISCUSSION

Recoveries and Correlation. Aqueous solutions containing 10, 15, 30, and 50 mg/l. of estriol-3-glucuronide and estriol-16-glucuronide (Sigma Chemical Co., St. Louis, Mo.) were assayed in replicate, and recoveries of 77–96% consistently obtained with an average recovery of 86%. The highest concentration of estrogen conjugate gave the lowest recovery indicating that samples of greater than 40 mg/l. concentrations be diluted and repeated. Estriol added to urine was recovered as shown in Table I. The data indicates excellent recoveries.

A series of urine specimens were assayed with the proposed method and compared with fluorometric (*12*) and gas chromatographic (*13*) procedures. The data are shown in Table II. Quite satisfactory correlations are obtained when the proposed procedure is compared with either of the other two methods.

Table II. Comparison of Proposed Method with Other Estrogen Methods[a]

Sample No.	MBTH	Fluorometric (*12*)	GC (*13*)
1	14.6	16.9	14.1
2	21.3	20.5	25.4
3	19.5	17.6	15.4
4	34.8	33.3	39.0
5	7.2	6.0	7.9
6	25.8	27.0	25.2
7	32.3	32.6	30.8
8	12.4	12.1	12.4
9	26.9	22.0	23.4
10	20.0	21.7	23.2
11	24.0	23.2	22.8
12	20.8	19.3	17.9
13	16.7	16.7	20.6
14	7.3	5.5	5.8
15	8.3	8.8	6.2
16	23.0	26.0	24.2
17	21.6	18.7	20.2
18	13.0	11.0	14.2
19	18.9	15.5	17.6
20	13.7	14.1	14.9
21	21.2	19.3	24.2
22	11.3	12.6	16.1
23	19.1	14.5	17.9
Average	18.9	18.0	19.1

[a] All values listed are mg/24 h. $Y_{(MBTH)} = 1.86 + 0.89 X_{(GC)}$; $r = 0.94$; $S_{xy} = 2.40$. $Y_{(MBTH)} = 1.62 + 0.96 X_{(fluor)}$; $r = 0.96$; $S_{xy} = 1.98$.

Table III. MBTH Reaction with Various Steroids[a]

Estriol	(+)
Estradiol	(+)
Estrone	(+)
Androsterone	(−)
Epiandrosterone	(−)
Dehydroepiandrosterone	(−)
Cortisol	(−)
Pregnanediol	(−)
Pregnanetriol	(−)

[a] Concentrations of all steroid solutions were 10 mg/liter in methanol.

Two commercially available urine control materials were assayed over a period of several months to yield a mean value of 5.3 mg/l. ± 1.4 (2σ), n = 42 (Lederle lot 2920-690 H6; values given: 4.0 ± 1.6 gas chromatography and 4.5 ± 1.6 Stanbio) and 7.3 ± 1.1 (2 σ), n = 28 (Hyland lot 0401 L001 AA; value given 6.6 ± 1.8 Brown colorimetric). A bias of approximately +0.8 mg/l. was found between the proposed method and the methods used for the commercial materials.

The recoveries and correlations suggest that the proposed method is suitable as an alternative method for the estimation of total estrogens in pregnancy urine.

Spectral Characteristics of the Chromogen. The reddish violet chromogen has two absorption maxima: one at 420–440 nm and the other at 530–560 nm. The 420–440 nm peak of the chromogen is slightly greater (Figure 2). The apparent molar absorptivity at 530 nm for estriol was 11 200 ± 600. The absorptivities for estradiol and estrone were similar, so that estriol was selected as the standard. The color followed Beer's law up to a concentration of 40 mg/l. estriol. Measurements were made at 530 nm for either automated or manual color development.

Color Reaction. The oxidative coupling of 3-methyl-2-benzothiazolinone hydrazone (MBTH) with phenols, aromatic amines, and active methylene compounds was reported by

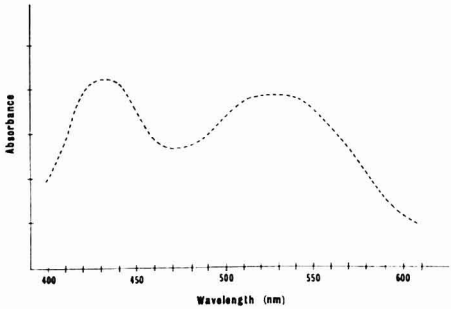

Figure 2. Spectrum of chromogen of estriol, MBTH, and ceric ion reaction

Hünig and Fritsch (*14*). The coupling was initially carried out under alkaline conditions with ferricyanide, but modification to use ceric ammonium sulfate in acid medium was successful with an increased sensitivity (*10*). The reaction is depicted in Figure 3.

Specificity and Interferences. The specificity of the color reaction with other representative steroids was investigated, and these data are given in Table III. Since the color reaction occurs with the phenol portion of the molecule, steroids not having this structure will not interfere. The most probable interferences in urine will be aromatic amines, phenolic acids, and neutral phenols. To eliminate interference from aromatic amine compounds, the isolation of the estrogens is carried out at an acid pH. Amines will be in the form of their acid salts which are relatively more water-soluble and not separated with the steroids. Phenolic acids are removed by washing the ether extract with potassium carbonate.

The most difficult compounds to remove are the neutral phenols of which p-cresol and catechol appear to be the predominant ones (*15*). Fortunately, two favorable factors minimize this interference: (a) phenols with a pK 7 are generally excreted as sulfate conjugates (*16*) (p-cresol pK = 10.3; catechol pK = 9.5), so that these salts would most likely remain in solution during the isolation of the steroids as well as being removed by the potassium carbonate wash; (b) substantial losses of both of these phenols would occur during the ether evaporation at 55 °C, since they are quite volatile (*15*). To determine the effects of p-cresol, samples containing 25 to 200 mg/l. [50 mg/l. is the normal amount found in urine (*15*)] were taken through the entire procedure. A concentration of 0.2–0.4 mg/l. of material was found at all concentrations of p-cresol. The concentration of residual phenolic substances of 25 nonpregnancy urine specimens was determined by the proposed method. An average concentration of 2.2 mg/l. was found with a range of 0.2–3.8 mg/l. Since the estrogen concentrations in the majority of urines analyzed by our laboratory are between 5–10 mg/l. and studies with two other established estrogen methods indicate good correlation, the residual phenolic substance concentration does not appear to interfere to any significant extent.

Because false positive results could occur, urine collections must be from pregnant subjects. Furthermore, this procedure is not suitable for estimating low concentrations of estrogens in urine from normal subjects.

Isolation and Purification. The first procedure for the isolation and purification of estrogens from urine using ammonium sulfate precipitation with high speed centrifugation was described by Cohen in a series of papers (*5, 17, 18*). Optimum conditions have been confirmed and defined (*19*).

The alternative procedure using an ether–ethanol extrac-

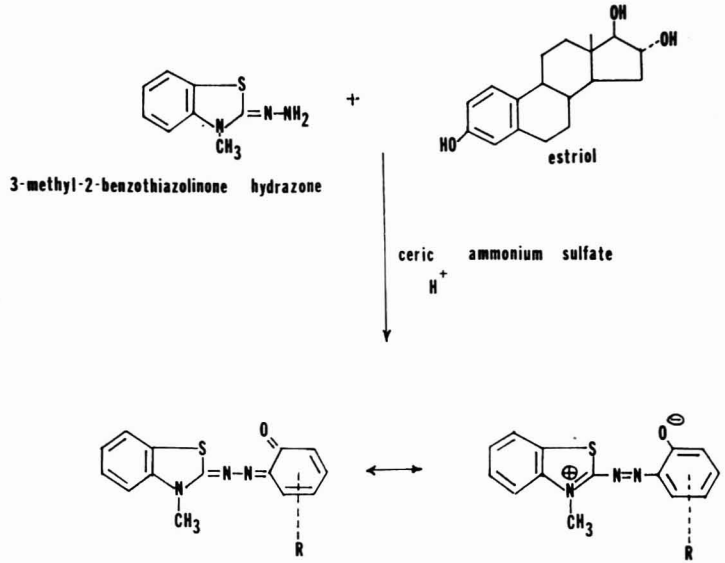

Figure 3. Oxidative coupling of MBTH with estriol in the presence of ceric ion

tion of urine containing 50% (w/v) ammonium sulfate was reported earlier (*4*).

A duplicate run (n = 20) using both procedures gave results for all samples that were within ±3 mg/l. with a correlation coefficient of 0.96. This evidence indicates that either means of separation is suitable for routine use. Because of greater variations in shaking with solvent in the initial extraction, the procedure employing ammonium sulfate and high speed centrifugation is preferred.

Amberlite XAD-2 separation, in our hands, was not satisfactory, especially with urine samples containing drugs of abuse. Colorimetric and fluorometric measurements gave extremely high results for these extracts. Direct analysis was also unsuitable, so that separation and purification must be carried out to ensure valid results.

The purification by solvent extraction or ammonium sulfate precipitation removed enzyme inhibitors, so that the rate of hydrolysis by the glucuronidase and sulfatase was increased (*17*). A large excess of enzyme was employed to make certain that specimens having high concentrations of estrogen conjugates were hydrolyzed within the 2-h incubation period.

Automated System. An alcoholic solution of the purified and hydrolyzed estrogens is diluted with 0.3% EDTA and 0.05% MBTH added. After mixing, 0.2% ceric ammonium sulfate is added. This final solution is mixed and pumped through the flow cell and measurements made at 530 nm. Carryover was 2% for a 5 mg/l. sample after a 20 mg/l. one and 2.5% after a 40 mg/l. one. Steady state reached was 94%. Sampling rate was 50/h with a sample wash ratio of 2:1. Slightly improved washout characteristics of 1.9% could be obtained at a rate of 50/h, 1:1, with a lower percent steady state reached and a diminishing of the peak heights. The peak heights could be restored by using a larger sample line to compensate for the shorter sampling time at the 1:1 ratio.

The ceric to MBTH ratio for the automated procedure is 1 ml 0.2% ceric:0.23 ml 0.05% MBTH and is critical. Increased amounts of MBTH without compensating increases in ceric ions will result in baseline drift. This drift is caused by the continuing formation of the greenish cerous ions. The drift can be controlled by maintaining the proper reagent ratio and by rapid passage of the reaction stream through the colorimeter before any substantial reduction of ceric ions takes place. Note that in the construction of the manifold, we have specified that the tubing from the last mixing coil be kept as short as possible in length.

LITERATURE CITED

(1) J. W. Green, Jr., and J. C. Touchstone, *Am. J. Obstet. Gynecol.*, **85**, 1 (1963).
(2) L. Lee and R. Hahnel, *Clin. Chem.* (*Winston-Salem, N.C.*), **17**, 1194 (1971).
(3) E. S. C. Quek, J. E. Buttery, and G. F. deWitt, *Clin. Chem.* (*Winston-Salem, N.C.*), **19**, 1204 (1973).
(4) R. W. Edwards and A. E. Kellie, *Acta Endocrinol.*, **27**, 262 (1958).
(5) S. L. Cohen, *J. Clin. Endocrinol. Metab.*, **26**, 994 (1966).
(6) W. P. Barnard and R. W. Logan, *Clin. Chim. Acta*, **29**, 401 (1970).
(7) D. G. Campbell and G. Gardner, *Clin. Chim. Acta*, **32**, 153 (1971).
(8) I. R. Hainsworth and P. E. Hall, *Clin. Chim. Acta*, **35**, 201 (1971).
(9) M. Lever, J. C. Powell, and S. M. Peace, *Biochem. Med.*, **8**, 188 (1973).
(10) H. O. Friestad, D. E. Ott, and F. A. Gunther, *Anal. Chem.*, **41**, 1750 (1969).
(11) P. D. Goulden, P. Brooksbank, and M. B. Day, *Anal. Chem.*, **45**, 2430 (1973).
(12) A. T. Howarth and D. B. Robertshaw, *Clin. Chem.* (*Winston-Salem, N.C.*), **17**, 316 (1971).
(13) J. Van de Calceyde, N. Scholtis, N. Schmidt, and A. Kuypero, *Clin. Chim. Acta*, **25**, 345 (1969).
(14) S. Hunig and K. H. Fritsch, *Justus Liebigs Ann. Chem.*, **609**, 143 (1957).
(15) S. L. Tompsett, *Clin. Chim. Acta*, **3**, 149 (1958).
(16) "Isolation and Identification of Drugs", E. G. C. Clarke, Ed., The Pharmaceutical Press, London, England, 1969, p 153.
(17) S. L. Cohen, *Can. J. Biochem.*, **46**, 563 (1968).
(18) S. L. Cohen, *J. Clin. Endocrinol. Metab.*, **29**, 47 (1969).
(19) G. S. Pinkus and J. L. Pinkus, *Clin. Chem.* (*Winston-Salem, N.C.*), **16**, 824 (1970).

RECEIVED for review January 20, 1976. Accepted June 25, 1976.

Gas Liquid Chromatographic Determination of Therapeutic and Toxic Levels of Amitriptyline in Human Serum with a Nitrogen-Sensitive Detector

John Vasiliades* and Kerry C. Bush

Department of Pathology, The University of Alabama in Birmingham, Birmingham, Ala. 35233

A gas liquid chromatographic (GLC) procedure is presented for the determination of therapeutic and toxic serum levels of amitriptyline or nortriptyline using a nitrogen sensitive detector. The drugs are extracted from an alkaline solution into *n*-heptane–4% isobutanol and back-extracted into 0.1 M HCl. After washing with *n*-heptane, the drugs are back-extracted into ether and analyzed by GLC. Protriptyline is used as the internal standard. The method is accurate, sensitive, and specific with no derivatization required prior to analysis. An advantage of the procedure is the small sample size needed for analysis and the selectivity and sensitivity of the detector, with the limit of detection for amitriptyline being 1 ng/ml.

Amitriptyline and its monomethyl metabolite, nortriptyline, are widely used therapeutic agents for the treatment of severe depression. A definite correlation between circulating blood levels of amitriptyline, nortriptyline, and therapeutic effect has been established (*1*). The more common use of these drugs has brought about an increase in tricyclic abuse and self-inflicted poisonings. Patients may take the drug for therapeutic purposes or suicide gestures. Because of cardiovascular complications, the identification and quantitation of amitriptyline and nortriptyline overdosage is important (*2*).

A number of procedures have been reported for the determination of amitriptyline and nortriptyline in serum (*3–7*). A gas liquid chromatographic (GLC) procedure using a nitrogen sensitive detector is presented in this report. An advantage of this procedure is the small sample size used for analysis and the sensitivity and selectivity of the detector. No derivatization is required and quantitation is achieved from therapeutic to toxic levels. Seven representative patients involved in amitriptyline poisonings are presented.

EXPERIMENTAL

Reagents. All reagents used were spectral grade: Chloroform (Fisher Scientific), methanol (Fisher Scientific), isobutanol (Eastman Organic Chemicals), *n*-heptane (Sargent Welch Scientific Company). Anesthetic grade ether (Merck and Co., Inc.) was used. Amitriptyline HCl (Merck, Sharp & Dohme Research Laboratories, Rahway, N.J.), nortriptyline HCl (Eli Lilly and Company, Indianapolis, Ind.), and protriptyline HCl (Merck, Sharp & Dohme Research Laboratories, West Point, Pa.) were used as the hydrochloride salts; however, all concentrations are expressed as the free base. The protriptyline internal standard was prepared in spectral grade chloroform–methanol 1:1 by weighing out the pure drug and dissolving in 1:1 chloroform–methanol. A 1 mg/ml stock aqueous solution of amitriptyline and nortriptyline was prepared in deionized distilled water; serum standards were made up by adding small amounts of aqueous amitriptyline or nortriptyline 10 μg/ml working standards to pooled human serum. A 0.5 M NaOH solution was prepared from solid sodium hydroxide and a 0.1 M HCl solution was prepared from concentrated HCl acid.

Apparatus. Analyses were performed on a Perkin-Elmer 3920 gas chromatograph equipped with flame ionization and nitrogen sensitive detectors (Perkin-Elmer, Norwalk, Conn. 06852). A 1.8 meter × 2 mm glass column packed with 3% OV-17 on 100/120 mesh Gas Chrom Q (Applied Science Laboratories, Inc.) was used to accomplish separation. The chromatographic conditions were as follows: carrier gas, helium with a flow rate of 100 ml/min; column oven temperature, 230 °C; injector temperature, 260 °C; interface temperature, 270 °C; air flow to detector, 40 psi; hydrogen flow to detector, 15 psi; and detector voltage, 5.5–5.8. A Perkin-Elmer 26 recorder set at a range of 1 mV and a chart speed of 10 mm/min was used to record all chromatograms.

The detector used in the analysis was the new nitrogen-sensitive detector developed by Perkin-Elmer. A discussion of the principle of its operation has been reported (*8*).

The long life of the rubidium bead is an advantage of this detector over other detectors using volatile alkali salts. Kolb and Bischoff (*8*) report that a single bead was used for over 6 months without any loss of sensitivity. We have used the same bead for over 4 months with little change in sensitivity.

Procedure. A 2-ml sample of human serum, 1 ml of 0.5 N NaOH, and 25 ml of *n*-heptane containing 4% isobutanol were combined in a 50-ml glass-stoppered centrifuge tube and shaken on a mechanical shaker for 5 min. The mixture was then centrifuged and the organic layer transferred to another 50-ml centrifuge tube containing 5 ml of 0.1 N HCl. This mixture was then shaken for 5 min, centrifuged, and the organic layer discarded. The remaining 5-ml aqueous phase was washed twice with 25 ml of *n*-heptane to remove the isobutanol. After discarding the *n*-heptane from the second wash, the acidic aqueous phase was transferred to a clean 45-ml glass stoppered centrifuge tube and made basic by the addition of 1.5 ml of 0.5 N NaOH. A 6-ml aliquot of ether was added and the mixture shaken for 5 min. After a light centrifugation, the ether layer was transferred to a 12-ml glass-stoppered centrifuge tube and evaporated to dryness at 40 °C. During evaporation, the tubes were occasionally chilled to wash down any material on the sides of the tube. The residue was then dissolved in 10 μl of protriptyline internal standard and subjected to duplicate analysis on the gas chromatograph. One microliter of the samples was injected for analysis.

Standard curves were obtained by analyzing serum standards containing known amounts of amitriptyline and nortriptyline. With patients whose clinical symptoms indicated that they might be in the toxic range, serum standards containing 200 to 800 ng/ml of amitriptyline or nortriptyline were used; samples from patients thought to be in the therapeutic range were run with amitriptyline and nortriptyline serum standards at the 50, 100, and 200 ng/ml level. The concentration of the protriptyline internal standard used for the toxic range was 220 μg/ml and the concentration for the therapeutic range was 100 μg/ml. Following chromatography, peak areas were measured using the formula height times width at half peak height, and the ratio of amitriptyline or nortriptyline peak area to internal standard peak area of each serum standard was calculated and plotted against its concentration. Peak height ratios were also calculated and gave essentially the same relative standard deviation. The origin and serum standard ratios were then used to draw the standard curve as a check on linearity. However, the amitriptyline or nortriptyline concentration in patients was not obtained from the curve, but rather by using the nearest serum standard.

RESULTS AND DISCUSSION

Figure 1 shows the excellent separation of amitriptyline, nortriptyline, and protriptyline under the described conditions of study. The retention times at 230 °C were 8.5, 10.0, and 11.7 min, respectively. Figure 1 also indicates the detector was most sensitive to amitriptyline, followed by nortriptyline, and then protriptyline. Sensitivity was governed by the ability of these three amines to form cyano free radicals.

Blank serum samples assayed in the same manner as standards and patients gave no significant peaks on the chroma-

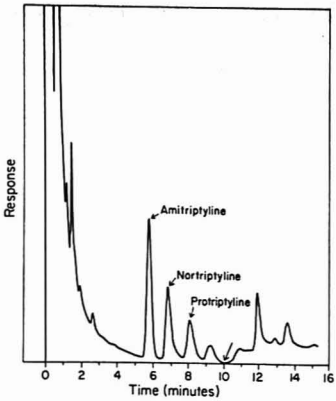

Figure 1. Gas–liquid chromatogram of blank serum with (20 ng/ml) of amitriptyline, nortriptyline, and protriptyline added after the serum was carried through the extraction

Chromatographic conditions: Column, 240 °C; carrier gas, helium, 100 ml/min; detector voltage, 5.8; and attenuation, 1 × 8

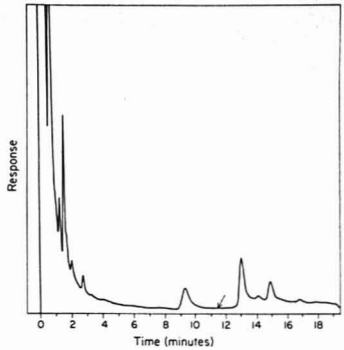

Figure 2. Gas–liquid chromatogram of drug-free pooled human serum assayed in the same manner as patients' samples and standards

Chromatographic conditions: Column, 240 °C; carrier gas, helium, 100 ml/min; detector voltage, 5.8; and attenuation, 1 × 32

tograph that might interfere with the analysis (Figure 2). The arrows in Figures 1 and 2 indicate where the temperature was raised after separation of the three drugs was accomplished; this was done to observe any endogenous peaks that might follow. Retention times of all three drugs could have been reduced had it not been for an unidentifiable peak that appeared after the protriptyline peak. Elevation of the temperature or increased carrier gas flow rate tended to move this peak beneath the protriptyline internal standard peak. It was also found that imipramine had a retention time approximating that of protriptyline. Thus, in the presence of imipramine, protriptyline could not be used as an internal standard.

The absolute percent recovery of amitriptyline by our method averaged 64 ± 10% for serum standards of 50, 100, 200, 400, and 800 ng/ml. The relative percent recovery for serum standards averaged 99 ± 10%. This compares well with the procedure described by Hucker and Stauffer (*3*) who reported 97 ± 8% relative percent recovery for amitriptyline, although they used plasma samples of lower concentration. The amount of drug recovered decreased slightly as concentration increased. Other researchers (*7*) have made the same observation using a different procedure. Recovery studies also indicated that a greater amount of drug was extractable from an aqueous matrix as compared to a serum matrix. Thus, when determining the levels in patients, we chose to carry serum instead of aqueous standards through the entire procedure. Since the patients' samples and the standards were in the same biological matrix, this helped to correct for experimental error and loss of drug during the extraction. The relative percent recovery for serum standards of nortriptyline at the 200, 400, and 800 ng/ml level averaged 99 ± 2%.

The linearity of the entire assay was demonstrated by extracting 2 ml of serum samples in duplicate containing 50, 100, 200, 400, and 800 ng/ml of amitriptyline and subjecting the extract to GC analysis after the addition of internal standard. Again the ratio of amitriptyline peak area to internal standard peak area was calculated and plotted against concentration. The range of linearity extended through 800 ng/ml. Standard curves run on separate days were linear. Excellent linearity was also observed for nortriptyline. Serum standards containing 300 and 800 ng/ml of amitriptyline were analyzed in quadruplicate for amitriptyline concentration. The within-run relative standard deviation (rel std dev) at the 300 ng/ml level was 4.1% while the within-run rel std dev at the 800 ng/ml level averaged 12.8%. There was no difference observed in extracting amitriptyline at pH 9.3 vs. pH 13 using this procedure. The percent difference of extracting at the two pH concentrations was 4%. Since the within run rel std dev is about 4%, it was concluded that there is no difference in extracting amitriptyline at the two pH concentrations.

The above procedure was used to determine serum amitriptyline levels in patients seen in the emergency room and suspected of having ingested amitriptyline. A review of seven patients seen by the emergency room is summarized in Table I. Shown in Table I is the patients' alleged drug ingestion, clinical symptom, and amitriptyline level. In all cases, amitriptyline was identified and confirmed by three separate methods. The metabolite nortriptyline was quantitated in serum in some cases. Amitriptyline was first identified in the urine and or gastric samples of each patient by UV spectrophotometry (*9–11*). The drug was extracted from a basic solution into ether; subsequent extraction of the drug into 2 N sulfuric acid left the drug in the protonated form. The sulfuric acid fraction was scanned and then made basic. The basic solution was then rescanned. The scans were compared with standard absorption curves for amitriptyline. Amitriptyline and nortriptyline were also identified in urine and gastric samples by thin layer chromatography (*12*). The drugs were extracted from basic solution into chloroform–isobutanol, spotted with pure standards and controls, and allowed to rise on the plate with the appropriate solvent. The plate was then dried, and visualization of amitriptyline and other drugs was obtained by spraying with iodoplatinate. Amitriptyline and two metabolites were observed. Amitriptyline has an R_f value of 71 and the first metabolite R_f = 46 was identified as nortriptyline.

GLC analysis was performed on the serum to qualitatively identify and quantitate the drug. Figure 3 shows the GLC spectra of a patient whose amitriptyline level in serum was 404 ng/ml. Table II gives the concentration of amitriptyline as determined using this procedure and the peak area ratio for calculating the patients' drug level. Also given in Table II is the amitriptyline serum level using peak height ratio for calculating the drug level. There appears to be good agreement between the two methods of calculation. A 300 ng/ml serum standard ran in quadruplicate gave a rel std dev of 4.1 and

Table I. Summary of Patients Involved in Amitriptyline Poisoning

Patient	Drugs allegedly ingested	Clinical symptoms	UV spectra for amitriptyline	TLC		Serum level of amitriptyline, ng/ml[a]
				Amitrip.	Nortrip.	
A. 34 yr W–M	2–3 beers, unknown amount of Triavil	Progressively obtunded, semicomatose	+	+	+	274 (73)
B. 34 yr W–F	2 empty bottles of Elavil (left a suicide note)	Obtunded with hypoactive reflexes	. . .	+	+	404
C. 24 yr W–M	Unknown amount of Elavil	Fully conscious with good reflexes, skin very flushed	+	+	+	113 (73)
D. 33 yr B–M	Unknown amount of Valium and Elavil or Triavil	Semicomatose but responding to pain	+	+	+	283 (115)
E.[b] 31 yr W–F	Unknown amount of Elavil, meprobamate, Artane, and Darvon	Stuporous and often combative	+	+	. . .	102
F. 39 yr B–F	Unknown amount of Elavil (left a suicide note)	Comatose with respiratory complications	+	+	+	471
G. 26 yr B–F	10–12 tablets of Elavil of unknown concentration	Fully awake with good reflexes	+	+	+	51

[a] The value in parenthesis after the amitriptyline level is the nortriptyline concentration in ng/ml. [b] Meprobamate level = 5 mg/dl, TLC very positive for Darvon), + = positive.

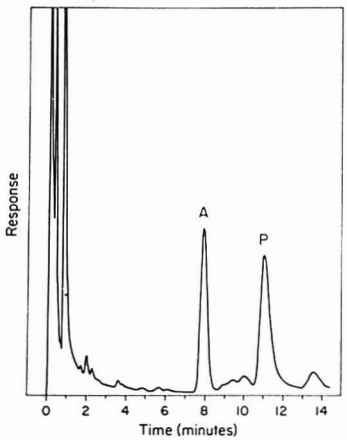

Figure 3. Gas–liquid chromatogram of amitriptyline extracted from the serum of a patient whose level was 404 ng/ml

Chromatographic conditions: Column, 230 °C, carrier gas, helium, 100 ml/min; detector voltage of 5.8; and an attenuation of 1 × 32. The protriptyline internal standard concentration was 220 μg/ml. A = Amitriptyline, P = Protriptyline

Table II. Concentration of Amitriptyline in Patients Using Peak Area and Peak Height Ratios

Patient	Concentration using peak area ratio, ng/ml	Concentration using peak height ratio, ng/ml
A	274	275
B	404	404
C	113	114
D	283	297
E	102	103
F	471	514
G	51	40

4.4%, respectively, for the two methods of calculation using peak area and peak height. The rel std dev at the 800 ng/ml level using peak area and peak height was 12.8 and 13.1%, respectively. Thus, either peak area or peak height can be used for calculating the drug level.

Current gas chromatographic procedures have established that serum levels of patients on therapeutic doses of amitriptyline hydrochloride (75–100 mg/day) range anywhere from 20 to 200 ng/ml (*1, 3*) depending upon dosage and the time that the sample was drawn and analyzed. The toxic range is generally accepted to be greater than 400 ng/ml. The patients analyzed in our study ranged from therapeutic through toxic levels. The serum levels quantitated by this method correlated well with the physical state of the patient; the higher the level, the more obtunded and comatose the patient. Hemolyzed samples did not affect the sensitivity of the procedure. The patients' urine samples were also analyzed for the presence of phenothiazines. This helped to determine whether the patient took Elavil or Triavil if that information was not already available, since Triavil is known to contain perphenazine.

The method described in this paper appears to have several advantages over current gas chromatographic procedures utilizing electron capture and flame ionization detectors. The technique is fairly rapid and small sample volumes, as low as 0.5 ml of serum provide sufficient biological material for amitriptyline detection and quantitation. Injection of 1 μl of extract dissolved in internal standard is sufficient for GLC analysis. The spectra are very clean with excellent separation of all three drugs. Sub-therapeutic levels can be quantitated and the lower limit of detection is approximately 1 ng/ml. No derivatization is involved, only simple extraction of the pure drug. In addition, amitriptyline, nortriptyline, and protriptyline are eluted from the column after a steady baseline has been obtained. Quantitation of drug levels can be easily accomplished by using peak height instead of peak area as shown in Table II. Hucker and Stauffer (*3*) have recently described a similar gas chromatographic method for quantitation of amitriptyline using a flame ionization detector. However, their method involves a large sample size, 3–5 ml of plasma. Furthermore, the drugs are eluted before a baseline is reached, and their lower limit of detection is approximately 20 ng/ml. Several investigators have quantitated tricyclic levels in serum by derivatizing the drug before GLC analysis. An example is the procedure described by Wallace, Hamilton, Goggin, and Blum (*7*) in which amitriptyline and nortriptyline are oxidized to their polyaromatic carbonyl derivative anthraquinone and analyzed using an electron capture detector. Their method is quite sensitive, as low as 2 ng/ml in a 0.5-ml specimen, but lacks the ability to differentiate between ami-

triptyline and nortriptyline. Watson and Stewart (*6*) have proposed a new high performance liquid chromatography technique for the determination of amitriptyline, nortriptyline, and protriptyline. They report a sensitivity level of 10 ng/ml for a 10-ml aqueous sample of amitriptyline; sensitivity levels in serum and urine were not reported. Jorgensen (*4*) reports a GLC method using a nitrogen-sensitive detector that has a lower limit of detection of 5 ng/ml for amitriptyline using a 2-ml serum sample. However, the addition of acetic anhydride is required to acetylate nortriptyline; otherwise the complete separation of amitriptyline and nortriptyline cannot be accomplished. In addition, the resolution of the drugs is not as great as demonstrated by our method.

The new method described here using the nitrogen-sensitive detector may be the most sensitive direct method to date for tricyclic analysis. Preliminary studies have shown that the identification and quantitation of many other drugs in biological materials may be achieved by this procedure or by a minor modification of it.

LITERATURE CITED

(1) R. A. Braithwaite, R. Goulding, G. Theano, J. Bailey, and A. Coppen, *Lancet*, 1297 June (1972).
(2) J. Vohra and G. D. Burrows, *Drugs*, **8**, 432 (1974).
(3) H. B. Hucker and S. A. Stauffer, *J. Pharm. Sci.*, **63**, 296 (1974).
(4) A. Jorgensen, *Acta Pharmacol. Toxicol.*, **36**, 79 (1975).
(5) H. B. Hucker and J. K. Miller, *J. Chromatogr.*, **32**, 408 (1968).
(6) I. D. Watson and M. J. Stewart, *J. Chromatogr.*, **110**, 389 (1975).
(7) J. E. Wallace, H. E. Hamilton, L. K. Goggin, and K. Blum, *Anal. Chem.*, **47**, 1516 (1975).
(8) B. Kolb and J. Bischoff, *J. Chromatogr. Sci.*, **12**, 625 (1974).
(9) E. G. C. Clarke, "Isolation and Identification of Drugs", The Pharmaceutical Press, London, 1969, pp 24–28.
(10) A. Curry, "Poison Detection in Human Organs," 2d ed., Charles C Thomas, Springfield, Ill., 1969, pp 76–81.
(11) S. Kaye, "Handbook of Emergency Toxicology," 3d ed., Charles C Thomas, Springfield, Ill., 1970, pp 58–61.
(12) M. M. Baden, N. N. Valanju, S. K. Verma, and S. N. Valanju, *Am. J. Clin. Pathol.*, **57**, 43 (1972).

RECEIVED for review April 26, 1976. Accepted June 21, 1976.

Intercalibration of Gas Chromatographic Analyses for Hydrocarbons in Tissues and Extracts of Marine Organisms

John W. Farrington,* John M. Teal, Gilbert C. Medeiros,[1] Kathryn A. Burns,[2] and E. Arthur Robinson, Jr.[3]

Woods Hole Oceanographic Institution, Woods Hole, Mass. 02543

James G. Quinn and Terry L. Wade

Graduate School of Oceanography, University of Rhode Island, Kingston, R.I. 02881

Gas chromatographic analyses of hydrocarbons separated from tuna meal samples and cod liver lipid extracts have been intercalibrated among three laboratories. Measurement of petroleum hydrocarbons spiked to samples of cod liver oil gave values as follows: $\hat{x}$, $(\hat{x} - \bar{x})/\hat{x}$, $s/\bar{x}$; distillate cut of South Louisiana crude oil—372 μg/g, 0.09, 0.06; No. 2 fuel oil—1163 μg/g, 0.50, 0.26; Wilmington crude oil—913 μg/g, 0.69, 0.34. The estimates of petroleum hydrocarbons in tuna meal subsamples gave $\bar{x} \pm s$ of 37.7 ± 4.6 μg/g dry weight. Measurements of pristane in cod liver lipid samples gave $\bar{x} \pm s$ of 35.7 ± 3.5 μg/g lipid and 271 ± 4.5 μg/g lipid. Measurements of pristane in tuna meal were less precise with $\bar{x} \pm s$ of 2.4 ± 1.5 μg/g dry weight. Some limitations to current methods of analysis as applied in this study and in several current oil pollution studies are demonstrated and discussed.

Petroleum and its refined products such as fuel oils and lubricating oils continue to be discharged to the world's oceans with little hope in the immediate future for substantial reduction of the quantities released (*1*). Studies of the inputs, effects, and fate of these discharges have recently been reviewed and recommendations for future studies set forth (*1*). These studies will require the efforts of many laboratories throughout the world because of the complexity and global nature of the oil pollution problem. This is already apparent to some degree in the oil pollution research literature.

An important factor in field or laboratory studies is the precision, accuracy, and intercomparability of the data gathered using the same or different methods of analyses in different laboratories (*1–3*). We initiated a program of intercalibration between our laboratories in 1971 as part of a study program to identify problems related to oceanic environmental quality under the auspices of the Office for the International Decade of Ocean Exploration, National Science Foundation. Three laboratories were involved in studying the distribution of hydrocarbons in the biota, water, air–sea interface and sediments of the North Atlantic Ocean. Unfortunately, suitable samples for intercalibration were not available, and we proceeded to develop our own. We choose to intercalibrate using a lipid material containing indigenous biogenic hydrocarbons and spiked petroleum hydrocarbons. Most current methods of extracting hydrocarbons from sediment, tissue, whole organism, or water involve an initial step of organic solvent extraction to obtain a lipid extract (*1–4*). Thus, it seemed that an initial intercalibration program with a lipid matrix sample would apply to a wide variety of marine samples. It also excluded the influence of initial lipid extraction which would have to be investigated at a later date if the first intercalibration program was successful.

We have reported the result of one phase of this intercalibration program (*5, 6*). Later we received a working intercalibration sample of tuna meal from the National Bureau of

[1] Present address, Department of Defense, Washington, D.C.
[2] Present address, Division of Agricultural Chemistry, Marine Chemistry Unit, Melbourne, Victoria, Australia.
[3] Present address, Chemistry Department, Tufts University, Medford, Mass. 02155.

Standards. We emphasize that this was not a standard reference material for hydrocarbon analysis. It was used only because it was a relatively homogeneous sample of marine tissue for which we had no knowledge of the hydrocarbon composition and concentration. A fourth laboratory participated in this phase of the intercalibration and we have issued a brief report on the results of this study (7).

We report here the result of our entire intercalibration program to date. We hope that by reporting our experience and data in detail, we will stimulate others to develop similar and even more comprehensive intercalibration efforts.

EXPERIMENTAL

Preparation of Intercalibration Samples. a) Cod liver oil sample A and sample B were manufactured by Squibb Pharmaceutical Company and purchased at a local pharmacy.

b) IDOE-1: Cod liver oil sample B was spiked with 1163 μg of No. 2 fuel oil/g cod liver oil.

c) IDOE-3: Cod liver oil sample B was spiked with 913 μg of Wilmington crude oil/g cod liver oil.

d) IDOE-5: Cod liver lipid extract was prepared by Virtis homogenization extraction in hexane (8) of a liver excised from a cod caught in the East Greenland Current on Cruise B-9-71 of *R/V Bjarni Saemudson* of the Marine Research Institute, Reykjavik, Iceland. The concentrated extract was spiked with 372 μg of a distillate fraction of a South Louisiana crude oil/g cod liver lipids. The distillate cut was prepared by vacuum distillation and had a boiling range between *n*-hexadecane (*n*-C_{16}, 287 °C, 760 mm Hg) and *n*-octacosane (*n*-C_{28}, 432 °C, 760 mm Hg).

e) Tuna meal sample: this was provided as a working intercalibration sample by the National Bureau of Standards, courtesy of Philip A. LaFleur.

Procedures. *IDOE-1 and IDOE-3,* QUINN AND WADE. Each subsample was transferred to a 50-ml centrifuge tube and 20 ml of 0.5 N KOH in absolute methanol was used to rinse out the sample vial and then added to the centrifuge tube. Three ml of distilled H_2O and 1 ml of methanol containing 100 μg of *n*-eicosane (internal standard) were added to the tube. The tube was flushed with nitrogen, capped, and heated at 100 °C for 10 min to ensure complete saponification of the sample. After cooling, 5 ml of distilled H_2O were added to the tube followed by 10 ml of ethyl ether. The contents of the tube were shaken and the phases separated by centrifugation.

The ether phase was removed and evaporated to dryness under reduced pressure at room temperature on a rotary evaporator. The residue was dissolved in a small amount of chloroform and applied to predeveloped (in chloroform) 0.37- or 0.50-mm thick silica gel G plates (20 × 20 cm). The solvent system was petroleum ether/ethyl ether/acetic acid (95/5/1). After development, the plates were visualized by brief exposure to iodine vapors. The total hydrocarbon band (corresponding to cochromatographed *n*-hexadecane and phenanthrene standards) was scraped from the plate and extracted with chloroform/methanol (9/1). After evaporation of the solvent under vacuum, the hydrocarbons were dissolved in a small volume of carbon disulfide and analyzed using a Hewlett-Packard Model 700 gas chromatograph equipped with a flame ionization detector (FID).

The chromatographic columns employed were 2.2-mm i.d. stainless steel and ranged in length from 1.8 to 2.0 m. The nonpolar column contained 2% Apiezon L on Anakrom Q (90/100 mesh), and the polar column contained 12% FFAP on Chromosorb W (H.P., 80/100 mesh). Both columns were temperature-programmed from 80 to 280 °C at 5°/min with nitrogen carrier gas at a flow rate of 10 ml/min. Quantitative analyses of samples involved comparison of the area of the chromatogram attributed to petroleum hydrocarbons with the area of the internal standard (IDOE-1) or pristane (IDOE-3, the concentration of pristane is known from analyses of the cod liver oil as described below). Peak areas were calculated by multiplying peak height times peak width at half height. The area of the unresolved complex mixture signal was determined by planimetry.

FARRINGTON. Subsamples of IDOE-1 and IDOE-3 were column-chromatographed on 10 g of alumina over 20 g of silica (both 5% deactivated with water) in a 1- to 1.5-cm i.d. column. Hydrocarbons were eluted with three column volumes of 5% benzene in pentane. The eluate was concentrated under reduced pressure to a volume of 10–15 ml and transferred to a 50-ml pear-shape flask. The eluate was then evaporated until the manometer in the vacuum line of the rotary evaporation unit showed a rapid drop in pressure indicating the last of the solvent had been evacuated from the flask. The residue was transferred to a small vial with ~0.5–1.0 ml of CS_2 and evaporated to dryness in the vial on the rotary evaporator. A known volume of CS_2 was added, usually 50–100 μl, and an aliquot was weighed on the Cahn balance to determine total hydrocarbon concentration. The hydrocarbons were analyzed by gas chromatography using a 2.3-m 3% Apiezon L on Chromasorb W 80/100 mesh column, 2.2-mm i.d. stainless steel, programmed from 80 to 290 °C at 6°/min. The column had 2160 plates as determined using *n*-C_{15} at 160 °C. Nitrogen carrier gas flow rate was 10–15 ml/min at the start of the program. Varian Aerograph Model 1200 and Model 1700 gas chromatographs equipped with FID's were used for these analyses.

The hydrocarbons were checked for purity by thin layer chromatography on silica gel G plates developed with 3% benzene in isooctane. No spots attributable to other lipids such as mono-, di-, and triglycerides, wax esters, sterol esters, methyl ketones, sterols, or fatty acids were found when plates were visualized in an iodine chamber. Several of the hydrocarbon samples were checked by infrared spectroscopy and no functional group absorption bands, which could be assigned to these other lipid compounds in the cod liver oil, were noted.

The concentration of petroleum hydrocarbons in the samples was determined as previously described in Quinn's section on methods using *n*-eicosane or *n*-docosane as an internal standard.

TEAL AND BURNS. Subsamples of IDOE-1 and IDOE-3 were analyzed by column chromatography using 20 g of 1/1 (v/v) deactivated alumina packed over silica in a 1-cm i.d. column. The columns were routinely eluted with three column volumes of pentane. Two analyses were also conducted by eluting the column with three column volumes of 5% benzene in pentane. Column eluates were concentrated by evaporation under reduced pressure. Aliquots of the residue, dissolved in CS_2, were weighed on the Cahn balance to determine total hydrocarbon concentration. The hydrocarbons were then analyzed by gas chromatography on a 3.0-m 3% Apiezon L on Chromasorb W column, 2.2-mm i.d. stainless steel, programmed from 80 to 280 °C at 5°/minute. Nitrogen carrier gas flow rate was 10–15 ml/min at the start of the program. The column had 4281 theoretical plates at the start of the analysis of the samples but had deteriorated to 1835 plates at the end of this series of analyses based on *n*-C_{14} analysis at 125 °C. A Hewlett-Packard Model 700 gas chromatograph with FID was used for these analyses.

The peak areas in chromatograms of a known portion of sample were calculated and multiplied by the quantity of hydrocarbons/unit area calculated from chromatograms of a series of standard *n*-alkanes of known amounts, i.e., external standard technique.

Cod Liver Oil—Samples A and B (Quinn, Wade, and Farrington). Samples of cod liver oil were analyzed to determine the concentration of pristane. Methods of analysis by Quinn were the same as those described above using *n*-eicosane as an internal standard. Farrington analyzed both saponified and nonsaponified samples using the same column procedure as described above. A thin-layer chromatography procedure employing silica gel G plates developed with 5% benzene in pentane was also used to analyze a saponified sample of cod liver oil. Samples were saponified under reflux for 2 h with 0.5 N KOH in methanol/benzene (1/1).

Comparison of the peak area of an internal standard of *n*-eicosane, *n*-docosane, *n*-tetradecane, or *n*-octacosane added prior to analysis, with the peak areas of the pristane was used as a means of determining concentrations. Gas chromatographic procedures were the same as described above.

IDOE-5 and Tuna Meal. The methods of analysis used to measure hydrocarbons in these samples have been presented in detail elsewhere (5–7, 9) and were in principle the same as those described above.

Measurement of Petroleum Hydrocarbons. The problems associated with distinguishing between pollutant hydrocarbons and those biosynthesized by organisms have been discussed elsewhere (1, 4). In our measurements, we have integrated the unresolved complex mixture signal,resolved and partially resolved peaks due to the petroleum spike (5).

RESULTS AND DISCUSSION

Pristane Concentration Measurements. The concentrations of pristane in the various samples analyzed are given in Table I. The agreement and precision of the measurement is good for the cod liver lipid samples where the pristane concentration was between 30 and 40 μg/g lipid and 260 to 280 μg/g lipid. The precision for the pristane in the tuna meal

Table I. Reproducibility of Pristane Analyses

Analyst	Technique	Pristane concn, μg/g Lipid
Cod Liver Sample A		
Quinn, Wade	Saponification–TLC, GC[a]	30.1
Farrington	Saponification–TLC, GC, 3 analyses by GC	35.8 ± 1.6
	Saponification–CC, 2 analyses by GC	39.4 ± 2.3[b]
	No saponification–CC, GC, Subsample A-1	36.4 ± 1.6[b]
	No saponification–CC, GC, Subsample A-2	37.3 ± 1.0[b]
	Mean =	35.7 ± 3.5
Cod Liver Sample B		
Farrington	No saponification–CC-GC	
	Subsample 1	38.7 (n-C_{14})[c]
		40.3 (n-C_{28})
	Subsample 2	37.1 (n-C_{14})
		39.7 (n-C_{28})
	Mean =	39.0 ± 1.2
IDOE-5		
Quinn, Wade	Saponification–TLC, GC, 2 analyses 259, 268; mean =	264
Teal, Burns	Saponification–CC, GC, 1 analysis	276
Farrington	Saponification–CC, GC, 6 analyses, range 225 to 308; mean =	272
	Mean for 3 laboratories	271 ± 4.5
Tuna meal		μg/g dry wt.
Quinn, Wade	Saponification–TLC, GC, 2 analyses 3.0, 3.6; mean =	3.3
Teal	Saponification–CC, GC, 1 analysis	2.0
Farrington	Saponification–CC, GC, 2 analyses; 1.9, 2.0; mean =	2.0
	Mean for 3 laboratories	2.4 ± 1.5

[a] TLC = Thin layer chromatography; CC = Column chromatography; GC = Gas chromatography. [b] Mean ± 1 σ estimated from 2 or 3 analyses by GC of hydrocarbons isolated from same sample. [c] Internal standard used to calculate concentration. Both n-C_{14} and n-C_{28} added to subsamples as internal standard.

Table II. Results of Hydrocarbon Analyses of IDOE-1 and IDOE-3 Intercalibration Samples, (μg hydrocarbons/g cod liver lipid)

		Gas chromatography analysis		
Sample	Analyst	Petroleum hyd. peaks + unresolved complex mixture	Total hyd.	Total hydrocarbons by weighing
IDOE-1	Quinn, Wade[a]	498 μg/g	770 μg/g	N.A.[b]
	Teal, Burns	782	823	1200 μg/g ± 310(2)[c]
	Farrington	449 ± 85 (4)	628 ± 131 (4)	2948 ± 192 (4)
	Mean	576 ± 147	740 ± 82	2074 ± 874
IDOE-1: $\bar{x}$ = 1,163 μg No. 2 fuel oil/g cod liver lipid[d]				
IDOE-3	Quinn, Wade[a]	410 μg/g	523 μg/g	N.A.
	Teal, Burns	178 ± 47 (2)	242 ± 54 (2)	1178 μg/g ± 313(2)
	Farrington	262 ± 122 (3)	438 ± 92 (3)	1080 ± 260 (5)
	Mean	283 ± 96	401 ± 118	1129 ± 49
IDOE-3: $\bar{x}$ = 913 μg Wilmington crude oil/g cod liver lipid[d]				

[a] The average coefficient of variation for total hydrocarbons estimated to be 20%. [b] N.A. = not analyzed or calculated. [c] Standard deviations calculated or estimated from number of analyses shown in parentheses. [d] An unknown but minor portion of the fuel oil and crude oil are not hydrocarbons.

sample was not as good. This may have been the result of the inclusion of the additional extraction procedure in the analysis. The starting mass of the lipid extract is not the reason because 200 to 600 mg of lipid were used for saponification, separation, and gas chromatographic analysis for both cod liver oil, IDOE-5, and tuna meal analyses.

IDOE-1 and IDOE-3 Measurements. The results of the analyses of samples of cod liver oil spiked with No. 2 fuel oil or Wilmington crude oil are given in Table II. The discrepancy between the actual amount of No. 2 fuel oil added to the sample (IDOE-1, 1163 μg/g lipid) and that found (576 ± 147 μg/g lipid) is probably due to losses by volatilization of hydrocarbons boiling below the C_{14} n-alkane during the isolation and concentration procedures. Comparison of the gas chromatograms of hydrocarbons isolated from IDOE-1 with the gas chromatogram of No. 2 fuel oil confirmed that there were losses of hydrocarbons boiling below n-tetradecane in the analysis of IDOE-1. This is consistent with previously reported recovery values of 70% by weight for No. 2 fuel oil from similar column chromatography procedures (8).

The values of total hydrocarbons by weighing are reasonably precise. However, the values found by Farrington were much higher than the calculated amounts of hydrocarbons in the sample. This is attributed to elution of cod liver oil com-

Table III. Results of Hydrocarbon Analyses of IDOE-5 Intercalibration Sample IDOE-5: $\bar{x}$ = 372 μg petroleum/g cod liver lipid (μg hydrocarbons/g cod liver lipid)

Analyst	(Petroleum hydrocarbons) Peaks and unresolved complex mixture	Peaks[c]	Unresolved complex mixture	Pristane
Subsamples date, January 1972. Analyses, January to October, 1972				
Quinn, Wade[a]	373	85.5	288	264
Teal, Burns[a]	438	87.7	350	276
Farrington[a]	407	64.4	343	272
Mean std dev	406 ± 26	79.2 ± 10.5	327 ± 27.7	271 ± 4.5
Subsample date, August 1972. Analysis, February 1974				
Medeiros, Robinson[b]	455	71	384	267
Subsample date, October 1972. Analysis, February 1974				
Medeiros, Robinson[b]	426	59	367	270
Subsample date, June 1974 Analyses, November 1974				
Quinn, Wade	474	78	396	262
	493	108	385	256
	676	63	613	272

[a] Data taken from Ref. (5). [b] Data taken from Ref. (6). [c] Does not include pristane or squalene.

Table IV. Results of Hydrocarbon Analyses of Tuna Meal[a] (μg/g dry wt tuna meal)

Analyst	Unresolved complex mixture n-C_{14} to n-C_{30}	Resolved peaks[b]	Total
Quinn, Wade	32.4	9.4	41.8
Teal, Burns	39.7	19.3	59.0
Farrington	41.0	6.5	47.5
Mean ± std dev	37.7 ± 4.6	11.7 ± 6.7	49.4 ± 8.8

[a] Taken from Ref. (6). [b] This does not include pristane or squalene.

ponents from the alumina–silica column which were not measured by gas chromatography because of its high molecular and very late elution, if at all, from the GC column. These components do not contain carbonyl, carboxyl, or carboxylate functional groups based upon infrared spectroscopy of the concentrated column eluate. Further analyses are needed to determine the nature of this material.

The petroleum hydrocarbon concentration in IDOE-3 as determined by gas chromatography has a greater relative standard deviation (34%) among the three laboratories than the analysis of IDOE-1 (26%). In addition, the measured IDOE-3 concentration values (283 ± 96 μg/g lipid) are much lower than the true value (913 μg/g lipid) compared to results of the analyses of IDOE-1.

The reported values for petroleum hydrocarbons can be explained as follows for the IDOE-3 analyses. Column and thin-layer chromatography as employed would exclude the more polar fractions of the crude oil from the hydrocarbon isolates. Also, the fraction of the crude oil which was obtained for gas chromatographic analysis would not include volatile low-boiling hydrocarbons which would be lost in the same manner as the volatile components of the No. 2 fuel oil in IDOE-1. Furthermore, the fraction analyzed by gas chromatography may contain high-boiling hydrocarbons which do not elute from the gas chromatographic column or elute at the end of the temperature program and during the isothermal operation at the upper limit. Their signal may be difficult to distinguish from the column bleed signal which is present at these high temperatures. This problem did not occur during analysis of the No. 2 fuel oil in IDOE-1 because its boiling range is such that the hydrocarbons elute from the column prior to the appearance of the column bleed signal.

There is evidence available to support our explanation of the low results obtained for IDOE-3 petroleum hydrocarbons. A comparison of the gas chromatograms of hydrocarbons in IDOE-3 with the gas chromatograms of the crude oil showed that lower-boiling hydrocarbons have been lost during the analysis. The recovery of Wilmington crude oil from the column chromatography procedure was 30–48% by GC analysis.

IDOE-5 Measurements. The results of the first series of intercalibrations with IDOE-1 and IDOE-3 led to the preparation of sample IDOE-5 as described previously. We prepared this sample to test our interpretation of the problems associated with analyses of IDOE-1 and IDOE-3. We reasoned our methods should lead to more precise and accurate measurements for the spike of the distillate fraction of South Louisiana crude oil because the spike contained only compounds with a molecular weight range within the range which could be measured by our methods, i.e., molecular weight range n-tetradecane to n-triacontane. Also, a check of the distillate fraction by column chromatography showed that 95+% of the components should be recovered by column chromatography and thin-layer chromatography as analyzed by weighing and GC.

The results of intercalibration with IDOE-5 were more precise and accurate as expected. The data are presented in Table III, as taken from our earlier reports (5, 6). The measured concentration of petroleum hydrocarbons is in fair agreement with the actual concentration spiked to the sample—372 μg/g lipid—with the exception of one measurement of the June 1974 subsample. We cannot explain this discrepancy except that it may represent inhomogeneity in this

Table V. Comparison of Results of IDOE-5 Analyses by One Laboratory Using Internal and External Standards (μg hydrocarbons/g lipid)

	Peaks and unresolved complex mixture	Resolved Peaks[a]	Unresolved complex mixture	Pristane
External standard method–6 subsample analyses	$41 \times 10^1 \pm 7 \times 10^1$	58 ± 18	$35 \times 10^1 \pm 6 \times 10^1$	$27 \times 10^1 \pm 3 \times 10^1$
Internal standard method–4 subsamples	400 ± 83	69 ± 28	331 ± 69	261 ± 24

[a] Does not include pristane or squalene.

sample. There are no large changes in the concentrations of hydrocarbons as a result of two years' storage in the dark, under N_2, at 0 °C. However, there appears to be a trend of a small increase in the concentration of petroleum hydrocarbons with time. The pristane concentration has remained constant within the interlaboratory variability. One explanation is that the bulk IDOE-5 sample has suffered some inhomogeneity imposed during subsampling. We intend further analyses and testing to establish if this trend is real.

Tuna Meal Measurements. The results of our analyses of tuna meal samples as reported elsewhere (*7*) are presented in Table IV. These analyses required extraction in addition to the procedures of analysis previously described in this paper. Despite this additional step, there is good agreement for the measurement of the unresolved complex mixture hydrocarbons. The agreement for the analyses of resolved peaks is not as good and is probably a result of the small ratio of peak signal to unresolved complex mixture signal for many of the peaks.

Comparison of Measurements Using Internal and External Standards. During the program of analyses of IDOE-5, we tested measurements of hydrocarbons by gas chromatography using both internal and external standards. Internal standards used for these experiments were the *n*-alkanes, *n*-tetradecane, *n*-eicosane, *n*-docosane, and *n*-octacosane. The gas chromatogram FID peak area of the internal standard was compared with the areas of the sample hydrocarbon peaks and unresolved complex mixture to quantitate the sample hydrocarbons. The second method employed was to analyze an accurately measured volume of a mixture of known concentrations of even carbon number *n*-alkanes from *n*-tetradecane to *n*-octacosane using the same gas chromatographic conditions as those used for analysis of the sample. The FID response is calibrated with the *n*-alkane standard and used to quantitate the hydrocarbon peaks and unresolved complex mixture signal of the sample.

A comparison of results obtained by analyzing subsamples spiked with an internal standard and quantitating hydrocarbons using this standard with results obtained by quantitation of hydrocarbons using external standards is presented in Table V. The results compare quite favorably.

There are advantages gained in using an internal standard. If the standard is added with a volumetric pipet under carefully controlled conditions, an accurate measurement of hydrocarbons in the sample to three significant figures is possible. In addition, the exact amount of sample injected into the GC need not be measured. The external standard method requires a more accurate measurement of the volume of external standard injected into the GC. The commonly used 10-μl Hamilton syringe or other similar syringes offer only two-figure volume measurements, thus limiting the accuracy and precision to two significant figures.

An additional advantage of the internal standard method is that once the standard is well mixed into the sample, any subsequent accidental losses do not negate the analysis. The disadvantage of the internal standard method is that it requires the analysis of a separate subsample without internal standard or with a different internal standard to determine which hydrocarbons present in the sample interfere with the measurement of a given internal standard. An error of this type results in calculation of a lower than true μg/unit area of peak. This disadvantage can be overcome by using ^{14}C-labeled hydrocarbon which would act as an internal standard for manipulations prior to the GC analysis and not interfere with FID-GC analysis due to the trace amount of label required.

GENERAL DISCUSSION

We have demonstrated the feasibility of interlaboratory calibration for hydrocarbon analyses in marine tissues and extracts. We have also shown that an intercalibration sample of marine lipids spiked with petroleum hydrocarbons can be stored for at least two years with minimal sample alteration as far as concentrations of hydrocarbons in lipid are concerned. The data suggest that after two years the sample may begin to deteriorate. However, we think that storage of subsamples under N_2 in sealed ampules at 0 °C could overcome this problem. We have stored the bulk sample under N_2 in a brown bottle with Teflon-lined screw cap at 0 °C in the dark. Subsamples were withdrawn in batches and it may be that, during the last subsampling, the homogeneity of the sample was altered and resulted in the data for one of the June 1974 subsamples.

The results of the first intercalibration effort confirms that the present methodology we employ and which is employed by others (*1–4*) has certain limitations. Some of these limitations have been discussed in this paper.

The agreement among three laboratories for the IDOE-5 and tuna meal samples was generally good and provides guidelines for comparing data reported by any of the laboratories and allows a more comprehensive interpretation of hydrocarbon biogeochemistry in the marine environment.

Despite these advances, we have only focused on a few aspects of the problem. A more thorough and widespread intercalibration effort is needed to investigate precision and accuracy from extraction through the entire analysis up to and including gas chromatography–mass spectrometry and other instrumental methods employed in oil pollution studies (*1*). Other methods of analyses for different molecular weight ranges and types of molecules need to be intercalibrated. Analyses for specific petroleum components, such as known carcinogenic polynuclear aromatic hydrocarbons, also need to be intercalibrated. These efforts would best be served if working intercalibration materials could be provided by an organization such as the United States National Bureau of Standards.

ACKNOWLEDGMENT

We thank J. M. Hunt and G. R. Harvey for comments, and B. W. Tripp for assistance.

LITERATURE CITED

(1) National Academy of Sciences, "Inputs, Fate and Effects of Petroleum in the Marine Environment", A Report of the Ocean Affairs Board, National Academy of Sciences, Washington, D.C., 1975.
(2) "Baseline Studies of Pollutants in the Marine Environment and Research Recommendations", Office of the International Decade of Ocean Exploration, National Science Foundation, Washington, D.C., 1972.
(3) "Marine Pollution Monitoring (Petroleum)", *Nat. Bur. Stand. (U.S.), Spec. Publ.*, **409**, 29 (1974).
(4) J. W. Farrington, and P. A. Meyers, Chapter 5 in "Environmental Chemistry, Vol. I", Specialist Periodical Report No. 35, The Chemical Society, U.K., 1975.
(5) J. W. Farrington, J. M. Teal, J. G. Quinn, T. Wade, and K. A. Burns, *Bull. Environ. Contam. Toxicol.*, **10**, 129 (1973).
(6) G. C. Medeiros and J. W. Farrington, in Ref. 3, p 167.
(7) J. W. Farrington, J. M. Teal, J. G. Quinn, P. L. Parker, J. K. Winters, T. L. Wade, and K. Burns, in Ref. 3, p 163.
(8) J. W. Farrington and G. C. Medeiros, "Proceedings, 1975 Conference on Prevention and Control of Oil Pollution", American Petroleum Institute, Washington, D.C., 1975, p 115.
(9) J. G. Quinn and T. L. Wade, Marine Memorandum Series No. 33, Graduate School of Oceanography, University of Rhode Island, Kingston, R.I. 02881, 1974.

RECEIVED for review March 4, 1976. Accepted July 9, 1976. This work was supported by the Office for the International Decade of Ocean Exploration Grants GX-28334 (WHOI), GX-28340 (URI), by grants from the National Science Foundation (GA-19472), and by the Office of Naval Research (N00014-66, Contract CO-241), and by Grant 802724 of the U.S. Environmental Protection Agency (WHOI). This is contribution No. 3729 of the Woods Hole Oceanographic Institution.

Gas Chromatographic Separation of Lower Aliphatic Amines

Yasuyuki Hoshika

Aichi Environmental Research Center, 7-6, Tsuji-machi, Kita-ku, Nagoya-shi, Aichi, Japan

A mixture of 13 lower aliphatic amines were separated by a TENAX-GC column in temperature programming gas chromatography. Primary amines were converted into corresponding Schiff bases by reaction with benzaldehyde. Residual secondary and tertiary amines were analyzed in the forms of their free amines. The amines separated are eight primary amines: methyl-, ethyl-, *n*-propyl-, isopropyl-, *n*-butyl-, isobutyl-, *n*-amyl-, and isoamylamines; three secondary amines: dimethyl-, diethyl-, and di-*n*-propylamines; and two tertiary amines: trimethyl- and triethylamines.

Qualitative and quantitative analysis of ammonia and lower aliphatic amines are problems commonly encountered in odor pollution analysis, because these compounds have odor threshold values at ppm or ppb levels in air (*1–3*).

Direct separation of the mixtures by gas chromatography (GC) with Lubrol MO, paraffin and undecanol (*4,5*), THEED and TEP (*6*), triethanolamine (*7*), PEG 1500 and 20 M (*8*), Amine 220 (*9*), squalane and glycerine (*10*), Chromosorb 103 (*11,12*), Pennwalt (*12*) have been used. However, in general when these columns are employed, the GC separation of the mixtures of ammonia and lower aliphatic amines, such as methyl-, dimethyl-, trimethyl-, ethyl-, diethyl-, triethyl-, and isopropylamines is poor.

In this study, to achieve complete chromatograms, separations of the mixtures of free amines and Schiff base derivatives of amines, the amines and derivatives were chromatographed simultaneously using TENAX-GC (*13*) column packing. Primary amines were converted into corresponding Schiff bases by reaction with benzaldehyde (*14*); residual secondary and tertiary amines were analyzed in the forms of their free amines, since they do not react with benzaldehyde. However, in this present method, ammonia was not analyzed, because ammonia only reacted with benzaldehyde but did not give the corresponding peak in the chromatograms.

EXPERIMENTAL

Reagents. Ammonia (28%, wt % aq. soln) and dimethylamine (40%, wt % aq. soln) were obtained from Katayama Chemical Industries, Ltd., Osaka, Japan. Methyl- (40%, wt % aq. soln), trimethyl- (30%, wt % aq. soln), ethyl- (70%, wt % aq. soln), diethyl-, triethyl-, and isopropylamines were obtained from Tokyo Kasei Kogyo Ltd., Tokyo, Japan. *n*-Propyl- and *n*-butylamines were obtained from Wako Pure Chemical Industries, Ltd., Osaka, Japan. Isobutyl-, *n*-amyl-, isoamyl-, and di-*n*-propylamines were obtained from PolyScience Corp., Niles, Ill. Benzaldehyde (95%, min.) was obtained from Wako Pure Chemical Industries Ltd., Osaka, Japan. *n*-Propylbenzene was obtained from Tokyo Kasei Kogyo, Ltd., Tokyo, Japan. *n*-Hexyl alcohol was obtained from PolyScience Corp. All reagents used were guaranteed or reagent grade chemicals.

Preparation of Schiff Base. The procedure for the preparation of all the Schiff bases listed in Table I was as follows. The amines ($1–6 \times 10^{-4}$ mol) and benzaldehyde (5×10^{-3} mol) were mixed in 2 ml of *n*-hexyl alcohol, at room temperature. The Schiff base formation reaction was rapid and exothermic; therefore the reaction time also was sufficient to form the derivatives of Schiff bases in a few minutes.

Apparatus. The gas chromatograph used was a Shimadzu Model GC5AP$_3$T (dual columns system) instrument equipped with on-column injection, a thermal conductivity detector (TCD), and a digital integrator (Shimadzu Model ITG-2A) for the determination of the

Table I. Relative Retention Times (RtR) of Ammonia and 13 Lower Aliphatic Amines in the Free Form, and the Schiff Base Derivatives (*n*-Propylbenzene = 1.00)

Compounds	RtR	Primary amine Schiff bases	RtR
Ammonia	0.07		
Class			
Primary in free			
Methylamine	0.15	Methylamine	1.14
Ethylamine	0.25	Ethylamine	1.19
n-Propylamine	0.41	*n*-Propylamine	1.28
Isopropylamine	0.33	Isopropylamine	1.20
n-Butylamine	0.58	*n*-Butylamine	1.40
Isobutylamine	0.53	Isobutylamine	1.32
n-Amylamine	0.72	*n*-Amylamine	1.54
Isoamylamine	0.68	Isoamylamine	1.47
Secondary in free			
Dimethylamine	0.24		
Diethylamine	0.48		
Di-*n*-propylamine	0.74		
Tertiary in free			
Trimethylamine	0.29		
Triethylamine	0.62		

relative retention times. The relative retention times of all the compounds listed in Table I were calculated using *n*-propylbenzene as an internal standard.

Chromatographic Conditions. The GC column consisted of a 3 m × 3 mm i.d. glass column, packed with TENAX-GC (made by Enka nv Arnhem/Holland), obtained from Shimadzu Ltd., Kyoto, Japan, 60/80 mesh, Lot No. 30704. The columns were preconditioned at 280 °C for 20 h with a constant flow of N_2 (50 ml/min) through the columns, before being connected with the TCD. The chromatographic conditions for the analysis were: carrier gas (N_2) flow rate, 50 ml/min; column temperature (programming), holding for 1 min at 100 °C and heating the column oven at a rate of 10 °C/min from 100 to 250 °C, maintaining this temperature for 15 min and then cooling to the starting temperature; injection port and detector temperatures, 250 °C; and bridge current, 66 mA.

Procedure. The sample solution was prepared by dissolving ammonia and 13 lower aliphatic amines and *n*-propylbenzene (4×10^{-4} mol) as an internal standard, in 2 ml of *n*-hexyl alcohol. One μl of sample was injected with a 10-μl Hamilton microsyringe (701-N) into the GC column. Benzaldehyde for Schiff base formation reactions was introduced directly to the sample solution.

RESULTS AND DISCUSSION

The relative retention times of ammonia and 13 lower aliphatic free amines and the derivatives of Schiff bases are listed in Table I. The retention time of *n*-propylbenzene was defined as unity.

Complete separation of ammonia and 13 lower aliphatic free amines were obtained, except for the overlap of *n*-amyl- and di-*n*-propylamines peaks, and the incomplete resolution of ethyl-, and trimethylamines. All primary amines were quantitatively converted to the corresponding Schiff bases by the reaction with benzaldehyde. Only the secondary and tertiary amines remained as free amines. The Schiff bases were resolved, except for the derivatives of ethyl- and isopropylamines. Analytical times for the GC determination of this method was about 25 min.

No evidence was found for the interference of water in the analysis.

Ammonia in the solution reacted with benzaldehyde in the mole ratio more than 2, quantitatively, but did not give the corresponding peak in 25 min, in the chromatogram. This was also confirmed from the chromatogram of the product by the direct reaction of ammonia with benzaldehyde, which was not used as solvent. It has been reported that aromatic aldehydes in general reacted with aqueous or alcoholic ammonia at room temperature to give the so-called "hydroamides" (*15*). These are high-melting, crystalline substances formed according to the following equation:

$$3ArCHO + 2NH_3 \rightarrow Ar(N{=}CHAr)_2 + 3H_2O$$

Particularly, in the case of benzaldehyde, an intermediate, crystalline addition consisting of 2 mol of benzaldehyde and 1 mol of ammonia has been isolated.

$$2C_6H_5CHO + NH_3 \rightarrow C_6H_5CHOHNHCHOHC_6H_5$$

Therefore, it is sufficiently considered that, when warmed at column temperature, the addition compounds break up into "hydroamide", aldehyde, and water.

$$2C_6H_5CHOHNHCHOHC_6H_5 \rightarrow (C_6H_5CH{=}N)_2CHC_6H_5 + C_6H_5CHO + 3H_2O$$

Therefore, in this present method, ammonia is not only analyzed, but in the case of large amounts present along with the amine mixtures may give the interfering effect. Because the ammonia will disappear benzaldehyde will react with the lower aliphatic primary amines. In such case in general, the addition to the amine mixtures of benzaldehyde of large amounts is necessary.

ACKNOWLEDGMENT

The author thanks G. Muto, University of Tokyo, and K. Yoshimoto, Aichi Environmental Research Center, for useful suggestions.

LITERATURE CITED

(1) W. Summer, "Methods of Air Deodorization", Elsevier Publishing Company, Amsterdam, 1963, p 46.
(2) G. Leonardos, D. Kendall, and N. Barnard, *J. Air Pollut. Control Assoc.*, **19**, 91 (1969).
(3) T. M. Hellman and F. H. Small, *J. Air Pollut. Control Assoc.*, **24**, 979 (1974).
(4) A. T. James, *Biochem. J.*, **52**, 242 (1952).
(5) A. T. James and A. J. P. Martin, *Analyst (London)*, **77**, 915 (1952).
(6) Y. L. Sze, M. L. Borke, and D. M. Ottenstein, *Anal. Chem.*, **35**, 240 (1963).
(7) R. E. Burks, Jr., E. B. Baker, P. Clark, J. Esslinger, and J. C. Lacey, Jr., *J. Agric. Food Chem.*, **7**, 778 (1959).
(8) A. DiCorcia and R. Samperi, *Anal. Chem.*, **46**, 977 (1974).
(9) S. R. Dunn, M. L. Simenhoff, and L. G. Wesson, Jr., *Anal. Chem.*, **48**, 41 (1976).
(10) Y. Kaburaki, Y. Mikami, Y. Okabayashi, and Y. Saida, *Bunseki Kagaku (Japn Anal.)*, **18**, 1100 (1969).
(11) C. E. Andre and A. R. Mosier, *Anal. Chem.*, **45**, 1971 (1973).
(12) A. R. Mosier, C. E. Andre, and F. G. Viets, Jr., *Environ. Sci. Technol.*, **7**, 642 (1973).
(13) J. M. H. Daemen, W. Dankelman, and M. E. Hendriks, *J. Chromatogr. Sci.*, **13**, 79 (1975).
(14) Y. Hoshika, *J. Chromatogr.*, **115**, 596 (1975).
(15) M. M. Sprung, *Chem. Rev.*, **26**, 297 (1939).

RECEIVED for review April 12, 1976. Accepted June 29, 1976

Coupled Gas Chromatography–Atomic Absorption Spectrometry for the Nanogram Determination of Chromium

Wayne R. Wolf

Nutrient Composition Laboratory, Nutrition Institute, Agricultural Research Service, U.S. Department of Agriculture, Beltsville, Md. 20705

A simple inexpensive interface to introduce the effluent from a gas chromatograph directly into the burner of a commercial atomic absorption spectrometer has been developed. Determination of chromium in the nanogram range by chelation–extraction of volatile chelates has been demonstrated, with a detection limit of 1.0 ng. Analysis of single samples is obtained in less than 1 min from injection into the GC-AAS. The use of this selective, relatively interference-free detection system was tested in recovery studies and in the determination of chromium content of NBS SRM 1571 Orchard Leaves.

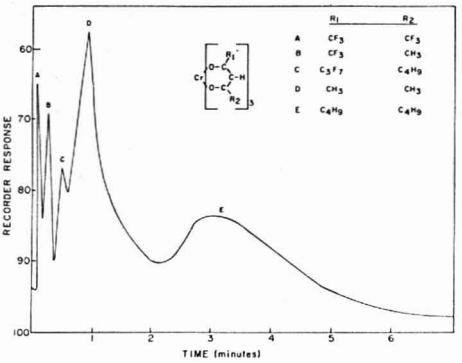

Figure 1. GC–AAS separation of chromium chelates

Amount of sample: (A) 0.15 μg Cr; (B) 0.20 μg; (C) 0.15 μg; (D) 2.90 μg; (E) 1.50 μg. Scale expansion, 3 on recorder readout; column temperature, 180 °C; N_2 flow, 65 ml/min

The gas chromatographic analysis of metals by formation of volatile metal chelates has been demonstrated for a wide variety of metals and matrices (*1, 2*). The analysis of chromium particularly has lent itself to this method because of the very stable, volatile chelates which are formed with the fluorinated derivatives of acetylacetone (2,4-pentanedione). Procedures have been reported for the analysis of chromium in several types of materials including biological materials (*3–5*). Because of the high sensitivity required in determination of naturally occurring chromium levels in biological samples, the electron capture detector has been used in these procedures. One major drawback to electron capture detection for this analysis is the relative nonspecificity of the detector to the metal, which is the analyte of interest. Electron capturing species extracted from the biological samples, or minor degradation products of the fluorinated ligand which are extracted into the organic phase during the separation give a detector response. This may result in an interfering signal, errors in analysis, and a very significant deterioration of the usable sensitivity of the method. Sensitive and specific detection of metals in gas chromatographic effluents by mass spectrometry has been demonstrated (*6*). However, the high cost, limited availability, and necessary minor modifications of existing equipment restricts its use on a routine basis.

An analytical method for chromium in biological materials by extraction with acetylacetone and analysis by flame atomic absorption spectrometry has been reported (*7*), but detection limits and sensitivities have not been sufficient to optimally meet the requirements of precise analysis at the naturally occurring levels. Atomic absorption spectrometry with carbon furnace atomization devices is a very sensitive, selective method for determination of trace elements. However, analyses with these devices have shown that many severe matrix effects exist. Particularly, the determination of chromium by carbon furnace atomic absorption has been shown to be very dependent upon the chemical form and matrix in which the chromium occurs (*8, 9*).

In order to determine an accurate amount of each chemical form of chromium in biological samples, it is necessary to have a procedure which will separate the form, and a detection system which is sensitive, precise, and selective. Therefore, I have examined the use of chelation–extraction and gas chromatography coupled with flame atomic absorption spectrometry. This paper describes a simple inexpensive interface which introduces the effluent from a gas chromatograph directly into the burner of the commercial atomic absorption spectrometer. This modification leaves the spectrometer unchanged in regards to sample introduction by aspiration which means that the instrument does not have to be dedicated to the GC-AAS mode, but can be used concurrently for conventional analysis of solutions.

EXPERIMENTAL

Instrumentation. This method was developed using a model 303 atomic absorption spectrometer (Perkin-Elmer Corp., Norwalk, Conn.) equipped with a model 56 recorder. Baseline stabilization was accomplished with a model 1021 electronic filter (Spectrum Scientific Corp., Newark, Del., 19711) with variable cut-off frequencies. The gas chromatograph was fabricated from a hot plate oven (OV10600, Thermolyne Corp.,Dubuque, Iowa) by drilling holes in the top and side for injection and exit ports. The injection port was fabricated from a ¼-inch Swagelok Tee. Nitrogen carrier gas was introduced through a flow meter into the stem of the tee. A septum was placed in the Swagelok nut on one arm and the ¼-inch o.d. Teflon column attached to the opposing arm. At the exit port of the oven, the effluent was carried to the burner of the atomic absorption spectrometer by ⅛-inch o.d. copper tubing. The injection port, exit port, and copper tubing were heated by wrapping heating tape around them, and the temperature was controlled by a variable power source (Powerstat, Fisher Scientific). Interface to the spectrometer was accomplished by tapping a threaded hole in the center of the side of the burner head to accept a 1/16-inch gold-plated Swagelok union. Both the standard 4-inch single slot and a 2-inch nitrous oxide burner head were successfully used with good results. Preliminary experiments with the triple slot burner head gave a significant decrease in sensitivity. The gas chromatographic column was 24 inches of 3-mm i.d. Teflon tubing, packed with 0.28 g of 10% SE-30 on Chromosorb W.H.P. 80/100 mesh (Hewlett-Packard, Avondale, Pa., 19311).

Reagents. Samples of pure chromium trifluoroacetylacetone ($Cr(tfa)_3$) were prepared by a previously published method (*1*) and purified by vacuum sublimation; the purity was checked by melting point. Trifluoroacetylacetone (Htfa) was obtained from a commercial source (Pierce Chemical Company, Rockford, Ill., 61105), redistilled before use, and stored in a polyethylene bottle at 4 °C. Standard solutions of $Cr(tfa)_3$ were prepared by dissolving weighed amounts of the pure chelate in hexane or benzene and diluting volumetrically to the desired concentration. Other chromium chelates were obtained from commercial sources or had been prepared previously (*1, 10*).

Chelation and Extraction. Samples of NBS SRM 1571 Orchard Leaves were digested in a reflux apparatus using sulfuric acid and hydrogen peroxide. This procedure has been developed to ensure quantitative recovery of total chromium content. Details of this digestion procedure will be described elsewhere. Aliquots of this digest (1.00 ml) were placed in reaction tubes fitted with Teflon valves (10 × 100 mm hydrolysis tubes, Kontes Glass, Vineland, N.J., 08360). The pH was adjusted to 5.5–6.0 with a concentrated solution of NaOH and 0.10 ml of Htfa added. The tubes were sealed and placed in an oven at 105 °C for 2 h. Tubes were removed from the oven and allowed to set at room temperature at least overnight until ready for extraction. The chelate was extracted into 0.500 ml of hexane, and aliquots of the hexane solution were injected into the GC-AAS for analysis. Up to 0.200-ml injections were used at times for samples of lower concentrations. Equal volume aliquots of various concentrations of the standards were injected intermittently with the samples to calibrate the system. Above 0.020 ml, there is a volume effect on observed peak height. Therefore, volume of sample and standard must be equal.

Solutions of inorganic chromium were prepared by fusion of pure Cr_2O_3 (Alpha Inorganics, Beverly, Mass., 01915) with Na_2CO_3 and dissolution with dilute acid. Chromium content of the solutions was checked by both flame and graphite furnace atomic absorption. Recovery studies were made with aliquots of these solutions carried through the chelation–extraction procedure described above for the Orchard Leaves digest.

RESULTS AND DISCUSSION

Preliminary trials were conducted with injection of solutions of chromium chelates into the mixing chamber of the AAS burner, by replacing the nebulizer with an injection port.

Table I. Recovery of Inorganic Chromium

Sample	Amount of Cr added, μg	First extraction,[a] μg	Second extraction,[b] μg	Total extracted, μg	Recovered, %
1	3.360	1.966	0.175	2.141	63.7
2	3.360	1.426	1.175	2.601	77.4
3	1.006	0.372	0.466	0.838	83.3
4	2.012	0.772	0.825	1.597	79.4
5	3.018	1.288	0.999	2.287	75.8
6	4.024	1.758	1.131	2.889	71.8
				mean ± SEM	75.2 ± 2.8

[a] Hexane. [b] Hexane + internal standard of $Cr(fod)_3$.

Table II. Chromium Content of NBS Orchard Leaves (SRM 1571)

Sample	First extraction, μg	Second extraction, μg	Total extracted, μg	Sample weight, g	Concentration measured, μg/g
1	0.144	0.065	0.209	0.0895	2.34
2	0.156	0.016	0.172	0.0895	1.92
3	0.077	0.002	0.079	0.0460	1.72
4	0.105	−0.013	0.092	0.0460	2.00
				mean ± SEM[a]	2.00 ± 0.13

[a] Mean is 76.9% of NBS value of 2.6 μg/g.

With chromium hexafluoracetylacetonate ($Cr(hfa)_3$) chelate, a precision of 4.2% relative standard deviation of 5.0 ng of Cr injected, was observed for peak height response, giving a detection limit of 0.4 ng Cr for twice the standard deviation. However, some limitations of this approach were readily apparent. The solvent passing through the flame gave a small instrumental response due to light scattering and momentary change of flame conditions. The magnitude of this response was volume-dependent and usable injection volumes were limited to 0.005 ml maximum. The solvent and chelate signals were not separated as both entered the flame at the same time; therefore, a correction had to be made for the solvent signal. Use of $Cr(tfa)_3$ or less volatile chelates necessitated heating the entire mixing chamber which is difficult to control.

Since the direct injections into the mixing chamber of the AAS burner were moderately successful, the possibility of separation of the solvent and chelate peaks in a gas chromatograph and introducing the effluent into the AAS burner became obvious. Therefore, the experimental setup described above was constructed and tested. With this system, a separation of $Cr(tfa)_3$ from the solvent and resolution of peaks for a mixture of five different volatile chromium chelates was realized as shown in Figure 1. In Figure 1, the solvent peak elutes at the same time as chelate A, which is $Cr(hfa)_3$. Note that fluorination of the chelates is not a prerequisite for detection by this system. The $Cr(tfa)_3$ chelate (peak B in Figure 1) is most suitable for analytical work, and was further studied for quantitation.

Peak height calibration curves for $Cr(tfa)_3$ were linear from 0.50 to 5.0 μg Cr/ml for 0.020-ml injection volumes, with curvature above 5.0 μg Cr/ml due to peak broadening in the GC. The calculated detection limit was 1.0 ng Cr injected, and precisions of less than 6% relative standard deviation for three or four injections of the same solution were routinely obtained.

Recovery studies of inorganic chromium and analysis of NBS Standard Reference Material SRM 1571 Orchard Leaves were performed to test the use of this detection system for the analysis of chromium in biological samples. The use of an internal standard in the organic phase and a measurement of the ratio of $Cr(tfa)_3$ to the internal standard significantly improved the quantitation and allowed more flexibility in the extraction and injection volume used for the analysis. The internal standard chosen was chromium–heptafluorodimethyloctandionate, ($Cr(fod)_3$) which elutes from the column at a later time than $Cr(tfa)_3$, (peak C in Figure 1). With a constant concentration of $Cr(fod)_3$ in the organic phase added to the extraction step and a variable concentration of $Cr(tfa)_3$, a calibration curve using the ratio of peak heights was generated. The curve is linear ($r = 0.997$) from 0.5 to 7.5 μg Cr/ml as $Cr(tfa)_3$ at a concentration of 2.50 μg Cr/ml as $Cr(fod)_3$. This ratio was independent of amount of sample injected into the GC-AAS, and calibration curves were reproducible from day to day (slope = 1.041 ± 0.017), intercept = 0.048 ± 0.013). Multiple injections of the same solution routinely gave precisions of less than 6% relative standard deviation, and single injections could be analyzed at the approximate rate of 1/min, giving a high speed system with good potential for automation.

Results of recovery of inorganic chromium and of measurement of chromium content of NBS Orchard Leaves are listed in Tables I and II. With a first extraction, the recoveries were low and, upon a second extraction, additional $Cr(tfa)_3$ was observed. Total extracted inorganic chromium was 75.2 ± 2.8% SEM, and the value obtained for the Orchard Leaves digest was 2.00 ± 0.13 SEM, which was 76.9% of the NBS certified value of 2.6 μg/g, in excellent agreement with the observed recovery of the inorganic standards. Thus, the detection system is seen to be accurate and the low recovery is in the chelation–extraction step. Subsequent experiments showed that optimum recovery is dependent upon the volume of the aliquot added to the reaction tube and that multiple extractions are necessary. Using 1.0-ml aliquots, adding a fixed amount of internal standard in the extraction step, extracting

the reaction mixture with three aliquots of 0.250 ml of hexane, and concentrating the combined extracts gave recoveries of 92.1 ± 2.5% SEM (n = 12). This procedure gave a value for the Orchard Leaves of 2.41 ± 0.12 SEM (n = 6) which is 92.7% of the NBS value.

In conclusion, the feasibility of introducing the effluent from a gas chromatographic column directly into the burner of an atomic absorption spectrometer has been successfully demonstrated. This selective detection system for the analysis of chromium has been shown to have high sensitivity, somewhat better than flame analysis by aspiration of sample solutions. This increased sensitivity is due mainly to the improved efficiency of introducing the metal into the flame as a volatile species. Although this system does not have the extremely high sensitivity of graphite furnace atomization systems, the freedom from interferences as a result of the separation of the metal from the bulk matrix in the chelation-extraction–chromatographic procedure is a very great advantage in working with complex samples. While this system has been developed for use in the analysis of the essential nutrient chromium in foods and other biological samples, a great number of other metals have previously been chromatographed as volatile chelates and should readily be detected by this system. Indeed, the entire area of metal analysis utilizing volatile chelates should find use for this simple method of obtaining a selective, sensitive, precise detection system that can be used with the procedures already established.

LITERATURE CITED

(1) R. W. Moshier and R. E. Sievers, "Gas Chromatography of Metal Chelates", Pergamon Press, New York, 1965.
(2) G. Guiochon and C. Pommier, "Gas Chromatography in Inorganics and Organometalics", Ann Arbor Science Publishers, Ann Arbor, Mich., 1973.
(3) J. Savory, P. Mushak, F. W. Snderman, Jr., R. H. Estes, and N. O. Roszel, *Anal. Chem.*, **42**, 294 (1970).
(4) L. C. Hansen, W. G. Scribner, T. W. Gilbert, and R. E. Sievers, *Anal. Chem.*, **43**, 349 (1971).
(5) G. H. Booth, Jr., and W. J. Darby, *Anal. Chem.*, **43**, 831 (1971).
(6) W. R. Wolf, M. L. Taylor, B. M. Hughes, T. O. Tierman, and R. E. Sievers, *Anal. Chem.*, **44**, 616 (1972).
(7) E. E. Cary and W. H. Allaway, *J. Agric. Food Chem.*, **19**, 1159 (1971).
(8) W. R. Wolf, W. Mertz, and R. Masironi, *J. Agric. Food Chem.*, **22**, 1037 (1974).
(9) W. R. Wolf, Federation of American Scieties for Experimental Biology, April, 1975, *Fed. Proc.*, **34**, 927 (1975).
(10) W. R. Wolf, R. E. Sievers, and G. H. Brown, *Inorg. Chem.*, **11**, 1995 (1972).

RECEIVED for review March 4, 1976. Accepted June 30, 1976. Mention of a trademark or proprietary product does not constitute a guarantee or warranty of the product by the U.S. Department of Agriculture, and does not imply its approval to the exclusion of other products that may also be suitable.

Optimization of Gas Chromatographic Analysis of Complex Mixtures of Unknown Composition

R. J. Laub and J. H. Purnell*

Department of Chemistry, University College of Swansea, Swansea, Wales SA2 8PP

The method is based on the principle that if unknown mixtures are chromatographed with columns of A, of S, and of their mixtures, the data points for individual solutes must accord with Equation 1, i.e. values of K_R must be linear in φ_A. Supplementary information such as peak height, peak width, etc. can be used to complete unambiguous linking of peaks from chromatogram to chromatogram. Subsequently, relative retentions (α) can be calculated and, via the previously described window diagram procedure, optimum column composition and length for complete resolution can be calculated. The method provides means to achieve resolution in ignorance of the nature of the mixture studied and can be applied to GLC or GSC with any type of column. The analysis of an industrial still residues sample of ten major and 33 minor unknown components is used to illustrate the method.

In a recent series of papers (*1–4*), we have established that the general solution law

$$K_R = \phi_A K^\circ_{R(A)} + \phi_S K^\circ_{R(S)} \quad (1)$$

is obeyed for 400 systems described in the literature. Here, K_R is the infinite dilution partition coefficient of any solute between a solvent mixture (A + S) and the gas phase, $K^\circ_{R(A)}$ and $K^\circ_{R(S)}$ are the corresponding quantities for the pure liquids, A and S, respectively, and ϕ represents a volume fraction. Self-evidently, Equation 1 must apply for a binary mixture of adsorptive solids. Subsequently, we showed (*5, 6*) that Equation 1 provides a quantitative basis for optimizing GC separations of known mixtures. We now describe how the method may be applied to optimize separations of complex mixtures of unknown components.

METHOD

The technique we describe below is based on the general validity of Equation 1, and for illustration we use binary stationary phases, although ternary mixtures, at least, can also be treated similarly (*6*). Briefly, the theory is that, for any given solute eluted from A, S, and A/S mixtures, the corresponding K_R/ϕ_A data *must* lie on a straight line.

First, two solvents, A and S, of differing type are chosen, and chromatograms of the unknown mixture are obtained with a column of each at some chosen and common temperature. The suitability of the two solvents can be assessed immediately, since, at this stage, the only matter of interest is to obtain symmetrical peaks corresponding to reasonable numbers of theoretical plates (N). If a satisfactory result, e.g., not less than 400 theoretical plates per foot with 100–120 mesh support, is achieved, we then assess the suitability of the chosen temperature from the point of view of both analysis time and of overall capacity factors (k'). Having then decided on a working temperature, the chromatograms are re-run. A standard solute for which $K^\circ_{R(A)}$ and $K^\circ_{R(S)}$ are accurately known is included in these and all subsequent runs which allows conversion of retention times to K_R values.

Hypothetical chromatograms for pure A and S columns are shown in Figure 1, (*a*) and (*e*). In each, four peaks appear, indicating, superficially, a four-component mixture, which is satisfactorily separated. The sample is then hypothetically run on three other columns containing, respectively, 2:1, 1:1, and 1:2 (vol/vol) mixtures of the two solvents, and chro-

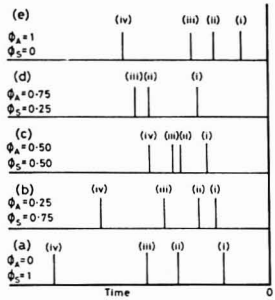

Figure 1. Hypothetical chromatograms of what appears to be an unidentified 4-component mixture

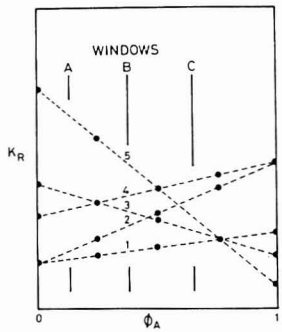

Figure 2. Plots of K_R vs. ϕ_A constructed from the data contained in Figure 1

matograms (*b*)–(*d*) illustrate possible results. Only three peaks appear in (*d*), but we cannot at this point assume that this is the only case where overlap has occurred. (We recognize that there will be changes in peak heights and areas which will be indicative of identities, but we shall return to this matter later.)

The data from Figure 1 are now represented as a plot of K_R vs. ϕ_A as shown in Figure 2, where each vertical set of points refers, from left to right, to chromatograms (*a*)–(*e*). Straight lines are drawn through the points, and we see for the first time that there are, in fact, at least five components.

A window diagram (*5, 6*) may now be constructed, since K_R for each component is known as a function of ϕ_A and so, α values for all component pairs can be calculated over the whole range ϕ_A = 0–1. Figure 3 shows the plot (window diagram) of α vs. ϕ_A wherein we see three almost equivalent optimum windows at the indicated values of ϕ_A and α. Figure 4 shows the skeletal chromatogram to be expected with columns of ϕ_A corresponding to each window peak composition, where, for convenience, we assume the column dead volume to be negligible. The order of elution is determined by reading up the window lines indicated in Figure 2. Further, each peak can unambiguously be assigned an identification number, even though their chemical identities are unknown. For example, we can now look back at Figure 1 and specify that the peaks shown correspond, in order of elution, to: (*a*) 1 + 2, 4, 3, 5; (*b*) 1, 2, 3 + 4, 5; (*c*) 1, 2, 3, 4 + 5; (*d*) 1 + 3 + 5, 2, 4; and (*e*) 5, 3, 1, 2 + 4. It will be appreciated that the foregoing example illustrates a situation of highly complex retention behavior, a feature which emphasizes the power of the technique.

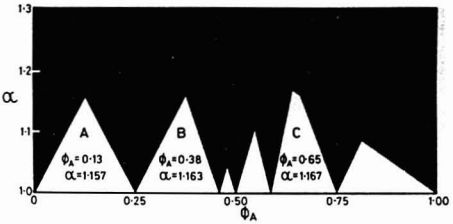

Figure 3. Window diagram for the 5 components identified via Figure 2

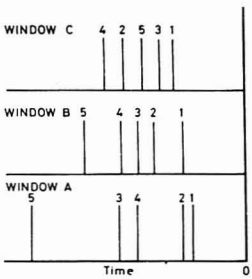

Figure 4. Hypothetical chromatograms for the 5 components of Figure 2 at the windows indicated in Figure 3

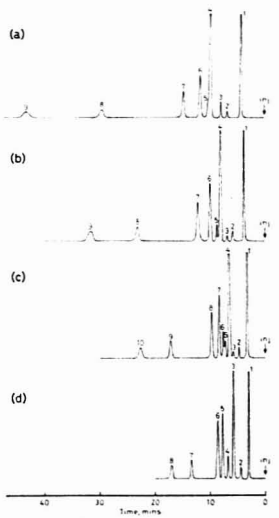

Figure 5. Chromatograms showing the major constituents of an industrial still residue mixture at 100 °C with columns of: (*a*) di-*n*-nonyl phthalate (DNNP); (*b*) squalane and DNNP (ϕ = 0.6276); (*c*) squalane and DNNP (ϕ = 0.3315); (*d*) squalane

Columns: 180 cm × 0.4 cm (i.d.) glass. Support: Chromosorb G (AW-DMCS, 100–120 mesh), wt % DNNP: 4.4024; wt % squalane: 3.7719. Inlet pressure: 30 psig. Packings (*b*) and (*c*) were made by mechanically mixing appropriate amounts of packings (*a*) and (*d*). Perkin-Elmer Model F-11. All off-scale peaks were singlets at lower sensitivity settings

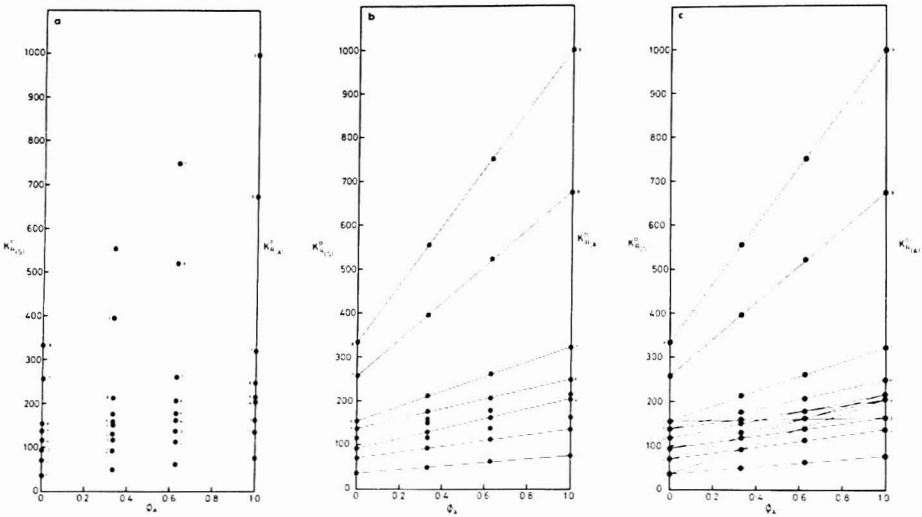

Figure 6. Partition coefficients for peaks of Figure 5 plotted vs. ϕ_{DNNP}: (*a*) without connecting lines; (*b*) lines drawn in for components identified by inspection; (*c*) all possibilities using all points

Table I. Partition Coefficients for Peaks of Figure 5

	K_R at ϕ_A =			
Peak No.	0.0000	0.3315	0.6276	1.0000
1	35.9	49.1	62.1	76.2
2	69.9	92.2	113	136
3	92.8	117	138	163
4	116	130	162	204
5	137	151	178	215
6	154	158	206	248
7	257	176	261	321
8	333	212	521	673
9	...	395	749	998
10	...	554	...	...
Toluene	108	117	127	138

Table II. Partition Coefficients for Peaks of Figure 7 (ϕ_A = 0.0749)

Peak No.	K_R	Peak No.	K_R
1	39.2	7	155
2	74.8	8	168
3	98.0	9	288
4	102	10	384
5	125	Toluene	110
6	146		

Finally, Figures 3 and 4 indicate that a column of $\phi_A = 0.65$ (window C), of sufficient length to provide the number of theoretical plates (N) required by the predicted window maximum α value, will provide marginally, the best separation. Furthermore, reference to Figure 2 shows that it provides the fastest analysis since the last emerging peak has the lowest K_R in this window.

It is recognized that from time to time a situation may arise where two or more solutes have virtually identical values of both $K°_{R(A)}$ and $K°_{R(S)}$ and so appear as a single peak at all times, irrespective of ϕ_A. However, this is not so difficult a problem as might seem since much ancillary information is contained in the original chromatograms. First, although it is not relevant to the above problem, unlike the situation depicted in Figure 1, all peaks will not be equal in height. For instance, we can now see that had we assumed equal amounts of components 1–5 in the data of Figure 1, the areas of the multiple peaks would have been: (*a* i) = 2, (*b* iii) = 2, (*c* iv) = 2, (*d* v) = 3, and (*e* iv) = 2, all other peaks being of unit area. Thus, inspection of the chromatograms will be a considerable aid in making the assignments involved in Figure 2 and in constructing Figure 3. Second, peak widths can also be useful, particularly in the context of the problem cited above. Any peak which is suspiciously broad, that is, shows a low value of N with respect to its neighbors, may indicate lack of separation. Finally, having optimized the separation, ancillary techniques, such as mass spectrometry, can be used both for identification and as an indication of lack of separation.

If, for any reason, it is still thought that the mixture may not have been completely resolved, the whole procedure can be repeated with other pairs of solvents. This is not a time-consuming matter, since, once a laboratory has a set of "standard" pure solvent columns, and has amassed the corresponding K_R data for the added standard solutes, the necessary data can be obtained quickly. Indeed, any solvent pair can be fully explored in a day or two for a mixture of almost any degree of complexity.

We now consider the final choice of working temperature. The foregoing procedure will have specified a column composition and length which will achieve complete separation of the mixture at the working temperature. What, then, might be the object of searching for an alternative temperature? First, overall analysis time may be undesirably long unless low solvent/support ratios are used. This however, may introduce one or both of two significant problems: (*a*) unacceptable solid and/or liquid surface adsorption effects and, even if these are absent, (*b*) the increasing N requirement for separation as the capacity factor (k') is reduced. Second, it is generally, although not always, true that reduction of analysis temperature increases α values which, in principle, allows separation with

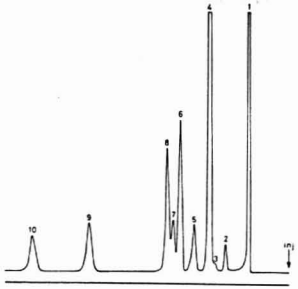

Figure 7. Chromatogram of the industrial still residue with a column of ϕ_{DNNP} = 0.0749; other conditions as specified in Figure 5

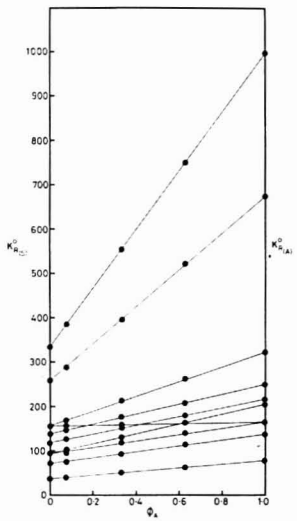

Figure 8. Correct K_R vs. ϕ_{DNNP} plot for the 10 unambiguously identified major components of the industrial still residue mixture at 100 °C

shorter columns. However, this corresponds to increased values of K_R which, since it means longer analysis times, takes us back to, and to some extent, exacerbates, the first of the problems listed. Thus, while we might consider repeating the entire optimization procedure at a lower temperature, the most profitable initial approach would be to carry out test runs with the already-optimized column at lower temperatures. The optimum volume fraction of the binary stationary phase may vary slightly with temperature but unless drastic temperature changes are used, this effect will be inconsequential.

Since α generally decreases with increased temperature, it is unlikely that the optimized column will provide complete (6σ) separation at a temperature *higher* than the test temperature, and so, only if column length is of no consequence and all materials are well below the point of thermal instability, should a move in this direction be undertaken.

Although a quantitative procedure for temperature optimization can be developed along the lines we indicate, we feel it to be of little value to discuss it further here, since the strategy is self-evident. We also note that the entire procedure could easily be computerized.

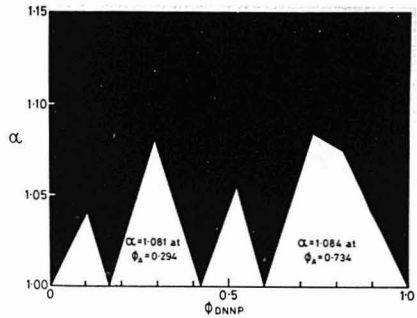

Figure 9. Window diagram for solutes constructed from data contained in Figure 8. Highest windows occur at ϕ_{DNNP} = 0.2940 (α = 1.081), and ϕ_{DNNP} = 0.7340 (α = 1.084)

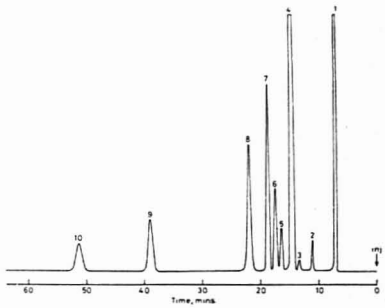

Figure 10. Chromatogram showing complete resolution at 100 °C of the major components of the industrial still residue mixture with column packing of ϕ_{DNNP} = 0.2940.

Column: 360 cm × 0.15 cm (i.d.). All other conditions as in Figure 5 except use of Pye 104

EXPERIMENTAL

All chromatograms were obtained at 100 °C with silanized glass columns which were packed with 100/120-mesh Chromosorb G (AW-DMCS). Both a Perkin-Elmer Model F-11 and a Pye Unicam Model 104 gas chromatograph were employed. The solvents, squalane (S) and di-*n*-nonyl phthalate (DNNP) (A), were reagent grade from B.D.H. Ltd., and were used without further purification. Liquid loadings for the pure solvent columns were 3.77 wt % (S) and 4.40 wt % (A) and binary stationary phases comprised mechanical mixtures of these. The mixture analyzed below is an industrial still residues sample of composition unknown to us. Other details and procedures have been published elsewhere (*5*, *6*).

RESULTS

Only very rarely does any mixture contain all components at about the same concentration level. Whatever the ultimate analytical objective, the first requisite is complete separation of the major components. Thus, the most suitable initial strategy is to work at detector attentuations which reveal only the majors and keep them "on scale" for accurate K_R measurement.

Figure 5 shows four chromatograms of the industrial still residues mixture, only the major constituents being shown. The DNNP column (Figure 5*a*) yields 9 peaks, a column of ϕ_A = 0.6276 (Figure 5*b*) gives 9 peaks also while one of ϕ_A = 0.3315 (Figure 5*c*) gives 10 peaks and a pure squalane column (Figure 5*d*) resolves only 8. Toluene was eluted from each of

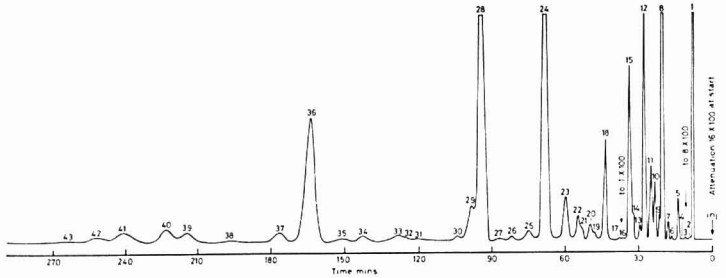

Figure 11. Chromatogram of the industrial still residue mixture with column as specified in Figure 10 at 75 °C

All conditions identical, except sensitivity increased by a factor of 16 and inlet pressure reduced to 15 psig. Numbering now sequential

the columns and, since its K_R for each was accurately known, those for the unknowns were calculated from relative retention data. The data for all peaks and columns are given in Table I, and Figure 6*a* shows the K_R values plotted vs. ϕ_A. The numbered data points in the figure correspond to the peak numbers in Table I and Figure 5.

By inspection of the chromatograms in Figure 5 and the points in Figure 6*a*, we can immediately draw several connecting lines between $K°_{R(S)}$ and $K°_{R(A)}$ values. As one example, the data for the peaks numbered 8 ($\phi_A = 0$), 10 ($\phi_A = 0.3315$), 9 ($\phi_A = 0.6276$), and 9 ($\phi_A = 1$) all lie on a single straight line and, furthermore, the peaks have the same area. Therefore, these peaks must be due to the same component. In contrast, we can draw a line which connects data point No. 9 ($\phi_A = 0.6276$) with data point No. 8 ($\phi_A = 1$), but extrapolation of such a line predicts a peak appearing after No. 10 at $\phi_A = 0.3315$; since no such peak was found, we eliminate this possibility.

Figure 6*b* shows the same data points as in Figure 6*a*, except that now, those points which, by inspection (as outlined above) have been shown to relate to a given component, have been connected by straight lines. We see that 7 components have, in this process, been unambiguously identified. We must now turn to a consideration of the several points left over and, as yet, unconnected. Clearly, the components involved must, at some value or other of ϕ_A, overlap others. To decide which ones they overlap, all possible straight lines are drawn through the various unconnected points such that each line has 4 points on it, as shown in Figure 6*c*. Previously-used points are used again, if necessary. We now see that there are 13 lines in total, i.e., 13 possible components.

Some of the lines in Figure 6*c* may be fictitious, that is, it may be coincidental that a straight line can be drawn through a set of points. To test this prospect, a column composition is selected by consideration of Figure 6*c*, such that all (possible) components would be at least partially resolved if present. Such a column composition occurs at $\phi_A = 0.075$; Figure 7 shows the corresponding chromatogram where, still, only 10 peaks are seen. The partition coefficients are given in Table II, and are shown plotted in Figure 8, where the three fictitious lines of Figure 6*c* have been eliminated.

We are now in a position to optimize the separation of these 10 components; Figure 9 shows the window diagram, where the two best α values indicated are 1.081 ($\phi_A = 0.294$) and $\alpha = 1.084$ ($\phi_A = 0.734$). Referring back to Figure 8, we find that analysis times for the latter window will be considerably longer than those for the first. Since the two windows are for all practical purposes identical in terms of α, thus offering no real choice on the basis of resolution, we choose the window at $\phi_A = 0.294$. Figure 10 shows the chromatogram obtained with a column containing packing made up at the indicated ϕ_A value, and of appropriate length to provide the number of theoretical plates demanded by the relevant value of α where all 10 components are resolved in 52 min. If the window at $\phi_A = 0.734$ had been used, the corresponding analysis time would have been about 80 min.

Finally, Figure 11 shows a chromatogram of the mixture with the column of $\phi_A = 0.294$ operated at lower flow rate but at a higher sensitivity setting at 75 °C. There are now 43 clearly visible peaks.

In order completely to resolve the entire mixture, the optimization procedure would have to be repeated at the higher sensitivity setting, but this is a relatively trivial task as was indicated earlier.

We have now applied the above approach to a number of complex mixtures of initially unknown composition with equal success. It seems likely that the method will prove a powerful addition to chromatographic technique since it can be applied to GLC and GSC and for any type of column, provided only that these can be accurately packed or coated.

We recognize, of course, that what we have provided is a solution specific for mixtures of two particular packings. Obviously, a better optimization might be achieved with some other pair in the sense of requiring shorter columns, faster analysis, or some other desirable feature. To some extent, the judgment will be subjective; to a further extent, it may be defined by physical limitations imposed by equipment. If, in the end, an unsatisfactory solution is achieved, even though it has provided the desired complete resolution, further studies according to our method can be carried out until an acceptable situation is found. As we have stated earlier, a binary packing can be exhaustively studied in a matter of days so no great time is involved.

Finally, although we have so far (*1–6*) been unable to find a solvent pair which does not behave in accord with Equation 1, the possibility exists and it might be argued that this destroys the generality of our method. Mechanical mixtures of packings of pure solvents always obey Equation 1; hence, their use avoids any ambiguity arising on this account.

LITERATURE CITED

(1) J. H. Purnell and J. M. Vargas de Andrade, *J. Am. Chem. Soc.*, **97**, 3585 (1975).
(2) J. H. Purnell and J. M. Vargas de Andrade, *J. Am. Chem. Soc.*, **97**, 3590 (1975).
(3) R. J. Laub and J. H. Purnell, *J. Am. Chem. Soc.*, **98**, 30 (1976).
(4) R. J. Laub and J. H. Purnell, *J. Am. Chem. Soc.*, **98**, 35 (1976).
(5) R. J. Laub and J. H. Purnell, *J. Chromatogr.*, **112**, 71 (1975).
(6) R. J. Laub and J. H. Purnell, *Anal. Chem.*, **48**, 799 (1976).

RECEIVED for review May 10, 1976. Accepted July 9, 1976. We acknowledge the support of the Science Research Council.

High-Pressure Liquid–Liquid Partition Chromatography of Metal Chelates of Tetradentate β-Ketoamines

Enrico Gaetani and Carlo F. Laureri

Istituto di Chimica Farmaceutica e Tossicologica, Università di Parma, 43100 Parma, Italy

Alessandro Mangia* and Giovanni Parolari

Istituto di Chimica Generale ed Inorganica, Università di Parma, 43100 Parma, Italy

High pressure liquid–liquid partition chromatography was applied to some metal chelates of the tetradentate β-ketoamines: *N,N'*-ethylenebis(acetylacetoneimine), (H_2(en)AA), *N,N'*-trimethylenebis(acetylacetoneimine), (H_2(tm)AA) and *N,N'*-ethylenebis(benzoylacetoneimine) (H_2(en)BA). The complexes Co^{II}, Ni^{II}, Cu^{II}, Pd^{II}(en)AA, Ni^{II}, Cu^{II}(en)BA, Cu^{II}(tm)AA have been considered. Nickel and copper were separated by using H_2(en)AA and H_2(en)BA on two different columns. Palladium was successfully separated from copper but not from nickel. The dependence of the response of the uv detector (254 nm) on the amount of metal in aqueous solutions is reported for Ni and Cu(en)AA. The detection limits are about 0.2 and 0.5 ng of metal injected for Ni and Cu, respectively.

High-pressure liquid chromatography is most widely employed in organic chemistry, but some examples of its application to inorganic and organometallic compounds have been reported. Ion exchange technique has been used for separation and determination of Fe^{III} (*1*), Sb^{III}, Bi^{III}, Cr^{VI}, Au^{III}, Hg^{II}, Pd^{II}, Pt^{IV}, Ru^{IV}, Tl^{III}, Sn^{IV} (*2*), Pb^{II} (*3*), Th^{IV}, Ca, Cu^{II}, Mn^{II}, Ni^{II} (*4*), rare earths (*5*), and transplutonium elements using di(2-ethylhexyl)orthophosphoric acid as a stationary phase (*6*). With liquid–solid high-pressure chromatography, the separation of Hg^{II}, Cu^{II} (*7*), Sn^{II} (*8*) has been achieved. The partition liquid–liquid technique, with direct or reversed phase, has been chosen for organometallic Cr^{III} (*9, 10*) and Fe^{III} (*11*) compounds and for the β-diketonates of several divalent and trivalent metals (*12*).

We applied the reversed phase liquid–liquid partition chromatography to some metal complexes of the tetradentate β-ketoamines

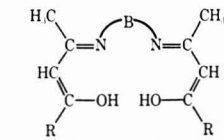

with B = $(CH_2)_2$ R = CH_3 (H_2(en)AA)
B = $(CH_2)_3$ R = CH_3 (H_2(tm)AA)
B = $(CH_2)_2$ R = C_6H_5 (H_2(en)BA)

Our aim was to study the behavior of metal chelates in high pressure partition chromatography and to evaluate the possibility of using this method in the determination of metals.

The separation of Ni and Cu using the ligand H_2(en)AA has been briefly reported by us (*13*). Independently and at the same time, other authors published the separation of Ni(en)AA and Cu(en)AA (*14*); in this case liquid–solid chromatography was used, with microparticulate silica as a stationary phase.

The present paper deals with the chromatographic behavior of Co^{II}(en)AA, Ni^{II}(en)AA, Cu^{II}(en)AA, Pd^{II}(en)AA, Ni^{II}(en)BA, Cu^{II}(en)BA, Cu^{II}(tm)AA. The dependence of the detector response on the amount of Ni and Cu in aqueous solutions is also reported.

EXPERIMENTAL

Preparation of Ligands and Metal Chelates. Described procedures were followed in the preparation of H_2(en)AA, H_2(tm)AA, H_2(en)BA, Ni(en)AA, Cu(en)AA, Cu(tm)AA, Cu(en)BA (*15*) and Pd(en)AA(*16*).

Except for H_2(tm)AA, the compounds were characterized by elemental analysis, mp, and mass spectra. The mass spectra of the complexes of H_2(en)AA and H_2(tm)AA agree with those reported (*17*). The mass spectra of Ni(en)BA and Cu(en)BA show the expected fragmentation patterns with parent ion peaks.

The cobalt(II) complex was not isolated, but prepared by adding small excess of cobalt acetate to the methanolic solution of H_2(en)AA in nitrogen atmosphere. The yellow solution obtained was directly used for the chromatographic analysis.

High-Pressure Liquid Chromatography. *Apparatus.* A Varian Aerograph 8500, with a single wavelength uv detector (254 nm) was used; the full-scale sensitivity was 0.005 absorbance unit; flow cell volume, 8 μl.

Columns. The columns used were stainless steel 25 cm × 0.2 cm i.d. MicroPak CH (Octadecylsilane on silica gel 10-μm diameter), stainless steel 50 cm × 0.2 cm i.d. slurry packed (*18*) with silica gel (10-μm diameter) bonded to 3-aminopropyltriethoxysilane (*19*) (–NH_2 column). As moving phase, methanol–6×10^{-3} M phosphate or borate buffer mixtures were used. The pH of the buffer solutions ranged between 7.0 and 11.0. The flow rate of the eluent was 1 or 1.5 $cm^3\ min^{-1}$ at a pressure of 225–300 atm. Spectroscopic grade solvents were used. Peak areas were measured by a Varian CDS 101 integrator.

Mass Spectrometry. Mass spectra of ligands and chelates were run on a Varian MAT CH5 spectrometer at the ionizing voltage of 70 eV. The solid samples were directly introduced into the source by means of a direct insertion probe. Source temperature was 220–240 °C.

Ultraviolet–Visible Spectrometry. Electronic spectra of the chelates were run on a Perkin-Elmer model 402 spectrophotometer. Methanol and tetrahydrofuran (spectroscopic grade) were used as solvents.

RESULTS AND DISCUSSION

N,N'-Ethylenebis(acetylacetoneimine) and its analogues, particularly the fluorinate ones, have been successfully employed in the gas chromatographic analysis (*17, 20–22*). Owing to the high values of the stability constants of their complexes ($\log K = 23$ for Cu(en)AA (*23*)), which are soluble in medium and low polarity solvents, these ligands are also suitable for liquid–liquid partition chromatography; at high pH, the values of the total distribution coefficient of the metals are approximately coincident with those of the partition coefficient of the complexes (*12*). Moreover the high values of the molar absorptivities in the uv region allow good sensitivity with photometric detectors. The low number of metals with which they form stable complexes (*24*), reduces the problem of interferences.

On the MicroPak CH column different moving phases were used, varying the volume ratio between methanol and the

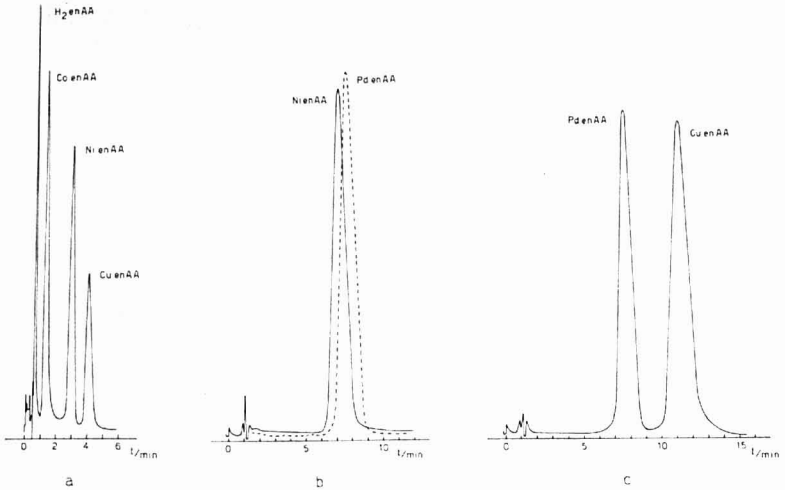

Figure 1. (a) Separation of H_2(en)AA, Co^{II}(en)AA, Ni^{II}(en)AA, Cu^{II}(en)AA. Column: MicroPak CH 25 cm × 0.2 cm; moving phase: methanol/phosphate buffer pH 7.8, 65/35 (v/v); flow rate: 1 cm^3 min^{-1}. Theoretical plate number for Cu(en)AA: 480. (b) Superimposed chromatograms of Ni(en)AA and Pd(en)AA. Moving phase: methanol/phosphate buffer pH 7.8, 45/55 (v/v); flow rate: 1 cm^3 min^{-1}. (c) Separation: of Pd(en)AA and Cu(en)AA at the same condition of b). Theoretical plate number for Cu(en)AA: 410

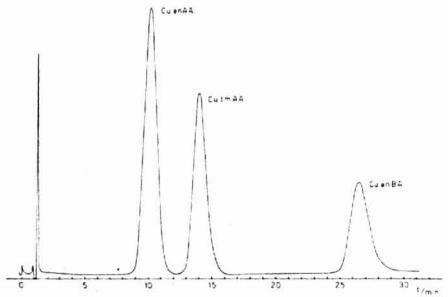

Figure 2. Separation of Cu(en)AA, Cu(tm)AA, and Cu(en)BA. Column: MicroPak CH; mobile phase: methanol/phosphate buffer pH 7.8, 50/50 (v/v). Flow rate: 1 cm^3 min^{-1}. Theoretical plate number for Cu(en)BA: 940

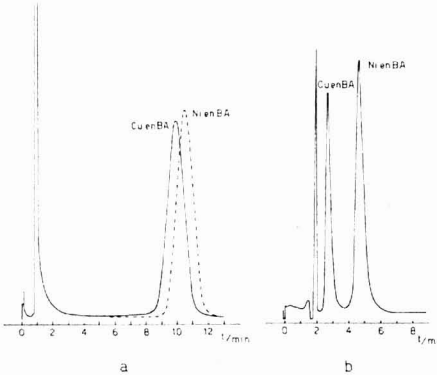

Figure 3. (a) Superimposed chromatograms of Cu(en)BA and Ni(en)BA. Column: MicroPak CH; mobile phase: methanol/phosphate buffer pH 7.0, 70/30 (v/v). Flow rate: 1.5 cm^3 min^{-1}. (b) Separation of Cu(en)BA and Ni(en)BA. Column: $-NH_2$ 50 cm × 0.2 cm; mobile phase: methanol/phosphate buffer pH 7.8, 40/60 (v/v). Flow rate: 1 cm^3 min^{-1}. Theoretical plate number for Ni(en)BA: 346

aqueous buffers and the pH value of the buffer. Separation of a methanol solution of H_2(en)AA, Co, Ni, Cu(en)AA was achieved by using a methanol/buffer volume ratio 65/35 and pH 7.8 (Figure 1a). The resolution factors are 1.44 for Cu/Ni(en)AA, 2.85 for Ni/Co(en)AA, 4.25 for Cu/Co(en)AA. The peaks were identified by injecting the single chelates. The cobalt chelate decomposes in solution, even in N_2 atmosphere; the solution turns brown, and successive injections show a second peak immediately after that attributed to Co(en)AA.

Separation of Ni(en)AA and Pd(en)AA was not successful, Pd(en)AA being only slightly more retained (Figure 1b) for every volume ratio between methanol and buffer solution. The separation of Pd(en)AA and Cu(en)AA in methanolic solution is shown in Figure 1c. The resolution factor for Cu/Pd(en)AA under the conditions quoted in the figure, is 1.94.

The behavior of CuenAA is not considerably influenced by the pH of the buffer on the range 7.0–11.0 (phosphate buffers up to 8.0 and borate buffers between 8.0 and 11.0 were used): in this pH range, the uncorrected retention time lengthens from 1.7 to 1.9 min for a methanol/buffer volume ratio 70/30; the area of the peak is constant for the same quantity of complex. The copper chelates Cu(en)AA, Cu(tm)AA, Cu(en)BA in THF solution are separated using a 50/50 methanol/buffer pH 7.8 mixture (Figure 2). The presence of the phenyl ring in Cu(en)BA determines a major affinity of the complex for the stationary phase and the retention time increases sensibly. With this ligand, nickel and copper are not separated; the superimposed chromatograms of Ni(en)BA and Cu(en)BA in chloroform solutions are shown in Figure 3a. On

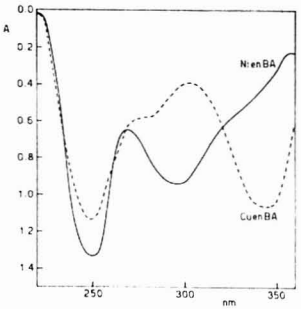

Figure 4. Ultraviolet spectra of 5×10^{-5} M solutions of Cu(en)BA and Ni(en)BA in tetrahydrofuran

the contrary, Ni(en)BA and Cu(en)BA are separated on the $-NH_2$ column, using a mobile phase with a volume ratio methanol/buffer pH 7.8, 40/60 (Figure 3b).

Both these chelates are stable and have high absorption in the uv region (Figure 4). Their molar absorptivities at 254 nm ($\epsilon \simeq 20\,300$ and $26\,000$ mol^{-1} l. cm^{-1} for Cu(en)BA and Ni(en)BA, respectively) could allow a good sensitivity in the chromatographic determination of traces of Ni and Cu.

The other complexes Ni, Cu, Pd(en)AA and Cu(tm)AA are not separated on the $-NH_2$ column for any composition of the mobile phase; their retention times are influenced very little by the volume ratio in the eluent mixture.

To estimate the possibility of an analytical application of the liquid–liquid partition chromatography of tetradentate ketoamines, the dependence of the detector response on the amount of the metal was verified for Ni(en)AA and Cu(en)AA. For this purpose, the MicroPak CH column was used; the mobile phase was a methanol/borate buffer pH 10, 70/30 mixture. Calibration curves were set up both with solutions of the pure chelates and starting from the metals in aqueous solution. In the latter procedure, methanolic solutions of an excess of the ligand (500–50 times) were added to equal volumes of aqueous solutions of the metal acetates in the range of concentration 0.2–2 and 10–100 ppm of metal, buffered at pH 10. The reaction was carried out three times for each sample; the mixed solutions were directly injected into the column. The injections were replicated five times and the peak area was determined by means of an integrator. Figure 5 shows a typical chromatogram of some injections of 5 μl of a 0.5-ppm solution of Ni^{2+}, i.e., corresponding to 2.5 ng of metal. The calibration curves obtained starting from the aqueous solutions of the metals are linear in both ranges of concentration, corresponding to 0.5–5 and 25–250 ng of metal injected; the relative standard deviation of each mean value of the peak area is about 2% in the higher range of concentration and between 3–6% in the lower one. The plots obtained by using methanolic solutions of the two chelates coincide with those obtained starting from the metals, within the experimental errors. The detection limits, corresponding to a signal-to-noise ratio 2:1, for Ni and Cu are about 0.2 and 0.5 ng. The lower detection limit for Ni is attributable to the higher molar absortivity at 254 nm of the nickel chelate (*13*) and especially to its lower retention time. Moreover, it is noticed that the metals can be extracted by means of a chloroform solution of the ligand and the extracts can be concentrated; in this way, it is possible to start from more dilute aqueous metal solutions.

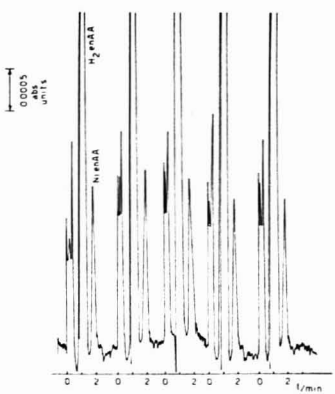

Figure 5. Chromatograms of successive injections of Ni(en)AA: methanol/water solution of 0.5 ppm of metal; 0.5-μl samples. Column: MicroPak CH; mobile phase: methanol/borate buffer pH 10, 70/30. Flow rate: 1.5 cm^3 min^{-1}

The results obtained confirm the possibility of a useful application of the HPLC to metal chelates; further studies on liquid–liquid partition chromatography of the metal complexes of β-ketoamines and other polydentate ligands are in progress.

LITERATURE CITED

(1) M. D. Seymour, J. P. Sickafoose, and J. S. Fritz, *Anal. Chem.*, **43**, 1734–1737 (1971).
(2) M. D. Seymour and J. S. Fritz, *Anal. Chem.*, **45**, 1394–1399 (1973).
(3) M. D. Seymour and J. S. Fritz, *Anal. Chem.*, **45**, 1632–1636 (1973).
(4) J. S. Fritz, *Anal. Chem.*, **46**, 825–829 (1974).
(5) D. O. Campbell, *J. Inorg. Nucl. Chem.*, **35**, 3911–3919 (1973).
(6) E. P. Horwitz and C. A. A. Bloomquist, *J. Inorg. Nucl. Chem.*, **35**, 271–284 (1973).
(7) P. Heizmann and K. Ballschmiter, *Fresenius Z. Anal. Chem.*, **268** (3), 206–207 (1973).
(8) J. S. Fritz and L. Goodkin, *Anal. Chem.*, **46**, 959–962 (1974).
(9) J. M. Greenwood, H. Veening, and B. R. Willeford, *J. Organomet. Chem.*, **38**, 345–348 (1972).
(10) J. F. K. Huber, J. C. Kraak, and H. Veening, *Chem. Commun.*, 1305 (1969).
(11) R. E. Graf and C. P. Lillya, *J. Organomet. Chem.*, **47**, 413–416 (1973).
(12) J. F. K. Huber, J. C. Kraak, and H. Veening, *Anal. Chem.*, **44**, 1554–1559 (1972).
(13) E. Gaetani, C. F. Laureri, and A. Mangia, Abstracts, 12th National Meeting of the Società Chimica Italiana, Cagliari, September 1975, pp 68–70.
(14) P. C. Uden and F. H. Walters, *Anal. Chim. Acta*, **79**, 175–183 (1975).
(15) P. J. McCarthy, R. J. Hovey, K. Ueno, and A. E. Martell, *J. Am. Chem. Soc.*, **77**, 5820–5824 (1955).
(16) "Gmelins Handbuch der Anorganische Chemie", 65, Verlag Chemie GBBH, Weinheim, 1942, p 403.
(17) R. Belcher, K. Blessel, I. Cardwell, M. Pravica, W. I. Stephen, and P. C. Uden, *J. Inorg. Nucl. Chem.*, **35**, 1127–1144 (1973).
(18) R. E. Majors, *Anal. Chem.*, **44**, 1722–1726 (1972).
(19) R. E. Majors and M. I. Hopper, *J. Chromatogr. Sci.*, **12**, 767 (1974).
(20) R. Belcher, M. Pravica, W. I. Stephen, and P. C. Uden, *Chem. Commun.*, 41–42 (1971).
(21) P. C. Uden and K. Blessel, *Inorg. Chem.*, **12**, 352–356 (1973).
(22) R. Belcher, R. J. Martin, W. I. Stephen, D. E. Henderson, A. Kamalizad, and P. C. Uden, *Anal. Chem.*, **45**, 1197–1203 (1973).
(23) G. Schwarzenbach and M. Honda, *Helv. Chim. Acta*, **40**, 27–40 (1957).
(24) R. H. Holm, G. W. Everett, Jr., and A. Chakravorty, "Progress in Inorganic Chemistry", Vol. 7, F. A. Cotton. Ed., Interscience, New York, 1966, p 180.

RECEIVED for review April 15, 1976. Accepted June 14, 1976. A part of this work was presented at the XII National Meeting of the Società Chimica Italiana, Cagliari, Italy, September 1975.

Liquid Chromatography of Aromatic Hydrocarbons on Ion-Exchange Resins

David M. Ordemann and Harold F. Walton*

Department of Chemistry, University of Colorado, Boulder, Colo. 80309

Polycyclic aromatic hydrocarbons and halogenated hydrocarbons, including chlorinated biphenyls, are separated chromatographically on columns of low-cross-linked polystyrene-type cation-exchange resins. The counterions affect retention, doubly- and triply-charged ions being more effective than singly-charged. Best results were obtained with Ca and Fe(III), using acetonitrile–water or methanol–water solvent mixtures.

Ion-exchange resins based on polystyrene absorb uncharged organic compounds, especially those having aromatic character. The charge type of the resin is of secondary importance. In 1957, Sherma and Rieman (*1*) described the "solubilization chromatography" of alcohols, esters, ketones, and aromatic hydrocarbons on columns of anion- and cation-exchange resins, using as eluents mixtures of water with methanol or acetic acid. The proportion of nonaqueous solvent was increased as elution proceeded. Recently Funasaka et al. (*2*) studied the chromatography of several substituted benzenes and naphthalenes on six different ion-exchange resins with six different solvents. Anion-exchange resin columns were used by Scott and others (*3, 4*) to analyze the polar organic constituents of body fluids and contaminated waters.

Polycyclic aromatic hydrocarbons and their chlorinated derivatives are of current interest because of their environmental importance. Chromatography on bonded packings (*5, 6*) and on silica gel (*7, 8*) has been used to analyze mixtures of these compounds. A combination of gas and liquid chromatography was used by May et al. (*9*) to analyze aromatic hydrocarbons in sea water. Gas chromatography on a liquid crystal stationary phase (*10*) is very effective for distinguishing isomers.

In our laboratory, we have studied the chromatography of various polar aromatic compounds on anion- and cation-exchange resins (*11, 12*) and noted, among other effects, the effect of the resin counterions. We have now extended these studies to polycyclic aromatic hydrocarbons and a few of their chlorinated derivatives, using both anion- and cation-exchange resins of the polystyrene type. Experiments with cation-exchange resins are described in this paper.

EXPERIMENTAL

Materials. Most of our work was done with the sulfonated polystyrene cation-exchange resins, Aminex 50W-X4, 20–30 μ, and Aminex A-7, 8% cross-linked, 7-11 μ, both supplied by Bio-Rad Laboratories, Richmond, Calif. A custom-made copolymer of 2-methyl-5-vinylpyridine with 9% divinylbenzene was supplied by the same company. The nonionic, macroporous styrene–divinylbenzene copolymer, Amberlite XAD-2 (Rohm and Haas Co., Philadelphia) was also tested. Pure phenanthrene, biphenyl, and chlorinated biphenyls were supplied by Analabs, Inc., North Haven, Conn., and other hydrocarbons by Aldrich Chemical Co., Milwaukee, Wis. High-quality solvents were used.

Columns, Chromatographic Equipment, Procedure. Water-jacketed glass columns, 6.3-mm i.d., fitted with adjustable Teflon (PTFE) plungers and tolerating pressures of 500–1000 psi (35–70 bars) were supplied by Glenco Scientific, Inc., Houston, Texas, and by Laboratory Data Control, Riviera Beach, Fla. Injections were made by septum or by sample-injection valves. Pumps were made by Waters Associates, Milford, Mass., and by Laboratory Data Control. Ultraviolet detectors were supplied by Spectra-Physics, Inc., Santa Clara, Calif., and were used at 254 nm.

The columns were normally kept at 55–65 °C by circulating water from a constant-temperature bath. The resin beds were 18–35 cm long. Mixed solvents were used, one component being water and the other either methanol, acetonitrile, or isopropyl alcohol. Solvent gradients were sometimes used. Flow rates were between 12 and 30 ml/h, with pressures up to 300 psi (20 bars). With the soft, 4% cross-linked resin, it was important not to use excessive pressure, or the resin bed collapsed, sometimes irreversibly. At moderate pressures, the columns could be operated continuously.

RESULTS

Comparison of Ionic and Nonionic Resins. The ionic functional groups of ion-exchange resins play no direct part in the absorption of uncharged organic compounds. Their main function is to become hydrated and cause the resins to swell and become permeable. Comparing the retention of biphenyl on a column of Aminex 50W-X4 ion-exchange resin with that on a column of nonionic, macroporous Amberlite XAD-2, we found much stronger retention on XAD-2. The capacity factor, k', was 2.5 at 65 °C with 80% acetonitrile as the solvent, compared to 1.6 with 33% acetonitrile for the ion-exchange resin (see Table III). The bands were much broader with XAD-2, because this resin was used in its normal commercial form, as porous granules 0.5 mm in diameter.

Counterion Effects. The absorption of hydrocarbons by cation-exchange resins depends on the counterions. Divalent ions give considerably stronger retention than univalent, and trivalent ions give somewhat stronger retention than divalent ions. This effect was first noticed in batch equilibration tests with 8% cross-linked resin in its sodium and calcium forms. The distribution ratio of biphenyl in isopropyl alcohol–water mixtures was almost twice as great for the calcium form of the resin than it was for the sodium form. Column elution tests confirmed this result. A selection from a large number of elution data with different counterions is given in Tables I and II.

Cross-Linking. Table II shows that the higher-cross-linked resin retains hydrocarbons more strongly. The bands were significantly broader with this resin, however. The effective plate height for fluoranthene, for example, was more than 1.5 times as great for the 8% cross-linked resin than for the 4% cross-linked resin with Mg as counterion. For this reason, the 4% cross-linked resin was chosen for more detailed study.

Comparison of Different Resins. The anion-exchange resin, Bio-Rad AG1-X4 37–75 microns, was tested. It retained hydrocarbons roughly twice as strongly as calcium-loaded Aminex 50W-X4, and the chloride form gave slightly stronger retention than the sulfate form. However, the plate height of AG1-X4 was about five times as great as that of 50W-X4.

Cross-linked 2-methyl-5-vinylpyridine resin retained hydrocarbons some four times as strongly as Aminex 50W-X4-Ca, but it, too, gave broad bands with marked reverse tailing.

Solvents. Mixtures containing water and up to 60% of an organic solvent were used. Acetonitrile and methanol gave the narrowest bands, corresponding to their low viscosities. Rel-

Table I. Elution of Phenanthrene from Aminex 50W-X4[a]

Counterion	2-Propanol 25% k′	2-Propanol 25% H	2-Propanol 37.5% k′	2-Propanol 37.5% H	Acetonitrile, 37.5% k′	Acetonitrile, 37.5% H
Na	4.8	...	3.8	1.0	...	...
Ag	...	...	...	...	6.3	0.3
NH_4	5.2	...	4.4	0.7	...	...
Ca	8.6	0.2	7.9	0.7	7.9	0.3
Al	9.1	0.3	7.4	0.8	...	...
Fe(III)	11.1	0.4	8.2	0.5	8.4	0.3
Th	...	...	...	...	9.1	1.3

[a] Flow rate, 24 ml/h; temp. 60 °C; k' = capacity factor; H = effective plate height, mm.

Table II. Comparison of Counterions and Cross-Linking[a]

Resin cross-linking	Counter-ion	k′ for Anthracene	k′ for Fluoranthene	k′ for Pyrene
8%	Mg	1.9	3.4	4.5
	Zn	2.4	...	5.1
4%	Na	0.9	1.8	2.3
	Mg	1.15	2.3	2.9
	Ca	1.3	2.6	3.2

[a] Solvent, 50% CH_3CN by volume; flow rate, 24 ml/h, temp. 55 °C; k' = capacity factor.

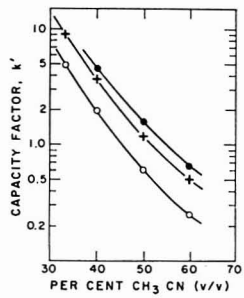

Figure 1. Capacity factor (column distribution ratio) and solvent composition

(+) fluoranthene; (●) pyrene; (○) phenanthrene. Resin, Aminex 50W-X4-Ca. Temp. 65 °C

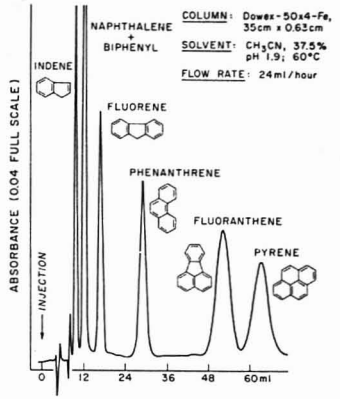

Figure 2. Isocratic elution on Fe-loaded resin

Resin, Aminex 50W-X4-Fe; solvent, acetonitrile, 37.5% (v/v); temp. 60 °C; flow rate, 24 ml/h. Column dimensions, 35 cm × 0.63 cm

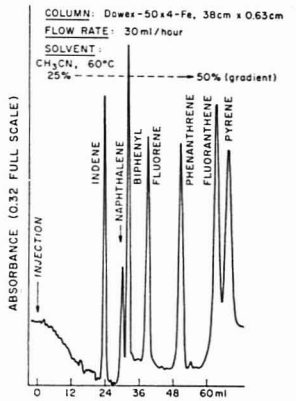

Figure 3. Gradient elution on Fe-loaded resin

Resin, Aminex 50W-X4-Fe; solvent, acetonitrile; gradient, 25% to 50% in 45 min; temp. 60 °C; flow rate, 30 ml/h. Column dimensions, 35 cm × 0.63 cm. Quantities injected (μg): indene 10, naphthalene 17, biphenyl 10, fluorene 7, phenanthrene 4, fluoranthene 24, pyrene 24

ative retention volumes of different hydrocarbons were almost unaffected by the choice of solvent, though we did notice that chlorinated naphthalenes were poorly resolved in isopropyl alcohol–water mixtures, compared to acetonitrile–water mixtures. Chlorinated biphenyls were resolved nearly as well in methanol–water (60% methanol by volume) as in acetonitrile–water (33% acetonitrile). Elution volumes were lower in acetonitrile–water mixtures than in methanol–water mixtures having the same proportion of organic solvent.

Elution volumes increased rapidly with decreasing proportion of organic solvent. Figure 1 shows an almost linear correlation between the logarithm of the corrected elution volume and the proportion of acetonitrile by volume ("50% by volume" means that equal volumes of acetonitrile and water were mixed). This is a common relationship, and shows that the energy of transfer of solute from the solution to a standard state is proportional to the volume fraction of the mixed solvents.

Elution Sequences and Separations. Two extended series of tests were made with the resin Aminex 50W-X4, one with Fe(III) counterions, the other with Ca(II).

Iron-Loaded Resin. With Fe(III), the solvents were made 0.01 M in nitric acid to prevent hydrolysis. A very small leakage of iron from the resin was observed, but it was steady, and stable baselines were obtained with the uv detector. Figures 2 and 3 show chromatograms obtained with this column.

With 20% acetonitrile as solvent, we separated a number of single-ring and two-ring aromatic hydrocarbons. They were eluted in this order: benzene, toluene, ethyl benzene, *ortho*-xylene, *meta*- plus *para*-xylene (not resolved), indene, naphthalene, biphenyl. Naphthalene and biphenyl were well resolved with good baseline separation. Anthracene and phenanthrene were not resolved.

Compounds with larger molecules than pyrene were sepa-

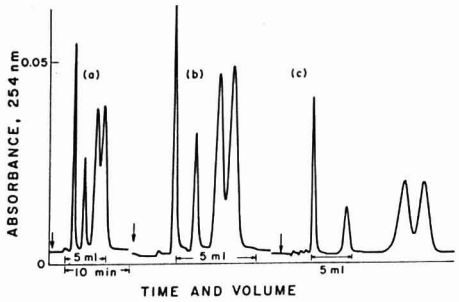

Figure 4. Elution on Ca-loaded resin

Resin, Aminex 50W-X4-Ca; temp. 65 °C; column dimensions, 18 cm × 0.63 cm. Peaks, in order of elution, are: biphenyl, 0.2 μg; phenanthrene, 0.025 μg; fluoranthene, 0.3 μg; pyrene, 0.6 μg. Curves (*a*) and (*b*), 50% acetonitrile (v/v); (*a*) 24 ml/h; (*b*) 12 ml/h. Curve (*c*), 37.5% acetonitrile (v/v), 24 ml/h

Table III. Effects of Chlorine Substitution[a]

Compound	k'	Absorptivity at 254 nm
Biphenyl	1.60	16 500
2-Chlorobiphenyl	1.30	5 400
2,2′-Bichlorobiphenyl	1.03	1 000
4-Chlorobiphenyl	2.00	32 000
4,4′-Bichlorobiphenyl	2.85	36 000
Naphthalene	1.7	...
1-Chloronaphthalene	2.6	...
Anthracene	8.0	10 000
9,10-Dichloroanthracene	15.5	50 000

[a] Resin, Aminex 50W-X4-Ca; solvent, 33% CH_3CN by volume; temp. 65 °C; k' = capacity factor. Molar absorptivities are approximate.

rated with a solvent mixture consisting of acetonitrile, tetrahydrofuran, and water, in ratios 4:1:5 by volume. These elution volumes were found at 55 °C on the same column used for Figures 1 and 2: fluoranthene 17, pyrene 19.5, chrysene 23.5, benzo[*a*]pyrene 29.5, perylene 34 ml. Effective plate heights were 1.5 mm at 24 ml/h, which is to say that the bands for the hydrocarbons beyond pyrene were undesirably broad.

A mixture of biphenyl, 4-bromobiphenyl, and 4,4′-dibromobiphenyl was cleanly separated on a column 18 cm × 0.63 cm, with 37% CH_3CN at 55 °C. Elution volumes were, respectively, 8.0, 10.5, and 14.0 ml. The presence of a halogen atom always increased the elution volume except in the case of 2-substituted biphenyls (see below).

Calcium-Loaded Resin. The advantage of calcium as a counterion, compared with iron, is that it is not hydrolyzed by water and there is no need to acidify the solvent. Retentions and bandwidths are comparable.

Representative chromatograms of a hydrocarbon mixture on a calcium-loaded 4% cross-linked resin are shown in Figure 4. They show the effects of solvent composition and flow rate. With 50% acetonitrile at 12 ml/h, acceptable resolution of biphenyl, phenanthrene, fluoranthene, and pyrene was achieved in 40 min. For fluoranthene, the plate number of the 18-cm column was 1050, and the effective plate number was 750.

A chromatogram of a mixture of chlorinated biphenyls and biphenyl itself appears in Figure 5. It shows that chlorine atoms in the 2 position decrease the retention rather than increasing it. They cause the two phenyl groups to be twisted out of their common plane, and as a result, π-electron overlap is lost and attachment to the aromatic resin polymer is reduced. Another consequence is reduced absorption of ultraviolet light. Where no steric interference occurs, however, the effect of chlorine substitution is to increase the retention by the resin and also to increase the ultraviolet absorption. These effects are seen in Table III.

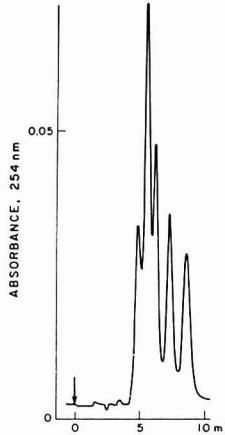

Figure 5. Biphenyl and chlorinated biphenyls

Resin, Aminex 50W-X4-Ca; temp. 65 °C; column dimensions, 18 cm × 0.63 cm; solvent, 33% acetonitrile (v/v); flow rate, 21.5 ml/h. Peaks, in order of elution, are: 2,2′-bichlorobiphenyl, 3 μg; 2-chlorobiphenyl, 1 μg; biphenyl, 0.2 μg; 4-chlorobiphenyl, 0.1 μg; 4,4′-bichlorobiphenyl, 0.1 μg

The 3- and 3,3′-substituted chlorobiphenyls were retained somewhat more strongly than their 4- and 4,4′-isomers.

DISCUSSION

An interesting feature of these results is the effect of the counterion. The stronger absorption found with divalent counterions, compared with univalent, may simply be due to the fact that one doubly-charged ion takes up less space than two singly-charged ions, and leaves more room for absorbed molecules. A more likely explanation is that electrostatic fields within the resin are stronger with doubly-charged ions. Their position of maximum stability is close to one of the singly-charged fixed ions, not midway between two of them. A strong electrostatic field would induce a dipole moment in an aromatic molecule and strengthen its absorption.

Silver ions are known to form π-bonded coordination complexes with aromatic hydrocarbons, but the few tests that we made showed little difference in retention between a silver-loaded and a sodium-loaded resin, probably because water is present and the silver ions are hydrated.

The major cause of the binding of aromatic hydrocarbons by polystyrene resins is, almost certainly, π-electron overlap. The behavior of 2-substituted biphenyls supports this idea.On a column packed with C_{18}-bonded silica, we found that 2-chlorobiphenyl was retained more strongly than biphenyl itself, whereas the reverse was true on the cation-exchange resin.

As to the practical utility of the 4% cross-linked cation-exchange resin for chromatography of these compounds, it would seem that, in most circumstances, a C_{18}-bonded packing would work better. Certainly this is true for molecules having more than four aromatic rings, for the transfer of big molecules in and out of a resin is just too slow. For molecules the size of pyrene and smaller, however, the resin may be a useful alternative. Resolution is as good as on the bonded packing, with

5000 plates per meter and better. Elution peaks on the resin are very symmetrical, even at high loadings, which makes it easy to detect small amounts of closely-eluted impurities. We found, for example, that our high-grade phenanthrene had a small trace of an impurity which eluted 0.6 ml after the phenanthrene peak.

The higher capacity of the resin makes it better for preparative purposes than the bonded packing. Columns of 4% cross-linked resin are easy to pack and to use. Chromatography is slower than on C_{18}-bonded packings, but not much slower, and if running times of 30–60 min are acceptable, resin columns may be of practical value.

LITERATURE CITED

(1) J. Sherma and W. Rieman, *Anal. Chim. Acta*, **20**, 357 (1957).
(2) W. Funasaka, T. Hanai, T. Matsumoto, K. Fujimura, and T. Ando, *J. Chromatogr.*, **88**, 87 (1974).
(3) C. D. Scott, *Sep. Purif. Methods*, **3**, 263 (1974).
(4) W. W. Pitt, R. L. Jolley, and C. D. Scott, *Environ. Sci. Technol.*, **9**, 1068 (1975).
(5) B. B. Wheals, C. G. Vaughan, and M. J. Whitehouse, *J. Chromatogr.*, **106**, 109 (1975).
(6) C. H. Lochmüller and C. W. Amoss, *J. Chromatogr.*, **108**, 85 (1975).
(7) B. Coq, C. Gonnet, and J. L. Rosca, *J. Chromatogr.*, **106**, 249 (1975).
(8) U. A. Th. Brinkman, J. W. F. L. Seetz, and H. G. M. Reymer, *J. Chromatogr.*, **116**, 353 (1976).
(9) W. E. May, S. N. Chesler, S. P. Cram, B. H. Gump, H. S. Hertz, D. P. Enagonio, and S. M. Dyszel, *J. Chromatogr. Sci.*, **13**, 535 (1975).
(10) G. M. Janini, K. Johnston, and W. L. Zielinski, *Anal. Chem.*, **47**, 670 (1975).
(11) P. Larson, E. Murgia, Tong-Jung Hsu, and H. F. Walton, *Anal. Chem.*, **45**, 2306 (1973).
(12) H. F. Walton, *J. Chromatogr.*, **102**, 57 (1974).

RECEIVED for review April 19, 1976. Accepted July 1, 1976. This work is taken in part from the M.A. Thesis of D.M.O. (University of Colorado, 1975). Support is acknowledged from the National Science Foundation grant MPS 73-08592.

Determination of Anhydrotetracyclines in Tetracycline by High-Pressure Liquid Chromatography

Richard F. Lindauer,* David M. Cohen,* and Kevin P. Munnelly*

Pfizer Inc., Quality Control Division, Brooklyn, N.Y. 11206

A method has been developed for determination of (4*S*)-anhydrotetracycline (ATC) and (4*R*)-anhydrotetracycline (EATC) by high-pressure liquid chromatography. The method uses a cation-exchange column and a neutral 0.3 M ethylenediaminetetraacetate buffer. Response is linear and the estimated limits of detection are 12 ng of ATC and 7 ng of EATC. At 429 nm, the recoveries of ATC and EATC added to tetracycline at the 0.6% level were quantitative with relative standard deviations of 0.7% and 1.4%, respectively. Preparation and characterization of a suitable assay standard is described and possible application to other tetracyclines is discussed.

Commercial preparations of the broad-spectrum antibiotic (4*S*)-tetracycline (TC) may develop varying levels of (4*S*)-anhydrotetracycline (ATC) and (4*R*)-anhydrotetracycline (EATC) if stored under adverse conditions—e.g., high temperature and humidity (*1*). Limits for EATC in TC bulks and products have been established by the Food and Drug Administration (*2*). Because ATC and EATC are readily interconverted (*3*), accurate determination of both epimers is desirable. Resolution of ATC and EATC from TC has been achieved by partition chromatography (*1, 2, 4, 5*), gel permeation chromatography (*6*), and gas chromatography (*7*), but these methods were not rapid. High-pressure liquid chromatography (HPLC) with certain reverse-phase systems gave poor resolution of ATC from EATC (*8, 9*). Shorter analysis times and good resolution of ATC, EATC, TC, (4*R*)-tetracycline (ETC), and chlortetracycline have recently been reported by isocratic reverse-phase ion-pair HPLC (*10*) and by gradient-elution reverse-phase HPLC (*11*); however, no evidence was presented to rule out formation of ATC and EATC by partial dehydration of TC and ETC in the highly acidic mobile phases used. Reproducibility data were not given for the ion-pair system, but in the gradient method the relative standard deviation for EATC was only ±6%.

Several ion-exchange HPLC systems with short analysis times and adequate efficiencies for the anhydrotetracyclines nevertheless appeared unsuitable for our purposes since the anhydrotetracyclines eluted on the tail of the main tetracycline peaks (*12*). However, a preliminary cation-exchange HPLC system (*13*) in which k' values for the anhydrotetracyclines were low appeared to be more promising. The latter system, which used a dilute phosphate/ethylenediaminetetraacetate (EDTA) buffer at pH 7 as the mobile phase, was investigated and modified in an effort to develop a suitable assay for ATC and EATC in TC bulks and products. This paper describes both the resulting system and methods of preparing and characterizing a suitable quantitative standard for ATC and EATC.

EXPERIMENTAL

Apparatus. For determinations at wavelengths greater than 260 nm, a Du Pont Model 843 pump module was used in conjunction with a Schoeffel Model SF 770 multiwavelength absorbance detector and a Spectrum Scientific Model 1020 electronic filter (operated at a nominal cutoff frequency of 0.1 Hz). At 254 nm, a Du Pont Model 840 liquid chromatograph was used. Injections were made with a (nominal) 10-μl loop injector valve (Du Pont No. 204590), and all connections were made with either stainless steel or Teflon capillary tubing. The temperature of the column was maintained to within ±0.2 °C by a Varian water jacket (No. 96-000048-00 and No. 37-000324-00) and a Lauda K-2/R circulator. Spectrophotometry was performed on a Cary 14 recording spectrophotometer.

Column. A straight 2.1-mm × 1-m stainless steel column (Du Pont No. 820983903) was thoroughly cleaned with hot detergent solution, rinsed with hot water, hot 30% nitric acid, hot deionized water, and methanol, and dried. Stainless steel column plugs (Du Pont: inlet porosity, 10 μm; outlet porosity, 2 μm) were used, and the column was packed with Zipax SCX (Du Pont No. 820960003) using the modified tap-fill procedure (*14*). A prepacked column of the same dimensions (Du Pont No. 820950002) gave comparable results. Prior to first use, columns were conditioned by elution with 150–200 ml of the mobile phase.

Mobile Phase. The nearly saturated mobile phase may be prepared readily in the following manner. Add 229 g of disodium EDTA dihydrate (Fisher Certified) to 1.8 l. of 0.27 M aqueous sodium hydroxide at 70 °C and stir to dissolve. Filter (1.2-μm membrane, Millipore type RAWP) and cool to room temperature under vacuum (100–150 Torr)

to degas the viscous liquid. Adjust to pH 7.00 with 50% aqueous sodium hydroxide and dilute to 2.00 l.

Qualitative Reference Standards. Tetracycline hydrochloride (USP Reference Standard), chlortetracycline hydrochloride (NF Reference Standard), "anhydrotetracycline hydrochloride" (ATC), and "4-*epi*-anhydrotetracycline hydrochloride" (BP Authentic Specimens) were used directly. Doxycycline hydrochloride, methacycline hydrochloride, and oxytetracycline were internal working standards of Pfizer Inc. (4*R*)-Tetracycline ammonium salt monohydrate was prepared by the method of McCormick et al. (*3*).

Preparation of EATC/ATC Assay Standard. Commercial sources for pure ATC and EATC are virtually nonexistent, and the BP Authentic Specimens are available in extremely limited quantities outside the UK. The following procedure affords an assay standard suitable for simultaneous determination of ATC and EATC.

With vigorous stirring 100 g of bulk tetracycline hydrochloride was added during 1 min to 1.0 l. of 2 N hydrochloric acid at 80 °C. Precipitation from the clear red-orange solution began within 5 min, and the suspension was cooled to room temperature. The precipitate was isolated by filtration and dried under vacuum (40 °C, 12 Torr), affording 97 g of crude anhydrotetracycline hydrochloride consisting mainly of the (4*S*)-epimer (HPLC analysis).

A solution of 130 g of crude product in 2.6 l. of 5% aqueous acetic acid was maintained at 75–80 °C for 75 min, cooled to ~10 °C during the next 50 min, and added to 500 ml of cold 12 N hydrochloric acid. The precipitate was filtered, air-dried, and freed from insoluble matter by methanol extraction in a Soxhlet apparatus. The solvent was removed in vacuo and the solid was finely ground. Drying for 4 h at 55 °C (<1 Torr) yielded 107 g of the standard mixture of EATC and ATC as the hydrochlorides.

Characterization of the Assay Standard. Inasmuch as neither the bulk purities nor the epimer ratios are specified by the BP, neither Authentic Specimen is suitable as a direct quantitative standard. Accordingly, the composition of the mixed assay standard described above had to be determined indirectly. HPLC analysis at 254 nm detected no components other than ATC and EATC, each of which exhibited the same retention volume and bandwidth shown by the appropriate Authentic Specimen. The bulk purity of the EATC/ATC standard was determined in quadruplicate by potentiometric titration in acetic acid containing 0.6% mercuric acetate, the titrant being 0.05 N perchloric acid in glacial acetic acid; the mean value ± the standard deviation s was 97.8 ± 0.3% as the hydrochlorides. Upon heating, the EATC/ATC standard was epimerically stable for >5 h at 115 °C (HPLC analysis). The volatile content of the standard mixture was determined in quadruplicate by heating under vacuum for 2 h at 80 °C: the mean value ± s was 2.1 ± 0.1%.

Because suitable quantitative standards were not available, the molar ratio ρ of ATC to EATC was determined by two alternative methods in order to increase the reliability of the values. Each method depends on the observation that epimerization of tetracycline at C-4 is reversible and catalyzed by buffers such as acetate (*3*). Since each epimer has a characteristic molar absorptivity ϵ under a given set of conditions, the molar absorptivity ϵ' of a mixture of ATC and EATC under the same conditions will be given by:

$$\epsilon' = \frac{\rho'\epsilon_a}{1+\rho'} + \frac{\epsilon_e}{1+\rho'} \quad (1)$$

where the subscripts a and e refer to ATC and EATC, respectively. In dilute hydrochloric acid, the values of ϵ_e (*15*) at the longwave maximum (~7×10^3 at 427 nm) and at the shortwave minimum (~15×10^3 at 238 nm) are similar to the corresponding values for ϵ_a, i.e., ~7×10^3 at 432 nm and ~16×10^3 at 237 nm (*16*). As a result, 430 nm and 237 nm may be taken as quasi-isosbestic points, at which ϵ' will be relatively insensitive to ρ'. Therefore, the ratio of the total anhydrotetracycline concentrations in two separate EATC/ATC mixtures can be determined quite accurately without knowing the individual concentrations if the mixtures are allowed to epimerize under the same conditions until $\rho'_1 \simeq \rho'_2$ and if the absorbances are then measured at one of the "isosbestic" points. In order to minimize systematic errors in the comparison study, spectrophotometry was performed at 430 nm in the partition method and at 237 nm in the HPLC method, peak areas being measured at 254 nm; however, 275 nm or 429 nm would be preferable for routine HPLC area measurements.

HPLC Method. If an aliquot of an EATC/ATC solution is analyzed by HPLC (vide infra) and the area A of each peak is determined, ρ for the mixture is given by:

$$\rho = \frac{A_a\beta_e}{A_e\beta_a} = \frac{R_A}{R_\beta} \quad (2)$$

where β_a and β_e are the individual detector response factors (peak area per μg injected), the response ratio R_β is β_a/β_e, and the area ratio R_A is A_a/A_e.

An iterative procedure using arbitrary mixtures of ATC and EATC was used to calculate R_β. Two stock solutions (No. 1 and 2) were prepared so that $R_{A1} \simeq 6$ and $R_{A2} \simeq 0.12$. The ratio C_1/C_2 of the total anhydrotetracycline concentrations C in the two stock solutions was determined by epimerization in hot acetic acid (vide infra) and spectrophotometry at 237 nm. A mixed solution (No. 3) prepared from equal volumes of the two stock solutions exhibited area ratio R_{A3}. Initially, it was assumed that $R_\beta = 1$, giving $\rho_1 = R_{A1}$ and $\rho_2 = R_{A2}$; ρ_3 was calculated by straightforward algebraic manipulation of C_1/C_2, ρ_1, and ρ_2. Since $R_\beta = R_{A3}/\rho_3$, a revised value of R_β could be calculated and used to improve ρ_1 and ρ_2; iteration was continued until successive values of R_β agreed to within 0.001. Two separate determinations of R_β gave 1.074 and 1.088 at 254 nm.

Using the mean value for R_β, quadruplicate determinations of R_A for the EATC/ATC standard gave $\rho = 0.942 \pm 0.005$ for the mean ± s.

Partition Method. A slurry of 20 g of acid-washed diatomaceous earth (*4*), 95 ml of 0.1 M EDTA (adjusted to pH 7.8 with ammonia), and 5 ml of glycerin was dried to a free-flowing powder at 105 °C. For each determination, ~2 mg of EATC/ATC standard was applied to the top of a short column (12-mm i.d.) containing a lightly tamped 5-cm bed of the EDTA-impregnated powder. ATC was eluted with methylene chloride, and then EATC was eluted with 5% acetic acid in methylene chloride. The two fractions were heated to dryness, dissolved in 25 ml of 5% aqueous acetic acid, heated at 75–80 °C for 100 min to ensure equilibration, cooled, and diluted to 50 ml with 5% aqueous acetic acid. Spectrophotometry at 430 nm afforded the ratio of absorbances for the two fractions and, hence, ρ for the EATC/ATC standard. Determination in quadruplicate gave $\rho = 0.941 \pm 0.023$ for the mean ± s.

Of the two procedures, the HPLC method is preferred because of its greater precision and speed, once R_β has been determined. From the combined analytical data, the EATC/ATC standard was assigned values of 48.5% ATC hydrochloride and 51.4% EATC hydrochloride when dried for 2 h at 80 °C under vacuum.

Procedure. With the column temperature at 35 °C and the flow rate at 0.5 ml/min (inlet pressure ~700 psig), allow the baseline to stabilize with the detector at ~0.2 AUFS (275 nm) or ~0.08 AUFS (429 nm). On the day of use, prepare a 0.32-mg/ml solution of the EATC/ATC standard in 0.1 N aqueous sodium hydroxide; store at 0–10 °C to stabilize the epimer ratio. Analyze the standard solution. Prepare a 16-mg/ml solution of tetracycline base or hydrochloride in 0.1 N or 0.2 N aqueous sodium hydroxide, respectively; analyze the sample solution within 1 h of preparation. Reanalyze the standard solution. For each anhydrotetracycline epimer, use the sample signal and the average standard signal in the calculations.

Table I. Effect of Temperature on System Performance for EATC and ATC

Temperature, °C	Capacity factor k'		Plate height H, mm	
	EATC	ATC	EATC	ATC
25.0	1.18	2.77	8.5	12.0
27.5	1.08	2.45	7.2	11.2
30.0	0.95	2.17	6.4	9.4
32.5	0.86	1.90	5.3	8.7
35.0	0.79	1.72	4.8	7.5

RESULTS AND DISCUSSION

Optimization for ATC and EATC. Because TC is unstable at either low or high pH (*3*), the mobile phase was maintained at a nominal value of pH 7.00 during the optimization studies. The usual formulas (*16*) for capacity factor k', separation factor α, resolution R_s, effective plate number N_{eff}, and plate height H were used in the evaluations, and limits of detection LD were estimated as twice the peak-to-peak noise level.

Chromatographic Conditions. Increasing the EDTA concentration from 0.005 M to 0.3 M decreased k' for EATC, ATC, and ETC, increased α for each epimeric pair, and substantially improved baseline stability at 254 nm. With 0.3 M EDTA flowing at an arbitrary rate of 0.9 ml/min, increasing

Table II. Linear Regression of Assay Response on Analate Concentration for EATC and ATC[a,b]

Wavelength, nm	Analate	Regression coefficients: Slope	Regression coefficients: Intercept	Standard error of estimate, s_{yx}	Correlation coefficient, r
254	EATC	0.982	0.034	0.050	0.998
254	ATC	0.985	0.003	0.016	1.000
275	EATC	0.991	0.018	0.019	1.000
275	ATC	0.998	−0.005	0.012	1.000
429	EATC	0.996	0.013	0.008	1.000
429	ATC	1.002	−0.014	0.012	1.000

[a] Two determinations for each analate at solution concentrations of 0.016, 0.05, 0.11, 0.16, and 0.32 mg/ml as the hydrochlorides. At the specified assay concentration, these would be equivalent to 0.01, 0.03, 0.07, 1.0, and 2.0% of analate in a hypothetical tetracycline bulk. [b] Amount found = slope × amount added + intercept, values expressed as absolute percentage of analate in a hypothetical tetracycline bulk.

the column temperature in the range 25–35 °C had no significant effect on the resolution of EATC and ATC ($R_s \simeq 1.29$) but decreased k' and H markedly for both epimers (Table I). However, at 50 °C overall column performance was notably poorer, and 35 °C was chosen as the best compromise. Since column efficiency and, hence, peak height per μg injected vary with temperature, the column should be operated isothermally. For accurate determination by peak height, maintaining constant flow was also found to be important; decreasing the flow rate in the range 1.12–0.35 ml/min increased N_{eff} for EATC from 37 to 87.

Sample Preparation. Increasing the amount of TC injected up to 250 μg did not significantly increase the assay time (~30 min at 0.5 ml/min) as indicated by return to baseline, although TC did begin to elute sooner as a result of the column being overloaded for TC. For adequate sensitivity without interference to the ATC peak, tetracycline (hydrochloride) samples were prepared at a concentration of 16 mg/ml in 0.1 N (0.2 N) aqueous sodium hydroxide. TC and ETC are known (*15, 16*) to undergo irreversible dehydrations readily under acidic conditions, forming ATC and EATC, respectively. Use of the alkaline solvent would be expected to minimize both anhydrotetracycline formation and interconversion of ATC and EATC (*3*) prior to analysis. In fact, at 5 °C the standard solution of ATC and EATC in 0.1 N sodium hydroxide is stable for at least 10 h.

Detection Wavelength. In the mobile phase ATC and EATC exhibit absorption maxima at 269 and 430 nm and at 268 and 428 nm, respectively. Since the absorptivities were roughly three times higher at the ultraviolet maxima, detection was expected to be more sensitive at 269 nm than at 429 nm. However, background absorbance from the mobile phase increases rapidly below 270 nm. The Du Pont unit used in the original studies operated only at 254 nm, and, as a result, the baseline was quite sensitive to flow variations and changes in the mobile phase composition due to injection of the alkaline solutions. The Schoeffel unit was unable to compensate for the high background absorbance below 260 nm. Baseline stability and short-term noise improved dramatically as the wavelength was increased to 285 nm, but response to ATC and EATC decreased at wavelengths greater than ~269 nm.

Selection of an analytical wavelength will depend on a variety of factors including the availability of suitable detectors and the presence of interfering substances in complex TC samples. In our hands, detection at 275 nm afforded the best compromise between noise and sensitivity. Commercial detectors operating at 280 nm would probably give adequate results for bulk TC samples. However, TC and many of the excipients commonly found in TC dosage forms—e.g., ascorbic acid, ethyl maltol, procaine or propyl paraben—absorb strongly only in the ultraviolet. Detection at the visible maxima for ATC and EATC, although less sensitive than at 275 nm, would increase the selectivity for anhydrotetracycline determination in such samples. Thus, 429 nm is the wavelength of choice for general use in determination of the anhydrotetracyclines.

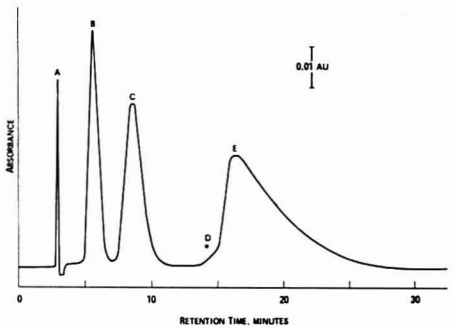

Figure 1. Chromatogram of tetracycline hydrochloride containing 0.6% (4*R*)-anhydrotetracycline and ~0.75% (4*S*)-anhydrotetracycline, detection at 429 nm

(A) Solvent peak; (B) (4*R*)-anhydrotetracycline; (C) (4*S*)-anhydrotetracycline; (D) (4*R*)-tetracycline; (E) tetracycline

Linearity and Accuracy for ATC and EATC. Preliminary studies of detector response at 254 nm showed comparable results either by peak height or by peak area. Accordingly, linearity of response by peak height was investigated at 254, 275, and 429 nm using ATC and EATC solutions in the concentration range 0–0.32 mg/ml; these would be equivalent to 0–2% of each epimer in a hypothetical tetracycline hydrochloride sample solution at 16 mg/ml. Two determinations were made at each of five concentrations, and the data were analyzed by linear regression (Table II). The correlation coefficients r were excellent at each of the three wavelengths, but comparison of the standard errors of estimate s_{yx} and the regression coefficients showed that 429 nm gave the best results. As expected from the spectral data, *LD* for either ATC (0.012 μg) or EATC (0.007 μg) was lower at 275 nm than at 429 nm (0.04 μg or 0.02 μg, respectively).

Following the procedure outlined in the Experimental, a sample of tetracycline hydrochloride was analyzed before and after having been spiked with 0.6% each of ATC and EATC (Table III). A typical chromatogram of the spiked sample (Figure 1) illustrates both the efficiency of the separation and the selectivity for ATC and EATC afforded by detection at 429 nm. The average recoveries ± s were 99.4 ± 0.7% for ATC and 101.0 ± 1.4% for EATC; neither average was statistically significantly different from 100% at the 95% confidence level (t-test).

Other Tetracyclines. In order to more fully evaluate the capabilities of the system, k' was determined for several

Table III. Analysis[a] of Tetracycline Hydrochloride[b] Spiked with 0.6% EATC[c] and 0.6% ATC[c]

	Spike Recovered, %	
Replicate No.	EATC	ATC
1	100.6	99.7
2	98.9	98.2
3	101.0	99.5
4	102.1	100.0
5	102.4	99.4
Mean ± stand dev	101.0 ± 1.4	99.4 ± 0.7

[a] Detector at 429 nm, flow at 0.5 ml/min, column temperature at 35.0 °C. [b] Quadruplicate analysis of the unspiked sample gave 0.146 ± 0.004% ATC hydrochloride and 0.007 ± 0.002% EATC hydrochloride. [c] As the hydrochlorides.

common tetracyclines using solutions of 0.5 mg/ml in order to avoid overloading the column. Detection at 359 nm afforded maximum sensitivity to TC with minimum response to either ATC or EATC. Methacycline ($k' = 0.87$), oxytetracycline ($k' = 1.39$), and doxycycline ($k' = 1.95$) were well separated from TC ($k' = 7.3$). ETC ($k' = 4.7$) exhibited adequate resolution from TC ($R_s = 1.0$) and was completely eluted before the TC maximum was reached. Chlortetracycline ($k' = 5.8$) was separated but not well resolved from TC ($R_s = 0.4$).

Potential usefulness as an assay for ETC and/or TC was also investigated. Both TC and ETC are slowly degraded in aqueous alkali (*3*), but solutions of either one in 0.01 N sodium hydroxide are suitable if analyzed within 5 min of preparation. For both ETC and TC, peak heights were determined once at each of five concentrations in the range 0.1–0.8 mg/ml, and the data were analyzed by linear regression using the 0.8 mg/ml solution as the standard. Each epimer showed excellent linearity ($r = 1.000$), the concentrations found (mg/ml) being given by the equations $y = 1.003\,x - 0.003$ (ETC) and $y = 1.004\,x - 0.003$ (TC); *LD* values were 0.06 μg and 0.07 μg, respectively. However, TC begins to elute slightly before the ETC maximum is reached, and low-level determination of ETC in TC would be somewhat inaccurate. Nevertheless, excellent quantitative results should be possible for TC with little or no modification of the HPLC system.

ACKNOWLEDGMENT

We wish to acknowledge the contribution of J. E. Wolleben, who carried out two of the linearity studies.

LITERATURE CITED

(1) V. C. Walton, M. R. Howlett, and G. B. Selzer, *J. Pharm. Sci.*, **59**, 1160 (1970).
(2) 21 CFR 436.309, *Fed. Regist.*, **39**, 18965 (1974).
(3) J. R. D. McCormick, S. M. Fox, L. L. Smith, B. A. Bitler, J. Reichenthal, V. E. Origoni, W. H. Muller, R. Winterbottom, and A. P. Doerschuk, *J. Am. Chem. Soc.*, **79**, 2849 (1957).
(4) R. G. Kelly, *J. Pharm. Sci.*, **53**, 1551 (1964).
(5) W. W. Fike and N. W. Brake, *J. Pharm. Sci.*, **61**, 615 (1972).
(6) B. W. Griffiths, R. Brunet, and L. Greenberg, *Can. J. Pharm. Sci.*, **5**, 101 (1970).
(7) K. Tsuji and J. H. Robertson, *Anal. Chem.*, **45**, 2136 (1973).
(8) "Application Highlights", No. 25, Waters Associates, Framingham, Mass.
(9) K. Tsuji, J. H. Robertson, and W. F. Beyer, *Anal. Chem.*, **46**, 539 (1974).
(10) J. H. Knox and J. Jurand, *J. Chromatogr.*, **110**, 103 (1975).
(11) K. Tsuji and J. H. Robertson, *J. Pharm. Sci.*, **65**, 400 (1976).
(12) A. G. Butterfield, D. W. Hughes, N. J. Pound, and W. L. Wilson, *Antimicrob. Agents Chemother.*, **4**, 11 (1973).
(13) C. Manning, Alza Corp., Palo Alto, Calif., personal communication, 1972.
(14) J. J. Kirkland, *J. Chromatogr. Sci.*, **10**, 129 (1972).
(15) B. Hoener, T. D. Sokoloski, L. A. Mitscher, and L. Malspeis, *J. Pharm. Sci.*, **63**, 1901 (1974).
(16) K. D. Schlecht and C. W. Frank, *J. Pharm. Sci.*, **64**, 352 (1975).
(17) L. R. Snyder and J. J. Kirkland, "Introduction to Modern Liquid Chromatography", John Wiley and Sons, New York, N.Y., 1974.

RECEIVED for review January 22, 1976. Accepted June 21, 1976.

Separation and Quantitation of Diazonium Salts as Heptanesulfonate Ion Pairs by High Pressure Liquid Chromatography

Edward Fitzgerald

GAF Corporation, 25 Ozalid Road, Johnson City, N.Y. 13790

Quantitative analysis of diazonium salts in formulations is important for the quality control of diazo reprographic products. Quantitative separations of several diazonium salts were obtained by reverse phase high pressure liquid chromatography of the heptanesulfonate ion pairs. Chromatography was performed with an octadecyl bonded phase column and a buffer–acetonitrile eluent using a uv detector. The precision was 0.2% standard deviation with good least squares linearity (0.9988 coefficient of determination) over a range of 0.07 to 0.14% diazonium salt. The chromatographic system provides good routine in-process quality control of diazonium salts and couplers in reprographic formulations.

Separation and analysis of diazonium sensitizers in reprographic formulations requires an efficient chromatographic system, especially in formulations containing more than one diazonium salt. Reverse phase high pressure liquid chromatography on octadecyl bonded phase columns has been reported to perform good separations for a variety of compounds (*1, 2*). This type of column yielded a good separation for a mixture of typical diazonium salts except for the formation of two peaks for one of the salts. This effect was not reproducible and was particularly troublesome in quantitative analysis of the diazonium salt. Reverse phase chromatography of organic ions paired with heptanesulfonate has been recently reported (*3*), and it was believed that this ion would form one peak with the diazonium ion in question. One reproducible peak was obtained using the heptanesulfonate permitting good separation and quantitation.

EXPERIMENTAL

Reagents. Acetonitrile was purchased from Burdick and Jackson,

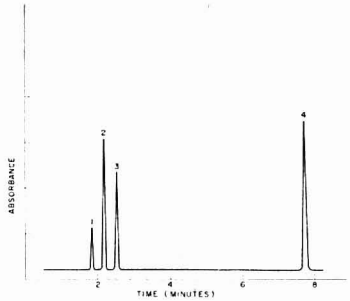

Figure 1. Separation of diazonium salts with acetonitrile–buffer eluent on μBondapak C-18

Peaks (1, 2), *p*-*N*,*N*-diethylaminobenzenediazonium chloride; (3), 3-methyl-4-pyrrolidinylbenzenediazonium chloride; (4), 2,5-di-*n*-butoxy-4-morpholinobenzenediazonium chloride

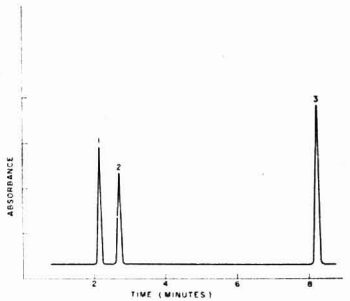

Figure 2. Separation of diazonium salts in acetonitrile–buffer with heptanesulfonate added

Peak (1), *p*-*N*-*N*-diethylaminobenzenediazonium chloride; (2), 3-methyl-4-pyrrolidinylbenzenediazonium chloride, (3) 2,5-di-*n*-butoxy-4-morpholinobenzenediazonium chloride

Muskegon, Mich. The diazonium salts were commercial sensitizers supplied by Philip Hunt and ABM Chemicals Ltd. and recrystallized several times.

Apparatus. Chromatography was performed on a Waters C-900 3000 PSI pumping system with a Valco CV-6-HPAX sampling valve and a Waters Model 440 ultraviolet detector. The column was a Waters 30 cm × 5 mm μBondapak C-18 column. Chromatograms were integrated with a Spectra Physics Minigrator.

Procedure. One-percent solutions of the diazonium salts were made up in water and stabilized with 1% citric acid. They were diluted 5:50 in acetonitrile along with a 10% toluene internal standard diluted 2:50 and injected in the 10-μl sample loop.

The buffer consisted of 2.5% potassium phosphate monobasic with phosphoric acid added to obtain a PH of 3.

RESULTS AND DISCUSSION

2,5-Di-*n*-butoxy-4-morpholinobenzenediazonium chloride, ½ (zinc chloride) and 3-methyl-4-pyrrolidinylbenzenediazonium chloride, ½ (zinc chloride) yielded sharp quantitative peaks on the octadecyl column using 45 acetonitrile–55 aqueous PH3 buffer as eluent at a flow rate of 1.3 ml/min. However, *p*-*N*,*N*-diethylaminobenzenediazonium chloride, ½ (zinc chloride) yielded two peaks, as in Figure 1. Addition of 0.005 M heptanesulfonic acid to the buffer–acetonitrile eluent resulted in one sharp peak, as in Figure 2. The precision was 0.2% standard deviation with good least squares linearity (0.9988 coefficient of determination) over a range of 0.07 to 0.14% diazonium salt after dilution. The quantitative data were obtained by area ratio of the peak to the toluene internal standard.

CONCLUSIONS

The diazonium ion probably exists as an ion pair in this system and the double peak of the *p*-*N*,*N*-diethylaminobenzenediazonium salt may be the result of ion pairs with two anions. Formation of the heptanesulfonate ion pair resulted in one peak. The retention time of the last salt, which was well retained, was increased significantly when heptanesulfonate was added as expected, but the first two salts which elute rapidly were not significantly more retained as heptanesulfonates.

This system is also useful for separation of diazonium salts and couplers in reprographic formulations. The degree of quantitation is excellent for quality control application.

LITERATURE CITED

(1) R. F. Borch, *Anal. Chem.*, **47**, 2437 (1975).
(2) M. Dong, D. Locke, and E. Ferrand, *Anal. Chem.*, **48**, 368 (1976).
(3) D. P. Wittmer, N. O. Nuessle, and W. G. Haney, *Anal. Chem.*, **47**, 1422 (1975).

RECEIVED for review May 19, 1976. Accepted July 6, 1976.

Analysis of Solid Materials by Laser Probe Mass Spectrometry

R. A. Bingham

AEI Scientific Apparatus Ltd., Barton Dock Road, Urmston, Manchester, England

P. L. Salter*

Department of Applied Physics, University of Hull, Hull, Yorkshire, England

Three types of laser have been examined as sources of ion production for trace element analysis of solid materials by mass spectrometry. Comparison is made between the lasers and with the conventional rf spark source. Their analytical qualities and potential are discussed for the examination of both conducting and nonconducting materials.

The conventional means of ionizing solid materials for the analysis of trace elements in mass spectrometry is by the radio-frequency spark (*1*). The laser has an appeal as a competitor because of its inert nature and because it provides the possibility of examining small regions of single specimens without the need for special preparation. In the case of the

Table I. Pulsed Laser Parameters

	CO_2 gas	Ruby	NdYAG
Pulse length, ns	>100	20	15
Energy, mJ	300	10	10
Q-switched	...	Dye—Vanadyl phthalocyanine	Pockells cell
Wavelength, μm	10.6	0.6943	1.06
Pulse repetition rate	Up to 1 Hz	10 s per pulse (max)	Up to 50 Hz
Mode	Multimode	Single TEM_{00}	Single TEM_{00}
Pulse reproducibility	...	±15%	±5%

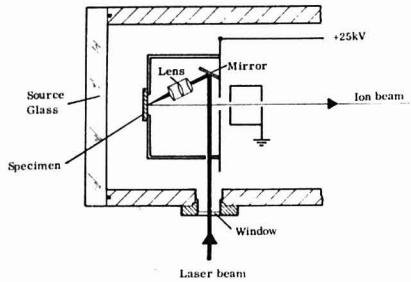

Figure 1. Mass spectrometer source arrangement

spark source, a pair of electrodes must be prepared which are electrically conducting. This can present problems for both solid and powder samples. For solids, the surfaces can be contaminated from handling or from chemical reagents used for etching and cleaning the surfaces. In the case of nonconducting powders, these have to be mixed with a high purity conducting powder, usually graphite, silver, or aluminum. This has two detrimental effects. First, the material for examination is atomically diluted by a function of the weight mix and the atomic weights of the two materials involved, thus reducing analysis sensitivity. Second, any trace elements in the conducting powder will limit the analysis sensitivity of these elements in the sample. The use of the laser as a means of ionizing the material overcomes these problems as the specimen may be examined directly and in many cases without any preparation. The electrical conductivity of the sample has little influence on ion production.

INSTRUMENTAL

In a previous paper (*2*), we have demonstrated the quantitative analytical capability of the ruby laser for solid materials and shown that it provides not only a microanalytical surface technique because of its small beam diameter capability but also offers the possibilities of both bulk and surface analysis with a focused or defocused beam. In this paper, we report on work carried out using three types of high power pulsed laser source; CO_2, ruby, and NdYAG; and we compare these with the conventional spark source. We have not used any secondary ionizing process in our work but have extracted ions directly from the laser-produced plasma into an AEI MS7 type double-focusing mass spectrometer. This instrument is of the Mattauch-Herzog design normally used with the spark source which is capable of coping with the large ion energy spread produced by the spark and it was expected to be more than adequate for the anticipated energy spread from ions of a laser plasma.

We have concluded that the ideal laser for materials analysis is a pulsed laser operated in the Q-switched mode. With a Q-switched laser, a high intensity short duration pulse interacts with the sample. Material is removed early in the pulse and the energy of the pulse is used in the efficient ionization of the evaporated material (*3*). A highly ionized plasma is produced which expands away from the sample surface. The use of a high intensity short duration pulse is advantageous for the following reasons. If the pulse length is long, the plasma temperature increases and so do the ionization states resulting in large numbers of multiply charged ions. Also, since the plasma lifetime is long, radiation from the plasma can cause local evaporation around the crater which can boil out volatile elements. Furthermore, a low laser power density ($<10^8$W cm^{-2}) can be shown to discriminate against higher boiling point elements to the advantage of the volatile elements.

Our work has been carried out mainly in the power density range 10^9–10^{11} W cm^{-2} and, at these high fluxes, the laser is found to be nonselective for a wide range of elements.

EXPERIMENTAL

Figure 1 is a schematic layout of the mass spectrometer source housing and shows how it has been modified for the ruby and NdYAG laser systems. The specimen is mounted with its plane normal to the mass spectrometer and the laser beam is passed through a window in the wall of the chamber, reflected from a mirror through a lens system to strike the specimen surface at an angle of approximately 45°. Both the lens and the specimen positions can be adjusted from outside the vacuum chamber to give control of the position of the specimen and focus of the beam. Generally, the focal point of the laser beam is arranged to coincide with the specimen surface in line with the optical axis of the mass spectrometer but this is not critical. As will be explained in more detail later, the experimental arrangement was slightly different when the CO_2 laser was used as at the wavelength of its radiation (λ = 10.6 μm) germanium optical components were necessary. A viewing system incorporating a microscope is also fitted to the source chamber and provides a large field of view of the region to be examined. The area for analysis is selected using a He–Ne C.W. laser which is aligned along the same optical path as the pulsed laser. This method of alignment is found to be quite accurate for selecting small regions for analysis. Crater diameters down to 20 μm have been obtained with the ruby and NdYAG laser systems.

All results reported in this paper have been recorded on Ilford Q2 photoplates. These are ideal detectors for experimental work as they can detect all isotopes over the mass range 6–240 simultaneously with the MS7 and enable the effects on all types of ion species to be observed. Photoplates do not have the sensitivity of electrical detection techniques but are much more useful for overall assessment purposes.

All three lasers used in the experiments produced large pulses of ions (of the order of several amperes) and it was necessary to support the accelerating voltage (25 kV) with capacitors. Shielding was necessary to screen the plasma from earthed parts of the source chamber to avoid accelerating voltage collapse which would reduce ion transmission through the mass spectrometer. Space charge problems were also experienced in the ion beam within the mass spectrometer and this was overcome by closing the object slit of the mass spectrometer (S3) down to 10-μm width. The resolving power thus obtained with all three lasers was similar to that of the spark source.

Details of the parameters of the three lasers are given in Table I.

CO_2 Laser. The laser used was a CO_2 solid cathode Transversely Excited Atmospheric gas laser. This type of laser has been described by Pearson and Lamberton (*4*). The main discharge occurred across two parallel electrodes with edges shaped to a Rogowski profile. Initial ionization is produced by field emission from a fine trigger wire which runs parallel to the two electrodes. Field emission induces a sheet

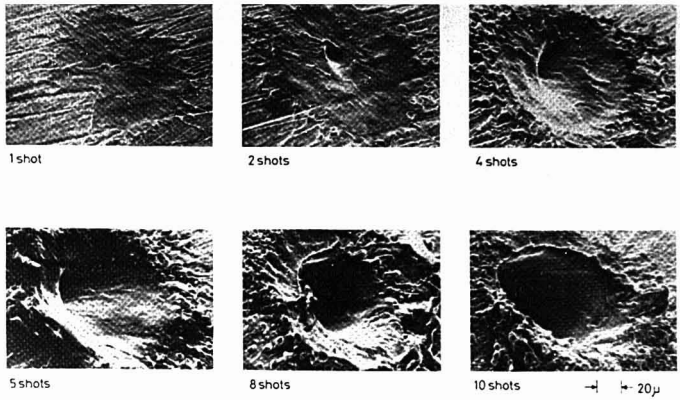

Figure 2. Ruby laser craters

Table II. Ruby Laser Power Density

Focused spot diameter μm	Power, density, W cm^{-2}
500	10^8
160	10^9
50	10^{10}
20	10^{11}

discharge across the whole length of the electrodes. The laser was a sealed unit having a discharge length of 28 cm. This meant that no control over the output mode structure was possible. The multimode output of the laser had a peak pulse of about 300 mJ. The pulse shape as observed using a photon drag detector has a fairly narrow initial peak (half width 100 ns) and a long tail of between 1 and 4 μs.

A considerable amount of energy occurred in the tail of the pulse. The laser was not Q-switched but the maximum power density in the initial peak of the pulse was of the order of 10^9 W cm^{-2}. As was noted earlier, it was necessary to use germanium optical components to transmit the radiation (λ = 10.6 μm) into the mass spectrometer source. The radiation was focused using a 1.5-in. (3.8-cm) focal length germanium lens and the crater sizes obtained were approximately 300 μm in diameter (on mild steel). Typical crater depths were 10 μm. Because of the multimode output of the laser, the intensity distribution across the focused beam was not uniform and "hot spots" or lobes occurred. The effects of these could be observed in the craters produced.

Visual element sensitivity on the photoplate was 2000 ppm atomic per laser shot from materials such as steel and was obtained from a crater 300 μ in diameter and 10 μm deep. By repeating a series of shots, all superimposed on the same spectrum, a higher sensitivity is obtained. Thus, 1000 shots produced sensitivity of 2 ppm and with a pulse repetition rate of 1 Hz the 1000 pulses took 16 min to record.

Using the CO_2 laser under these conditions, volatile elements were found to be preferentially emitted and some substances, such as copper, were low in ion production. This could be expected as copper is known to be highly reflective to the longer wavelengths.

Semiquantitative analysis could be carried out but the relative sensitivity factors of the elements covered a wide range. These aspects will be discussed later. The large amounts of material removed showed an ionization efficiency of about 1% despite there being several levels of multiply charged ion species present in the spectra.

Ruby Laser. Some of the work carried out with the ruby laser has been reported in a previous paper (*2*). In this paper we will present further results and highlight its differences with the other laser sources. The NdYAG and ruby laser are found to be very similar in most respects and their parameters are given in Table I. The ruby laser had a low pulse repetition rate of 1 pulse every 10 s and gave a photoplate sensitivity of 1000 ppm per shot. So to fire 300 shots (the largest number recorded) in order to reach a visual photoplate sensitivity of 3 ppm required a time of 50 min.

The reproducibility of the pulse output was estimated to be ±15% using a photodiode measuring system. The amount of material evaporated, for the same element sensitivity was considerably lower with the ruby laser than with the CO_2 laser. This is to be expected for a Q-switched laser (*3*). A single laser pulse on mild steel evaporated about 10^{-8} g of steel compared with 6×10^{-7} g with the CO_2 laser.

NdYAG Laser. This was a commercial laser system which had a pulse repetition rate which could be controlled over the range from single pulses to 50 Hz. This feature provided several advantages over the other lasers. The major advantage was the greater speed of analysis, but it also offers the possibility of using electrical detection methods for either spectrum scanning or peak switching. With the higher pulse repetition rate, it was possible to use the ion monitor signal on the MS7 as a measure of transmission, and it was reasonably steady at repetition rates above 20 Hz. This stable signal made it much easier to tune the mass spectrometer for optimum transmission.

A single shot from the NdYAG laser gave a visual sensitivity on the photoplate of 1000 ppm and the spectra showed good quantitative features.

The power density at the specimen surface is a function of the focus conditions for a fixed pulse energy, and Table II gives an indication of the levels used in these experiments. Most work has been carried out in the power density range 10^9–10^{11} W cm^{-2}. Latest work has shown that pulses of about 10^{14} ions are produced in each laser pulse and the ionization efficiency measured approaches 100%.

Crater dimensions can be varied over the range 20–300 μm diameter with depths of 5 μm at 20 μm diameter in steel down to 0.5 μm at 300 μm. Figure 2 shows a set of six electron microscope photographs of the ruby laser craters produced by increasing numbers of laser shots on steel.

The laser beam is incident at an angle of 45° to the steel surface and was "in focus" on the surface.

The output of both the ruby and NdYAG lasers is single mode. The beam intensity profile is Gaussian and, therefore, the highest power density occurs in the center of the laser produced crater. The power density falls off at the edges of the beam and consequently there is a region around the rim of the crater where only melting occurs. Material which is explosively removed from the center of the crater also re-solidifies around the edge of the crater. This is seen in the electron microscope photographs shown in Figure 2. The outer region produced by melting can be reduced by using an aperture in the laser beam. This is illustrated in Figure 3 which shows a single shot ruby crater in steel. The outer molten region has been almost completely eliminated. No detectable reduction in ion pulse intensity was noticed using this technique and it tended to confirm our observations that few ions are produced from the outer regions of the crater.

It is not important for specimen surfaces to be flat. We have examined such things as irregular fractured rock surfaces selecting individual mineral grains with little loss in ion signal; but if the angle between the specimen and the optical axis of the mass spectrometer is large, then ion extraction does suffer. This aspect and also the small probe size enables very small specimens to be examined either embedded in some other bulk material or mounted on the end of a pin or rod.

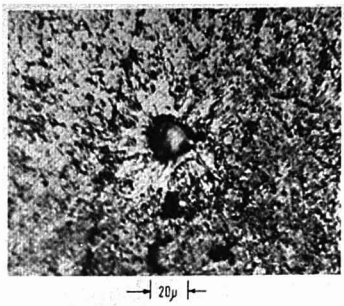

Figure 3. Single shot ruby laser crater in steel

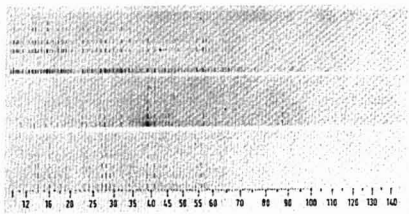

Figure 4. Rock specimen of slate

With the ruby and NdYAG lasers, ion extraction is just as efficient with electrically nonconducting as with conducting materials. Substances such as glass produce ion pulses of the same magnitude as metallic samples, and no problems are encountered due to surface charging as found in other probe techniques. We have also examined solid organic materials directly although the lasers rapidly dig deep holes.

We have obtained good spectra from rubber and have examined plastics, wood, walnuts, and other similar substances. We have only detected carbon and oxygen in these fairly pure organic materials. This feature could open up new fields of application in the mass spectrometry of organic solids.

Sensitivity of element detection is achieved by superimposing several laser pulses on one spectrum. A single ruby or NdYAG laser shot has a sensitivity of 1000 ppm and in the case of steel this removes 10^{-8} g of material. We have found this relationship to be linear up to the maximum number of shots recorded of 300 pulses for the ruby laser. Using the NdYAG system with a well focused beam over a large number of shots, the ion signal falls as the crater deepens because of the angle between the laser beam and specimen surface with respect to the optical axis of the mass spectrometer. As the crater deepens, the ions expand back along the laser beam. With a defocused beam, this effect is reduced; and extrapolating from our figures for a single shot of 1 pulse removing 10^{-8} g for 1000-ppm detection level, one may expect that at 50 Hz then 10^5 pulses would remove 1 mg to give a sensitivity of 0.01 ppm in 33 min. These figures are similar to that currently achieved by the spark source for the same exercise. In practice, it is unlikely to compare as favorably because of the cratering effects previously discussed, but could certainly compete on shorter less sensitive analyses.

Although electrical detection techniques have not yet been employed for analysis of the laser ion beams, a higher instantaneous sensitivity for individual elements could be obtained giving up to a factor 10^3 gain and providing a detection limit of about 1 ppm for a single shot. With a repetition rate of 30–50 Hz, the spectrum could be scanned over a large mass range or selected elements peak switched in a similar manner to that currently used with the spark source and with detection limits of the same order (0.1 ppm scanning; 0.01 ppm peak switching).

RESULTS AND DISCUSSION

The spectra obtained with the laser sources are not as complex as the spark source, and the resolving power is similar

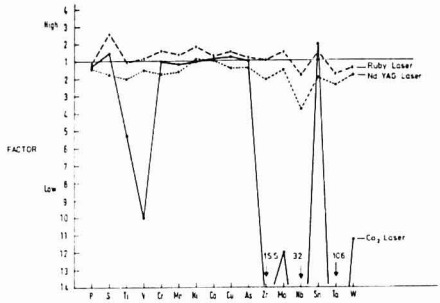

Figure 5. Laser sensitivity of elements relative to matrix-steel

giving around 3000 at mass 60 (50% peak height definition) under present conditions. Multiply charged ions are present in the laser spectra but are at lower levels than the spark.

Figure 4 shows spectra over the mass range 10–150 obtained from a specimen of slate using spark, CO_2, and ruby laser ion sources. Each set of spectra are from a separate photoplate, each recorded in steps 1–3–10, etc. The spark spectra have been recorded as charge over the range 0.01–3 nC, the CO_2 laser spectra over the range 1–1000 shots, and the ruby laser 1–300 shots.

The dispersions of the three sets of spectra are not quite the same and so have been lined up at m/e 40. It can be seen that the spark spectra are rich in lines at the lower mass range because of multiply charged ions compared with those of the lasers. For example, the doubly charged ion species ^{39}K and ^{41}K found at m/e 19.5 and m/e 20.5 are very much less dense in the laser spectra than the spark. Molecular species have rarely been found in the laser spectra, even in such complex substances as this rock indicating the high energy processes taking place in the plasma.

Slate is a good example of a nonconducting complex mineral mixture and demonstrates well the differences between these sources. The major elements are oxygen, silicon, aluminum, and potassium with smaller amounts of magnesium, sulfur and iron. An interesting feature of these spectra is that the small probe size of the ruby laser has picked out a small crystal of iron pyrite (FeS). The second spectrum (3 shots) of the ruby series shows strong ^{56}Fe and ^{32}S compared with their absence in the single- and ten-shot spectra. The crystal must have weighed less than 3×10^{-8} g and been of the order of a 20-μm cube in size. The CO_2 laser and spark sources cover a much larger surface area and are unable to discriminate to such small dimensions.

The CO_2 laser spectra show the typical thermal effects on element selectivity of the more volatile elements as can be seen for potassium (m/e 39/41), rubidium (m/e 85/87) and cesium (m/e 133). They are grossly enhanced in comparison with the spark and ruby spectra and can be attributed to the lower peak power density and long tail of the laser pulse.

The problem of element sensitivity (normally termed the relative sensitivity factor) is a measure of the sensitivity of an element with respect to the matrix element(s). For example, a volatile element such as sodium in aluminum could show a high value of sodium with respect to the aluminum, whereas an element like tungsten could appear unexpectedly low. The relative sensitivity factors for a range of elements in a steel standard have been measured for the CO_2, ruby, and NdYAG lasers and are shown in Figure 5. To retain linearity of comparison the measurements below unity are reciprocals of the value Calculated Value/Nominal Value used to obtain the factors. It can be seen that the relative sensitivity factors for

Table III. Visual Analysis of NBS Steel Standard 467 with the MS7/NdYAG Laser (ppm weight)

Element	Concentrations	
	Given	Calculated
Pb	6	11
W	2000	2300
Ta	2300	970
Sn	1000	1260
Mo	210	350
Nb	2900	1660
Zr	940	490
Ag	40	116
As	1400	1340
Ge	30	77
Cu	670	1030
Ni	880	1580
Co	740	1050
Mn	2800	2950
Cr	360	460
V	410	460
Ti	2600	5150
S	100	57
B	2	0.7

Table IV. Visual Analysis of Johnson-Matthey Copper Standard CAO with the MS7/NdYAG Laser (ppm weight)

Element	Concentration	
	Given	Calculated
Bi	500	326
Pb	400	323
Sb	500	381
Sn	480	276
Ag	470	338
Ga	350	387
Cr	220	120

the ruby and NdYAG lasers are close to unity. They are very similar to each other and to those obtained for the spark source. However the CO_2 laser shows poor sensitivity for the high boiling point elements, particularly niobium and tantalum where the latter is over a factor of 100 down.

High relative sensitivity factors are not serious if they are constant, and can be quantitative. But if they are due to thermal processes wich are dependent on a plasma temperature which can vary, then they cannot form the basis for a quantitative technique. In this respect, the CO_2 system tested is not such a suitable analytical source as the ruby and NdYAG systems.

In order to assess the analytical capabilities of the technique we have analyzed several well known standard materials. Table III shows the results obtained by visual photoplate analysis of NBS standard 467 using the NdYAG laser. The series of spectra were recorded over the range 0.01–3 nC charge as measured at the monitor of the mass spectrometer. This gives a measure of the ions passing through the instrument and is the conventional method of recording spectra with the spark source.

The concentrations were calculated using an estimated photoplate sensitivity obtained from the matrix isotope ^{58}Fe. No element correction factors were used. Despite the fact that the analysis was made visually, which gives an accuracy of the order of ±50% with the line extinction method, it can be seen that the elemental sensitivities vary over at most a factor 3.

Table V. Visual Analysis of NBS Glass Standard 611 with the MS7/NdYAG Laser (ppm atomic)

Element	Concentration	
	Given	Calculated
U	117	80
Th	119	60
Pb	124	120
Ag	142	200
Sr	354	200
Rb	298	300
Zn	407	400
Cu	418	600
Ni	468	1000
Co	398	400
Fe	492	600
Mn	531	600
Ti	548	1000
K	712	1000
B	1920	600

Table VI. Visual Analysis of Steel Standard NBS 464 with the MS7/CO_2 Laser (ppm atomic)

Element	Concentration	
	Given	Calculated
Pb	54	<4
W	67	<6
Ta	213	<2
Sn	204	180
Ag	16	<4
Nb	223	12
Mo	166	<20
Zr	62	<4
As	134	200
Ge	12	25
Cu	823	500
Co	266	300
Ni	1280	1200
Mn	13200	3000
Cr	840	600
V	3240	400
Ti	47	15
S	350	400
P	307	300
B	255	200

By using element correction factors and microdensitometry of the lines, this accuracy should be improved.

Table IV gives the analysis figures obtained from a Johnson-Matthey copper standard CAO using the NdYAG laser and recorded in the same way as with the steel analysis. The photoplate sensitivity taken was that estimated from the steel analysis and no element correction factors were made.

Table V shows the visual analysis of a nonconducting material, NBS glass standard 611 with the NdYAG laser. The specimen was in the form of a solid disc and the laser fired directly onto the surface. The series of spectra were again recorded over the range 0.01–3 nC charge and plate sensitivity taken from the steel analysis. No element correction factors were used and it can be seen that the accuracy of the results is similar to those of the metallic samples.

Analysis figures obtained with the ruby laser for the same materials have been reported in a previous paper (2), and are very similar in accuracy to those with the NdYAG laser. Table VI gives the analysis results for NBS steel standard 464 using

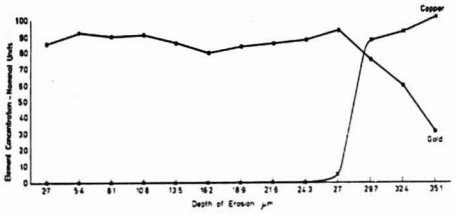

Figure 6. Layer analysis of gold plated brass

the CO_2 laser and shows again the poor comparison and lack of sensitivity for many of the elements.

The results of these and other standard samples examined show that the laser is capable of semiquantitative analysis of many types of materials without a similar type of standard as a comparison.

The reproducibility of element analysis for single laser shot spectra has been measured to be ±20% with the ruby laser which compares favorably with a variation of ±15% in the peak power energy. For the NdYAG laser, reproducibility of analysis was <10% for single shots compared with the manufacturers quoted peak power reproducibility of ±5%. It would be expected that the reproducibility of multiple shot spectra would limit at that of the photoplate emulsion (about ±4%).

In the results we have presented, we have not attempted to demonstrate that the laser source is or can be superior in accuracy to the spark source. This would involve considerably more work to be carried out than has so far been undertaken in these preliminary experiments. First, longer exposures of spectra would be required to be able to densitometer the lines (the human eye is far more sensitive in the detection of a weak line than a photometer) and many more standards would need to be run to determine accurate relative sensitivity factors. Using these methods, there is no reason to doubt that the laser could analyze to an accuracy at present attained by the spark source of about ±10% using photoplates. Electrical detection could improve this further due to its higher sensitivity and more precise measuring capability.

We have so far discussed the use of laser probes mainly from their semiquantitative analysis capability but it must be remembered that the amount of material removed to achieve this accuracy is small. By defocusing the beam, thinner layers can be removed down to approximately 0.2 μm per shot, [Eloy et al. (*5, 6*)]. To demonstrate this, we have examined a specimen of brass sheet, which has a gold layer on the surface, with the ruby laser. The beam diameter was adjusted to 200 μm and the erosion rate of the gold surface was measured to be 0.9 μm per shot. A series of spectra were recorded each spectrum being composed of three laser shots.

Figure 6 shows densitometer measurements of the gold and copper as the laser eroded into the material. It can be seen from the curves that the interface is about 27 μm deep and, by examination of the specimen cross section by microscope, the mean gold depth was measured to be 29 μm.

Each recorded spectrum of three shots gave an element sensitivity of 300 ppm and so all elements present in the layer removed for each spectrum could be detected down to this level. The distribution of elements through surface layers could be measured using this method.

Conversely by focusing the laser to a fine focus, spatial analysis can be obtained across the specimen surface. Line scans or area mapping can be obtained by recording a series of spectra across the area of interest and the photoplate will record all elements above 1000 ppm simultaneously for a single shot. More than one shot in each position will increase the sensitivity according to the number of shots. By using electrical detection, individual elements could be monitored to much lower detection levels and the surface analysis method would be analogous to that undertaken at present by the ion probe.

Solution analysis could be carried out by evaporating the liquid on a flat surface of polythene. With a defocused laser beam, the surface deposit would be analyzed along with some of the polythene but this would only contribute carbon and oxygen lines (assuming high purity material) because of the low molecular formations of the laser source. Higher element sensitivity would be obtained than with the spark source because the liquid deposit would not require mixing with graphite as previously discussed. A moving tape with one or several deposits on the surface could be run through the ion source providing on-line analysis. The laser also offers the possibility of multiple sample loading in the source chamber. This is difficult with the spark source as two small electrodes have to be carefully aligned with each other and the optical axis of the mass spectrometer, and there is thus a danger of contamination from sputtered material. However, with a single specimen which only requires moving into a fixed position for analysis it should be possible to design a source chamber capable of holding several specimens at one loading and to move each one into the analysis position in turn. This would speed up the analysis cycle by saving on the pumping time normally necessary between each sample.

CONCLUSIONS

The laser can now take its place as an analytical source in mass spectrometry for the examination of solid materials. It has been shown to be capable of providing semiquantitative analysis on different types of materials and can produce spectra from unusual specimens such as organic substances. It is yet to be seen if the latter can provide meaningful analytical results.

The laser source competes directly with the conventional spark source in all respects and offers the further advantages of surface analysis, analysis of nonconducting materials, minimal sample preparation, negligible molecular contributions, and simple spectra.

ACKNOWLEDGMENT

The authors wish to note their appreciation to those who loaned laser equipment for these experiments. The CO_2 laser was supplied by GEC-Elliott Automation, Borehamwood, London, England; the ruby laser was supplied by the University of Hull, Hull, England; and the NdYAG laser was supplied by J. K. Lasers, Rugby, England. The authors also acknowledge the keen interest in the work shown by S. A. Ramsden and G. J. Pert of the Department of Applied Physics, The University of Hull.

LITERATURE CITED

(1) A. J. Ahearn, "Mass Spectrometric Analysis of Solids", Elsevier, Amsterdam, 1966, p 5.
(2) R. A. Bingham and P. L. Salter, *Int. J. Mass Spectrom. Ion Phys.*, to be published.
(3) J. F. Ready, "Effects of High Power Laser Radiation", Academic Press, New York; Library of Congress Catalog Card No. 77-137597.
(4) P. R. Pearson and H. M. Lamberton, IEEE/USA, Conference on Laser Engineering and Applications, Washington, D.C. June 2–4, 1971, *IEEE J. Quantum Mechanics*, Special Conference Issue.
(5) J. F. Eloy and J. L. Dumas, *Methods Phys. Anal.*, **2**, 251, (1966).
(6) J. F. Eloy, *Methods Phys. Anal.*, **5**, 157 (1969).

RECEIVED for review February 26, 1975. Accepted April 19, 1976. One of the authors (PLS) acknowledges the receipt of a Science Research Council C.A.S.E. studentship during the period in which this work was carried out and is based on work supported in part by A.W.R.E., Procurement Executive, Ministry of Defence.

Concentration Instabilities in Liquid Chromatography

John C. Helmer

Varian Instrument Division, Palo Alto, Calif. 94303

Chromatography with mixed solvents may produce concentration oscillations when the viscosity of the mixture varies with the concentrations of the liquid components. The characteristics of the oscillation depend on the solvent system. Two kinds of solvent systems have been identified, depending on whether the solvents are water based or non-associating. A mathematical model is derived which describes the experimentally observed oscillations in a dual-pump gradient system. Systems may be stabilized by several methods. These include using larger mixers, using a circuit design which utilizes the limited frequency response of the column, using a constant pressure valve, and using pressure derivative feedback on the liquid flow rates.

High sensitivity in high pressure liquid chromatography (HPLC) requires a pulseless, constant flow rate from the solvent delivery system. Problems in pulse damping on systems employing reciprocating pumps of small volume (less than 1 ml) have led to the design of constant flow syringe pumps of larger volume (e.g. 250 ml) (for example, the System 8500 HPLC, Varian Aerograph, Walnut Creek, Calif.) As used in gradient elution, two syringe pumps containing different solvents are connected to a mixer, such that the volume flow rate out of the mixer is constant, while the concentration varies according to a predetermined schedule. The mixer is connected to a chromatographic column whose resistance to flow depends on the viscosity of the liquid stream. When solvents of different viscosity are mixed, it is evident that the column resistance will vary with concentration of the mixture. This effect, coupled to the compressibility of the reservoirs, has been identified as the probable cause of oscillations occasionally observed in using water–methanol gradients, (*1*, *2*).

The effect of fluid compressibility on isocratic (single solvent) HPLC has been previously treated by M. Martin et al. (*3*), and will not be discussed in this paper.

SINGLE RESERVOIR MODEL

Imagine a situation in which two fluids, 1 and 2, are mixed and passed through a column, as in Figure 1. Fluid 2 is incompressible and is delivered to the mixer at a constant flow rate. Fluid 1 is compressible in its reservoir, and the reservoir fluid is replaced at a constant rate by a pump at its inlet. Fluid 2 is more viscous than 1, and 2's concentration after mixing is 90% by volume.

The mechanism of instability is as follows. Suppose the pressure across the column drops slightly. This will allow fluid 1 to expand out of the reservoir to increase the concentration of 1 relative to 2. This produces a *decrease* in viscosity of the mixture which can further lower the pressure across the column. The process may be cumulative and the composition of the mixture may refuse to stabilize at the 90% 2, 10% 1 setpoint. The form taken by the concentration–pressure fluctuations depends on the fluid circuit parameters which will be analyzed.

The water–methanol instability is one in which 2 is methanol and 1 is water, except the viscosity *increases* as the percent of water increases. In this case, the concentration oscillation exists as a wave traveling down the line between the mixer and the column. If there is 180° phase change in the oscillation, between mixer and column, then the column will see a reduced viscosity as the viscosity is increasing at the output of the mixer. Then the condition that the pressure decrease as the concentration of water increases (at the output of the mixer) will be satisfied. In this case, it is the time delay between mixer and the column which is the primary frequency determining element of the fluid circuit.

In the following sections, we analyze the elements of the fluid circuit. We put these elements together in a mathematical model and derive the characteristics of the oscillation. We examine the conditions for stability and present experimental evidence in support of the theory.

MODELING THE CIRCUIT ELEMENTS

Syringe Pump. Figure 2 shows a syringe pump. We suppose the pump is full and the piston is traveling inward with velocity v. The volume V is a function of the length L of the cylinder, and the fluid density ρ is a function of the pressure P. Thus the mass flow rate out of the pump is given by

$$\frac{dM}{dt} = -\frac{d}{dt}(\rho V) = -\rho\frac{\partial V}{\partial L}\frac{dL}{dt} - V\frac{\partial \rho}{\partial P}\frac{dP}{dt} \qquad (1)$$

We have $\partial V/\partial L = A$ = cross section area, $dL/dt = -v$, and $\partial\rho/\partial P = k\rho_0$, where k is the compressibility of the fluid and ρ_0 is its density. Thus Equation 1 becomes

$$\frac{dM}{dt} = \rho A v - \rho_0 k V\frac{dP}{dt} \qquad (2)$$

The volume flow rate is given by

$$Q = \frac{1}{\rho}\frac{dM}{dt} = Av - \frac{\rho_0}{\rho}kV\frac{dP}{dt} \qquad (3)$$

For small fluctuations, it is sufficient to set $\rho = \rho_0$. Also $Av \equiv Q_0$ = equilibrium flow rate, and Equation 3 becomes

$$Q = Q_0 - kV\frac{dP}{dt} \qquad (4)$$

Equation 4 shows that the flow rate out of the pump is influenced by pressure changes, due to the compressibility k of the liquid and the volume V of the reservoir.

Although V is reduced in time due to the motion of the piston, we make the approximation that the change in V is negligible over a period of oscillation. In the oscillation analysis, V is taken to be constant, and, from this viewpoint, the syringe pump appears as a reservoir of constant volume connected to a pump which forces liquid through it at rate Q_0 as in Figure 1.

Mixer. If two pumps containing different solvents are connected to a mixer of volume V_m, as in Figure 3, how does the output concentration change with pressure? Solvents 1 and 2 are input to the mixer at rates $Q_1(t)$ and $Q_2(t)$, respectively. Mixing is instantaneous. Let c be the concentration of Solvent 1 in the mixer. This is defined as the volume in the mixer of Solvent 1, divided by the volume of the mixer. We do not know c, but we can calculate its change Δc in an interval Δt. In the derivative limit, this is given by

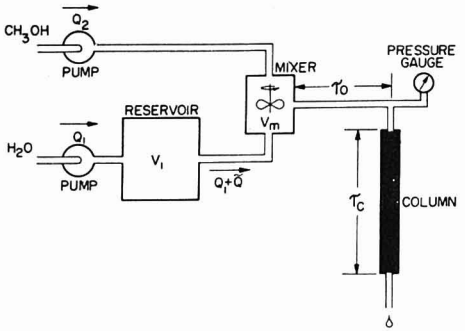

Figure 1. Model LC oscillator with single reservoir

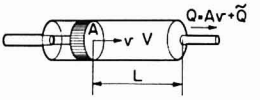

Figure 2. Model of a syringe pump

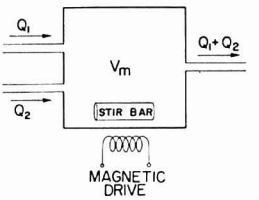

Figure 3. Model of a fluid mixer

$$\frac{dc}{dt} = \frac{Q_1 - c(Q_1 + Q_2)}{V_m} \tag{5}$$

Each parameter is given an equilibrium value x plus a variable value $\tilde{x}$. Thus

$$Q_1 = Q_{10} + \tilde{Q}_1, \quad Q_2 = Q_{20} + \tilde{Q}_2, \quad Q_{10} + Q_{20} = Q_0$$

$$c = c_1 + \tilde{c}, \quad c_1 = \frac{Q_{10}}{Q_{10} + Q_{20}} \tag{6}$$

When Equation 5 is expanded to first order in the variable quantities, we obtain

$$\frac{d\tilde{c}}{dt} + \frac{\tilde{c}}{\tau_m} = \frac{\tilde{Q}_1 c_2 - \tilde{Q}_2 c_1}{V_m} = \frac{\tilde{c}_0}{\tau_m} \tag{7}$$

where $\tau_m = V_m/Q_0$ is the volume exchange time of the mixer and $c_2 = 1 - c_1$. In Equation 7 we find that

$$\tilde{c}_0 = \frac{\tilde{Q}_1 c_2 - \tilde{Q}_2 c_1}{Q_0} \tag{8}$$

is the concentration variation produced by a mixer of zero volume, $V_m = 0$.

Roughly speaking, an analysis of Equation 7 shows that, at time t, the mixer outputs a concentration which is an average of all concentrations entering it in the time interval $t - \tau_m$ to t. The response to a delta function input is an exponential $\exp(-t/\tau_m)$, and the response to a general input $\tilde{c}_0(t)$ is

$$\tilde{c}(t) = \int_{\tau=-\infty}^{t} \tilde{c}_0(\tau) \exp\left(\frac{\tau - t}{\tau_m}\right) \frac{d\tau}{\tau_m} \tag{9}$$

Double input ports for Q_1 and Q_2 are not conceptually necessary, and a single port is sufficient to input the concentration function $\tilde{c}_0(t)$, previously generated by a mixer of zero volume.

If the mixer is driven by two syringe pumps of volumes V_1 and V_2, such that $\tilde{c}_0$ arises from the expansion of these reservoirs during pressure changes, then $\tilde{Q}_1$ and $\tilde{Q}_2$ are obtained from equations of the form of Equation 4. Thus

$$\tilde{Q}_1 = -k_1 V_1 \frac{d\tilde{P}}{dt} \tag{10}$$

$$\tilde{Q}_2 = -k_2 V_2 \frac{d\tilde{P}}{dt} \tag{11}$$

where k_1 and k_2 are the compressibilities of the two solvents, and $\tilde{P}$ is the pressure variation. Then from Equation 8, we obtain,

$$\tilde{c}_0 = -\frac{k_1 V_1 c_2 - k_2 V_2 c_1}{Q_0} \cdot \frac{d\tilde{P}}{dt} \tag{12}$$

Column. The pressure across the column varies because of changes in flow rate and changes in concentration of the mixed fluid passing through it.

$$\tilde{P} = \tilde{Q}\frac{\partial P}{\partial Q} + \tilde{c}\frac{\partial P}{\partial c} = \tilde{Q}R_d + Q_0\tilde{R} \tag{13}$$

The term $R_d = \partial P/\partial Q$ is the differential column resistance. $\tilde{R}$ is the variation in column resistance due to changes in concentration $\tilde{c}$. If $R_0 = P_0/Q_0$ is the equilibrium column resistance, we have from Equation 13

$$\tilde{R} = R_0 \left(\frac{1}{P_0}\frac{\partial P}{\partial c}\right)_{Q=\text{const.}} \tilde{c} = R_0 b\tilde{c}, \quad b \equiv (1/P_0)\partial P/\partial c \tag{14}$$

The constant b is a critical parameter, since the fluid system can be unstable if $|b| > 1$. The value of b depends on the operating point on the curve of pressure vs. concentration.

In the glass bead columns used in the experimental part of this work (Bio Glas–1500 Å, 40-μ particles), the resistance to flow rate is constant, $R_d = R_0$, and we will assume that this condition holds.

Equation 14 will be used when changes in $\tilde{c}$ are slow enough in comparison to the void volume exchange time of the column, that $\tilde{c}$ is approximately uniform throughout the column. In general it is necessary to assume that $\tilde{c} = \tilde{c}(t - x/v)$, where v is the fluid velocity and x is a position along the length of the column. If the column is homogenous, which we assume, then b is constant along its length. Then the variation in column resistance is given by

$$\tilde{R} = R_0 b \int_0^L \tilde{c}\left(t - \frac{x}{v}\right)\frac{dx}{L} = R_0 b \int_{t-\tau_c}^{t} \tilde{c}(\tau)\frac{d\tau}{\tau_c} \tag{15}$$

where $\tilde{c}(t)$ is the concentration variation at the entrance to the column, L is the column length, and τ_c is the column void volume exchange time.

If $\tilde{c}$ is a steady state oscillation represented by $\tilde{c} = \exp j\omega(t - x/v)$, then from Equation 15, we have

$$\tilde{R} = R_0 b \left(\frac{\sin \omega\tau_c/2}{\omega\tau_c/2}\right) \exp j\omega(t - \tau_c/2) \tag{16}$$

We conclude that with steady-state oscillations, a distributed column is equivalent to a point resistance with the following properties. The resistor is located downstream from the column entrance by a time equal to $\tau_c/2$, and the effective value of b is reduced by the factor $(\sin \omega\tau_c/2)/\omega\tau_c/2)$. We note that $\omega/2\pi = 1/\tau_c$ is the cutoff frequency for the column response to variations in concentration.

Length of Tubing. We assume that as a circuit element a length of tubing is represented by a simple delay time τ_0 equivalent to its volume exchange time. Thus if the concentration entering the tube is $\exp j\omega t$, the concentration leaving is $\exp j\omega(t - \tau_0)$. This assumption implies that plug flow exists in the tube.

The parameter τ_0 is very useful in the interpretation of experimental observations. However, some degree of laminar flow must exist, depending on the tube diameter and wall finish. In relation to the present subject, the concentration transfer equations for laminar flow are somewhat intractable and, in any case, they do not seem to be necessary for interpretation of the oscillations.

SYSTEM ANALYSIS

Pressure is uniform throughout the system preceding the column, and it varies at the column according to Equation 13, with $\bar{R}$ given by Equation 15. If $c(t)$ is the concentration output of the mixer, and there is a delay time τ_0 between mixer and column, then the concentration input to the column is $c(t - \tau_0)$. Thus the pressure variation is given from Equations 13 and 15 by

$$\bar{P} = \bar{Q}R_d + P_0 b \int_{t-\tau_c}^{t} c(\tau - \tau_0)\frac{d\tau}{\tau_c} \tag{17}$$

$P_0 = R_0 Q_0$ is the equilibrium condition, and we set $R_d = R_0$. From Equations 10 and 11, we have

$$\bar{Q} = \bar{Q}_1 + \bar{Q}_2 = -(k_1 V_1 + k_2 V_2)\frac{d\bar{P}}{dt} \tag{18}$$

When Equation 18 goes into Equation 17, we recognize the system time constant

$$T = R_0(k_1 V_1 + k_2 V_2) \tag{19}$$

so the general form of Equation 17 is

$$\bar{P} = -T\frac{d\bar{P}}{dt} + P_0 b \int_{t-\tau_c}^{t} \bar{c}(\tau - \tau_0)\frac{d\tau}{\tau_c} \tag{20}$$

At the output of the mixer, $\bar{c}(t)$ is given by

$$\frac{d\bar{c}}{dt} + \frac{\bar{c}}{\tau_m} = \frac{\bar{c}_0}{\tau_m} \tag{21}$$

and from Equations 12 and 19, we obtain

$$\bar{c}_0 = -\left(\frac{k_1 V_1 c_2 - k_2 V_2 c_1}{k_1 V_1 + k_2 V_2}\right)\frac{T}{P_0}\frac{d\bar{P}}{dt} \tag{22}$$

Equation 22 shows that expansion of the fluid in the reservoirs produces no change in concentration if

$$k_1 V_1 c_2 = k_2 V_2 c_1 \tag{23}$$

This condition will stabilize the system against oscillations, but it is too restrictive on the operating conditions to be of practical use in chromatography.

If $V_2 = 0$ in Equation 22, it reduces to a form representative of the single reservoir system shown in Figure 1.

$$\bar{c}_0 = -\frac{c_2 T}{P_0}\frac{d\bar{P}}{dt} \tag{24}$$

We will use this form because, without loss of generality, c_2 may also be employed to designate the general term,

$$c_2 \rightarrow \frac{k_1 V_1 c_2 - k_2 V_2 c_1}{k_1 V_1 + k_2 V_2} \tag{25}$$

Equations 20, 21, and 24 provide a complete system of equations which may be solved to obtain the transient response of the system.

Analysis by Exponential Functions. We anticipate a solution of the form $\exp(pt)$, where $p = \alpha + j\omega$, with α being the growth constant and ω the angular frequency. Thus, the previous variables are represented by a set of complex amplitudes s, c, and c_0, such that

$$\frac{\bar{P}}{P_0} = Re(se^{pt}), \quad \bar{c} = Re(ce^{pt}), \quad \bar{c}_0 = Re(c_0 e^{pt}) \tag{26}$$

The term Re means "real part of." When Equations 26 are substituted into Equations 20, 21, and 24, we obtain

$$s = -pTs + bce^{-p\tau_0}\int_{-\tau_c}^{0} e^{p\tau}\frac{d\tau}{\tau_c} \tag{27}$$

$$c = \frac{c_0}{1 + p\tau_m}, \quad c_0 = -c_2 pTs \tag{28}$$

When Equation 28 goes into Equation 27, we obtain an equation which may be solved for p,

$$-\frac{1}{pT} = 1 + \frac{bc_2 e^{-p\tau_0}}{1 + p\tau_m}\left(\frac{1 - e^{-p\tau_c}}{p\tau_c}\right) \tag{29}$$

This general equation includes the mixer-to-column time delay τ_0, the mixer integration time τ_m, the column volume exchange time τ_c, and the system time constant T. Special cases will now be examined.

General Solution to 1st Order in α. Equation 29 may be rewritten

$$0 = (1 + p\tau_m)\left(1 + \frac{1}{pT}\right) + bc_2 e^{-p\tau_0}\left(\frac{1 - e^{-p\tau_c}}{p\tau_c}\right) \tag{30}$$

If we set $p = j\omega$ and solve for ω, we get the steady-state oscillation frequency together with the required value of bc_2 such that $\alpha = 0$. To include the attenuation rate α, we expand each p function in Equation 30 about $p = j\omega$ to first order in α. If for $\alpha = 0$, each function is represented by an amplitude and a phase, then α introduces a real expression which changes the amplitude and an imaginary expression which changes the phase. Thus, we obtain the following quantities.

Time delay:

$$e^{-p\tau_0} = (1 - \alpha\tau_0)e^{-j\theta_0} \tag{31}$$

where $\theta_0 = \omega\tau_0$.

Mixer: Let $A_m = \sqrt{1 + \omega^2\tau_m^2}$, $\tan\theta_m = \omega\tau_m$, then

$$1 + p\tau_m = (A_m + \alpha\tau_m\cos\theta_m) \times \exp j\left(\theta_m - \frac{\alpha\tau_m}{A_m}\sin\theta_m\right) \tag{32}$$

Reservoir: Let $A_r = \sqrt{1 + 1/(\omega^2 T^2)}$, $\tan\theta_r = 1/\omega T$, then

$$1 + \frac{1}{pT} = \left(A_r + \frac{\alpha\cos\theta_r}{\omega^2 T}\right)\exp j\left(-\theta_r + \frac{\alpha\sin\theta_r}{\omega^2 T A_r}\right) \tag{33}$$

Column: Let $A_c = (\sin\theta_c/2)/(\theta_c/2)$, $\theta_c = \omega\tau_c$, then

$$\frac{1 - e^{-p\tau_c}}{p\tau_c} = \left(A_c - \frac{\alpha}{\omega}\sin\theta_c/2\right) \times \exp j\left(\frac{-\theta_c}{2} + \frac{\alpha}{\omega} - \frac{\alpha\cos\theta_c/2}{\omega A_c}\right) \tag{34}$$

On substituting Equations 31–34 into Equation 30, it is required that the phases sum to give zero or a multiple of π, if they are combined in the same exponent.

$$n\pi = \theta_0 + \frac{\theta_c}{2} + \theta_m - \theta_r + \alpha\left(\frac{-\tau_m\sin\theta_m}{A_m} + \frac{\sin\theta_r}{A_r\omega^2 T} - \frac{1}{\omega} + \frac{\cos\theta_c/2}{A_c\omega}\right) \tag{35}$$

where $n = 0, 1, 2, 3 \ldots$

The α term in Equation 35 represents a small correction to the steady-state phase condition. This correction is of no particular interest. Taking $\alpha = 0$, we write $\tan(\theta_0 + \theta_c/2 - n\pi)$

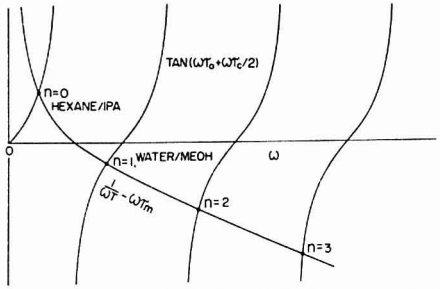

Figure 4. Graphical solution for the oscillation frequency ω, at $\alpha = 0$

$= \tan(\theta_r - \theta_m)$, from Equation 35. Thus, the steady-state frequency of oscillation is given by

$$\tan(\omega\tau_0 + \omega\tau_c/2) = \frac{(1/\omega T) - \omega\tau_m}{1 + \tau_m/T} \tag{36}$$

Equation 36 has an infinite number of solutions for ω, and the graphical solution is indicated in Fig. 4. The even-order roots, $n = 0, 2, 4, \ldots$ require that bc_2 be a negative quantity, whereas the odd-order roots, $n = 1, 3, 5, \ldots$ require that bc_2 be positive, as shown below. These two sets of solutions correspond to the two types of solvent mixtures, e.g., hexane-isopropanol (negative b) and water-methanol (positive b).

There are two special cases of interest, because these are the oscillations which have been observed. These are the $n = 0$ (negative b) and $n = 1$ (positive b) modes. The $n = 0$ mode gives very low frequency oscillations involving the system time constant T. For $\omega\tau_0 + \omega\tau_c/2 < 1$ and $\tau_m/T \ll 1$, Equation 36 gives the solution

$$\omega = \left(\frac{1}{T(\tau_0 + \tau_m + \tau_c/2)}\right)^{1/2} \tag{37}$$

The $n = 1$ mode may be observed under the conditions $\omega T \gg 1$, $\omega\tau_m < 1$; such that from Equation 35

$$\omega(\tau_0 + \tau_m + \tau_c/2) = \pi \tag{38}$$

The period of oscillation, $2\pi/\omega$, is equal to twice the net transit time, $\tau_0 + \tau_m + \tau_c/2$, and the frequency is directly proportional to flow rate. This condition provides a simple test of the oscillation mechanism.

When the phase sum in Equation 35 is satisfied, then Equation 30 is real and the coefficient of b is negative or positive depending on the total phase, $n\pi$. When the magnitudes of Equations 31–34 are multiplied in Equation 30, we retain only 1st powers of α. This process yields the following solution for α.

$$\alpha = \frac{|bc_2|A_c - A_mA_r}{\left(\tau_0A_c + \frac{\sin\theta_c/2}{\omega}\right)|bc_2| + \tau_mA_r\cos\theta_m + \frac{A_m\cos\theta_r}{\omega^2T}} \tag{39}$$

Undamped oscillation exists when $\alpha \geq 0$. Thus, the condition for stability is $\alpha < 0$, or

$$|bc_2| < \frac{A_mA_r}{A_c} = \frac{\sqrt{1+\omega^2\tau_m^2}\sqrt{1+1/\omega^2T^2}}{\frac{\sin\omega\tau_c/2}{\omega\tau_c/2}} \tag{40}$$

If the expected value of $|bc_2|$ for different solvent systems is known, then the parameters of the fluid circuit may be chosen to achieve stability. These parameters are $\omega\tau_m$, ωT, and $\omega\tau_c$.

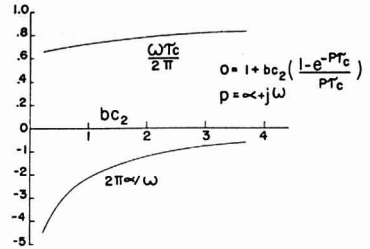

Figure 5. The phase angle $\omega\tau_c$ and attenuation per cycle for positive b oscillations generated only by the column transit time τ_c. $n = 1$

An effective method of quenching the $n = 1$ mode of oscillation is to minimize the volume of the mixer and the connecting tube such that $\tau_0 + \tau_m \ll \tau_c/2$. Then Equation 38 gives the frequency of oscillation by $\omega\tau_c/2 = \pi$. But then $(\sin\omega\tau_c/2)/(\omega\tau_c/2) = 0$ and Equation 40 indicates stability for all values of bc_2.

For negative values of bc_2 in the $n = 0$ mode, the frequency will tend to be so low that $(\sin\omega\tau_c/2)/(\omega\tau_c/2) \simeq 1$. If $\tau_m \gg \tau_0 + \tau_c/2$, then Equations 36 and 40 reduce to

$$\omega = \frac{1}{\sqrt{T\tau_m}}, \quad |bc_2| < 1 + \tau_m/T \tag{41}$$

This oscillation (as well as the previous one) is quenched by increasing the volume of the mixer and reducing the volume of the reservoir.

Exact Analysis of Column Oscillations for the $n = 1$ Mode, (positive b) and $\tau_0 = \tau_m = 0$, $T = \infty$. The previous analysis of column damping violates the assumption of small α. An exact treatment is possible when the column is the only frequency dependent circuit element.

The non-steady state behavior is given by solution of Equation 29 with $\tau_m = \tau_0 = 0$. In addition, we take $T = \infty$, as this is often a good approximation. Thus Equation 29 becomes

$$0 = 1 + bc_2\left(\frac{1 - e^{-p\tau_c}}{p\tau_c}\right) \tag{42}$$

We multiply through by $p\tau_c$ and separate real and imaginary parts of Equation 42.

$$0 = \alpha\tau_c + bc_2(1 - e^{-\alpha\tau_c}\cos\omega\tau_c) \tag{43}$$

$$0 = \omega\tau_c + bc_2e^{-\alpha\tau_c}\sin\omega\tau_c \tag{44}$$

By inspection, a particular solution is $\omega\tau_c = 3\pi/2$, $bc_2 = -\alpha\tau_c = 1.3$. We can expand Equations 43 and 44 about this solution, such that $\omega\tau_c = 3\pi/2 + \theta$, $\cos\omega\tau_c = \theta$, $\sin\omega\tau_c = -1$. We then eliminate θ between Equations 43 and 44 to obtain a quadratic solution for bc_2 as a function of $\alpha\tau_c$. Given bc_2 and $\alpha\tau_c$ we can then calculate θ and $\omega\tau_c$. This solution is given in Figure 5.

As expected, damping is obtained for all values of bc_2. As bc_2 exceeds the value 3, the damping per cycle becomes rather small and approaches zero as $bc_2 \to \infty$. At $bc_2 \simeq 2$, the ringing amplitude is reduced by a factor of e in each successive cycle, and the damping is very rapid for smaller values of bc_2.

Especially if bc_2 is not too large, the elimination of the connecting volumes to make $\tau_m, \tau_0 \simeq 0$ is an effective way to stabilize the system against $n = 1$ oscillations.

Analysis of Instabilities for $n = 0$ (negative bc_2) and Large Damping. For $n = 0$, the frequency is very low and a useful approximation is that $e^{-p\tau_0} = 1 - p\tau_0$. We set $p\tau_c \simeq 0$, and then Equation 30 yields the quadratic equation

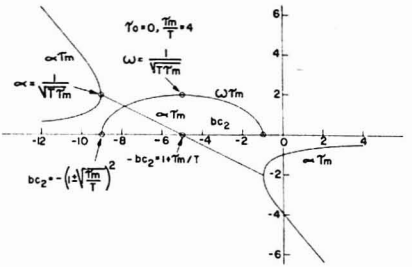

Figure 6. The frequency ω and attenuation α for negative b oscillations in which the mixer is connected directly to the column ($\tau_0 = 0$). $n = 0$

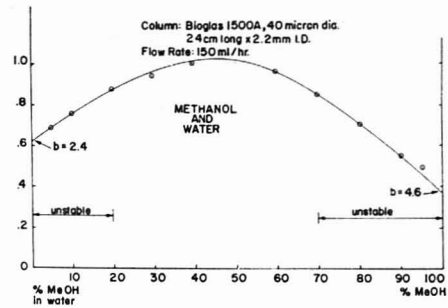

Figure 7. Pressure vs. concentration CH_3OH/H_2O at constant flow rate

$$0 = (1 + p\tau_m)(p + 1/T) + bc_2p(1 - p\tau_0)$$

or

$$p^2(\tau_m - bc_2\tau_0) + p\left(1 + \frac{\tau_m}{T} + bc_2\right) + 1/T = 0 \quad (45)$$

Figure 6 gives the solution for $\tau_0 = 0$, $\tau_m/T = 4$, and also gives the formulas for values of certain characteristic points of the solution. Thus the region of undamped motion is defined by $bc_2 \leq -(1 + \tau_m/T)$. For any given solvent system characterized by a maximum negative value of bc_2, the mixer volume may be chosen to give a value of τ_m such that the transient motion of the system is damped.

In the non-oscillating regions, for $bc_2 < -(1 + \sqrt{\tau_m/T})^2$ and $bc_2 > -(1 - \sqrt{\tau_m/T})^2$, the motion is characterized by two time constants, both positive or both negative, respectively. At $b = 0$, these correspond to the time constants T and τ_m of the reservoir and the mixer. Experimentally it is the longest time constant (smallest α) which is observed, and this leads to a clear distinction in the behavior of negative b vs. positive b systems. Beginning in a stable region (small value of bc_2), as the concentration ratio is changed to take bc_2 into an unstable region, if bc_2 is going negative the observed time constant will get shorter, whereas if bc_2 is going positive the time constant will get longer.

Saturation Oscillations. For sufficiently negative values of bc_2, Figure 6 indicates a nonoscillating motion of unbounded exponential growth, which is physically impossible. This growth is limited by "saturation" which reduces the effective magnitude of bc_2. By setting $\tau_0 = \tau_m = \tau_c = 0$, we eliminate all phase shifts which dominate the previous analyses and expose the exponential instability that occurs when $bc_2 < -1$.

In general, the equilibrium pressure is a nonlinear function of concentration, and the concentration is a nonlinear function of $\bar{Q}$. Thus Equations 13 and 18 should be written

$$\frac{\bar{P}}{P_0} = \sum_{n=1}^{\infty} a_n \left(\frac{\bar{Q}}{Q_0}\right)^n, \quad \frac{\bar{Q}}{\bar{Q}_0} = -\frac{T}{P_0}\frac{d\bar{P}}{dt} \quad (46)$$

where $P_0 = R_0Q_0$ is the equilibrium condition and the a_n's are constants. The term a_1 corresponds to $1 + bc_2$ in previous notation. a_2 gives rise to a shift in average pressure and the generation of second harmonics. a_3 is important for saturation, since the effective value of $a_1\bar{Q}/Q_0$ can be taken from the 1st and 3rd terms in the summation.

$$\left(a_1\frac{\bar{Q}}{Q_0}\right)_{\text{eff}} = a_1\frac{\bar{Q}}{Q_0}\left[1 + \frac{a_3}{a_1}\left(\frac{\bar{Q}}{Q_0}\right)^2\right] \quad (47)$$

If a_3/a_1 is negative, the $\bar{Q}^2$ term in Equation 47 has a dc component which reduces the effective value of a_1 as the amplitude $\bar{Q}$ increases. The physical situation with respect to HPLC has not been analyzed in detail. We find that the solution of Equation 46 with a_1 negative and a_3 positive gives rise to oscillation with a *sawtooth* waveform, in which the amplitude is proportional to $(-a_1^3/a_3)^{1/2}$, and the period is equal to $1.5\,a_1T$:

Experimentally, such oscillations would be most easily investigated by using a zero volume mixer, no time delay τ_0, and by replacing the column with a valve so that $\tau_c = 0$. Also, as $\tau_0 + \tau_m \to 0$ in the previous analysis, that solution must make a smooth transition into the solution described here. This area has not been experimentally investigated.

RESULTS

Water–Methanol Solvent System. Water–methanol mixtures have been described by Hettinger, Pertuit, and Munk, (*1, 2*). A measurement of normalized pressure vs. concentration at constant flow rate is shown in Figure 7, which is interpreted with the aid of Equation 14. The magnitude of b in Equation 14 is maximum at the end points of the concentration scale. If c measures the concentration of methanol, then $b = 1/P_0(\partial P/\partial c)$ is maximum positive at $c = 0\%$ and maximum negative at $c = 100\%$. However, both ends represent a positive b instability in the single reservoir representation of Figure 1. This is because the coefficient which multiplies b, represented by c_2 in Equation 25, changes sign in passing from one end of the concentration scale to the other. In the single reservoir model, the reservoir contains the minor fluid component, and the sign of b is determined by the variation of pressure with this minor component. The major fluid concentration is now designated by c_2, and it can be seen in the term bc_2 that the instability is enhanced by working at $c_2 \simeq 1$. Thus, positive b oscillations are generated at 95% H_2O–5% MeOH or at 5% H_2O–95% MeOH.

Experiments were done with a Varian Model 8500 HPLC. For V (H_2O) = 200 ml, V (MeOH) $\simeq$ 20 ml, $Q_0 = 100$ ml/h, $P_0 = 200$ atm, $\tau_0 \simeq 1.5$ min, $\tau_m = 0.24$ min, and a fluid composition of 5% H_2O–95% MeOH, harmonic pressure oscillations are generated with a period of about 3 min. The influence of the system time constant, $T \simeq 2$ min in Equation 6, is negligible and Equation 38 for the $n = 1$ mode applies. The frequency of this mode is accurately proportional to flow rate, as predicted by Equation 38. When $c_2 = c$ (MeOH) is varied in stepwise fashion from a stable region at 50% toward 100% MeOH, the active time constant *increases* in approaching the unstable region, according to the discussion of Figure 6.

Equation 38 for the frequency of oscillation was verified by placing various lengths of tubing between the mixer and the column, to get various values of τ_0. The total delay time $\tau_s = \tau_0 + \tau_m + \tau_c/2$ from mixer to column was measured by intro-

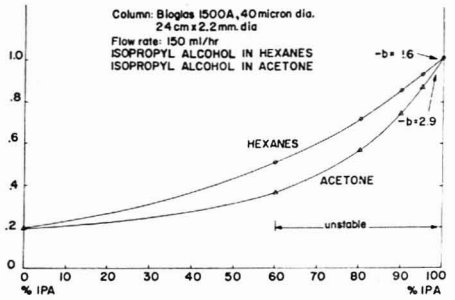

Figure 8. Pressure vs. concentration of isopropyl alcohol in hexanes and acetone, at constant flow rate

ducing a step change in concentration, and noting the time for this step to reach the column and change the pressure across it. Taking ω as the observed frequency, we obtained in all cases the value $\omega\tau_s \simeq \pi$, in agreement with Equation 38.

Theoretically a value $b > 1$ is necessary for undamped oscillation. Figure 7 shows that b values of 2.4 and 4.6 are available at the ends of the scale. Thus, undamped and growing oscillations can be obtained. The proposal to damp these oscillations with $\tau_0 = 0$, by connecting the mixer directly to the column, as discussed in regard to Figure 5, was tested. With a mixer of about 10^{-3} ml volume, no ringing could be obtained (*4*).

Isopropanol–Hexane or Acetone Systems. Postive b systems as described in the previous section apparently occur only in water based mixtures in which there is a high degree of molecular coordination. Isopropanol with acetone or hexane forms a negative b system which is characteristic of non-associating (Kneser) liquids (*5*). In these systems, the viscosity is always less than a linear extrapolation between the concentration end points. This behavior can be described as a linear combination of viscosities which are themselves a function of concentration.

Let c_1 be the concentration of one liquid with viscosity η_{11}, and $c_2 = 1 - c_1$ be the concentration of the other liquid with viscosity η_{22}. We have found that the total viscosity η of a binary mixture of Kneser liquids is approximately described by the following relations.

$$\eta = c_1\eta_1 + c_2\eta_2 \tag{48}$$

where

$$\frac{1}{\eta_1} = \frac{c_1}{\eta_{11}} + \frac{c_2}{\eta_{12}}, \quad \frac{1}{\eta_2} = \frac{c_1}{\eta_{21}} + \frac{c_2}{\eta_{22}} \tag{49}$$

and $\eta_{12} = \eta_{21}$ is the intermolecular viscosity of liquid No. 2 with respect to No. 1. Equations 49 are suggested by gas phase viscosity relations. Equations 48 and 49 may be fitted to experimental data to yield a value of η_{12}. For example, the slope, $d\eta/dc_1$ at $c_1 = 0$, is given by $\eta_{12} - \eta_{22}^2/\eta_{21}$. Given the value of η_{22}, the experimental slope determines η_{12}. This formulation may be compared to the one by Herzfeld and Litovitz (*5*).

A measurement of normalized pressure vs. flow rate for hexane/isopropanol and acetone/isopropanol systems is shown in Figure 8. Maximum negative b values of 1.6 and 2.9 are indicated at 100% isopropanol. Weak oscillation may be obtained with hexane, and stronger oscillation with acetone, which has a higher b value. A period of oscillation in excess of 8 min was measured with the shortest possible delay time between mixer and column. The frequency predicted by Equation 37 seems to be roughly correct, although no detailed verification was made.

As the transit time $\tau_0 + \tau_m + \tau_c/2$ is reduced towards zero, the behavior of the $n = 0$ mode should pass progressively from the oscillating condition expressed by Equation 37 to the saturation oscillation described in the text. Further experimental and theoretical work is warranted to describe this region of operation.

Higher Order Modes, $n > 1$. The preceding sections describe observation of the $n = 1$ and $n = 0$ modes of oscillation, respectively. In principle, one could observe the $n = 0, 2, 4, 6, \ldots$ modes simultaneously, and the $n = 1, 3, 5, 7, \ldots$ modes simultaneously. These higher order modes have not been seen, and the reason is probably that the system picks that mode with the highest gain and oscillates solely in that mode. The higher order modes might be observable under brief, transient conditions.

Examination of Equation 40 suggests that a higher odd-order mode might be generated by minimizing the mixer volume and increasing the transit time τ_0 to lower the frequency. This will increase the threshold value of bc_2 through the term $1/\omega^2T^2$. At some point, the system will choose to reduce the threshold by jumping to a higher frequency at a higher n value.

CONDITIONS FOR STABILITY

This text has shown that, under certain special conditions, it is possible to obtain concentration oscillations in gradient chromatography. Although observation of these oscillations has been infrequent, it is worthwhile to have a system which is stable under all conditions. Overall stability can be achieved by the following means.

Use of a Constant Pressure Valve. This technique was first suggested by M. Munk (*2*). If an automatic valve is installed at the outlet of a reservoir, such that the reservoir pressure is held constant, then $dP/dt = 0$. This eliminates the transient fluid flow described by Equation 4 and quenches all oscillations. In addition, the use of a constant pressure valve enhances the general performance of the system (*6*).

Elimination of Connecting Volume between Mixer and Column. As described in the text, if $\tau_0 = 0$, then the $n = 1$ mode in the water–methanol system will not oscillate. This plumbing configuration has improved the gradient performance of the system (*6*).

Pressure Derivative Feedback. Equation 40 shows that the system may always be stabilized by reducing the reservoir time constant T. One method would be to reduce the reservoir volume. Another method is to feed back to the reservoir piston, a velocity which is proportional to both the pressure derivative dP/dt and the reservoir volume V. In the right proportion, this will introduce a transient flow which will cancel the pressure generated transient flow in Equation 4. Complete cancellation cannot be achieved because it is impossible to measure the instant value of dP/dt. Some measuring time delay τ_e is required, in which case the minimum achievable reservoir time constant is about $\sqrt{T\tau_e}$. This still allows a significant reduction. It can be shown that this method is equivalent to a reduction in the fluid compressibility.

Increase in Mixer Volume. Equation 40 also shows that the system may be stabilized by increasing the mixer volume. This technique is less desirable than the others because it tends to introduce an unacceptable time lag between the gradient program as delivered by the pumps and the gradient program as received by the column.

ACKNOWLEDGMENT

I am indebted to A. Abu-Shumays for several stimulating discussions and creative experiments.

LITERATURE CITED

(1) J. Hettinger and R. Pertuit, unpublished work, Varian Associates, Palo Alto, Calif.
(2) M. Munk and S. Reifsneider, private communication, Varian Associates, Walnut Creek, Calif.
(3) M. Martin, G. Blu, C. Eon, and G. Guiochon, *J. Chromatogr.* **112**, 399 (1975).
(4) A. Abu-Shumays, private communication, Varian Associates, Palo Alto, Calif.
(5) K. F. Herzfeld and T. A. Litovitz, "Absorption and Dispersion of Ultrasonic Waves," Academic Press, New York, 1959, pp 425–427.
(6) S. Abbott, J. Berg, P. Achener, and R. Stevenson, *J. Chromatogr.*, to be published.

RECEIVED for review April 28, 1976. Accepted June 30, 1976.

Liquid Chromatographic Identification of Oils by Separation of the Methanol Extractable Fraction

W. A. Saner,* G. E. Fitzgerald, and J. P. Welsh

U.S. Coast Guard Research and Development Center, Avery Point, Groton, Conn. 06340

A liquid chromatographic oil spill identification technique employing dual ultraviolet detection was developed. The methanol-extractable fraction was removed from the oil samples and separated on a reverse-phase column using a water/methanol gradient. Ratios of the peak heights of two closely eluting bands (α = 1.01; detector λ = 254 nm), common to all oils studied, were reproducible to within ±3.0%. This ratio was used for screening improbable oil spill source samples. A series of intra-chromatographic peak-height ratios was then used to define a "fingerprint" region (detector λ = 210 nm). The spill chromatogram was used as a standard to which all suspects were compared for matching purposes. This matching technique showed that, as an oil weathered, the standard error of the standard deviations between any two chromatograms (weathered and unweathered) increased proportionately to exposure time. This permitted the calculation of an estimated time of spillage (±8 h) based on the linear increase of the standard error with time, for nine of the eleven oils tested.

The potential of separating high molecular weight compounds, which are presumably more resistant to weathering than more volatile compounds separable by gas chromatography, has made liquid chromatography a powerful complementary technique to an oil spill source identification system (*1, 2*).

Carmin and Raymond (*3*) traced the historical development and increasing use of chromatography in the petroleum industry. Oil analysis employing liquid chromatography has primarily involved gel-permeation and straight-phase systems (*4–9*). These separations, however, were generally applied to classify oils by type or for class composition analysis of major petroleum components. Applications of reverse-phase liquid chromatography for separation of polyaromatics present in oils has been demonstrated (*10, 11*). Other reverse-phase separations of aromatics have been restricted to automobile exhaust condensates and air pollution samples (*12, 13*). Frankenfeld and Schulz (*14*) reported the solvent extraction of petroleum with acetonitrile followed by reverse-phase liquid chromatography of the solvent extract. Schulz (*15*) also reported the effect of weathering on the reverse-phase liquid chromatograms of extracted oils. Jadamec, Saner, and Porro (*16*) reported the use of methanol for extracting petroleum; the solvent extracts were chromatographed on a reverse-phase column followed by fluorescence spectroscopic identification of some major peaks. The methanol-extractables from the API (American Petroleum Institute) No. 2 fuel oil standard included two and three fused-ring aromatics (naphthalene, 2-methylnaphthalene and fluorene were identified). In addition, many peaks possessed comparable fluorescence emission spectra very similar to carbazole. Drushel and Sommers (*17*) have demonstrated the presence of carbazoles, quinolines, and indoles, using GLC in a light catalytic-cycle oil. McKay and Latham (*18*) have identified carbazole and benzocarbazoles present in the 400–500 °C distillates of Wilmington, Calif., and Wasson, Texas, crude oils by employing thin-layer, gel permeation, and anion-exchange chromatography. The present study was undertaken to evaluate the ability of reverse-phase liquid chromatography to separate the methanol-extractable aromatics from petroleum oils and to evaluate the specificity of this oil fraction for "fingerprinting" spills. Although it was realized that heterocyclic aromatics in general have some solubility in water, and could diffuse into the aqueous layer from an oil spill on water (*19, 20*) this condition was not found to be serious.

EXPERIMENTAL

Apparatus. A Perkin-Elmer Model 1220 high pressure liquid chromatograph with two screw-driven piston pumps capable of 3000 psi solvent delivery was interfaced with a Perkin-Elmer Model 250 Ultraviolet Absorption Detector and a Coleman Model 55 UV-Vis Digital Spectrophotometer (variable wavelength). The methanol-soluble fractions from petroleum oils were chromatographed using gradient elution on two 0.64 × 30 cm columns packed with Waters Associates μ Bondapack C_{18}. This column packing has a monomolecular layer of octadecyltrichlorosilane chemically bonded to small diameter (*21*) (<10 μm) silica particles. The columns were connected by reducing end fittings containing a 5-μm stainless-steel frit and were maintained isothermally in an air bath at 60 ± 0.1 °C. Column effluent was monitored at 254 nm in a 12-μl cell. The detector signal (linear from 0.01 to 0.5 absorbance units full scale) was recorded on a Perkin-Elmer Model 56 recorder. After passing through this uv photometric cell, the column effluent was then transferred via 0.015-in. i.d. stainless-steel tubing to a Coleman Model 55 Spectrophotometer; its 8-μl photometric cell was monitored at 210 nm and recorded on a Perkin-Elmer Model 56 recorder.

Procedure. A solution of degassed spectroquality methanol (MCB MX475) and distilled water was used as the gradient-elution mobile phase programmed for a linear 1% per minute increase in methanol concentration from a starting mixture of 50/50 (v/v) methanol/water taken to 100% methanol (50-min gradient time). A 1400-psi head was developed at a flow rate of 1.5 ml/min. The oil samples were dried with calcium sulfate. Methanol-extractables were removed from the oil by a liquid–liquid extraction using acidified methanol (0.4% acetic acid/methanol by volume). The ratio of oil sample volume to extracting solution volume was unity. The oil–methanol mixture was shaken on a vortex mixer for 1 min, then centrifuged at 1000 RCF for 10 min. The methanol phase was removed and retained. Sample

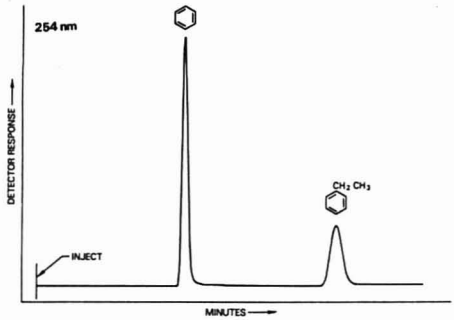

Figure 1. Isocratic separation of benzene and ethyl benzene

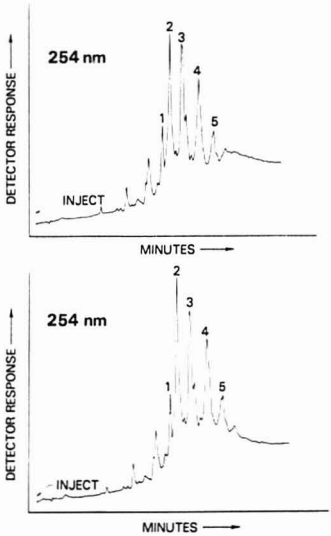

Figure 2. Replicate chromatograms of the American Petroleum Institute No. 2 fuel oil

saturation was achieved by vacuum evaporation of the methanolic extract at 60 °C to the point where visible oil droplets precipitated. Four microliters of the sample was stop-flow injected through septum using a 5-μl side port Auto Sampler Syringe (Precision Sampling Corp.).

Column Efficiency. Figure 1 shows the isocratic (nongradient) separation of benzene and ethylbenzene using 50/50 methanol/water (v/v) as the carrier at 1.5 ml/min flow rate. Utilizing the benzene peak, a value to 3600 plates was calculated representing HETP, H (cm) of 0.0167. The basic separation mode by this particular column packing is reverse-phase liquid–liquid (RPLL) (*22*).

Reproducibility. Figure 2 shows replicate chromatograms (254-nm uv absorption) of the API No. 2 fuel oil standard, utilizing gradient elution. Retention times for the five major peaks indicated in Figure 2 are listed in Table I. The variability of retention times of these duplicate runs is about ±0.5%. The major contributing factors to cause this variability were the precision of solvent delivery by the dual pump system (±1% of the indicated flow rate), and, of lesser importance, the precision of the air bath temperature (±0.1 °C). A difference of 1% in flow rates between replicate chromatograms has significant effect on retention volumes, particularly for peaks eluting after substantial time frames.

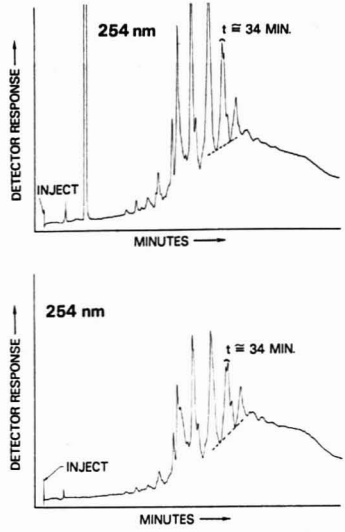

Figure 3. Chromatograms of two No. 6 fuel oils refined from the same feedstock

Table I. Reproducibility of Retention Times (Minutes) of Major Peaks on Replicate Chromatograms of the American Petroleum Institute No. 2 Fuel Oil Standard

Chromatogram	Peak 1	Peak 2	Peak 3	Peak 4	Peak 5
A	27.9	29.4	32.0	35.7	39.2
B	28.2	29.6	32.0	36.0	39.5
Mean	28.05	29.5	32.0	35.85	39.35
Maximum deviation from mean (%)	0.5%	0.3%	0%	0.4%	0.4%

Table II. Repeatability of Peak Height Ratios of the $t \simeq 34$-Minute Doublet for Replicate Injections with No Weathering Differences

	254 ratios			$\bar{x}$	Std dev (S)	$(S/\bar{x}) \times 100$, % rel std dev
API No. 2 fuel oil	0.83	0.89		0.86	0.04	4.7
Trinidad fuel oil	1.08	1.07	1.06	1.07	0.01	1.3
Italy fuel oil	1.28	1.33		1.31	0.03	2.4
Italy fuel oil	1.15	1.10		1.125	0.035	3.1
Finland fuel oil	0.83	0.84		0.835	0.007	0.8
Venezuela fuel oil	1.19	1.18		1.185	0.007	0.6
Venezuela fuel oil	0.83	0.84		0.835	0.007	0.8
No. 5 fuel oil	0.96	0.98		0.97	0.014	1.4
Diesel oil	1.19	1.20		1.195	0.007	0.6
No. 2 fuel oil	1.14	1.17		1.155	0.02	1.7

Table III. Repeatability of Peak Height Ratios of the $t \simeq 34$-Minute Doublet for Replicate Injections with Weathering Differences

Oil sample number	254 Ratios: Unweathered	Increasing weathering time →			Std dev	% Rel std dev
1. Massachusetts (Spill)		1.32[a] (28 May)	1.30[a] (29 May)		0.014	1.1
2. New Hampshire (Spill)		1.32[a] (21 May)	1.34[a] (22 May)	1.29[a] (23 May)	0.025	1.9
3. Artificially weathered	1.42	1.39[b] (4 h)	1.43[b] (72 h)		0.021	1.5
4. Artificially weathered	1.21	1.24[b] (96 h)	1.22[a] (96 h)		0.015	1.2
5. Artificially weathered	1.09	1.12[b] (36 h)			0.019	1.9
6. Artificially weathered	1.18	1.20[b] (40 h)			0.014	1.2
7. Artificially weathered	1.10	1.11[b] (24 h)			0.007	0.6
8. Artificially weathered	1.09	1.08[b] (24 h)			0.007	0.7
9. Artificially weathered	0.95	0.98[b] (70 h)			0.02	2.2
10. Artificially weathered	1.18	1.20[b] (48 h)			0.014	1.2
11. Artificially weathered	1.18	1.14[b] (48 h)			0.028	2.4

[a] Weathering substrate = sand. [b] Weathering substrate = salt water.

Baseline drift is evident in these chromatograms. Although spectroquality methanol was used throughout, some absorption in the uv was demonstrated due to impurities. The increasing methanol concentration in the eluting solvent as the gradient proceeded caused an increasing uv absorption.

RESULTS

Distinguishing Oils: Comparing Peak Height Ratios of a $t = 34$ Min Doublet (254-nm uv Detection). The liquid chromatograms of two No. 6 fuel oils are shown in Figure 3. Both of these residual oils were manufactured by Gulf Oil from the same Caribbean crude feedstock. The resulting 254-nm chromatograms are very similar. However, the peak-height reversal of the two closely eluting bands at about $t = 34$ min is readily apparent. The separation factor (α) for these particular peaks is 1.01. Although this value is low, meaningful resolution of peaks eluting with an α value as low as 1.05 has been reported (*23*). (No attempt was made to compare directly the peak heights of the $t = 34$ doublet interchromatographically since a relatively large quantitative error is introduced with peak height measurements by incomplete peak separation, $Rs < 1$.)

Baseline drift was compensated by interpolating the baseline between the start and finish of both peaks, considered collectively, as shown by the dashed line in Figure 3. Peak height, rather than peak area was used because the height measurement is both intrinsically simpler and more accurate when resolution (Rs) is low. The reason for this is that peak heights are much less affected by neighboring, overlapping peaks than are peak areas (*24*). Furthermore, regardless of the resolution between peaks, Janik (*25*) has shown that for quantitative GC analysis, the variance for peak heights measured with a ruler and peak areas measured with an electronic integrator are of the same order. The peak height measurements provide ratios of 0.97 and 1.13 for the chromatograms shown in Figure 3.

In order to determine both the range of this ratio for different oils and to estimate the precision of this calculation, ten different oils were extracted and chromatographed. Three oils were weathered before chromatographing. The remaining seven oils were all unweathered. All replicates, regardless of weathering history, were taken from the same methanolic oil extracts. In this way, this set of experiments tested the precision of the instrumentation (and of septum injections by hand) in reproducing the 254-nm ratio for oils with no weathering differences ($\Delta T = 0$). Table II lists these data. Examination of the range in the ratio shows a low of 0.83 and a high of 1.33. The relative standard deviations (Pearson's coefficient of variation) for the ratios range from 0.6 to 4.7%. The median relative standard deviation is 1.35%: two times the median standard deviation ($2.7 \simeq 3\%$) was taken as the allowable error for the ratio. Because of both the limited range of the ratio and the limits of its reproducibility (±3%) much overlap between oils occurs. In fact, duplication of a ratio (0.83–0.84) occurred for two distinct fuel oils manufactured from Venezuelan and Finnish Crude feedstocks. It became apparent that the ratio could, at best, only be used as a primary screening technique, since it lacked sufficient specificity for oil spill identification.

Effect of Weathering on Peak Height Doublet Ratios (254-nm uv Detection). Although loss of the 34-min doublet peak was noticed with increasing weathering time, if the peaks decreased proportionally then the ratio of their heights should remain constant to provide a suitable mathematical description of an oil for screening purposes.

In order to determine weathering effects on the ratio, a second series of chromatograms was studied (Table III). Various types of oils were used, i.e., crude, No. 6 fuel oil, No. 5 and No. 4 fuel oil, No. 2 fuel oil, and diesel oil. The oils were weathered outside in open containers on the rooftop of a one-story building during the months of May, June, and July. Because past experience demonstrated that 95% of all significant oil spills were detected and sampled within 48 h of the spill time, weathering exposure was limited to four days or less.

Admadjian et al. (*26*) found that natural weathering conditions can be closely simulated by weathering oils in containers on land; generally high water temperatures reached in the rooftop containers were found to cause accelerated oil weathering, regardless of the oil type. Furthermore, Brown et al. (*27*) have observed that the greatest change in the in-

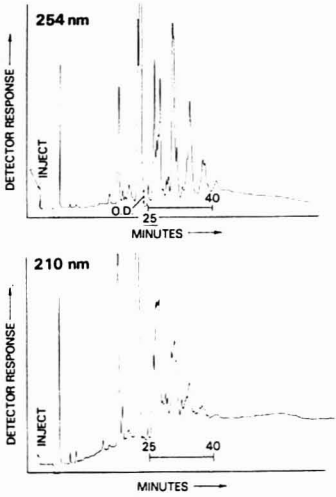

Figure 4. Chromatogram of a No. 4 fuel oil

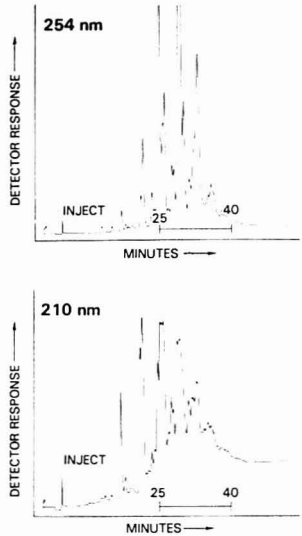

Figure 5. Chromatogram of diesel oil

frared spectrum of an oil takes place during the first two days of weathering.

The present study corresponds to accelerated weathering conditions which would hardly be commonplace for most real world spill situations. The acceleration of weathering by the rooftop simulated weathering procedure has been estimated to proceed at five to ten times the rate of natural weathering in real world spill situations (*28*). As a result, the oils weathered four days in the present study could represent oils weathered between 20 and 40 days under more natural conditions.

Examination of Table III shows that there were no significant changes in the ratios for any of the in-house weathered oils regardless of whether sand or water substrates were used for weathering. Furthermore, no significant changes were detected in the ratios for any of the real world oil spill samples. An error of 2.4% relative standard deviation was the maximum ratio difference for all in-house weathered oils. This represented the standard deviation for the ratio of a No. 2 fuel oil weathered on water for 48 h vs. the unweathered oil. Furthermore, the Massachusetts spill showed only a 1.1% standard deviation between samples weathered for x and $x + 24$ h. The New Hampshire spill demonstrated a 1.9% standard deviation for the ratios among samples weathered y, $y + 24$ h, and $y + 48$ h.

The median relative standard deviation of 1.20% for these eleven weathered oil ratios compares closely with the median value of 1.35% relative standard deviation for ten unweathered oil ratios (Table II). Any real differences in the ratios caused by disproportionate losses of one peak relative to the other were within the reproducibility limits for the ratio itself irrespective of the weathering variable. Therefore, any changes in the ratios caused by weathering are less than 3% related to the original unweathered oil. Even though this ratio demonstrated stability through weathering, it could only be used to indicate possible matches between spill and source oil samples.

Matching Oils: Serial Ratioing of Peaks Eluting between 25 and 40 Min (210-nm uv Detection). In an effort to expand the capability of this liquid chromatographic technique for also assigning oil spill matches, a variable wavelength uv detector monitoring column effluent at 210 nm, was added behind the 254-nm uv detector. Figure 4 shows the chromatograms of a No. 4 fuel oil using both 254-nm and 210-nm uv detection. From inspection, it is apparent that for some regions of the chromatogram, particularly for those peaks eluting between 25 and 40 min, the 210-nm absorption trace showed an increased number of bands. In addition, Figure 5 shows the chromatogram of a diesel oil using dual uv detection. Those peaks absorbing at 210 nm which eluted between approximately 25 and 40 min seem characteristic for the oil. The 0- to 25-min regions of the chromatograms were found to be grossly affected by weathering. For these abovementioned reasons, only those peaks which eluted between 25 and 40 min were investigated further for the purpose of matching oils statistically.

Peak heights were utilized rather than peak areas due to the incomplete separation of bands in the 25- to 40-min elution range. Since the peak separation, however, throughout this entire region is marginal at best, rather than direct interchromatographic peak height comparisons for all bands, a series of intrachromatographic ratios was generated for each chromatogram by ratioing the first peak to the second, second to the third, third to the fourth, etc. [i.e., $n/(n + 1)$, $(n + 1)/(n + 2)$, $(n + 2)/(n + 3)$] for these peaks (i.e., those peaks within the 25–40 min range, eluting after the major naphthalene peaks). Only those peaks with both a positive and a negative slope and with a minimum peak height of 5 mm were considered. In this way, each 210-nm chromatogram was reduced to an ordered set of ratios which served as a numerical description of each oil. It was realized that substantial errors in peak-height measurements were possible due to the fact that small "rider" peaks present on larger peaks cause displacement of the true band centers of these smaller peaks. However, if the chromatograms displayed constant repeatable peak center displacements, then the error introduced into the peak height measurement would be lessened. In addition, the ratioing of directly adjacent peaks served to lessen further the peak height error caused by band center displacement for incompletely separated peaks. For instance, any two adjacent

Table IV. Ratio Series for Replicate Chromatograms of a No. 2 Fuel Oil

Original run	Replicate run
1.13	1.39
2.57	2.57
0.07	0.07
0.99	1.01
2.94	2.88
0.93	0.87
0.76	0.75
1.07	1.07
3.31	3.39
0.83	0.84
1.16	0.94

peaks, eluting on either the front or back side of a larger peak, display band center displacements in the same direction. Since the resulting peak-height measurements would be overestimates, then a series of ratios using adjacent peaks would tend to minimize this error. Last, since the detector response is variable for different compounds, the ratioing of even adjacent peaks in a chromatogram is in no way a direct measurement of the quantitative relationship of these peaks since their molar absorptivities at 210 nm are unknown and probably different. Rather, the above method of reducing a chromatogram to a set of numbers was envisioned simply as a possible means of reducing chromatographic data in order to compare two oils objectively for matching purposes. As such, the 25–40 min elution range of the spill oil chromatogram was used to establish a typical profile as a standard.

It was realized that in order to study the reproducibility of this series of ratios for a particular oil, it would be necessary to study the reproducibility of each individual ratio in the series. Because any one oil generated between 10 and 15 peaks which eluted between 25 and 40 min, this alternative meant studying the reproducibility of between 9 and 14 ratios per oil. Instead all ratios in the series were considered collectively by a statistical method.

Statistical Method of Comparing of Any Two Ratio Series (210-nm uv Detection). This method compares any two chromatograms and assigns a numerical degree of "match". This method can be directly applied to ascertaining the proximity of a spill sample/suspect sample pair for matching purposes. The procedure involves: 1) Computation of the standard error of the standard deviations of the serial ratios (collectively considered) for any two oils, and 2) computation of the correlation coefficient between the individual ratios of the two oils.

For any two chromatograms (X and Y) the correlation coefficient (*29*) (r) was calculated from the formula:

$$r_{XY} = \frac{n\Sigma xy - \Sigma x \Sigma y}{\sqrt{[n\Sigma x^2 - (\Sigma x)^2][n\Sigma y^2 - (\Sigma y)^2]}} \quad (1)$$

where chromatogram X produces an ordered set of x's (intrachromatogram peak height ratios = n) and chromatogram Y produces an ordered set of y's (intrachromatogram peak height ratios = n). The correlation coefficient is then used to test the hypothesis that the serial ratios of the X chromatogram and the Y chromatogram are not significantly different:

$$S_D = \sqrt{S_{\theta X}^2 + S_{\theta Y}^2 - 2r_{XY}S_{\theta X}S_{\theta Y}} \quad (2)$$

where $S_{\theta X}$ = standard error of chromatogram X, $S_{\theta Y}$ = standard error of chromatogram Y, and r_{XY} = coefficient of correlation between X and Y.

The standard error, S_θ (for the separate sets of serial ratios), was calculated from:

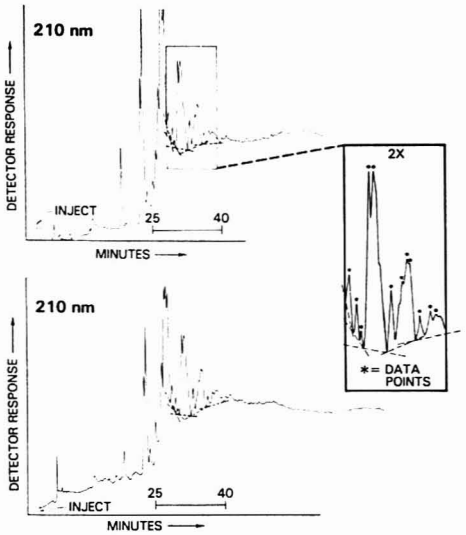

Figure 6. Replicate chromatograms of a No. 2 fuel oil

$$S_\theta = \frac{S}{\sqrt{2n}} \quad (3)$$

$$S = \sqrt{\Sigma(x_1^2) - \frac{(\Sigma x_1)^2}{n-1}} \quad (4)$$

where x_1 represents the individual ratios in the series for peaks eluting after napthalenes and between 25 and 40 min.

Figure 6 shows replicate chromatograms of a No. 2 fuel oil indicating those peaks meeting the above-mentioned criteria within the 25–40 min elution range, and baseline interpolation. Table IV lists the two ratio series for these particular chromatograms. The two series yielded a correlation coefficient of (r = 0.994). The test of the standard errors of the standard deviations, S_D, was 0.10. Furthermore, a replicated diesel oil S_D value of 0.09 compared closely with the S_D of 0.10 calculated for replicate chromatograms of a second No. 2 fuel oil. The individual standard deviations, r values, and S_D values are summarized in Table V. These results indicated that minor differences existed between duplicate runs of the same oil. These differences, however, were consistent. A perfect match indicating no differences would, of course, be zero. The calculated value of 0.10 ± 0.01, then, is a measure of the instrumental precision. This value was accepted as the numerical definition of a match between two oils with no weathering differences.

In-House Oil Spill Testing. The effect of weathering on the S_D values was studied by a set of in-house oil spill identification tests developed by an independent team. These tests consisted of weathering the "spill" oil sample from 24 to 96 h on both salt water and sand. All suspect sources provided were unweathered. Various oils, No. 2, No. 4, No. 5, and No. 6 fuel oils in addition to crude and diesel oils were used. The oils were weathered in containers on the rooftop of a one-story building, explained previously. In any one test, the same type of suspect oil and spill oil was supplied. In addition, the source samples were chosen on the basis of physical and chemical similarities (i.e., flash point, percent sulfur, viscosity, insolubles, asphalt content) to the spill sample. Last, the majority

Table V. Standard Deviations (S_θ), Coefficients of Correlation (r), and Standard Errors of the Standard Deviations (S_D) Calculated from Replicate Chromatograms

	No. 2 Fuel Oil (A)		Diesel Oil		No. 2 Fuel Oil (B)	
	Unicate	Duplicate	Unicate	Duplicate	Unicate	Duplicate
(S_θ)	0.70	0.69	0.64	0.725	1.36	1.46
(r)	0.994		0.998		0.9995	
(S_D)	0.10		0.09		0.10	

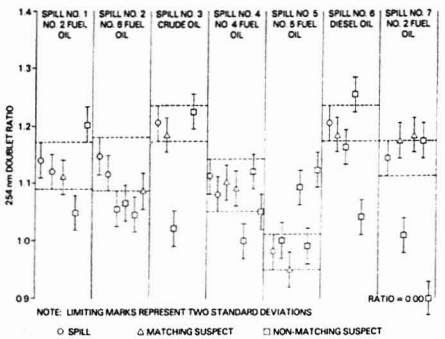

Figure 7. Comparison of the 254-nm doublet ratios for seven in-house oil spill tests

of suspect sources provided in any particular spill test was from the same processor.

In the application of the ratio series for differentiating oils, the spill samples provided were used as comparison standards and only those suspects having a 254-nm doublet ratio within ±3% of the spill sample were considered for ratio series comparisons. In this way, the 254 detection served as a means of screening out improbable source samples. However, since qualitative differences between spill and suspect chromatograms in the 25- to 40-min region of the 210-nm chromatogram occurred frequently, the spill sample was arbitrarily made the standard for comparison. Only corresponding peaks common to both spill and suspect were used for the ratioing and calculation of r and S_D. Extraneous peaks existing in the 25–40 min elution range of the suspects were ignored in calculating the series of ratios for that suspect if no such peak existed in the spill chromatogram because these could be attributed to losses as the result of weathering. In this way, zero values were not included in the series of ratios for any of the spill or suspect oils. Where more than one spill sample was provided in the same spill test, each was considered as a distinct oil and used separately as standards for comparison to the suspect samples or remaining spill samples.

Figure 7 plots the 254-nm doublet ratios for the spill and suspect samples for the seven in-house oil spill tests. Any suspect oil whose 254-nm peak ratio overlapped the spill ratio is considered a potential match to be further evaluated by means of the 210-nm peak ratio series. Conversely, any sample whose ratio did not meet these requirements was considered a definite mismatch and was not evaluated further. It is obvious that the ratios plotted in Figure 7 are clustered closely to the spill samples for each test. Nevertheless, the minimum percentage of suspects which were eliminated in any one oil spill test was 20%, while, in two cases, the 254 ratio screened out 50% of the suspects.

Table VI. Paired Comparisons (S_D) for Spill Cases with Two Spill Samples

Spill sample	Spill/spill	Spill/suspect 1	2	3	4	5
Test 1						
From water	0.10	0.21	2.07	X[a]		
From sand	0.10	0.21	2.08	X[a]		
Test 2						
From water	0.51	X[a]	X[a]	X[a]	0.56	
From sand	0.50	0.58	4.86	X[a]	0.10	
Test 4						
From water (A)	0.42	0.49	0.14	0.39	0.28	X[a]
From water (B)	0.35	0.14	0.37	0.50	0.49	X[a]

[a] Screened out as possible spill match on basis of 254-nm doublet ratio.

Three of the in-house spill tests provided more than one spill sample; i.e., Tests 1, 2, and 4. Tests 1 and 2 each provided two spill samples, one on salt water and one on sand. Test 4 provided two spill samples, both of which were on salt-water.

Table VI shows the results of the S_D calculations for these multiple spills and the potential matches for them. The S_D value of 0.10 between the spill on water and the spill on sand for Test 1 indicates that these two samples were the same oil, with no determinate weathering differences during 96 h of exposure. Using either spill sample as the standard for comparison, the table also shows the suspect sample with the least difference to the spill sample (S_D = 0.21) is Suspect 1. This suspect was, in fact, the source of the spills.

On the other hand, the S_D calculations between the two spill samples for Test 4 (0.42 and 0.35) indicated that they were either different oils, or the same oil with weathering differences present. Additionally, the minimal S_D value for the comparison of Spill 1 to all probable suspects is 0.14, indicating a match to Suspect 2. Similarly, Spill 2 vs. Suspect 1 produced a minimal S_D value of 0.14. The conclusions, therefore, were that the spill samples (1 and 2) consisted of different oils which matched Suspect 2 and Suspect 1, respectively.

Oil spill Test 2 (consisting of No. 6 fuel oils) also provided two spill samples, one on sand, another on salt water. The S_D value for these was large. The spill on sand vs. Suspect 4 S_D value of 0.10 was the minimal value possible for replicate chromatograms of the same oil with no weathering differences. The conclusions were that the spill samples consisted of different oils, and only the spill on sand was identical to Suspect 4. These results, however, were incorrect, probably due to contamination. Suspect 4 had been used to generate both spill samples. Table VII lists the S_D values for the remaining spill tests which provided one spill sample each (on salt water). In

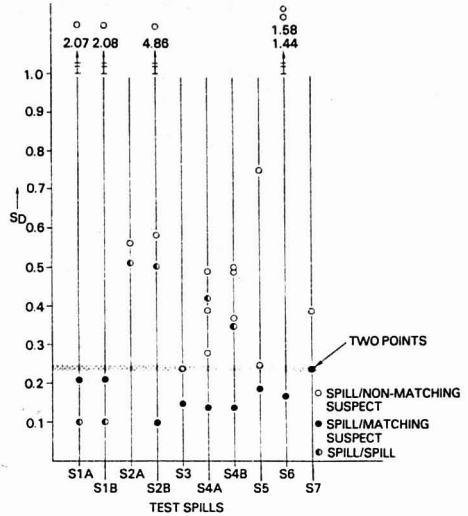

Figure 8. Distribution of S_D values of all possible sample pairs (i.e., spill/suspect, spill/spill not eliminated by 254-nm screening) for seven in-house oil spill identification tests

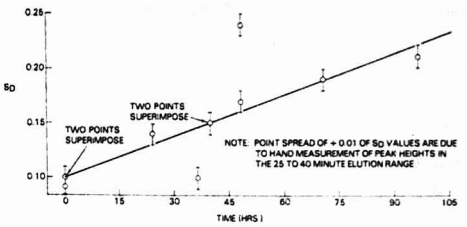

Figure 9. Best fit curve defining increasing S_D with time

Table VII. Paired Comparisons (S_D) for Spill Cases with One Spill Sample

Spill on water test	Spill/suspect 1	2	3	4	5
3	0.15	0.24	X[a]	X[a]	
5	0.25	0.19	X[a]	0.75	X[a]
6	0.17	1.58	1.44	X[a]	
7	0.24[b]	X[a]	0.24[b]	0.39	X[a]

[a] Screened out as possible spill match on basis of 254-nm doublet ratio. [b] Suspect 1 vs. Suspect 3, S_D value = 0.20.

each of these tests, the minimal S_D value predicted the correct match between spill and source. Table VII, however, shows that for Test 7, two source suspects (1 and 3 with comparable S_D values of 0.24) are equally good matches for the spill. Furthermore, the S_D value for Suspect 1 vs. Suspect 3 was 0.20. The S_D value for the same oil, with no weathering differences between replicates, is 0.10 ± 0.01. The observed value of 0.20 for suspect samples 1 and 3 could possibly represent differences in handling these two oil samples over 1½ years. (Suspects 1 and 3 were the same oil, stored in different, but identical containers.)

These oil spill tests provided a total of 47 possible spill/sample correlations; 33 negative correlations (spill and spill or spill and suspect do not match) and 14 positive correlations (spill and spill or spill and suspect match). By employing both the 254-nm doublet ratio to screen improbable matches and the 210-nm ratio series to assign numerical differences between chromatograms, a total of 12 correct positive correlations and 33 correct negative correlations between oils was made. This is equivalent to 0.957 (45/47) probability for correctly matching oils. However, since this procedure is based on a "best fit" method, that is, one which "matches" a spill to whatever suspect happens to show the least difference to the spill (minimal S_D), it would be highly dependent on complete sampling of all possible pollution sources in real world cases.

Because all real world spill cases do not include all possible sources, it becomes necessary to assign a maximum limit to the value of S_D for defining a suspect/spill match. The S_D values from the seven oil spill tests are plotted in Figure 8. All correct positive correlations between spill and source (solid dots) are either equal to or less than 0.24. However, since the S_D value for any two chromatograms is reproducible to ±0.01 (a fact due primarily to errors in hand measurement of peak heights), the recognition of a "gray area" (0.24 ± 0.01) is necessary. For any oil spill sampled within 96 h of spillage, an S_D value < 0.22 will define a match, while an S_D value > 0.26 will define a mismatch.

Figure 8 shows that for Spills 3 and 5, one nonmatching suspect falls within the inconclusive S_D range, for each. Furthermore, two matching suspects (later shown to be the same oil, S_D = 0.20) for Spill 7 also fall in this S_D range. For this reason, the range $0.22 \leq S_D \leq 0.26$ is defined as inconclusive for spill matching purposes. Utilizing this inconclusive range as the border between a match ($S_D < 0.22$) an nonmatch ($S_D > 0.26$), then of a possible eight unique positive correlations, seven clearly fall within the match range for S_D; one, Test 7, falls within the inconclusive range. This is equivalent to a 0.875 probability of correctly matching oils based solely on the numerical value of S_D.

Figure 9 plots the S_D values of spill sample vs. matching suspect for each of the seven oil spill tests, using the best fit curve for defining the increase in S_D with time for different oil types. Only the spill on sand vs. matching suspect for oil spill Test 2 was used, since the spill on water was suspected of having been contaminated during the course of weathering. (See Table VI.) A value of 0.10 was taken as the minimal S_D defining the reproducibility between chromatograms of the same oil with no weathering differences. (See Table V.)

A range of ±0.01 has been indicated for each data point established for the precision of the S_D calculation. This curve shows that as weathering exposure time increases, the S_D value for comparing the same oil unweathered vs. weathered also increases. A limit of the 96 h maximum exposure time is indicated in order that a weathered oil and its unweathered source may be "matched" ($S_D < 0.22$). The equation

$$y = 0.5x + 10 \tag{5}$$

defines this best-fit line. Correcting for differences in the scales of x and y, this equation becomes

$$y^1 = (1.25 \times 10^{-3})\, x^1 + 0.1 \tag{6}$$

where $y^1 = S_D$, and x^1 = exposure time in h.

Solving for x^1 and substituting S_D for y^1,

$$\text{Exposure time (in h)} = \frac{(S_D - 0.1) \times 10^3}{1.25} \tag{7}$$

Because of the ±0.01 precision limit for S_D, the calculated

values for x^1 are within ±8 h. Consequently, for an unknown oil spill sampled within 4 days of spillage, the S_D value can, alone, establish the identity of the spill. However, the calculation of x^1 will additionally assign an approximate time of spillage. This information can be very useful as corroborative evidence where a "passing ship in the night" is identified as the spill source and yet is 4 days' steaming time distant from the actual spill site. Additionally, as was pointed out above, the artificial weathering scheme used to produce "weathered" oils for this set of in-house tests has been known to cause greatly accelerated weathering of oils compared to actual real world weathering situations. Consequently, the 96-h time limit imposed on the weathering framework in order that S_D values remain less than 0.22 is a significant underestimate for real world weathering situations.

Environmental parameters in real world situations are unique; as such, the weathering of spilled oils will proceed at various rates for different locations and for different times of the year. This problem will be addressed in future work.

LITERATURE CITED

(1) C. B. Koons, P. H. Moneghan, and G. S. Baylis, "Pitfalls in Oil Spill Characterization: Needs for Multiple Parameter Approach and Direct Comparison of Spill Material With Specific Parent Oils", Esso Production Research Co., Houston, Texas.
(2) "Oil Spill Identification System", Department of Transportation, United States Coast Guard, Office of Research and Development, Washington, D.C., Report No. CG-D-41-75. (Available to the public through the National Technical Information Service, Springfield, Va. 22161.)
(3) D. L. Carmin and A. J. Raymond, *J. Chromatogr. Sci.*, **11**, 625 (1973).
(4) Waters Associates, Milford, Mass., Bulletin AN154, February 1975.
(5) Waters Associates, Milford, Mass., Bulletin AN108, December 1973.
(6) R. L. Stevenson, *J. Chromatogr. Sci.*, **9**, 251 (1971).
(7) D. M. Jewell, R. G. Ruberto, and B. E. Davis, *Anal. Chem.*, **44**, 2318 (1972).
(8) K. H. Altgelt and E. Hirsch, *Sep. Sci.*, **5(b)**, 855 (1970).
(9) T. E. Cogswell, J. F. McKay, and D. R. Latham, *Anal. Chem.*, **43**, 645 (1971).
(10) "Modern Practice of Liquid Chromatography", J. J. Kirkland, Ed., Wiley-Interscience, New York, 1971, p 188.
(11) J. B. F. Lloyd, *Analyst (London)*, **100**, 529 (1975).
(12) Waters Associates, Milford, Mass., Bulletin AN131, September 1973.
(13) J. A. Schmitt, R. A. Henry, R. C. Williams, and J. F. Dickman, *J. Chromatogr. Sci.*, **9**, 648 (1971).
(14) J. W. Frankenfeld and W. Schulz, "Identification of Weathered Oil Films Found in the Marine Environment", DOT, USCG Office of Research and Development, Washington, D.C., Report No. DOT-CG-23,035-A. (Available to the public through the National Technical Information Service, Springfield, Va. 22161.)
(15) W. Schulz, Abstracts, 26th Pittsburgh Conference on Analytical Chemistry and Applied Spectroscopy, Cleveland, Ohio, March 1975, No. 459.
(16) J. R. Jadamec, W. Saner, and T. Porro, Abstracts, 26th Pittsburgh Conference on Analytical Chemistry and Applied Spectroscopy, Cleveland, Ohio, March 1975, No. 456.
(17) H. V. Drushel and A. L. Sommers, *Anal. Chem.*, **38**, 19 (1966).
(18) J. F. McKay and D. R. Latham, *Anal. Chem.*, **44**, 2132 (1972).
(19) J. W. Frankenfeld, "Weathering of Oil at Sea", DOT, USCG Office of Research and Development, Washington, D.C., Report No. CG-D-7-75. (Available to the public through the National Technical Information Service, Springfield, Va. 22161.)
(20) S. P. Wasik, *J. Chromatogr. Sci.*, **12**, 845 (1974).
(21) Waters Associates, Milford, Mass., Bulletin DS042, February 1974.
(22) R. E. Leitch and J. J. DeStefano, *J. Chromatogr. Sci.*, **11**, 105 (1973).
(23) Waters Associates, Milford, Mass., Bulletin AN114, September 1973.
(24) L. R. Snyder and J. J. Kirkland, "Modern Liquid Chromatography", John Wiley and Sons, Inc., New York, 1974, p 435.
(25) A. Janik, *J. Chromatogr. Sci.*, **13**, 93 (1975).
(26) M. Ahmadjian, C. Baer, P. Lynch and C. Brown, *Environ. Sci. Technol.*, in press.
(27) C. Brown, P. Lynch, M. Ahmadjian, and C. Baer, *Am. Lab.*, December, 59 (1975).
(28) C. Brown, University of Rhode Island, Kingston, R.I., personal communication, February 1976.
(29) E. L. Crow, F. A. Davis, and M. W. Maxfield, "Statistical Manual", Dover Publication, Inc., New York, 1960, p 158.

RECEIVED for review May 13, 1976. Accepted July 1, 1976.

Determination of the Specific Surface of Adsorbents by the Dynamic Adsorption Method

Henryk Golka and Boguslawa Jeżowska-Trzebiatowska*

Institute of Chemistry, University of Wroclaw, Wroclaw, Poland

Logarithmic equations were derived for the adsorbate distribution among the sequential adsorbent samples in a column during the dynamic adsorption from the flowing mixture of carrier gas and benzene. To check the equations, a series of benzene adsorption measurements on several Al_2O_3 samples were carried out. It has been found that the derived equations properly describe the adsorption course and that the specific surfaces of examined samples determined by them are identical to those determined by other methods.

Studies on the adsorption of volatile compounds of rhenium, molybdenum, and selenium (*1, 2*) require a special method for analysis of the adsorbate distribution along the adsorbent packed in a column, because of the specific conditions such as high temperature, adsorption at dynamic conditions, and unusually long retention times. Theoretically derived equations for the distribution of an adsorbate on an adsorbent allowed: a) the determination of the specific surface of solids and b) calculation of the dimensions of adsorption columns at a fixed efficiency.

In order to check the accuracy of the derived equations, adsorption measurements of benzene on adsorbents of known surface were carried out at dynamic conditions.

EXPERIMENTAL

The measurements were carried out on the apparatus shown in Figure 1. Its most important element consists of a multisectional, dismantable adsorption column (8, Figure 1). At first, samples of studied adsorbents(0.02–0.1 g) were placed in each section. Samples of Al_2O_3 of different specific surfaces, made from ignited $Al(OH)_3$ (*3*), called Al_2O_3(I), Al_2O_3(II), Al_2O_3(III) and adsorbent B (*1, 2*) ($MgO + Al_2O_3$) were used in our studies as adsorbents. The number of sections in a column was usually 5–6. A neutral gas current (hydrogen, 20 ml/min) was passed through the column. The carrier gas flow was maintained constant by use of a three-stage reducing valve (2a–c, Figure 1). Hydrogen was purified by passing through a column (3, Figure 1) packed with A-4 molecular sieve and a liquid nitrogen trap (4, Figure 1). Before starting the measurements, the adsorbent samples, placed in the column (8a–e, Figure 1), were heated for 1 h at 200 °C. After the impurities (*4*) were removed from the adsorbent surface and equilibrium in the system was reached (decay of the recorder baseline drift), the column was cooled down to 25 °C. That temperature was kept constant using an ultrathermostat. Then the thermostated column (8, Figure 1) was cut from the path I of carrier gas (valve 6, Figure 1) and put into the circuit of gas (path I) saturated with benzene in a bubbler (7, Figure 1). The volume of the gas which was passed through the column was measured with a gas burette (12a,

Table I. Results of the Dynamic Adsorption Measurement of Benzene on Al_2O_3 (I)

Section	Sample weight, g	Peak area, mm^2			Adsorbed amount of benzene, N cm^3		
		1[a]	2[a]	3[a]	1[a]	2[a]	3[a]
a	0.0704	3307	5140	5315	1.1582	1.7966	1.8564
b	0.0692	2016	1102	1484	0.7053	0.3852	0.5183
c	0.0641	837	438	868	0.2933	0.1504	0.3031
d	0.0407	187	81	460	0.0654	0.0283	0.1607
e	0.0870	4	43	316	0.0014	0.0151	0.1105
sum	0.3314				2.2246	2.3756	2.9490

[a] Corresponds to individual measurement series.

Table II. Results of the Dynamic Adsorption Measurement of Benzene on Al_2O_3 (II)

Section	Sample weight, g	Peak area, mm^2			Adsorbed amount of benzene, N cm^3		
		1[a]	2[a]	3[a]	1[a]	2[a]	3[a]
a	0.0289	2060	2263	2323	1.689	2.105	2.528
b	0.0248	511	593	752	0.418	0.554	0.819
c	0.0256	449	414	605	0.368	0.386	0.658
d	0.0532	407	398	858	0.334	0.371	0.936
e	0.0503	132	128	596	0.108	0.119	0.649
f	0.0576	48	28	326	0.040	0.026	0.357
sum	0.2404				2.957	3.561	5.947

[a] Corresponds to individual measurement series.

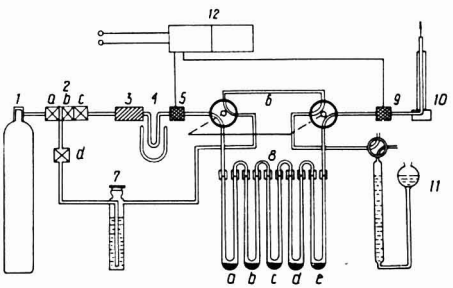

Figure 1. Apparatus used for studies of the dynamic adsorption of benzene

(1) Carrier gas container, (2) (a, b, c, d) reducing valves, (3) molecular sieve, (4) liquid nitrogen trap, (5) comparative catharometer cell, (6) valve, (7) bubler containing benzene, (8) (a, b, c, d, e) multisection adsorption column, (9) catharometric measurement cell, (10) flow meter, (11) gas burette, (12) power supply and recorder

Figure 1). After a given amount of benzene–H_2 mixture was passed through, the adsorption column was connected again to path I. To avoid any perturbation of measurements, which might be caused by the adsorbed benzene migration, the column was cooled simultaneously to −72 °C (dry ice–EtOH). Next, the column sections were subsequently heated up to 100 °C in the following order—section 8e, 8d, 8c, 8b, and 8a, causing fast and complete desorption of benzene from a given adsorbent sample. By passing various volumes of benzene-saturated H_2 through the column, various amounts of the adsorbate were injected on the column and therefore (at a given amount of the adsorbent) different amounts of benzene were adsorbed on subsequent sections of the column. The amounts of adsorbed benzene in individual measurement series are given in Tables I–IV (also see Figures 3a and 4a). The benzene desorbed was determined quantitatively using a Sorptiograph S-272 (made by ICSO Blachownia Slaska–Poland), operating on a chromatograph principle. A catharometer of 1000 mV/mg/ml sensitivity was used in this unit as detector. The amounts of desorbed benzene were determined from peak areas. The calibration indicated that the relation, $P = f(n)$, where P = peak area in mm^2 and n = amount of benzene, is linear in the applied concentration range. To find the total amount of adsorbed benzene, the determination of two calibration points for each measurement series was sufficient. The results of benzene adsorption on

Table III. Results of the Dynamic Adsorption Measurement of Benzene on Al_2O_3 (III)

Section	Sample weight, g	Peak area, mm^2		Adsorbed amount of benzene, N cm^3	
		1[a]	2[a]	1[a]	2[a]
a	0.0468	9096	6512	7.959	5.696
b	0.0750	2800	2994	2.450	2.619
c	0.0983	1843	2211	1.612	1.934
d	0.1063	766	678	0.671	0.757
e	0.1140	110	126	0.096	0.141
f	0.0887	16	17	0.014	0.019
sum	0.5291			12.802	11.167

[a] Corresponds to individual measurement series.

Table IV. Results of the Dynamic Adsorption Measurements of Benzene on Sorbent B

Section	Sample weight, g	Peak area, mm^2		Adsorbed amount of benzene, N cm^3	
		1[a]	2[a]	1[a]	2[a]
a	0.0204	1761	1952	1.5156	1.6798
b	0.0291	363	504	0.3120	0.4336
c	0.0254	138	315	0.1184	0.2711
d	0.0255	43	190	0.0374	0.1638
e	0.0340	30	74	0.0258	0.0637
sum	0.1324			2.0092	2.6120
a	0.0578	2858		0.9962	
b	0.0525	1098		0.3833	
c	0.0590	1062		0.3707	
d	0.0549	636		0.2219	
e	0.1082	123		0.0429	
sum	0.3324			2.0151	

[a] Corresponds to individual measurement series.

the adsorbents Al_2O_3(I), Al_2O_3(II), Al_2O_3(III), and B are given in Tables I–IV. Figure 2 presents one of the chromatograms of benzene distribution among the adsorbent B samples, placed in subsequent column sections.

CALCULATION METHODS

In order to find mathematical relations in the examined

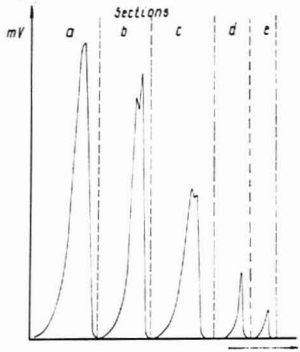

Figure 2. Chromatogram of benzene distribution among the sample weights of the sorbent B, placed in subsequent column sections, during the thermal benzene desorption. The arrow indicates the direction of the gas mixture flow

process, and to find quantitative relations between the amount of substance adsorbed in a given volume (dv) of an adsorbent and its distance from the start of filling of the column, equilibrium conditions of the adsorption and desorption processes were assumed. Since the experiment was carried out a) at low carrier gas flow rates and b) using short, lightly packed columns, the following assumptions were made: 1) Carrier gas pressure decay along the column is very small. 2) The adsorption process is running under the equilibrium conditions. 3) The amount of substance adsorbed on the adsorbent surface is determined only by the adsorption isotherm. For further calculations the Langmuir isotherm was applied:

$$a = \frac{a_m b p}{1 + bp} \tag{1}$$

The amount of substance adsorbed in each volume element dv of the adsorbent packed in the column is given by

$$a = \frac{dn_s}{dv} \tag{2}$$

Balancing the adsorbed substance flowing through a given volume element ($dv = dx \cdot dy \cdot dz$) of the filling, it should be considered that, because of the gas phase flow forced in the macroscopically favored direction, e.g., along the z axis, an additional transfer of the sorbed substance along the two remaining directions x and y occurs. That transfer is caused by the diffusion, convection, and turbulence of the main gas stream. At limited cross sections of a column, these phenomena lead to the decay of the adsorbate concentration gradient in those two directions (x, y). That makes possible a balancing of the adsorbate in one favored direction—the gas phase flow direction.

Therefore,

$$-\frac{dn_s}{r \cdot dl} = a \tag{3}$$

The negative value was used to denote the decrease of the amount of substance adsorbed in a given volume element at an increasing distance from the beginning of the column. Following Dalton's law, the partial pressure of adsorbate was expressed by concentration. Since the total carrier gas pressure in the column during the experiment was equal, p_c = const = 1 atm,

$$-\frac{dn_s}{r dl} = \frac{a_m b n_g / V}{1 + b n_g / V} \tag{4}$$

Defining $x = n_s/n_o$,

$$1 - x = n_g/n_o \tag{5}$$

and since $n_s + n_g = n_o$

$$-\frac{n_o dx}{r dl} = \frac{a_m b n_o (1 - x)}{V + b n_o (1 - x)} \tag{6}$$

Integration of Equation 6 at limiting conditions:

$$p = p_o, x = 0 \text{ at } l = 0$$

$$p = p_i, x = x_i \text{ at } l = l_i$$

results in

$$-\ln (1 - x_i) + \frac{b n_o x_i}{V} = \frac{a_m b r}{V} l_i \tag{7}$$

At low partial pressures of the adsorbate, $b n_o x_i / V \approx 0$. To prove this, Equation 7 was rewritten

$$Y = AX + B \tag{8}$$

where $Y = [\ln (1 - x_i)]/x_i$, $X = l_i/x_i$, $B = b n_o/V$.

Differences between the results obtained from Equation 7 at $b n_o x/V = 0$ and Equation 8 were negligible. Therefore, for further calculations Equation 7 was used in its simplest form:

$$-\ln (1 - x) = A \cdot l \tag{9}$$

where $A = b \cdot C$, b = adsorption–desorption equilibrium constant, and C = constant value at given experimental conditions.

If gas pressures are differing from 1 atm, Equation 7 becomes

$$-N \ln (1 - x_i) + b n_o p_c x_i = a_m b p_c r l_i \tag{7a}$$

Equation 7a should be linearly dependent on the absolute value of the total gas pressure.

However, if the pressure gradient along the column becomes $\Delta p_c / \Delta l \neq 0$, Equation 7a should behave nonlinear. The influence of pressure gradients was not examined in detail.

The polylayer adsorption could be thought of as a series of parallel systems (*5, 6*). Each of them could be defined by the reactions:

$$\text{sorbate} + \text{free surface} \underset{k_{-1}}{\overset{k_1}{\rightleftharpoons}} \text{single adsorption complex}$$

$$\text{sorbate} + \text{single adsorption complex} \underset{k_{-2}}{\overset{k_2}{\rightleftharpoons}}$$

double adsorption complex, etc.

where $k_1/k_{-1} = b_1$, $k_2/k_{-2} = b_2$, $k_3/k_{-3} = b_3$, etc. Usually, the equilibrium constant b_1 for the first layer is remarkably higher than $b_2, b_3, \ldots$ for the second and next layers, because the sorbent–sorbate interaction is decreasing rapidly with increasing distance. It is usually assumed that

$$b_1 \gg b_2 \geq b_3 \approx \ldots \tag{10}$$

In the case of multilayer adsorption, the assumption of the applicability of the Langmuir isotherm for each layer independently, as in the BET theory, leads to the conclusion that differences among the subsequent equilibrium constant values (Equation 10) should influence the slope ($A \cdot b$) of Equation 9 (if experimental data are presented as log $(1 - x)$ vs. l). In the ideal case the plot of log $(1 - x)$ vs. l should be composed of linked straight-line sectors of various slopes. Their joint points called L_m (Figure 3.) are situated at distance l_m in the coordinate system, and should correspond to the adsorbent coverage completion/beginning by adsorbate molecules within a given monoenergetic surface section of adsorbent. The layer

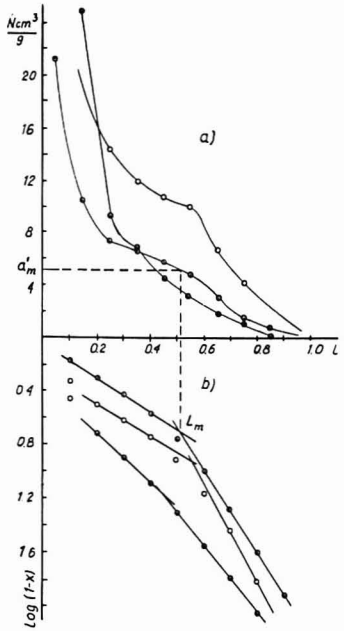

Figure 3. Dynamic adsorption of benzene on sorbent B

(a) Distribution of benzene among the sequential sorbent samples in the column for injected benzene doses: (in $N\,cm^3$) ◒ = 13.217, ○ = 17.180, ⊙ = 6.063. (b) Application of Equation 9 to describe the adsorption.

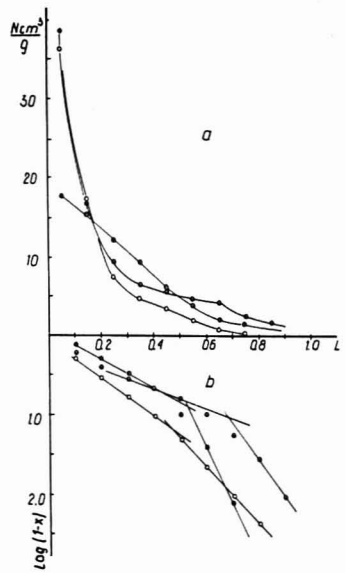

Figure 4. Dynamic adsorption of benzene on Al_2O_3 (I).

(a) Distribution of benzene among the sequential sorbent samples in the column for injected benzene doses: (in $N\,cm^3$) ⊙ = 6.715, ○ = 7.169, ◒ = 8.899. (b) Application of Equation 9 to describe the adsorption

capacity at that point may be determined from the plot of a vs. l. That dependence determines the adsorbate quantity (calculated for the adsorbent mass unit) adsorbed in a given element ΔV on its distance from the beginning of a column. The capacities of layers at distances l_m will be given by the corresponding a_m values.

Because of the simultaneous existence of several adsorption–desorption equilibria (Equation 10.) the plot of $\log(1-x)$ vs. l for experimental data would be a curve composed of linear sectors. The distance l_m could in that case be evaluated by the extrapolation of the straight-line sectors of that curve. Differences in the slopes of those sectors should occur for those layers only which differ in the equilibrium constants (Equation 10).

That method can be much simplified. Differentiation of Equation 9, given in its exponential form and substituting differentials by increments leads to Equations 12 and 13, which relate directly the amount of adsorbed molecules in a given layer element to its distance from the beginning of adsorbent filling in the column:

$$1 - x = \exp(A \cdot b \cdot l) \tag{11}$$

$$d(1-x) = A \cdot b \cdot e^{Abl} dl \tag{12}$$

$$\ln \frac{\Delta x}{\Delta l} = A \cdot b \cdot l + \text{const} \tag{13}$$

The slope of Equation 13 also contains the equilibrium constant b and, hence, the plot of $\ln(\Delta x/\Delta l)$ vs. l should exhibit a bending in the formation area of the completed adsorbate layer on the adsorbent.

RESULTS

The results of the benzene adsorption measurements on sorbents B, Al_2O_3(I), Al_2O_3(II), Al_2O_3(III) are listed in Tables I–IV. For a convenient direct comparison, these results were recalculated introducing the adsorption degree (x) and weight fraction of the adsorbent (g_i). The adsorption degree of the examined compound at a given distance (l_i) of the column packing is defined as the sum of ratios of adsorbate amounts in subsequent layers to the total amount injected to the column:

$$x_i = \Delta x_1 + \Delta x_2 + \ldots + \Delta x_i$$

$$\Delta x_i = n_i/n_o \tag{14}$$

The weight fraction of the ith layer of the adsorbent was defined as the ratio of its mass to the total mass of an adsorbent in a column:

$$g_i = m_i/m_o \tag{15}$$

One may prove that the weight fraction g_i of the ith layer of adsorbent is equal to the volume and length fractions of the given layer, respectively:

$$g_i = \Delta v_i = \Delta l_i$$

and therefore

$$\sum_i g_i = v_i = l_i = \Delta l_1 + \Delta l_2 + \ldots + \Delta l_i \tag{16}$$

The equivalence of the weight, volume, and length fractions allowed the easy illustration of changes in the amounts of adsorbed molecules along the column packing. It allows also the use of the very illustrative term of distance of ith adsorbent layer from the column start.

Table V. Determined Values of the Specific Surface of Examined Samples

Sorbent	Injected amount of benzene, N cm³/g	Specific surface determined, m²/g: From Eq. 9 a'_m	From Eq. 9 S_o	From Eq. 13 a'_m	From Eq. 13 S_o	By other methods S_o
Al_2O_3 (I)	6.715	5.50	64.6	5.07	59.5	
	7.169	5.10	60.0	...	...	60.2[a]
	8.899	5.20	61.0	5.15	60.5	
Al_2O_3 (II)	12.290	9.76	114.9	9.88	117.0	
	14.813	9.76	114.9	...	...	116.0[b]
	24.798[c]	10.4	122.0	21.4	252.0	
Al_2O_3 (III)	24.196	13.5	159.0	...	...	
	21.106	13.6	160.0	13.5	159.0	297[b]
Sorbent B	6.063	5.20	61.0	5.15	60.6	
		5.17	60.7	5.19	61.0	62.0[b]
	13.217[c]	...	...	10.37	122.0	
	17.180[c]	10.4	122.0	10.30	121.2	

[a] Specific surface determined by the classic BET method from the benzene adsorption isotherm. [b] Specific surface determined by the thermal desorption of nitrogen method (7,8). [c] Benzene injected in excess vs. capacity of sorbent sample used.

On the basis of such calculated data, plots of x vs. l, showing the mean increase x in sequential adsorbent layers for increments $\Delta l = 0.1$, were drawn. The resulting averaged data were used in the graphic solution of derived Equations 9 and 13.

Determination of the Specific Surface from Equation 9. From intersections of the extrapolated straight line sectors of the log $(1 - x)$ vs. l plots, only the l_m distance of those points from the start of the column packing were determined directly. The amount a_m' of adsorbed molecules at this L_m point, at the distance l_m, was determined indirectly from plots a_i vs. l_i where $a_i = \Delta x_i \cdot n_o / \Delta l_i \cdot m_o$. Examples of plots log $(1 - x_i)$ vs. l_i and a_i vs. l_i for the dynamic benzene adsorption on Al_2O_3(I), and on adsorbent B are given in Figures 3 and 4. The x_m and a_m' values read from the diagrams and calculated on the basis of surfaces occupied by the adsorbed benzene molecules are listed in Table V; these values correspond to the cross-points (L_m) of straight-line sectors of the log $(1 - x)$ vs. l dependence. The surface occupied by the benzene molecules was calculated from the formula:

$$S_o = \frac{a_m \cdot N \cdot \omega}{22{,}414} \qquad (17)$$

Determination of the Specific Surface from Equation 13. Equation 13 can be transformed:

$$\log a_i = \alpha \cdot l_i + C' \qquad (18)$$

Examples of log a_i vs. l_i plots for the dynamic benzene adsorption on Al_2O_3(I) and on adsorbent B are given in Figures 5 and 6. These plots are not straight lines, according to assumption. From the L_m points, determined by extrapolation of their linear parts, the log a_m' values were determined. The calculated layer capacity a_m' and, calculated from Equation 17, surface C_o occupied by the adsorbed benzene molecules are listed in Table V.

Extensive simplification of Equation 9, given by Equation 13, might lead to inaccurate results and therefore we would recommend the use of Equation 9 to determine the S_o values.

DISCUSSION

The capacity a_m' of the layer determined from the L_m points on logarithmic plots and, hence, calculated surface occupied by the adsorbed benzene molecules proved to be practically equal to the specific surface values of studied adsorbents determined by another method (thermal desorption of nitrogen (7, 8)). That agreement of specific surface values for the examined samples seems to confirm our assumptions and derived equations.

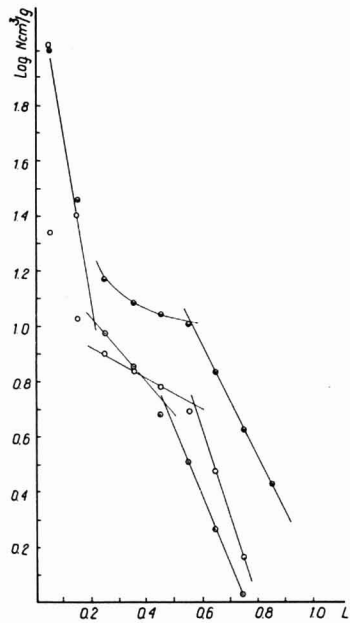

Figure 5. Dynamic adsorption of benzene on sorbent B

Application of Equation 15 to the determination of the specific surface of the examined sample, for injected benzene doses: (in N cm³) ⊙ = 13.217, ◒ = 17.180, ○ = 6.063

The results obtained indicate that the deflection areas of logarithmic plots correspond to the formation of the complete adsorbate layer on the adsorbent surface in the case of benzene. The slope of straight-line sectors of a logarithmic plot is proportional to the equilibrium constant of the sequential adsorption stages. The deflection point on the log $(1 - x)$ vs. l plot appears at the change of equilibrium constant, i.e., at transition from monomolecular to polymolecular adsorption. The observed discrepancies of the specific surface values determined for the Al_2O_3(III) adsorbent from thermal desorption and our method are most likely due to the molecular sieve effect.

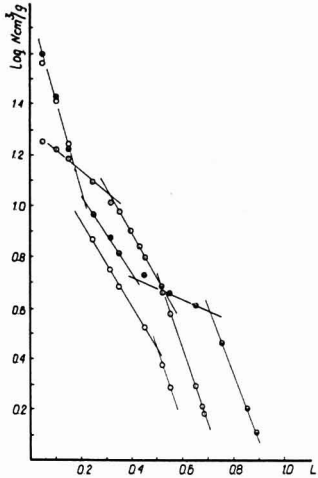

Figure 6. Dynamic adsorption of benzene on sorbent Al_2O_3 (I)

Application of Equation 15 to the determination of the specific surface of the examined sample for injected benzene doses: (in N cm^3) ⊙ = 6.715, ○ = 7.169, ◒ = 8.899

The layer capacity a_m' determined from the deflection point of the discussed plots is in some cases twice as large as normally observed. That was observed only if relatively large amounts of benzene were injected to a column. It seems likely that, in those cases, the deflection point appeared either as the results of completion of the second layer or because of the layer capacity increase. An increase of the layer capacity might be due to the reorientation of adsorbed molecules. It seems that the possibility of observing the deflection point on a logarithmic plot at higher surface concentrations of adsorbed molecules could be considered as a confirmation of the sensitivity of our method.

The influence of the gas carrier flow rate on the slope and L_m distance makes some difficulty in application of that method. The optimal setting of the carrier gas flow rate was found at 20–80 cm^3/min for our column (80–280 cm^3/min·cm^2). For such flow rates, the most reproducible results were obtained because the l_m values were ranging from 0.3 to 0.5. Flow rates outside those limits are unfavorable because they are leading to an increase of the cross-angle of extrapolated straight-line sectors of logarithmic plots. The benzene dose affects the accuracy as well. We have found that the dose of benzene should be sufficient to find as small as possible, but quantitatively detectable, amounts of benzene adsorbed in the last column section (see Figure 2.). At this condition, we found that $a_m = a_m'$. The appropriate dose is usually determined within 3 runs at varying amounts of the adsorbate.

At measurements of the dynamic adsorption of benzene, an interesting phenomenon was observed: on the desorption chromatogram of benzene, at higher carrier gas flow rates of 30 ml/min and for adsorbent samples of higher surface occupancy, a splitting of peaks was observed. That splitting was not observed at the benzene desorption from samples placed in more remote column sections—at smaller surface coverages. For those samples, the slopes of relations log a_i vs. l_i and log $(1 - x)$ vs. l differed from those determined for samples of higher coverage. Those peak splittings are not due to benzene impurities. The high purity of benzene used was confirmed by gas chromatography. It seems that the peak splitting is analogous to that described by Kuge and Yoshikawa (*9*). According to those authors, the peak splitting corresponds to the point B on the Second Type Isotherm, following the Brunauer classification (*3*).

It should be noted that unpublished results (*10*) on dynamic adsorption of selenium(IV) and rhenium(VII) oxides indicate that the appearance of a deflection point on log $(1 - x)$ vs. l plots has to be interpreted as the filling of the monoenergetic surface section on the adsorbent surface, and not as the formation of a complete monolayer of the adsorbate molecules.

NOMENCLATURE

a = amount of a substance adsorbed in N cm^3/g.
a_i = amount of benzene adsorbed on the sorbent sample in a given column section per 1-g sample.
a_m = monolayer capacity in N cm^3/g.
a_m' = amount of adsorbed benzene in N cm^3/g of the adsorbent determined from L_m points.
$A = b \cdot C$.
α = slope, including the expression for the equilibrium constant b.
b = adsorption–desorption equilibrium constant.
C = constant value at given experimental conditions.
C' = constant, including also the expression for the equilibrium constant b.
l = column length.
l_i = distance of the sorbent sample from the beginning of the packing in a column.
l_m = distance of L_m points from the packing start of the column.
L_m = cross point of the extrapolated straight-line sectors of the log $(1 - x)$ vs. l dependence.
m_o = total mass of a sorbent in the column.
m_i = mass of ith analyzed sorbent sample in a given column section.
n_o = total amount of adsorbate injected in the column.
n_i = amount of adsorbed substance on ith analyzed sorbent sample in a given column section.
n_s = amount of adsorbed substance.
n_g = amount of adsorbate in gaseous phase.
N = Avogadro number.
ω = the surface occupied by the benzene molecule.
p = pressure of the sorbed component.
r = cross section of a column.
S_o = specific surface of the examined sample in N cm^3/g.
v = sorbent volume.
V = carrier gas volume.

LITERATURE CITED

(1) H. Golka, T. Mikulski, and B. Jeżowska-Trzebiatowska, *Przem. Chem.*, **51**, 99 (1972).
(2) B. Jeżowska-Trzebiatowska and H. Golka, *Przem. Chem.*, **53**, 101 (1974).
(3) S. Brunauer, L. S. Denning, W. E. Denning, and E. Teller, *J. Am. Chem. Soc.*, **62**, 1723 (1940).
(4) N. E. Bujanova, G. B. Gudkova, and A. P. Karnaukhov, *Kinet. Katal.*, **6**, 1085 (1965).
(5) J. Ościk, "Adsorpcja", PWN, Warszawa, 1973.
(6) S. Brunauer, P. H. Emmett, and E. J. Teller, *J. Am. Chem. Soc.*, **60**, 309 (1938).
(7) O. G. Grubner, *Z. Phys. Chem.*, **216**, 287 (1961).
(8) F. M. Nelsen, and F. T. Eggertsen, *Anal. Chem.*, **30**, 1387 (1958).
(9) Y. Kuge and Y. Yoshikawa, *Bull. Chem. Soc. Jpn.*, **38**, 948 (1965).
(10) H. Golka, unpublished results.

RECEIVED for review January 2, 1975. Accepted May 21, 1976.

Correlation between Electron Capture Response and Chemical Structure for Alkyl Halides

Tsugio Kojima* and Yasukazu Tanaka

Department of Industrial Chemistry, Faculty of Engineering, Kyoto University, Yosida, Kyoto, Japan

Masaru Satouchi

Department of Industrial Chemistry, Shiga Prefectural Junior College, Hikone, Shiga, Japan

The dissociative electron capture reaction for alkyl halides was measured by use of an electron capture detector and the activation energy was obtained by means of the Arrhenius plot of the electron capture coefficient. The free electron in this reaction can be regarded as a nucleophile and the halide anion as a leaving group; then it is considered that the dissociative electron capture reaction proceeds by a mechanism similar to bimolecular nucleophilic substitution (SN2). The relationship between the chemical structure and the activation energy for alkyl halides can be completely explained by assuming the transition state of an SN2 reaction. A gas chromatograph–electron capture detector system can afford the retention index and the activation energy simultaneously, and both closely relate to the chemical structure of the sample molecule. Therefore, it can be expected to facilitate the qualitative analysis of alkyl halides by measuring these values.

Various organic compounds, containing a halogen, oxygen, or sulfur atom, and polynuclear aromatic hydrocarbons exhibit strong electron capture characteristics. By taking advantage of this property, the gas chromatographic trace analysis of a wide variety of environmental pollutants such as poly(chlorobiphenyl), alkyl mercuric chloride, and peroxyacetyl nitrate became possible with an electron capture detector connected to a chromatographic column. The principle of this detection method is summarized as follows.

The background current I_b which is the current observed when the detector is operating with no solute passing through it, is proportional to the concentration of secondary electrons produced through inelastic and elastic collisions between primary electrons from the β-source and molecules or atoms of carrier gas. When an electron-capturing solute entering into the detector captures a near-thermal secondary electron, the current across the cell decreases to I_e because of the consumption of the free electron, and the difference in the detector current, $I_b - I_e$, is observed as the output of the detector on the recorder.

Wentworth and co-workers (*1, 2*) have described the electron attachment phenomenon on the basis of kinetic derivations using the steady-state approximation and related the electron capture response to the concentration of a capturing species in terms of the electron capture coefficient K. According to Wentworth's theory, the molecular electron affinity or the activation energy for an electron attachment accompanying a bond dissociation is obtained from K.

A free electron in an electron capture detector can be regarded as the simplest nucleophile or radical, and then it is possible to consider that the electron attachment is a kind of organic reaction between the simplest reagent and a reactive substrate, both suspended in an inert gas. Since the electron affinity or the activation energy is the potential energy difference between the neutral state and the anion radical of a sample molecule or the electron-attached transition state of a sample molecule, variations in these energies can be explained in terms of the stabilization of the anion radical or the transition state through the inductive and resonance effects, and the molecular strain. Since the effects are closely correlated with the chemical structure of the sample molecule, the electron affinity and the activation energy obtained could be used as information for identification. It has been proved that the structure of various compounds can be estimated by measuring the electron affinity and the activation energy (*3–5*).

Although an electron capture detector is constructed from very simple units compared with other instruments for identification, it functions not only as a highly sensitive detector but also as a qualitative detector.

This paper describes the correlation between the activation energy and the chemical structure of haloalkanes on the basis of the transition state model analogous to that in an SN2 reaction and proposes its applicability to qualitative analysis.

EXPERIMENTAL

The gas chromatograph used in this investigation was a modified Shimadzu GC-2C model. The electron capture detector employed was a concentric type with 15 mCi nickel-63 as a radioactive source. Applied voltage was supplied as a pulse through a pulse generator with an amplitude of 28 V, a pulse width of 3.2 μs and a pulse time of 3200 μs, and then electron capture reaction proceeded under field-free conditions.

Glass columns (0.4 cm × 240 cm) were packed with Shimalite W 80/100 mesh, coated with 15% Apiezon L or 20% TCP for separation of the chlorides and the bromides and their temperatures were maintained at 80 °C or 100 °C. For the iodides, a glass column (0.4 cm × 100 cm) was packed with Durapak (Carbowax 400/Porasil C) and its temperature was maintained at 70 °C. Nitrogen was used as a carrier gas. In most cases, methane at a concentration of 5–10% is added to argon as a quenching gas for thermalization of fast electrons. Using methane, Wentworth et al. (*6*) estimated that an electron with an energy of 10 keV was cooled to 10% above thermal energies ($2–5 \times 10^{-2}$ eV) in 0.076 μs. Although the activation energies obtained in this study were somewhat smaller than those with argon–methane by Wentworth, it would not be unreasonable to assume that in the time of 3200 μs with no voltage applied, a near-thermal distribution could be obtained.

Since van de Wiel and Tommassen have described that an oxygen molecule as an impurity in nitrogen gas captures a free electron (*7*), the oxygen in the carrier gas was removed by passing it through an absorption tube packed with cuprous chromate pellets. When this tube is inserted between the cylinder of the carrier gas and the GC inlet, an increase in the detector current is observed. Another tube packed with Molecular Sieve 5A was used for the removal of moisture.

The temperature of the detector cell was measured by insertion of a thermocouple in the detector bath. The reagents used were all commercially available and some of them were redistilled before use. The sample solution was prepared by dilution with pentane, hexane, or benzene to a concentration such that the detector current decreases to about a half of the background current.

The electron capture coefficient K was calculated from the following equation derived by Wentworth (*1, 2*):

$$\frac{F}{S}\int \frac{I_b - I_e}{I_e}\,dx = Kn$$

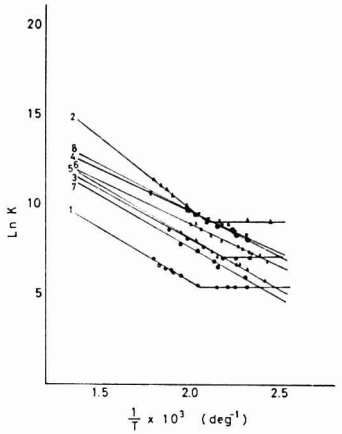

Figure 1. Arrhenius plots of electron capture coefficients for alkyl chlorides

(1) Isopropyl chloride, (2) *n*-butyl chloride, (3) *sec*-butyl chloride, (4) *tert*-butyl chloride, (5) *n*-pentyl chloride, (6) *tert*-pentyl chloride, (7) *n*-hexyl chloride, (8) cyclohexyl chloride

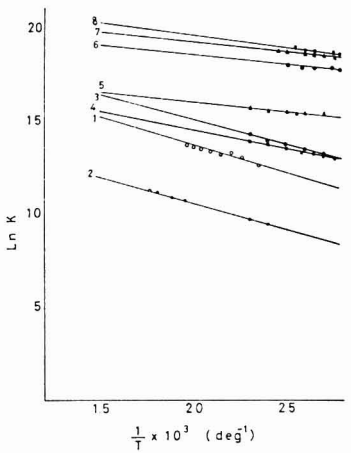

Figure 2. Arrhenius plots of electron capture coefficients for alkyl bromides and alkyl iodides

(1) *n*-Propyl bromide, (2) isopropyl bromide, (3) *n*-pentyl bromide, (4) *sec*-pentyl bromide, (5) *tert*-pentyl bromide, (6) ethyl iodide, (7) *n*-propyl iodide, (8) *n*-butyl iodide

where F is the carrier gas flow rate in l./min, S is the chart speed in cm/min, n is the amount of sample injected in moles. I_b and I_e are the detector current without and with a capturing species in the detector, respectively. Since the detector signal proportional to $(I_b - I_e)$ was converted to the signal proportional to $(I_b - I_e)/I_e$ through an analog convertor, the integral term of the above equation corresponds to the peak area on the chromatogram.

RESULTS AND DISCUSSION

According to Wentworth's theory, there are roughly two reaction modes in an electron capture reaction; a nondissociative reaction where an anion radical is produced from a sample molecule and a dissociative reaction where an anion and a radical are produced (*1*, *2*).

$$AB + e^- = AB^- \text{ (nondissociative)} \quad (1)$$

$$AB + e^- = A + B^- \text{ (dissociative)} \quad (2)$$

Wentworth and co-workers have correlated the electron capture coefficient K to the electron affinity of a sample molecule in the nondissociative reaction or the activation energy for the dissociative reaction as expressed in the following equations:

$$\ln KT^{3/2} = Z + EA/RT \text{ (nondissociative)} \quad (3)$$

$$\ln K = Z - E^*/RT \text{ (dissociative)} \quad (4)$$

where EA and E^* are the electron affinity and the activation energy in kcal/mol, R is a gas constant, and T is the absolute temperature in the detector. Z is a pre-exponential factor. The Arrhenius plot of K may be linear with a positive slope of EA/R for the nondissociative case or with a negative slope of E^*/R for the dissociative case.

The Arrhenius plots of ln K for alkyl chlorides, alkyl bromides, and alkyl iodides are shown in Figures 1 and 2. Since all the plots are linear with negative slopes, it can soon be seen that alkyl halides capture free electrons dissociatively. In Table I are given the activation energies calculated by the least-squares method. The activation energy for an alkyl halide evidently depends primarily upon the halogen species contained, and secondarily upon the carbon skeleton. The activation energies fall in the range of about 12 to 9 kcal/mol for the chlorides, of about 7 to 2 kcal/mol for the bromides, and of nearly 2 kcal/mol for the iodides. The activation energies decrease in the order of the length of the carbon chain and in the order of primary > secondary > tertiary and in the order of chloride > bromide > iodide. This order is the same as that of the dissociation energy for the carbon–halogen bond and is contrary to the order of electron affinity for the halogen atom. This fact shows that the activation energy is predominantly determined by the bond dissociation energy. Since the magnitude of the activation energy is the measure of the sensitivity of an electron capture detector to the sample molecule, it will be concluded that if the dissociation energy

Table I. Activation Energies E^* for Alkyl Halides

Compound	E^*
Isopropyl chloride	10.9 ± 0.3[a]
n-Butyl chloride	12.1 ± 0.3
sec-Butyl chloride	11.5 ± 0.3
tert-Butyl chloride	10.0 ± 0.3
n-Pentyl chloride	10.8 ± 0.3
tert-Pentyl chloride	9.1 ± 0.3
n-Hexyl chloride	10.7 ± 0.3
Cyclohexyl chloride	9.6 ± 0.3
n-Propyl bromide	6.4 ± 0.3
Isopropyl bromide	5.6 ± 0.3
n-Butyl bromide	5.7 ± 0.3
sec-Butyl bromide	4.6 ± 0.3
tert-Butyl bromide	2.4 ± 0.3
n-Pentyl bromide	5.8 ± 0.3
sec-Pentyl bromide	3.6 ± 0.3
tert-Pentyl bromide	1.6 ± 0.3
Ethyl iodide	1.8 ± 0.3
n-Propyl iodide	2.0 ± 0.3
n-Butyl iodide	2.3 ± 0.3
Benzyl chloride	3.6 ± 0.1
m-Methylbenzyl chloride	3.4 ± 0.2
p-Methylbenzyl chloride	3.2 ± 0.2
	in kcal/mol

[a] Standard deviation.

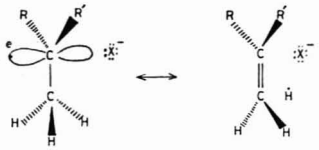

Figure 3. Resonance structure in transition state

of the A–B bond is low, a sample molecule AB containing an electrophilic group B may be detected by an electron capture detector with a high sensitivity even if the electron affinity of group B is low.

Wentworth et al. have described a linear relationship between the activation energy and the change in internal energy with a slope of unity for some alkyl halides as expressed in Equation 5 (*8*).

$$E^* = \Delta E + 15.3 \quad (5)$$

where ΔE is the change in internal energy (the difference between the dissociation energy of the C–X bond and the electron affinity of group X). In this study, the relationship between E^* and ΔE obtained is expressed by the following equation.

$$E^* = 0.89\ \Delta E + 14 \quad (6)$$

Since a standard error of about 2 kcal/mol is involved in the C–X bond dissociation energy, it seems that this empirical relationship is essentially identical with that obtained by Wentworth. This is a very convenient relation for estimating E^* from ΔE or vice versa.

As the activation energy is concerned with the difference of the potential energy between the neutral state and the transition state of a sample molecule, it is interesting to consider the structure of the transition state and to correlate the stability of the transition state to the value of the activation energy shown in Table I. The dissociative electron capture reaction of the alkyl halide could be assumed to be similar to a bimolecular nucleophilic substitution in solution. According to this assumption, the sp^3 orbital on the α-carbon atom should change to an sp^2 orbital as a free electron is approaching. Therefore, the stability of the transition state depends upon the extent to which the accepted odd-electron in the p orbital on the α-carbon atom is delocalized by resonance. In such a case, it can be considered that the resonance effect is based on the hyperconjugation in which the hydrogen atoms attached to the β-carbon atom participate (Figure 3).

From this model, it can be explained that the activation energies for alkyl halides decrease in the order of primary > secondary > tertiary. In addition, it is expected that the delocalization of the odd electron on the α-carbon atom through the phenyl ring in benzyl halide gives an additional resonance energy and the activation energies for benzyl halides will be lower than those for alkyl halides. This assumption, in fact, was confirmed by comparison of the activation energies for alkyl halides and benzyl chloride as shown in Table I. Because of the contribution of the *p*-methyl group to the hyperconjugation through the phenyl ring, it is also shown in Table I that *p*-methylbenzyl chloride has greater reactivity in the electron capture reaction than benzyl chloride or *m*-methylbenzyl chloride.

While the reactivity of alkyl halides with a free electron decreases in the order of tertiary > secondary > primary, the reverse order has been found to hold in SN2 reactions in solution. This difference may be explained by considering the steric hindrance between the alkyl groups around the α-carbon atom and a nucleophile. Since such an effect is negligible when a free electron is a nucleophile, the reactivity in the electron capture reaction is influenced only by the electronic effect. On the other hand, the steric hindrance between the alkyl groups around the α-carbon atom and the leaving group X contributes to weakening the C–X bond in analogy with an SN2 reaction.

In the dissociative electron capture reaction, the hyperconjugation also contributes to the stabilization of the resulting radical. Then the factor contributing to the stabilization of the product parallels that found in the transition state. This fact is an explanation for the linear relationship between the activation energy and the change in internal energy.

Our proposal on the mechanism of the electron capture reaction will be helpful for understanding the relationship between the activation energy measured and the chemical structure of the sample molecule and then the identification of a peak on the chromatogram in the GC–ECD system.

CONCLUSION

An extensive study has been made of the structural effects on the electron capture reaction of alkyl halides. We concluded that the electron capture reaction of alkyl halides is a kind of SN2 reaction. The reactivity in the electron capture reaction of alkyl halides is fully interpreted on the basis of the mechanism for the SN2 reaction. The validity of the activation energy for the estimation of the chemical structure was suggested.

If an electron capture detector is used in gas chromatographic analysis of alkyl halides, the activation energy E^* and the retention index I for each compound are measured simultaneously. These values could conceivably aid in elucidating the structure of an unknown component. For example, the carbon number could be estimated from I, the kind of halogen atom from ΔI and E^*, the number and the kinds of substituents on the α-carbon atom from ΔI and E^*.

LITERATURE CITED

(1) W. E. Wentworth, E. Chen, and J. E. Lovelock, *J. Phys. Chem.*, **71**, 1652 (1967).
(2) W. E. Wentworth and E. Chen, *J. Gas Chromatogr.*, **5**, 170 (1967).
(3) M. Satouchi and T. Kojima, *Anal. Lett.*, **5**, 931 (1972).
(4) T. Kojima and M. Satouchi, *Jpn Anal.*, **22**, 1428 (1973).
(5) T. Kojima and M. Satouchi, *Jpn Anal.*, **23**, 79 (1974).
(6) W. E. Wentworth, E. Chen, and J. E. Lovelock, *J. Phys. Chem.*, **70**, 445 (1966).
(7) H. J. van de Wiel and P. Tommassen, *J. Chromatogr.*, **71**, 1 (1972).
(8) W. E. Wentworth, R. George, and H. Keith, *J. Chem. Phys.*, **51**, 1791 (1969).

RECEIVED for review April 5, 1976. Accepted June 24, 1976.

Comparison of Positive Ions Formed in Nickel-63 and Corona Discharge Ion Sources Using Nitrogen, Argon, Isobutane, Ammonia and Nitric Oxide as Reagents in Atmospheric Pressure Ionization Mass Spectrometry

I. Dzidic, D. I. Carroll, R. N. Stillwell, and E. C. Horning*

Institute for Lipid Research, Baylor College of Medicine, Houston, Texas 77025

Ions with a short residence time were observed with an API (atmospheric pressure ionization) corona discharge source by locating the discharge point 0.5 mm from the sampling aperture. Nitrogen ions (N^+ and N_2^+) and argon ions (Ar^+) were observed when nitrogen and argon (0.1% in ultrahigh purity helium) were reagents. The nitrogen ion N_4^+ was the major reactant ion observed in nitrogen alone. Ions with long residence times in a corona source were observed by changing the distance from the discharge point to the sampling aperture to 4.0 mm. The formation and reactions of $t\text{-}C_4H_9^+$, NO^+, and NH_4^+ with several organic compounds are described for both corona discharge (4 mm) and ^{63}Ni sources.

The technique of API (atmospheric pressure ionization) mass spectrometry using a ^{63}Ni or a corona discharge ionization source has been described in previous publications (*1–9*). Several methods of sample introduction have been employed. Samples may be introduced by direct injection in common organic solvents (*1, 2*), or in the effluent stream from a liquid chromatograph (*3, 4, 6*). Under these conditions, the reactant ion species are determined by the organic solvent. For example, $C_4H_9^+$ is the major reactant ion produced when isooctane is used (*6*). The sample may also be introduced by volatization from a platinum wire probe inserted into the heated flowing gas stream (*5*), or in the effluent stream from a gas chromatograph. Previously, reactant ion species employed in the absence of solvents were generated from water or oxygen present as trace impurities in the carrier gas. As indicated in this paper, the addition of small amounts of isobutane, ammonia, or nitric oxide to the carrier gas yields the reactant ions $t\text{-}C_4H_9^+$, NH_4^+, and NO^+, and these ions can be used in the same manner at atmospheric pressure as in conventional chemical ionization (CI) mass spectrometry at pressures around 1 Torr. The order of basicity is $NH_3 > C_4H_8 > H_2O$.

It is possible to generate and to observe short lived reactant ions in a corona discharge source of new design. This source has an axially adjustable discharge point. Ion residence times can be effectively controlled by adjusting the distance from the discharge to the sampling aperture. With a distance of 0.5 mm, ions with very short residence times in the source can be observed. This circumstance makes it possible to demonstrate experimentally the presence of high energy reactant ions in an API source, and to define in greater detail the sequence of ion molecule reactions that are involved in the ionization of organic compounds in these sources.

The work reported in this paper is primarily directed to defining reactions and conditions leading to the formation of useful reactant ions. It should be noted that product ions observed with both a ^{63}Ni and a corona discharge source, when the discharge is several mm distant from the aperture, are identical. The product ions observed under these conditions are stable and relatively long lived. With a corona discharge source of appropriate design, however, initial, intermediate, and product ionic species involved in API processes can be detected.

EXPERIMENTAL

Instrumentation. Details of the design and operation of the API mass spectrometer under a variety of conditions have been published (*1–9*). The spectra of high energy ions reported in this paper were obtained using a source designed for a gas chromatograph–mass spectrometer–computer (GC-MS-COM) analytical system. A schematic diagram of this source is shown in Figure 1. For this study, the source was connected directly to the reagent gas supply, without an intervening gas chromatograph. The distance from the corona discharge point to the sampling aperture was 0.5 mm, the corona potential was 800–1000 V, and the discharge current was maintained at 10^{-5} A. Under these conditions, the major reactant ion peaks saturated the electron multiplier. Single ion currents, measured using the multiplier as a Faraday cup, were up to 10^{-10} A. The high energy ion spectra were taken using the multiplier as a Faraday cup with a full scale recorder deflection of 10^{-10} A.

The API source used for the comparison of ^{63}Ni and corona discharge spectra, for ions with relatively long lifetimes, was designed for use in a prototype liquid chromatograph–mass spectrometer–computer (LC-MS-COM) analytical system (*4*). The reaction chamber contained both a ^{63}Ni and a corona discharge source. In this instance, the distance of the corona discharge point to the sampling aperture was 4 mm. Samples were introduced by platinum wire probe (*5*). Spectra of the reactant ions $t\text{-}C_4H_9^+$, NO^+, and NH_4^+, and ionic products from these ions, were determined in conventional manner using pulse counting techniques (*1*).

Reagents. Nitrogen or argon (0.1% in ultrahigh purity helium), ammonia (0.01% in ultrahigh purity helium), ultrahigh purity helium, and high purity nitrogen were obtained from Linde Division, Union Carbide Corp. Research grade isobutane (0.1% in high purity nitrogen) was obtained from Matheson Gas Products. *n*-Heptylamine and 4-heptanol were from Aldrich Chemical Co. Heptanoic-γ-lactone was from Pfaltz and Bauer, Inc. Nicotine was from Eastman Organic Chemical Co.

RESULTS AND DISCUSSION

Nitrogen Ions in Nitrogen and in Nitrogen/Helium. In the initial API study (*1*) it was proposed, primarily on the basis of kinetic data (*10*), that the $H^+(H_2O)_n$ ions observed as reagent ions in an API source (with nitrogen as the carrier gas) were formed by a sequence of ion molecule reactions originating with the formation of N_2^+ by electron bombardment:

$$N_2 + e \rightarrow N_2^+ + 2e \quad (1)$$

$$N_2^+ + 2N_2 \rightarrow N_4^+ + N_2 \quad (2)$$

$$N_4^+ + H_2O \rightarrow H_2O^+ + 2N_2 \quad (3)$$

$$H_2O^+ + H_2O \rightarrow H_3O^+ + OH \quad (4)$$

$$H_3O^+ + H_2O + N_2 \rightarrow H^+(H_2O)_2 + N_2 \quad (5)$$

$$H^+(H_2O)_{n-1} + H_2O + N_2 \rightarrow H^+(H_2O)_n + N_2 \quad (6)$$

The ions N_2^+, N_4^+, and H_2O^+ can be observed only if ion residence times in the source are reduced to less than the half

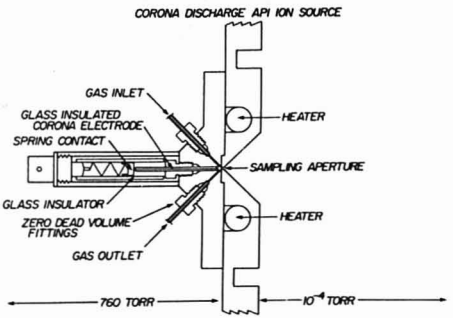

Figure 1. Schematic diagram of a corona discharge source with an adjustable distance between point and sampling aperture

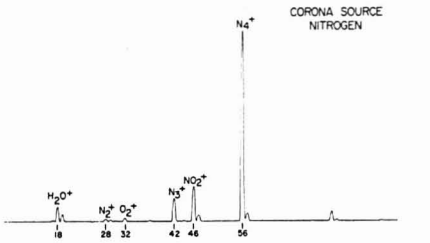

Figure 2. Mass spectrum of nitrogen obtained with the corona discharge point located at a distance of 0.5 mm from the sampling aperture. Source temperature, 200 °C

life of the reactions in which they participate. Assuming that the water concentration is 1 part per million (1.6×10^{13} molecules cm^{-3} at 200 °C), and using the experimentally determined reaction rate constant (*10*) of 1.8×10^{-9} cm^3 $molecule^{-1}$ s^{-1}, the half life of reaction 4 is:

$$t_{1/2} = \frac{1}{(1.6 \times 10^{13}) \times (1.8 \times 10^{-9})} = 3.5 \times 10^{-5}\ \text{s}$$

Thus, an experimental demonstration of the presence of H_2O^+ (the product of reaction 3) requires a sampling procedure that will remove ions from the source chamber in about 10^{-5} s or less. These conditions were achieved with a corona discharge source of the design shown in Figure 1, with a distance of 0.5 mm from the corona discharge point to the sampling aperture. With nitrogen as the carrier gas, and with this source, the major reactant ion at 200 °C was observed to be N_4^+. The ions present in the source chamber under this condition of operation are shown in Figure 2; N_2^+ is also present, along with some N_3^+.

It is generally assumed that ions formed at atmospheric pressure are brought to thermal equilibrium very rapidly. This may not be the case for a corona discharge. It is not possible at this time to determine directly the rate of transfer of ions from the corona point to the mass analyzer region, but estimates can be made. If the field from the corona discharge point to the aperture is uniform, the velocity of an N_4^+ ion generated with an applied voltage of 10^3 and present in a field of 2×10^4 V cm^{-1} would be 5×10^4 cm s^{-1} (*11*), and the transit time from the corona point to the aperture would be about 10^{-6} s. This value can be compared with estimates for the half life of reaction 2. The forward reaction rate constant is 8×10^{-29} cm^6 $molecule^{-2}$ s^{-1} (*12*), and the half life is:

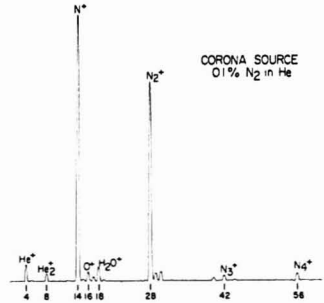

Figure 3. Mass spectrum of 0.1% nitrogen in helium, obtained with the corona discharge point located at a distance of 0.5 mm from the sampling aperture. Source temperature, 200 °C

$$t_{1/2} = \frac{1}{8 \times 10^{-29}\,[N_2]^2}$$

where $[N_2]$ is the nitrogen gas density. At 200 °C the density is 1.6×10^{19} molecules cm^{-3}, leading to a value for the reaction half life of about 5×10^{-11} s. These relationships suggest that at 200 °C, and with a transit time of about 10^{-6} s, it should not be possible to observe N_2^+ ions. If the equilibrium constant for reaction 2 is calculated from Figure 2, using the equation:

$$K_{2,4} = \frac{I_4}{I_2 \times P_{N_2}}$$

where I_2 and I_4 are the observed ion intensities for N_2^+ and N_4^+, respectively, P_{N_2} is the pressure of the nitrogen carrier gas (760 Torr), and $K_{2,4}$ is the equilibrium constant for Equation 2 in $Torr^{-1}$, the value is found to be 0.1 $Torr^{-1}$. The data of Payzant and Kebarle (*12*) give a value of $K_{2,4} = 0.1$ $Torr^{-1}$ for a temperature (at thermal equilibrium) of 540 °C. The ions are evidently not in thermal equilibrium with the ion source walls (which are at 200 °C). The high energy of the ions is probably due to the high electric field present in the discharge which leads to high ion velocities and thus through collisions to much higher vibrational and rotational energy, i.e., "high effective temperature" of the ions. These ions have ion lifetimes that permit their observation when transit times of 10^{-6} to 10^{-5} s are attained through appropriate source design.

A convenient way to reduce the concentration of nitrogen in the source is to use a nitrogen/helium mixture; this reduces the concentration of N_4^+ ions, and N_2^+ and N^+ ions become the principal high energy reactant ions. Figure 3 shows the positive ions observed for a 0.1% nitrogen in helium reagent gas mixture. The initial reactant ions are He^+ and He_2^+:

$$He + e \rightarrow He^+ + 2e \quad (7)$$

$$He^+ + 2He \rightarrow He_2^+ + He \quad (8)$$

and the N^+ and N_2^+ ions are produced by charge transfer:

$$He^+ + N_2 \rightarrow N^+ + He + N \quad (9)$$

$$He^+ + N_2 \rightarrow N_2^+ + He \quad (10)$$

The ions N_3^+ and N_4^+ are the products of subsequent reactions of N^+ and N_2^+ with N_2. The equilibrium constant for reaction 2, calculated as described from the observed (Figure 3) ion intensities for N_2^+ and N_4^+ indicates an effective temperature of 570 °C. This result is in agreement with observations made for nitrogen alone: the high energy, short

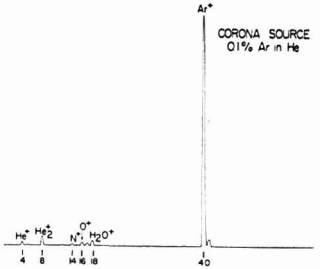

Figure 4. Mass spectrum of 0.1% argon in helium obtained with the corona discharge point located at a distance of 0.5 mm from the sampling aperture. Source temperature, 200 °C

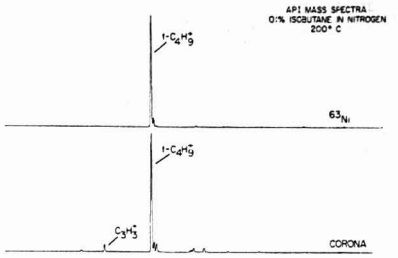

Figure 5. API mass spectra (^{63}Ni and 4-mm corona discharge) showing reactant ions obtained from isobutane (0.1% in nitrogen) at 200 °C

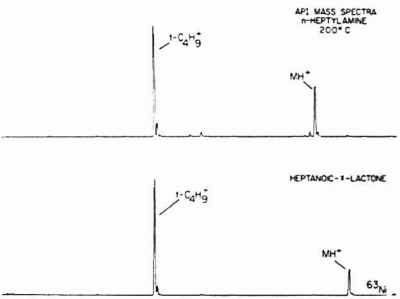

Figure 6. API mass spectra of reaction products for *n*-heptylamine and heptanoic-γ-lactone in the presence of t-$C_4H_9^+$ at 200 °C (^{63}Ni source)

lived reactant ions N^+, N_2^+, and N_4^+ are not in thermal equilibrium within the source.

These reactants will generate ions from any substance with an ionization potential below that of nitrogen that is introduced into the source. For example, Figures 2 and 3 show ions due to impurities in the gases. The ions at 16 and at 32 amu are due to O^+ and O_2^+; ions at 18 amu are due to H_2O^+. The ion at 46 amu was identified by Shahin (*13*) as being due to NO_2^+.

Other Highly Reactive Ions. When a reagent/carrier gas mixture of 0.1% argon in helium was employed, the major reactant ion was Ar^+, as shown in Figure 4. Water was not added to nitrogen or helium to provide additional reactant ions, although this could be done. The initial ionic product from water is H_2O^+ (reaction 3).

Reactions of High Energy Ions. The use of 0.1% of nitrogen or argon in helium, as a reagent/carrier gas results in a sequence of ionization reactions. The initial step is the formation of helium ions (ionization potential, 24.6 eV) (reactions 7 and 8). This is followed by ionization of the reagent to yield argon ions (ionization potential, 15.7 eV) or nitrogen ions (N_2^+, ionization potential, 15.6 eV). These highly reactive, short lived ions will react by charge transfer with organic compounds introduced into the source. It is not yet known if argon charge transfer spectra will prove to be of practical value in applications of GC-MS(API)-COM analytical systems. Preliminary experiments with *n*-alkanes have shown that hydrocarbon radical ions can be observed, but this aspect of API processes remains to be investigated.

Inorganic substances introduced into the source chamber may also be ionized under these conditions, but potential uses of API mass spectrometry in inorganic chemistry have not been investigated.

The introduction of appropriate organic or inorganic reagents has the effect of providing a new ion or group of ions which in turn may serve as reactants. In these instances, the carrier gas may be helium, argon, or nitrogen, and reagents of current interest are isobutane, ammonia, and nitric oxide. The ions derived from isobutane, ammonia, and nitric oxide are relatively stable and long lived, but sufficiently reactive with most organic compounds to provide product ions that are also relatively stable and long lived. An advantage gained in using these reactants is that water, which is unavoidably present as a trace impurity, is not ionized to a detectable extent in the presence of these reagents. The reagent and product ions are in thermal equilibrium in 4-mm corona discharge and ^{63}Ni sources.

Formation of t-$C_4H_9^+$ Ions in 0.1% Isobutane in Nitrogen. Figure 5 shows the reactant ions observed at 200 °C for nitrogen carrier gas containing 0.1% isobutane. The corona discharge (4 mm) and ^{63}Ni spectra are essentially identical, but the corona spectrum shows in addition a low concentration of the $C_3H_3^+$ ion. This ion was also observed in the CI (1 Torr) spectrum of isobutane (*14*); it is a relatively stable ion. In both sources the t-$C_4H_9^+$ ion is probably produced by charge transfer with hydrogen radical loss:

$$N_4^+ + C_4H_{10} \rightarrow t\text{-}C_4H_9^+ + 2N_2 + H \qquad (11)$$

The t-$C_4H_9^+$ ion is produced over a wide range of isobutane concentrations. The upper limit of useful concentration depends chiefly upon the impurities in the reagent; with research grade isobutane, the upper limit is around 1%. The lower limit of useful concentration is determined by the water present in the source. Reaction 3 forms H_2O^+ ions from traces of water present in the carrier gas. Assuming that the charge transfer reaction rates for reactions 3 and 11 are of the same order of magnitude, a useful limit would be about 10^2 above the water concentration. For this reason, a range of isobutane concentration from 0.01 to 1.0% is suitable for the generation of t-$C_4H_9^+$ ions. The half-life of reaction 11 is approximately 5×10^{-7} s for a 0.01% concentration of reactant.

Reactions of t-$C_4H_9^+$ Ions. The usual reaction observed under conventional isobutane CI conditions with organic compounds containing nitrogen or oxygen atoms is ionization by proton transfer (*15*).

$$M + t\text{-}C_4H_9^+ \rightarrow MH^+ + C_4H_8 \qquad (12)$$

This reaction is illustrated in Figure 6 for two compounds with a ^{63}Ni source; identical corona discharge spectra were observed. The t-$C_4H_9^+$ ion will also participate in hydride abstraction reactions with saturated aliphatic hydrocarbons, and will add to some compounds to form $(M + 57)^+$ (*15*). These reactions were not investigated.

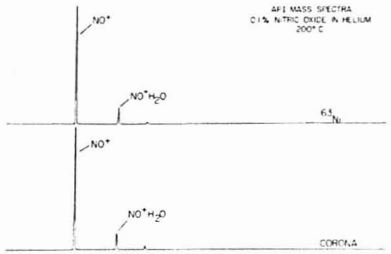

Figure 7. API Mass spectra (^{63}Ni and 4-mm corona discharge) showing reactant ions obtained from nitric oxide (0.1% in helium) at 200 °C

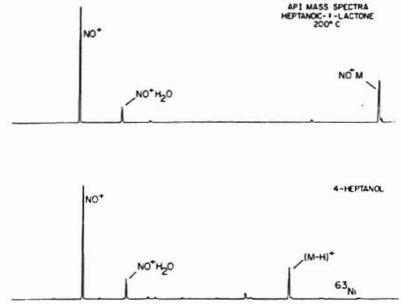

Figure 8. API mass spectra of reaction products for a secondary alcohol and for a lactone in the presence of NO^+ at 200 °C (^{63}Ni source)

Formation of NO^+ Ions in 0.1% Nitric Oxide in Helium. Figure 7 shows the corona discharge and ^{63}Ni spectra of 0.1% nitric oxide in helium at 200 °C. The NO^+ ions are formed directly or by charge transfer from He^+ ions:

$$He^+ + NO \rightarrow NO^+ + He \qquad (13)$$

The ionization potential of nitric oxide (9.2 eV) is below that of water (12.5 eV) so that charge transfer from H_2O^+ would also give NO^+ ions. The concentration range of nitric oxide in helium is not highly critical; the lower limit should be several orders of magnitude greater than sample concentrations, while the useful upper limit is set by dimer ion formation. In the concentration range of 0.1 to 1%, the major reactant ion species is NO^+. The concentration of cluster ions $NO^+(H_2O)_n$ will be dependent upon the source temperature and the water concentration. The expected ratios of NO^+ to NO^+H_2O at different temperatures and partial pressures of water can be calculated from the data of French, Hills, and Kebarle (*16*). The variation in ion intensities for N_2/NO mixtures under CI conditions (0.9 Torr, 100 °C), as a function of NO concentration, was studied by Jelus, Munson, and Fenselau (*17*). A similar study cannot be made with a 4-mm corona discharge source, since the short lived nitrogen ions which are present in the source are not observed.

Reactions of NO^+ Ions. The use of NO^+ ions in conventional CI mass spectrometry has been recommended as a means of identifying certain functional groups (*18–22*). For example, hydride abstraction from a secondary alcohol leads to $(M\text{-}H)^+$:

$$R_1CHOHR_2 + NO^+ \longrightarrow R_1\overset{\overset{+OH}{\|}}{C}R_2 + HNO \qquad (14)$$

This reaction is illustrated in Figure 8 for 4-heptanol.

Hydride transfer to NO^+ from hydrocarbons has been studied (*23–25*); when the hydrocarbon contains a tertiary hydrogen atom, the reaction occurs readily.

Reaction by addition may also occur. In instances where the reacting compound has a high dipole moment, NO^+ may add:

$$M + NO^+ + He \rightarrow NO^+M + He \qquad (15)$$

The extent of formation of NO^+M depends upon the structure of M and the source temperature; increasing the temperature decreases the ion yield. An example of reaction 15 is in Figure 8 for heptanoic-γ-lactone.

Charge transfer may also occur (*17*); relatively few examples of this type have been studied. Identical spectra for all reactions were obtained with ^{63}Ni and corona discharge sources.

Formation of NH_4^+ Ions in Ammonia in Helium. Formation at 250 °C of the reactant ion NH_4^+, and the cluster ion $NH_4^+NH_3$, in helium containing approximately 30 ppm of ammonia, is shown in Figure 9. This concentration was obtained by dilution of 0.01% ammonia in helium. The ^{63}Ni and corona discharge spectra are identical. The initial ionization reactions are assumed to involve charge transfer from He^+ to form NH_3^+, NH_2^+, and NH^+ ions. The reactant ion NH_4^+ is formed as a product of further reaction, for example:

$$NH_3^+ + NH_3 \rightarrow NH_4^+ + NH_2 \qquad (16)$$

The cluster ion $NH_4^+NH_3$ is formed by the reaction:

$$NH_4^+ + NH_3 + He \rightarrow NH_4^+NH_3 + He \qquad (17)$$

The cluster ion $NH_4^+NH_3$ has a proton affinity that is 24.8 Kcal greater than that of NH_4^+, and it is not suitable for general use as a reactant ion species. For this reason, the concentration of ammonia in the carrier gas must be held within relatively narrow limits. The lower limit of concentration is set by the requirements that reaction 16 be completed. Assuming a reaction rate constant for reaction 16 of 10^{-9} cm^2 molecule^{-1} s^{-1}, and a reaction half life of 10^{-4} s for reaction 16, gives a lower limit of about 10^{13} molecules cm^{-3} or about 0.6 ppm of ammonia. At this concentration, the ratio of $NH_4^+NH_3$ to NH_4^+ ions can be calculated from the relationship:

$$K_{0,1} = \frac{I_c}{I \times P_{NH_3}}$$

where I_c is the cluster ion intensity, I is the NH_4^+ ion intensity, P_{NH_3} is the ammonia pressure in Torr and $K_{0,1}$ is the equilibrium constant in Torr^{-1}. The equilibrium constant at various source temperatures can be determined from the data of Payzant, Cunningham, and Kebarle (*26*). At 250 °C, it is 100 Torr^{-1}. Assuming an upper limit of 2:1 for the ratios of $NH_4^+NH_3$ to NH_4^+, as shown in Figure 9, the upper limit of ammonia concentration is 27 ppm. At 200 °C, the equilibrium constant increases to 700 Torr^{-1} and the upper limit would be reduced to 4 ppm, just slightly above the useful lower limit. Thus, in API studies, the useful range of ammonia concentration is rather limited.

Reactions of NH_4^+ Ions. Figure 10 shows the ionization of *n*-heptylamine and nicotine by reaction with NH_4^+ ions. The ^{63}Ni and corona discharge spectra were identical.

Numerous examples have been published of the use of NH_4^+ as a reactant ion in conventional CI mass spectrometry (*27–33*). The proton affinities of amines (*34–37*), amides (*36*), pyridines (*34, 35*) and some ketones (*29*) are higher than ammonia, so that a variety of compounds can be ionized by proton transfer from NH_4^+. Two examples of amine protonation are in Figure 10.

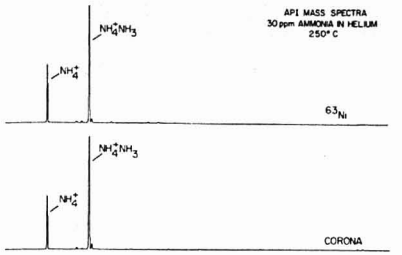

Figure 9. API mass spectra (^{63}Ni and 4-mm corona discharge) showing reactant ions obtained from ammonia (30 ppm in helium) at 250 °C

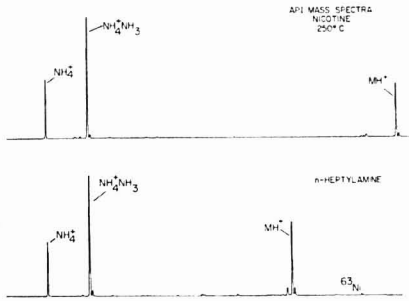

Figure 10. API mass spectra of reaction products for *n*-heptylamine and for nicotine in the presence of NH_4^+ at 250 °C (^{63}Ni source)

The cluster ion $NH_4^+NH_3$ is relatively unreactive, since proton transfer from this ion is 24.8 Kcal/mol more endothermic than proton transfer from NH_4^+ (*26*); if the concentration of NH_4^+ ions is greatly depressed by the use of 0.1% ammonia in helium, the capability of ionization by NH_4^+ is virtually lost.

Low Energy Ions as Reactants. No differences have been observed in ^{63}Ni and corona discharge (4 mm) spectra for reactions of relatively low energy ions with organic compounds. Both reactant and product ions are less reactive than ions such as N^+, N_2^+, or Ar^+. The transit time from the corona point to the sampling aperture is estimated to be about 10^{-4} to 10^{-3} s, and highly reactive carrier gas ions, although present in the source, are not detectable under these conditions.

Only a few representative reactions were studied; the results are in accord with present knowledge of CI reactions. The reactant ions $t\text{-}C_4H_9^+$, NH_4^+, and NO^+ should show the same chemical properties in an API source as in a conventional CI source.

Comparison of Sensitivity of Detection with Different Sources. The sensitivity of detection observed with the usual 4-mm corona discharge source has been shown to be the same as that of a ^{63}Ni source (*6*). The sensitivity of detection with the corona discharge source (0.5 mm) designed for studies of high energy ions has not been determined. The ion residence times are reduced, while the total ion current is increased by about 10^2. It is expected that the sensitivity of detection attainable with this source will probably be less than that observed for ^{63}Ni and 4-mm corona discharge sources; this question is under investigation.

Use of Mixed Gases in API Sources. The use of mixed gases in a conventional CI source has been proposed (*38, 39*) in order to provide a composite spectrum made up of charge transfer fragmentation ions and one or more relatively stable ions resulting from proton transfer. These spectra have been recommended for use in structural studies.

The purpose of using mixed gases in API mass spectrometry is entirely different. Only small amounts of reagent are needed to produce a suitable reactant ion concentration. The ionization sequence is carrier gas → reagent → product ions, and concentrations of 0.01–0.1% of reagent are adequate for this purpose. Other advantages in using a low concentration of reagent are that cluster ion formation is reduced (this is an important effect for ammonia) and that the effects of small amounts of impurities are minimized. The upper limit of reagent concentration is usually determined by the impurities in the reagent. There is no implication that a charge transfer and a proton transfer spectrum should be observed in composite form as a consequence of the use of mixed gases with a ^{63}Ni or 4-mm corona discharge source.

CONCLUSIONS

The reactant ions N_2^+ and N_4^+, whose formation in an API source was originally proposed on the basis of kinetic data, can be observed in a corona discharge source with a corona point-to-sampling aperture distance of 0.5 mm. Other high energy ions such as He^+, He_2^+, Ar^+, N^+, O^+, and H_2O^+ can also be observed under these conditions. With a corona point-to-sampling aperture distance of 4 mm or greater, the ion residence times are longer and the corona discharge and ^{63}Ni spectra of reactant ions are essentially identical.

Ionization reactions in API mass spectrometry leading to positive ions are not limited to water- or solvent-mediated ion molecule reactions.

The reactant ions $t\text{-}C_4H_9^+$, NH_4^+, and NO^+ can be generated easily in ^{63}Ni and corona discharge (4 mm) API sources. Identical mass spectra of product ions were observed for these two sources when positive ions were generated by reaction of samples with reagent ions. Although only a limited number of reactions were investigated, the results suggest that reactions which have been observed under conventional CI conditions employing the same reagents will also be observed under API conditions.

LITERATURE CITED

(1) E. C. Horning, M. G. Horning, D. I. Carroll, I. Dzidic, and R. N. Stillwell, *Anal. Chem.*, **45**, 936 (1973).
(2) D. I. Carroll, I. Dzidic, R. N. Stillwell, M. G. Horning, and E. C. Horning, *Anal. Chem.*, **46**, 706 (1974).
(3) E. C. Horning, D. I. Carroll, I. Dzidic, K. D. Haegele, M. G. Horning, and R. N. Stillwell, *J. Chromatogr. Sci.*, **12**, 725 (1974).
(4) E. C. Horning, D. I. Carroll, I. Dzidic, K. D. Haegele, M. G. Horning, and R. N. Stillwell, *J. Chromatogr.*, **99**, 13 (1974).
(5) I. Dzidic, D. I. Carroll, R. N. Stillwell, and E. C. Horning, *Anal. Chem.*, **47**, 1308 (1975).
(6) D. I. Carroll, I. Dzidic, R. N. Stillwell, and E. C. Horning, *Anal. Chem.*, **47**, 2369 (1975).
(7) D. I. Carroll, I. Dzidic, R. N. Stillwell, and E. C. Horning, *Anal. Chem.*, **47**, 1956 (1975).
(8) I. Dzidic, D. I. Carroll, R. N. Stillwell, and E. C. Horning, *J. Am. Chem. Soc.* **96**, 5258 (1974).
(9) E. C. Horning, M. G. Horning, D. I. Carroll, R. N. Stillwell, and I. Dzidic, *Life Sci.*, **13**, 1331 (1973).
(10) A. Good, D. A. Durden, and P. Kebarle, *J. Chem. Phys.*, **52**, 212 (1970).
(11) E. W. McDaniel, "Collision Phenomena in Ionized Gases", S. C. Brown, Ed., Wiley, New York, N.Y., 1964, p 476.
(12) J. D. Payzant and P. Kebarle, *J. Chem. Phys.*, **53**, 5723 (1970).
(13) M. M. Shahin, *J. Chem. Phys.*, **45**, 2600 (1967).
(14) F. H. Field, "Ion Molecule Reactions", Vol. 1, J. L. Franklin, Ed., Plenum Press, New York, N.Y., 1972.
(15) G. W. A. Milne, H. M. Fales, and T. Axenrod, *Anal. Chem.*, **43**, 1815 (1971).
(16) M. A. French, L. P. Hills, and P. Kebarle, *Can. J. Chem.*, **51**, 456 (1973).
(17) B. L. Jelus, B. Munson, and C. Fenselau, *Biomed. Mass Spectrom.*, **1**, 96 (1974).
(18) N. Einolf and B. Munson, *Int. J. Mass Spectrom. Ion Phys.*, **9**, 141 (1972).
(19) D. F. Hunt and J. F. Ryan, *J. Chem. Soc., Chem. Commun.*, 620 (1972).
(20) B. L. Jelus, B. Munson, and C. Fenselau, *Anal. Chem.*, **46**, 729 (1974).
(21) B. L. Jelus, B. Munson, K. A. Babiak, and R. K. Murray, Jr., *J. Org. Chem.*, **39**, 3250 (1974).
(22) D. F. Hunt, C. N. McEwen, and T. M. Harvey, *Anal. Chem.*, **47**, 1730 (1975).

(23) P. Ausloss and S. G. Lias, "Ion Molecule Reactions", Vol. 2, J. L. Franklin, Ed., Plenum Press, New York, N.Y., 1972.
(24) S. K. Searles and L. W. Sieck, *J. Chem. Phys.*, **53**, 794 (1970).
(25) A. D. Williamson and J. L. Beauchamp, *J. Am. Chem. Soc.*, **97**, 5714 (1975).
(26) J. D. Payzant, A. J. Cunningham, and P. Kebarle, *Can. J. Chem.*, **51**, 3242 (1973).
(27) M. S. Wilson, I. Dzidic, and J. A. McCloskey, *Biochim. Biophys. Acta*, **240**, 623 (1971).
(28) I. Dzidic, *J. Am. Chem. Soc.*, **94**, 8333 (1972).
(29) I. Dzidic and J. A. McCloskey, *Org. Mass Spectrom.*, **6**, 939 (1972).
(30) D. F. Hunt, C. N. McEwen, and R. A. Upham, *Tetrahedron Lett.*, 4539, (1971).
(31) A. M. Hogg and T. L. Nagabhushan, *Tetrahedron Lett.*, 4827 (1972).
(32) K. D. Haegele and D. M. Desiderio, *J. Antibiot.*, **26**, 215 (1973).
(33) R. C. Dougherty, J. D. Roberts, W. W. Binkley, O. S. Chizhov, V. I. Kadentsev, and A. A. Solovyov, *J. Org. Chem.*, **39**, 451 (1974).
(34) M. Taagepera, W. Q. Henderson, R. C. T. Brownless, J. L. Beauchamp, D. Holtz, and R. W. Taft, *J. Am. Chem. Soc.*, **94**, 1369 (1972).
(35) J. P. Briggs, R. Yamdagni, and P. Kebarle, *J. Am. Chem. Soc.*, **94**, 5128 (1972).
(36) R. Yamdagni and P. Kebarle, *J. Am. Chem. Soc.*, **95**, 3504 (1973).
(37) D. H. Aue, H. M. Webb, and M. T. Bowers, *J. Am. Chem. Soc.*, **94**, 4726 (1972).
(38) D. F. Hunt and J. F. Ryan III, *Anal. Chem.*, **44**, 1306 (1972).
(39) D. F. Hunt, *Adv. Mass Spectrom.*, **6**, 517 (1974).

RECEIVED for review October 31, 1975. Accepted June 21, 1976. This work was aided by Grant GM-13901 of the National Institute of General Medical Sciences, Grants HL-05435 and HL-17269 of the National Heart and Lung Institute, and Grant Q-125 of the Robert A. Welch Foundation.

Large-Scale Mass Spectral Analysis by Simplex Pattern Recognition

T. Fai Lam, Charles L. Wilkins,* Thomas R. Brunner, Leonard J. Soltzberg, and Steven L. Kaberline

Department of Chemistry, University of Nebraska–Lincoln, Lincoln, Neb. 68588

In the present work, the simplex optimization procedure is examined as a means of producing high quality linear discriminant functions for recognition of eleven functional group categories from low resolution mass spectra. Classifier performance is evaluated with test sets totaling over 1900 compounds; and a new performance measure—the figure of merit—is employed in the evaluation. For linearly separable data, simplex-derived weight vectors are not superior to those obtained by the simpler error-correction-feedback methods. For inseparable data, however, a simplex with initial vertices at weight vectors derived by error-correction-feedback does indeed generally converge on a set of weight vectors with superior performance. It is found that those weight vectors showing poorest performance correspond to the more difficult chemical discriminations.

Studies of chemical pattern recognition have shown the promise of the method for eventual routine application to spectral analysis (*1–4*). Previous work has been open to the criticism that it was based on relatively small data sets unrepresentative of practical analytical problems. Therefore, a primary objective of the work presented here was to investigate the applicability of linear discriminant analysis to a larger data set. Accordingly, 2140 mass spectra drawn from a larger collection of 18 806 spectra (*5*), were used in this study.

BACKGROUND

The linear learning machine method of pattern recognition is an empirical approach to data analysis (*6*). Using error correction feedback (*7*) and known training sets, weight vectors are trained to make binary decisions. In principle, if enough different sets of sufficiently accurate weight vectors were accumulated, they could be used to identify molecular structures from mass spectra, even in the absence of knowledge of the theory of mass spectrometry. The linear learning machine method has been used with some success in determining empirical formulas (*8*) and for some substructure determinations (*9*), although with relatively small data sets. However, one problem of the technique is its inability to deal adequately with linearly inseparable data. The particular weight vector obtained is dependent in a complicated way upon the details of the feedback process and the order of pattern presentation during training. In the case of inseparable data, convergence to 100% recognition of the training set is impossible and, even worse, the final weight vector may bear little relationship to class identities. Consequently, unreliable predictions can result. Even for separable data, there is no assurance that a vector giving perfect recognition of a training set will yield optimum prediction results.

The simplex method, a procedure for optimization, has been used in several areas of analytical chemistry such as experimental design (*10*), data reduction (*11*), and automated instrument control (*12*). More recently, this technique has been found attractive for pattern recognition because it may provide a means for generating near-optimum linear discriminant functions for inseparable data (*13*). Accordingly, it could be a more reliable tool for obtaining these functions for use in mass spectral interpretation than previous methods (*13*). In this paper, that premise is examined using a large data set to develop functions for eleven structural questions.

EXPERIMENTAL

Data Base. For initial training and testing, a set of 1252 mass spectra (Set A) was drawn from a computer-readable file of 18 806 spectra (*5*). These spectra were so selected that each compound represented contained only one of eleven functional groups chosen for the development of weight vectors (an exception to this was the phenol category, which obviously contains a substituted phenyl). For each of the eleven categories, a training set containing up to 200 spectra was chosen from the 1252 spectrum set. Wherever possible, training sets were comprised of approximately equal numbers of class member and nonmember spectra. The remaining spectra, unused in training, were used as test sets to determine the prediction capabilities of the weight vectors developed. After weight vectors had been calculated, additional spectra were drawn from the 18 806 spectrum file to serve as further unknowns. Spectra of deuterated compounds were rejected. In this way, a set of 888 additional unknowns was obtained.

Computations. Programs for modified sequential simplex and linear learning machine calculations were written in FORTRAN IV and all computations performed using an IBM 360/65 computer. The simplex method was that described previously (*13*), except that the spanning constant, a, was 4000 for all questions except amine, where it was 100.

Preprocessing and Feature Selection. Intensities in the master file were encoded to 1 part in 9999, with the base peak in each spectrum being assigned the value 9999 and the others assigned values

Table I. Composition of Training Sets Used[a]

Training set	Phenyl 1	Ketone/ Aldehyde 2	Ether 3	Alcohol 4	Phenol 5	Acid 6	Thiol[b] 7	Ester 8	Amine 9	Amide 10	Nitrile 11
Number in class	249	96	103	185	84	51	135	125	131	56	37
Class											
1	100	31	31	18	32	40	28	30	30	40	35
2	12	56	13	12	14	15	10	10	12	15	15
3	11	16	60	11	16	15	11	12	12	15	15
4	18	19	16	100	20	25	15	18	18	15	20
5	8	15	12	6	44	15	10	10	10	15	15
6	8	8	10	8	10	30	8	8	8	15	25
7	12	15	15	14	16	15	80	17	17	15	15
8	9	13	13	9	12	15	12	80	13	15	15
9	12	15	14	12	16	15	13	13	70	15	15
10	6	8	10	6	10	10	7	7	7	30	10
11	4	4	6	4	10	5	5	5	5	10	20

[a] Training sets are listed as columns; e.g., the training set for phenyl contained 100 phenyl compounds, 12 ketones and/or aldehydes, 11 ethers, etc. [b] Thioethers were also included in this category.

Table II. Comparison of Simplex and Linear Learning Machine Predictions for 1052 Monofunctional Unknowns

Functional group vector	Presence or absence (% correct) SIM	RED-SIM	LLM	RED-LLM	Features[a]	Merit (M)[b] SIM	RED-SIM	LLM	RED-LLM	$\bar{M}$ (av)
Phenyl	91.2	94.9*[c]	92.0	91.2	20	0.55	0.63	0.53	0.34	0.51
Aldehyde and ketone	88.9	89.3	95.4*	88.5	35	0.31	0.27	0.50	0.25	0.33
Ether	81.6	83.4	84.4*	88.1	45	0.23	0.20	0.21	0.07	0.18
Alcohol	87.1	79.4	88.5*	87.1	30	0.36	0.23	0.34	0.18	0.28
Phenol	91.7	94.8*	91.9	87.1	20	0.32	0.53	0.42	0.38	0.41
Acid	93.0*	90.9	91.3	86.3	25	0.25	0.23	0.23	0.18	0.22
Thiol or thioether	93.9	94.4*	93.3	86.1	20	0.53	0.55	0.49	0.36	0.48
Ester	83.0	86.2*	90.5	82.4	25	0.26	0.23	0.15	0.14	0.20
Amine	87.9	95.1*	94.4	77.8	20	0.49	0.55	0.57	0.09	0.43
Amide	86.3	90.2	94.3*	81.3	25	0.15	0.20	0.32	0.19	0.22
Nitrile	90.8	96.1	96.6*	94.3	25	0.33	0.42	0.49	0.36	0.40

[a] The number of features used in the reduced-feature simplex and linear learning machine training, designated RED-SIM and RED-LLM, respectively; 60 features were used, otherwise. [b] The figure of merit, defined as the ratio of information gain in bits to possible information gain in bits. See Equation 14. [c] The best weight vectors, selected by considering merit figures and % correct prediction are indicated by *. Average percent correct for these is 92.5%.

relative to that one. For this study, metastable peaks and those with less than 1% relative intensity were not used. The square roots of intensities of remaining peaks were used for subsequent calculations. For computational convenience, feature selection (i.e., choice of the *m/e* values to be used in weight vector development) was accomplished by selecting the 60 most frequently appearing peaks for each of the eleven functional group categories. Following feature selection, members of the training sets possessing peaks at none of the selected *m/e* values were eliminated. This resulted in elimination of 1 spectrum from each of four training sets, 2 spectra from one training set, and 10 spectra from one training set.

RESULTS AND DISCUSSION

It was a primary objective of the research to obtain, if possible, reliable weight vectors capable of achieving reasonably high levels of accuracy in detecting the presence or absence of selected functional groups in molecules by examination of their mass spectra. A second objective was to evaluate the relative merit of the simplex and linear learning machine approaches, both generally and for the present applications. For these reasons, the training was conducted using both simplex pattern recognition (*13*) and the linear learning machine method on the preprocessed data selected for training. It seemed logical to develop weight vectors which could discriminate between specific well-defined classes (the functional group categories) and all other classes. Accordingly, the training sets were purposely comprised of spectra from compounds whose spectra would be uncomplicated by the presence of more than one kind of functional group (with the exception of phenyl and phenol). Although this is certainly a defensible strategy *for training*, use of such a set of spectra, where ambiguity is minimized, is unlikely to provide realistic tests of the prediction ability for actual unknowns, where no such artificial restrictions exist. Therefore, in addition to testing the prediction performance with monofunctional compounds not used in training, 888 additional spectra (Set B) arbitrarily selected from the master file, were employed to evaluate the potential performance on realistic problems. Table I shows the distribution of compound types for the entire 1252 spectrum set (Set A) which served as the source of training sets. Also included in Table I is the distribution of compounds within each of the eleven training sets. As mentioned earlier, several of the training sets have slightly fewer than 200 members because of the elimination of compounds having no peaks at the 60 *m/e* positions chosen for the particular questions.

Table II summarizes the recognition and prediction performance for all simplex and linear-learning machine weight vectors developed in this study. In each case, all Set A nonmembers of the respective training sets were used as prediction set unknowns. Recognition of training set members was, with three exceptions, 98% or better for the simplex and 60 feature linear learning machine weight vectors. Table V presents the prediction percentages of the weight vectors for the additional 888 unknowns. Here, the percentage of correct predictions is somewhat lower, as expected, and averages 82.3% correct, if the best vectors are considered.

For the present study, the Fisher ratio (*14*) feature selection technique employed previously for mass spectral vector de-

Table III. 60-Feature Simplex Recognition and Prediction Results, Percent Correct 1052 Monofunctional Unknowns[a]

Weight vector	1	2	3	4	5	6	7	8	9	10	11
Recognition	98.0	99.5	99.0	95.0	99.5	99.0	99.5	96.0	99.5	97.8	99.5
Class											
1	94.6	97.2	98.2	99.1	82.9	98.1	98.6	86.8	96.8	94.3	95.6
2	98.8	82.5	78.3	92.9	98.8	96.3	91.9	83.7	70.9	95.1	92.6
3	88.0	83.9	83.3	59.8	100.0	94.3	78.3	76.9	89.0	88.6	88.6
4	91.6	86.7	62.0	87.1	95.8	91.9	94.7	83.2	89.8	94.7	92.7
5	46.1	95.4	100.0	92.3	77.5	98.6	97.3	86.5	94.6	97.1	95.7
6	90.7	86.0	92.7	72.1	100.0	71.4	93.0	44.2	83.7	66.7	97.2
7	95.1	88.3	88.3	91.7	92.4	92.5	92.7	67.8	94.9	94.2	91.8
8	96.6	87.5	64.3	67.2	86.7	73.3	94.7	87.3	91.0	86.4	72.7
9	98.3	86.2	72.4	99.2	98.3	99.1	99.2	98.3	100.0	52.6	87.1
10	96.0	85.4	80.4	94.0	95.7	89.1	100.0	93.9	57.1	65.4	91.3
11	100.0	87.9	100.0	81.8	81.5	84.4	71.9	90.6	37.5	66.7	88.2
Overall prediction	91.2	88.9	81.6	87.1	91.7	93.0	93.9	83.0	87.9	86.3	90.8

[a] The columns contain the detailed performance of the weight vectors for unknowns belonging to each of the classes.

velopment (*13*) and in a parallel carbon-13 NMR spectra study (*15*) was not used. Instead, features (*m/e* positions to be used for each weight vector) were selected simply on the basis of the frequency of peak appearance within each training set. That is, for each set, those 60 *m/e* positions where peaks (excluding metastables and those with less than 1% relative intensity) were most often found, were selected as the features to be used. This method gave significantly better results than the use of Fisher ratios in a few trial comparisons.

In those cases where fewer than 60 features were used, feature selection was accomplished by successively discarding groups of five features from the frequency-ordered set of 60 features, until the data became linearly inseparable in the training sets within the computational constraints imposed. As before, the least frequently appearing features were discarded first.

Because a primary objective of the study was to produce the best possible weight vectors for incorporation into an on-line pattern recognition system, methods of improving the simplex weight vectors obtained were of interest. Additionally, it was of interest to investigate the premise suggested by earlier work (*13, 15*) that simplex-derived weight vectors would be superior for linearly inseparable data. It seemed possible that, in the latter case, a preprocessing step to produce a beginning weight vector via the linear learning machine method might provide a better means for initializing the simplex process. To examine these matters, the number of features used were reduced until the training sets became inseparable, as described above. Linear learning machine weight vectors obtained from these reduced-feature training sets were then used as starting points for each of the eleven simplex calculations, instead of the mean value starting vectors (*13*) utilized for the 60 feature simplex calculations.

Classifier Evaluation. In the past, the most common single measure of prediction reliability for pattern recognition predictions of functional group category from spectral data has been the overall percent correct prediction. Because this figure can sometimes obscure the performance when predicting class membership, as opposed to nonmembership, percent correct performance on class and nonclass members commonly has also been reported. In a study, such as the present one, with one objective being selection of the most reliable of a number of binary classifiers, it is particularly important to use an appropriate means of determining which classifiers are the best for the application.

One matter of concern in applying the percent correct performance criterion, especially when derived from a large diverse test set, is the significant dependence of this measure upon test set composition. In an effort to minimize this dependence, Rotter and Varmuza (*16*) have proposed that the information gain, $I(A,B)$, be used as an objective measure of performance. This quantity measures the amount by which a classifier reduces the uncertainty in class membership and is measured in bits.

Specifically, information gain is defined as difference in entropy, H, before ($H(A)$) and after ($H(A|B)$) application of the classifier (*17*). As Rotter and Varmuza reemphasized (*16*), the convenient formulation of Equation 2

$$I(A,B) = H(A) - H(A|B) \tag{1}$$

$$I(A,B) = \sum_{i=1,2} \sum_{k=j,n} p(i,k) \log_2 \frac{p(i,k)}{p(i)p(k)} \tag{2}$$

allows easy computation of the quantity.

However, even this information-theoretic approach retains a measure of dependence on test set composition. Accordingly, we have proposed an alternate measure of classifier performance (*18*) based on recognition of the fact that the maximum possible information gain of a classifier is limited by the initial uncertainty, $H(A)$, which in turn depends on the composition of the test set as shown in Equation 3. This new measure (Equation 4), which we have called the figure of merit, M, is the information gain relative to the maximum possible information gain imposed by the test set composition.

$$H(A) = -p(1) \log_2 p(2) \tag{3}$$

$$M = \frac{I(A,B)}{H(A)} \tag{4}$$

In the present study, we have calculated M for all 44 classifiers developed for the eleven functional group questions, using for this purpose test sets of over 1000 spectra.

Prediction Reliability. When the results contained in Tables II through V are considered, a number of interesting facts are observed. First, if one compares the performances tabulated in Table II, it is seen that, on the basis of percent correct predictions for the 60 feature data sets, the linear learning machine (LLM) weight vectors were superior to the simplex (SIM) weight vectors for 9 of the 11 questions and only slightly worse for the remaining 2 questions. For these separable or near-separable training sets, there is no pronounced advantage from the use of the simplex method. However, examination of the merit figures, M, in Table II reveals that the case is not quite as clear-cut as prediction percentages might suggest. Here, only six of the LLM categorizers had higher ratings than the simplex discriminants, suggesting that prediction performance for members and nonmembers was sometimes less balanced than might be desired. For example, even though the overall prediction performance for the ester question is over 7% better for the

Table IV. 60-Feature Linear Learning Machine Recognition and Prediction Results, Percent Correct 1052 Monofunctional Unknowns[a]

Weight vector	1	2	3	4	5	6	7	8	9	10	11
Recognition	100.0	100.0	97.0	99.0	100.0	99.0	100.0	100.0	99.5	99.5	100.0
Class											
1	92.0	99.1	94.0	97.8	84.3	99.0	95.5	97.3	97.7	99.5	97.2
2	97.6	87.5	80.7	89.3	93.9	96.3	100.0	90.7	94.2	96.3	95.0
3	100.0	96.6	76.7	65.2	98.9	84.1	79.4	75.8	97.8	94.3	100.0
4	99.4	97.6	76.3	82.4	98.8	90.0	99.4	87.4	100.0	98.2	97.0
5	53.3	98.6	94.4	94.9	90.0	95.7	90.5	96.0	96.0	100.0	95.7
6	100.0	88.4	92.7	90.7	95.1	71.4	88.4	79.1	88.4	91.7	96.2
7	99.2	99.2	90.0	97.5	89.9	95.8	90.9	99.2	94.1	100.0	98.3
8	99.1	92.0	52.7	75.0	86.7	80.0	84.1	50.9	100.0	99.1	95.5
9	78.2	89.7	91.5	95.0	99.1	96.6	99.2	98.3	95.1	69.0	93.1
10	92.0	87.5	97.8	90.0	97.8	84.8	100.0	98.0	65.3	73.1	100.0
11	90.9	100.0	93.6	72.7	70.4	68.8	84.4	100.0	62.5	96.3	88.2
Overall prediction	92.0	95.4	84.4	88.5	91.9	91.3	93.3	90.5	94.4	94.3	96.6

[a] The columns contain the detailed performance of the weight vectors for unknowns belonging to each of the classes.

LLM discriminant, M for that discriminant is only 0.15, while the M for the corresponding simplex discriminant is 0.26. When the detailed performance tabulations of Tables III and IV are compared, it is obvious that there is a large discrepancy between class performance (row 8, column 8) and overall prediction for the LLM discriminant. Of course, a judgment of whether higher overall correct prediction or balanced prediction is more desirable is only possible when considered in terms of the proposed application. In the present context, evaluating the discriminant for inclusion in an on-line pattern recognition system, a somewhat lower overall prediction performance appears to be the better choice if, thereby, better prediction of class membership results. That is, we judge a positive prediction about possible presence of a group more useful to the spectroscopist than the suggestion of its absence.

Turning now to consideration of the results from the reduced-feature data sets, where linear inseparability was purposely introduced by systematic elimination of features from the training sets, it is possible to verify the earlier conclusion (*13, 15*) that, for inseparable data, the simplex-derived weight vectors are, in general, superior to LLM weight vectors. Here, when percent correct performance for the reduced feature simplex vectors (RED-SIM) are compared with the corresponding learning machine performances (RED-LLM), it is seen that, for 9 of the 11 questions, the simplex performance was better. In every case the merit figure was higher. Even more revealing is the fact that for 7 of the 11 questions, *the reduced feature simplex vectors performed as well (within 1%) as, or better than, the 60-feature LLM vectors.* Similar trends are displayed by their comparative merit figures. This reflects the success of the strategy of using the linear learning machine weight vectors obtained from inseparable data as the *starting vectors*, suitably modified by addition of the spanning constant, a (*13*), for definition of starting simplex figures, which are the basis of the reduced simplex weight vectors ultimately obtained. It is found that those weight vectors are equal or superior to the original 60 feature simplex vectors on either a percent correct prediction basis or if figures of merit are considered. We interpret this as verification of the importance of correct selection of the starting points for the simplex optimization procedure, if local extrema in the response surface are to be avoided (although it certainly could be argued that the reduced feature space had a different and more favorable response surface). Nevertheless, it is clear that the 60 feature simplex vectors were those corresponding to local response maxima, as recognition percentages for the training sets (also listed in Tables III and IV) establish that the linear learning machine vectors were located at higher response regions for the training sets in almost every case. Reduced feature predictors behaved similarly when their details were considered in the same way as in Tables III and IV for the 60 feature predictors.

Table V. Prediction Percentages for 888 Unknowns

	Presence or Absence (% Correct)			
Functional group	60-Feature simplex	60-Feature LLM	Red-simplex[a]	Red-LLM[a]
Phenyl	83.8	80.3	82.8*[b]	76.7
Aldehyde or ketone	79.4	87.8*	70.6	64.9
Ether	83.6	80.5*	72.2	71.8
Alcohol	79.8	79.6*	64.1	73.8
Phenol	63.3	61.4	64.8*	59.2
Acid	85.4*	82.5	80.4	80.5
Thiol or thioether	82.5	75.9	85.1*	80.8
Ester	71.9	85.7	74.6*	79.9
Amine	92.3	81.8	88.8*	60.1
Amide	75.2	91.4*	84.2	78.6
Nitrile	83.2	84.1*	83.8	77.8
Av	80.0	81.0	77.4	73.1

[a] For reduced-feature weight vectors, the numbers of features used are those given in Table II. [b] Best weight vectors, included in Appendix A, are indicated by *. Average percent correct for these is 82.3%

One other question of interest is whether the results for those questions where categorization was consistently more difficult can be understood in chemical terms. One convenient index of this is the average merit figure, $\overline{M}$ (Table II), for all categorizers applied to each particular question. Because of the lack of any dramatic spread in the value M among the different discriminant functions for each question, a low value for $\overline{M}$ indicates that they all encountered difficulty. Using $\overline{M}$ values of below 0.30 as an arbitrary choice of "difficult" categorization questions, we can examine Tables III and IV containing the typical detailed results to ascertain whether there are chemically reasonable bases for the difficulty in classification. Five of the eleven questions are difficult by this criterion: ether, alcohol, acid, ester, and amide are the functional group categories involved. When the appropriate sections of the tables are examined, it is seen that significantly lower than average prediction performance is found for alcohols and esters when encountered by the ether categorizer. Conversely, the alcohol categorizer generally shows decreased

Table VI. Appendix

Class[a] m/e	1	2	3	4	5	6	7	8	9	10	11
18		0.9395	−1.4230	1.4120		21.7400			1.2100	−0.4649	−0.2983
26		0.1889	−0.7663	−0.5443		200.1000				−0.1922	0.8643
27	−0.2159	−0.3812	−0.3360	1.4980	−0.5811	−84.8600	0.4970	0.8056	0.3578	−1.3470	0.7423
28		−0.8767	−0.3483	−1.6510		34.9100		−0.5643	−0.1694	0.0214	−0.2184
29		1.6740	−0.0678	−1.1000		−8.7600	−0.3302	−0.1565	−1.0280	0.4374	−0.6870
30		−1.3720	0.0697	−1.3410		−57.5100			5.6820	0.7397	0.1351
31		−2.127	1.0550	2.1170		0.9030		−0.3276	−0.2217	−1.1670	−0.7821
32			0.6007	0.3908							
37											
38		0.4380	−1.1830	0.9865		189.5000				0.5452	0.5377
39	53.5500	−0.6658	1.0430	−0.9577	−7.160	−25.6200	−0.8257	−0.8574	−3.3830	−0.3601	−0.1036
40		0.1401	0.5918	0.4737		84.6000	1.0990	0.4938		0.5822	0.6129
41	−0.2780	−0.9351	−0.1506	−1.2480	−1.0160	−142.7000	−0.7020	−1.2930	0.8308	−1.1350	−0.0752
42		0.0834	0.6476	−0.4929		−29.5200	−1.0630	1.0540	3.6510	−0.4972	0.0130
43	−37.5900	0.7310	−0.1825	−0.3479	−0.4975	−42.4900	0.0373	1.0840	−4.0570	−0.4052	0.2207
44		0.1089	−0.4054	−0.6401		−40.6800	−0.9890	−1.2060	1.1040	0.7387	−0.8946
45		−0.8361	0.9015	0.6905		16.90	0.0021	−0.5052	−1.8150	−1.1600	−1.3110
46		−0.8348	−1.7140	−0.7014		63.2600	0.1055			−0.0052	0.6758
47			0.3795				4.2750				
49							1.0110				
51	−0.7387	0.5907	−0.2518	0.0892	1.1170	−21.8100				−0.8034	0.2357
52											1.2080
53	0.0431	0.7661	−1.6160	0.6451	2.839	−5.4950				−1.0060	0.7068
54		0.0941	0.1386	0.9431		39.8400				0.6722	3.0110
55	−0.6445	−1.1400	−1.9380	1.4960	−0.1233	6.0490	−0.2468	−1.3880	−1.3410	−0.1101	−0.7014
56		0.3311	−0.1696	−0.0847		11.63	−0.8057	1.1010	−1.9530	1.3110	1.1220
57		0.6818	1.2680	0.0323		1.0780	0.5309	0.3893	−1.3150	−0.5703	−0.9768
58		−0.1025	−0.3532	−0.0168		−29.5700	0.0277	−3.0150	2.1740	0.0035	−0.4099
59		−1.2250	0.5913	−0.2102		−33.80	−0.7692	0.0247	−3.7210	1.4030	−0.4288
60		−0.3180	−1.2490	−1.4750		304.0000	0.6833			0.4329	0.1802
61		−1.2080	0.0470	−0.1210		−62.7000	1.2040			−0.3451	−0.0896
63	−1.5090	0.4777	−2.3170		−0.7860	−31.61				−0.0372	0.2037
65	−0.4451	−0.3194	0.0768		1.2030	−127.9000				−0.6685	−0.8918
66					1.4300						
67		0.1353	0.0502	−0.5426		−20.6100				−0.2232	−0.2714
68		0.4330	0.7896	−0.7721		90.70					1.0700
69		−0.6883	−2.1360	1.2540		1.6440		0.9972		−1.0140	−1.1110
70		−0.0832	2.0230	0.0221		−5.750		1.6610	3.6690	−1.6950	0.2260
71		0.2113	0.9274	−0.4068		−14.3210		−0.6139		0.1610	−1.0560
72		1.5190	−1.2750	1.1830		−18.4300			−3.9160	0.0565	−0.0141
73		−1.1850	0.3246	−0.3241		40.6300		−0.3060		1.5170	−1.7200
74		0.0699	−0.0784	−1.1170		37.0300		1.5570		0.5979	−0.0623
75		−0.1533	0.5645			−22.9500	−0.2308			−0.6644	0.4764

76											
77	1.9400	−0.9922	−0.4369	−0.8008	0.2431	−95.4900				−1.2090	−1.0290
78		−0.3686	0.0541		−2.9640	−39.0000				−0.3025	−0.1877
79	−2.0740	−1.0830	−0.4291	−1.5070	−0.2620	−53.4200				−1.2600	−0.5589
81		1.2250	−0.9867	−0.0028		−5.3430					1.0480
82		0.6631	2.7350	−0.1094		35.5800				1.1220	1.4710
83		−0.1715	−0.2138	−0.0523		2.4650				−0.7651	−0.6906
84		0.0699	0.6368	−1.0750		75.4200				2.1670	0.0255
85		−0.0502	0.7619	−0.6124		−24.6000		0.6512		−0.9688	−0.4715
86		0.5274	−0.6255	1.7390		33.5900			−2.1770	−0.3481	0.5365
87		−1.2620	0.2272	−0.5636		40.3700		0.5868		0.6218	0.4080
88			−0.8100	0.0384		31.2700				0.9234	0.9031
89		0.4849	0.4757			−36.0200				−0.7092	0.2299
91	0.3589	−3.2210	−1.4810	−3.4560	−0.6766	−66.4900				−3.2930	−3.2090
92	0.1351					47.5100				0.0124	
95				0.7441							
96				0.6202							
97		−0.7164	−0.9072	0.6038		43.2900				−0.1995	0.6725
98		0.2727		−0.9838		129.5000					−0.2915
99		0.7030	0.8596	−0.4754		−191.5000				1.0090	−0.0412
100		0.2451								−0.0104	
101		−0.8226	−0.2984	0.9490		27.4000		1.5470		0.0422	0.5066
103	−1.7410	−0.7283	1.5120		0.4118	−84.6600				−0.5164	−0.3596
104	1.063		0.0476							0.1783	
105	1.0240	−3.383	−0.4789		−0.5933	61.2600				−3.5360	−3.4310
107					2.5240						
108					1.9840						
111				1.4000							
112				0.2107							0.6598
113		0.6295		0.5486							
115	0.2425	−0.9116	0.8050	−0.8102	0.2861	−65.4000		−0.8301		−0.3458	−0.6004
116											
117	−0.5969	−0.6836	0.1563			−72.6700				−0.6185	−0.6718
118											
119	−0.1886										
121					1.0510						
122											
126				0.9223							
128		−0.2480								0.3730	
129				−0.4388		−54.4500				−0.3962	
130											
133	1.375										
134											
139				0.0476							
140				1.3320							
141											
$d+1$	−1.1070	0.7681	−1.0620	0.7601	−1.2750	100.0	−0.1025	−0.2414	1.0240	0.7168	−0.9671
d[b]	20	60	60	60	20	60	20	25	20	60	60

[a] Classes are designated as in Table I. [b] Number of data features used.

performance when ethers, esters, and nitriles are encountered. Chemically and mass spectrometrically, this is neither surprising nor totally unexpected. In fact, it provides further assurance that the discrimination being achieved is a function of mass spectral information, rather than being fortuitous. In a similar way, it can be seen that esters, amides, and acids are confused with each other by their respective discriminant functions. Once again, this is a kind of confusion which is chemically understandable and, in fact, to be expected. An understanding and verification of the specific sources of confusion, as made possible by analysis of the kind presented here, will permit design of machine-assisted interpretation systems to circumvent the difficulties posed, and it is expected that this will be done.

As a final test of the discriminant functions, they were applied to 888 unknowns (Set B) drawn at random from the 18 806 spectrum file, subject only to the restriction that they not be deuterated compounds. Table V presents the results of this trial. For all but two of the categories, the prediction performance was worse than for the more specifically selected Set A. For the one category where performance was far worse than previously (phenols), the misclassification of other phenyl compounds was primarily responsible for the poor performance. Average prediction performance for the best vectors (vide infra) was approximately 82%, irrespective of whether class or nonclass unknowns were considered. As we had hoped, performance of these vectors on this less carefully-selected test set paralleled that found earlier.

Implications for On-Line Mass Spectral Pattern Recognition. It appears that among the weight vectors obtained in the present study are ones sufficiently reliable for incorporation in a mass spectral pattern recognition system for routine use by analysts. We have therefore selected the best weight vector for each functional group question, based on the joint consideration of percent correct prediction on the 1052 spectrum test set and the figure of merit, M, for inclusion in Appendix A, along with instructions for their use. In most, but not all, of the cases, the classifier with the best percentage prediction performance had a merit figure about as high (within 0.02) or higher than other classifiers and was therefore chosen. The two exceptions were the reduced feature LLM classifier for ethers and the 60-feature LLM classifier for esters, where low merit figures prompted selection of the second best (by the percentage correct criterion) predictors. It is worth noting that one of the eleven weight vectors chosen (that for acid categorization) was a 60-feature simplex vector, five were reduced-feature simplex vectors (those for phenyl, phenol, thiol, ester, and amine), and the remainder were 60-feature linear learning machine vectors.

It does not appear possible, at the present time, to develop weight vectors which are perfect in their performance. However, that should not prohibit the effective use of linear discriminant functions, including those presented here, *as a diagnostic aid to the practicing spectroscopist*. Because of the minimal computer storage requirements and the ease of applying weight vectors to spectra obtained on computer-controlled systems, it seems both realistic and practical to incorporate such capabilities into existing laboratory minicomputer systems. It is not expected that such developments will immediately permit the fully automated computer interpretation of unknown spectra. Rather, such a system will offer the analyst suggestions which can be accepted or rejected upon the basis of other information available; in this manner, the task of interpretation will be assisted by the easy availability of guidelines which may point the way toward solution of structure determination problems. It does seem self-evident that, as multidata-source information becomes available (e.g., gas chromatography, NMR, and infrared spectra), it should be possible to employ this information synergistically in on-line pattern recognition systems to further aid the analyst. Perhaps then, the desirable objective of rapid, reliable, and automatic analysis may be achieved.

SUMMARY

It has been shown that a selection of eleven weight vectors derived by the simplex and linear learning machine methods and tested with 1940 test spectra for prediction performance can achieve an average of 88% correct prediction. This level seems sufficiently high to warrant use of the vectors in an on-line mass spectra interpretation system. It has also been further verified that, when inseparable data sets are used for training, simplex pattern recognition is to be preferred to the linear learning machine approach. Furthermore, a new strategy for obtaining near-optimum weight vectors in such cases by using the linear learning machine method as a preprocessing step to provide a basis for the initial simplex, has been shown effective. Additional work is under way to compute more weight vectors for other important functional group categories and to incorporate them in an on-line system.

APPENDIX A

This appendix contains the best weight vectors obtained in this study (Table VI); these correspond to the classifiers marked with asterisks in Table II. The features correspond to the m/e values listed in the left hand column. Thus, feature 1 is associated with mass spectral peaks at $m/e = 18$, and so forth.

To classify a mass spectrum, the summation

$$\sum_i x_i w_i + (d + 1)$$

is carried out over all features. Here, x_i is the preprocessed peak intensity corresponding to the ith feature, and w_i is the corresponding weight vector component. A positive sum indicates that the compound producing the spectrum contains the functional group represented by the weight vector.

LITERATURE CITED

(1) T. L. Isenhour and P. C. Jurs, *Anal. Chem.*, **43** (10), 20 A (1971).
(2) T. L. Isenhour, B. R. Kowalski, and P. C. Jurs, *Crit. Rev. Anal. Chem.*, July 1974, pp 1–44.
(3) P. C. Jurs and T. L. Isenhour, "Chemical Applications of Pattern Recognition", John Wiley and Sons, New York, N.Y., 1975.
(4) B. R. Kowalski, *Comput. Chem. Biochem. Res.*, **2**, 1–76 (1974).
(5) E. Stenhagen, S. Abrahamssen, and F. W. McLafferty, "The Registry of Mass Spectral Data", Wiley-Interscience, New York, N.Y., 1974.
(6) N. J. Nilsson, "Learning Machines", McGraw-Hill, New York, N.Y., 1965.
(7) P. C. Jurs and T. L. Isenhour, Ref. 3, pp 13–15.
(8) P. C. Jurs, B. R. Kowalski, and T. L. Isenhour, *Anal. Chem.*, **41**, 21 (1969).
(9) P. C. Jurs, B. R. Kowalski, T. L. Isenhour, and C. N. Reilley, *Anal. Chem.*, **42**, 1387 (1970).
(10) S. N. Deming and S. L. Morgan, *Anal. Chem.*, **45**, 278A (1973).
(11) D. M. Olsson and L. S. Nelson, *Technometrics*, **17**, 45 (1975).
(12) R. R. Ernst, *Rev. Sci. Instrum.*, **39**, 998 (1968).
(13) G. L. Ritter, S. R. Lowry, C. L. Wilkins, and T. L. Isenhour, *Anal. Chem.*, **47**, 1951 (1975).
(14) R. O. Duda and P. E. Hart, "Pattern Classification and Scene Analysis", Wiley-Interscience, New York, N.Y., 1973, p 116.
(15) T. R. Brunner, C. L. Wilkins, T. F. Lam, L. J. Soltzberg, and S. L. Kaberline, *Anal. Chem.*, **48**, 1146 (1976).
(16) H. Rotter and K. Varmuza, *Org. Mass Spectrom.*, **10**, 874 (1975).
(17) C. H. Chen, "Statistical Pattern Recognition", Hayden Book Co., Inc., Rochelle Park, N.J., 1973, p. 57.
(18) L. J. Soltzberg, C. L. Wilkins, S. L. Kaberline, T. F. Lam, and T. R. Brunner, *J. Amer. Chem. Soc.*, in press, 1976.

RECEIVED for review April 5, 1976. Accepted June 25, 1976. Support of this research by the National Science Foundation under Grant MPS-74-01249 is gratefully acknowledged. A grant from the University of Nebraska Research Council provided partial support for the purchase of the mass spectra data set used. L. J. Soltzberg is Visiting Associate Professor, 1975–76, from Simmons College, Boston, Mass.

Comparison of Continuum Models in Quantitative Diffuse Reflectance Spectrometry

Harry G. Hecht

Department of Chemistry, South Dakota State University, Brookings, S.D. 57006

Model systems containing soluble dyes in scattering media are considered in this article dealing with quantitative diffuse reflectance spectroscopy in highly absorbing media. Several continuum models are used to interpret the data, including those of Kubelka and Munk, Pitts, and Rozenberg, as well as exact solutions to the radiative transfer equation for various phase factors. The Pitts' formula is a two-parameter representation which gives a good fit to the experimental data. It does, however, require the use of very anisotropic phase functions. The large deviations from the Kubelka–Munk and similar formulas are due to the anisotropy of scatter. Thus, the two-parameter formula is not just an empirical means of fitting the data but has the potential of distinguishing between nonlinear effects and instrumental errors, and thus extending the range of reflectance measurements for quantitative analytical purposes.

Numerous diffuse reflectance theories have been proposed, and they may be quite different depending on the interests of the author(s). Astrophysicists have usually been concerned with radiative transfer theory, whereas spectroscopists have tended toward the use of various layer models. It has become traditional to group the theories into two categories, the continuum models and the statistical models. There are many parallels which can be drawn between the theories, and these have recently been reviewed (*1*).

In general, it may be stated that the statistical theories require the use of a rather specific model for the medium. By summing contributions to the reflectance from the individual particles or layers, one can derive an expression for the reflectance from which the absorptivity can be determined. The success of this approach depends, of course, on how closely the model corresponds with reality.

The continuum theories, on the other hand, are more general. They do not depend on a detailed knowledge of the medium since the scattering and absorbing processes are described by two phenomenological constants. The absolute absorbance cannot be determined using continuum theories. For analytical purposes, this is not a severe limitation, since determinations are usually made from comparative measurements.

Reflectance spectrometry is now recognized as a valuable companion technique to transmission spectrometry (*2*). It is, in fact, the preferred technique in some highly absorbing media, and the only applicable technique for many surface studies, color measurements, and in situ analyses of thin-layer chromatograms.

The most widely used method of interpreting diffuse reflectance data on a quantitative basis is the Kubelka–Munk theory (*3–5*). This theory was advanced in 1931 (*6*), but, in fact, constitutes a re-discovery of the earlier treatment by Schuster (*7*). The form given by Kubelka and Munk is convenient for analytical purposes, and this is probably the reason that spectrometrists continue to use it so widely and refer to it as the K-M theory.

The K-M function can be applied for quantitative analysis by reflectance measurements in much the same way that the Beer–Lambert law is applied to transmission measurements (*3–5*). As is well known, the Beer–Lambert law is a limiting law which is obeyed only in dilute solutions. The K-M function should also be regarded as a limiting law for essentially the same reasons (*8*).

In practice, it is found that the K-M function is valid only over a very limited concentration range (*9*). The primary reasons for this appear to be two basic assumptions which are not valid. Namely, it is assumed that homogeneous scattering layers are involved in which scatter and absorption are proportional to the layer thickness. Differential equations are then written for these layers, although one would not expect them to be valid in the limit of small differential layer thicknesses (*10*). Furthermore, as the medium becomes more strongly absorbing, anomalous dispersion effects should play an increasingly significant role (*11*). These effects would also lead to deviations from the ideal K-M behavior, since they are not included in the theory.

The K-M theory represents an approximate solution to the radiative transfer equation for a medium which scatters isotropically (*2*). The exact solution for this case has been given by Chandrasekhar (*12*). An exact solution for scatter according to the phase function $\omega_0(1 + x \cos \Theta)$ is also available (*12*). ω_0 is defined in terms of the absorption (α) and scattering (σ) coefficients by $\omega_0 = \sigma/(\alpha + \sigma)$, and is known as the albedo of single scatter. Θ is the angle of scatter referred to the direction of incidence assuming a radial distribution, and x is a parameter representing the degree of anisotropy. The various solutions have been put into a useful form by Giovanelli (*13*) and compared with an approximate solution due to Pitts (*14*). Another useful approximation is that of Rozenberg (*15*).

It appears that some of the other solutions mentioned above might give a more accurate description of the reflectance of strongly absorbing media than the K-M function, and would allow such measurements to be used for quantitative analytical purposes over a more extended concentration range. It is felt that this approach is preferable to the use of the numerous ad hoc relationships which have been proposed in the past to linearize reflectance data simply as an analytical expedient (*16*), since these experiments have at least the potential of suggesting reasons for departure from the simple K-M theory. It is unlikely that a new relationship can be found which linearizes reflectance data much better than the K-M theory over an extended concentration range, but the simple calculational procedures which the other theories involve cannot be regarded as a serious deterrent in a modern analytical laboratory.

Several model systems will be used to quantitatively compare the various continuum reflectance theories in strongly absorbing media. This paper reports the results for systems of one type; namely, those containing a soluble absorbent in a scattering medium.

EXPERIMENTAL

Two model systems were chosen for the present study: eosin B in magnesia suspensions, and methylene blue in cow's milk. The samples were prepared by quantitative addition from stock dye solutions to

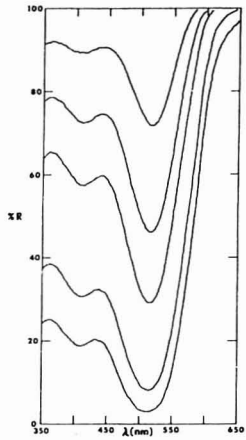

Figure 1. Some representative diffuse reflectance spectra for samples of eosin B in milk of magnesia

Each sample contained 10 ml of Phillips' Milk of Magnesia and was made up to a total volume of 20 ml. The molar concentrations of dye for the various curves (from top to bottom) are: 4.06×10^{-6}, 1.62×10^{-5}, 4.06×10^{-5}, 1.62×10^{-4}, 3.25×10^{-4}

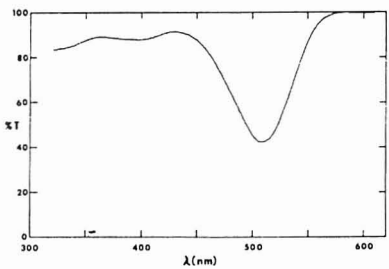

Figure 2. Transmission spectrum of a 8.12×10^{-6} M aqueous solution of eosin B recorded with a Beckman Model DB spectrophotometer

suspensions which contained a fixed volume of the scattering medium. Commercial Phillips' Milk of Magnesia was used in the former case, and fresh whole cow's milk in the latter.

Reflectance measurements were made using a Beckman Model DK-2A spectrophotometer equipped with an integrating sphere reflectance attachment. Similar suspensions to which no dye had been added were used as reflectance standards. Ten-mm silica cells were used. It was verified that the condition of "infinite layer thickness" was satisfied by noting that the reflectance was not altered by the addition of a white backing. A dark current adjustment was made before each measurement. Periodic checks vs. the reflectance standard showed that instrumental drift was no more than 1% throughout the course of the measurements. Those reflectances which were less than 0.1 R are reported as averages of several scans using an expanded scale.

RESULTS

The Eosin B in Magnesia Model System. Some typical reflectance curves are shown in Figure 1. By comparison with the transmission spectrum of the dye solution (Figure 2), the peak at shorter wavelength is considerably accentuated. This effect is attributed to increased scatter at the shorter wavelengths. This same effect is probably responsible for some apparent shifts in the peak positions as well. The two absorption peaks involved are identified by their reflectance maxima at ca. 411 and 516 nm.

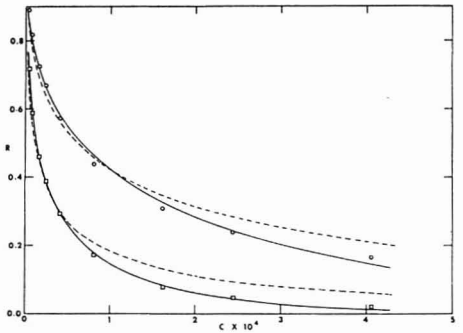

Figure 3. Reflectance of eosin B in milk of magnesia suspensions at the two wavelengths 411 nm (○) and 516 nm (□) as a function of the reduced concentration, C

The dashed curves are least squares fits using an isotropic phase function (Equation 7), and the solid curves are least squares fits using the Pitts formula (Equation 9)

The absorption and scatter of the samples are represented by the two constants α and σ, respectively, where

$$\alpha = C_1\alpha_1 + C_2\alpha_2 \quad (1)$$

$$\sigma = C_1\sigma_1 + C_2\sigma_2 \quad (2)$$

The subscript 1 refers to the magnesia particles and the subscript 2 refers to the dye molecules. It is assumed that $\alpha_1 = 0$ and $\sigma_2 = 0$. The reflectance is expressed in terms of the single independent variable $C = C_2/C_1$, where C_1 is a relative concentration determined by the dilution factor. The absolute concentration of scattering particles is not reported here. The measured reflectance values as a function of C are shown in Figure 3 for the two peaks at 411 nm (○) and 516 nm (□).

In Figure 4, the data are plotted according to the K-M function $f(R)$,

$$f(R) = \frac{(1-R)^2}{2R} = \frac{K}{S} = \frac{2\alpha}{\sigma} = 2\gamma C \quad (3)$$

where $\gamma \equiv \alpha_2/\sigma_1$. A least squares fit to the data is represented by the solid lines whose slopes yield the parameters $\gamma_{411} = 2534$ and $\gamma_{516} = 24168$. The ratio $\gamma_{411}/\gamma_{516} = 0.104$ is smaller than the corresponding ratio of molar extinction coefficients determined from the solution spectrum, 0.148. This is presumably due to the different magnitude of the scattering constant at the two wavelengths, as previously mentioned. As might have been anticipated, the K-M theory fails to give a good account of the reflectance for the more intense band, although that for the weaker band is satisfactory.

Rozenberg (*17*) has argued that models of the K-M type are too crude to give anything but a fortuitous agreement with actual reflectance data. Using methods developed by Kuznetsov (*18*), Rozenberg (*15*) showed that the reflectance is given by

$$C_iR = \sum_{t=1}^{\infty} \frac{a_{it}}{(1+\beta)^t} \quad (4)$$

where t is the multiplicity of scatter, C_i is a parameter describing the polarization of the reflected radiation, and the a_{it} are constants which depend upon the scattering indicatrix. As $\beta \equiv \alpha/\sigma$ increases, terms of higher multiplicity become less important. Ambartsumian (*19*) has shown that the mean multiplicity of scatter in a semi-infinite turbid medium is in

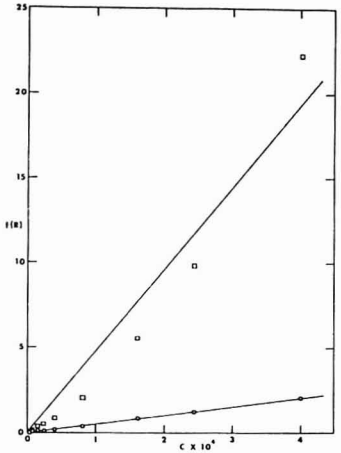

Figure 4. Kubelka–Munk function for eosin B in milk of magnesia suspensions at the two wavelengths 411 nm (O) and 516 nm (□) as a function of the reduced concentration, C. The lines are least squares fits using Equation 3

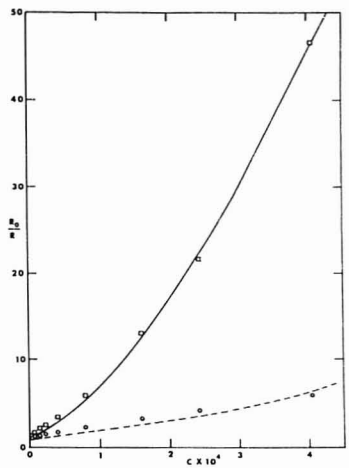

Figure 5. Rozenberg function for eosin B in milk of magnesia suspensions at the two wavelengths 411 nm (O) and 516 nm (□) as a function of the reduced concentration, C

The solid line is a least squares fit to the 516-nm data using Equation 5, and the dashed curve is a least squares fit to the 411-nm data using the same fixed value of $Q = 16.18$

fact given by $\sqrt{1 + 1/\beta}$. Thus when $\beta \geq 1/3$, a sufficiently accurate solution is obtained by inclusion of terms up to second or third degree. Assuming scatter to be independent of β, the reflectance is then given by

$$\frac{R_0}{R} = \frac{(1+\beta)^2}{1 + \dfrac{\beta}{Q}} \tag{5}$$

where

$$Q = 1 + \sum_{t=1}^{\infty} \frac{a_{1,t+1}}{a_{11}(1+\beta_0)^t}$$

is a constant characteristic of the scattering medium in the absence of absorption ($\beta = \beta_0$). Equation 5 can also be derived in terms of a simple layer model (*20*), in which case

$$\beta = \frac{a}{r+t} \text{ and } Q = 1 + \frac{t}{r+t} \tag{6}$$

a, t, and r are the absorption, forward scatter, and reflection constants of the layer, respectively.

Figure 5 shows the reflectances at 411 and 516 nm plotted according to the Rozenberg formula (Equation 5). The solid line is a least squares fit to the 516 nm peak with $Q_{516} = 16.18$ and $\gamma_{516} = 17687$. The fit is seen to be quite satisfactory in general, although there is an obvious trend in the data at low concentrations which is not represented by the Rozenberg curve. No convergence was obtained in an attempt to fit the 411-nm band. The curvature is so slight that Q is not uniquely determined. If it is fixed at the value of the 516-nm band; i.e. at 16.18, a rather poor fit is obtained with $\gamma_{411} = 4125$ (dashed line).

An attempt was made to fit the reflectance data using the exact solution to the radiative transfer equation for isotropic scatter in the form given by Giovanelli (*13*) for our $R_{0°,D}$ measurements:

$$R(1) = 1 - H(1)(1 - \omega_0)^{1/2} \tag{7}$$

where $\omega_0 = \sigma/(\alpha + \sigma)$ and $H(1)$ is an integral given by Chandrasekhar (*12*). The least squares fit gives $\gamma_{411} = 1148$ and $\gamma_{516} = 5964$, and is shown by the dashed curves in Figure 3. The fit is rather poor; the curvature is obviously not correct.

The exact solution for the phase factor $\omega_0(1 + x \cos \Theta)$ has also been given by Giovanelli (*13*),

$$R(1) = 1 - H(1)\{1 - [(\omega_0/2)(\alpha_0 - c\alpha_1)]\} \tag{8}$$

where

$$c = x(1 - \omega_0)\omega_0[\alpha_1/(2 - \omega_0\alpha_0)]$$

and α_0 and α_1 are moments of the H-integrals. It is generally assumed that $0 \leq x \leq 1$. An attempt was made to fit the data of Figure 3 using $x = 1$. The result was somewhat better than with $x = 0$ (isotropic solution), but still unsatisfactory. This suggests that a fit with $x > 1$ might be better, but the necessary integrals have been tabulated by Chandrasekhar (*12*) only for $x = 0$ and $x = 1$.

It was shown by Giovanelli (*13*) that an approximate solution given by Pitts (*14*) is in excellent agreement with the exact solution at $x = 0$ and $x = 1$. The Pitts formula is obtained using the Eddington approximation and can be expressed in the form,

$$R(\mu_0) = \frac{\omega_0}{2\sqrt{\chi} + 3 - \omega_0 x}\left\{-x + \frac{3 + (1 - \omega_0)x}{1 + \mu_0\sqrt{\chi}}\right\} \tag{9}$$

where

$$\chi = (3 - \omega_0 x)(1 - \omega_0)$$

This formula represents a convenient analytic expression for non-integral x values, and makes possible the investigation of systems with very anisotropic scatter without the cumbersome calculation of H-integrals and moments. It will be shown elsewhere (*21*) that the Pitts approximation is in very good agreement with the exact solution for non-integral x values, including those in range $x > 1$.

A nonlinear least squares fit of Equation 9 to the data is shown by the solid curves of Figure 3. The parameters determined are $\gamma_{411} = 127.5$, $x_{411} = 2.52$, $\gamma_{516} = 1278$, and $x_{516} =$

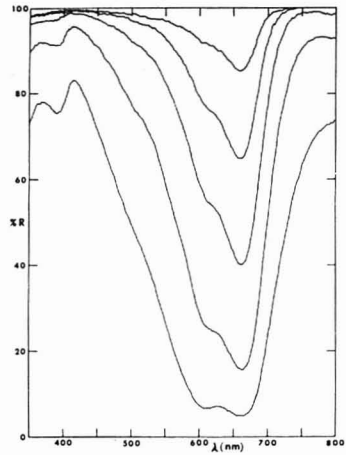

Figure 6. Some representative diffuse reflectance spectra for samples of methylene blue in cow's milk

Each sample contained 25 ml of fresh whole milk to which varying volumes of a stock dye solution were added. The reduced molar concentrations for the various curves (top to bottom) are: 5.35×10^{-6}, 2.67×10^{-5}, 1.07×10^{-4}, 5.35×10^{-4}, 2.67×10^{-3}

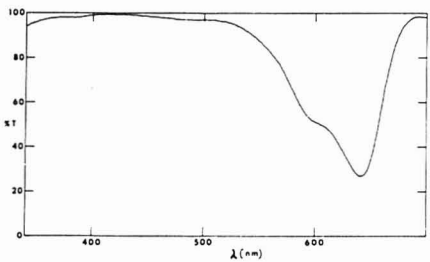

Figure 7. Transmission spectrum of a 6.69×10^{-5} M aqueous solution of methylene blue recorded with a Beckman Model DB spectrophotometer

2.06. The agreement is obviously quite good and the ratio $\gamma_{411}/\gamma_{516} = 0.0998$ is very nearly the same as that determined by the K-M theory.

The Methylene Blue in Cow's Milk Model System. Analogous measurements were made for the second model system. Some typical reflectance curves are shown in Figure 6. Once again a comparison with the solution spectrum of methylene blue (Figure 7) reveals some changes in intensity and position which may be attributed to an increase in the scattering constant at shorter wavelengths. Measurements were made for the peak at ca. 660 nm, the shoulder at ca. 610 nm, and the small peak at ca. 390 nm. Reflectance values for these three features are shown in Figure 8 by the symbols □, ○, and △, respectively. A relative concentration is once again used, since the absolute concentration of scattering particles has not been determined.

A plot of the reflectance data according to the K-M theory is shown in Figure 9. The least squares analysis gave the values of $\gamma_{660} = 1911$, $\gamma_{610} = 1490$, and $\gamma_{390} = 8.5$. The lines determined by these slopes are given also in Figure 9, and once

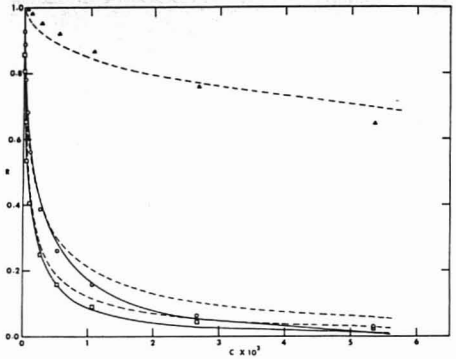

Figure 8. Reflectance of methylene blue in milk suspensions at the wavelengths 660 nm (□), 610 nm (○) and 390 nm (△) as a function of the reduced concentration, C

The dashed curves are least squares fits using an isotropic phase function (Equation 7) and the solid curves are least squares fits using the Pitts' formula (Equation 9)

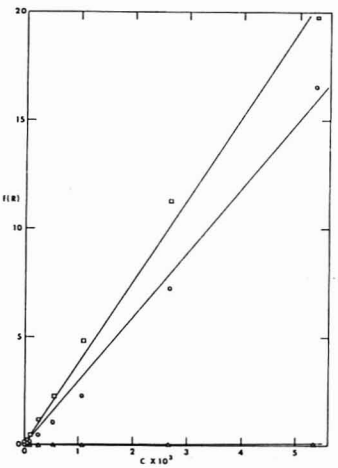

Figure 9. Kubelka–Munk function for methylene blue in milk at 660 nm (□), 610 nm (○), and 390 nm (△) as a function of the reduced concentration, C. The lines are least squares fits using Equation 3

again the model is satisfactory for the weak band but gives a very poor fit to the stronger bands.

The reflectance data for methylene blue in milk are shown in the Rozenberg form in Figure 10. A nonlinear least squares fit to these data was convergent only for the 610-nm shoulder for which $\gamma_{610} = 2188$ and $Q_{610} = 3.24$. The other bands have curvatures which are not consistent with the Rozenberg formula (Equation 5).

A fit of the data with the exact solution for isotropic scatter (Equation 7) is shown by the dashed curves of Figure 8. The corresponding γ-values are $\gamma_{660} = 1061$, $\gamma_{610} = 468$, and $\gamma_{390} = 3.4$. It is apparent once again that the curvature of the isotropic solution is too small, and a better fit can be obtained if anisotropic scatter is assumed. Using the Pitts formula (Equation 9) with both γ and x treated as parameters yielded

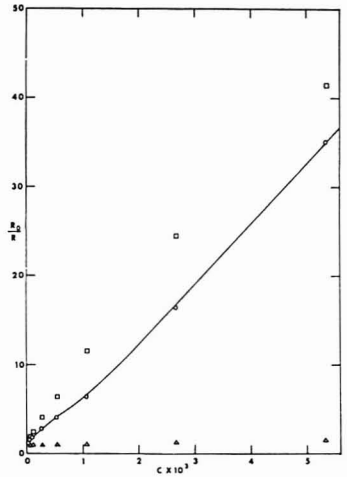

Figure 10. Rozenberg function for methylene blue at 660 nm (□), 610 nm (○), and 390 nm (△) as a function of the reduced concentration, C. The solid line is a least squares fit to the 610 nm data using Equation 5

the values $\gamma_{660} = 388$, $x_{660} = 1.61$, $\gamma_{610} = 112$, and $x_{610} = 2.02$. The least squares fit was nonconvergent for the weak band at 390 nm, showing in fact very little x-dependence. The solid curves of Figure 8 show the optimum fit to the 660- and 610-nm bands.

CONCLUSIONS

Because the K-M theory leads to a simple one-parameter equation (Equation 3), it is a very attractive model and is very useful where applicable. In accordance with previous observations (*3–5, 9*), this study shows that it can be used to quantitatively describe the concentration of an absorbing species in scattering media only over a very limited concentration range.

The Rozenberg formula (Equation 5) has been derived for strongly absorbing media, and is claimed to give very good agreement with reflectance data obtained using a filter-photometer system (*22*). Perhaps the crude filter system masks some effects, for we find that the Rozenberg equation gives a good description of the reflectance data in some cases, but fails completely in others. It appears that the formula is of little value for a weak band, because the slope is too small for Q to be uniquely determined. An examination of Equation 5 shows that, at high concentrations, R_0/R should become linear in concentration with slope $Q\gamma$. On the other hand, it appears that additional difficulties are encountered for strong, overlapping bands as in the case of methylene blue. Because of anomalous dispersion effects, these bands perturb one another and they do not show the expected concentration-dependence of an isolated band.

The magnitudes of the Q's which fit our data also raise some questions about the general validity of the Rozenberg theory. According to the approximate parameters of Chekalinskai (Equation 6), we would expect $1 \lesssim Q \lesssim 2$, since $a + r + t = 1$. The value reported by Il'ina and Rozenberg (*22*) for several systems is 2.3. However, our values of 3.24 and 16.18 are too large to be given any reasonable physical interpretation.

The use of an exact solution to the equation of radiative transfer for isotropic scatter offers no advantage over the simple K-M theory. This is not surprising, as it has previously been shown that the solutions differ very little (*2*). It is significant to observe that solutions which are based upon anisotropic scatter give a much better account of the reflectance of strongly absorbing media. The Pitts formula (Equation 9) has been shown to be a convenient two-parameter equation which fits our data well. It requires large x-values, which implies that the scatter in these model systems is highly anisotropic.

In condensed media, the apparent scatter is a result of multiple scattering processes, each of which is known to be anisotropic. It is generally assumed that the net result can be represented by an isotropic phase factor (see, for example, Ref. *17*). This is apparently not true of the model systems studied here.

It appears that quantitative analysis by diffuse reflectance spectrometry is possible in strongly absorbing media if proper account is taken of the anisotropy of scatter. Some variation in the anisotropy of the bands reported in this study is obvious. There is insufficient data at present to show whether the degree of anisotropy correlates with the magnitude of the absorbance and/or with the wavelength of the band. Further measurements will be made in an attempt to clarify this point and better define the scattering properties of the model systems. It seems intuitively obvious that the degree of anisotropy within a given elemental sample layer must depend upon the absorbance of that layer. The present reflectance theories do not include a concentration-dependent anisotropy of scatter, but it is suggested that proper account of this effect might lead to an improved model.

LITERATURE CITED

(1) H. G. Hecht, *J. Res. Nat. Bur. Stand.*, in press.
(2) H. G. Hecht, in "Modern Aspects of Reflectance Spectroscopy", W. W. Wendlandt, Ed., Plenum Press, New York, 1968, pp 1–26.
(3) W. W. Wendlandt and H. G. Hecht, "Reflectance Spectroscopy", Interscience Publishers, New York, 1966.
(4) G. Kortüm, "Reflectance Spectroscopy", Springer-Verlag, New York, 1969.
(5) R. W. Frei and J. D. MacNeil, "Diffuse Reflectance Spectroscopy in Environmental Problem-Solving", CRC Press, Cleveland, Ohio, 1973.
(6) P. Kubelka and F. Munk, *Z. Tech. Phys.*, **12**, 593 (1931).
(7) A. Schuster, *Astrophys. J.*, **21**, 1 (1905).
(8) Ref. 4, p 181.
(9) G. Kortüm and G. Schreyer, *Z. Naturforsch. A*, **11**, 1018 (1956).
(10) E. L. Simmons, *Appl. Opt.*, **14**, 1380 (1975).
(11) A. L. Companion, in "Developments in Applied Spectroscopy", Vol. 4, E. N. Davis, Ed., Plenum Press, New York, 1965, pp 221–234.
(12) S. Chandrasekhar, "Radiative Transfer", Clarendon Press, 1950 (reprinted by Dover Publications, Inc., 1960).
(13) R. G. Giovanelli, *Opt. Acta*, **2**, 153 (1955).
(14) E. Pitts, *Proc. Phys. Soc., London, Sect. B*, **67**, 105 (1954).
(15) G. V. Rozenberg, *Dokl. Akad. Nauk SSSR*, **98**, 201 (1954).
(16) C. A. Lermond and L. B. Rogers, *Anal. Chem.*, **27**, 340 (1955).
(17) G. V. Rozenberg, *Usp. Fiz. Nauk*, **69**, 666 (1959).
(18) E. S. Kuznetsov, *Izv. Akad. Nauk SSSR, Ser. Geogr. Geofiz.*, **5**, 247 (1943).
(19) V. A. Ambartsumian, *Dokl. Akad. Nauk Arm. SSR*, **8**, 101 (1948); *J. Phys. USSR*, **8**, 65 (1944).
(20) I. I. Chekalinskaia, *Izv. Akad. Nauk SSSR, Ser. Fiz.*, **21**, 1494 (1957).
(21) H. G. Hecht, *Appl. Spectrosc.*, in press.
(22) A. A. Il'ina and G. V. Rozenberg, *Dokl. Akad. Nauk SSSR*, **98**, 365 (1954).

RECEIVED for review March 10, 1976. Accepted July 6, 1976.

Determination of Ammonia by Mercury-Sensitized Luminescence

William Ho* and A. B. Harker

Science Center, Rockwell International, Thousand Oaks, Calif. 91360

A method using the principle of mercury-sensitized luminescence was developed and demonstrated for the detection and quantitative analysis of ammonia. The method is based on observing the emission from the decay of a bound state of the mercury–ammonia exciplex formed by reacting ammonia with metastable 6^3P_0 mercury atoms. The emission is specific in frequency for ammonia. For samples containing low concentrations of interfering gases such as O_2, real-time measurements were shown feasible at sensitivities well below the picogram level. For ambient measurements, gas chromatographic separation techniques were used to isolate the ammonia samples and a sensitivity of 3 pg with a signal-to-noise ratio of 5 was achieved. In addition, the linearity of the emission signal was established for ammonia samples between 3 and 5000 pg.

Evidence is accumulating that ammonia, though present in ambient air at low concentrations (0.1 to 100 ppb), plays a significant role in the formation and stabilization of ambient pollution aerosols, and that such aerosol particles can potentially cause adverse health effects in humans. In response to the need for a sensitive method of continuously monitoring gaseous NH_3 at ambient levels, a detection method has been developed based on the observation of the emission intensity from the decay of the excited mercury–ammonia complex (exciplex).

The exciplex is produced by the reaction of NH_3 with Hg atoms in the excited metastable 6^3P_0 state which can be formed by irradiating Hg vapor with 253.7-nm light in the presence of N_2. The emitted light from the exciplex is in a continuum band centered at 345 nm with a half-width of approximately 20 nm. An extensive examination of the physics and chemistry of the process has been carried out and the rate constant of the exciplex formation reaction as well as the lifetimes of the exciplex and $Hg(6^3P_0)$ atoms have been measured (*1, 2*).

In this previous study, it was found that the exciplex emission is linear with concentration and for NH_3 in N_2, measurements can be made to well below the part-per-billion by volume level. For ambient measurements, it was found that specific gases, primarily molecular oxygen, lowered the sensitivity of the method through the quenching of the excited Hg atoms. Therefore, gas chromatographic techniques capable of separating NH_3 at ppb concentrations were developed and used in conjunction with the exciplex emission detection method for the purpose of measuring NH_3 in ambient air.

Since other compounds also form emitting mercury exciplexes, this technique can potentially also be employed to detect such species as amines, alcohols, hydrazine, and water.

PRINCIPLE OF DETECTION

Several investigators (*3, 4*) have established that the metastable mercury (6^3P_0) state forms an excited complex (exciplex) with ammonia in the gas phase which primarily decays via the emission of light in a continuum centered at 345.0 nm. This emission band is specific for the ammonia exciplex and does not overlap any other known mercury exciplex emissions such as those for water vapor, alcohols, or other amines.

Mercury (6^3P_0) metastable atoms are created by the quenching (usually by N_2) of mercury in the 6^3P_1 state which can be produced by irradiating mercury vapor with 253.7-nm light. The proposed mechanism for the formation and decay of the exciplex are given by the reactions:

$$Hg + h\nu(253.7\text{ nm}) \rightarrow Hg(6^3P_1) \quad (1a)$$

$$Hg(6^3P_1) + N_2 \rightarrow Hg(6^3P_0) + N_2^* \quad (1b)$$

$$Hg(6^3P_0) + NH_3 \rightarrow (Hg \cdot NH_3)^* \quad (1c)$$

$$Hg(6^3P_0) + NH_3 + N_2 \rightarrow (Hg \cdot NH_3)^* + N_2 \quad (1d)$$

$$(Hg \cdot NH_3)^* \rightarrow Hg + NH_3 + h\nu(345.0\text{ nm}) \quad (1e)$$

$$(Hg \cdot NH_3)^* + N_2 \rightarrow Hg + NH_3 + N_2^* \quad (1f)$$

$$(Hg \cdot NH_3)^* + M \rightarrow \text{Products} \quad (1g)$$

$$Hg(6^3P_0) + N_2 \rightarrow Hg + N_2^* \quad (1h)$$

$$Hg(6^3P_0) + M \rightarrow Hg + M^* \quad (1i)$$

$$Hg(6^3P_1) + M \rightarrow Hg + M^* \quad (1j)$$

where M denotes any gas species present other than nitrogen.

The intensity of the emission produced in reaction 1e is given by,

$$\text{Emission (345.0 nm)} = k_e[(Hg \cdot NH_3)^*] \quad (2)$$

where the steady-state exciplex concentration for the mechanism given above can be expressed as,

$$[(Hg \cdot NH_3)^*]_{ss} = \frac{(k_c + k_d[N_2])[Hg(6^3P_0)][NH_3]}{k_e + k_f[N_2] + k_g[M]} \quad (3)$$

At milliTorr Hg concentrations, the absorptivity is sufficiently large such that in a few cm pathlength, virtually all 253.7-nm radiation is absorbed. Hence, the $Hg(6^3P_1)$ production rate is proportional only to the incident 253.7-nm light. This allows the spatial and time averaged steady-state $Hg(6^3P_0)$ concentration in a flow reaction cell to be written as,

$$[Hg(6^3P_0)]_{ss} = \frac{k_b[\alpha I][N_2]}{\{k_h[N_2] + k_i[M] + [NH_3](k_c + k_d[N_2])\}\{k_b[N_2] + k_j[M]\}} \quad (4)$$

where α is a constant of proportionality.

For low concentrations of NH_3, $k_h[N_2] + k_i[M] \gg (k_c + k_d[N_2])[NH_3]$. In addition, at high N_2 concentrations and low impurity levels $k_b[N_2] \gg k_j[M]$. Therefore, the expression for the emission intensity of the exciplex can be approximated by,

Emission (345.0 nm)

$$\sim \frac{k_e(k_c + k_d[N_2])[\alpha I][NH_3]}{[k_e + k_f[N_2] + k_g[M]][k_h[N_2] + k_i[M]]} \quad (5)$$

Alternatively, Equation 5 can be expressed in the form,

Emission (345.0 nm)

$$\sim k_e(k_c + k_d[N_2])[NH_3][\alpha I]\tau[Hg(6^3P_0)]\tau(Hg \cdot NH_3)^* \quad (6)$$

where $\tau[Hg(6^3P_0)]$ is the lifetime of the metastable Hg atom in the system, and $\tau(Hg \cdot NH_3)^*$ is the lifetime of the exciplex.

These two expressions show that the exciplex emission intensity is directly proportional to the ammonia concentration, with its overall sensitivity controlled by magnitude of the rate constants, incident excitation light intensity, and the level of impurities, or M gases, existing in the reaction cell. Therefore, for a given set of operating conditions and for a constant level of trace contaminants, the emission intensity at 345.0 nm provides a simple measure of the ammonia concentration present.

The presence of impurities in the system influences the observed ammonia exciplex emission primarily via the quenching reactions 1j and 1i which reduce the steady-state concentration of the $Hg(6^3P_1)$ and $Hg(6^3P_0)$ atoms necessary for the formation of the ammonia exciplex. From the data given in Table I, the relative importance of these two processes can be estimated.

For the first process, if it is assumed that less than 10% of the $Hg(6^3P_1)$ state produced is quenched to the ground state, i.e., $k_j[M]/k_b[N_2] \leq 0.1$, then the maximum allowable concentrations for some common gases listed are: $O_2 \leq 1.4\%$; $CO_2 \leq 7.9\%$; $H_2 \leq 3.3\%$; $NO \leq 0.8\%$.

The estimates for the second effect, whereby the mercury atoms in the $^3P_0$ state are quenched to the ground state, require a slightly different approach. Since the $Hg(^3P_0)$ state is metastable and the transition to the ground state is doubly forbidden, the major mechanisms controlling the lifetime of the $Hg(^3P_0)$ state in a given system are quenching by trace contaminants from outgassing and by wall reactions. What one wishes to compare, therefore, is not the quenching rate constant of various gases relative to NH_3 and N_2, but rather to compare them to the effective quenching rate in a clean system which can be determined by measuring the lifetime of the $Hg(^3P_0)$ state.

The observed lifetime of the $Hg(^3P_0)$ state for a typical reaction cell containing 1 atm of pure N_2 was found to be of the order of 100 μs corresponding to a first-order rate constant of 10^4 s^{-1} for the quenching of $Hg(^3P_0)$ to the ground state. Using the data in Table I, the required concentrations for the various gases in order to give a rate constant equal to or less than 10^4 s^{-1} are given by: $O_2 \leq 2$ ppm; $H_2 \leq 6.5$ ppm; $NO \leq 1.5$ ppm; $CO \leq 34$ ppm; $C_2H_6 \leq 3000$ ppm; $C_2H_4 \leq 0.8$ ppm. These values correspond to the impurity level for a given contaminant gas such that the lifetime of the $Hg(^3P_0)$ state, and therefore the emission intensity of the ammonia exciplex, is reduced by a factor of 2. For other atmospheric trace gases such as SO_2 and NO_2, it is expected their quenching rate constant would be comparable to that for O_2. Consequently, they can also be tolerated at the parts-per-million level. As can be seen, the conditions imposed by the quenching of the $Hg(^3P_0)$ state by the impurity gases via reaction 1i are much more critical than those for the quenching of the $Hg(^3P_1)$ state.

For ambient monitoring, molecular oxygen removal is by far the most critical problem, owing to its abundance and relatively large quenching rate constant. Its concentration in a sample obtained from ambient air must be reduced by approximately a factor of 10^5 in order to maintain the same detection sensitivity as that achieved in measurements made with NH_3 in pure N_2. It should be noted, however, that the presence of O_2 only decreases the sensitivity and does not change the linearity of the emission intensity with NH_3 concentration so long as the O_2 concentration remains constant. Therefore, the degree to which it can be tolerated is largely dependent on the required sensitivity for a given application.

A feasible method for separating NH_3 from other gases in ambient samples is by the use of chromatographic columns. The described detection method can then be used as a highly sensitive and specific detector in a gas chromatograph for the measurement of NH_3 as well as other species such as amines and alcohols. It is in this context that the use of the proposed technique for the detection of NH_3 was most thoroughly investigated in a series of experiments.

Table I. Quenching Rate Constants of Various Gases Reacting with the Excited States of Mercury

	Bimolecular Rate Constants		
	Hg $6(^3P_1)$ at 298 K (From Cvetanović (5)) k(cm^3 molecule^{-1} s^{-1})		Hg $6(^3P_0)$ at 295 K (From Callear and McGurk (6)) k(cm^3 molecule^{-1} s^{-1})
Gas	Procedure I[a]	Procedure II[a]	
N_2	3.02×10^{-12}	4.31×10^{-12}	Very small
O_2	2.08×10^{-10}	2.98×10^{-10}	1.8×10^{-10}
H_2	3.36×10^{-10}	4.81×10^{-10}	5.37×10^{-11}
NO	3.85×10^{-10}	5.45×10^{-10}	2.51×10^{-10}
CO	6.48×10^{-11}	9.27×10^{-11}	1.035×10^{-11}
NH_3	5.91×10^{-11}	8.37×10^{-11}	3.1×10^{-13}
H_2O	1.94×10^{-11}	2.77×10^{-11}	Very small
CO_2	3.25×10^{-11}	4.64×10^{-11}	4.39×10^{-13}
N_2O	1.66×10^{-10}	2.37×10^{-11}	1.12×10^{-10}
CH_4	1.3×10^{-12}	1.8×10^{-12}	5.9×10^{-15}
C_2H_4	4.2×10^{-10}	6.0×10^{-10}	4.2×10^{-10}
C_2H_6	1.7×10^{-12}	2.5×10^{-10}	8.88×10^{-14}

$Hg/NH_3/N_2$ system (*1*)

k_c(cm^3 molecule^{-1} s^{-1})	k_d(cm^6 molecule^{-2} s^{-1})	$\tau(Hg \cdot NH_3)^*$	$\tau[Hg\,6(^3P_0)]$
3.1×10^{-13}	$2.2 \pm 0.2 \times 10^{-31}$	1.7 ± 0.1 (μs)	80–120 (μs)

[a] The two procedures reviewed by Cvetanović give absolute bimolecular quenching rate constants which differ by about a factor of 1.43. The relative values are in good agreement.

EXPERIMENTAL

The experimental apparatus used for the measurements consisted of a standard gas chromatograph column and injection system, and an emission cell with its associated optical system. A schematic of the arrangements of the components is shown in Figure 1. The chromatographic system consists of a dual-coil microvalve suitable for on-column injection. The column best suited to the present purpose was experimentally determined to be a 1.5-meter, 0.32-cm o.d. Teflon column packed with 60–80 mesh Chromosorb 104 which was treated with a 10% by weight solution of tetrahydroxyethylethylenediamine (THEED). The injection valve and column were enclosed in a constant temperature oven maintained at 80 °C. Ultrapure grade N_2 was used as the carrier gas and the flow rate through the column was set between 80 to 100 cm^3/min. The elution from the column was then mixed with a 500 cm^3/min flow of N_2 which was passed through a Hg bubble saturator thermostated at 22 ± 1 °C. The column effluent and saturator flow were then passed into a quartz (Suprasil) reaction cell whose dimensions were 1.25 cm in diameter and 5 cm long. The cell was concentrically irradiated with three (Ultra-Violet Products) low-pressure mercury pen-ray lamps.

It was observed in preliminary tests that during prolonged operation of the system, the walls of the cell become coated with products (primarily HgO) formed from reactions taking place within the cell involving trace contaminants. However, it was experimentally discovered that by introducing a very small concentration of methanol

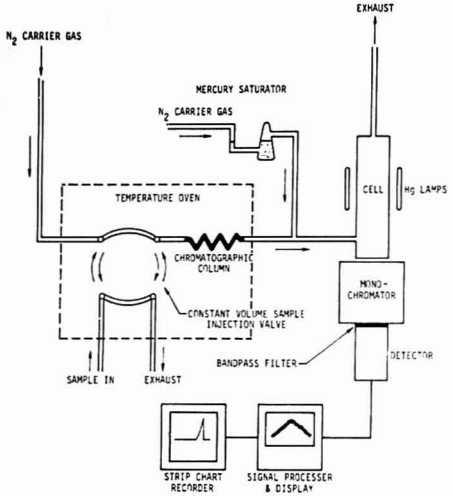

Figure 1. Schematic diagram of experimental apparatus

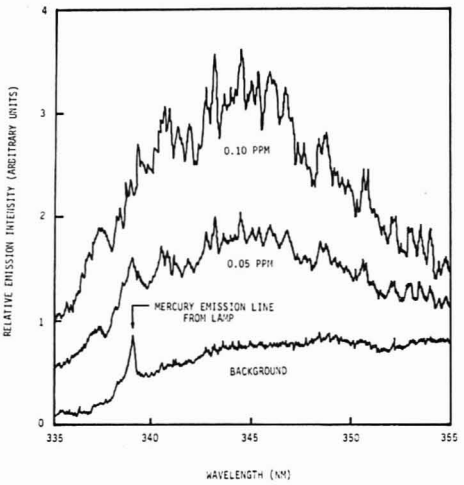

Figure 2. Measured $(Hg{\cdot}NH_3)^*$ emission spectra for a continuous flow of N_2 containing 0.1 and 0.05 ppm NH_3 through the reaction cell at an integration time of 1 s. The 348-nm filter was not used

vapor into the main N_2 flow, this product buildup can be virtually eliminated. Presumably, methanol acts as a gas phase scavanger of reaction products which can combine to form condensable materials. Since the exciplex emission from the $(Hg{\cdot}CH_3OH)^*$ exciplex occurs at 295 nm, it is isolated from the $(Hg{\cdot}NH_3)^*$ emission and does not interfere with the measurements for the NH_3. Therefore, a small concentration of methanol vapor was added to the system with a saturator which permitted very stable long term operation of the system with no detectable degradation of the signal intensity.

The spectral emission from the reaction cell was measured with a ¼-meter Jarrell-Ash grating spectrometer whose exit slit was modified in the standard manner to interface with a PAR model 1205A optical multichannel analyzer (OMA). This 500-element multichannel analyzer was set up to have a 20-nm display width with a resolution of 0.04 nm per channel element. This system was chosen because it is capable of performing simultaneous real-time, as well as integrated time-average, sampling of the emission over the entire spectral region of interest while maintaining sensitivity approaching that obtainable by direct photon-counting techniques for each optical element.

To reduce the scattered light background from the Hg emission lines in the photolysis lamp (see Figure 2), the emission radiation from the reaction cell was passed through an interference band-pass filter centered at 348 nm, with a 5-nm half-width. The resulting emission signal detected for this experimental arrangement is the convolution of the exciplex emission bandshape with the transmission characteristics of the interference filter.

Gas samples containing ammonia at various concentrations were prepared by passing nitrogen or air over permeation tubes of various lengths located in a constant temperature bath. Concentrations ranging from 20 ppm to 100 ppb were generated by adjusting the temperature and the flow rate accordingly. For the low concentrations in the range of a few ppb, the flow from the permeation tube enclosure was further diluted by mixing with additional clean gas. It was found that after an initial equilibration period of about 1 h, the concentration of ammonia generated remained stable to within a few percent.

For experiments performed with samples of ammonia in nitrogen, Matheson ultrapure grade nitrogen gas was used. Further purification of the gas as delivered from the manufacturer, performed by passing the flow from the cylinder through a cryogenic trap cooled to liquid argon temperature, produced negligible change in the results. For the case of ammonia in air samples, both room air and zero gas were used.

The described experimental apparatus were utilized to make three different types of measurements. The injection system was by-passed and gas samples of ammonia in nitrogen generated by the permeation tube were flowed continuously through the reaction cell. The resulting real-time signal displayed by the OMA were used to study the spectral content and intensity of the exciplex emission, as well as scattered light background interferences. The signals was integrated for various time intervals to establish the achievable sensitivity and the signal-to-noise of the system.

Known volumes of sample containing ammonia at various concentrations were also injected directly into the cell to study the time dependence of the emission as a function of carrier flow rate and reaction cell configuration. The data obtained were used to verify the degradation in sensitivity due to trace gas contaminants.

Finally, using samples of ammonia in nitrogen and ammonia in air, and injecting known volumes into the cell through the column, studies were carried out to test the feasibility of the system for ambient ammonia concentration measurements, as well as the degradation of the signal due to column effects such as incomplete separation, and loss of material due to irreversible wall absorption.

RESULTS

Some typical data obtained with continuous flow of N_2 containing various concentrations of NH_3 through the reaction cell are shown in Figure 2. The upper curve represents the measured emission spectrum for 0.1 ppm by volume NH_3 in N_2 while the middle curve is that for 0.05 ppm. The bottom curve is the background emission and scattered light signal without the presence of NH_3 and shows the presence of scattered light emission from the photolysis lamp. The structure on top of the emission spectra is not noise but, rather, emission lines from the mercury atoms in the cell due to its interaction with the ammonia exciplex. Since this emission signal is also proportional to ammonia concentration, it represents additional signal which enhances the sensitivity of the detection scheme. The real signal-to-noise ratio per channel of the optical multichannel analyzer was measured and found to be 70 to 1 at 0.1 ppm, or 10 to 1 at 14 ppb. By placing the previously mentioned 348-nm interference filter in the optical path between the cell and the monochromator, the background scattered light interferences were greatly reduced, and a further improvement in the signal-to-noise ratio of an order of magnitude or better was achieved.

The results obtained by injecting known volumes of samples containing NH_3 at various concentrations are shown in Figure 3. Figure 3a represents the real-time signal for a single channel of the OMA corresponding to the peak frequency of the

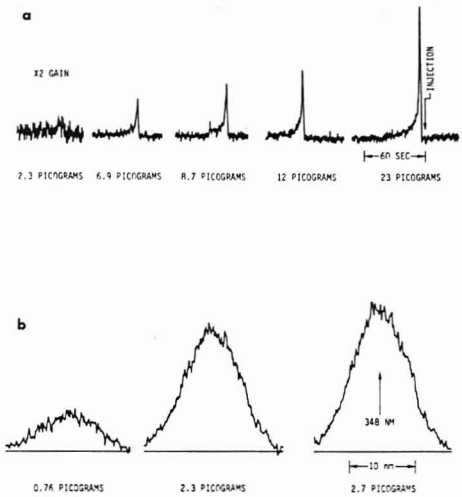

Figure 3. Real-time single channel (348 nm) emission signal and time-integrated intensity of the NH_3 emission band for direct injections of samples of NH_3 in N_2 into the reaction cell

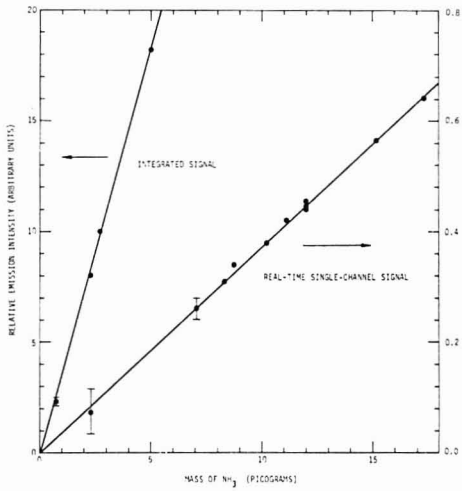

Figure 4. Relative intensity of measured emission as a function of injected NH_3 mass for direct injections of samples of NH_3 in N_2

emission spectra. Figure 3b represents the intensity of the emission band integrated over the residence time of the sample while flowing through the detector cell. The shape of these spectra is mainly dominated by the frequency response of the measurement system. As can be seen by comparing the areas under these curves, the frequency and time integration enhances the emission signal by about two orders of magnitude. Figure 4 shows the relative intensity of the signals detected as a function of NH_3 concentration. The signal was found to be linear in the mass of NH_3 gas injected over the

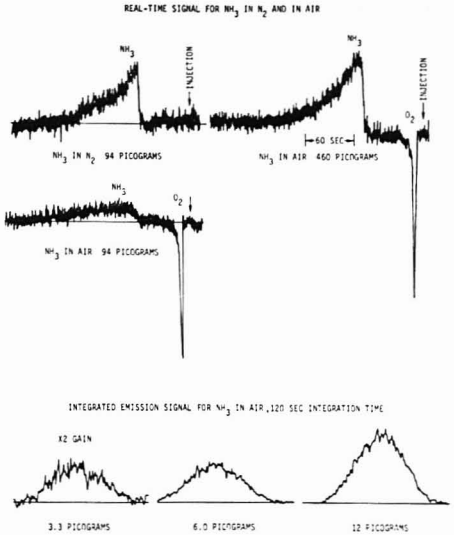

Figure 5. Real-time and integrated signals from NH_3 emissions for injections of NH_3 in N_2 and NH_3 in ambient air through the chromatographic column

range of measurements, and a sensitivity of the order of a few tenths of a picogram was achieved.

Extensive tests were carried out with injections of NH_3 in N_2 and in ambient air through the chromatographic column. Figure 5 shows some typical real-time and integrated signals for the two cases under similar conditions. As can be seen, the retention time of NH_3 for the conditions used was about 1 min, and the time necessary for complete elution of the NH_3 peak was of the order of 2 min. The retention for O_2 is about 10 s, which can be measured from the position of the strong negative signal caused by O_2 quenching of the background Hg fluorescence from the cell. A comparison of the two results indicates that the emission signal is lowered by about a factor of 6 for air samples. This is most likely caused by residual O_2 contamination of the system from the tailing of the air peak. It was, however, found that, by the use of methanol vapor as a gas phase scavenger, excellent repeatability can be obtained for measurements made over long periods of time.

The integrated emission signals are also shown as a function of frequency in Figure 5. Again, an enhancement of about a factor of two orders of magnitude in signal was achieved over the real-time single channel measurements. The integrated areas under these curves are shown in Figure 6 for both samples of NH_3 in N_2 and in air. The signal was shown to be linear for NH_3 concentrations up to 5000 pg. The achieved sensitivity in the present system for samples of NH_3 in air is about 3 pg (with a signal-to-noise of 5), which corresponds to a detection limit of the order of 4 parts per billion in a 1 cm^3 sample.

DISCUSSION

The results of this study have shown the technique of mercury-sensitized luminescence to be capable of determining ambient NH_3 in the 1- to 100-ppb range with linearity in concentration over three orders of magnitude. The ultimate sensitivity of the method is limited by the stringent requirement on the level of allowable interfering gases such as molecular oxygen. For specific applications where these gases are

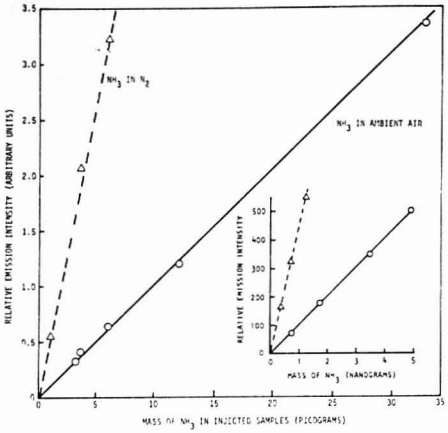

Figure 6. Relative intensity of the measured integrated emission signal as a function of injected NH_3 mass for samples of NH_3 in N_2 and NH_3 in ambient air through the chromatographic column

not present, the potential sensitivity of the described technique for detecting NH_3 exceeds that for other competitive methods. For ambient air monitoring, the practical limitation on sensitivity is determined by the degree with which chromatographic techniques can be developed to reliably separate samples containing NH_3 at concentrations below 1 ppb.

The detection principle itself has a number of fundamental advantages. The mercury–ammonia exciplex has a high efficiency for emission, with about 70% of the exciplexes decaying through dissociation with photon emission (*3*). Second, the exciplex emission occurs in a relatively narrow spectral range in the near ultraviolet, allowing high-efficiency photomultiplier tubes to be used for the measurements. Third, the emission is specific in frequency and the spectral information may be used to distinguish the signal from emissions due to various other gases which form excited mercury complexes. Fourth, the exciplex emission reaction is proportional to the total pressure of the system so that measurements can be carried out at atmospheric pressures or higher. Finally, the exciplex reaction mechanism does not remove NH_3 from the system except via secondary product formation. Therefore, with proper choice of reaction conditions, each NH_3 molecule can, in principle, react and emit many times, thus enhancing the sensitivity of the method. For example, if the lifetime of the $Hg(6^3P_0)$ in a cell is 100 μs and the incident photolysis power density is 250 mW per cm^3, then the NH_3 exciplex emission rate is of the order of 100 photons-molecule^{-1} s^{-1}. Hence, for an average residence time in a reaction cell of 1 s, a signal enhancement of 2 orders of magnitude can be realized over other emission measurements involving degenerative processes.

Work is currently being continued to utilize the method as an analytical tool in laboratory research programs as well as to adapt the technique to the detections of other gas species.

LITERATURE CITED

(1) Alan B. Harker and C. S. Burton, *J. Chem. Phys.*, **63**, 885 (1975).
(2) C. S. Burton, A. B. Harker, and W. W. Ho, Science Center Technical Report, Rockwell International Science Center, SCTR-74-3 (1974).
(3) R. H. Newman, C. G. Freeman, M. J. McEwan, R. F. C. Claridge, and L. F. Phillips, *Trans. Faraday Soc.*, **66**, 2827 (1970).
(4) A. B. Callear and J. H. Connor, *Chem. Phys. Lett.*, **13**, 245 (1972).
(5) R. J. Cvetanović, "Mercury Photosensitized Reactions", Progress in Reaction Kinetics, Vol. 2, G. Porter, Ed., The Macmillan Co., New York, 1964, p 39.
(6) A. B. Callear and J. McGurk, "Flash Spectroscopy with Mercury Resonance Radiation", Part 5: Formation and relaxation of Hg $6(^3P_0)$, *J. Chem. Soc. Faraday Trans. II*, No. 1, 97 (1973).

RECEIVED for review April 5, 1976. Accepted June 28, 1976.

Determination of *p*-Aminobenzoic Acid by Room Temperature Solid Surface Phosphorescence

R. M. A von Wandruszka and R. J. Hurtubise*

Department of Chemistry, University of Wyoming, Laramie, Wyo. 82071

***p*-Aminobenzoic acid and several other molecules were found to phosphoresce at room temperature when adsorbed on sodium acetate. A unique phosphorimetric method is described for determining *p*-aminobenzoic acid without separation in multicomponent vitamin tablets. The reflected phosphorescence of *p*-aminobenzoic acid adsorbed on sodium acetate was measured in the quantitation step. The method is rapid, very selective, and sensitive for *p*-aminobenzoic acid. The limit of detection is about 0.5 ng per sample spot and the relative standard deviation is 2.4% at 5 mg per tablet. *p*-Hydroxybenzoic acid, folic acid, and the benzamide of *p*-aminobenzoic acid also exhibited room temperature phosphorescence when adsorbed on sodium acetate. Phosphorescence data on these molecules are reported.**

Room temperature phosphorescence of adsorbed ionic organic molecules was first reported by Schulman and Walling (*1, 2*) and later by Paynters et al. (*3*) who put the phenomenon to its first analytical use. Also, Wellons et al. have reported on room temperature phosphorimetry of biologically-important compounds (*4*). Some solid surfaces that have been used are filter paper, silica, alumina, and asbestos. In all instances, it was stressed that extensive drying of the surface was required.

p-Aminobenzoic acid (PABA) was found to phosphoresce at room temperature when adsorbed on a surface of sodium acetate, even when the system was in contact with a solution of absolute ethanol.

The new method of PABA determination discussed in this paper is insensitive to moisture and utilizes a thin-layer densitometer for rapid, sensitive determinations. The method is much more sensitive than the USP XVIII method (*5*) and it can be used for samples to which the USP method is not applicable. It compares favorably with a recently reported uv absorption method (*6*).

EXPERIMENTAL

Apparatus. Phosphorescence excitation and emission spectra and phosphorescence lifetimes were determined with a Perkin-Elmer MPF-2A Fluorescence Spectrophotometer with a phosphorescence accessory. The source was a 150-watt Xe arc and the detector a 1P28 photomultiplier with S-5 response. Quantitation was achieved with a Schoeffel SD3000 Spectrodensitometer using a 150-watt Xe arc and a 1P28 photomultiplier. The samples that were measured with the densitometer were placed in a series of 12 circular depressions of $\frac{3}{16}$-inch diameter and $\frac{1}{100}$-inch depth that were milled into a brass plate along a line parallel to the edge. The plate was blackened to a dull, nonreflecting finish. In all subsequent quantitative determinations, it was placed on the moving stage of the densitometer.

Reagents. Ethanol was purified by distillation as described by Winefordner and Tin (*7*). Other solvents were reagent grade and used without further purification. The PABA was reagent grade and purified by recrystallization from ethanol. The other compounds tested were reagent grade and used without further purification. All PABA solutions were prepared with absolute ethanol unless stated otherwise. The vitamin B complex tablets analyzed were distributed by Plus Products, Irvine, Calif., and purchased from a local health food store.

Procedure. Standards and unknown samples were prepared as follows: 25-μl volumes of ethanol were introduced into 4 × 0.4 cm test tubes from a micropipet and 1–6 μl volumes of standard or sample solution were added from a 10-μl Hamilton syringe. The amounts of PABA thus delivered to each tube ranged from 10 to 200 ng. A fixed amount of sodium acetate was added to each tube with a measuring spoon that had the same volume as the depressions in the plate described above. The tubes were placed in an oven at 80 °C until all the ethanol had evaporated. The dry solid was quantitatively transferred to a small mortar and a pestle was used to gently break up conglomerate particles. The powder was then transferred to the depressions in the plate and smoothed over with a spatula.

A stock PABA-containing solution was prepared from vitamin tablets by grinding 20 tablets with a mortar and pestle and then extracting with ethanol for 1 h. The extract was filtered and the filtrate diluted to 250 ml with ethanol. This solution was used to prepare all other extract solutions used in subsequent PABA determinations.

After introduction of the powder into the depressions in the plate, the latter was placed on the stage of the densitometer. The phosphorescence intensity was measured with the excitation monochromator set at 290 nm and the emission monochromator set at 426 nm. The excitation monochromator was a prism, the emission monochromator a wedge monochromator, and all measurements were obtained in the single beam reflection mode.

Unless indicated otherwise for the phosphorescence excitation and emission spectra and lifetime determinations, the powder was introduced into a phosphorescence cell which was placed in the phosphorescence accessory of the fluorescence spectrophotometer.

RESULTS AND DISCUSSION

Sodium Acetate Suspension. The sodium acetate surface was formed and suspended as a gelatinous precipitate in absolute ethanol by addition of 0.5 ml of acetic anhydride to a 50-ml solution of ethanol saturated with sodium hydroxide and containing 0.10 mg PABA. This mixture was shaken for several minutes and a thick white precipitate of sodium acetate was formed. Upon excitation with a uv lamp, the PABA, presumably adsorbed on the suspended precipitate, was visibly phosphorescent. This was indicated by a strong blue signal that persisted for several seconds after the uv lamp was shut off. The precipitate was introduced into a phosphorescence cell, and the phosphorescence excitation and emission spectra were obtained using the phosphorescence accessory. These spectra were identical to the room temperature phosphorescence spectra obtained for a PABA sample prepared as described under Procedure. The excitation and emission maxima obtained were 290 and 426 nm, respectively. Liquid nitrogen temperature phosphorescence spectra of PABA in ethanol showed an excitation maximum at 315 nm and an emission maximum at 415 nm. Reported values are 310 nm for the excitation maximum and 430 nm for the emission maximum for ethanolic PABA solutions (*8*). The maximum room temperature phosphorescence excitation and emission wavelengths of PABA adsorbed on dried filter paper are reported to be 273 nm and 426 nm, respectively (*4*).

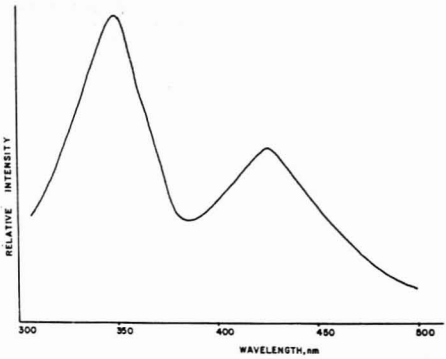

Figure 1. Total luminescence emission spectrum of PABA on sodium acetate. Excitation wavelength, 290 nm

Sodium Acetate Powder. The room temperature phosphorescence lifetimes of a PABA sample, prepared as described under Procedure and measured following the description in the Hitachi N-619E phosphorimeter manual, was found to be 3 s. The reported liquid nitrogen temperature phosphorescence lifetime of PABA in ethanol is 3.2 s (*8*). The fluorescence excitation and emission maxima of an ethanolic PABA solution are reported to be 290 nm and 350 nm, respectively (*9*). The lifetime of the luminescence signal and the position of the maximum emission wavelength from the solid surfaces indicate that phosphorescence from PABA was observed. With a PABA sample prepared as described and placed in the brass plate, the total luminescence emission spectrum was taken with the densitometer, using a scanning grating emission monochromator. Figure 1 clearly shows the fluorescence and the phosphorescence emission spectra of PABA.

Sodium Acetate Crystal. In another experiment, a single crystal of sodium acetate was grown from aqueous solution and placed in an ethanolic PABA solution (50 μg/ml). Strong blue phosphorescence, similar to that described above, was observed from the crystal surface, using a uv lamp for excitation. When the crystal was removed from solution and dried, phosphorescence could be observed upon excitation with a uv lamp even after the crystal was exposed to the atmosphere for several days.

Sodium acetate is slightly soluble in ethanol and its surface is affected by this solvent. This was indicated by the opaqueness that developed on the surface of the sodium acetate crystal after it was placed in ethanol. Several other solvents were used to prepare PABA solutions to be brought in contact with a sodium acetate crystal surface. The solvents tested were methanol, diethyl ether, isopropanol, isobutanol, acetone, and water and the choice of solvent was found to be of utmost importance. A crystal of sodium acetate, introduced into a solution of PABA in diethyl ether, appeared to be unaffected by the solvent and no phosphorescence was observed from the crystal surface. Sodium acetate crystals exposed to PABA dissolved in methanol, isopropanol, and isobutanol did not give rise to phosphorescence on the crystal surface although the crystal was affected to some extent by these solvents. Relatively weak phosphorescence was observed in all cases after the crystals were removed from solution and dried. It disappeared after prolonged exposure to the atmosphere. A sodium acetate crystal put in an acetone solution of PABA

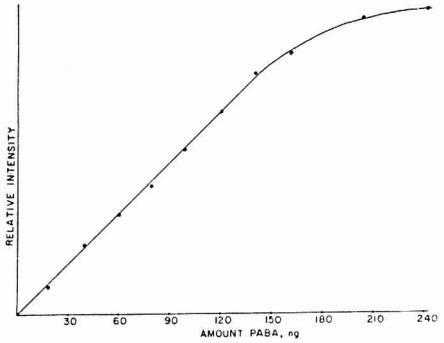

Figure 2. Calibration curve: phosphorescence intensity vs. amount of PABA

showed no surface phosphorescence whatever. Sodium acetate crystals grown from aqueous solution containing PABA did not yield phosphorescent crystal surfaces.

Other species tested on a sodium acetate crystal surface were benzoic acid, aniline, *p*-aminophenol, *o*-aminobenzoic acid and *m*-aminobenzoic acid, all dissolved in absolute ethanol. The first four showed no phosphorescence; the *m*-aminobenzoic acid gave a weak signal, but only after thorough drying.

Other Surfaces. PABA was applied to a number of other surfaces—silica gel, alumina, sodium carbonate, sodium iodide, potassium acetate, ammonium acetate, lead acetate, and lithium carbonate—but the phosphorescence observed was weak and the surfaces required thorough drying, notably in the case of potassium acetate.

The phosphorescence effect described is highly specific with respect to three factors: adsorbed molecule, adsorbent, and solvent. Of the systems described above, only the combination PABA–sodium acetate–ethanol gave rise to strong phosphorescence from the adsorbed PABA. Moreover, this combination presented the only case in which phosphorescence persisted after the crystal was removed from solution, dried, and exposed to the atmosphere for extended periods of time. Work is continuing to explain these facts.

Quantitative Determinations. A series of 10 identical PABA samples, each containing 100 ng PABA, was prepared and the phosphorescence signals were measured with the densitometer. The average peak height of the recorder response was taken to represent 100 ng PABA. The amount of PABA corresponding to each individual peak was computed and the relative standard deviation of the series was found to be 5%. A similar determination was made with a series of 10 ng samples of PABA and the relative standard deviation in that case was 7%. The linear range of a typical calibration curve extended from 0–200 ng PABA per sample. Above 200 ng, the curve became nonlinear (Figure 2), but was shown to be reproducible, and analytically useful results could be obtained up to 0.5 μg of PABA. The smallest amount of PABA in a sample spot that gave a phosphorescence signal equal to twice the background signal was 0.5 ng.

To demonstrate the analytical usefulness of this new phenomenon, PABA was determined in vitamin tablets labeled to contain 5 mg PABA per tablet. A list of tablet ingredients is given in Table I. The PABA content of these tablets was considerably less than the 94% specified in USP XVIII (*5*) as the minimum content of tablets to which the USP method can be applied. The tablet extract solution was prepared as described and a 0.2-ml aliquot of this solution was taken and diluted to 10 ml with ethanol. Two-microliter volumes of this final solution were introduced into the test tubes with a microsyringe and treated as described. The results of replicate determinations are shown in Table II. The average amount of PABA per tablet was found to be 5.0 mg.

Table I. Tablet Ingredients

Ingredient	Quantity per 6 tablets (as labeled)
Vitamin B_1	5 mg
Vitamin B_2	5 mg
Vitamin B_6	5 mg
Folic acid	0.1 mg
PABA	30 mg
Pantothenic acid	100 mg
Niacinamide	50 mg
Inositol	1000 mg
Choline bitartrate	1000 mg
Vitamin B_{12}	15 μg
Biotin	25 μg

Table II. PABA in Vitamin Tablets

Determination	PABA per tablet, mg
1	5.1
2	5.0
3	4.8
4	4.9
5	5.0
6	5.0
7	4.9
8	5.0
9	5.0
10	4.8
11	5.2
12	5.1
13	5.1
	Av 5.0 mg PABA/tablet
	Std dev, σ = 0.12
	Rel std dev 2.4%

Table III. Percentage PABA Recovery in Spiked Extract Samples[a]

ml extract in 10-ml solution	PABA determined in series 1, ng/μl	PABA added in series 2, ng/μl	total PABA present in series 2, ng/μl	total PABA determined in series 2, ng/μl	Recovery, %
0.1	4.2	49.5	53.7	54.2	101
0.2	8.0	49.0	57.0	57.0	100
0.3	11.5	48.5	60.0	61.0	102
0.4	16.2	48.0	64.2	62.9	98
0.5	20.5	47.5	68.0	70.0	103
					Av 101%

[a] Average values from duplicate determinations.

Interferences. A study was made to determine possible interferences with PABA determinations by other tablet ingredients. For this work, two series of aliquots ranging from 0.1–2.5 ml were taken from the extract. Each of the aliquots in the first series was diluted to 10 ml with ethanol. In the second series, the aliquots were diluted to 10 ml with a 50 μg/ml standard PABA solution so that each of the resulting solutions contained a different, known amount of PABA in addition to the extract. It was found that in both series the

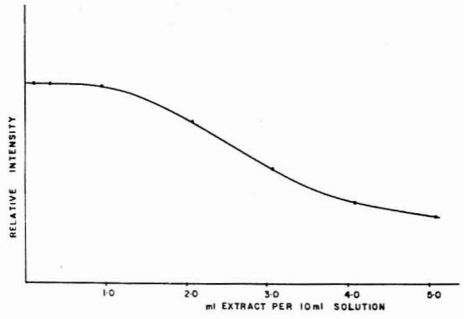

Figure 3. Reduction of PABA phosphorescence intensity with increasing amount of extract

PABA could be determined accurately in the solutions containing less than 1.0 ml of extract per 10 ml of solution. For the solutions more concentrated in extract, a strong reduction in PABA phosphorescence intensity was noted. Also, the amount of PABA determined no longer varied in accordance with the amount of extract present in the solutions. To find the range of extract concentrations that could be used without leading to reduction in the PABA phosphorescence signal, a number of solutions were prepared containing 0.1–5.0 ml of extract, diluted to 10 ml with a concentrated standard PABA solution and/or pure ethanol, such that all solutions contained 225 ng/μl PABA. One-microliter volumes of these solutions were treated as for a PABA determination, and the PABA phosphorescence intensities were measured. A plot of PABA phosphorescence intensity vs. amount of extract was made (Figure 3). The resulting curve showed that extract volumes greater than about 0.8 ml will give erroneous results.

In the two series of solutions described above, the PABA contents were determined for the solutions containing 0.5 ml of extract and less per 10 ml of solution. The percent recovery of PABA was computed and the results are shown in Table III.

It is clear from Figure 3 and the data in Table III that accurate results can be achieved when the amount of extract is less than 5% of the volume of the final solution. This does not present a problem as the sensitivity of the method allows for the determination of extremely small amounts of PABA with good precision. For example, test tubes containing 1.0 μl of an extract solution at 8 ng/μl PABA were spiked with 5.0, 10.0, and 20.0 ng PABA in ethanol solution and the samples determined for PABA. The PABA recovery was 100% in all three cases.

To investigate the cause of the reduction in PABA phosphorescence intensity at higher extract concentrations, a reflection spectrum of extract on sodium acetate was taken with the densitometer set in the double beam mode (Figure 4). It can be seen that the extract absorbs at the phosphorescence emission wavelength of PABA, which would be one factor leading to the observed reduction in phosphorescence intensity for the more concentrated extract solutions. Also, the absorption of exciting radiation by other tablet ingredients would cause a reduction in PABA phosphorescence intensity. As indicated by Tables II and III, these factors are not important at the level of extract used in the analytical procedure.

Luminescence spectra of the extract on sodium acetate were also taken with the fluorescence spectrophotometer. With the phosphorescence accessory in place, the extract gave excitation and emission spectra virtually identical to pure PABA on sodium acetate, with maxima at 300 nm and 425 nm, respectively. The total luminescence emission spectrum of extract on sodium acetate obtained with the fluorescence spectrophotometer is shown in Figure 5. It is evident that the phosphorescence peak at 426 nm corresponds closely to that of pure PABA, whereas the fluorescence peak has shifted to shorter wavelengths, indicating the presence of other fluorescent species in the extract. The shoulder centered around 460 nm must also be due to other fluorescent species since emission spectra of extract on sodium acetate obtained with the phosphorescence accessory show a single peak with the maximum at 426 nm.

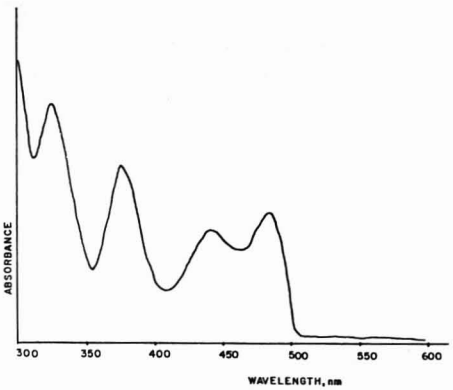

Figure 4. Absorbance–reflection spectrum of extract on sodium acetate. Readings taken every 10 nm

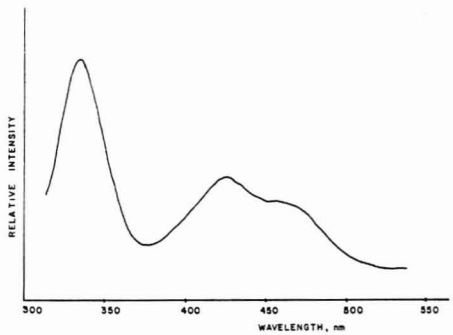

Figure 5. Total luminescence emission spectrum of extract on sodium acetate. Excitation wavelength, 300 nm

Finally, an ethanolic solution containing 20 ng/μl PABA as well as 200 ng/μl *m*-aminobenzoic acid and a solution containing 20 ng/μl PABA and 200 ng/μl *o*-aminobenzoic acid were prepared and the PABA contents were measured. It was found that the PABA determinations were in both cases free from interference.

Other Molecules. In a preliminary study, *p*-hydroxybenzoic acid, folic acid, and the benzamide of PABA were investigated. Phosphorescence excitation and emission spectra were obtained for these molecules on sodium acetate and their respective phosphorescence excitation maxima were 340, 320, and 300 nm and the corresponding emission maxima 404, 465, and 430 nm. Investigations into the behavior of other molecules are continuing.

LITERATURE CITED

(1) E. M. Schulman and C. Walling, *Science*, **178**, 53 (1972).
(2) E. M. Schulman and C. Walling, *J. Phys. Chem.*, **77**, 902 (1973).
(3) R. A. Paynters, S. L. Wellons, and J. D. Winefordner, *Anal. Chem.*, **46**(6), 736 (1974).
(4) S. L. Wellons, R. A. Paynter, and J. D. Winefordner, *Spectrochim. Acta, Part A*, **30**, 2133 (1974).
(5) "The United States Pharmacopeia", 18th rev., Mack Publishing Co., Easton, Pa., 1970, p 999.
(6) W. L. Paul, *J. Pharm. Sci.*, **62**(4), 660 (1973).
(7) J. D. Winefordner and M. Tin, *Anal. Chim. Acta*, **31**, 239 (1964).
(8) G. G. Guilbault, "Practical Fluorescence, Theory, Methods and Technique", Marcel Dekker, Inc., New York, N.Y., 1973, p 190.
(9) J. J. Aaron and J. D. Winefordner, *Talanta*, **19**, 21 (1972).

RECEIVED for review October 24, 1975. Resubmitted May 10, 1976. Accepted June 28, 1976.

Determination of Tin by Gas Phase Atomization and Atomic Absorption Spectrometry

Prem N. Vijan* and Chris Y. Chan

Air Quality Laboratory, Ministry of the Environment (Ontario), Toronto, Ontario, Canada

A semiautomated method for the determination of tin in suspended air particulate matter is described. The dissolved tin is reacted with sodium borohydride solution and converted into gaseous hydrides. The resulting gaseous mixture is combusted in a tube furnace and the atomic absorption of tin is measured at 286.3 nm. More than 20-fold concentrations of copper, nickel, antimony, and arsenic interfere. The interferences are eliminated by the addition of sodium oxalate to the sample solutions or by prior coprecipitation with hydrated manganese dioxide. Fifty Hi-Vol air filters can be analyzed per day. The relative standard deviation of the method is 6% with a sensitivity of 0.45 μg/l. and a detection limit of 0.1 μg/l.

There is a need for a simple and sensitive method for measuring tin concentrations in environmental, food, and geological materials. The colorimetric methods for the determination of tin are tedious, nonspecific and involve lengthy distillation (*1*). The sensitivity of the conventional flame atomic absorption methods for tin is approximately 0.5 μg/ml which is insufficient for accurate analysis. Besides, they are prone to chemical, spectral, and molecular interferences (*2–4*). Tin belongs to a family of metals and metalloids that form gaseous hydrides with a fair degree of ease. The research papers based on the use of gaseous hydrides for atomic absorption measurements by flame and nonflame atomization devices have shown a considerable increase over the past few years. Improvements of sensitivity by several orders of magnitude have been reported compared with conventional atomic absorption methods. Fernandez (*5*) reported an absolute sensitivity of 7 ng/ml for tin in dilute hydrochloric acid solution using sodium borohydride pellets for hydride generation and a balloon reservoir for collection. He used an argon–hydrogen–entrained air flame and measured the atomic absorption signal at 224.6 nm.

Heated quartz tubes are stable atomizers as compared with flames. They do not require the use of high pressure gases and are better suited for unattended operations (*6*). Schmidt et al. (*7*) have briefly listed the advantages of the automated approach. They used an argon–hydrogen–entrained air flame to establish the precision and the detection limits for arsenic, selenium, bismuth, antimony, and tin in aqueous solutions. Pierce et al. (*8*) applied the same idea to the determination of selenium and arsenic in surface waters using a tube furnace, as in Ref. 6, together with a stripping column used by Goulden et al. (*9*).

Smith (*10*) carried out a systematic study of the interferences encountered in the determination of volatile hydride-forming elements using the manual method and the argon–hydrogen flame. Very little work, however, was done on tin, and large blanks were obtained. No attempt has been made to investigate the elimination of these interferences.

Burke (*11*) successfully used the scavenging properties of the oxide of Mn(IV) for quantitative coprecipitation of traces of antimony, bismuth, lead, and tin from solutions of nickel prior to their determination by atomic absorption spectrometry.

The present paper describes a method for determination of tin in airborne dust collected on a glass fiber filter, and a few other matrices by a continuous hydride generation technique with special emphasis on the study and elimination of interferences.

EXPERIMENTAL

Apparatus. A Techtron Model AA-5 atomic absorption spectrophotometer was used to obtain all the data. The analytical wavelength used was 286.3 nm and the light source was a tin hollow cathode tube (Westinghouse) operated at recommended current. Argon gas flow rate was regulated at 240 ± 30 ml/min by means of a calibrated flow meter. An electrically heated open ended quartz tube, 10 cm long and 10-mm i.d. with a 4-mm diameter inlet tube was used for atomizing tin in the gaseous stream. The temperature of the tube furnace was controlled by a Variac transformer. A Technicon sampler, proportioning pump, and manifold were used in conjunction with a 10-mV variable range recorder for achieving an automatic operation as previously reported (*6*). The system diagram is shown in Figure 1. The optimum instrumental parameters are summarized in Table I.

Reagents. Tin standard solutions were prepared by diluting 1000 ppm stock solution (BDH) and 1% HCl. (All other acids and salts used were reagent grade.) A 1% solution of sodium borohydride (98% Fisher Scientific) was used for hydride generation. Demineralized distilled water was used for preparing all the reagent and sample solutions.

Procedure. *Sample Decomposition.* Hi-Vol Filters. Circular filter disks measuring 5 cm^2 were cut from 33 exposed Hi-Vol glass fiber filters by means of a stainless steel punch. They were placed in 18 × 150-mm test tubes held in a 40-hole aluminum heating block. Seven blank disks were placed in the remaining test tubes and 0, 0.05, 0.10, 0.20, 0.30, 0.50, and 1.00 ml of 15 μg/ml tin solution were added by means of a microburet. Two-ml portions of concentrated hydrochloric acid were added to each test tube. The loaded aluminum block was transferred to a hot plate and the contents of the test tubes were maintained at near boiling temperature for 2 h. The digestates were diluted to 15 ml with demineralized distilled water and mixed thoroughly. The test tubes were centrifuged and 1:10 dilutions of the clear solutions were transferred to the sampling cups for automated tin analysis. The final solutions contained approximately 1% hydrochloric acid. If lower reportable limits are desired, the dilution step is eliminated and instead the sample digestates are neutralized with sodium hydroxide, reacidified with 1.5 ml of 10% hydrochloric acid and made up to 15 ml with distilled water using one drop of phenolphthalein as indicator.

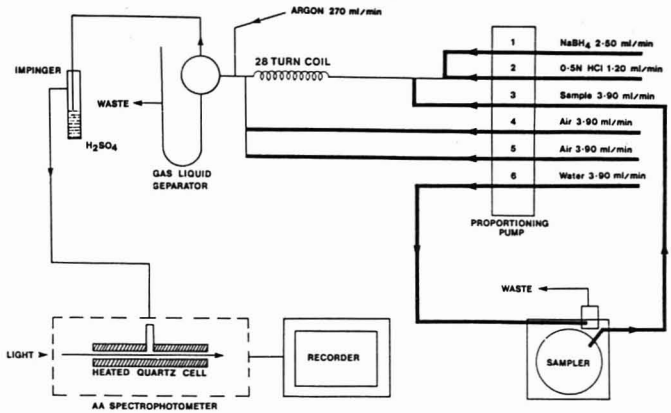

Figure 1. AutoAnalyzer–AAS system for tin

Minerals. The samples were fused with sodium peroxide in vitreous carbon crucibles. The fusions were dissolved in 1:1 hydrochloric acid and diluted to known volumes. The prepared solutions were further diluted with 1% hydrochloric acid to bring their concentrations within the optimum range of working standards.

Rocks. About 100 mg of accurately weighed sample was heated with 2 ml of 5:2:10 mixture of H_2SO_4:HNO_3:HF in a 25-ml Teflon beaker. The contents were taken to fuming. The residue was dissolved in distilled water and neutralized with 5% sodium hydroxide until a precipitate appeared. The solution was acidified with 1 ml of 1:1 hydrochloric acid and the volume was made up to 50 ml with distilled water.

Sludges. About 100 mg of accurately weighed sample was digested with 2 ml of 1:4 perchloric–nitric acid mixture in a covered 25-ml beaker. The contents were heated until white fumes appeared. The digestate was made up to 100 ml with 1% hydrochloric acid. The prepared solution was further diluted with 1% hydrochloric acid as required.

Liquid Food and Water Samples. No sample preparation was required. Samples were diluted with 1% hydrochloric acid and analyzed. For solid foods, decomposition procedures recommended by Sandell (*1*) may be used.

Coprecipitation with Hydrous Manganese Dioxide. A suitable aliquot of the prepared sample solution containing 0.3 to 1.0 μg of tin was transferred to an 18- × 150-mm test tube and diluted with 10 to 12 ml of distilled water. One-ml volume of 1% manganese sulfate solution was added and the contents were heated to boiling. A half-ml portion of 0.25% potassium permanganate solution was added dropwise to the contents of the test tube and heated to boiling again. The test tube was set aside for 30 min at room temperature. The precipitated manganese dioxide was filtered, under gentle suction, through a disk of glass fiber or Whatman 40 filter fitted into a Gooch crucible. The test tube was rinsed 3 to 4 times with small volumes of distilled water and the rinsings were passed through the same Gooch crucible. The precipitate was wetted with 0.3 ml of 6 M hydrochloric acid followed by 2 ml of 10% hydrogen peroxide to dissolve it completely. The solution was received in the same test tube in which the precipitation was performed. The filter and Gooch crucible were washed several times with small quantities of water so as not to exceed the volume of 15 ml. The final volume was made to the 15-ml mark on the test tube.

RESULTS AND DISCUSSION

Effects of Experimental Parameters. *Manifold Design.* The tube sizes required to build the manifold shown in Figure 1, were determined by the trial and error method to provide optimum flow rates of various reagents. Use of a two-lobe sampler cam allowed 1 min for sampling and 2 min for wash cycles. These intervals were best suited for obtaining well formed signal peaks returning smoothly to a reasonably stable baseline. A draught- and smoke-free environment around the ends of the quartz tube, and a minimum opening of the exhaust pipe damper were necessary to reduce the baseline drift to half a chart paper division (0.001 absorbance). A sudden drop in sensitivity was always attributed to either the condition of the quartz cell or the manifold tubes. After a prolonged use, a greyish powdery deposit built up on the inner walls of the cell, possibly due to a reaction between quartz and hydrogen at high temperature. This affected the performance of the system. An occasional brushing with a mild detergent and heating the quartz tube to a high temperature restored its performance. The manifold tubes required occasional replacement or cleaning with hydrochloric acid.

Table I. Optimum Instrumental Parameters

Damping	Maximum (D)
Wavelength	286.3nm
Slit width	100 μm
Sample time	1 min
Wash time	2 min
Recorder span	5-mV Full scale
Recorder speed	0.5 cm/min
Atomizer temp.	850 °C

Introduction of air into the system was necessary. Complete blockage of air tubes produced signal peaks which were irregular in shape and took a longer time to return to the baseline. Use of two manifold tubes for air supply gave slightly better performance than one tube. The system was found to be quite rugged and trouble free over an operating period of 3 to 4 months. The presence of sulfuric acid dryer was not essential but was desirable because it prevented the condensation of water vapor in the gas delivery tube.

Carrier Gases. The optimum argon flow rate was between 220 to 280 ml/min depending on the size of the quartz cell. A continuous decrease of argon flow rate from 600 ml/min to 100 ml/min increased the signal progressively by approximately 60%. However, lower flow rates produced distorted peaks with unstable baseline and higher flow rates decreased sensitivity partly due to dilution and partly due to the shortened residence time in the heated atomizer. The use of nitrogen as sweep gas at the same flow rate as argon gave approximately the same response (*12*).

Atomizer Temperature. The temperature of the quartz tube was 850 ± 10 °C for maximum sensitivity and precision.

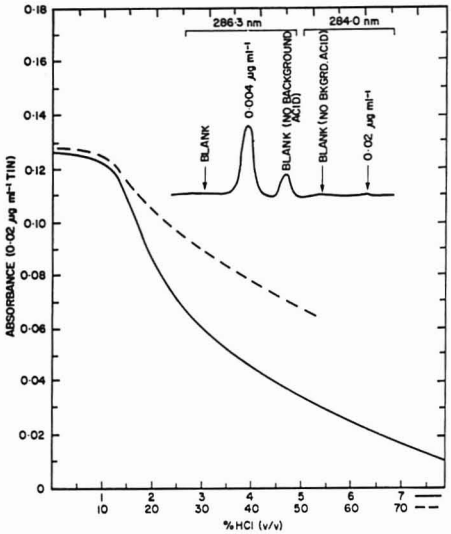

Figure 2. Effect of acid concentration on the absorbance signal of tin; (—) sample acid concentration vs. absorbance; (- - -) background acid concentration vs. absorbance

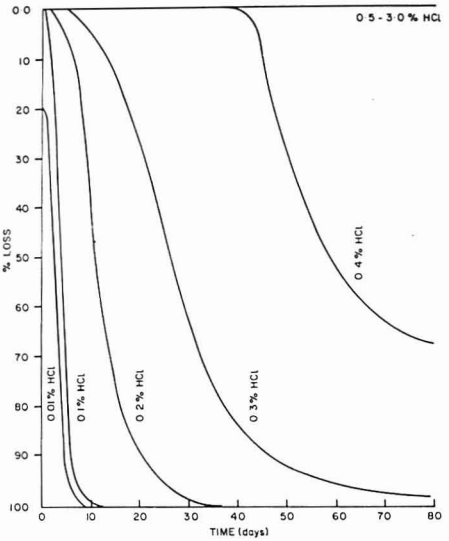

Figure 3. Effect of acid concentration on the stability of a standard solution of tin (0.1 μg per ml)

Table II. Effect of Foreign Elements on Recovery of Tin[a]

Interfering element	Amount added, μg ml^{-1}	% Recovery: Direct	% Recovery: With copptn[b]	% Recovery: With $Na_2C_2O_4$, 600 μg ml^{-1}
Ni	0.5	100	100	100
	2.0	90	100	100
	5.0	60	100	100
	10.0	30	100	100
Cu	0.5	100	100	100
	2.0	85	100	100
	5.0	75	100	85
	50.0	50	100	65
As[c]	0.3	100	100	100
	0.5	82	100	82
	5.0	50	98	50

[a] All solutions contained 0.03 μg ml^{-1} tin in 1% HCl. 10 000 μg ml^{-1} Na, K; 1000 μg ml^{-1} PO_4^{3-}, SO_4^{2-}, NO_3^-, Cl^-; 40 μg ml^{-1} Pb, Ca, Mg, Zn, Fe, Al; 5 μg ml^{-1} Se, Cr, Mo do not interfere. [b] 1000 μg ml^{-1} of Cu, Ni, Cr, Zn, Fe, Al gave 100% recoveries. [c] Sb behaves similarly.

Raising the temperature to 950 °C caused progressive reduction in response by 25% and lowering the temperature to 700 °C increased the sensitivity slightly but caused peak distortion and baseline instability. A 10- × 100-mm quartz tube was found to be twice as sensitive as an 18- × 140-mm tube.

Sodium Borohydride Solution Concentration. The increase of sodium borohydride solution concentration from 0.5% to 5%, w/v, did not change the sensitivity significantly. A 1% concentration chosen for this work allowed for some spontaneous decomposition of the reagent solution without affecting the calibration. A fresh solution was prepared before use. The solution of sodium borohydride stored overnight at room temperature produced a lower response. Storage in a refrigerator maintained the strength of this solution.

Acid Concentration. The sensitivity of the present method was found to be strongly dependent on the concentration of hydrochloric acid present in the sample and of the acid pumped through line 2 of the manifold diagram. This relationship is illustrated in Figure 2. The small plateau of the curve allows some variation in the acidity of the sample solution without adverse effect on the quality of results. Presence of some acid is essential for initiating the reaction. The background acid (line 2 of manifold) was necessary to obtain good signal peaks with stable baseline and to continuously subtract the reagent blank by setting the recorder pen to zero. On substituting distilled water for 0.5N hydrochloric acid in line 2, a reagent blank signal peak corresponding to 1.2 ng per ml tin was obtained. This peak was confirmed to be due to tin by the use of a neighboring 284.0-nm non-absorbing line (Figure 2). Acids such as nitric, hydrochloric, sulfuric, perchloric and their mixtures of equivalent concentration gave equal absorbance signals for 0.1 μg per ml tin.

Matrix Effects. The effect of several matrix elements likely to occur in Hi-Vol filters and other samples was investigated. Of the common elements studied only nickel, copper, antimony and arsenic interfered. Up to 20-fold concentrations of these four elements did not suppress the signal. The amounts of nickel, copper, antimony and arsenic present in air, in excess of 0.5, 2.5, 1.0 and 2.0 μg/m^3 respectively, would interfere. These concentrations are uncommon in typical air samples. Interference due to higher amounts of nickel and copper was effectively removed by the use of coprecipitation procedure and to a lesser degree by providing 600 μg per ml of sodium oxalate in the final sample solutions. The results are summarized in Table II. Tin impurity was not detected in 600 μg per ml solution of sodium oxalate. All results reported in this paper were obtained without the use of coprecipitation or addition of sodium oxalate. The inherent sensitivity of the method allows very high dilutions of the sample solutions thereby reducing the concentration of interferents to a point

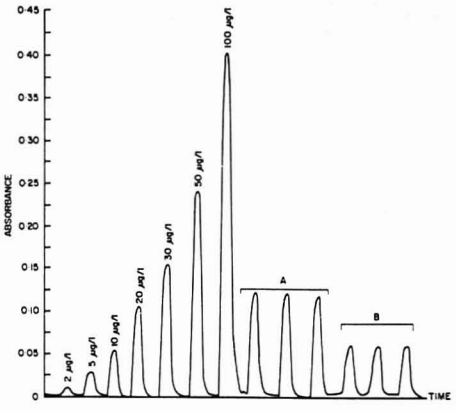

Figure 4. Typical recorder tracings of tin; (A) triplicate peaks for sample No. 1; (B) triplicate peaks for sample No. 2

Table III. Precision Data for Determination of Tin in Three Hi-Vol Filters

Sample No.	I	II	III
No. of detns	12	12	12
Mean (ng ml^{-1})	21.3	48.2	24.3
Mean ($\mu g/m^3$)	0.126	0.285	0.143
Std dev	0.86	2.86	1.30
Std error	0.25	0.83	0.38
Rel std dev	4.06	5.94	5.37

of insignificance. Tolerance of high concentrations of sodium and potassium permits neutralization of the digested samples for proper adjustment of their acidity. No molecular absorption effects were noticed in this study.

The coprecipitation of tin with hydrated manganese dioxide was very effective in removing interferences. Standard solution of tin (0.1 µg per ml) taken through the coprecipitation procedure produced absorbance peaks which were equal in height to those produced by untreated solution. The coprecipitation procedure used was essentially that of Burke (*11*) except for a slight modification. He performed coprecipitation in nitric, perchloric and sulfuric acid solutions but in our hands hydrochloric acid was found to work just as well. Hydrochloric acid was chosen because it was the preferred solvent for tin in air particulate matter as well as other matrices. The acidity of the sample solution before coprecipitation was found to be very critical and must be maintained below 0.16N. Higher acidity caused the precipitated MnO_2 to redissolve resulting in low and imprecise recoveries of tin. The use of up to 0.3 ml of 50% hydrochloric acid for dissolution of manganese dioxide, resulted in an optimum acidity of the prepared solution. Strict adherence to the procedural details were necessary to obtain good results.

Stability. The stability of 0.1 µg per ml tin solutions prepared in different concentrations of hydrochloric acid was investigated. The results are depicted in Figure 3. Standard solutions of tin containing 0.5% hydrochloric acid were found to be stable for more than 80 days. Those prepared in 0.01% hydrochloric acid lost tin to the walls of the container within a few hours. Storage in glass and polyethylene containers were found to be equally good. Nitric acid gave results similar to hydrochloric acid. Standard solutions prepared in 2% and 3% hydrochloric acid gave constant but lower signal peaks due to the effect of increased acidity (Figure 2).

Table IV. Determination of Tin in Hi-Vol Filter Samples by Two Methods

Mean of Duplicates	
Present method (µg/m³)	Flame AAS[a] (µg/m³)
206.1 ± 0	215.2 ± 21.2
20.6 ± 0	20.0 ± 0
183.1 ± 7.0	184.9 ± 9.1
260.7 ± 0	266.8 ± 0
104.3 ± 4.2	97.0 ± 0
151.6 ± 0	145.5 ± 0
104.9 ± 1.2	106.1 ± 3.0

[a] Nitrous oxide–acetylene.

Table V. Determination of Tin in Different Sample Matrices

Foods	Manufacturer I, µg ml^{-1}[a]		Manufacturer II, µg ml^{-1}	
Orange juice	55	66	0.15	0.15
Apple juice	4.2	4.2	<0.1	<0.1
Apple cherry juice	<0.1	<0.1	1.40	1.35
Apple pineapple juice	50	62	<0.1	<0.1
Orange banana juice	70	55	2.0	1.8
Mixed fruit juice	30	50	1.9	2.1
Tomato juice	89	90	50	52
Cola	0.5	0.6	0.3	0.3
Tap water	0.00008			

Sludges	Present method, µg ml^{-1}	Emission spec, µg ml^{-1}
1	2.9	3.0
2	4.6	4.8

Rocks and minerals	Found	Certified value
USGS-W-1 rock	3.0 ± 0.33 ppm	3.2 ppm
CCRMP-KC-1	0.68 ± 0.20%	0.68%
CCRMP-MP-1	2.43 ± 0.15%	2.50%

[a] The two sets of results shown under each manufacturer are not duplicates but values obtained on two different cans.

Sensitivity, Detection Limits, Precision and Accuracy. Figure 4 shows the typical recorder tracings obtained for the calibration curve. The curve is linear up to 0.04 µg per ml tin. Sensitivity and detection limit (signal equal to twice the standard deviation of blank) of the method were 0.45 ng per ml and 0.05 ng per ml respectively. The triplicate sample peaks for two different Hi-Vol filters (Figure 4) give a visual indication of the repeatability of the method. The sensitivity measured at 224.6 nm was 66% higher but the baseline drift increased considerably.

The precision of the method was measured by replicate analysis of three typical Hi-Vol filter samples. The results are shown in Table III. A relative standard deviation of between 4.06 and 5.94% was obtained at the concentrations shown.

Recoveries of tin added to six different Hi-Vol samples averaged 99% with a relative standard deviation of 6.0%.

A set of Hi-Vol filters containing high concentrations of tin were analyzed by the present method and by flame atomic absorption method using nitrous oxide acetylene flame. The results obtained are summerized in Table IV. The results also indicate that in spite of high dilution of the prepared sample solutions the precision and accuracy of the present method are quite satisfactory.

The use of concentrated nitric acid, concentrated sulfuric

acid, 1:1 hydrochloric:hydrofluoric acid mixture for digestion of Hi-Vol samples gave results which agreed within 3% of those obtained by concentrated hydrochloric acid. Unexposed glass fibre filters from different lots showed no detectable amounts of tin. The average tin concentration of urban air around Toronto was found to be 18 μg per thousand cubic meters, based on analysis of 32 Hi-Vol filters, with a maximum of 122 μg and a minimum of 3 μg per thousand cubic meters.

The concentrations of tin were higher in air particulate matter in and around lead refineries and can manufacturing operations. The lead:tin ratio in these areas was about 300 as against 50 for traffic locations. As low as 0.5 μg tin per thousand cubic meters of air can be measured by this method. Up to 50 samples can be easily analyzed in one man-day.

Application to Other Materials. The results of tin determination in a few other sample matrices are listed in Table V. The certified tin concentrations in the Canadian Certified Reference Materials Project (CCRMP) Samples KC-1 and MP-1 and USGS W-1 rock sample show close agreement with the results obtained by the present method. The CCRMP samples are minerals containing very high levels of nickel, copper, iron, sulfur etc., and yet did not require either coprecipitation of tin or addition of sodium oxalate before analysis. Food samples were appropriately diluted with 1% v/v, hydrochloric acid and analyzed.

LITERATURE CITED

(1) E. B. Sandell, "Colorimetric Determination of Traces of Metals", 3d rev. ed., Interscience Publishers, New York, 1959, p 854.
(2) P. O. Juliano and W. W. Harrison, *Anal. Chem.*, **42**, 84 (1970).
(3) J. R. Levine, S. G. Moore, and S. L. Levine, *Anal. Chem.*, **42**, 412 (1970).
(4) I. Rubaska and M. Miskowsky, *At. Absorpt. Newsl.*, **11**, 57 (1972).
(5) F. J. Fernandez, *At. Absorpt. Newsl.*, **12**, 93 (1973).
(6) P. N. Vijan and G. R. Wood, *At. Absorpt. Newsl.*, **13**, 33 (1974).
(7) F. J. Schmidt, J. L. Royer, and S. M. Muir, *Anal. Lett.*, **8**, 123 (1975).
(8) F. D. Pierce, T. C. Lamoreaux, H. R. Brown, and R. S. Fraser, *Appl. Spectrosc.*, **30**, 38 (1976).
(9) P. D. Goulden and P. Brooksbank, *Anal. Chem.*, **46**, 1431 (1974).
(10) A. E. Smith, *Analyst (London)*, **100**, 300 (1975).
(11) B. E. Burke, *Anal. Chem.*, **42**, 1536 (1970).
(12) K. C. Thompson and D. R. Thomerson, *Analyst (London)*, **99**, 595 (1974).

RECEIVED for review April 12, 1976. Accepted July 6, 1976. Presented at the 1976 Pittsburgh Conference on Analytical Chemistry and Applied Spectroscopy, Cleveland, Ohio.

Studies on the Mechanism of Atom Formation in Graphite Furnace Atomic Absorption Spectrometry

R. E. Sturgeon, C. L. Chakrabarti,* and C. H. Langford

Metal Ions Group, Department of Chemistry, Carleton University, Colonel By Drive, Ottawa, Ontario, Canada K1S 5B6

The mechanism of atom formation for a number of elements in a Perkin-Elmer HGA 2100 has been studied using a combined thermodynamic and kinetic approach. Assuming that an analyte surface–gas phase equilibrium exists within the furnace and the production of observable atoms is characterized by a unimolecular rate constant, a plot of the logarithm of the absorbance as a function of the inverse of the absolute temperature yields a straight line from which the activation energy, E_a, of the limiting step in the atomization pathway can be obtained. These E_a values reveal that three major atomization mechanisms are operative: thermal dissociation of the analyte oxide or halide, and carbon reduction of the oxide followed by atomization of the free metal.

The formation of analyte atoms in various flames has been discussed by many workers. As convenient cells for the study of high-temperature reactions, flames have been used to obtain spectroscopic evidence of reaction intermediates and bond dissociation energies of stable species (*1–10*). However, little has been reported regarding the atomization processes in graphite furnace atomizers. Whereas it is generally conceded that local thermodynamic equilibrium exists at various points throughout a flame (*1*), it may be questionable to assume that equilibrium is attained in electrothermal atomizers. The possibility of high thermal gradients, the rapid rates of rise of temperature and the transient signals generated by these atomizers (*11, 12*) may not allow adequate time for physical and chemical processes to reach equilibrium before the atomic species have been lost. Despite the possibility that equilibrium may not be attained in electrothermal atomizers, several researchers have attempted to gain insight into the dominant processes of atom production based on the assumption that equilibrium has been attained. For example, Campbell and Ottaway (*13*) have assumed that reduction of metal oxides by carbon is rapid, and have correlated the appearance temperature (the temperature at which atom formation is first observed (*11*) with the temperature at which reduction of analyte oxides with solid carbon (the surface of the graphite cell) becomes thermodynamically favorable ($\Delta G^0_{\text{reaction}} \leq 0$):

$$M_xO_{y(s)} + yC_{(s)} \longrightarrow xM_{(g)} + yCO_{(g)} \qquad (1)$$

Their study suggests that a large number of analyte species produce gaseous atoms through such a reduction reaction. Although correlation between the temperature and $\Delta G°$ of the above reduction reaction was observed for 18 of the 27 elements investigated, their data for the appearance temperature reflects the temperature of the cell wall at the point in time at which the peak, rather than the beginning, of the analyte signal occurs. Many of their appearance temperature values therefore tend to be too high. The difference between their reported temperature and the true appearance temperature for each element is a function of the heating rate of the graphite cell, the geometry of the cell, and the analyte species. On the other hand, Aggett and Sprott (*14*) have compared the appearance temperatures of various analytes in both graphite and tantalum atomizers. Comparison of these two appearance temperatures from each atomizer for the same analyte species indicates whether or not oxide reduction plays a role in the formation of analyte atoms. Lower appearance temperatures from the graphite atomizer are indicative of a reduction process. The free energy change for Equation 1 was evaluated at the appearance temperature to determine if re-

duction was thermodynamically possible. Of the 16 elements studied, only 4 (Fe, Ni, Co, and Sn) offered evidence of a reductive mechanism. These authors (*14*) have implicitly assumed the surface of the tantalum atomizer to be coated with an inert Ta_2O_5 layer. Thermodynamically, tantalum reduction of analyte oxides at the temperatures employed is highly favorable:

$$2Ta_{(s)} + 5MO_{(s)} \longrightarrow Ta_2O_{5(s)} + 5M_{(s,l,g)}$$

The assumption that this reduction reaction can be ruled out is valid only if Ta_2O_5 forms a coherent stable film on the surface of the metal. It has been determined (*15*, p 339) that growth of the surface oxide proceeds by a mechanism of diffusion of the metal through the film to the surface. Provided this step is slow in comparison to the atomization time of the analyte, reduction by tantalum is not likely to occur. The fact that a change in the appearance temperature was noted can be interpreted as confirmation of the fact that the reduction of analyte oxides by Ta is hindered by the presence of a surface film of Ta_2O_5 (assuming that accurate measurements of the temperature were obtained for both atomizers). Fuller (*16, 17*) has criticized the thermodynamic approach to atom production because it does not explain the fact that several elements may form thermodynamically stable carbides at and below the temperatures at which $\Delta G^\circ_{\text{reduction}}$ for Equation 1 is zero. In addition, the thermodynamic approach cannot give any indication of the rates of atomization and, consequently, predict absorbance peak shapes. As a result, he has attempted to explain the dynamics of these transient signals using a kinetic approach. With copper as a working model, he obtained rate constants for the production and dissipation of atoms in a heated graphite atomizer and assigned an activation energy of 13.8×10^4 J mol^{-1} (33 kcal mol^{-1}) to the production of copper atoms. Whereas such treatment has the potential for predicting peak shapes and activation energies governing the production and dissipation of atoms, it is a necessary condition that an isothermal environment exist within the atomizer, preferably throughout the entire duration of the signal. In addition, accurate atomic vapor temperatures are required. Commercially available atomizers cannot provide an isothermal environment over the entire duration of the absorbance pulses (*11, 12*). As a result, a purely kinetic treatment of the entire absorption pulse is very difficult. In addition, Fuller (*16, 17*) has implicitly assumed that the atomic vapor temperature is equal to that of the graphite surface. Deviations from thermal equilibrium will cause large errors in the estimation of rate constants and activation energies, particularly when activation energies of the order of 100 kcal mol^{-1} are involved. Johnson et al. (*18*) have examined the nature of atom production from a nonmechanistic viewpoint. By assuming that a simple Boltzmann factor governs the vaporization of solid analyte and, hence, the equilibrium concentration of gaseous analyte species, these authors have succeeded in modeling a single transient signal (molybdenum) arising from atomization with a West-type carbon filament atomizer. Unfortunately, poor agreement was obtained for those metals which vaporized at low temperatures. These authors (*18*) have implied that various energies are associated with the vaporization process, these energies being characteristic of the analyte and related to either the heat of vaporization of the metal or the metal oxide bond dissociation energy, whichever is larger. A comprehensive kinetic model for atomization developed by Torsi and Tessari (*19–22*) details the determination of such atomization energies using a filament type device. These authors have obtained an activation energy of 405 kJ mol^{-1} (96 kcal mol^{-1}) for the production of Ni atoms, suggesting that the atomic species arises as a result of sublimation of the metal.

The major problem with such studies is that electrothermal atomizers do not function as cuvettes (with the exception of those used by L'vov (*23*) and Woodriff (*24*)) in which isothermal conditions exist, but rather as furnaces in which an isothermal environment cannot be achieved over the time required for the production of the signal (*11, 12*). As such, the characteristics of the transient signals are largely determined by kinetic parameters (rates of production and dissipation of atoms) as is evidenced by the magnitude of the effect of the heating rate on the resulting peak absorption (*11, 12, 18, 19*). Despite this limitation, it is interesting to examine the results of those models for atom formation which are based on the assumption that thermodynamic equilibrium exists. From such studies, however, only indirect evidence of the possible dominant reactions which lead to free atom formation has been provided, and no evidence of any intermediates in such reactions has been published.

It is important to establish the relationship of such energy values, as arise from the above models (*16–22*) to the nature of the atomization processes, and to quantitatively evaluate their magnitudes from the measurement of basic system parameters. This paper attempts to provide some evidence as to the nature of the major atomization processes for a number of elements in a heated graphite atomizer (HGA-2100).

THEORY

After studying the model presented by Fuller (*16, 17*), it was decided that the absorbance signals arising from analyte atomization in the HGA-2100 cannot be properly handled by a kinetic technique, since a knowledge of accurate vapor temperatures is required. The model developed by Torsi and Tessari (*19–22*) is applicable only to those atomizers in which the region above the vaporizing analyte behaves as an infinite sink for atomic species, i.e., an open system. No provision has been made in their model for analyte condensation and subsequent reevaporation, which occur in tube-type furnaces used in commercial apparatus. As a result, their treatment is applicable only to those cases in which atomization occurs from a rod or filament device. With tube-type atomizers, such as the Perkin-Elmer HGA-2100 employed in this study, analyte condensation and reevaporation can be shown to occur. It is for this reason that an entirely new approach to the problem was undertaken. The model presented here was designed to account for both the thermodynamic and kinetic aspects of atomization in a Perkin-Elmer HGA-2100.

There are a number of potential pathways by which gas phase atoms may be formed. When the sample is in the form of a nitrate or sulfate, the metal oxide usually results on heating; even when the sample is in the form of a halide, this may still be true, since hydrolysis to oxygen-containing species frequently occurs. The majority of precursors to gas phase atoms are therefore either metal oxides (generally monoxides (*23*, p 129)) or halides which, in the most general cases, may partake in such reactions as the following:

$$M_xO_{y(s,l)} \rightleftharpoons M_xO_{y(g)} \longrightarrow xM_{(g)} + yO_{(g)} \qquad (2)$$

$$M_xO_{y(s,l)} + yC_{(s)} \longrightarrow xM_{(s,l)} + yCO_{(g)}$$

$$\Downarrow$$

$$x/2M_{2(g)} \longrightarrow xM_{(g)} \qquad (3)$$

$$MX_{m(s,l)} \rightleftharpoons MX_{m(g)} \longrightarrow M_{(g)} + mX_{(g)} \qquad (4)$$

in the heated graphite atomizer. We will use these equations to form our simplified model. The validity of this model will be tested, finally, by its ability to make predictions and to produce numbers coherently related to other experiments.

The oxygen and halogen atoms resulting from the dissociation of the metal compounds in Equations 2 and 4 have

been shown in the monatomic form. The reason for this is that the partial pressures of these species (as well as the metal) in the gas phase are exceedingly low. Since the analyte masses atomized are of the order of 10^{-9} g, the partial pressure exerted by any liberated oxygen or chlorine within the furnace at a temperature of 1500 K is approximately 10^{-7} atm. Over the initial portion of the signal, where measurements are taken, these partial pressures are closer to 10^{-8} atm. As such, the probability of collision of analyte fragments and their resulting recombination is negligible. The reactions postulated in Equations 2–4, and throughout the remainder of this paper, are therefore not written with the conventional double-headed reversible equilibrium arrow. It has been assumed that equilibrium with respect to bimolecular gas phase collisions does not exist (i.e., there is no formation of Cl_2, O_2, etc.). Gas phase–condensed phase equilibria are assumed to be established for such species as M_xO_y, MX_m, and $M_{(s,l)}$–$M_{2(g)}$ (the latter system will be further discussed in a subsequent section). The gas phase–condensed phase equilibrium should more properly be labeled a quasi-equilibrium. Such equilibria (Equations 2–4) may be written as (using Equation 2 as a typical example):

$$MO_{(s,l)} \underset{k_b}{\overset{k_f}{\rightleftharpoons}} MO_{(g)} \longrightarrow M_{(g)} + O_{(g)}$$
$$\downarrow k_d$$

where k_f/k_b is simply the equilibrium constant for the phase equilibrium, and k_d has been introduced to account for diffusional losses of gas phase molecules. The viability of the model presented here rests on the assumption that k_b competes favorably with k_d. This is not an unreasonable assumption when one considers the total internal area of the furnace walls on which condensation and reevaporation of MO may occur as compared to the velocity and mode of permanent molecular loss from the analysis volume (limited to diffusional losses to relatively cool condensation points within the furnace).

At this point, it is convenient to introduce an additional concept closely related to the above argument. It is implicitly assumed throughout the remainder of this paper that gas phase molecular species have a longer lifetime in the furnace than the corresponding metal atoms. This is due to the latter's intrinsically higher reactivity towards the hot carbon (leading to carbide formation (25)) and any gas phase scavengers present in this system.

It can be shown that the energy associated with the production of free atoms of the analyte may be obtained directly from atomic absorption measurements. Nikolaev and Nemets (26), for example, have determined the heats of sublimation of Ti and Mo from measurements made with a graphite cuvette. By lining the cuvette with a thin layer of metal foil of the appropriate element and allowing equilibrium to be attained at each temperature, the heat of sublimation of the metal was calculated from the slope of a plot of the logarithm of the absorbance as a function of the inverse of the absolute temperature. Although these were "static" measurements, made with a graphite cuvette which is capable of maintaining an isothermal environment, it will be shown in the following sections that this same information may be obtained from "dynamic" measurements of the absorbance by metal vapors produced in a commercial graphite furnace whose temperature is constantly rising.

Consider the most general atomization processes illustrated by Equations 2–4. If the final step in the atomization processes is characterized by a unimolecular rate constant k_1, then, according to Equation 2, the rate of production of $M_{(g)}$ at any temperature is given by:

$$dP_{M_{(g)}}/dt = xk_1P_{M_xO_{y(g)}} \quad (5)$$

$$= k_1K_pa_sx \quad (6)$$

where $K_p = P_{M_xO_{y(g)}}/a_s$, a_s is the activity of the condensed phase on the surface of the carbon furnace, and P is the partial pressure of the species denoted by the subscript of P. The activity of the surface phase will be maintained as a variable throughout the remainder of this model, since it is quite conceivable that the activity of the surface phase will vary with both temperature and analyte mass. For small analyte masses, the sample can penetrate the pores of the graphite surface. In such cases, the activity of the surface phase will be different from that which would result if sufficient analyte mass were introduced to both saturate the pores and form a homogeneous surface layer. Under these conditions, it is also easy to visualize variations of a_s with temperature. As the temperature rises, the surface layer is stripped off, exposing the subsurface layer of different activity.

The loss of atomic vapor from the furnace is associated with a number of different processes. Among these must be included the diffusive and convective losses of vapor through the injection port, diffusive loss through the porous walls of the furnace, expulsion of excess atomic vapor from the furnace, and loss of vapor due to condensation on the cooler parts of the furnace (at the ends where the water-cooled cones make electrical contact with the furnace tube). The expulsion of excess vapor from the furnace may be ignored because of the small volume occupied by nanogram quantities of the atomic vapor compared with the volume of the furnace. Convectional and diffusional losses of vapor through the injection port of the furnace account for only about 10% of the total vapor loss (the results will be presented in a subsequent publication) The process of diffusion of atomic vapor through the relatively porous furnace walls, as in many cases of this nature, is generally governed by an activation energy barrier (27). As a result, this type of vapor loss will have minimum influence at low temperatures, whereas loss due to condensation of the vapor on the cooler ends of the furnace occurs at all temperatures. Consequently, the net rate of appearance of metal vapor, as given by Equation 6, must be modified to account for such diffusive losses, i.e.,

$$dP_{M_{(g)}}/dt = k_1K_pa_sx - R_D \quad (7)$$

where R_D is introduced to account for such losses. The distribution of atomic vapor within the graphite tube is governed by Fick's second law—there is a roughly Gaussian distribution of atomic vapor along the axial length of the tube. By making the simplifying assumption that the vapor density falls linearly from its maximum at the center of the furnace where the sample is atomized, to zero where, the vapor leaves the graphite tube (by condensation at either end), it can be shown (23, p 204) that the rate of diffusional loss from the furnace may be approximated by a simple first order process:

$$R_D = k_DP_{M_{(g)}}$$

in which k_D is a (slightly temperature dependent) rate constant for loss of vapor. Under conditions such as these, the atomization process in the furnace may be likened to a reaction in a flow system in which reactants ($M_xO_{y(g)}$) enter the reaction volume continuously while the product mixture ($M_{(g)}$ and $O_{(g)}$) is withdrawn. During the short period when a_s is nearly constant, a steady state is achieved in which the number density of all species no longer changes with time. Equation 7 may thus be written as (at any given temperature):

$$dP_{M_{(g)}}/dt = 0 = k_1K_pa_sx - k_DP_{M_{(g)}} \quad (8)$$

which upon rearrangement yields:

$$P_{M_{(g)}} = k_1 K_p a_s x / k_D \tag{9}$$

In atomic absorption spectroscopy, the measured absorbance is directly proportional to the concentration of atomic vapor, hence:

$$A_T = k_A P_{M_{(g)}} = k_A k_1 K_p a_s x / k_D \tag{10}$$

where A_T is the absorbance by metal vapor at any temperature T and k_A is simply the proportionality constant relating absorbance to metal vapor concentration. According to transition-state theory, the rate constant k_1 can be formulated in thermodynamic terms by introducing the standard free energy change for the reaction:

$$k_1 = \frac{kT}{h} e^{-\Delta G^{\circ\ddagger}/RT}$$

V. Ph. 22 June 1977

$$= (kT/h) e^{\Delta S^{\circ\ddagger}/R} e^{-\Delta H^{\circ\ddagger}/RT} \tag{12}$$

where k and h are Boltzmann's and Planck's constants, respectively, and the quantities $\Delta G^{\circ\ddagger}$, $\Delta S^{\circ\ddagger}$, and $\Delta H^{\circ\ddagger}$ are the free energy, the entropy, and the enthalpy of activation, respectively. To a first approximation, the enthalpy of activation may be equated to the activation energy E_a for the reaction (*28*). Not only is k_1 a function of temperature, but so also is K_p, the equilibrium constant for the gas-condensed phase equilibrium. The relationship of K_p to temperature is given by the well-known van't Hoff equation (*29*)

$$\left(\frac{\partial \ln K_p}{\partial(1/T)}\right)_p = -\frac{\Delta H^\circ}{R} \tag{13}$$

where ΔH° is the standard enthalpy change accompanying the phase transition (reactants and products at 1 atm). In the integrated form, using common logarithms, Equation 13 may be written as

$$\log K_p = -\Delta H^\circ / 2.3RT + C \tag{14}$$

where C is an integration constant, and ΔH° has been assumed to be temperature-independent (i.e., the product $\Delta T \Delta C_p$ is small compared to ΔH°). Substituting Equations 12 and 14 in 10 yields:

V. Ph. 22 June 1977

$$\log A_T = -\frac{E_a + \Delta H^\circ}{2.3RT} + \frac{\Delta S^{\circ\ddagger}}{2.3R} + \log \frac{k_A a_s kTxC'}{hk_D} \tag{15}$$

$$= -\frac{E_a + \Delta H^\circ}{2.3RT} + A_0 \tag{16}$$

Equation 16 expresses the relationship of the measured absorbance to the energy associated with the production of atomic vapor as a function of temperature. A plot of the logarithm of the absorbance as a function of the inverse of the absolute temperature should yield a straight line with a slope of $-(E_a + \Delta H^\circ)/2.3R$ and an intercept of A_0. In addition to the basic assumptions of this model which have been introduced up to this point, the construction of a log A_T vs. $1/T$ plot requires that the temperature of the gas phase be equal to that of the surface of the graphite tube over the data range employed, that atomization of the analyte is of a thermal nature only, that E_a (as well as ΔH°) is approximately independent of the temperature over the temperature range employed in the above plot, and that the temperature-dependence of k_D is sufficient to compensate for that introduced by the last term in Equation 15 (i.e., the linear T factor and that arising from the fact that $k_A \propto T^{0.7}$ (*23*, p 221)). This last assumption is a reasonable approximation based on the different temperature-dependencies reported for gas phase diffusion (i.e., $T^{1/2} \rightarrow T^{3/2}$).

Although the slope of the log A_T vs. $1/T$ plot yields an activation energy, the magnitude of E_a is an excellent approximation to the bond dissociation energies of gaseous species (*30*), and throughout this paper will be so identified.

The above model for atom production, which leads to the energy relationship expressed in Equation 16, is based on reaction sequence 2. It is straightforward to see that consideration of either reaction sequence 3 or 4 will lead to an identical equation. Treatment of the absorbance data is therefore quite generalized—it is not necessary to know the reaction sequence a priori. By correlating the energy value obtained from the log A_T vs. $1/T$ plot with a very limited set of possible primary steps in the atomization sequences (Equations 2–4), the utility of the model may be tested and the major precursors to free analyte atoms identified. More specifically, the energy term may be correlated for best agreement with one of the following values: (a) the dissociation energy of the metal oxide, which would imply that gaseous free atoms of analyte arise predominately from the thermal dissociation of an oxide intermediate; (b) the dissociation energy of metal halide; (c) the heat of atomization of the metal, which would infer that carbon reduction of a metal oxide intermediate has occurred to yield a solid or liquid metal species that may proceed through reaction sequence 3; (d) the metal–metal bond dissociation energy, which would imply a reaction sequence similar to that described above in (c) with an appreciable formation of dimeric metal species, or (e) the metal–carbon bond dissociation energy, which would require that carbide formation has occurred. Throughout the remainder of this paper the log A_T vs. $1/T$ plot will be referred to as an E_a plot, and the associated energy obtained from the slope will simply be identified, for convenience, as E_a.

At this point, it is necessary to examine the behavior of the E_a plot in more detail. From a consideration of reaction sequences which involve more than one potential source of $M_{(g)}$, such as that outlined in Equation 3, it becomes evident that as the temperature of the system is increased, certain steps in the path to $M_{(g)}$ will be replaced by others and hence disappear from the E_a plot. As a result, the E_a plot may appear as a composite of two or more intersecting straight line segments of different slope, reflecting the transition which occurs when the major supply of $M_{(g)}$ changes from one species to another. Consider, once again, reaction sequence 2

$$M_zO_{y(s,l)} \rightleftharpoons M_zO_{y(g)} \longrightarrow xM_{(g)} + yO_{(g)}$$

At relatively low temperatures, when little of the oxide has been vaporized and a_s may be considered a constant, production of $M_{(g)}$ arises by way of the following path;

$$M_zO_{y(s,l)} \rightleftharpoons M_zO_{y(g)} \dashrightarrow xM_{(g)} + yO_{(g)}$$

the energy associated with $M_{(g)}$ production being the combined energies of vaporization (the contribution from the K_p term, i.e., ΔH°) and dissociation (the contribution from k_1, i.e., E_a) of the oxide. At higher temperatures, when almost all of the surface phase oxide has vaporized ($a_s \rightarrow 0$), the major supplier of $M_{(g)}$ becomes $M_xO_{y(g)}$;

$$M_zO_{y(g)} \longrightarrow xM_{(g)} + yO_{(g)}$$

with the result that the energy now associated with $M_{(g)}$ production is that arising only from oxide dissociation (i.e., the contribution from k_1). It is evident, from this simplified discussion, that as the temperature of the system increases,

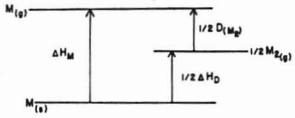

Figure 1. Energy level diagram for the sublimation of a metal

ΔH_M is the heat of vaporization of the monomeric species, ΔH_D the heat of vaporization of the dimeric species and $D_{(M_2)}$ the dissociation energy of $M_{2(g)}$

certain steps in the sequence to $M_{(g)}$ may "fall out", just as the temperature dependence of K_p was lost when a sufficiently high temperature was reached to vaporize the surface oxide. It can also be appreciated, that, in this simple model, if the sample mass is greatly increased, such that the $M_xO_{y(s)} \rightleftharpoons M_xO_{y(g)}$ equilibrium is maintained over the full range of temperature employed in these studies (i.e., the saturated vapor pressure of M_xO_y is attained within the graphite tube over the temperature range in which measurements are made), then the temperature dependence arising from both the K_p and k_1 terms will be measured. This concept of energy terms being lost at high conversion of the reaction may be further illustrated by considering reaction sequence 3. The first step of the sequence in this reaction, carbon reduction of the metal oxide, leaves the free metal on the surface of the furnace in a physical state (prior to atomization) that is determined by the temperature of the graphite tube. The energy involved in this step is obviously not observable by the proposed technique. At the first appearance of free metal, the following equilibrium is immediately established, the concentrations of the vapor phase species being determined by the temperatures:

$$M_{(s/l)} \rightleftharpoons \tfrac{1}{2}M_{2(g)} \longrightarrow M_{(g)}$$

Initially, the concentration of $M_{2(g)}$ is very low and the measured energy corresponding to the production of $M_{(g)}$ is the heat of atomization of $M_{(s/l)}$, i.e., $M_{(s/l)} \rightarrow M_{(g)}$. When the temperature has reached a sufficiently high value such that the bulk of $M_{(s/l)}$ has been evaporated and the dominant precursor to $M_{(g)}$ is the dimer, the production of $M_{(g)}$ arises predominately from the reaction $M_{2(g)} \rightarrow M_{(g)}$, the measured energy corresponding to the dissociation energy of the dimer. As a net result, the log A_T vs. $1/T$ plot will appear as a composite of two intersecting straight lines of different slope. It is obvious that those energy steps which drop out of the atomization process as the temperature is raised (or those which do not appear at all, e.g., reduction) are those for which reaction equilibria, as written, lie so far to the right that equilibria no longer exist.

The formation of gaseous metal dimers upon evaporation of metals has been well documented (*31–33*). Honig (*31*) has shown that formation of dimeric and larger clusters of atoms in the gas phase must take place during the evaporation process itself; they are not restricted to forming in the gas phase at high monomer partial pressures. Figure 1 presents the energy level diagram for the sublimation of a metal (*32*). For $M_{(s/l)}$, $M_{(g)}$, and $M_{2(g)}$ in equilibrium,

$$\frac{d \ln P_M}{d(1/T)} = -\frac{\Delta H_M}{R} \quad \text{and} \quad \frac{d \ln P_D}{d(1/T)} = -\frac{\Delta H_D}{R}$$

If $\Delta H_D > \Delta H_M$, the dimer may be present in small amount at low temperatures but will become increasingly important the higher the temperature. Thus, unstable molecules with little probability of forming at low temperatures can become significant at high temperatures (*32*).

Just as energy steps may be lost from the reaction sequence because of high conversion of the reactants to another form, new reaction pathways may arise because of low conversion. An example of such a case is the carbon reduction of metal oxides followed by sublimation of the element. This is the result of the low "conversion" of the oxide to the gas phase below the temperature at which the reduction reaction becomes thermodynamically favorable.

Having obtained a value of E_a and a possible atomization sequence, it is necessary to make sure that the resulting intermediate also satisfies additional physicochemical criteria. For example, if it is implied (from the E_a data) that the free metal was the immediate precursor to gaseous analyte atoms, then reduction by carbon of the metal oxide must have occurred. The reduction reaction must therefore be thermodynamically favorable at or prior to the temperature at which the atomic absorption commences (called the appearance temperature (*11, 12*)—the corresponding time is called the appearance time). Often accurate, high temperature thermodynamic data are lacking and, at best, only approximate agreement between calculated and experimental results can be expected in many cases. In addition, the selected reaction sequence (Equations 2–4) must reflect the physical and chemical form of the analyte at the appearance temperature, as indicated by melting and boiling point data and results of differential thermal analysis.

The second parameter arising from the above model is the intercept (log A_0) of the log A_T vs. $1/T$ plot, which, according to Equation 15, contains a number of physical constants, the largest being the entropy factor for production of atomic vapor. Since the intercept also includes temperature-dependent parameters (k_A, k_{D_2}, a_s, and T), its magnitude cannot be evaluated by a linear extrapolation of the log A_T vs. $1/T$ curve (i.e., $1/T \rightarrow 0$ as $T \rightarrow \infty$). As a result, this term will not be considered further in this discussion.

EXPERIMENTAL

Apparatus. Details of the apparatus have been presented in a previous publication (*12*). A Perkin-Elmer heated graphite atomizer, HGA-2100, was used throughout this study. All surface temperatures were measured with an automatic optical pyrometer (Ircon Inc., Niles, Ill., series 1100) calibrated by the manufacturer and confirmed by measurements with thermocouples and by the melting points of selected pure metals to cover the entire range of temperature used. A 1000-watt xenon-arc lamp (Hanovia, Canrad Precision Ind., Model 976C-1) was employed for measurement of the atomic vapor temperatures.

Reagents. All chemicals used were of certified ACS grade or of the highest purity commercially available. The stock solutions of metal standards were prepared as follows for each metal separately, and contained 1000 μg/ml of that metal only. Solutions of Cu, Sn, Al, Zn, Ni, Mg, Mn, Fe, Cr, and Co were prepared from the metals; Cd, Pb, and Ca from their carbonates, and Mo and V from molybdenum trioxide and vanadium pentoxide, respectively. The above metals or their compounds were dissolved in pure acids or bases where required and diluted with ultrapure water obtained direct from a Milli-Q water system (Millipore Corporation). All test solutions were prepared immediately prior to their use by dilution with ultrapure water. Polystyrene–2% divinylbenzene copolymer beads (200–400 mesh, Eastman Kodak Co.), anhydrous oxalic acid (Fisher Scientific) and triply-distilled mercury were employed as matrices for "dilution" of solid samples.

Gases. Except where noted otherwise, argon gas (99.95% purity) was employed to sheath the atomizer. Nitrogen gas (99.95% purity) was also used for some selected studies.

Procedure. Temperature–time curves of the HGA-2100 graphite surface were obtained using the automatic optical pyrometer. As the heating rate of the atomizer is dependent upon the quality of the electrical contacts between the graphite tube and the cones, care was taken to ensure a reproducible temperature profile by measuring the furnace resistance prior to each study and maintaining it at a set arbitrary value of 22 mΩ by suitably adjusting the contact tension between the cones and the tube. It was noted that, as the graphite tube aged, the resistance increased up to a value of 26 mΩ. Atomic vapor temperatures were measured according to the method prescribed by L'vov (*34, 35*) using Fe and Sn as the thermometric species with their respective hollow cathode lamps as radiation sources, and also by the

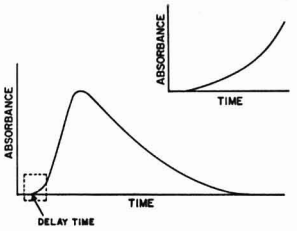

Figure 2. Typical absorbance–time profile with the inset indicating the magnified portion of the curve over which the data was taken

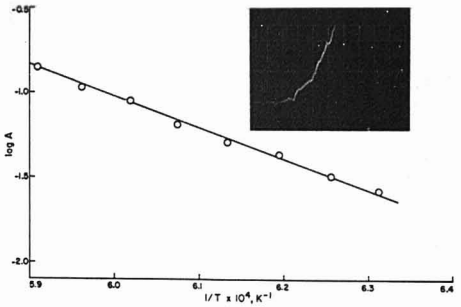

Figure 3. E_a plot for 5.0×10^{-9} g iron taken as the chloride under atomize conditions of: dry 100 °C, ash 300 °C; atomize 2700 °C

Oscilloscopic trace of absorbance–time data used: vertical scale: absorbance, 0.05/scale unit. Horizontal scale: sweep speed, 50 ms/scale unit

two-line absorption method of Browner and Winefordner (*36*) using In and Ga as the thermometric species and the xenon-arc continuum as the radiation source.

Aqueous test solutions of Cd, Zn, Mn, Ni, Sn, Pd, Cr, Cu, Fe, Co, Ca, Al, and Mg taken as the chlorides containing 5% (v/v) HCl, and aqueous solutions of Cd, Zn, Mn, Ni, Cr, Pb, Cu, Fe, Co, Ca, Al, and Mg taken as the nitrates containing 5% (v/v) HNO_3 were prepared. Aqueous test solutions of Sn and V in 5% (v/v) NaOH and Mo in 5% (v/v) NH_4OH were also prepared. All aqueous samples were introduced in 5-μl volumes into the atomizer with an Eppendorf pipet fitted with disposable plastic tips.

A copper amalgam was prepared by saturating triply-distilled mercury with copper metal. A lead amalgam was prepared following the procedure given by Vogel (*37*). After further dilution of these "stock amalgams", sampling was accomplished in the same manner as for aqueous solutions.

Solid samples of various copper and aluminum compounds were also atomized in the HGA-2100 furnace. Copper was taken in the following compound forms: CuI, $CuBr_2$, $CuCl_2$, Cu_2O, $CuSO_4$, $Cu(NO_3)_2$, and CuCN. Aluminum was taken as $AlCl_3$, Al_2O_3, and $Al_2(SO_4)_3$. Polystyrene beads were acid-leached free of copper and mixed with the above copper compounds as an inert matrix to provide a 10^6-fold dilution for the test sample introduced into the atomizer (at the ng level). This was accomplished by homogenizing a mass of each compound containing a mg of the metal into 1 g of matrix. A mg portion of this sample was further "diluted" with an additional 1 g of matrix, thus ensuring a 10^6-fold dilution. As the polystyrene beads could not be acid washed free of Al, an oxalic acid matrix was employed for sampling the solid Al compounds. The oxalic acid was purified by sublimation under vacuum and mixed with the aluminum samples in a manner identical to that described above for Cu in polystyrene. Sampling was accomplished by placing approximately 1 mg of this mixture into the center of the furnace by removing an end window cap from the atomizer and introducing the sample with a microspatula. The 217.9-nm and 256.8-nm lines were used for copper and aluminum solid sampling analysis, respectively—these lines were employed instead of the more sensitive lines because the latter gave high absorbance signals.

Absorbance–time profiles for each of the elements studied were obtained in the following manner: using a storage oscilloscope for signal recording and a sufficient mass of each analyte to obtain a peak absorbance of approximately 1, a high sensitivity (0.05 absorbance/cm), fast-scan 20–50 ms/cm) absorbance–time trace was photographed. From this trace and the temperature–time profile of the furnace, a plot of the logarithm of the absorbance vs. the reciprocal of the absolute temperature over a range of 100–300 ms (depending on the element) beyond the appearance time (covering absorbance values ≤ 0.25) was drawn. The activation energy, E_a, was evaluated from the slope of this plot by a least squares analysis. The E_a data reported in this study are the average of at least three separate determinations for each element.

Except where otherwise stated, all absorbance traces were obtained under the following temperature program, as indicated by the temperature setting on the HGA-2100 control unit: dry, 100; ash, 300; and atomize, 2700. When copper solid samples were atomized, the temperature setting of the ash stage was increased to 500 in order to remove completely all traces of the polystyrene matrix. The oxalic acid used for aluminum solid sampling was completely removed prior to atomization at the temperature setting 300 for the ash stage. In all cases, the HGA-2100 was operated in the internal purge gas interrupt mode during atomization.

A nominal spectral bandpass of 0.08 nm was used for all elements except calcium, cobalt, and tin, for which 0.16 nm was used (to maintain a suitable signal-to-noise ratio at the high recording sensitivities used). The following resonance lines were used for measurement (nm): Al 309.3, Ca 422.7, Cd 228.8, Co 240.7, Cu 324.7, Cr 357.8, Fe 248.3, Mg 285.2, Mn 279.5, Mo 313.3, Ni 232.0, Pb 283.3, Sn 224.6, V 318.4, Zn 213.9.

RESULTS AND DISCUSSION

Atomic vapor temperatures obtained with Fe, Sn, In, and Ga as thermometric species (*38*) indicated that over a range of 200–300 ms beyond the appearance time, there is no lag in the temperature between the atomic vapor and the atomizer surface. Beyond this range, however, the atomic vapor temperature deviated linearly from the surface temperature as the time increased, the deviation reaching up to 900 K toward the end of the absorbance trace. This pattern was observed for each of the thermometric species. Similar atomic vapor temperature–time behavior has recently been reported by Adams and Kirkbright (*39*). Provided efficient thermal contact exists between the condensed phase and the furnace wall, thermal energy is rapidly transferred throughout a condensed phase by vibrational interaction involving frequency factors of the order of 10^{12} s^{-1} (*40*). The rapidity of this energy transfer step is greatly facilitated when the analyte is present as a surface layer. Once such intimate thermal contact with the furnace wall is lost (i.e., on the completion of analyte evaporation), the atomic vapor temperature begins to lag behind that of the atomizer surface. Since the ability of the model to predict is based on the requirement of the surface temperature of the atomizer being equal to the atomic vapor temperature (and the fact that reaction equilibria will shift, once the surface temperature has become high enough for a_s to become very small), absorbance measurements were restricted to the initial few hundred ms of the absorption pulse. For example, a typical absorbance profile (*11, 12*) with respect to time arising from sample atomization in the heated graphite atomizer is presented in Figure 2. Also shown is the expanded initial portion of such a curve covering the first 200–300 ms of the profile following the appearance of the signal. From the temperature–time characteristics of the atomizer surface, the temperature of the atomizer surface at each point in time over the absorbance profile may be obtained. The temperature of the atomizer surface at the delay time (*11, 12*) in Figure 2 is called the appearance temperature.

Figure 3 is a typical E_a plot of $\log A_T$ vs. $1/T$ obtained from the atomization of 5.0 ng of iron taken as the chloride. As predicted by the theory, a straight line relationship is observed from which E_a is evaluated.

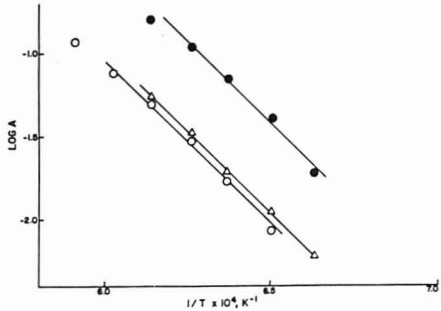

Figure 4. E_a plots for varying masses of manganese (taken as the nitrate) under atomize conditions of: dry 100 °C; ash 300 °C; atomize 2700 °C

(○) 2.5×10^{-10} g, (△) 3.0×10^{-10} g, (●) 7.5×10^{-10} g

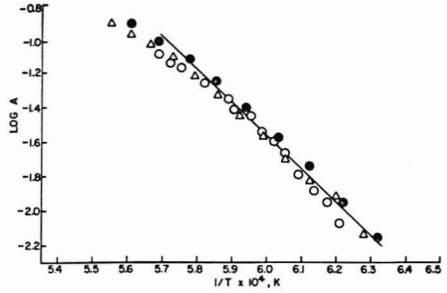

Figure 5. E_a plots for 4.0×10^{-10} g of magnesium taken as the nitrate under atomize conditions of: dry 100 °C; ash 300 °C; atomize,

(●) 2700 °C, (△) 2500 °C, (○) 2100 °C

As expected from Equations 15 and 16, the E_a values were found to be independent of both the initial mass of the sample atomized and the rate of atomization (i.e., the rate of rise of temperature of the atomizer (*11, 12*)). Figure 4 is a E_a plot obtained for the atomization of 0.25, 0.30, and 1.0 ng of manganese (taken as the nitrate). Within the standard deviation of the slopes, the E_a values are equal. Below a certain critical analyte mass (≃0.1 ng for Mn), accurate quantitative measurements could not be made. Under such conditions, the absolute mass of analyte is too small to provide a substantial atomic population for measurement before curvature of the E_a plot becomes appreciable. A further discussion of the influence of mass on these measurements will be presented in a subsequent section.

Figure 5 is a E_a plot obtained by atomizing 0.4 ng Mg (taken as the nitrate) using meter settings of 2700, 2500, and 2100 on the HGA control unit. These arbitrary settings correspond to initial furnace heating rates of 1.23, 1.06, and 0.74 K ms^{-1}. Within the standard deviation of the slopes, the E_a values are independent of the rate of heating of the atomizer. It can be seen from this plot that at the higher absorbance values, toward the higher temperature portion of the plot, the straight line begins to show negative curvature. This bending, characteristic of all these plots, may be the result of a number of factors, including the fact that the atomic vapor temperature begins to deviate from the graphite surface temperature, the variation with temperature of the activity of the analyte on the surface of the furnace, the decrease in the flux of material entering the vapor phase as the area of the evaporating surface decreases with time, i.e., with increasing temperature, and the possibility that E_a is not a temperature-independent parameter, as assumed.

In order to consider the possible role of reduction reactions in the production of free atoms, the overall free energy change per mole of metal, $\Delta G^\circ_{\text{reaction}}$, for the reduction of the oxide at the "appearance temperature" for each element was calculated. The required thermodynamic data were obtained from a number of sources (*41–44*). The results of these calculations are presented in Table I. The subscript given to each of the $\Delta G^\circ_{\text{reaction}}$ values is the temperature closest to the appearance temperature for which the calculation was made. The final physical state of the reduced metal was, in contrast with the treatment given by Campbell and Ottaway (*13*), considered as being governed solely by the temperature of the furnace and the melting and boiling points of the element in question. Only in those cases for which $\Delta G^\circ_{\text{reaction}} \leq 0$ is the reduction reaction thermodynamically feasible at the appearance temperature.

It should be noted that although the standard free energy change, ΔG°, was evaluated assuming the solid components to be at unit activity and gases at unit fugacity, this is not the case in the furnace (where the partial pressure of CO is not 1 atmosphere). As a result, the ΔG° values, as written, should be much more favorable than indicated. It is for this reason that the standard state free energy change $\Delta G^\circ \leq 0$ should not be used as the criterion for spontaneity, but simply $\Delta G \leq 0$. The equilibrium constants (calculated from the relationship $G^\circ_T = -RT \ln K_p$) have also been listed in Table I. The magnitudes of these constants enable one to appreciate more easily the extent to which such reduction reactions occur. Thermodynamic calculations, however, provide no information as to the rates of the reactions involved. A slightly favorable reaction, in the context of reaction energetics, may actually prove to be unfavorable because of kinetics and, hence, the extent of the reaction may be limited.

Experimentally, it has been found that the "appearance temperature" of each analyte is a characteristic of that analyte and is independent of the analyte mass (*11, 12*). These observations are only to be expected as a natural consequence of the model presented. A minimum temperature must be attained for extensive dissociation of the analyte to occur, this temperature being independent of the analyte mass but dependent upon the activation energy for the process.

Table II lists the E_a values obtained for the elements atomized from aqueous solutions, the appearance temperature for each element and the corresponding literature values for the dissociation energy. The E_a values have a standard deviation of the order of 8–10%, which represents the sum of the uncertainties in the measurement of temperature (≃2.5%), the absorbance signal with respect to time (≃1–2%), and the least square slope of the E_a plot (≃5%). For those cases in which the sequential processes contributing to the production of atomic vapor were measurable, the resulting E_a values and selected intermediates have been presented in Table II as being separated by a slash.

The activation energies obtained in these studies arise from the fact that a unimolecular rate constant governs the production of observable atoms. Under normal circumstances, rate constant data are obtained from a number of discrete isothermal runs in which total vibrational, rotational, and dissociation relaxation is maintained. In the present system, isothermal data points cannot be plotted because the temperature is continuously rising at a high rate. Even under conditions such as these, however, it is probable that thermal equilibrium at each temperature over all degrees of freedom is approximately established (indeed, the data indicate that this must be the case). Data obtained from measurements in

Table I. Free Energy of Reduction Reactions

Oxide	Element mp, K	Element bp, K	Compound mp, K	Compound bp, K	Appearance temp, K	$\Delta G°$ reaction, kcal mol^{-1}	log K_{eq}	Form of metal
CdO	594	1038	d 1173	subl 1832	720	3_{700}	−0.9	Liquid
ZnO	693	1180	2248	...	1140	6_{1100}	−1.2	Liquid
PbO	601	2013	1161	...	1040	-22_{1050}	4.6	Liquid
CuO	1356	2848	1599	...	1270	-44_{1300}	7.4	Solid
CoO	2690	3143	2208	...	1430	-24_{1400}	3.7	Solid
MnO	1517	2235	>1923	...	1480	7_{1500}	−1.0	Solid
FeO	1808	3023	1693	...	1500	-16_{1500}	2.3	Solid
Fe_3O_4	1808	3023	d 1811	...	1500	-27_{1500}	3.9	Solid
MgO	922	1363	3073	3873	1510	43_{1500}	−6.3	Gas
SnO_2	505	2543	1400	subl 2073	1560	-69_{1600}	9.5	Liquid
NiO	1728	3005	2263	...	1590	-37_{1600}	5.1	Solid
Cr_2O_3	2163	2755	2708	4273	1660	-12_{1700}	1.6	Solid
CaO	1112	1757	2853	3123	1850	35_{1900}	−4.0	Gas
Al_2O_3	933	2740	2318	3253	2080	16_{2100}	−1.7	Liquid
MoO_3	2890	4885	1068	subl 1428	2100	-154_{2100}	16.0	Solid
V_2O_3	2163	3653	2243	...	2200	-26_{2200}	2.6	Liquid

Table II. Heats of Atomization of the Elements

Element/form	Appearance temp., K	E_a, kcal mol^{-1}	Selected literature values: Intermediate[a]	Selected literature values: Energy, kcal mol^{-1}	Ref.
Pb/HCl, Pb/HNO_3	1040	46/28	$Pb_{(l)}$/Pb–Pb	42.5/24	(77)
Cu/HCl, Cu/HNO_3	1270	77/44	$Cu_{(c)}$/Cu–Cu	80.7/46.6	(77)
Co/HCl, Co/HNO_3	1430	97/44	$Co_{(c)}$/Co–Co	102.4/40	(77)
Sn/HCl, Sn/NaOH	1560	74/47	$Sn_{(c)}$/Sn–Sn	72.2/46.7	(77)
Ni/HCl, Ni/HNO_3	1590	99/50	$Ni_{(c)}$/Ni–Ni	102.8/55.5	(77)
Mo/NH_4OH	2100	165	$Mo_{(c)}$	157.3	(77)
V/NaOH	2200	153/116	V-O/$V_{(l)}$	154/109.9	(77)
Fe/HNO_3	1500	97	$Fe_{(c)}$	99.3	(77)
Cr/HNO_3, Cr/HCl	1660	99	$Cr_{(c)}$	95	(77)
Mg/HCl, Mg/HNO_3	1510	90	Mg–O	94	(*33*)
Cd/HNO_3	720	65	Cd–O	67	(77)
Zn/HNO_3	1140	65	Zn–O	66	(77)
Mn/HCl, Mn/HNO_3	1480	92	Mn–O	96	(77)
Ca/HCl, Ca/HNO_3	1850	90	Ca–O	84	(77)
Al/HCL, Al/HNO_3	2080	234/114	[b]ΔH_r/Al–O	[b]221/116	(68)
Cd/HCl	670	50	Cd–Cl	49.9	(77)
Zn/HCl	940	48	Zn–Cl	49	(*33*)
Fe/HCl	1400	86	Fe–Cl	84	(77)

[a] Subscript (c) denotes the heat of atomization of the element from its standard state at 298 K. Subscript (l) denotes the heat of vaporization of the element. [b] ΔH_r is the heat of reaction: $Al_2O_{3(s)} \rightarrow Al_{(g)} + O_{2(g)} + AlO_{(g)}$.

shock tubes (*45*, *46*) on the vibrational and rotational relaxation times of many molecular species indicate that chemical equilibrium can be established despite the extreme rates of rise of temperature that accompany the shock wave. Dissociation relaxation times for many molecules are on the μs time scale (*45*, pp 189–212), while the maximum rate of rise of temperature employed here is only 0.001 K μs^{-1}.

MECHANISMS FOR ATOMIZATION OF THE ELEMENTS

Three major pathways leading to gaseous free atoms have been identified: carbon reduction of the analyte oxide with subsequent sublimation of the metal, thermal dissociation of the metal oxide, and thermal dissociation of the metal chloride. Examples of the three mechanisms are given in the following sections. No attempt has been made to maintain mass balance with respect to the physicochemical transformations in the equations given. Only products for which evidence is available appear.

Carbon Reduction–Vaporization. *Lead.* Two sequential atomization energies have been obtained for lead, 46 and 28 kcal mol^{-1}, regardless of whether the analyte is taken as the nitrate or chloride. Figure 6 is the E_a plot for lead. It may be decomposed into two straight-line segments which intersect at a temperature of approximately 1160 K. In the low temperature region, the slope corresponds to an E_a value of 46 kcal

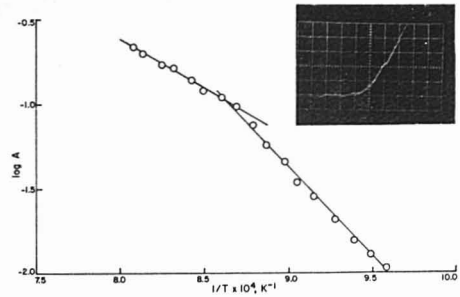

Figure 6. E_a plot for 2.0×10^{-9} g lead taken as the nitrate under atomize conditions of: dry 100 °C; ash 300 °C; atomize 2700 °C

Oscilloscopic trace of absorbance–time data used; vertical scale: absorbance, 0.05/scale unit. Horizontal scale: sweep speed, 50 ms/scale unit.

Table III. Heats of Atomization of Solid Samples

Compound	Appearance temp., K	E_a, kcal mol^{-1}	Selected Literature Values: Intermediate[a]	Selected Literature Values: Energy, kcal mol^{-1}
CuI	1300	87/48		
$CuBr_2$	1310	83/43		
$CuCl_2$	1250	86/40		
Cu_2O	1310	88/46	$Cu_{(c)}/Cu_2$	80.7/46.6
$CuSO_4$	1300	76/43		
$Cu(NO_3)_2$	1310	89/39		
CuCN	1310	85/43		
Cu/Hg	1510	89/–	$Cu_{(c)}$	80.7
Al_2O_3	2190	202/111		
$Al_2(SO_4)_3$	2010	193/109	[b] ΔH_r/AlO	[b] 221/116
$AlCl_3$	2150	211/115		
Pb/Hg	930	52.28	$Pb_{(l)}/Pb_2$	42.5/24

[a] Subscript (c) denotes the heat of atomization of the element from its standard state at 298 K. Subscript (l) denotes the heat of vaporization of the element. [b] ΔH_r is the heat of the reaction: $Al_2O_{3(s)} \rightarrow Al_{(g)} + O_{2(g)} + AlO_{(g)}$.

mol^{-1}. In the higher temperature regions, a value of 28 kcal mol^{-1} is obtained. These energies can be attributed to the heat of vaporization of lead and the bond dissociation energy of Pb–$Pb_{(g)}$, having values of 42.5 and 24 kcal mol^{-1}, respectively. The appearance temperature recorded for $Pb(NO_3)_2$ and $PbCl_2$ is 1040 K. Below this temperature, $PbO_{(s)}$ (mp = 1161 K) is present as a result of decomposition of the nitrate (*47*): $Pb(NO_3)_{2(s)} \rightarrow$ (925 K) $PbO_{(s)}$. Hydrolysis of lead chloride may also lead to production of the oxide. In the absence of reducing agents, $PbO_{(s)}$ is known to sublime to $PbO_{(g)}$ (*48*). Therefore, in the present system $Pb_{(g)}$ must be formed from reduction of $PbO_{(s)}$. This is a favorable reaction at 1050 K (Table I). Atomization of the lead is therefore a sequence of two processes: the energies, in kcal mol^{-1}, associated with each of the processes are shown above or below the lines.

$$PbO_{(s)} \xrightarrow{\text{reduction}} Pb_{(l)} \rightleftharpoons Pb_{2(g)} \xrightarrow{28} Pb_{(g)}$$
$$\qquad\qquad\qquad\qquad\qquad\qquad\qquad\qquad\qquad\qquad 46$$

Consideration of the ΔH_M and ΔH_D values for Pb suggest that there is an increase in $Pb_{2(g)}$ species with increasing temperature. The existence of $Pb_{2(g)}$ in equilibrium with Pb(l) has also been confirmed mass-spectrometrically (*31, 32, 49, 50*).

Introduction of lead as an amalgam does not change its atomization characteristics (Table III). The appearance temperature for lead in the amalgam, however, is approximately 100 K lower than that obtained for the nitrate or chloride. This may be due to the fact that a reduction reaction is not required in this system to form $Pb_{(l)}$, this species being present as a surface layer having an activity different from that of $Pb_{(l)}$ resulting from oxide reduction (*51*, cf. Equation 15).

Copper. The atomization of copper proceeds in a manner similar to that for lead. For both the nitrate and the chloride forms of copper, a single appearance temperature of 1270 K and E_a values of 77 and 44 kcal mol^{-1}, corresponding to the heat of atomization of copper and the Cu–Cu bond energy, respectively, were obtained. The temperature at the point of intersection of the two slopes of the E_a plot is approximately 1400 K. Below the appearance temperature, $CuO_{(s)}$ is formed (*47*): $CuCl_2 \cdot 2H_2O_{(s)} \rightarrow$ (1000 K) $CuO_{(s)}$; $Cu(NO_3)_2 \cdot 6H_2O_{(s)} \rightarrow$ (1220 K) $CuO_{(s)}$. Brewer and Mastick (*48*) have reported that $CuO_{(g)}$ is the gas phase species in equilibrium with $CuO_{(s)}$ in the temperature range 873–1223 K. The production of $Cu_{(g)}$, therefore, may be accounted for only by a reductive decomposition of the solid oxide (mp 1600 K), which is a favorable reaction at 1200 K (Table I). The proposed atomization mechanism for copper is therefore:

$$CuO_{(s)} \xrightarrow{\text{reduction}} Cu_{(s)} \rightleftharpoons Cu_{2(g)} \xrightarrow{44} Cu_{(g)}$$
$$\qquad\qquad\qquad\qquad\qquad\qquad 77$$

The existence of $Cu_{2(g)}$ is well documented in the literature (*49, 52, 53*) and has been observed in emission from a King furnace (*52*).

In contrast to this mechanism, Aggett and Sprott (*14*) have concluded from their study that, despite a favorable $\Delta G°$ reaction for the carbon reduction of the oxide at the appearance temperature, $Cu_{(g)}$ results from the thermal dissociation of the oxide. This conclusion has been based on their observation that the appearance temperature for copper is higher with a graphite than with a tantalum atomizer and the assumption that the reduction kinetics are slow relative to that for the thermal dissociation.

Table III presents the E_a results obtained for the atomization of various solid copper compounds, the average values being 85 and 43 kcal mol^{-1}. Thermogravimetric data (*47*) for the following compounds: Cu_2O, $CuCl_2$, CuI, $CuSO_4$, and $Cu(NO_3)_2$ indicate that $CuO_{(s)}$ is the common decomposition product below a temperature of 1250 K. It may therefore be concluded that copper salts are also atomized as described earlier, aqueous sampling playing no recognizable physicochemical role in the processes.

When copper is introduced as an amalgam, an E_a value of 89 kcal mol^{-1} is obtained, which corresponds to the heat of atomization of solid copper. In this case, only a single E_a value was observed over the temperature range studied. Because of the large mass of Cu present, vaporization of the surface deposit was not completed in the temperature range studied. As a result, the transition from condensed phase metal to gaseous dimer as the major supplier of $Cu_{(g)}$ did not occur. No explanation can be offered for the increase in the appearance temperature observed for the atomization of the copper amalgam.

Cobalt. Two E_a values have been obtained for Co, 97 and 44 kcal mol^{-1}, corresponding to the heats of atomization of

solid cobalt metal and the dissociation energy of Co–Co, respectively. These values are identical for both the nitrate and chloride forms of the analyte. Below the appearance temperature (1430 K), the nitrate and chloride are converted to the oxide (*47*): $Co(NO_3)_2{\cdot}6H_2O_{(s)} \rightarrow$ (970 K) $CoO_{(s)}$; $CoCl_2{\cdot}6H_2O_{(s)} \rightarrow$ (430 K) $CoO_{(s)}$. Reduction of $CoO_{(s)}$ to $Co_{(s)}$ is favorable at the appearance temperature (Table I). Thus, atomization of Co occurs in a manner similar to that for lead and copper:

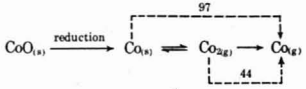

$Co_{2(g)}$ has been observed, mass-spectrometrically, as a vapor phase species effusing from a Knudsen cell containing $Co_{(l)}$ (*54*).

Tin. Two sequential atomization energies have been obtained for tin, 74 and 47 kcal mol^{-1}, irrespective of whether it is taken as the chloride or hydrous oxide. These energies correspond to the heat of atomization of the metal and the Sn–Sn bond dissociation energy, respectively. $Sn_{2(g)}$ has been widely observed (*31, 49, 50*) in the gas phase above $Sn_{(l)}$.

Below the appearance temperature the following reactions occur (*47*): $SnO_2{\cdot}H_2O_{(s)} \rightarrow$ (1110 K) $SnO_{2(s)}$; $SnCl_2{\cdot}2H_2O_{(s)} \rightarrow$ (780 K) $SnCl_2{\cdot}SnO_{(s)}$. In neutral media, over the temperature range 994–1166 K, $SnO_{(g)}$ is the gas phase species in equilibrium with $SnO_{(s)}$ (*48*); consequently, $Sn_{(g)}$ must be accounted for by the reductive decomposition of $SnO_{2(l)}$ (mp 1400 K). The data in Table I show that at the appearance temperature, carbon reduction of the oxide is very favorable. The following mechanism for the production of $Sn_{(g)}$ is therefore postulated:

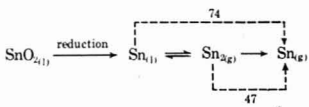

Aggett and Sprott (*14*) have also indicated that carbon reduction plays a major role in the production of $Sn_{(g)}$. These authors reported a 260 K lower appearance temperature for the atomization of tin from a graphite atomizer as compared to that from a tantalum atomizer.

At the appearance temperature, tin is in the liquid state. It would be reasonable to expect the E_a to correspond to the heat of vaporization of $Sn_{(l)}$ and not the heat of atomization of $Sn_{(s)}$. If the enthalpy change involved in heating the liquid from the appearance temperature to its boiling point is added to its heat of vaporization, an atomization energy of 63 kcal mol^{-1} is obtained. This is in reasonable agreement with the observed E_a value.

Nickel. Two sequential atomization energies have been obtained for nickel, 99 kcal mol^{-1} and 50 kcal mol^{-1}, in close agreement with the heat of atomization of $Ni_{(s)}$ ($Ni_{(s)} \rightarrow Ni_{(g)}$; $\Delta H° = 102.8$ kcal mol^{-1}) and the dissociation energy of the dimer, $Ni_{2(g)}$ (55.5 kcal mol^{-1}). $Ni_{2(g)}$ has been observed mass-spectrometrically in the gas phase (*55*). The temperature at the intersection point of the two segments of the E_a plot is approximately 1690 K.

Below the appearance temperature (1590 K), $NiO_{(s)}$ results from the thermal decomposition of the nitrate (*47*): $Ni(NO_3)_2{\cdot}6H_2O_{(s)} \rightarrow$ (615 K) $NiO_{(s)}$. $NiO_{(s)}$ is also formed by the hydrolysis of the chloride, since no difference was observed in the appearance temperature of nickel taken as either the chloride or nitrate. $NiO_{(s)}$ is readily reduced (Table I) at a temperature of 1600 K to produce $Ni_{(s)}$. It is reasonable to conclude, therefore, that $Ni_{(g)}$ arises from the following reaction sequence:

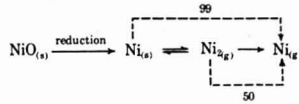

It is appropriate at this point to reconsider the assumption made in the model concerning the establishment of a gas phase–condensed phase equilibrium. The activation energy for Ni reported by Torsi and Tessari (405 kJ mol^{-1}, (*22*)) is in agreement with that obtained in this study for the heat of atomization of the metal. Torsi and Tessari (*22*) however, have not reported any energy values relating to the dissociation of $Ni_{2(g)}$, the reason being that condensed phase–gas phase (dimer) equilibrium cannot be attained in their open filament system, but is established in the HGA-2100.

Molybdenum. The E_a value obtained for molybdenum (165 kcal mol^{-1}) is in agreement with the heat of atomization of the element, 157.3 kcal mol^{-1}.

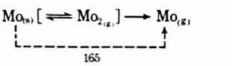

Unlike Pb, Cu, Co, Sn, and Ni, the dimeric metal species (i.e., $Mo_{2(g)}$) written into the above atomization sequence has been enclosed in brackets because no E_a value could be obtained from the high temperature region of the E_a plot (because of curvature of the plot as a result of factors discussed earlier) corresponding to the dissociation of $Mo_{2(g)}$. This lack of observation, however, does not preclude the possibility of the presence of the dimer; it simply means that not all of the $Mo_{(s)}$ vaporized within the measurement period. As a result, only the energy associated with the heat of atomization was obtained.

Table I indicates that reduction of molybdenum trioxide is a thermodynamically favorable process well below the appearance temperature. In fact, reduction of the trioxide may be shown to be possible below its sublimation temperature (1428 K). If this were not the case, sublimation of the trioxide would result in polymeric gas phase species (*56*), making reduction quite improbable even at higher temperatures.

The magnitude of the E_a value does not rule out the formation of an involatile molybdenum carbide species over the initial temperature range studied. Runnels et al. (*25*) however, have determined, by energy dispersive x-ray analysis, that Mo does form a carbide through surface reactions with the graphite of the furnace wall. The E_a value obtained for Mo does suggest, however, that any carbide that has formed is not dissociated to an appreciable extent throughout the temperature range used in this study (<2350 K).

One thousand-fold increases in sensitivity have been reported for molybdenum in graphite atomizers as compared to tantalum- and tungsten-lined atomizers (*57*). It is possible that, in the latter cases, an involatile alloy between molybdenum and tantalum or tungsten may be formed (*58*; *15*, p 462).

Vanadium. Two E_a values are reported for vanadium, 153 kcal mol^{-1} in the low temperature portion of the E_a plot (2200–2360 K) corresponding to the V–O energy, and 116 kcal mol^{-1} above 2360 K corresponding to the heat of vaporization of the metal.

Above 2020 K, $V_2O_{5(s)}$ decomposes to $V_2O_{3(s)}$ (mp 2240 K). On further heating, $V_2O_{3(s)}$ decomposes (*59*): $V_2O_{3(s)} \rightarrow 2VO_{(g)} + O_{2(g)}$ liberating $VO_{(g)}$. Subsequent dissociation of $VO_{(g)}$ will

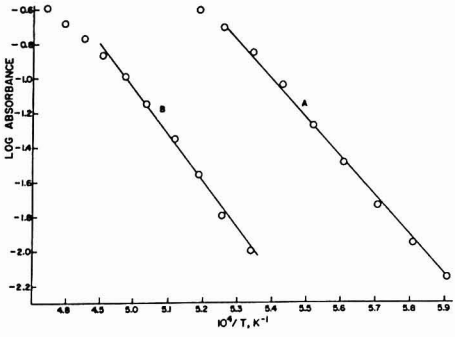

Figure 7. E_a plot for the atomization of chromium under atomize conditions of: dry 100 °C; ash 300 °C; atomize 2700 °C

(A) 2.5×10^{-9} g Cr at 357.8 nm; E_a = 99 kcal mol^{-1}. (B) 2.5×10^{-7} g Cr at 520.8 nm; E_a = 120 kcal mol^{-1}

yield an E_a value equal to the V–O bond energy, as observed:

$$VO_{(g)} \xrightarrow{153} V_{(g)} + O_{(g)}$$

The data in Table I indicate that reduction of $V_2O_{3(s)}$ at the appearance temperature (2200 K) is a thermodynamically favorable reaction. It would appear from the above data, however, that the reduction kinetics are slow. Only above 2360 K is an E_a value obtained which is in agreement with the heat of vaporization of liquid vanadium:

$$VO_{(s)} \xrightarrow{\text{reduction}} V_{(l)}\,[\rightleftharpoons V_{2(g)}] \longrightarrow V_{(g)} \qquad (116)$$

As in the case of Mo, an energy value corresponding to the dissociation of $V_{2(g)}$ was not obtained because all of the condensed phase had not vaporized within the time interval of the measurement. At 2360 K, the metal, if pure, should be in the liquid form (mp 2163 K). It is known (*60*), however, that small amounts of interstitial carbon can greatly increase the melting point of V (10% C increases the mp by approximately 1000 K). As a result, $V_{(s)}$ can just as likely (in the present circumstances) be substituted for $V_{(l)}$ in the above equation. Although this necessitates reinterpretation of the E_a value as the heat of atomization of the solid metal (123 kcal mol^{-1}), the uncertainty of the experimental results (±10%) does not rule out such a correlation.

As with molybdenum, no dissociation of involatile vanadium carbide was observed over the initial temperature range studied. This, of course, does not rule out its formation.

Iron. As indicated in Table II, two E_a values have been obtained for the atomization of iron: 97 kcal mol^{-1} and 86 kcal mol^{-1} for iron taken as the nitrate and chloride, respectively. The atomization behavior of the chloride will be discussed in a later section. When iron is taken as the nitrate, the E_a value may represent either the dissociation energy of Fe–O (96 kcal mol^{-1}) or the heat of atomization of iron ($Fe_{(s)} \rightarrow Fe_{(g)}$; ΔH°_0 = 99.3 kcal mol^{-1}). The correct choice must be based on the physicochemical behavior of the analyte, as follows. Below the appearance temperature (1500 K), $Fe(NO_3)_3$ is converted to the oxide (*47*): $Fe(NO_3)_3{\cdot}9H_2O_{(s)} \rightarrow$ (585 K) $Fe_3O_{4(s)} \equiv (FeO{\cdot}Fe_2O_3)$. Table I indicates that carbon reduction of both FeO and Fe_3O_4 at 1500 K is very favorable. In addition, Aggett and Sprott (*14*) have observed a 220 K decrease in the appearance temperature of iron from a graphite atomizer as compared to that from a tantalum atomizer. These data strongly suggest that atomic iron must result from the sublimation of solid iron, and the observed E_a value of 97 kcal mol^{-1} corresponds to the energy of the reaction:

$$FeO_{(s)} \xrightarrow{\text{reduction}} Fe_{(s)}\,[\rightleftharpoons Fe_{2(g)}] \longrightarrow Fe_{(g)} \qquad (97)$$

Because all of the iron on the surface of the furnace did not vaporize during the time taken in the measurement, no E_a value corresponding to the dissociation energy of $Fe_{2(g)}$ was observed.

Chromium. The E_a value of 99 kcal mol^{-1} obtained for chromium (taken as either the chloride or nitrate) is in agreement with the heat of atomization of the element, 95 kcal mol^{-1}. Below the appearance temperature of 1660 K, $Cr_2O_{3(s)}$ is the most stable oxide of chromium (*47*). Carbon reduction of the oxide is highly favorable at the appearance temperature (Table I). Atomization of the elemental metal is therefore to be expected:

$$Cr_2O_{3(s)} \xrightarrow{\text{reduction}} Cr_{(s)}\,[\rightleftharpoons Cr_{2(g)}] \longrightarrow Cr_{(g)} \qquad (99)$$

As in the cases of Mo, V, and Fe, no dimeric $Cr_{2(g)}$ species was observed.

To gain greater insight into the processes which are actually being investigated and the energy values obtained from this type of measurement, the energy required to produce gaseous metal atoms in an electronic excited state was measured. All of the elements examined in this study were monitored with electronic ground state lines. The energy so measured was that required to produce the atomic vapor in its electronic ground state. If the atomic population in an electronic excited state is monitored, the energy measured should equal the sum of the energies for the formation of atomic vapor and the energy of the electronic excited state. Such a determination may only be made with an element which possesses a transition from an electronic nonground state line of energy not less than 20 kcal above the electronic ground state (in order that this energy difference can be reliably measured). Such a precaution is necessary because of the ±10% uncertainties in the measurement methods. Additional requirements of the transition selected are that the line be strong in emission (from the source hollow-cathode lamp), must have an appreciable gf value and not be much above 20 kcal in energy (or else the population of the electronic excited state would be too small). Finally, elements which meet these criteria must also satisfy the temperature requirement as follows. The atomization of the element must take place at such a sufficiently high temperature that the electronic excited state is adequately populated. Elements that have an appearance temperature of 1000 K are poor choices for this reason, even though all other criteria may be satisfied. All of these criteria are satisfied by the chromium 520.8-nm line (at 7593 cm^{-1}, 21.7 kcal above the electronic ground state). Figure 7 is an E_a plot obtained from the atomization of chromium. Curve A represents the production of the electronic ground state atoms at 357.8 nm (E_a = 99 kcal mol^{-1}), whereas, curve B represents the production of the electronic excited state atoms (21.7 kcal above the electronic ground state) at 520.8 nm (E_a = 120 kcal mol^{-1}). The observed 21 kcal mol^{-1} energy difference is in excellent agreement with the expected 21.7 kcal mol^{-1} energy difference. This observation lends support to the credibility of the energy measurements obtained by this technique and also to

the assumption that a Boltzmann distribution of population has been attained. Recently, Ottaway and Shaw (*61*) have described a graphite furnace atomic emission spectrometric technique in which elemental detection limits were found to vary in the expected Boltzmann order with respect to the wavelength and the temperature.

Oxide–Dissociation. *Magnesium.* The energy of atomization obtained for magnesium is 90 kcal mol^{-1}, regardless of whether the chloride or the nitrate is taken for analysis. This value correlates well with the bond dissociation energy of Mg–O (94 kcal mol^{-1}). Thermogravimetric analysis (*47*) indicates that $MgO_{(s)}$ (mp 3073 K) is a common intermediate in the decomposition of both the chloride and the nitrate below the appearance temperature (1510 K): $MgCl_2 \cdot 5H_2O_{(s)}$ → (890 K) $MgO_{(s)}$; $Mg(NO_3)_2 \cdot 6H_2O_{(s)}$ → (750 K) $MgO_{(s)}$. Carbon reduction of $MgO_{(s)}$ at 1500 K is very unfavorable (Table I), suggesting that the presence of $Mg_{(g)}$ is due to thermal dissociation of the oxide in the gas phase. It is known, however, that $Mg_{(g)}$ and $O_{2(g)}$ are the principal gas phase species in equilibrium with $MgO_{(s)}$ (*62*). This type of sublimation process often occurs when the heat of sublimation of the oxide is greater than the dissociation energy of the oxide. In order to establish the kind of transition undergone by a compound upon vaporization, it is necessary to compare the changes in the free energy of formation of the compound from the gaseous components with the free energy of vaporization. To a first approximation, the bond energy of the gaseous compound may be compared with the heat of vaporization of the compound. If the bond energy is much higher than $^2/_3$ of its heat of vaporization, the substance may be expected to vaporize without undergoing dissociation. If the bond energy is much less than the heat of vaporization, the compound will be partly or wholly dissociated in the gas phase, depending on the relative magnitudes of these two energies (*63*, p 38). The high heat of sublimation of $MgO_{(s)}$, 158 ± 4 kcal mol^{-1} (*62*), accounts for its dissociation upon vaporization. With the knowledge that MgO dissociates upon vaporization, it remains to rationalize the E_a value of 90 kcal mol^{-1}, which is in close agreement with the Mg–O bond energy. It would be reasonable, in light of the above, to expect the atomization energy to correspond to the negative of the heat of formation of $MgO_{(s)}$ at and above the appearance temperature (1510 K), i.e., 175 kcal mol^{-1} (calculated from (*44*) for $MgO_{(s)} \rightarrow Mg_{(g)} + {}^1/_2O_{2(g)}$ at 1600 K). When excessively high masses of the analyte were atomized (100-fold larger than those used to obtain the above data), an E_a value of 174 kcal mol^{-1} was obtained. The only reasonable explanation for these observations involves the equilibrium vapor pressure of MgO at and above the appearance temperature. Vapor pressure data (*64*) reveal that, at the appearance temperature and with the analyte masses used in this study (approximately 10^{-10} g for Mg), all of the oxide has vaporized. As a result, vapor phase magnesium atoms are formed by the gas phase dissociation reaction:

$$MgO_{(g)} \xrightarrow{90} Mg_{(g)} + O_{(g)}$$

leading to the observed agreement between the Mg–O bond energy and the E_a value. If high concentrations of analyte are atomized, however, then the partial pressure of $MgO_{(g)}$ may equal its saturated vapor pressure. Under such conditions, the atomization behavior of MgO is similar to that discussed earlier for lead:

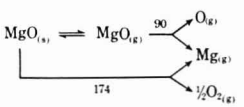

The E_a value should correspond to the negative of the heat of formation of $MgO_{(s)}$, as is experimentally observed. At higher temperatures, when almost all of the $MgO_{(s)}$ has vaporized, the E_a value should simply correspond to the Mg–O bond energy. It is of particular interest to point out that the predictive ability of the model now stands verified by the above result, which also confirms the assumption of gas–solid equilibrium made earlier.

Cadmium. Two values for E_a have been reported in Table II (50 and 65 kcal mol^{-1}), depending on whether the metal is taken as the chloride or the nitrate. These values are in agreement with the Cd–Cl and Cd–O bond dissociation energies, respectively. The discussion of the chloride system will be presented in a later section. At the appearance temperature of the signal (720 K), $CdO_{(s)}$ is formed when the analyte is taken as the nitrate (*47*): $Cd(NO_3)_2 \cdot 4H_2O_{(s)}$ → (617 K) $CdO_{(s)}$. It is evident from Table I that, at the appearance temperature, carbon reduction of $CdO_{(s)}$ is not thermodynamically favorable. Aggett and Sprott (*14*) have also shown that there is no significant difference in the atomization behavior of cadmium from carbon and tantalum atomizers. Reduction reactions with graphite may therefore be ruled out (the possibility of the reduction of the analyte by Ta has been discussed earlier). Gaseous Cd may therefore be accounted for only by dissociation of the oxide. Brewer and Mastick (*48*) have reported that, in the absence of a reducing atmosphere, $Cd_{(g)}$ and $O_{2(g)}$ are the major gas phase species in equilibrium with solid CdO. The atomization behavior of CdO is identical to that encountered for MgO. It would be expected from the above that the atomization energy should correspond to the sum of the energies of the negative of the heat of formation of $CdO_{(s)}$ (at the delay temperature of 700 K) and the heat of vaporization of $Cd_{(l)}$, these being approximately 62.5 (calculated from (*44*)) and 23.9 kcal mol^{-1}, respectively, corresponding to the reaction:

$$CdO_{(s)} \xrightarrow{86.4} {}^1/_2O_{2(g)} + Cd_{(l)} \longrightarrow Cd_{(g)}$$

As in the case of MgO, it is unlikely that the masses of analyte used in this study were sufficient to yield the equilibrium partial pressure of the analyte within the graphite tube. When very large masses of analyte were introduced (500-fold larger than that normally employed) into the graphite tube, an E_a value of 81 kcal mol^{-1} was obtained corresponding to the ΔH°_{700} of the above reaction (86.4 kcal mol^{-1}, calculated from data in (*44*)). It is evident from such studies that, at low analyte concentrations, all of the analyte has been transferred to the gas phase below the appearance temperature. As a result the measured E_a value corresponds to the gas phase dissociation of $CdO_{(g)}$:

$$CdO_{(g)} \xrightarrow{65} Cd_{(g)} + O_{(g)}$$

Zinc. The heats of atomization obtained for zinc are 65 and 48 kcal mol^{-1} when the analyte is taken in the nitrate or the chloride form, respectively. These values are in close agreement with the Zn–O and Zn–Cl bond dissociation energies, respectively. The atomization behavior of the chloride will be presented in a later section.

Thermogravimetric analysis (*47*) of $Zn(NO_3)_2$ indicates that the monoxide is formed below the appearance temperature (1140 K): $Zn(NO_3)_2 \cdot 6H_2O_{(s)}$ → (623 K) $ZnO_{(s)}$. Carbon reduction of the oxide is unfavorable below the appearance temperature; $Zn_{(g)}$ must therefore be formed from oxide dissociation. As in the case of MgO and CdO, ZnO is decomposed upon vaporization. $Zn_{(g)}$ and $O_{2(g)}$ are the major gas phase species in equilibrium with $ZnO_{(s)}$ (*48*, *65*). The agreement of

E_a with the Zn–O bond energy, when Zn is taken as the nitrate, can be rationalized only by an argument identical to that invoked for CdO. The production of $Zn_{(g)}$ directly from $ZnO_{(s)}$ would require not only the energy equal to the negative of the heat of formation of $ZnO_{(s)}$ at 1100 K but also the heat of vaporization of $Zn_{(l)}$, i.e.,

$$ZnO_{(s)} \xrightarrow{111.8} \tfrac{1}{2}O_{2(g)} + Zn_{(l)} \longrightarrow Zn_{(g)}$$

the total of such energy, $\Delta H^{\circ}_{1100} = 111.8$ kcal mol^{-1}. As in the cases of MgO and CdO, atomization of very large masses of ZnO yields an E_a of 103 kcal mol^{-1}, in agreement (within experimental uncertainty) with the above ΔH°_{1100}. It can be shown that the masses of Zn analyte normally employed in this study are too low to yield a saturated partial pressure of $ZnO_{(g)}$ within the graphite tube at 1100 K (from vapor pressure data, (*64*)). As a result, all of the ZnO is transferred to the gas phase where dissociation occurs:

$$ZnO_{(g)} \xrightarrow{65} Zn_{(g)} + O_{(g)}$$

Manganese. The energy of atomization obtained for manganese is 92 kcal mol^{-1}, corresponding to the bond dissociation energy of MnO. Below the appearance temperature, $MnO_{(s)}$ is present on the graphite surface irrespective of whether it has been introduced as the chloride or the nitrate (*47*):

$$MnCl_2{\cdot}2H_2O_{(s)} \xrightarrow{925K} Mn_2O_{3(s)} \xrightarrow{1215K} Mn_3O_{4(s)} \underset{1435K}{\rightleftharpoons} MnO_{(s)}$$

$$Mn(NO_3)_2{\cdot}6H_2O \xrightarrow{575K} MnO_{2(s)} \xrightarrow{975K} Mn_3O_{4(s)} \xrightarrow{1435K} MnO_{(s)}$$

Brewer and Mastick (*48*) have reported that at a temperature of 1767 K, $Mn_{(g)}$ and $O_{2(g)}$ are the major gas phase species in equilibrium with $MnO_{(s)}$. The heat of vaporization of $MnO_{(s)}$ is 121.4 kcal mol^{-1} (*63*, p 177). As in the cases of MgO, CdO, and ZnO, the monoxide molecule (MnO) is expected to be a minor species in the gas phase compared to its dissociation products. In such circumstances, the atomization energy would be expected to correlate with the sum of the energies of the negative of the heat of formation of $MnO_{(s)}$ at 1500 K and the heat of vaporization of the metal, i.e.,

$$MnO_{(s)} \xrightarrow{146} \tfrac{1}{2}O_{2(g)} + Mn_{(s)} \longrightarrow Mn_{(g)}$$

corresponding to a ΔH°_{1500} of 146 kcal mol^{-1}. When very large masses of the analyte were atomized, an E_a of 155 kcal mol^{-1} was obtained, in agreement with the above value. As has been the case with metal oxides discussed earlier, the normal masses of analyte employed in this study are too small to yield the equilibrium partial pressure of the oxide in the gas phase (*64*); consequently, all of the analyte is transferred to the gas phase below the appearance temperature, where subsequent dissociation occurs leading to the agreement between the observed E_a and the Mn–O bond energy:

$$MnO_{(g)} \xrightarrow{92} Mn_{(g)} + O_{(g)}$$

At high analyte masses, the equilibrium partial pressure of $MnO_{(g)}$ may be attained but the formation of atomic $Mn_{(g)}$ requires the total energy of 146 kcal mol^{-1}, as discussed above:

$$MnO_{(s)} \rightleftharpoons MnO_{(g)} \xrightarrow{92} O_{(g)} + Mn_{(g)}$$
$$MnO_{(s)} \xrightarrow{155} Mn_{(g)} + \tfrac{1}{2}O_{2(g)}$$

At higher temperature (where the data cannot be obtained by the technique presented here because of obvious constraints) when almost all of the surface phase $MnO_{(s)}$ has disappeared, it is expected that the atomization energy will correspond to only the Mn–O bond energy as indicated earlier.

Calcium. The observed energy of atomization of calcium, 90 kcal mol^{-1}, is in reasonable agreement with the Ca–O bond dissociation energy of 84 kcal mol^{-1}. Below the appearance temperature (1850 K), $CaO_{(s)}$ is formed by thermal decomposition of the nitrate (*47*): $Ca(NO_3)_2{\cdot}4H_2O \rightarrow$ (700 K) $CaO_{(s)}$. Hydrolysis of the chloride can also form the oxide. Since carbon reduction of $CaO_{(s)}$ is not favorable at 1900 K (Table I), it must be concluded that $Ca_{(g)}$ is formed by thermal dissociation of CaO. The heat of vaporization of CaO is 147 ± 15 kcal mol^{-1} (*66*), and as a result $CaO_{(g)}$, compared to the gaseous products of its dissociation, is a minor gas phase species in equilibrium with $CaO_{(s)}$ (*63*). As found in the cases of the oxides of Zn, Cd, Mg, and Mn, it is to be expected that, under these conditions, the atomization energy of CaO should correspond to the negative of the heat of formation of $CaO_{(s)}$ from the elements in their standard states at 1900 K, i.e., $CaO_{(s)} \rightarrow Ca_{(g)} + \tfrac{1}{2}O_{2(g)}$; $\Delta H^{\circ}_{1900} = 188$ kcal mol^{-1}. At high analyte masses, an E_a of 184 kcal mol^{-1} was obtained. These E_a values may, again, be rationalized by considering that, at low analyte masses, all of the CaO has been transferred to the gas phase where dissociation occurs:

$$CaO_{(g)} \xrightarrow{90} Ca_{(g)} + O_{(g)}$$

resulting in an atomization energy corresponding to the Ca–O bond energy. Under the conditions of high analyte masses the following reaction occurs:

$$CaO_{(s)} \rightleftharpoons CaO_{(g)} \xrightarrow{90} O_{(g)} + Ca_{(g)}$$
$$CaO_{(s)} \xrightarrow{184} Ca_{(g)} + \tfrac{1}{2}O_{2(g)}$$

At higher temperatures, when almost all of the $CaO_{(s)}$ has disappeared, the E_a value should correspond to the Ca–O bond energy.

Aluminum. Two sequential atomization energies have been obtained for Al, 234 kcal mol^{-1} and 114 kcal mol^{-1}. Below the appearance temperature, Al_2O_3 is the common intermediate for the nitrate and the chloride (*47*): $Al(NO_3)_3{\cdot}9H_2O_{(s)} \rightarrow$ (1020–1270K) $Al_2O_{3(s)}$; $AlCl_3{\cdot}6H_2O_{(s)} \rightarrow$ (770K) $Al_2O_{3(s)}$. Since reduction of this oxide is not thermodynamically favorable at the appearance temperature, $Al_{(g)}$ must be formed by the thermal decomposition of an oxide. This conclusion is supported by observations by Aggett and Sprott (*14*) that the appearance temperature for atomization of aluminum is the same from both a carbon and a tantalum atomizer. A reasonable interpretation of the results is based on the following reaction:

$$Al_2O_{3(s)} \rightleftharpoons Al_2O_{3(g)} \xrightarrow{234\ (a)} Al_{(g)} + AlO_{(g)} + O_{2(g)}$$
$$AlO_{(g)} \xrightarrow{(b)\ 114} Al_{(g)} + O_{(g)}$$

Initial formation of Al occurs through sequence (a). The heat of this reaction, calculated from the heat of sublimation of

$Al_2O_{3(s)}$ (*67*) and the bond energies of $AlO_{(g)}$ (*66, 68*) and $O_{2(g)}$, is 221 kcal mol^{-1}, in good agreement with the observed E_a value. When most of the $Al_2O_{3(s)}$ has vaporized, thereby depleting the supply of $Al_2O_{3(g)}$, $AlO_{(g)}$ becomes the dominant precursor of $Al_{(g)}$. The heat of this reaction is simply the bond dissociation energy of $AlO_{(g)}$, i.e., 116 kcal mol^{-1}, in agreement with the observed E_a value. It is important to emphasize that the above reaction sequences leading to the experimental E_a values, result in two well-defined slopes in the E_a plot and do not require any bimolecular gas phase recombination reactions.

It is also of interest to examine the results of atomization of some selected aluminum compounds introduced into the atomizer in an oxalic acid medium. The results are presented in Table III. As in the case of the chloride and the nitrate, the sulfate also is converted to the oxide below the appearance temperature (*47*): $Al_2(SO_4)_3 \cdot 16H_2O_{(s)} \rightarrow$ (880–1270 K) $Al_2O_{3(s)}$. The heats of atomization of the solid compounds are consistent with the atomization pattern described above.

In all these atomization studies, argon gas has been used as a sheath gas. When nitrogen gas is substituted for argon gas, the peak and integrated sensitivities for aluminum decrease by a factor of three, as indicated in Figure 8. Sensitivity losses such as these cannot be simply ascribed to an increase in the rate of diffusional loss in nitrogen gas as compared to argon gas. Formation of an appreciable amount of aluminum nitride at high temperatures, however, may account for this effect. Atomization of aluminum from tantalum- and tungsten-lined atomizers equalizes the sensitivities obtained in argon and nitrogen gases, whereas substitution of pyrolytic graphite for regular graphite decreases the above difference by 25% (*57, 69*). The above studies indicate that carbon plays a role in the formation of the nitride:

$$Al_2O_{3(s)} + 3C_{(s)} + N_{2(g)} \longrightarrow 2AlN_{(s)} + 3CO_{(g)}$$

This reaction is thermodynamically favorable because carbon forms a stable volatile oxide (CO) but does not form as stable a compound with aluminum as does nitrogen (*70*). The above reaction is generally carried out at a temperature of 1973–2273 K (*71*), the $AlN_{(s)}$ formed being stable in the solid phase up to 2500 K (*72*). It is evident that the nitride is not formed in tungsten or tantalum atomizers, and the extent of the nitride formation may possibly be reduced in pyrolytic graphite atomizers, probably as a result of the denser structure of this material as compared to regular graphite. However, this latter explanation is only a speculation. An energy of atomization for aluminum corresponding to dissociation of $AlN_{(g)}$ has not been observed in these studies because $AlN_{(g)}$ is not produced in a measurable quantity as a result of the stability of $AlN_{(s)}$ in the solid phase. Since very little $AlN_{(s)}$ is vaporized until the temperature exceeds approximately 2500 K (mp > 2473 K), the range of temperature required for the study of $AlN_{(s)}$ is beyond the capability of the technique used in this study. For this reason, the E_a values obtained for Al_2O_3 in both argon and nitrogen sheath gases are identical.

Chloride–Dissociation. *Cadmium.* When Cd is taken as the chloride, an E_a value fo 50 kcal mol^{-1} was obtained, in agreement with the Cd–Cl bond energy of 49.9 kcal mol^{-1}. At the appearance temperature of the signal (720 K), cadmium is present as the chloride if it is introduced into the atomizer as a solution in 5% (v/v) hydrochloric acid (*47*): $CdCl_2 \cdot 5H_2O_{(s)} \rightarrow$ (873K) $CdO_{(s)}$. Mass spectrometric studies of the vapor above liquid $CdCl_2$ over the temperature range 785–838 K indicate that $Cd_{(g)}$, $CdCl_{2(g)}$, and $CdCl_{(g)}$ are the major species (*73*). The formation of $CdCl_{(g)}$ was accounted for by dissociation of $CdCl_{2(g)}$ by ion-source electron impact and, as such, was not considered to be a direct sublimation product. The results of the present study can be rationalized only by assuming that $CdCl_{(g)}$ is a direct evaporation product of $CdCl_{2(l)}$ since gas-phase dissociation of $CdCl_{2(g)}$ should yield an E_a value twice as large as that obtained. The authors can offer no satisfactory alternative interpretation.

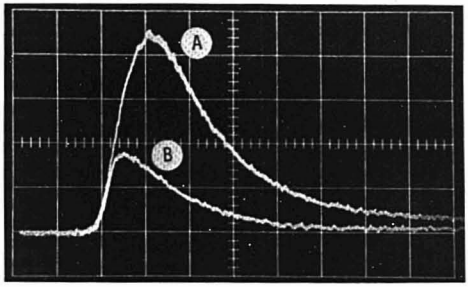

Figure 8. Oscilloscopic trace of the absorbance–time profile for 1.5 × 10^{-11} g aluminum taken as the nitrate under atomize conditions of: dry 100 °C; ash 300 °C; atomize 2700 °C

Vertical scale: absorbance 0.10/scale unit. Horizontal scale: sweep speed 500 m/scale unit. (A) Argon sheath; (B) Nitrogen sheath

Zinc. When zinc is atomized from hydrochloric acid media, an appearance temperature of 940 K is obtained. Although thermogravimetric data were not available, the 200 K decrease in the delay temperature with respect to that of the nitrate is indicative of a radical change in the atomization behavior; hence, the atomization appears to proceed via thermal dissociation of the chloride. The agreement obtained between the E_a value and the Zn–Cl bond energy can only be accounted for by the gas phase dissociation of $ZnCl_{(g)}$. As in the case of cadmium chloride, this reaction presupposes the existence of $ZnCl_{(g)}$ in the vapor above $ZnCl_{2(l)}$. However, mass spectrometric studies (*74*) of the equilibrium vapor above $ZnCl_{2(l)}$ have not reported $ZnCl_{(g)}$ as a major species.

Iron. Atomization of the chloride commences at 1400 K with an E_a value of 86 kcal mol^{-1}, in close agreement with the reported Fe–Cl bond energy. At a temperature of approximately 590 K (*75*), $FeCl_{3(s)}$ is reduced to $FeCl_{2(s)}$. Above 674 K, $FeCl_{2(s)}$ sublimes. It has been reported (*76*) that the major gas phase species in equilibrium with $FeCl_{2(s)}$ are $FeCl_{2(g)}$ and $(FeCl_2)_{2(g)}$. Despite this fact, the only reasonable explanation of the observed E_a is that $FeCl_{(g)}$ must be present in the gas phase over $FeCl_{2(2)}$. The E_a value obtained in this study could only be achieved by atomizing large masses of the analyte (i.e., above 10 ng Fe).

RELATIONSHIP OF THE APPEARANCE TEMPERATURE TO E_a

In agreement with the findings of Johnson et al. (*18*), a linear relationship between the appearance temperature and the heat of atomization of the analyte was observed. The slope of such a plot, shown in Figure 9, is approximately 0.06 kcal mol^{-1} K^{-1} and is in agreement with that calculated from the data of Johnson et al. (*18*). No point is shown for Al in this figure because its coordinates (2080 K, 234 kcal mol^{-1}) are anomalous with respect to the linear relationship observed with the other elements. Atomization of Al (low analyte mass) occurs predominately by a solid-state decomposition reaction. When the coordinates for Al (2080 K, 234 kcal mol^{-1}) are plotted on a graph containing the data for CdO, ZnO, MnO, MgO, and CaO which were obtained using high analyte masses, a straight line of slope 0.1 kcal mol^{-1} K^{-1} results. The common feature to each of these oxides is that atom formation is the result of a solid-state oxide decomposition. Figure 9 is

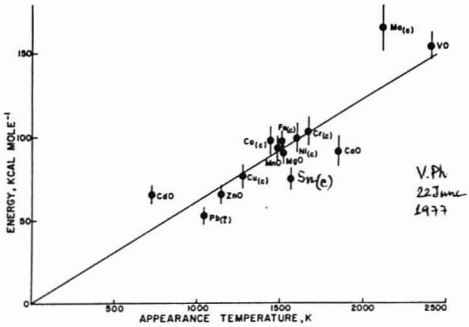

Figure 9. Plot of the appearance temperature vs. the energy relating to the atomization step

$M_{(c)}$ energy = heat of atomization of the metal. MO energy = bond dissociation energy of the metal monoxide

useful for the purposes of prediction. In those cases where the activation energy barrier to analyte vaporization is small (i.e., for the sublimation of metals or for small masses of analyte oxides where all of the monoxide is transferred to the gas phase), there is a linear relationship between the atomization energy and the appearance temperature of the analyte. The conditions stipulated above are those normally operative in atomic absorption analysis, and the predictive power of this relationship is thus limited to the atomization of small analyte masses. With a knowledge of the experimental appearance temperature of the anlayte, an atomization energy may be obtained. By correlating this energy with that of some possible atomization processes, as outlined earlier, a reasonable guess as to the identity of the immediate precursor to analyte atoms may be made. The correlation between the atomization energy and the appearance temperature also appears to be independent of the type of atomizer used (cf. the data of Johnson et al. (*18*), as reported above in which analyte atomization was carried out in a carbon filament atomizer). It is possible that the correlation between the appearance temperature and the atomization energy is universal.

From the data presented, it is possible to formulate some general mechanisms of analyte atomization in a graphite furnace, based on those trends which have emerged here. From a consideration of the physiochemical properties of the analyte, coupled with available thermodynamic data and the appearance temperature of the analyte, a reasonable mechanism for atomization may be postulated. The first point which must be considered is the thermal behavior of the analyte as it crystallizes from the test solution during the dry and ash heating periods. Here, it is necessary to examine available thermogravimetric data for the analyte and its matrix (e.g., nitric or hydrochloric acid media) to determine whether or not hydrolysis to oxides or oxygen-containing species occurs below the appearance temperature. For example, if hydrolysis in hydrochloric acid medium does not occur, atomization of the analyte will likely proceed through dissociation of the chloride. On the other hand, if an oxide is formed, two alternate atomization mechanisms are likely: dissociation of the metal oxide or carbon reduction of the oxide followed by vaporization of the elemental metal. This latter possibility may be conveniently checked by considering the free energy of the carbon reduction reaction. If $\Delta G_{\text{reaction}} \leq 0$, the reaction is a thermodynamically favorable process. However, thermodynamics gives no indication of the kinetics of such reactions. Barring slow reactions, however, one may be reasonably confident in assuming that reduction has occurred at the appearance temperature, or will occur at a slightly higher temperature, particularly in those cases having large negative values for free energy changes. Under such conditions, the reduced metal (whose state of aggregation is determined by the appearance temperature) may vaporize directly into the gas phase predominantly as the monomer or substantial quantities of the dimer may also be formed. This possibility may be considered by examining the energetics of such a process, as illustrated in Figure 1. In such cases where carbon reduction proves unfavorable, dissociation of the oxide occurs. Here again, however, there are two alternative mechanisms of atomization available. For those oxides whose heats of vaporization are substantially lower than their dissociation energies, the substance is vaporized without being dissociated. In such cases, gas phase dissociation of the oxide will predominate. For those oxides whose dissociation energies are lower than their heats of vaporization, vaporization will occur with dissociation, giving rise to a solid-state dissociative process. Finally, by reference to an energy vs. temperature plot whose slope is approximately 0.06 kcal mol^{-1} K^{-1}, a reasonable estimate of E_a may be obtained simply from a knowledge of the appearance temperature of the species. The E_a value may then be correlated with that which would arise from the suspected process. At this point, the resources for prediction are exhausted. The final solution to a still unresolved mechanistic problem must be found by further experimental investigation by methods including those outlined in this paper.

CONCLUSIONS

Quantitative evidence has been presented regarding the mechanism of atomization of a number of elements. The major pathways leading to gaseous atoms have been found to be thermal dissociation of the metal oxide, carbon reduction of the oxide followed by atomization of the free metal, and thermal dissociation of the metal halide.

The energy values obtained by the methods outlined in this study provide information only as to the major suppliers of gas phase atoms over the initial states of signal production. Generation of atoms by other species at significantly higher temperatures, not handled by this technique, (e.g., carbides of Fe, Cr, Ni, Mo, V, etc., which may give rise to the characteristically long decay regions associated with these signals) cannot be investigated and, consequently, formation and decomposition of other species cannot be ruled out.

Further experimental work is required to substantiate many of the conclusions drawn. In this respect, it would also be of interest to obtain experimental confirmation of some of the suggested gas phase molecular species and their concentration–time profiles for correlations with atomic absorption profiles. It would be also of interest to study atomization in tungsten and tantalum atomizers in order to evaluate the relative importance of suggested reduction reactions.

Determination of the energies of atomization in those cases where solute vaporization interferences or chemical interferences are present, will provide energy values which may serve as quantitative measures of such effects.

ACKNOWLEDGMENT

The authors thank K. J. Laidler and E. A. Flood for helpful discussion and for providing valuable comments, and P. Bertels for technical assistance.

LITERATURE CITED

(1) C. Th. J. Alkemade and P. J. Th. Zeegers, in "Spectrochemical Methods of Analysis", Vol. 9, J. D. Winefordner, Ed., Wiley-Interscience, New York, N.Y., 1971, pp 3–125.
(2) P. J. Kalff and C. Th. J. Alkemade, *J. Chem. Phys.*, **59**, 2572 (1973).

(3) D. E. Jensen and G. A. Jones, *J. Chem. Soc., Faraday Trans., 1*, **69**, 1448 (1973).
(4) N. J. Friswell and D. R. Jenkins, *Combust. Flame*, **19**, 197 (1972).
(5) R. N. Newman and F. M. Page, *Combust. Flame*, **17**, 149 (1971).
(6) D. H. Cotton and D. R. Jenkins, *Trans. Faraday Soc.*, **65**, 1537 (1969).
(7) R. W. Reid and T. M. Sugden, *Discuss. Faraday Soc.*, **33**, 213 (1962).
(8) E. M. Bulewicz and T. M. Sugden, *Trans. Faraday Soc.*, **55**, 720 (1959).
(9) E. M. Bulewicz and T. M. Sugden, *Trans. Faraday Soc.*, **54**, 830 (1958).
(10) T. M. Sugden, *Trans. Faraday Soc.*, **52**, 1465, 1475, 1481 (1956).
(11) R. E. Sturgeon, C. L. Chakrabarti, I. S. Maines, and P. C. Bertels, *Anal. Chem.*, **47**, 1240 (1975).
(12) R. E. Sturgeon, C. L. Chakrabarti, and P. C. Bertels, *Anal. Chem.*, **47**, 1250 (1975).
(13) W. C. Campbell and J. M. Ottaway, *Talanta*, **21**, 837 (1974).
(14) J. Aggett and A. J. Sprott, *Anal. Chim. Acta*, **72**, 49 (1974).
(15) F. T. Sisco and E. Epremian, "Columbium and Tantalum", J. Wiley and Sons Inc., New York, 1963.
(16) C. W. Fuller, *Analyst (London)*, **99**, 739 (1974).
(17) C. W. Fuller, *Analyst (London)* **100**, 229 (1975).
(18) D. C. Johnson, B. L. Sharp, T. S. West, and R. M. Dagnall, *Anal. Chem.*, **47**, 1234 (1975).
(19) G. Torsi and G. Tessari, *Anal. Chem.*, **45**, 1812 (1973).
(20) S. L. Paveri-Fontana, G. Tessari, and G. Torsi, *Anal. Chem.*, **46**, 1032 (1974).
(21) G. Torsi and G. Tessari, *Anal. Chem.*, **47**, 839 (1975).
(22) G. Tessari and G. Torsi, *Anal. Chem.*, **47**, 842 (1975).
(23) B. V. L'vov, "Atomic Absorption Spectrochemical Analysis" (Engl. Trans. by J. H. Dixon), Adam Hilger, London, 1970.
(24) R. Woodriff, R. W. Stone, and A. M. Held, *Appl. Spectrosc.*, **22**, 408 (1968).
(25) J. H. Runnels, R. Merryfield, and H. B. Fisher, *Anal. Chem.*, **47**, 1258 (1975).
(26) G. I. Nikolaev and A. M. Nemets, *Zh. Prikl. Spectrosk.*, **13**, 695 (1970).
(27) R. M. Barrer, "Diffusion in and Through Solids", Cambridge University Press, London, 1951.
(28) W. J. Moore, "Physical Chemistry", 4th ed., Prentice-Hall Inc., Englewood Cliffs, N.J., 1972, p 386.
(29) G. N. Lewis and M. Randall "Thermodynamics", 1st ed., McGraw-Hill Co. Inc., New York, 1923, p 299.
(30) M. Szwarc, *Chem. Rev.*, **47**, 75 (1950).
(31) R. E. Honig, *J. Chem. Phys.*, **21**, 573 (1953).
(32) I. E. Campbell and E. M. Sherwood, "High Temperature Materials and Technology", John Wiley and Sons, New York, 1967, p 22.
(33) A. G. Gaydon, "Dissociation Energies and Spectra of Diatomic Molecules", 3d ed., Chapman and Hall, London, 1968.
(34) B. V. L'vov, *J. Quant. Spectrosc. Radiat. Transfer*, **12**, 651 (1972).
(35) B. V. L'vov, D. A. Katskov, and L. P. Kruglikova, *Zh. Prikl. Spectrosk.*, **14**, 784 (1971).
(36) R. F. Browner and J. D. Winefordner, *Anal. Chem.*, **44**, 247 (1972).
(37) A. I. Vogel, "A Textbook of Quantitative Inorganic Analysis", Longmans Green and Co. Ltd., 1962, p 335.
(38) R. E. Sturgeon and C. L. Chakrabarti, submitted to *Spectrochim. Acta, Part B.*
(39) *M. J. Adams and G. F. Kirkbright, Anal. Chim. Acta*, **84**, 79 (1976).
(40) E. A. Moelwyn-Hughes, "Physical Chemistry", 2d ed., Pergamon Press, Oxford, 1965.
(41) JANAF Thermochemical Tables, D. R. Stull, Ed., Dow Chemical Co., Midland, Mich., 1965, 1966, and 1967 and subsequent supplements.
(42) H. L. Schick, "Thermodynamics of Certain Refractory Compounds", Vol. II, Academic Press, New York, 1966.
(43) D. R. Stull and G. C. Sinke, "Thermodynamic Properties of the Elements", American Chemical Society, Washington, D.C., 1956.
(44) I. Barin and O. Knacke, "Thermochemical Properties of Inorganic Substances", Springer-Verlag, New York, 1973.
(45) A. G. Gaydon and I. R. Hurle, "The Shock Tube in High Temperature Chemical Physics", Reinhold Publishing Co., New York, 1963.
(46) "Proceedings of the Ninth International Shock Tube Symposium", D. Bershader and W. Griffith, Ed., Stanford University Press, Stanford, Calif., 1973.
(47) C. Duval", Inorganic Thermogravimetric Analysis", 2d ed., Elsevier Publishing Co., New York, 1963.
(48) L. Brewer and D. F. Mastick, *J. Chem. Phys.*, **19**, 834 (1951).
(49) J. D. Drowart and R. Honig, *J. Phys. Chem.*, **61**, 980 (1957).
(50) J. L. Margrave in "Physicochemical Measurements at High Temperatures", J. O'M. Bockris, J. L. White, and J. D. MacKenzie, Ed., Butterworths, London, 1959, p 225.
(51) J. J. Lingane, "Electroanalytical Chemistry", 2d ed., Interscience Publishers, Inc., New York, 1966, p 232.
(52) R. W. B. Pearse and A. G. Gaydon, "The Identification of Molecular Spectra", Chapman and Hall Ltd., 3d ed., London, 1963, p 151.
(53) J. D. Drowart and R. Honig, *J. Chem. Phys.*, **25**, 581 (1956).
(54) A. Kant and B. Strauss, *J. Chem. Phys.*, **41**, 3806 (1964).
(55) A. Kant, *J. Chem. Phys.*, **41**, 1872 (1964).
(56) J. Berkowitz and M. G. Inghram, *J. Chem. Phys.*, **26**, 842 (1957).
(57) Perkin-Elmer Corporation, personal communication.
(58) L. Northcott, "Molybdenum", Butterworths, London, 1956, p 126.
(59) E. Rutner, P. Goldfinger, and J. P. Hirth, "Condensation and Evaportion of Solids", Gordon and Breach Publications, New York, 1964, p 299.
(60) F. A. Cotton and G. Wilkinson, "Advanced Inorganic Chemistry", 3d ed., John Wiley and Sons, New York, 1972.
(61) J. M. Ottaway and F. Shaw, *Analyst (London)*, **100**, 438 (1975).
(62) R. L. Altman, *J. Phys. Chem.*, **67**, 366 (1963).
(63) I. S. Kulikov, "Thermal Dissociation of Chemical Compounds" (Engl. Trans. by J. Schmorak), Israel Program for Scientific Translations, Jerusalem, 1967.
(64) "The Characterization of High Temperature Vapors", J. L. Margrave, Ed., John Wiley and Sons, New York, 1967.
(65) D. F. Anthrop and A. W. Searcy, *J. Phys. Chem.*, **68**, 2335 (1964).
(66) T. P. J. H. Babeliowsky, *J. Chem. Phys.*, **38**, 2035 (1963).
(67) L. Brewer and A. Searcy, *J. Am. Chem. Soc.*, **73**, 5308 (1951).
(68) D. L. Hildenbrand, *Chem. Phys. Lett.*, **20**, 127 (1973).
(69) Unpublished works of the present authors.
(70) A. W. Searcy, *Proc. Inorg. Chem.*, **3**, 71 (1962).
(71) "Handbook of the Physicochemical Properties of the Elements", G. V. Samsonov, Ed., Plenum Press, New York, 1968, p 769.
(72) G. V. Samsonov, "Handbook of High Temperature Materials—Properties Index", Plenum Press, New York, 1964, p 75.
(73) F. J. Keneshea and D. Cubicciotti, *J. Chem. Phys.*, **40**, 1778 (1964).
(74) F. J. Keneshea and D. Cubicciotti, *J. Chem., Phys.*, **40**, 191 (1964).
(75) C. M. Cook, Jr., *J. Phys. Chem.*, **66**, 219 (1962).
(76) R. C. Shoonmaker and R. F. Porter, *J. Chem. Phys.*, **29**, 116 (1958).
(77) "Handbook of Chemistry and Physics", 55th ed., R. C. Weast, Ed., Chemical Rubber Co., Cleveland, Ohio, 1975.

RECEIVED for review May 24, 1976. Accepted August 2, 1976. The authors are grateful to the National Research Council of Canada for financial support of this research project. One of us (RES) is grateful to the National Research Council of Canada for a postgraduate scholarship. This work was presented in part at the 5th International Conference on Atomic Spectroscopy, Clayton, Victoria, Australia, August 25–29, 1975, and will be presented at the 3d FACSS meeting and the 6th International Conference on Atomic Spectroscopy, Philadelphia, Pa., November 14–19, 1976.

Sulfate Formed by Interaction of Sulfur Dioxide with Filters and Aerosol Deposits

Sir: There is concern and some evidence (*1, 2*) that atmospheric aerosol samples collected on filters contain spurious sulfate as a consequence of SO_2 oxidation in the filter and/or the sample deposit. We report here a simple technique by which we show that 1) poly(tetrafluoroethylene) membrane filters and pH-neutral quartz-fiber filters cause very minor SO_2 conversion to sulfate, 2) glass-fiber filters and alkaline quartz-fiber filters cause considerable SO_2 conversion to sulfate, and 3) the aerosol deposit itself causes—in four tests—very little SO_2 conversion to sulfate.

The experiments were conducted in 1974, 1975, and 1976 in the Allegheny Tunnel of the Pennsylvania Turnpike and in the rural air near the tunnel as a part of programs reported elsewhere (*3–6*) and preparatory to a field study of sulfuric acid emissions from catalyst-equipped vehicles in this tunnel. For our purpose, it was important to address the question of spurious sulfate at the site that was of interest to us, with its particular gas composition and so forth, rather than i the laboratory. However, to lend some generality to our results, some experiments were conducted also in the ambient air near the tunnel. Since it was anticipated the water absorbed on the filter and/or aerosol deposit might promote SO_2 oxidation, the relative humidity was monitored; it was found to range from 34 to 97% in the tunnel and in the ambient air (all years combined). Temperature was 1 to 23 °C.

(There is also a possibility that SO_2 could be adsorbed and oxidized to spurious sulfate not immediately but rather during the analysis; in the experiments to be described, this pathway to spurious sulfate is indistinguishable from the other, and our results should be taken to refer to the sum of the two. Because the extent of oxidation of adsorbed SO_2 during analysis can depend on the analytical method, our results should be considered in the context of our chemical procedures to be described later.)

Method. An efficient filter which is reasonably inert to SO_2 conversion is placed upstream of the filter to be tested. The upstream filter removes the particulate matter and allows the gases, including most or all of the SO_2, to reach the second filter. The extent to which the SO_2 can react on the second filter to form spurious sulfate can be determined subsequently by sulfate analysis. If, in addition, the second filter has an aerosol deposit on it, the SO_2 can react also on this particulate matter to form spurious sulfate.

The following experimental procedure was used to determine the amount of spurious sulfate formed by both processes: a) Mount a pH-neutral quartz-fiber filter (which is a very efficient filter and also proves to be reasonably inert with respect to SO_2 conversion) on top of the filter to be tested in a standard HiVol sampling unit. Sample for a period t_1. Remove the top filter, lay a thin polyethylene sheet over one half of the bottom filter, and lay a new pH-neutral quartz-fiber filter over both halves. Sample for a period t_2. b) Simultaneously, in a second HiVol, collect a particulate sample on the filter to be tested in the usual way for the period t_1. Cover one half with a thin polyethylene sheet and lay a new pH-neutral quartz filter over both halves. Sample for period t_2. c) Determine ambient SO_2 levels during t_1 and t_2 using H_2O_2 impingers.

The sulfate (minus blank correction) found on the bottom filter of procedure (a) above (i.e., the bottom filter which had not been exposed to particulate matter) will be the spurious sulfate formed by reaction with the filter alone, all particulate matter having been stopped by the upstream filter. For the half under the polyethylene mask, the sulfate will be formed during t_1 and for the other half, it will be formed during t_1 and t_2. The difference between the two halves will be the spurious sulfate formed during t_2—that is to say, on a filter which already had been exposed to SO_2 for t_1. In this way, especially with the repetition of the experiment with different values of t_1 and t_2, the conversion rate as a function of time can be measured.

The sulfate (minus blank correction) found on the bottom filter of procedure (b) above (i.e., the bottom filter which had been exposed to particulate matter) will be the spurious sulfate formed by reaction with the filter plus particulate matter—together with the "honest" sulfate present in that particulate matter. Under the polyethylene, the sulfate will be that found by the usual method of sampling, i.e., particulate sulfate plus sulfate from SO_2-filter reaction and SO_2-particulate reaction (during t_1). The sulfate on the half not covered with polyethylene will be that found by the usual method during t_1 plus that due to further exposure to SO_2 alone during t_2. A comparison of the results from the two HiVols yields the amount of spurious sulfate formed during t_2 by the reaction with the particulate matter alone, since the spurious sulfate formed in the filter during t_2, and the particulate sulfate plus all spurious sulfate formed during t_1, both will have been measured.

It should be noted that this method requires that the filters be uniform over their entire collection surface. Uniformity in flow characteristics is necessary so that the SO_2 (and/or the SO_4^{2-}) exposure per unit of filter area is uniform across the filter in period t_1; and uniformity in chemical composition is necessary so that uniform SO_2 exposure results in uniform spurious sulfate formation. The uniformity was checked by determining the sulfate found on replicate quarters of 52 HiVol filters collected in the usual way. The standard deviation between quarters for quartz-fiber filters was 2% of the sulfate found on a quarter, i.e., too small to be a problem in this work.

To recapitulate, the strategy outlined above gives: (1) the spurious sulfate formed by SO_2 exposure of particulate matter, subsequent to collection of the particulate matter; (2) the spurious sulfate formed by SO_2 exposure of a filter already exposed to SO_2; and (3) the spurious sulfate formed by SO_2 exposure of a virgin filter. The strategy does not give the spurious sulfate formed by SO_2 exposure to a fresh aerosol deposit, although in principle one could approach this condition to any arbitrary degree.

The procedures for chemical analysis in this work were as follows. The sulfate in the filters was extracted with water in the presence of strong-acid cation exchange resin at 60 °C for 2 h, and determined by $Ba(ClO_4)_2$ titration to the Thorin dye-indicator endpoint (*7, 8*) with photometric endpoint detection (*9*); the function of the resin was to remove cations from the sample and thus bring out dissolution of all sulfate including those of Ba, Pb, etc. (*10*). Sulfur dioxide, oxidized to sulfate in the H_2O_2 impingers, was determined straightaway on the impinger solutions by $Ba(ClO_4)_2$-Thorin titrimetry.

Table I. Data on $SO_2 \rightarrow SO_4^{2-}$ Conversion in pH-Neutral Quartz-Fiber Filters

	Tunnel aerosol		Rural aerosol	
	Run 1	Run 2	Run 3	Run 4
First exposure period (t_1)				
Minutes	183	729	183	737
SO_2 concentration, $\mu g/m^3$	—	150	—	(<7?)
Sulfate concentration,[a] $\mu g/m^3$	14.8	12.2	12.5	6.7
Spurious sulfate formed in bottom filter:				
μg per cm^2 filter	0.62	0.61	0.48	0.60
Equivalent $\mu g/m^3$	1.6	0.41	1.2	0.37
SO_2 exposure; μg per cm^2 filter	—	225	—	(<20?)
Second exposure period (t_2)				
Minutes	730	1648	730	1645
SO_2 concentration, $\mu g/m^3$	129	67	—	<10
Sulfate concentration,[a] $\mu g/m^3$	8.0	19.3	4.3	21.1
Spurious sulfate formed in bottom filter:[b]				
μg per cm^2 filter	0.17	0.088	0.34	0.19
Equivalent $\mu g/m^3$	0.076	0.018	0.11	0.025
SO_2 exposure, μg per cm^2 filter[c]	290	329	—	<75
Combined exposure periods ($t_1 + t_2$)				
Spurious sulfate in bottom filter, μg per cm^2 filter	0.79	0.69	0.82	0.79

[a] Sulfate found in top filter. [b] Sulfate increment during t_2. [c] Exposure during t_2.

Conversion of SO_2 in Quartz-Fiber Filters. It has been pointed out that the top filters in these experiments were pH-neutral quartz fiber to minimize SO_2 conversion therein. The inertness of these filters toward SO_2 was demonstrated by the procedure described above, using quartz-fiber filters for the top and bottom filters. The results of four tests are shown in Table I. Two of the the four tests were conducted inside of the Allegheny Tunnel where SO_2 levels on the order of 100 $\mu g/m^3$ are encountered. The other two tests were run in the ambient air near the tunnel where the SO_2 levels were substantially lower ($\lesssim$10 $\mu g/m^3$). Initially the filter is quite active for SO_2 conversion and the spurious sulfate builds up with a time constant depending on the SO_2 available until a level of about 0.7 to 0.8 μg per cm^2 of filter is reached. From then on, little or no further SO_2 is converted. If the sampling time is only a few hours or if the true sulfate level is low, the spurious sulfate from this cause can be considerable (e.g., 10% of the total sulfate in the t_1 period of Runs 1 and 3, Table I). For protracted exposures, the spurious sulfate from this cause would be insignificant (~300 μg in the case of a standard 8-in. × 10-in. HiVol filter) compared to the true sulfate or the SO_2 exposure.

Implicit in these experiments is the premise that none of the sulfate found on the bottom filter was due to aerosol penetration of the top filter, i.e., that the filtration efficiency of the quartz-fiber filter is essentially 100%. This premise was verified by running three quartz-fiber filters in a stack on one Hivol. If the sulfate on the second filter is due to penetration, there should be very much less sulfate found on the third filter. However, if the sulfate found on the second filter is due to SO_2 conversion, the third filter should have approximately the same amount of sulfate as the second (provided that the second filter has not removed a large fraction of the SO_2 reaching it).

Table II shows that the third filter has about as much sulfate as the second, implying that aerosol penetration is unimportant. This result, at a linear flow velocity of 37 cm/s or a volume flow rate of 0.9 m^3/min, does not support the claim (*11*) of substantial penetration by submicron aerosols through fiber filters at high flow rates. The data of Reference *11*, on glass-fiber filters, cannot distinguish between penetration and SO_2 conversion, and we suspect that the latter, together with possible loss of the largest particles by impaction on the inlet louvers of the filter housing as suggested by First (*12*), is the real cause of the reported "penetration".

Table II. Data on Filter Efficiency for pH-Neutral Quartz-Fiber Filters

	Sulfate found, μg per cm^2 filter
Top filter	46.85
Middle filter	0.38
Bottom filter	0.45

Conversion of SO_2 in Aerosol Deposits. During the same t_1 periods and at the same locations as those depicted in Table I, aerosol deposits also were collected on quartz-fiber filters in a second HiVol. For the t_2 period, one half of the aerosol deposit was covered with polyethylene and both halves of the filter were covered with a second quartz-fiber filter, as described above. The data, shown in Table III, show that the halves which were exposed to the SO_2 during t_2 have *less* sulfate than would be expected if the SO_2 did not react with the deposit to form sulfate. There was a problem of transfer of the particulate matter from the bottom filter to the top one by contact, with a corresponding transfer of ~0.5 μg sulfate per cm^2. (This was checked by the following experiment in the Allegheny Tunnel: A quartz-fiber filter with an aerosol deposit containing 20.4 μg sulfate per cm^2 was used as the third filter of a 3-filter stack in a subsequent run. The transfer was evaluated by sulfate analysis of the middle filter taking SO_2 interaction with the middle filter into account.)

Even with transfer taken into account, the estimate of spurious sulfate formed in the deposit during t_2 (i.e., the sulfate found minus the minimum sulfate expected, Table III) is greater than zero in only half of the runs. Apparently there is a 5% random error between sulfate found and the minimum expected; part of the error consists of the ±2% error due to filter nonuniformity. Because of the uncertainty in the amount of sulfate transferred in the four runs, it *cannot* be asserted

Table III. Data on $SO_2 \rightarrow SO_4^{2-}$ Conversion in Aerosol Deposits

	Tunnel aerosol		Rural aerosol	
	Run 1	Run 2	Run 3	Run 4
Aerosol collection period (t_1)				
Particulate deposited, $\mu g/cm^2$	126	303	85	219
Sulfate found, $\mu g/cm^2$	6.7	20.2	5.0	10.0
SO_2 exposure, $\mu g/cm^2$	—	224	—	(<10?)
Aerosol-deposit SO_2 exposure period (t_2)				
Sulfate found, $\mu g/cm^2$	6.5	19.1	5.1	9.0
Sulfate expected,[a] $\mu g/cm^2$:				
Maximum[b]	6.9	20.3	5.3	10.2
Minimum[c]	6.4	19.8	4.8	9.7
SO_2 exposure, $\mu g/cm^2$	293	321	—	<62

[a] Sulfate expected on the assumption that no spurious sulfate was formed in the deposit during t_2. [b] Consists of the sulfate found for period t_1 (above) plus the spurious sulfate formed in the filter during t_2 (see Table I). [c] Minimum equals maximum minus allowance for the possibility that 0.5 μg sulfate per cm^2 was transferred to the top filter during t_2.

Table IV. Data on $SO_2 \rightarrow SO_4^{2-}$ Conversion in Various Filters

	pH-neutral quartz fiber[a]	Strengthened quartz fiber[b]	Glass fiber[c]				Membrane[d] Cellulose Ester[e]	Membrane[d] Fluoropore[f]	
Sampling site	Tunnel	Tunnel	Tunnel	Tunnel	Rural	Rural	Tunnel	Tunnel	Rural
Sampling time, min	605	393	5816	5697	5858	5873	633	8301	7778
Sample volume, m^3	547	391	3294	4712	5308	5571	28.3	509	467
SO_2 concentration, $\mu g/m^3$	136	143	125	125	12	16	187	155	26
Sulfate concn[g], $\mu g/m^3$	34.8	24.9	13.2	13.2	10.5	8.7	19.1	10.0	7.3
Gross particulate,[g] $\mu g/m^3$	313	320	154	154	23.4	26.1	284	141	37.7
Spurious sulfate formed:									
μg per cm^2 filter	0.42[h]	15.2	4.3	2.0	14.6	33.7	~0.8[i]	0(<0.07)[j]	0.04
Equivalent $\mu g/m^3$	0.31[h]	15.8	0.53	0.18	1.12	2.46	~2.8[i]	0(<0.013)[j]	0.008
SO_2 exposure, μg per cm^2 filter	183	137	1011	1449	160	216	54.6	815	125
pH of blank filter	5.6[k]	9.7[k]	9.9[k]	9.9[k]	9.9[k]	9.9[k]	6.5[l]	5.6[m]	5.6[m]

[a] Tissuquartz 2500 QAO, Pallflex Corp., standard 8-in. × 10-in. HiVol filter, deposit area 406 cm^2; second and third filters of a 3-filter stack of pH-neutral quartz-fiber filters. [b] Tissuquartz 2500 QAOS, Pallflex Corp., standard 8-in. × 10-in. HiVol filter, deposit area 406 cm^2; third filter, behind two pH-neutral quartz-fiber filters in a 3-filter stack. [c] Gelman Type A standard 8-in. × 10-in. HiVol filter, deposit area 406 cm^2; second filter of a 2-filter stack; top filter is pH-neutral quartz fiber. All 4 runs were during the same period in 1974. [d] 142-mm diameter filters, 0.2-μm pore flow diameter, Millipore Corp.; deposit area 97 cm^2. [e] Second of two mixed cellulose-ester filters. [f] Third, or second and third averaged, of three stacked Fluoropore filters. "Fluoropore" is Millipore Corp. trademark for filters of poly(tetrafluoroethylene) (Teflon) backed with polyethylene. [g] By analysis of the first filter of the stack. [h] Average of the second and third filters of the 3-filter stack. [i] Average of 4 determinations. Uncertainty is 50% of the number shown. [j] From 3 determinations. [k] Whole 8-in. ×-10 in. filter extracted with 200 ml deionized water of pH 5.9. [l] Whole 142-mm filter extracted with 100 ml deionized water of pH 5.9. [m] Whole 142-mm filter extracted with 100 ml deionized water of pH 5.5.

that *no* SO_2-to-sulfate conversion occurred in the aerosol deposits; but it can be said that the data show no evidence of such conversion.

For the tests conducted in the Allegheny Tunnel, the aerosol deposit is typical of that from vehicle (both gasoline and diesel) traffic (*6*). The other tests deal with a rural aerosol. The conclusion that SO_2 conversion on the aerosol deposit is unimportant should hold for aerosols in other locations that are similar. It should be noted, however, that the low SO_2 levels in the rural air render the null result less definitive than it could have been if higher SO_2 levels had been encountered.

Conversion of SO_2 in Other Types of Filters. By including various filter types as backup filters in regular aerosol sampling runs, behind a pH-neutral quartz-fiber filter or a membrane filter, other filter types were evaluated with the results shown in Table IV. Conversion in pH-neutral quartz-filters is again seen (perhaps less than before, judging from the μg per cm^2 of filter). The cellulose-ester membrane filter appears comparable in terms of μg per cm^2 of filter, but the spurious effect seems greater as a fraction of the actual sulfate or the SO_2 exposure, owing to the flow-rate penalty of the membrane filter; this should be checked further, as the uncertainty is large.

The spurious conversion is at a minimum in the case of the poly(tetrafluoroethylene) (Teflon) membrane filters. The advantage over pH-neutral quartz is less than meets the eye because of the flow-rate penalty but it is still true that Teflon membrane filters (Fluoropore) give the least conversion of SO_2 to spurious sulfate of all filter types tested. (It should be added that sulfate penetration in the 0.2-μm pore size Fluoropore filters was found to be effectively zero, by use of the 3-filter-stack technique described earlier for the pH-neutral quartz-fiber filters.)

One of the glass-fiber filters gave good results on a $\mu g/m^3$ basis (0.18), but apparently only because of the protracted sampling; the spurious sulfate per cm^2 (2.0 μg) would be serious in a run of, say, 12 h. We have sought to rationalize the incoherent pattern of spurious sulfate formation on glass-fiber

filters as seen in Table IV. One can imagine that a difference in the trace-gas composition in the tunnel relative to the ambient air might result in the obvious greater propensity to spurious sulfate formation in the ambient case. We have no rationale for the other anomalies in the glass-fiber results.

In some of the instances shown in Table IV, the amount of spurious sulfate renders the glass-fiber filter unacceptable not only for sulfate but even for gross mass determination. The strengthened quartz-fiber filter is as bad or worse; spurious sulfate can be seen to have been 64% as much as the true sulfate and 5% as much as the amount of gross particulate matter, by virtue of conversion of 7% of the SO_2 to which the filter was exposed.

The data suggest that egregious amounts of spurious sulfate are a consequence of filter alkalinity. This should be studied further, because certain procedures (*13*) for imparting strength to glass- or quartz-fiber filters involve treatment with alkali. The filter types that give the most spurious sulfate (Table IV) are also the ones that give aqueous extracts that are alkaline.

Summary. We find that the formation of spurious sulfate in filter sampling can be quite minimal or can be quite extensive. It has to do primarily with the filter medium and not the aerosol deposit. The amount formed depends very much on the type of filter. Of the types evaluated, poly(tetrafluoroethylene) membrane and pH-neutral quartz fiber filters are the best. At least in the case of the latter type of filter, a saturation effect seems to exist so that, given the opportunity for a sufficiently long sampling period, the error relative to the true sulfate can be brought within bounds.

ACKNOWLEDGMENT

We thank William H. Sherlock, former Executive Director, Pennsylvania Turnpike Commission, and the many members of his organization who helped us in carrying out these experiments. We also thank Douglas E. McKee, of the Ford Research Staff, for his assistance with the experiments.

LITERATURE CITED

(1) R. E. Lee, Jr., and J. Wagman, *J. Am. Ind. Hyg. Assoc.*, **27**, 266–271 (1966).
(2) J. W. Coffer, "SO_2 Oxidation to Sulfate on a High Volume Air Sampler", M.S.E. Thesis, University of Washington, 1974; J. W. Coffer, C. McJilton, and R. J. Charlson, Paper No. 102, Division of Analytical Chemistry, American Chemical Society, 167th National Meeting, Los Angeles, Calif., April 3, 1974.
(3) W. R. Pierson and W. W. Brachaczek, *Rubber Chem. Technol.*, **47**, 1275–1299 (1974).
(4) W. R. Pierson and W. W. Brachaczek, "Airborne Particulate Debris from Rubber Tires", in Proceedings of Conference on Environmental Aspects of Chemical Use in Rubber Processing Operations (Akron, Ohio, March 12–14, 1975), Franklin A. Ayer, compiler, EPA-560/1-75-002 (Office of Toxic Substances, U.S. Environmental Protection Agency, July 1975), pp 217–273, 306–311.
(5) W. R. Pierson and W. W. Brachaczek, *J. Air Pollut. Control Assoc.*, **25**, 404–405 (1975).
(6) W. R. Pierson and W. W. Brachaczek, Paper 760039 presented at SAE Automotive Engineering Congress, Detroit, Mich., February 1976.
(7) J. S. Fritz and S. S. Yamamura, *Anal. Chem.*, **27**, 1461 (1955).
(8) R. S. Fielder and C. H. Morgan, *Anal. Chim. Acta*, **23**, 538 (1960).
(9) J. W. Butler and D. N. Locke, *J. Environ. Sci. Health—Environ. Sci. Eng.*, **A11**, 79 (1976).
(10) O. Samuelson, "Ion Exchange Separations in Analytical Chemistry", John Wiley & Sons, New York, 1963, pp 247–249.
(11) A. L. Cohen, *Environ. Sci. Technol.*, **7**, 60–61 (1973).
(12) M. W. First, *Environ. Sci. Technol.*, **7**, 181 (1973).
(13) A. L. Benson, P. L. Levins, A. A. Massucco, D. B. Sparrow, and J. R. Valentine, *J. Air Pollut. Control Assoc.*, **25**, 274–277 (1975).

William R. Pierson*
Robert H. Hammerle
Wanda W. Brachaczek

Ford Motor Company
Research Staff
P. O. Box 2053
Dearborn, Mich. 48121

RECEIVED for review February 18, 1976. Accepted July 6, 1976.

Modified Buffer for Use with Fluoride-Selective Electrodes

Sir: The addition of a total-ionic strength buffer (TISB) containing Na salts (1.9 M) to solutions when estimating F^- using a fluoride-selective electrode is now a well-established procedure (*1*). The purposes of this buffer are: (i) to provide a background of high-ionic strength, (ii) to adjust the pH, (iii) to release any fluoride bound to metals by the inclusion of a stronger complexing agent (*trans*-1,2-diaminocyclohexane-*N,N,N',N'*-tetraacetic acid (CDTA)). However, several workers (*2–4*) have measured association between Na^+ and F^- and their results would suggest the formation of an appreciable concentration of NaF^0 in TISB, thus partially negating some of the decomplexing function. The degree of association between K^+ and F^- is much less than with the Na salt (*2*) so that replacement of Na salts by K salts in TISB should be an improvement. To assess the degree of ion-pairing, measurements were made with an Orion Research Inc. fluoride-selective electrode (94-90) and double-junction reference (90-02-00) 3.5 M KCl in outer compartment, immersed in TISB made to the following compositions: XCl = 1.0 M, acetic acid = 0.25 M, X acetate = 0.75 M, CDTA = 0.011 M, with X = Na or K buffers were mixed with an equal volume of NaF solutions to give concentrations 5×10^{-7}–5×10^{-3} M. Other measurements were also made in solutions 5×10^{-4} M without buffer but containing 4 M NaCl or KCl because it should be easier to detect ion-pairing at these high concentrations.

For concentrations 5×10^{-5}–5×10^{-3} M NaF, an excellent fit to the Nernst equation was found with both buffers (see Figure 1). There was a shift between the two lines with $E_{Na} - E_K = 6.0 \pm 0.4$ mV. A larger difference was observed between the emf's in 4 M NaCl and KCl with $E_{Na} - E_K = 19.7 \pm 0.4$ mV. The sign of these differences is consistent with greater ion-pairing in the Na salt solutions than in the K salt solutions. By making some reasonable assumptions about activity coefficients, the magnitude of these differences can be shown to be in agreement with previous estimates of association constant and suggest that 15–20% of total fluoride is present as NaF^0 in TISB prepared from Na salts. Measurements made at concentrations below 5×10^{-5} M were of lower precision because of slow equilibration of the electrode. The time to reach a slow drift (0.1 mV/5 min) often exceeded 30 min and there was no significant difference between the Na and K buffers in this respect. Omission of CDTA from the buffers did not reduce this time markedly. At concentrations below 5×10^{-5} M in the Na buffer, the results deviated from the linear graph (see Figure 1). This deviation was much less for results from the K buffer. Other workers have noted a similar nonlinearity using TISB and have attributed the effect to the presence of F as an impurity in the buffer salts (*5, 6*). To estimate the impurities, measurements were made in buffers diluted with an equal volume of water not containing

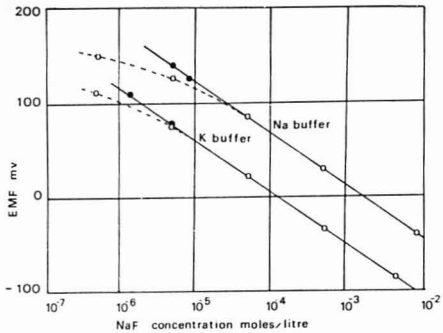

Figure 1. Emf vs. log(NaF concentration mol/l.) for Na and K buffers

All points from the K buffer have been displaced 60 mV downward for greater clarity. (O) Experimental points; (●) points in the region $<10^{-5}$ M NaF for which the nominal concentrations have been corrected for the presence of F impurity in the buffer

intentionally-added F. By extrapolation of the linear portion of the graphs values of 4×10^{-6} and 1×10^{-6} M were derived as the contributions from impurities in the Na and K buffers, respectively. When correction was made to the nominal concentrations, the linear region of the graph was extended down to 10^{-6} M. Although a generalization cannot be made on the basis of results with one batch of salts, it may be noted that Mesmer (*6*) in a similar experiment found less F in 1 M KCl than in 1 M NaCl.

It follows from this comparison that in order to avoid possible complications from ion-pairing and to be consistent with the use of KF as primary standard (*2*) that TISB or other high-ionic strength solutions be prepared from K salts rather than Na salts. As a possible additional benefit from this change, K salts may introduce lower F impurity than Na salts resulting in an extended linear calibration and reduction in the minimum detectable concentration.

LITERATURE CITED

(1) J. E. Harwood, *Water Res.*, **3**, 273 (1969).
(2) R. A. Robinson, W. C. Duer, and R. G. Bates, *Anal. Chem.*, **43**, 1862 (1971).
(3) W. C. Duer, R. C. Robinson, and R. G. Bates, *J. Chem. Soc., Faraday Trans., 1*, **68**, 716 (1972).
(4) J. N. Butler and R. Huston, *Anal. Chem.*, **42**, 1308 (1970).
(5) M. S. Frant and J. W. Ross, *Anal. Chem.*, **40**, 1169 (1968).
(6) R. E. Mesmer, *Anal. Chem.*, **40**, 443 (1968).

J. Bagg

Department of Industrial Science
University of Melbourne
Parkville, Victoria 3052
Australia

RECEIVED for review May 3, 1976. Accepted June 30, 1976.

Chromatographic Analysis of Gaseous Products from Pyrolysis of Organic Wastes with a Single Column

Sir: The operation and optimization of a pilot plant at which organic wastes, such as wood shavings, solid municipal waste, or rice hulls are pyrolyzed requires a method of analysis of the gaseous products. The gases detected were H_2, N_2, CO, CO_2, H_2O, CH_4, C_2H_4, C_2H_6, C_6H_6, and C_7H_8. Our objective was to obtain a method of determination for these gases as simply and rapidly as possible.

A search of the literature failed to show a simple separation of this particular combination of gases. Hollis and Hayes (*1*) showed that H_2, N_2, O_2, Ar, and CO could be separated at −78 °C on a Porapak Q column. In the same paper, they indicated that the column could also separate H_2, air, CO, CH_4, CO_2, C_2H_4, C_2H_6, and H_2O in that order at room temperature. This separation was made by Cross (*2*). Papic (*3*) later separated C_1 through C_4 hydrocarbons, also on a column of Porapak Q. Many people have combined columns to achieve better separations (*4–7*). Stufkens and Bogaard (*8*) made a separation of N_2, O_2, CO_2, C_2H_6 and heavier hydrocarbons, including C_6H_6 and C_7H_8 using a Porapak R column operated between −10 °C and 230 °C. This correspondence describes a method whereby the above mentioned gases may be separated for determination employing a single column.

EXPERIMENTAL

Apparatus. A Hewlett-Packard 5750 gas chromatograph equipped with temperature programming and a 0.5-ml gas sampling valve was used. The dual stainless steel columns (10 ft × ⅛ in. i.d.) were packed with 50–80 mesh Porapak QS and modified with 2% terephthalic acid.

Method. The separation was carried out as follows: prior to sample injection, the oven was cooled to room temperature (~26 °C). This was best achieved by opening the oven door and leaving it open

Table I. Analytical Conditions

Sample	
Size:	0.5 ml
Column	
Length:	10 ft
Diameter:	⅛-in. i.d.
Material:	Stainless steel
Packing:	Porapak QS
Packing size:	50–80 mesh
Packing modifier:	2% Terephthalic acid
Carrier gas:	Helium
Temperatures	
Column:	Room temperature (~26 °C) to 200 °C
Primary isothermal period:	2 min
Programming rate:	60 °C/min
Final isothermal rate:	Balance of analysis
Injection port:	230 °C
Detector:	260 °C
Sample loop:	Room temperature (~26 °C)
Recorder	
Chart speed:	2.00 in./min for 4 min 0.25 in./min for balance
Detector	
Type:	Thermal conductivity
Bridge current:	160 mA

Table II. Individual Analyses (mol %)

Sample	H_2	N_2	CO	CH_4	CO_2	C_2H_4	C_2H_6	C_6H_6	C_7H_8
120275 R1	17.7	1.3	37.6	17.9	25.0	3.8	0.9	1.2	0.3
120275 R2	19.8	0.5	39.6	19.4	22.4	3.7	0.9	1.3	0.3
120275 R3	11.5	0.8	41.8	18.8	20.9	3.6	0.8	1.0	0.2
120375 R1	18.0	0.7	30.1	18.6	19.4	3.5	0.8	1.2	0.2
120375 R2	19.0	0.6	34.4	17.9	19.7	3.6	0.9	1.4	0.3
120375 R3	19.5	0.7	33.8	19.1	21.6	3.5	0.9	1.3	0.3

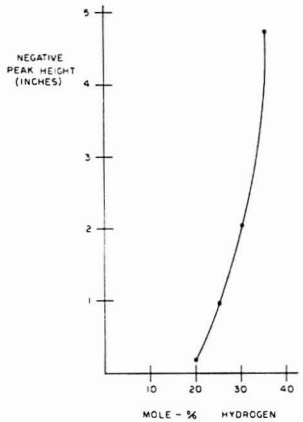

Figure 1. Typical negative peak height curve

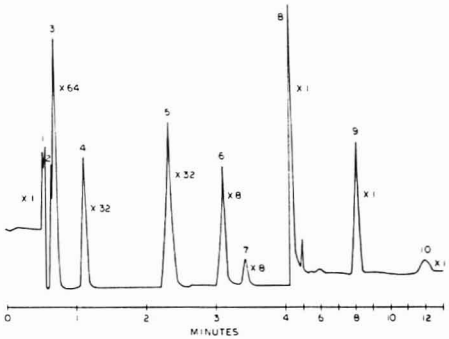

Figure 2. Typical chromatogram of pyrolysis gas

Peak identification: (1) hydrogen, (2) nitrogen (includes oxygen), (3) carbon monoxide, (4) methane, (5) carbon dioxide, (6) ethylene, (7) ethane, (8) water, (9) benzene, (10) toluene

throughout the initial isothermal period. The gas sample, collected at the pilot plant in a 40-ml Whitey stainless steel gas sampling bulb, was allowed to purge through the 0.5-ml gas sampling valve until the system came to atmospheric pressure. The sample was then quickly injected.

The oven was held at room temperature with the oven door open for 2 min. Temperature was then raised at 60 °C/min to a maximum of 200 °C. In order to save paper, the chart speed which had been run at 2 in./min was reduced to 0.25 in./min 4 min into the analysis. Complete analytical conditions may be found in Table I.

Calibration. The system was calibrated by analyzing a purchased (Union Carbide Corporation, Linde Division Primary Standard) calibration mixture. The relationship between peak area and mole percentage was found using the cut and weight method (*9*). Because of the nonlinearity of the hydrogen response (*10*), a calibration curve was made for this gas employing separate standards (Alltech Associates Calibration Gas). The relationship between the negative peak height (*10*) and the mol % was plotted, as shown in Figure 1, and compared to samples. Finally, aromatics were calibrated using a 3-μl injection of a solution of benzene (50 ml/l.) and toluene (10 ml/l.) in chloroform. A relationship between liquid volume and mol % was developed employing the ideal gas law. Water was neither calibrated nor calculated for.

RESULTS

A typical chromatogram is shown in Figure 2. Resolution between peak 2 (nitrogen) and peak 3 (carbon monoxide) is increased as the room temperature is lowered. Results of the analysis of some samples collected from the pyrolysis of rice hulls are shown in Table II.

ACKNOWLEDGMENT

The authors express their deep gratitude to W. Martin Fassell, Donald W. Bridges, and Richard C. Dietz for their assistance and encouragement in preparing this work.

LITERATURE CITED

(1) O. L. Hollis and W. V. Hayes, "Gas Chromatography 1966", A. B. Littlewood, Ed., Institute of Petroleum, London, 1967, pp 57–70.
(2) R. A. Cross, *Nature (London)*, **211**, 409 (1966).
(3) M. Papic, *J. Gas Chromatogr.*, **6**, 493 (1968).
(4) R. R. Forsey, *J. Gas Chromatogr.*, **6**, 555 (1968).
(5) R. I. Jerman and L. R. Carpenter, *J. Gas Chromatogr.*, **6**, 298 (1968).
(6) H. W. J. Sears, *AMDEL Bull.*, **6**, 47 (1968); as cited in *Anal. Abstr.*, **18**, Abstr. 1033 (1970).
(7) J. S. Archer, *J. Inst. Fuel*, **43**, 56 (1970).
(8) J. S. Stufkens and H. J. Bogaard, *Anal. Chem.*, **47**, 383 (1975).
(9) H. M. McNair and E. J. Bonelli, "Basic Gas Chromatography", 5th ed., Varian Aerograph, Walnut Creek, Calif., 1969, p 154.
(10) J. E. Purcell and L. S. Ettre, *J. Gas Chromatogr.*, **3**, 69 (1965).

Peter T. Brodowski
Norma B. Wilson
William J. Scott* [1]

Resource Recovery Systems Division
Barber-Colman Company
Irvine, Calif. 92714

RECEIVED for review May 10, 1976. Accepted June 24, 1976.

[1] Present address, 515 Palmetto, Pasadena, Calif. 91105.

Free Energy Correlations with Solvatochromic Red Shifts for Indicators in Aprotic Solvents

Sir: In a recent communication to this journal (*1*), experimental evidence was presented for empirical correlations between the red shifts for a set of solvatochromic indicators and the Gibbs free energy values (ΔG_f) for the equilibrium in Equation 1.

$$p\text{-}FC_6H_4OH + :B \rightleftharpoons p\text{-}FC_6H_4OH \ldots :B \text{ (in } CCl_4 \text{ soln)} \quad (1)$$

It was suggested that the observed trend can be interpreted in terms of a systematic response of the solvatochromic dye to changes in the Lewis basicity for polar aprotic species (:B). Since the completion of that project, related reports have appeared elsewhere which necessitate an extension of my preceding discussion and conclusions.

Kamlet and Taft (*2*) have identified relationships between solvatochromic shifts for 4-nitroanilines and 4-nitrophenols interacting with a wide range of hydrogen bond donor-acceptor pairs (HBA) in equilibrium 2.

$$X\text{-}C_6H_4\text{-}NH_2 + HBA \rightleftharpoons X\text{-}C_6H_4\text{-}NH_2 \ldots HBA \quad (2)$$

They found that their β-scale for solvent basicities derived from Equation 2 is linearly related to pK_f values for the same equilibrium. However, by using published data for *bathochromic dyes* (i.e., Phenol blue, Nile blue A oxazone, and Brooker's dye VII) in 22 solvents, it can be verified that no general correlation exists between the transition energies (E_T) of the indicators and the β-values of Kamlet and Taft. It should be noted that a nonlinear increasing trend does occur between E_T for Brooker's dye VII and β for five hydrogen bond donor solvents (i.e., the lower alcohols and dimethylformamide).

A second paper which more closely relates to my previous communication is the report of Spencer, Harner, and Penturelli (*3*) on the determination of thermodynamic differences attributable to solvation effects upon the hydrogen bonding equilibrium in Equation 3.

$$C_6H_5OH \ldots S_A + (CH_3)_2SO \rightleftharpoons C_6H_5OH \ldots OS(CH_3)_2 + S_A \quad (3)$$

They concluded that detectable specific interactions by the acceptor solvent (S_A) occur in all instances, including cyclohexane and carbon tetrachloride. Their choice of DMSO as the reference base appears to have been an excellent one since the results of Arnett, Mitchell, and Murty indicate that the alkyl sulfoxides and phosphates are among the stronger Lewis bases in hydrogen bond donor–acceptor equilibria (*4*); and likewise, for a given bathochromic indicator, the lowest E_T value was recorded in DMSO among all of the aprotic solvents investigated to date (*1*). However, Spencer, Harner, and Penturelli (*3*) found no general trends between ΔH, ΔS, or K_f for Equation 3 and the dielectric constant or other macroscopic properties of the solvent (S_A).

Equilibrium constant values for Equation 3 are listed in Table I along with the transition energies (E_T) for Phenol blue and related solvatochromic indicators in each of the six aprotic bases as S_A. The graphs in Figure 1 were derived from those data but expressed as E_T vs. $-\Delta G_f$. Slopes for the lines range from as low as 1.18 for Phenol blue derivatives to 1.65 for Phenol blue and 2.72 for Brooker's dye VII.

It is not fully unexpected that the empirical linear free energy (LFE) plots in Figure 1 would include within the same function the broad range of solvent types from nonpolar to polar aprotic Lewis bases as well as the weak hydrogen bond

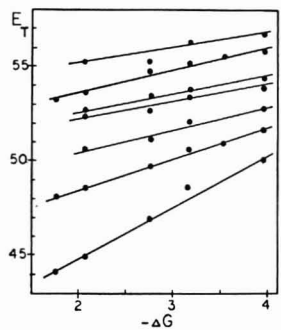

Figure 1. Correlation of the transition energy (E_T) for the indicators in Table I with the ΔG_f for the C_6H_5OH:DMSO complex in the solvents: chloroform; 1,2-dichloroethane; benzene; carbon tetrachloride; carbon disulfide; cyclohexane

Table I. Summary of Data Used in Correlations with Hydrogen Bonding Donor–Acceptor Equilibria

	Transition Energies (kcal/mol) in the solvents					
Bathochromic dye	C_6H_6	CS_2	CCl_4	$CHCl_3$	C_6H_{12}	$ClCH_2CH_2Cl$
Phenol blue (PB)[a]	49.72	50.87	50.60	48.13	51.61	48.58
PB derivatives: *N*-(4-substituted phenyl)quinone monoimimes[b]						
$-NH_2$ (4)	55.2	...	56.3	...	56.7	55.2
-3,5-R,R-NH_2 (5)	52.6	...	53.4	...	53.8	52.4
$-NHCH_3$ (3)	53.5	...	53.8	...	54.3	52.7
$-N(CH_3)_2$ (2)	51.1	...	52.1	...	52.7	50.7
Nile blue A oxazone (NBAO)[c]	54.87	55.58	55.09	53.24	55.78	53.54
Brooker's dye VII[d]	46.9	...	48.7	44.2	50.0	45.0
K_f for C_6H_5OH–DMSO complex in solv.[e]	106	381	215	19.4	811	33.0

[a] Data from J. Figueras (*5*) except new exptl value in CS_2. [b] Derivatives numbered (2–5) as designated by Figueras (*5*). [c] Results obtained by M. Davis and H. Hetzer, *Anal. Chem.*, **38**, 451 (1966). [d] Values from L. Brooker et al., *J. Am. Chem. Soc.*, **87**, 2443 (1965). [e] Formation constants (at 20 °C) reported by J. Spencer et al. (*3*).

donor, $CHCl_3$. The fundamental work on Phenol blue by Figueras (5), as well as ours (6), has demonstrated that the solvent polarity contribution to the free energy transition (E_T) of the dye can be derived from the two-parameter McRae equation; and the influence of a given hydrogen bond donor (*m*-cresol or $CHCl_3$) conforms to a simple additivity as a perturbation energy contribution. However, in equilibrium 3, chloroform serves as an acceptor (HBA) toward phenol and shows the regular behavior in the LFE function of the aprotic solvents. Because of the high correlation coefficients between the E_T values for all of the structurally related dyes in Table I, it appears that this whole series of bathochromic dyes may share a common phenomenological response to the Lewis basicity of the solvent.

Finally, it should be clear that the equilibria in Equations 1 and 3 are nonequivalent chemical processes and should have dissimilar E_T vs. ΔG_f plots. The solvent displacement reaction with DMSO assigns a measurable Lewis base strength to CCl_4 with reference to phenols as hydrogen bond donors. The available thermodynamic data for the two equilibria are not overlapping so that direct comparisons of solvent basicity between the two processes cannot be made at the present time. When a weaker Lewis base (i.e., pyridine) is substituted for DMSO in equilibrium 3, the two hydrogen bond donor solvents, chloroform and 1,2-dichloroethane, compete more effectively with phenol to interact with the HBA; and the LFE relationship fails (7). Although the LFE function for reaction 3 includes only the weaker aprotic bases, similar correlations have *not* been observed between thermodynamic parameters related to solvent basicity and the blue shift scales proposed in the past as measures of solvent polarity in aprotic media.

LITERATURE CITED

(1) O. W. Kolling, *Anal. Chem.*, **48**, 884 (1976).
(2) M. Kamlet and R. W. Taft, *J. Am. Chem. Soc.*, **98**, 377 (1976).
(3) J. Spencer, R. Harner, and C. Penturelli, *J. Phys. Chem.*, **79**, 2488 (1975).
(4) E. Arnett, E. Mitchell, and T. Murty, *J. Am. Chem. Soc.*, **96**, 3875 (1974).
(5) J. Figueras, *J. Am. Chem. Soc.*, **93**, 3255 (1971).
(6) O. Kolling and J. Goodnight, *Anal. Chem.*, **45**, 160 (1973).
(7) J. N. Spencer et al., *J. Phys. Chem.*, **80**, 811 (1976).

Orland W. Kolling

Chemistry Department
Southwestern College
Winfield, Kansas 67156

RECEIVED for review May 17, 1976. Accepted July 14, 1976.

Application of a Vidicon Tube as a Multiwavelength Detector for Liquid Chromatography

Sir: In this report, we describe preliminary data for the application of a silicon target vidicon as a multiwavelength detector for liquid chromatography (LC). Most photometers currently used as uv detectors in LC are limited to one or two wavelengths. For these systems, the selectivity of any analysis is limited to that which can be obtained via the chromatographic process, and the analytical wavelength is seldom optimized for all components to be detected. The vidicon detector, when used with appropriate optics, is capable of monitoring many wavelength resolution elements simultaneously (*1–3*), and as such should serve as a very versatile detector for liquid chromatography (*4, 5*).

The vidicon spectrometer system used in this work has been described in detail previously (*1, 2*). The liquid chromatograph was assembled from commercially available components and is similar to that described earlier (*6*) except that the flow cell from a stopped-flow mixing system (Aminco-Morrow Model B30-68109; American Instrument Co., Silver Spring, Md. 20910) modified by replacing the Teflon input chamber by a Teflon exhaust chamber, was used as the observation cell. No attempt was made to optimize the performance of the chromatographic system. Spectral data were collected, processed, and displayed by an on-line computer.

An aqueous mixture of uric acid, theophylline, and phenobarbital was selected as an illustrative example (*7*). Uric acid is an important biological compound and phenobarbital is often included in theophylline preparations. These compounds were eluted from an anion exchange column with an ammonia buffer at pH 10. The performance of the column had been degraded by previous operation. Spectra in the range of 225 to 450 nm were recorded every 10 s. Figure 1 represents the spectra after 220, 330, and 350 s for uric acid, theophylline, and phenobarbital, respectively, added to and eluted from the column separately. Figure 2 represents the absorbance measured at 10-s intervals at the absorbance maximum for each of the respective components. The spectra show that there is no wavelength within this range at which phenobarbital is free of interference from the other two components and, similarly, that there is no wavelength at which theophylline is free of interference from uric acid. The elution peaks show that uric acid is reasonably well separated from the other two components, but that the two drugs are poorly separated. These observations will be useful in interpreting data presented below.

Figures 3*A* and 3*B* represent spectra at selected times during the elution of a mixture (0.83 μg each) of the compo-

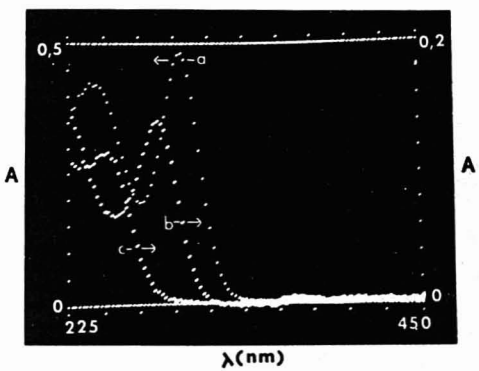

Figure 1. Absorption spectra of uric acid, theophylline, and phenobarbital.

All compounds were added to and eluted from the cation exchange column separately. Eluting reagent was 0.1 M ammonia buffer at pH 10. (*a*) Uric acid (5 μg) at 220 s, (*b*) Theophylline (2 μg) at 330 s, and (*c*) Phenobarbital (2 μg) at 350 s

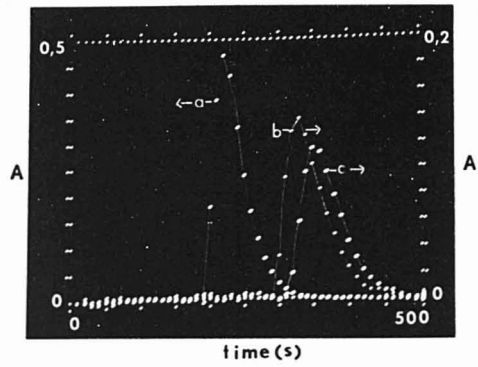

Figure 2. Absorbance vs. time for elution of pure samples of uric acid, theophylline, and phenobarbital

(*a*) Uric acid monitored at 290 nm, (*b*) Theophylline monitored at 275 nm, and (*c*) Phenobarbital monitored at 245 nm

nents. The spectra at 220 and 300 s in Figure 3*A* correspond closely to the spectra of uric acid and theophylline in Figure 1, suggesting that reasonably pure components are eluting at these times (see Figure 2). Figure 3*B* represents spectra at times when theophylline and phenobarbital are eluting together. The peak near 275 nm results almost exclusively from theophylline (see Figure 1) while the absorbance at shorter wavelengths result from both drugs.

Figures 4*A* and 4*B* represent absorbance vs. elution time at selected wavelengths. Figure 4*A* represents the absorbance at 290 nm (curve *a*) and at 275 nm (curve *b*). Curve *a* is recorded at the absorption maximum for uric acid and curve *b* is recorded at the absorption maximum of theophylline where phenobarbital does not interfere. Thus, uric acid could be determined with maximum sensitivity from the first peak in curve *a* and theophylline could be determined from the second peak in curve *b* without interference from phenobarbital even though the two drugs are not well separated. If either 275 or 290 nm were selected for both uric acid and theophylline, then small fluctuations in wavelength settings would have greater effects on one of the components than is the case when absorption maxima are used. Figure 4*B* represents the elution curves recorded at 245 nm where all components absorb. Uric acid could be quantified from the first peak, and some functions of the sum of the two drugs could be quantified from the second peak. Actually, since theophylline could be determined at each point from the peak at 275 nm in Figure 4*A*, the second peak in Figure 4*B* could be "corrected" for absorbance due to this component, leaving at least an estimate of the absorbance due to phenobarbital. These data were not treated in this fashion because the concept is relatively straightforward, but more importantly because we do not feel it would represent the best use of the data which are available from this type of experiment.

It should be noted that the data displayed in Figures 3 and 4 were selected from a large volume available in the computer. In other words, during a 400-s run, we would have collected 40 complete spectra and these spectra would be more effective in differentiating quantitatively between the two drugs than would the simpler two-wavelength approach mentioned above. For example, we have used multiwavelength data and matrix algebra to resolve two-, three- and four-component mixtures of compounds whose spectra overlap significantly (*8*). We suggest that the most effective use of the data available from the experiments described above, would be to use such a multiwavelength approach to resolve the effluent quantitatively at different points in time and then to use numerical integration methods to quantify each component in the original sample. In fact, if one were attempting to resolve these components in an otherwise clean matrix, then there would be little advantage in attempting to separate them on the ion-exchange column used in this work. On the other hand, if they were in a complex matrix, then the separation step could be useful in isolating the drugs into a two-component mixture and the multiwavelength detector could alleviate the need for a complete separation. We are presently working on software which will permit us to combine the mutliwavelength approach with numerical integration methods for chromatographic applications.

We have already suggested that one potential advantage of the rapid scanning detector for components which are well separated from others is the ability to monitor these components at or near their absorption maxima. We believe there are other useful features of the multiwavelength data. Kissinger et al. (*9*) have suggested that liquid chromatography

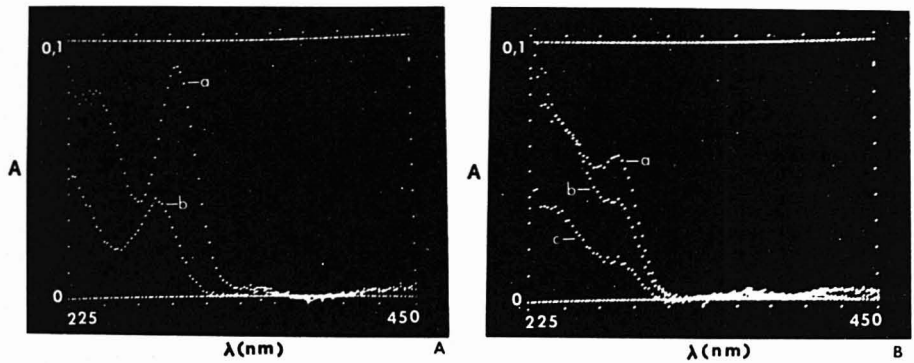

Figure 3. Absorption spectra during elution of a mixture of uric acid, theophylline, and phenobarbital (0.83 μg each)

(*A*) Spectra at 220 (*a*) and 300 (*b*) s and (*B*) Spectra at 330 (*a*), 350 (*b*), and 380 (*c*) s

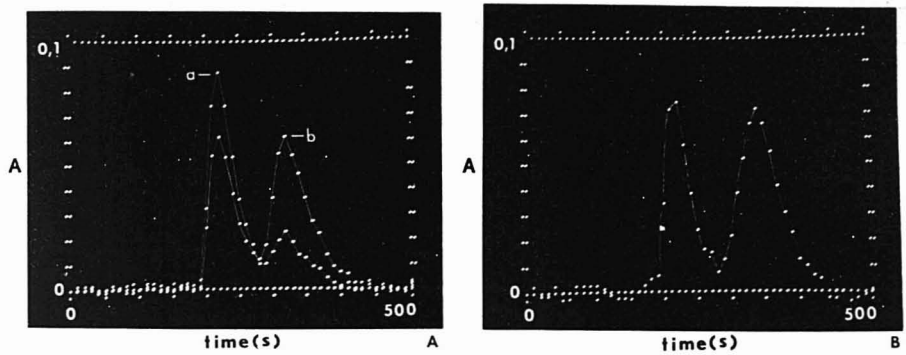

Figure 4. Elution peaks for a mixture of uric acid, theophylline, and phenobarbital

(*A*) Peaks monitored at 290 (*a*) and 275 (*b*) nm and (*B*) Peaks monitored at 245 nm

with electrochemical detection (LCEC) may represent a good choice as a reference method for uric acid. We believe multiwavelength spectral detection could represent a complementary approach because the spectral data could be used to evaluate the purity of the aliquots which were being monitored in the effluent. For example, if one selected some wavelength in the uric acid spectrum (e.g., 290 nm) as a reference, then the ratio of the absorbance at any other wavelength to that at the reference wavelength (or the difference in log *A*) should be a concentration independent constant for pure uric acid. Such ratios (or differences) evaluated at multiple wavelengths should prove very useful in evaluating the efficiency of a separation process. Such procedures could be useful both in semiroutine applications and in more basic chromatographic studies.

We do anticipate some limitations to this approach. The detection system, including the requirement of computing equipment to take full advantage of it, will certainly be more expensive than a single wavelength detector monitored by a strip-chart recorder. More important, there is little chance that a rapid scanning multiwavelength detector can be operated with the same reliability as the well regulated single wavelength detectors (*10, 11*). Accordingly, detection limits will most certainly be less impressive for multiwavelength detectors than with highly regulated single wavelength detectors. Accordingly, we view these as complementary approaches which will fill different needs for different workers.

LITERATURE CITED

(1) M. J. Milano, H. L. Pardue, T. E. Cook, R. E. Santini, D. W. Margerum, and J. M. T. Raycheba, *Anal. Chem.*, **46**, 374 (1974).
(2) M. J. Milano and H. L. Pardue, *Anal. Chem.*, **47**, 25 (1975).
(3) H. L. Pardue, A. E. McDowell, D. M. Fast, and M. J. Milano, *Clin. Chem. (Winston-Salem, N.C.)*, **21**, 1192 (1975).
(4) M. S. Denton, T. P. DeAngelis, A. M. Yacynych, W. R. Heineman, and T. W. Gilbert, *Anal. Chem.*, **48**, 20 (1976).
(5) R. E. Dessy, W. G. Nunn, C. A. Titus, and W. R. Reynolds, *J. Chromatogr. Sci.*, **14**, 195 (1976).
(6) P. T. Kissinger, L. J. Felice, R. M. Riggin, L. A. Pachla, and D. C. Wenke, *Clin. Chem. (Winston-Salem, N.C.)*, **20**, 992 (1974).
(7) M. Weinberger and C. Childsey, *Clin. Chem. (Winston-Salem, N.C.)*, **21**, 834 (1975).
(8) A. McDowell and H. L. Pardue, *Clin. Chem., (Winston-Salem, N.C.)*, submitted for publication.
(9) W. D. Slaunwhite, L. A. Pachla, D. C. Wenke, and P. T. Kissinger, *Clin. Chem., (Winston-Salem, N.C.)*, **21**, 1427 (1975).
(10) J. J. Kirkland, *Anal. Chem.*, **40**, 391 (1968).
(11) T. E. Hewitt and H. L. Pardue, *Clin. Chem. (Winston-Salem, N.C.)*, **21**, 249 (1975).

Alan McDowell
Harry L. Pardue*

Department of Chemistry
Purdue University
West Lafayette, Ind. 47907

RECEIVED for review May 17, 1976. Accepted July 2, 1976. This work was supported by USPHS Research Grant No. GM-13326-10 from the National Institutes of Health.

Determination of Low Concentrations of Hydrogen Chloride in Moist Air

R. R. Bailey, P. E. Field, and J. P. Wightman*

Department of Chemistry, Virginia Polytechnic Institute and State University, Blacksburg, Va. 24061

Hydrogen chloride, while not considered a major air pollutant, has received considerable attention recently as regards its effect on the environment (*1–4*). The quantitative detection of hydrogen chloride present in the atmosphere at ppm levels is important for several reasons including the assessment of environmental impact on such events as solid rocket launches (*4*), incineration of chlorinated hydrocarbons (*5*), and manufacture of products resulting in hydrogen chloride as a by-product or air pollutant (*5*). Analysis of low concentrations of HCl is a formidable experimental problem due to the chemical reactivity of hydrogen chloride in the presence of ambient moisture. Many techniques (*6, 7*) and instruments (*8*) have been used for the analysis of hydrogen chloride including selective ion electrode (*9*), chemiluminescence (*10*), correlation spectrophotometry and coulometric methods (*11*). These techniques for HCl analysis, while useful for many analysis problems are not applicable for ultra-low doses of HCl when a large number of monitoring stations are needed. Inexpensive collection methods employing pre-evacuated grab sample containers, condensation traps, adsorption tubes and/or plastic grab bags, commonly used for atmospheric gas analysis, are not suitable to HCl analysis because of sample loss prior to analysis (*8*). This paper describes an inexpensive, simple collection technique for the quantitative analysis of ppm level concentrations of hydrogen chloride in moist air.

EXPERIMENTAL

Instrumentation. A microcoulometer (Dohrmann Model C 200B) was used to analyze the 1–10 μl chloride samples. The microcoulometer consisted of an electrochemical titration cell, a differential amplifier, and recorder. The titration cell contained two pairs of silver electrodes. One pair monitored the titrant ion concentration (Ag^+) and the other pair replenished the silver ion lost by reaction with chloride entering the cell. The coulombs required to restore the original silver ion concentration were recorded and related to the amount of chloride introduced into the cell. A typical calibration curve obtained by the direct injection of NaCl standard solutions into the cell is shown in Figure 1.

Hydrogen Chloride–Air Mixture. A Matheson hydrogen chloride (42 ppm)–nitrogen mixture was further diluted with wet air in the flow system shown schematically in Figure 2. The effluent HCl concentration was typically 4.2 ppm. Wet air was produced by passing cylinder air (Airco) through a bubbler (B) containing distilled water. The HCl and air lines were Teflon and Tygon, respectively. The wet air flow was 1 l. min^{-1} while the HCl + N_2 flow was 100 cm^3 min^{-1}. The bulk of this mixture was vented to the atmosphere via a Teflon tee (T). The flow lines were passivated by flowing the HCl–air mixture for at least 30 min before a collector tube (CT) was placed in the system. The HCl sample was introduced into the collector tube by opening valve (V) to an air diaphragm pump (Universal Electric Co.) (P). The flow (99.3 cm^3 min^{-1}) through the collector tube was controlled by the needle valve (NV) and measured by the flow meter (FM3). The concentration of HCl in the gas stream was calculated from the measured flow rates. After dosing, the collector tube was set aside for later analysis.

Collector Tubes. The 1-m Pyrex collector tubes (1.04 ± 0.01 mm i.d.) were cleaned using concd HNO_3, detergent, and then rinsed with triple deionized water. The tubes were coated by repeated wetting with 10^{-2} M $NaNO_3$ solution, drained in a vertical position, and allowed to dry at ambient temperature overnight. The tubes were then placed in a 68% relative humidity (RH) chamber (maintained by a saturated KNO_3 solution) for at least 24 h prior to use.

HCl Analysis. The end of the HCl-dosed collector tube nearest the source was dipped into triple deionized water. The height of the water column (via capillarity) (1.5–3.5 cm) was measured precisely. The tube was alternately tilted to allow the column to transverse the tube repeatedly. A microsyringe was inserted to withdraw a measured sample which was then injected directly into the microcoulometer.

RESULTS AND DISCUSSION

The results for the analysis of 5 $NaNO_3$-coated tubes each loaded with 189 ng of chloride are shown in Table I. This loading was achieved by passing 4.2 ppm HCl (in moist air) through a collector tube for 20 s at a flow rate of 100 cm^3 min^{-1}. The height refers to the water column prior to analysis. The chloride concentration in ng/μl was determined using the calibrated microcoulometer. The amount of chloride on the tube was taken as the product of the measured concentration and the volume of water column. The relative accuracy of the technique is 0.1 and the relative standard deviation is 3%. For comparison, 15 ng of chloride were obtained for coated tubes not dosed with HCl which represents a minimal background contribution. A standard deviation of 8 ng was obtained for these blank tubes.

Further investigations of the effects of temperature, humidity, and time were made. Eight tubes were capped with rubber septums and stored in the laboratory from 2–14 days prior to dosing with HCl (189 ng of chloride). Subsequent analysis showed no time dependence of measured chloride on the storage time of the capped, coated tubes. An average value of 176 ng chloride with a standard deviation of 24 ng was obtained. Thirteen tubes were placed in the laboratory uncapped

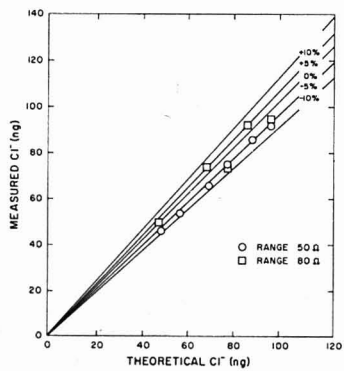

Figure 1. Calibration of microcoulometer

Error lines represent deviation from theoretical peak area calculated by using $[Cl^-] = A((4.4 \times 10^2)/\Omega)$ where $[Cl^-]$ is the amount of chloride introduced into the cell, A is the area of the peak produced, and Ω and 4.4×10^2 are factors based on the gain setting of the instrument

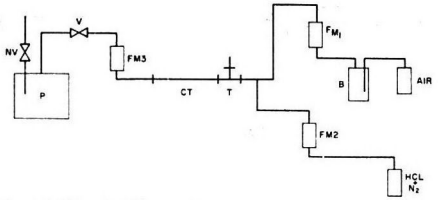

Figure 2. Diagram of flow system

Table I. Reproducibility of the Technique for 189 ng Chloride on Coated Tubes

Tube No.	Height, cm	Concn, ng/μl	Cl^- on tube, ng
43	2.9	7.1	174
47	3.3	6.1	171
44	4.0	4.9	166
57	2.5	8.1	172
10	3.6	5.3	162
		Av 169 ± 5 ng (± 3%)	

for 12–132 h prior to dosing with HCl. Again, subsequent analysis showed no time dependence of measured chloride on the storage time of the uncapped, coated tubes. An average value of 161 ng of chloride with a standard deviation of 46 ng was obtained.

A post exposure experiment was done with seven tubes dosed with HCl and stored uncapped for 2.5 h in three different locations (67% RH, 28 °C; 70% RH, 22 °C; 87% RH, 28 °C) to determine loss of any analyzable chloride. An average value of 158 ng of chloride was obtained. The standard deviation in this experiment was significantly more than for the previous ones (50 ng). On the other hand, no definite effect of relative humidity or temperature could be ascertained. Three tubes were dosed with HCl, capped, and then stored for several days. No loss of analyzable chloride was noted. An average value of 170 ng of chloride and a standard deviation of 32 ng was obtained.

All the previous experiments were performed with 20-s doses of 4.2 ppm HCl at 100 cm^3/min which corresponds to 189 ng of chloride. Studies of the ability of the coated tubes to trap smaller and larger doses of HCl were performed and the results are shown in Figure 3. The analysis of 10–90 s doses of 4.2 ppm HCl at 100 cm^3 min^{-1} can be made. The curve in Figure 3 begins to level off at 90 s indicating that the 1-m coated tubes have a analyzable chloride concentration of 400 ng maximum. This maximum value could presumably be increased by lengthening the coated tube.

The demonstrated trapping ability of the $NaNO_3$-coated tubes for HCl may be based on the hygroscopic nature of $NaNO_3$. The water associated with the $NaNO_3$ coating would have a larger capacity for HCl than an uncoated capillary. Such a mechanism would also be expected to be insensitive to the time, temperature, and humidity ranges studied as shown experimentally. The results obtained with $NaNO_3$-coated tubes suggest their use as inexpensive field collectors

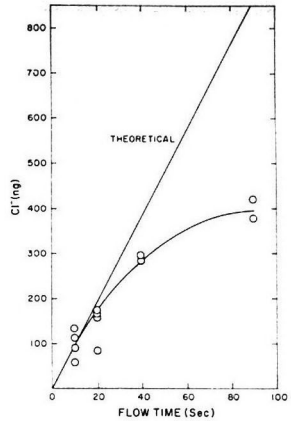

Figure 3. Chloride analysis of $NaNO_3$-coated tubes as a function of dose time to moist air containing 4.2 ppm HCl at a flow rate of 100 cm^3 min^{-1}

for ultra-low doses of HCl with later chloride analysis (>5 ng/μl) by a microcoulometer or other instruments.

ACKNOWLEDGMENT

The authors thank C. A. Potter for his assistance in the preliminary work with the microcoulometer. The advice of B. R. Emerson, Jr., G. L. Gregory, and C. H. Hudgins concerning the operation of the microcoulometer and the glassblowing services of A. Mollick are recognized.

LITERATURE CITED

(1) *Chem. Eng. News*, **52** (49), 16 (1974).
(2) G. Ayrey, B. C. Head, and R. C. Potter, *J. Polym. Sci., Macromol. Rev.*, **8**, 1 (1974).
(3) K. L. Paciorek, R. H. Kratzer, J. Kautamn, J. Nakahara, and A. M. Hartstein, *J. Appl. Polym. Sci.*, **18**, 3723 (1974).
(4) "Environmental Statement for the Space Shuttle Program", NASA, Washington, D.C., 1972.
(5) "Disposal of Organochlorine Wastes by Incineration at Sea. U.S. Environmental Protection Agency", Washington, D.C., July 1975, EPA-430/9-75-014.
(6) M. I. Brittan, N. W. Hanf, and R. R. Liebenberg, *Anal. Chem.*, **42**, 1306 (1970).
(7) M. G. Meador and R. M. Bethea, *Environ. Sci. Technol.*, **4**, 853 (1970).
(8) "Hydrogen Chloride: A Survey of Methods for Detecting, Measuring and/or Monitoring HCl Resulting from Combustion of Propellants", JANNAF, Jan. 75, Safety and Environmental Protection Working Group, Environmental Protection Committee, Subcommittee on Instrumentation.
(9) T. G. Lee, *Anal. Chem.*, **41**, 391 (1969).
(10) L. Gregory, B. R. Emerson, and C. H. Hudgins, "Evaluation of a Chemiluminescent Hydrogen Chloride and a N.D.I.R. Carbon Monoxide Detector for Environmental Monitoring", JANNAF Propulsion Meeting, Oct. 1974.
(11) R. L. Miller, "Hydrogen Chloride; A Study of Methods for Detection, Measurement and/or Monitoring HCl Resulting from Combustion of Propellants", JANNAF Propulsion Meeting, Oct. 1974.

RECEIVED for review March 17, 1976. Accepted May 27, 1976. Financial support for this work under NASA Contract NAS1-13175-1 including a graduate research assistantship for one of us (RRB) is gratefully acknowledged.

Determination of Methacrylic Acid by Coulometric Titration

D. H. Grant* and V. A. McPhee

Department of Chemistry, Mount Allison University, Sackville, N.B., Canada EOA 3C0

For a projected study of the pyrolysis of poly(methacrylic acid), we required a method of analyzing sub-milliliter samples of aqueous poly(methacrylic acid) solutions to determine their monomer concentration, expected to be about 10^{-2} F.

Although gas chromatography can be used to determine monomer during poly(methyl methacrylate) pyrolysis in solution (*1*), we rejected this method on the following grounds: polymer build-up at the injection port is always a nuisance, preliminary esterification would probably be necessary, and solvent–solute peak separation would be much more difficult in the present situation.

On a macro-scale, "bromine titration" is a routine method for determining residual monomer in polymers and is applicable to methacrylates (*2*). More often than not the term is misleading, as the actual titration is an iodine/thiosulfate determination of the excess bromine remaining after it has been allowed to react with the unsaturated species.

Coulometric titration using electrogenerated bromine seemed to offer a suitable micro-scale adaptation, particularly as there is an appropriate bi-amperometric method of end-point detection (*3*). It seemed likely that up to a 1000-fold dilution of sample between reaction vessel and titration cell could be tolerated.

Such monomers as styrene, α-methyl styrene, and vinyl acetate (*4*) and methyl vinyl ketone (*5*) have been determined satisfactorily by coulometric titration by bromine.

EXPERIMENTAL

The constant current power supply used was constructed substantially to Stock's design (*6*). It provides currents of either 9.65 or 0.965 mA. The bi-amperometric polarizing voltage was 150 mV.

Methacrylic acid (Matheson, Coleman and Bell) was re-distilled before use. Standard dilute solutions in electrolyte/solvent were prepared on a weight basis. BDH Reagent Grade glacial acetic acid was used. Potassium hydrogen phthalate and all inorganic reagents were of Fisher Certified Reagent quality.

The conventional technique of coulometric titration was followed. The electrolyte/solvent was pretitrated until a specific galvanometer reading was reached, significantly above fluctuations about zero. Then the sample was added and the titration continued till the same galvanometer reading was reached. Further samples can be added to the same batch of electrolyte and the titrations repeated.

RESULTS AND DISCUSSION

Crucial to the development of a satisfactory coulometric titration procedure is the selection of an electrolyte/solvent system.

As a starting point, we used the typical system of 0.2 F KBr in 50% aqueous acetic acid (*7*), but found it unsatisfactory because the rate of bromine addition is too slow. No significant improvement was observed in the presence of $AlCl_3$, $AlBr_3$, $HgCl_2$, $FeCl_3$, $NiCl_2$, LiCl, or LiBr, all of which are reported to catalyze bromine additions. More promising, but still unsatisfactory, results were obtained in 1 F HCl in 80% acetic acid where the electrogenerated species is presumably chlorine (*8*).

Relatively slow bromine addition is less of a problem in those macro-scale methods where the actual titration involves iodine/thiosulfate. While comparable "back titration" procedures can be developed for coulometry, they can result in a loss of some of its advantages. It seemed preferable to try to increase the rate of bromination.

According to Ingold (*9*), halogen addition to the double bond in methacrylic acid is slowed by the electron-withdrawing character of the carboxylic –COOH group. Since the carboxylate $-COO^-$ group is electron-releasing, addition to the methacrylate anion is much more rapid. Only Critchfield (*10*) seems to have modified macro-scale analytical procedures to take advantage of this. Even his method still has a final iodine/thiosulfate step.

The pK_A of methacrylic acid is 4.66 (*11*). Methacrylate anions will therefore be the predominant species at a pH over 4.7. However, solutions that are much more alkaline must also be avoided. Bromine reacts with hydroxide to form hypobromide. One result that has been reported is that the bi-amperometric detection method becomes unsatisfactory (*12*). A pH in the range 5 to 6 therefore seemed the best compromise.

The electrolyte that we found to be satisfactory was 0.05 F in potassium hydrogen phthalate, 0.035 F in sodium hydroxide and 0.2 F in potassium bromide. It has a pH of 5.5. No added catalysts are necessary; the bromine addition is sufficiently fast that either generator current can be used. Blanks are low.

Eleven samples of methacrylic acid between about 0.2 and 3.0 mg in 150 ml of electrolyte were titrated with an average error of $+0.029 \pm 0.013$ mg at a current of 9.65 mA. This calculation assumes 100% efficiency of bromine generation and addition. Similarly, at 0.965 mA, with 20 samples between about 0.02 and 0.70 mg, the average error was -0.009 ± 0.015 mg.

Additions of pure poly(methacrylic acid) do not interfere with the analyses.

It cannot be assumed that the method will be easily applicable to all α,β unsaturated acids. We found that acrylic acid does not brominate fast enough, and that with cinnamic acid, although the titration is possible, the precision is substantially less.

LITERATURE CITED

(1) S. Bywater and D. H. Grant, *Trans. Faraday Soc.*, **59**, 2105 (1963).
(2) L. S. Luskin, "High Polymers", Vol. XXIV, Part 1, Wiley-Interscience, New York, 1970, p 161.
(3) D. H. Evans, *J. Chem. Educ.*, **45**, 88 (1968).
(4) D. B. Gurvich, V. A. Balandina, and L. M. Palkina, *Zavod. Lab.*, **30**(3), 278–81 (1964); *Chem. Abstr.*, **60**, 13890e (1964).
(5) A. P. Zozulya and E. V. Novikova, *Zavod. Lab.*, **29**(5) 543–5 (1963); *Chem. Abstr.*, **59**, 4548e (1963).
(6) J. T. Stock, *J. Chem. Educ.*, **46**, 858 (1969).
(7) D. G. Marsh, D. L. Jacobs, and H. Veening, *J. Chem. Educ.*, **50**, 626 (1973).
(8) F. Cuta and Z. Kucera, *Chem. Listy*, **47**, 1166–72 (1953); *Chem. Abstr.*, **48**, 3850b (1954).
(9) C. K. Ingold, "Structure and Mechanism in Organic Chemistry", Bell, London, 1953, p 665.
(10) F. E. Critchfield, *Anal. Chem.*, **31**, 1406 (1959).
(11) E. Larsson, *Z. Phys. Chem. A*, **159**, 316)1932).
(12) G. M. Arcand and E. H. Smith, *Anal. Chem.*, **28**, 440 (1956).

RECEIVED for review April 15, 1976. Accepted June 11, 1976.

Performance Test for Direct Reading Balance

Don H. Anderson* and N. B. Woodall

Eastman Kodak Company, Kodak Park Division, Industrial Laboratory, Building 34, Rochester, N.Y. 14650

Although our analytical balances are maintained on a regular basis by a service group, it is still the laboratory's responsibility to be sure that the day-to-day measurements are correct. To this end, a fast, simple way to evaluate direct reading balances has been developed. The direct reading balance has obviated the necessity of handling weights and this improvement has unfortunately reduced the operator's awareness of the need for checking calibration. We have over 25 balances in our laboratory areas; and since we operate 15 remotely located service laboratories, our needs to assure uniform quality testing are especially critical. The use of National Bureau of Standards calibrated sets of weights is time consuming and the repetitive handling poses the danger of wear and damage to the calibrated reference weights.

The method devised serves to check the linearity of the balance, provides a direct intercomparison with all balances, and relates all balances to a Bureau of Standards reference. This is accomplished using the regular balance operators and results in a minimum of handling of our National Bureau of Standards reference weights. The entire operation is accomplished in a short period of time and makes no unusual demands on the laboratory staff. Three test objects were prepared by drilling out random amounts of metal from the bottoms of some old weights. These gave us a set of test objects weighing about 14, 29, and 56 g. They were carried to each balance station where an operator who normally used the balance weighed them individually and collectively. The data from each balance were recorded and no calculations made until all balances were checked. When the data for each balance had been compared with the mean, the balance closest to the mean was used to weigh the National Bureau of Standards certified weights and thus by handling these calibrated weights only once, the entire lot of balances was checked.

Table I. Data for 25 Balances

	Av from 25 balances, wt in g	Std dev, g	Rel std dev, %
A. First weight	13.9565	0.000 49	0.003 51
B. Second weight	29.4151	0.000 37	0.001 26
C. Third weight	56.4625	0.000 35	0.000 62
D. 3 Weights simultaneously[a]	99.8343	0.000 54	0.000 54
E. Sum of 3 weights[a]	99.8341		

[a] The difference between D and E provides an estimate of the linearity of the balance.

Table I summarizes the data for 25 balances.

A malfunctioning balance is quickly detected. It is a tribute to contemporary balance design that, out of the 25 balances checked, only 2 were suspect and required attention. Some of the balances have been in use for 15 years. In general, we are quite pleased with their overall performance.

RECEIVED for review April 16, 1976. Accepted June 1, 1976.

Sniffer to Determine the Odor of Gas Chromatographic Effluents

T. E. Acree,* R. M. Butts, R. R. Nelson, and C. Y. Lee

Department of Food Science and Technology, Cornell University, New York State Agricultural Experiment Station, Geneva, N.Y. 14456

Sniffing the effluent of a gas chromatograph (GC) is the most useful means of determining which components of a complex mixture of volatiles have odor. Although such a bioassay procedure is both qualitative and subjective, it is the only simple procedure for selecting those volatiles to isolate, identify, and evaluate for odor significance (*1*). Unfortunately, sniffing the effluent of a GC is both uncomfortable and inaccurate because of the irritating effects of the hot dry carrier gas and the lingering presence of strong odors in the environment of the GC output. Although the dryness of the carrier gas can be reduced by adding water to it upstream of the GC (*2*), this procedure limits the flexibility of the chromatography. This communication describes a simple inexpensive "sniffer" which improves the comfort and accuracy of sniffing GC effluents. The principle is to mix the GC effluent with a larger volume of rapidly moving humid air.

EXPERIMENTAL

The gas chromatography was done in a 4 m × 2 mm glass column packed with 5% SP 1000 on 100/120 mesh Chromasorb W installed in a Packard model 800 gas chromatograph. The column was operated isothermally at 100 °C and with a helium carrier gas flow of 20 ml/min. A nominal 50 to 1 splitter was installed in the flame ionization detector oven with the larger portion of the effluent going to the sniffer.

Figure 1 shows a diagram of a sniffer constructed from a brass laboratory filter pump (A). The air supply is deodorized by an in-line charcoal (Pittsburgh activated, 12–40 mesh) filter (H) and humidified by passing the air over the surface of distilled water in a half filled

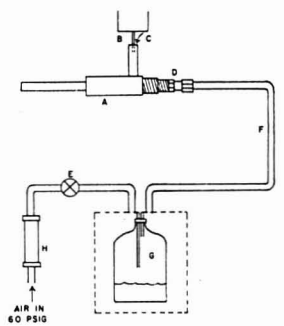

Figure 1. Diagram of the sniffer constructed from a laboratory filter pump

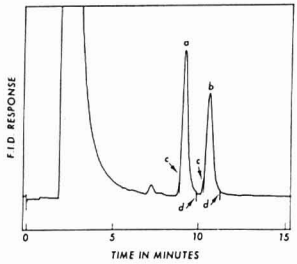

Figure 2. Gas chromatogram of *n*-hexylacetate (*a*) and 2-heptanol (*b*). The event marks (*c*) represent the first detection of odor while the marks (*d*) represent the disappearance of detectable odor

gallon jug (G). A piece of 1/16-in. stainless steel tubing from a nominal 50 to 1 splitter in the flame ionization detector oven extends 1 cm into the room and 2 mm into the vacuum port (B) of the filter pump. A 1/4-inch male Swagelok fitting was threaded into the filter pump at D to facilitate plumbing, and the ball check valve in the vacuum port was removed. Nylon tubing (1/4-in. o.d.) (F) was used to connect the components and a Whitey B-1RS4 (Whitey Co., Oakland, Calif.) valve was installed at E to control the air flow.

RESULTS AND DISCUSSION

Good results were achieved with a 12 l./min air flow through the filter pump and this caused 250 ml/min room air to flow into the vacuum port at C. Although this represented a 500-fold dilution of the gas chromatographic effluent, it did not appear to result in a severe reduction in odor intensity as compared to directly sniffing the effluent. Without the sniffer, the low velocity of the effluent carrier gas was subjected to room drafts which complicated the detection of peak odors. Figure 2 shows a gas chromatogram of *n*-hexylacetate (*a*) and 2-heptanol (*b*) which were simultaneously sniffed blindly. Each peak represented approximately 5 μg of material and the event marks (*c*) represent the first detection of odor and (*d*) the last detectable odor. This sniffer results in a marked improvement in the sensory resolution of gas chromatographic peaks compared with sniffing the effluent directly. Table I shows a comparison between the sensitivity of the sniffer and sniffing the GC output directly. Both methods yielded an apparent threshold of approximately 10 ng for both *n*-hexylacetate and 2-heptanol with less than a factor of 10 difference between them.

Table I. Comparison between the Detection of Odors Using the Sniffer and by Directly Sniffing the GC Output[a]

Amount injected, ng	Method	*n*-Hexylacetate	2-Heptanol
100	Sniffer	++	++
	Direct	++	++
10	Sniffer	0	0
	Direct	+	0
1	Sniffer	0	0
	Direct	0	0

[a] ++ indicates the compound was clearly detected; +, only faintly detected; and 0, no detectable odor.

When certain odorous compounds were present in high concentrations in the gas chromatographic effluent (e.g., phenyl ethyl alcohol in grape essence) or had an extremely low odor threshold (e.g., geosmin in beets), the sniffer became contaminated and it was necessary to clean the filter pump. Washing with water followed by isopropyl alcohol and then 1,1,2-dichloro-1,2,2,-difluoroethane (i.e., Freon 113) worked well. Contamination of the sniffer was also minimized by removing the sniffer from over the gas chromatographic effluent when strongly absorbant peaks emerged or by replacing it with a clean duplicate.

The sniffer worked equally well when attached to the effluent from a Llewellyn (*3*) type helium separator on a gas chromatograph–mass spectrometer interface.

LITERATURE CITED

(1) R. Teranishi, P. Issenberg, I. Hornstein, and E. L. Wick, "Flavor Research: Principles and Techniques," Marcel Dekker, New York, N.Y., 1971.
(2) H. S. Knight, *Anal. Chem.*, **30**, 2030 (1958).
(3) R. A. Flath, D. R. Black, D. G Guadagni, W. H. McFadden, and T. H. Shultz, *J. Agric. Food Chem.*, **15**, 29 (1967).

RECEIVED for review February 27, 1976. Accepted June 23, 1976.

Modification of Graphite Furnace Power Supply to Allow Interruption of Analytical Cycle

E. W. Cooper* and J. V. Dunckley

Electronic Engineering Department, Dunedin Hospital, Dunedin, New Zealand

The graphite furnace is now well established as a useful atom generator for the analysis of cations by atomic absorption spectrometry (*1–3*). Some of the variety of experimental furnaces described in the literature (*4–17*) have been developed and marketed by manufacturers of atomic absorption spectrometers either as an integral part of the instrument or, more commonly, as an "add on" accessory. These usually operate by automatic sequential switching of the furnace power in accordance with a preset program, generally in three or more steps with increasing current loadings for specific time intervals. For adequate control of the analytical process, it is desirable that time, temperature, and rise rates be reproducible.

A common operating sequence is dry–ash–atomize wherein the sample (e.g., 5 μl of solution) is applied to the furnace, dried at low temperature, ashed at a higher temperature, and finally atomized. It seemed that the graphite furnace had considerable unexploited potential as a chemical reaction vessel. This was realized by placing switches to interrupt the analytical cycle at the end of the drying and ashing cycles. One of these switches (Sx) at the end of the drying cycle would allow for multiple sample application to the furnace as well as the application of reagents to the dried specimen, while a further switch (Sy) to interrupt at the end of the ash cycle would allow for the addition of a variety of reagents to render ash constituents more or less volatile, or to modify the influence of matrix cations. Thus, in operation the sample would be placed in the furnace, the selected cycle interrupt switch closed, and the cycle "start" button pressed. The analytical cycle would then proceed automatically to the interrupt stage

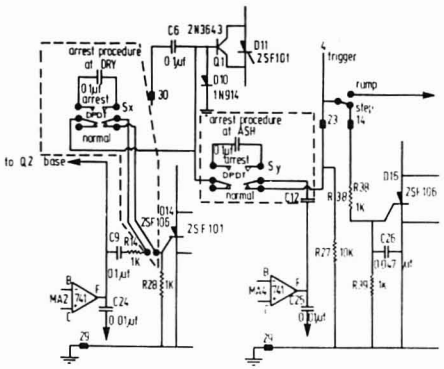

Figure 1. Circuit modifications which permit interruption of the analytical cycle are enclosed within dotted lines

and then shut down. On again pressing the start button, this sequence would be repeated. After opening the interrupt switch and pressing the start button, the full analytical sequence will take place.

The power supply—Varian Techtron Model 63—was modified as follows: Timer Board Assembly (Instruction Manual Figure 5-3.4c) was altered as shown in Figure 1. The operating sequence is commenced by pressing the START button which completes the circuit for a pulse from capacitor C28 (0.047 µf) to trigger the two SCR's D11 and D12, thus energizing relays A and B whose contacts B1 of relay B close, the timing sequence is commenced for the period as set by the DRY time control. At this same instant, relay A is energized, switching on the transistor Q10 (Figure 5-3.2 block diagram) to complete the circuit for the rectified pulses from T2 to operate the triac control for the carbon rod voltage from transformer, T3.

On completion of the DRY time cycle, the positive pulse from the differential output of MA2 is applied to the base of Q2, which switches off the SCR D12, thus de-energizing relay B, while at the same time Q3 is turned on resetting the ramp generator MA1 whose output will return to zero.

Without interruption by the switch Sx (Figure 1), the pulse at the output of MA2 would switch on the SCR D14 for the analysis to proceed. Because of the similar circuitry used for the ASH timing circuit, a corresponding modification has been applied in the circuit immediately following the I.C. MA4.

Two switches were interposed in the circuit, the first (Sx) at the junction of R14, R28, and the gate of SCR D14, leaving R28 and the gate connected at all times, but allowing the circuit to be broken at this point to prevent the pulse from switching on D14. The second break is made by switch Sy at the junction between C12, R27, and the RAMP/STEP switch, but again allowing R27 and the RAMP/STEP switch to remain in normal circuit. These two switches allow each step in the analysis to be interrupted to allow chemical manipulation of the analytical environment.

It is likely that the power supply-timer units of other manufacturers' furnaces may be similarly modified to extend their analytical capability in like manner.

LITERATURE CITED

(1) F. J. M. J. Maessen, F. D. Posma, and Johannes Balke, *Anal. Chem.*, **46**, 1445 (1974).
(2) F. J. M. J. Maessen and F. D. Posma, *Anal. Chem.*, **46**, 1439 (1974).
(3) B. C. Begnoche and T. H. Risby, *Anal. Chem.*, **47**, 1041 (1975).
(4) H. Massmann, *Spectrochim. Acta, Part B*, **23**, 215 (1968).
(5) R. Woodriff and G. Ramelow, *Spectrochim. Acta, Part B*, **23**, 665 (1968).
(6) T. S. West and X. K. Williams, *Anal. Chim. Acta*, **45**, 27 (1969).
(7) M. P. Bratzel, R. M. Dagnall, and J. D. Winefordner, *Anal. Chim. Acta*, **48**, 197 (1969).
(8) B. V. L'vov "Atomic Absorption Spectrochemical Analysis", Adam Hilger, London, 1970.
(9) M. Donega and T. E. Burgess, *Anal. Chem.*, **42**, 1527 (1970).
(10) H. T. Delves, *Analyst (London)*, **95**, 431 (1970).
(11) M. D. Amos, P. A. Bennet, K. G. Brodie, P. W. Y. Lung, and J. P. Matousek, *Anal. Chem.*, **43**, 211 (1971).
(12) J. B. Headridge and D. R. Smith, *Talanta*, **18**, 247 (1971).
(13) J. P. Matousek, *Am. Lab.*, June, 45 (1971).
(14) J. P. Pemsler and E. J. Rapperport, *Anal. Chim. Acta*, **58**, 15 (1972).
(15) Y. Talmi and G. H. Morrison, *Anal. Chem.*, **44**, 1455 (1972).
(16) C. J. Molnar, R. D. Reeves, J. D. Winefordner, M. T. Glenn, J. R. Ahlstrom, and J. Savory, *Appl. Spectrosc.*, **26**, 606 (1972).
(17) Tibor Kantor, S. A. Clyburn, and Claude Veillon, *Anal. Chem.*, **46**, 2205 (1974).

RECEIVED for review April 2, 1976. Accepted June 16, 1976.

External Reference Signal in X-ray Energy Spectrometry

P. J. Van Espen and F. C. Adams*

Department of Chemistry, University of Antwerp (U.I.A.), B2610 Wilrijk, Belgium

The precise and accurate analysis by x-ray fluorescence spectrometry requires a well stabilized high voltage supply to ensure a constant and easily reproducible fluorescing beam intensity. This condition is generally fully recognized in wavelength dispersive fluorescence spectrometry. Most generators used in energy-dispersive systems are much less stabilized. The rationale for this is that a very high precision cannot be reached anyway with this type of instrument. The reasons cited are lower counting rates and thus higher statistical errors and the occurrence of increased background levels and interferences. In many situations, the generator instability is the dominant source of error and, hence, represents the major limitation on precision and the accuracy. The remedy to this situation is quite simple, if one is willing to exchange the generator for a better stabilized one and, consequently, to considerably increase the total cost of the system. As an alternative, methods have been proposed which rely on the measurement of a spectral component which bears a relation to the primary beam intensity. The coherently and incoherently scattered primary beam have been proposed for this. It can only serve the purpose, however, when the sample is either infinitely thick or of strictly the same weight and composition because the scattered intensity is proportional to the primary beam intensity times the number of scattering atoms in the beam. Alternatively, an internal standard incorporated into the sample can be used, as is often done in ion induced x-ray emission (*1*). This is not possible when the sample has to be measured nondestructively without any preseparations or pretreatment. Moreover, the internal standard should be distributed very homogeneously throughout the sample.

We have successfully solved the stability problem by using a thin wire as an external standard which is reproducibly positioned in the radiation path just below the sample. Similar

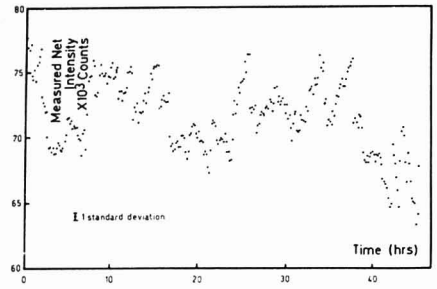

Figure 1. Intensity fluctuations of Br Kα as a function of time after 2-h warmup of the spectrometer.

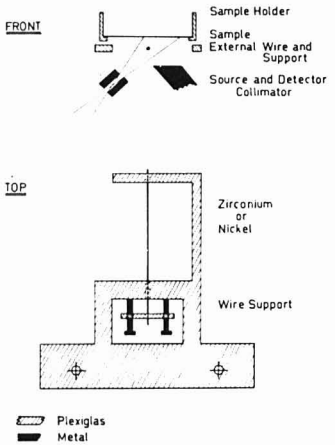

Figure 2. Schematic of external wire. (a) Location; (b) wire holder

normalization procedures have been used in wavelength dispersive fluorescence analysis. Jones (*2*) employed an iron rod which was attached to the cover of a standard Philips sample holder. Burke et al. (*3*) and Gunn (*4*) suspended disks of an appropriate reference element within the sample. The technique is used in these cases as an internal reference for the sample and serves the purpose of correcting for absorption effects and interelemental effects.

EXPERIMENTAL

The fluorescence spectrometer includes a Kevex x-ray system consisting of a tungsten anode water-cooled x-ray tube (Siemens Kristalloflex 2), a set of secondary targets, and a sample changer. The spectrum is measured with a high-resolution Si(Li) detector and associated electronics for amplification and storage. The equipment is fully described elsewhere (*5*). The Kristalloflex 2 generator is magnetically stabilized. It was originally developed for x-ray diffraction and is of the least stable type in use for fluorescence work.

RESULTS AND DISCUSSION

The stability of the spectrometer was tested by measuring repeatedly the same sample which was placed in one position of the sample changer, over periods ranging from 50 min to several days. The sample used consists of 64 μg of CsBr vacuum deposited onto Mylar foil. The spectrometer was allowed

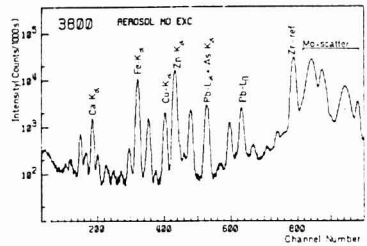

Figure 3. Fluorescence spectrum of aerosol loaded filter with molybdenum excitation and zirconium external reference

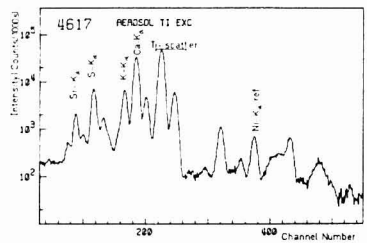

Figure 4. Fluorescence spectrum of aerosol loaded filter with titanium excitation and nickel external reference

to warm up for 2 h before each series of measurements. The short time instabilities over 50 min were investigated with the multichannel analyzer in the multiscaling mode at 0.9 s per channel. The integral radiation intensity was counted in this case. For longer time periods, repetitive measurements were performed and the intensity of the Br Kα peak was used with correction for the continuum radiation background. The mean square successive difference method (*6*) introduced by Hooton and Parsons was used on the repetitive measurements. The results shown in Figure 1 indicate that the spectrometer is highly unstable and subject to drift and to oscillations. Sudden increases or decreases of the intensity which are readily apparent from the graphical display do not appear to be correlated with any working condition in the laboratory. It appeared, however, that the intensity variations were roughly proportional to the current indication of the high voltage supply.

A suitable element can be selected in a physical form with appropriate dimensions and weight to provide an easily recognizable calibration peak in the spectrum for the correction of the primary radiation intensity fluctuations. For excitation with radiation from a molybdenum secondary target, a pure zirconium metal wire with a diameter of 50 μm was selected (Goodfellow Metals Ltd., Cambridge Science Park, Cambridge CB44DJ, England). When positioned reproducibly at 1.5 mm below the sample surface, a section 7-mm long is readily excited and its fluorescence radiation is measured sensitively. It gives rise to Kα/Kβ fluorescence radiation corresponding to 14 μg of zirconium in the sample. It does not interfere with the detection of the other elements except by a 20% increase in the detection limit for a 10 mg/cm^2 sample. The primary or secondary radiation absorption due to the presence of the wire is obviously neglible. Figure 2 shows schematically how the wire is positioned.

Zirconium was an obvious choice because: 1) It is very efficiently excited so that a very thin wire can be used which

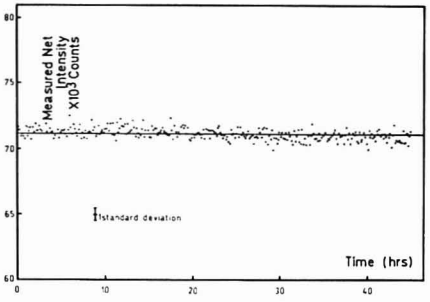

Figure 5. Data of Figure 1 after normalization through zirconium external reference

does not obstruct the radiation beams. Its L radiation is of sufficiently low energy around 2 keV and does not interfere with the detection of the elements from $Z = 17$. Its K radiation is only slightly below the Compton scatter peak in energy and, hence, also gives rise to few interferences. 2) It is available with a high purity as a metal except for possible niobium and hafnium impurities. 3) It can safely be assumed to be present at very low concentration in most samples to be measured, and especially in the environmental type samples for which the XES-method is particularly suited (5).

A nickel wire of the same diameter can be used in the case of germanium and titanium excitation. In the latter case, its K fluorescence is excited by the Bremsstrahlung continuum of the primary radiation. The spectrum of an aerosol loaded filter paper obtained with molybdenum excitation and the zirconium wire reference and that obtained with titanium excitation and nickel wire reference are shown in Figures 3 and 4.

The internal reference peak obtained in the manner fulfils several very useful functions: 1) It allows an easy and accurate correction for the spectrometer instabilities due to the high-voltage generator. Also, the frequent resetting of the x-ray tube current to some calibrated position becomes unnecessary.

The intensities shown in Figure 1 were corrected with the integral intensity of the zirconium Kα radiation and are shown in Figure 5. The analysis of these results shows that oscillations and instabilities are now absent to within the counting statistics which amount to 0.3% but that there remains a small statistically significant drift contribution of 0.2%/h as obtained through least squares fitting through the data. This drift proved relatively reproducible for a number of measurements. This increase in stability of the normalized counting rate proves that the high voltage generator is subject to instabilities of the anode tube current and to a much lesser extent of the high voltage. Indeed, the correction by normalization through the reference peak can be expected to be applicable fully for the first type of instability but only partially for the latter type, as the deviations of the high voltage change the primary radiation spectrum and, consequently, the secondary radiation production efficiency as a function of atomic number.

The dependence of the normalized radiation intensity of the elements titanium, copper, and bromine with the high voltage setting of the instrument was determined at 40 kV. The mean deviation of the intensity amounts to ca. +7% per kV and drops to − 0.3% per kV after normalization. This indicates roughly a decrease of the generator high voltage by 1 kV over the 45-h period.

The ultimate precision of the analysis has been increased

Table I. Reproducibility of Analysis of Aerosol Sample Shown in Figures 3 and 4 (11 Measurements)

	Element and radiation used (direct results)				
	Fe K$_\alpha$	Cu K$_\alpha$	Zn K$_\alpha$	Br K$_\alpha$	Pb L$_\beta$
Mean intensity (counts/3000 s)	95 360	18 946	166 785	12 967	27 661
Standard deviation on one measurement (s %)	2.73	2.73	3.07	3.00	2.87
Counting statistics (σ %)	0.33	0.80	0.25	1.06	0.68
Standard deviation[a] due to instabilities	2.71	2.61	3.06	2.81	2.79
	Element and radiation used (normalized to Zr wire)				
Standard deviation (s %)	0.35	0.84	0.22	1.19	0.84
Counting statistics (σ %)	0.38	0.82	0.31	1.09	0.72
Chi-square[b]	8.66	10.37	4.85	11.98	13.76

[a] Supposed equal to $s^2 - \sigma^2$. [b] with $\chi^2_{0.95}(\infty, 10) = 18.31$.

with the wire internal reference from about ± 3% to better than 0.3% (one standard deviation). This appears readily from the results of a daily repeated analysis of the aerosol filter of Figures 3 and 4 over a 10-day period shown in Table I. The first part of the table lists the results and the precision after the analysis of a number of elements. In the second part, the results are corrected with the aid of the zirconium standard.

2) A correction for counting rate losses is automatically applied because the losses in the reference peak should accurately match those in the other peaks. This allows the safe use of the maximum allowable fluorescence counting rates with the result of increased counting statistics and a higher precision of the analysis. This is an interesting feature because, even when pulse pileup rejection and dead time correction circuits are used, inaccuracies may easily remain undetected. These, then, give rise to high and irreproducible errors. The external reference radiation serves the same purpose as a purely random pulse generator (7).

With the wire holder shown in Figure 2, it became possible to reposition the zirconium wire with a precision of 0.33%.

CONCLUSION

Energy dispersive x-ray equipment is especially prone to generator output fluctuations. It appears that this source of error if it is due to current fluctuations, can be accurately corrected by the use of a thin wire external reference which gives rise to a reference photo peak in the spectra. The total gain in precision depends on the characteristics of the x-ray equipment used, namely, on the relative proportion of current and voltage instability which proved to be favorable with the instrumentation used. When pure bichromatic secondary target radiation could be used for excitation of the sample, all instabilities should be removed with the method even when the generator is highly unstable in regards to voltage.

For the automatic data reduction using computer calculations, the reference peak may serve a number of valuable diagnostic functions: easy recalibration of the energy and a check for an abnormal counting time of a sample. Also, useful spectral characteristics such as energy resolution and peak

symmetry are easily measurable. In combination with coherently and incoherently scattered radiation, it may be used to detect samples of abnormal size and samples placed at an incorrect measurement geometry.

LITERATURE CITED

(1) T. B. Johansson, R. E. Van Grieken, J. W. Nelson, and J. W. Winchester, *Anal. Chem.*, **47**, 855 (1975).
(2) R. A. Jones, *Anal. Chem.*, **22**, 1258 (1958).
(3) W. E. Burke, L. S. Hinds, G. E. Deodato, E. D. Sager, Jr., and R. E. Borup, *Anal. Chem.*, **36**, 2404 (1964).
(4) E. L. Gunn, *Appl. Spectrosc.* **19**, 99 (1965).
(5) R. Dewolfs, R. De Neve, and F. Adams, *Anal. Chim. Acta*, **75**, 47 (1975).
(6) K. A. H. Hooton, and M. L. Parsons, *Anal. Chem.*, **45**, 2218 (1973).
(7) H. H. Bolotin, M. G. Strauss, and D. A. McClure, *Nucl. Instrum. Methods*, **83**, 1 (1970).

RECEIVED for review May 18, 1976. Accepted June 28, 1976. This work was financially supported by the "Nationaal Fonds voor Wetenschappelijk Onderzoek", Belgium.

Dual Column Operation for Gas Chromatograph–Mass Spectrometer

Leo Kazyak

Division of Biochemistry, Walter Reed Army Institute of Research, Washington, D.C. 20012

At no other time, since the concept was introduced by Golay in 1958 (*1*), have capillary gas chromatographic columns been used more extensively than during the past few years. This new interest may be due, in part, to the comparatively inexpensive support-coated open tubular (SCOT) glass capillary columns that are quite easy to produce with the commercially available Hupe-Busch apparatus (Hewlett-Packard Co., Avondale, Pa.). A number of publications (*2–4*) give complete instructions on how to coat the inner surface of glass capillary tubing with a liquid phase and, in general, the procedure is fairly simple for nonpolar liquid phases such as SE-30 (or OV-1). With a little care and attention to detail, 50-meter columns with at least 30 000 to 50 000 theoretical plates can be made without much difficulty.

No matter how effective capillary columns may be, and regardless of how convincing the argument is to promote their use, it would be unrealistic to assume that there would be no further need of packed columns or to expect anyone to completely exclude them in favor of capillary columns. Nevertheless, the laboratory investigator with a gas chromatograph–mass spectrometer who decides to use capillary columns is confronted with this dilemma. Unlike the more common situation where several gas chromatographs exist in a laboratory and both types of columns could be utilized simultaneously, very few laboratories are equipped with more than a single combined gas chromatograph–mass spectrometer. Admittedly, columns can be exchanged (*5, 6*) to satisfy the requirements for one or the other, but capillary columns can be a nuisance to connect properly. However, the option to interchange columns is not very much of an inducement to use them. To be able to operate both types of column at the same time, by merely switching from one to the other without removing either column, would be more desirable. Thompson and Goode described such a modification (*7*) for two packed columns in a gas chromatograph–mass spectrometer. In our laboratory, a much simpler modification was devised for a capillary and a packed column in the LKB 9000 gas chromatograph–mass spectrometer, and quite possibly this adaptation can be made in similar equipment of other manufacturers.

DISCUSSION

Linnarson and Blomkvist, in the application laboratory of LKB Produktor AB, studied the use of capillary columns in the LKB 9000 gas chromatograph–mass spectrometer. They described a modification whereby the addition of carrier gas to the column effluent at the terminal end of the column (make-up gas) permitted the instrument to be used without removal of the molecular separator (*8*). The make-up gas reduced the loss of components transferred through the molecular separator to the analyzer tube of the mass spectrometer. Since make-up gas was necessary to improve the amount of component transported through the separator, and no apparent loss resulted in the resolution of those components during separation, it seemed reasonable to expect that carrier gas passing through a packed gas chromatographic column could serve as well to provide the make-up gas for a capillary column. In the manner suggested by Linnarson and Blomkvist, a Swagelok reducer fitting was drilled to accommodate a short length of 1.6-mm stainless steel capillary tubing that was silver soldered in place. The stainless steel capillary tubing formed a "tee" junction to merge the effluent from the packed column into the effluent from the capillary column. The columns were assembled (Figure 1) so that the packed column provided a frame and reinforcement for the more fragile capillary column as well as to supply the necessary carrier gas make-up. A few pieces of copper wire were used to fasten the columns together. To regulate carrier gas to the capillary column, a separate flow controller (Condyne Model 200, Condyne Instruments, La Canada, Calif. 91011) was installed. With this arrangement, either packed or capillary columns could be used at any time without changes or alterations.

Contrary to conventional applications of capillary columns, carrier gas stream splitting at the inlet was not used in our

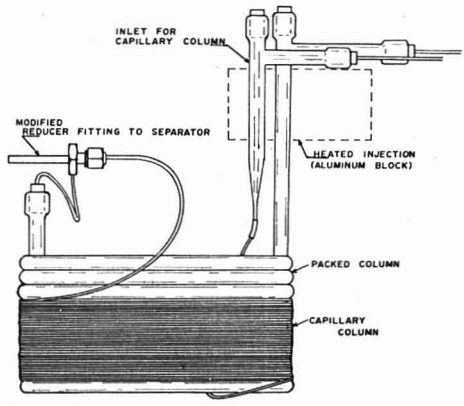

Figure 1. Dual column arrangement

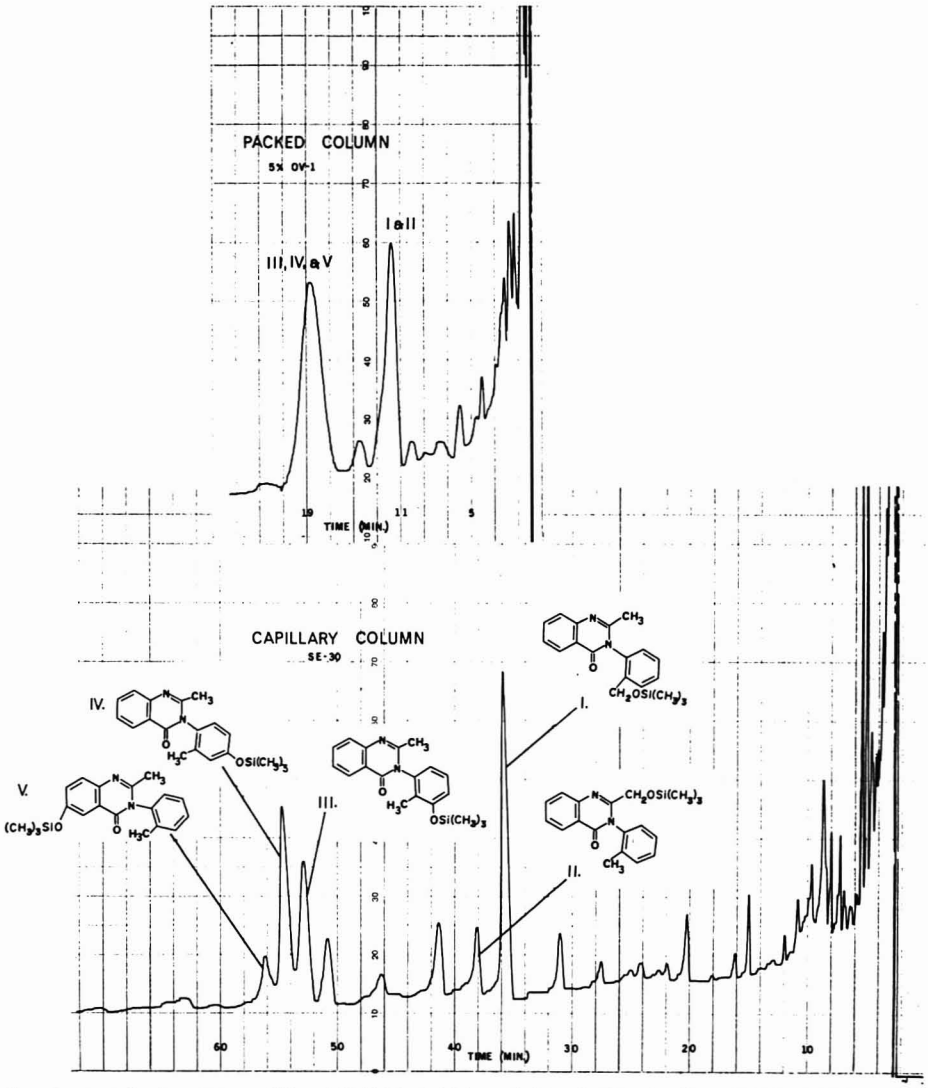

Figure 2. Comparative chromatograms of (I) 2-methyl-3-[2-(trimethylsilyloxymethyl)phenyl]-4(3*H*)-quinazolinone. (II) 2-(trimethylsilyloxymethyl)-3-*o*-tolyl-4(3*H*)-quinazolinone, (III) 2-methyl-3-[2-methyl-3-trimethyloxy)phenyl]-4(3*H*)-quinazolinone, (IV) 2-methyl-3-[2-methyl-4-(trimethylsilyloxy)phenyl]-4(3*H*)-quinazolinone, and (V) 2-methyl-3-*o*-tolyl-6(trimethylsilyloxy)-4(3*H*)-quinazolinone

applications. Many procedures are not amenable to stream splitting where injection volumes are considerably reduced before they enter the column. In Figure 1, the injection port and inlet design is shown that is recommended for nonsplitting injections of up to 1 μl of sample.

Very simply, the inlet is little more than 6-mm (o.d.) glass tubing with an inside diameter of 2 mm and a length of 15–20 cm. The tip is drawn to a capillary to be easily connected to the SCOT column with Teflon tubing. An alternative to drawing the end of the tube into a capillary is to use a Swagelok reducing union if leak-tight connections can be maintained between the glass inlet and the capillary column.

If the aluminum heating block can be replaced with one that accommodates a second inlet, the modification will be neater, and the heat to the inlet can be better controlled and more evenly distributed along the entire body of the tube. Otherwise, the glass inlet can be wrapped in three or four thicknesses

Table I. Replication of Peak Areas

Metabolite	Sample A Integrator counts	Sample A Mean and std dev	Sample B, integrator counts	Sample C, integrator counts	Sample D, integrator counts
I	88 840				
	92 120				
	92 370		126 400	60 490	25 060
	86 610	89 618 ± 2 532	132 000	59 580	24 690
	88 150				
II			48 870	2 183	6 991
			48 300	2 057	7 174
III	45 400				
	47 690				
	46 760		41 640	51 960	3 201
	42 060	44 754 ± 2 678	43 290	50 440	3 416
	41 860				
IV	86 070				
	89 590				
	87 400		72 690	19 540	49 400
	86 190	87 490 ± 1 469	73 230	19 490	46 540
	88 200				
V	126 000				
	130 400				
	128 200		26 480	17 890	345
	126 500	128 180 ± 1 945	26 430	17 600	338
	129 800				

of aluminum foil and secured to the existing heating block with glass heat-resistant tape. Enough heat is conducted to the inlet to maintain a temperature fairly close to that of the heating block, and sufficient to produce the necessary vaporization of the sample.

Apparently, the capacity of SCOT capillary columns is much greater than previously anticipated (*9*), and it was found that injections of up to 2 μl did not adversely affect the performance or the condition of the column. In the interest of optimum resolution and efficiency, however, the smallest sample volume injection is always to be preferred, and 1 μl is considered adequate. With injections of this magnitude, the columns can withstand continuous use of several months without noticeable deterioration. By continuous use is meant an average time cycle of 1 h for a chromatographic run, and sample injections are repeated automatically throughout a 24-h period for up to 5 days at a time. When column deterioration was evident, the column was removed and rejuvenated with a new coating of the liquid phase (2 g of SE-30 in 100 ml of isooctane). The recoated column was good for several more months of continuous operation.

Although some efficiency may be lost as a consequence of larger sample injection volumes, the precision is better than that of many stream splitting inlets. In Table I, sample A represents a synthetic mixture of methaqualone metabolites, and samples B, C, and D are extracts of human urine that contained these metabolites. Since the quantities of urine specimens were limited, duplicate analyses only were performed, whereas the synthetic sample was run repeatedly to demonstrate the reproducibility of the peak areas. (Synthetic metabolite II was not available, and for that reason was not included in the synthetic metabolite mixture.) The more important consideration is the advantage of a larger sample volume for those applications where the sample has been dissolved in a solvent, and constitutes only a small fraction of the entire injection volume. Stream splitting tends to diminish the actual concentration of the sample on column to the point where it might not be detected. In effect, nonsplitting improves the sensitivity of a procedure or application, since more of the sample is available to the detector.

Figure 2 shows chromatograms of the same specimen that was injected first into a 1-m, 5% OV-1 packed column, and followed by a similar injection in a SCOT capillary column coated with SE-30. Both columns were connected in the LKB 9000 gas chromatograph–mass spectrometer as described. The carrier gas of the packed column provided the make-up gas for the capillary column. The oven temperature was increased 10 °C (200 °C) for the capillary column to reduce the length of time for the run. These chromatograms represent comparative separations of an extract of hydrolyzed urine from an individual who had ingested a therapeutic dose of methaqualone. The peaks indicated are trimethylsilyl ether derivatives of the five principal methaqualone metabolites. The first two metabolites have coalesced into a single peak on the packed column chromatogram. In the same manner, the second large peak corresponds to the last three metabolites. In marked contrast, all five metabolites are well separated on the SCOT capillary column. Before capillary columns were attempted for these metabolite separations, packed columns of up to 1.5 m were employed without success.

Although the superiority of capillary columns is not difficult to demonstrate where resolution is a matter of concern, the prospect of having to change columns when packed columns are required, and the limitations of sample injection volume associated with stream splitting often discourages their use. The alternatives that have been presented here are simple and effective solutions to these problems. More importantly, these transformations can be accomplished easily without extensive alteration to the equipment involved.

LITERATURE CITED

(1) M. J. E. Golay, "Gas Chromatography 1958," D. H. Desty., Ed., Butterworth, London, 1958, p 36; U.S. Patent 2,920,478.
(2) G. Alexander and G. Garzó, *J. Chromatogr.*, **91**, 25 (1974).
(3) A. L. German, C. D. Pfaffenberger, J-P. Thenot, M. G. Horning, and E. C. Horning, *Anal. Chem.*, **45**, 930 (1973).
(4) E. C. Horning, M. G. Horning, J. Szafranek, P. Van Hout, A. L. German, J-P. Thenot, and C. D. Pfaffenberger, *J. Chromatogr.*, **91**, 367 (1974).
(5) K. Grob and H. Jaeggi, *Anal. Chem.*, **45**, 1788 (1973).
(6) J. G. Leferink and P. A. Leclercq, *J. Chromatogr.*, **91**, 25 (1974).
(7) C. J. Thompson and C. N. Goode, *Sci. Tools*, **19**, 33 (1972).
(8) A. Linnarson and G. Blomkvist, "LKB Application Note", August 1971.
(9) K. Grob and G. Grob, *J. Chromatogr. Sci.*, **7**, 584 (1969).

RECEIVED for review May 17, 1976. Accepted July 1, 1976. Any reference to manufacturer or equipment is for the purpose of information and does not constitute an endorsement by the Department of the Army.

Gas Chromatograph–Mass Spectrometer with Dual Electron Impact/High Pressure Ion Source

Ragnar Ryhage

Laboratory for Mass Spectrometry, Karolinska Institute, S-104 01 Stockholm 60, Sweden

Many applications of chemical ionization have been described since Munson and Field published their first paper in 1966 (*1, 2*). The construction of ion sources has changed slightly since that time, but experiments with many different reagent gases have been made by chemists working in the field of mass spectrometry, which has resulted in a more versatile and comprehensive application of this method for ionization.

Magnetic sector instruments, in which the ion source is at high potential, were mainly used in the first work with chemical ionization and the sample was introduced by the direct insertion probe or via the heated inlet system (*3–5*). However, during recent years, several articles have been published where gas chromatography–chemical ionization–mass spectrometry has been used (*6, 7*). Quadrupole mass spectrometers have frequently been used both for direct insertion probe and GC-CI-MS operation (*8, 9*). Some authors have used single ion sources designed for CI operation to produce EI spectra where helium was used as the reagent gas. These spectra show similar fragmentation as normal EI spectra (*10*). Because of the small aperture of the exit slit and of the electron beam entrance hole, EI mass spectra of optimal sensitivity cannot be obtained using CI ion source conditions. Other publications describe a fast changing EI/CI mode of operation (*11*). In this case, two ionization chambers with different slit widths were used to obtain optimal sensivity.

The work reported here illustrates how a GC-MS instrument for EI is modified to produce optimal conditions both for the EI and CI mode and to show the advantage in using two different reagent gases when the instrument is operating in the CI mode.

EXPERIMENTAL

Instrumentation. All experiments were performed with an LKB 2091 GC-MS instrument. The ion source and inlet system were modified as follows: A new ion source was constructed (patent applied for) so that the apertures of the ion exit slit, the electron beam entrance, and the exit to trap, which are included on a movable, gold-plated stainless steel band (8 × 0.03 mm), could be changed to permit either the electron impact or chemical ionization mode of operation. The slit size for the ion exit in the EI mode is 5 × 0.3 mm; for the filament electron entrance, 2 × 1 mm; and for the electron exit to trap, 2 × 2 mm. In the CI mode, the dimension of the exit slit is 3 × 0.03 mm; for the electron entrance holes, 0.3 mm in diameter; and there is no exit to the trap. Figure 1 shows the operational principle of the new ion source in the CI mode. By moving the band 21 mm to the other slit dimension, the ion source is ready for operation in the EI mode. It is important that the ion source is gas tight and that leaks around the movable band are small as compared to the apertures in the band. For this reason, the ionization box has been given suitable radii and the surface is well polished.

A differential pumping system is used which employs Edwards high vacuum pumps Ed 300 and Ed 150 at the ion source housing and the analyzer, respectively. The pumping speed around the ion source is about 200 l/s for a pressure of about 10^{-4} Torr and the pressure in the analyzer is about 10^{-6} Torr for an ion source pressure of about 0.5 Torr. By installing a cold trap at the top of the ion source housing and by using liquid nitrogen, the pumping speed will increase and the pressure for isobutane in the ion source housing drops to 10^{-5} Torr for an ion source pressure of 0.5 Torr. The pressure in the ion source is measured by a Pirani gauge connected to a special probe made of glass which can be used in the same position as the direct probe inlet. The emission control unit for the dual EI/CI source consists of two regulating circuits, one for the trap current (25 to 200 μA) and one for the total electron emission current (0.25–4 mA) in the EI and CI modes, respectively. The ion source has two extraction plates and two repellers. The voltage potentials on the extraction plates and the two repellers are adjusted separately for EI and CI and are switched, together with the electron energy, between the two modes of operation. The electron voltage can be continuously changed from 10 to 100 eV for EI and by steps from 50 to 600 eV in the CI mode. An integrator is connected to the galvanometer amplifier at the collector of the mass spectrometer. The circuit has start/stop integrate option programmed to sum up the ion intensities within a chosen mass range. The scan of the mass spectrometer can operate independent of the integrator and the output from the integrator produces the ion current gas chromatogram.

Operation. Figure 2. shows a schematic diagram of the combined gas chromatograph–mass spectrometer for EI/CI operation. Magnetic valves are used for the selection of the reagent gas along with a needle valve and glass capillary to limit the gas flow. Each reagent gas container has a separate pressure regulator, and a gas flow of 1 to 2 ml/min is sufficient to keep the pressure in the ion source between 0.4 and 0.8 Torr. In the EI mode, magnetic valves 1 and 2 are open and the other magnetic valves are closed. In the CI mode, valves 1 and 2 are closed and one of the valves to the reagent gases, 5, 6, or 7, is open. The pressure of the reagent gas in the ionization chamber can also be adjusted by needle valve 3. To reduce the time required to reach the operating pressure in this case, a magnetic valve, 4, can be opened for short periods which are determined by the setting of a timer.

The exchange of reagent gases during continuous operation can be done as follows: As soon as a scan of a mass spectrum with the first reagent gas is completed, the magnetic valves 1 and 2 are opened and the inlet line is evacuated in less than 0.5 s. Immediately afterwards, these valves are closed and another reagent gas is introduced into the ionization chamber and, after 0.5 s, when this gas has reached the operating pressure, a new mass spectrum can be taken in 1.5 s covering a mass range of *m/e* 5–500 (*12*). In this way, the GC-MS instrument can be operated in the CI mode and two complete 1.5-s scan spectra would then take about 5 s. To obtain both EI and CI mass spectra of the same GC peak, a proper timing of the required adjustments is necessary. The slits must be changed between scans which takes about 3 s and, at the same time, a readjustment of the electrical parameters must be made. The required time for two complete 1.5-s scan spectra would them be 7 to 9 s. For the results presented here, methane and isobutane were used as reagent gases with helium as carrier gas through the gas chromatographic column with a flow rate of 10–20 ml/min for all experimental studies. The mass spectra were recorded on uv paper since no computer was available for this project.

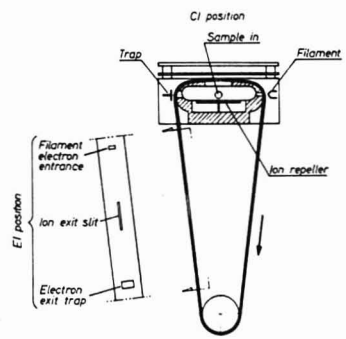

Figure 1. Schematic drawing of the combined EI/CI ion source

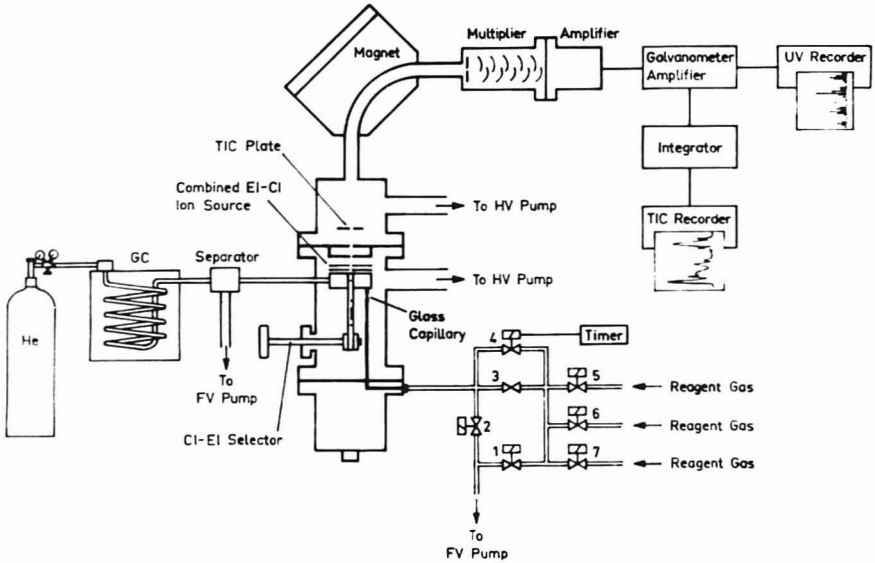

Figure 2. Schematic diagram of the combined gas chromatograph–mass spectrometer and reagent gas inlet system for EI/CI operation

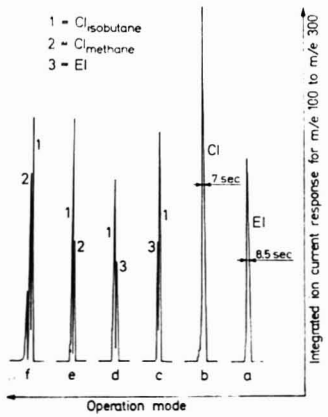

Figure 3. Chromatograms of the integrated ion current of pentobarbitone at different modes of operation

a = EI (only GC), *b* = $CI_{i\text{-but}}$ (only GC). Two complete mass spectra, one for each mode of operation were recorded for GC peaks *c* to *f*

RESULTS AND DISCUSSION

As a demonstration of the switching time from the conventional EI mode to the CI mode and vice-versa, and of the exchange of reagent gases in the CI mode, 2 μg of pentobarbitone were injected into the SE-30 column. The retention time for pentobarbitone was adjusted to be approximately 1 min. Figure 3 shows the GC peaks of the integrated ion current where *a* and *b* correspond to the EI and $CI_{i\text{-but}}$ modes of operation. No mass spectra were recorded for these peaks. The width of the GC peaks at half-height are about 7 to 9 s and, during this time, two complete mass spectra, one for each mode of operation, could be recorded for each GC peak. GC peaks *c* to *f* were checked to determine if any cross-residual effect could be observed from one mode of operation to another. Mass spectra of GC peak *c* were recorded in the CI mode with isobutane as the reagent gas, C1, and in the EI mode, C3. After the CI spectrum was recorded(C1), the reagent gas was switched off and the electron energy, repeller, and extraction voltages were switched over to the EI position as well as the movable band for a change to a larger exit slit and electron entrance hole into the ion source. After the EI mass spectrum (C3) was recorded, the voltages and movable band were reset for the CI mode. GC peak *d* was recorded in reversed mode, EI to $CI_{i\text{-but}}$. Two CI mass spectra were recorded for GC peaks *e* and *f*. The first mass spectrum of peak *e* was recorded with methane and the second with isobutane as a reagent gas. Peak *f* was first recorded with isobutane and then methane as the reagent gas.

The mass spectra of GC peaks *c* and *d* in Figure 3 are shown in Figure 4. The EI and $CI_{i\text{-but}}$ spectra show that even a fast change of the operating mode does not indicate any differences in the fragmentation pattern. In both cases, the EI spectra have a base peak at *m/e* 156 and in the CI mode *m/e* 227 (M + 1) is the base peak. No cross contamination was observed in the mass spectra of GC peaks *e* and *f* in Figure 3. Figure 5 shows the switching time for GC-MS analysis for benzophenone between the EI and $CI_{i\text{-but}}$ modes which was checked through the use of a multiple ion detector (MID) LKB 2091-710. The molecular ion (*m/e* 182) and the $(M + H)^+$ ion at *m/e* 183 with the isotope peak at *m/e* 184 were focused on the MID. As soon as the peak appeared for a few seconds in the EI mode, the movable band and the ion source voltages were changed to the CI mode. This procedure was repeated during the time the GC peak eluted from the column. The mode of operation was changed from EI-CI-EI-CI in about 15 s. During this time, it should be possible to obtain

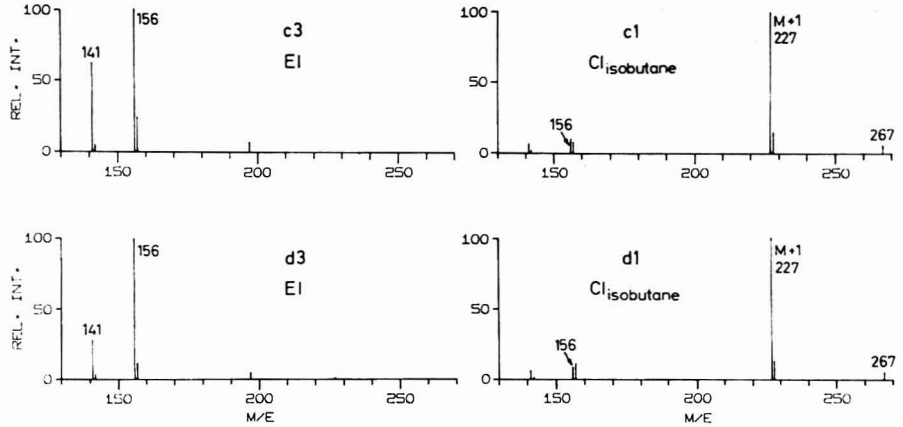

Figure 4. Mass spectra of pentobarbitone obtained from GC peaks *c* and *d* (Figure 3)

*c*3 and *d* 3 were obtained in the EI mode and *c*1 and *e*1 were obtained in the CI mode with isobutone as a reagent gas

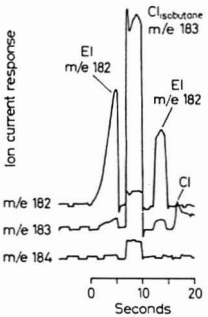

Figure 5. Intensities of ions at *m/e* 182, 183, and 184 of benzophenone as a function of the recording and switching time between the EI-CI-EI-CI modes

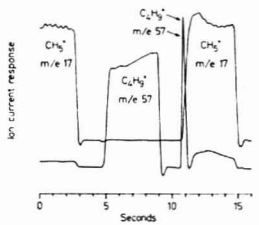

Figure 6. Intensities of the reactant ions CH_5^+ and $C_4H_9^+$ in the CI mode as a function of the recording and switching time when methane or isobutane, respectively, was used as a reagent gas

three complete 1.5-s scan mass spectra. To check the switching time of the reagent gases, the reactant ions *m/e* 17 (CH_5^+) and *m/e* 57 ($C_4H_9^+$) were focused on the MID. The intensity of these ions was recorded when the reagent gases used were methane, isobutane, and methane, consecutively. Figure 6 shows the intensity of these ions as a function of the switching and recording time. After the first mass spectrum was taken, the reagent gas methane was switched off and a pumping time of 2 s was allowed before isobutane was introduced into the ion source. Thus, during a period of about 5 s, two CI mass spectra could be obtained. When methane was introduced a second time, a sharp peak of isobutane was seen, which means that the inlet line contained a small amount of isobutane. However, this did not influence the mass spectra obtained with methane as the reagent gas.

From these experiments it could be concluded that, through a reduction in volume of the reagent gas inlet line, the influence of the remaining gas from the prior operation will be negligible. Furthermore, a reduction of the time required for two 1.5-s scan mass spectra using different reagent gases can be accomplished if proper synchronization of scan initiation and gas switching is made. Then the required time would be about 4 s as compared to 5 s with the semiautomatic procedure reported above. Similarly, the required time to obtain two 1.5-s scan mass spectra can be reduced to 6 s as compared to 7 to 9 s if automatic control of EI/CI switching and scan initiation were employed. The moveable band which permits rapid changing of the operation mode can easily be exchanged for one having smaller or larger slits suitable for the type of samples to be studied and the reagent gas used.

It is advantageous to run the mass spectrometer in the EI/CI mode of ionization for most of the compounds which show a low molecular ion intensity in the EI mode. A fast change of the ionization mode is advisable when such samples are flashed from the direct probe inlet or when special components in a gas chromatographic analysis must be thoroughly investigated. Additional mass spectrometric data which can be obtained from such an instrument will greatly increase the certainty of identification. In particular, this could be of importance in molecule identification when computerized "library search" routines are used to assist analysts in obtaining correct answers.

Since the GC-MS instrument used for this experiment is one of the first prototypes of LKB 2091, no time was spent on determing the maximum sensitivity and resolution. However, similar modifications which were made on this instrument have later been used for other LKB 2091 instruments. The specifications for these instruments regarding resolution and

sensitivity are similar to the standard model in the EI mode. In the CI mode, the resolution is the same as in the EI mode but the sensitivity has not been established.

LITERATURE CITED

(1) M. S. B. Munson and F. H. Field, *J. Am. Chem. Soc.*, **88**, 1621 (1966).
(2) M. S. B. Munson, *Anal. Chem.*, **43** (13), 28A (1971).
(3) H. M. Fales, G. W. A. Milne, and M. L. Vestal, *J. Am. Chem. Soc.*, **91**, 3682 (1969).
(4) H. M. Fales, G. W. A. Milne, and R. S. Nicholson, *Anal. Chem.*, **43**, 1785 (1971).
(5) I. Dzidic, D. M. Desiderio, M. S. Wilson, P. F. Crain, and J. A. McCloskey, *Anal. Chem.*, **43**, 1677 (1971).
(6) H. Miyazaki and Y. Hashimoto, *J. Chromatogr.*, **99**, 575 (1974).
(7) F. D. Hileman, T. A. Elwood, M. L. Vestal, and J. H. Futrell, 22nd Annual Conference on Mass Spectrometry and Allied Topics, Philadelphia, Pa, May 19–24, 1974.
(8) G. P. Arsenault, J. J. Dolhun, and K. Biemann, *Anal. Chem.*, **43**, 1720 (1971).
(9) I. O. Oswald, D. Parks, T. Eling, and B. J. Corbett, *J. Chromatogr.*, **93**, 47 (1974).
(10) D. M. Schoengold and M. S. B. Munson, *Anal. Chem.*, **42**, 1811 (1970).
(11) W. Kruger, N. Kuypers, and J. Michnowicz, 21st Annual Conference on Mass Spectrometry and Allied Topics, San Francisco, Calif., May 20–25, 1973.
(12) B. Hedfjall and R. Ryhage, *Anal. Chem.*, **47**, 666 (1975).

RECEIVED for review May 20, 1976. Accepted July 7, 1976. This work was made possible by grants from the Swedish Board for Technical Development, Knut and Alice Wallenbergs' Foundation and the Hedlund's Foundation.

Self-Positioning Anti-Vortex Plug for Nuclear Magnetic Resonance Sample Tubes

LeRoy F. Johnson

Nicolet Technology Corporation, Mountain View, Calif. 94041

When it is desired to use a minimum volume of solution in an NMR sample tube, anti-vortex plugs are generally used to prevent formation of a vortex when the sample tube is spun. This is particularly important when sample tubes of diameter near 20 mm are used (*1*). Commercial anti-vortex plugs (such as made by Wilmad Glass Co.) are designed to be a press-fit through action of pliable fins on the central part of the plug. The plug, which has an axial hole for air escape, tapped at one end, is positioned in the tube with the use of a threaded rod.

When used with large diameter (15–25 mm), thin wall (0.5 mm) tubes, a press-fit plug can rather easily break the tube during insertion. Also, variable temperature operation is a problem because expansion of the plastic plug during high temperature operation can break the tube, while contraction of the plug during low temperature operation can cause the plug to slide to the bottom of the tube.

An anti-vortex plug which overcomes the problems mentioned above is illustrated in Figure 1. A cylinder of Teflon of length about 35 mm is machined to a smooth diameter about 0.2 mm less than the inner diameter of the sample tube. The top 10-mm section of the cylinder is turned-down to a diameter of about 5 mm and a small radial hole is drilled through this section. The bottom of the plug is made slightly convex.

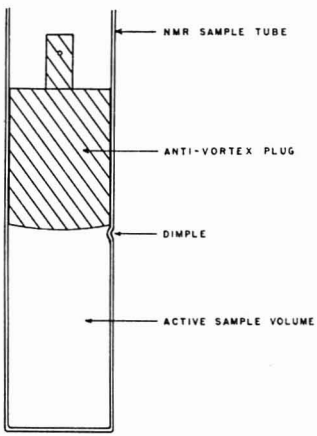

Figure 1. Diagram of anti-vortex plug in an NMR sample tube

The sample tube is spot-heated using a torch with a very small flame at an appropriate distance up from the bottom, and dimpled using a small metal rod. In use, the sample tube is filled to a depth just higher than the dimpled spot. The plug, inserted in the sample tube, will float down to the point where it rests on the indented spot. Any trapped air bubbles can be moved out of the active sample volume by shaking the sample tube as if it were a clinical thermometer. To remove the plug, a long piano wire with a 90° hook at the end is inserted in the radial hole of the plug.

In extended use, the anti-vortex plug described here has proved to be very convenient to use. Spin rates up to 100 rps have been used without formation of an air bubble below the plug. Dynamic balance of the loaded sample tube is not appreciably affected since the dimple region is quite small compared to the overall sample volume. Although initially conceived for use with 18–25 mm tubes, this plug design has also been quite practical with 12-mm tubes as well. Of course, with smaller diameter tubes, care must be exercised in generating the dimple in the tube so as to not distort the straightness of the tube.

LITERATURE CITED

(1) A. Allerhard, R. F. Childers, and E. Oldfield, *J. Magn. Reson.*, **11**, 272 (1973).

RECEIVED for review July 16, 1976. Accepted August 9, 1976.

CORRECTION

Kinetically Assisted Equilibrium Based Repetitive Determinations of Iron(II) with Ferrozine in Flow-Through Systems

The authors of this article [V. V. S. Eswara Dutt, A. Eskander-Hanna, and H. A. Mottola, *Anal. Chem.*, **48**, 1207 (1976)] would like to point out the omission of a necessary assumption for Equations 7 and 8 to be valid. Conditions leading to these equations require that $k_2' \gg k_{-1}$ as well as the stated $k_1 \gg k_{-1}$.

Author Index

Future Articles

Neutron Activation Analysis Program for Multielement Trace Determination with Absolute Counting
P. F. Schmidt and D. J. McMillan

Theoretical Considerations in Stable Istope Dilution–Mass Spectrometry for Organic Analysis
J. F. Pickup and K. McPherson

Simultaneous Multielement Determination with a Computer-Controlled Flameless Atomic Absorption Spectrophotometer
E. Lundberg and G. Johansson

Elemental Analysis of Obsidian Artifacts Using Proton-Induced X-ray Emission
K. K. Nielson, M. W. Hill, N. F. Mangelson, and F. W. Nelson

Determination of Cobalt, Molybdenum, and Nickel in Hydrodesulfurization Catalysts by Neutron Capture γ-Ray Spectrometry and Neutron Activation Analysis
M. Heurtebise, H. Buenafama, and J. A. Lubkowitz

Direct Analysis of Metals and Alloys by Atomic Absorption Spectrometry
D. S. Gough

Noise at Detection Limit Levels in Atomic Absorption Flame Spectrometry
P. R. Liddell

Coulometric Determination of Palladium in Hydrocracking Catalysts
J. N. Story

Holographic Interferometric Microscopy
R. F. Cournoyer, M. B. Rhodes, and S. Siggia

Detection of Lead via Lead-207m Using Cyclic Activation and a Modified Sum-Coincidence System
A. Egan and N. M. Spyrou

Instrument for the Generation of Reactive Gases
W. Tsang and J. A. Walker

Improving the Reliability of Factor Analysis of Chemical Data by Utilizing the Measured Analytical Uncertainty
D. L. Duewer, B. R. Kowalski, and J. L. Fasching

Just flip a switch and do an entire titration automatically, even the calculations.

It could be just one, or as many as 44 acid/base, redox, colorimetric, conductometric or coulometric titrations.

It could be an end point, a pH stat or a Karl Fischer titration.

It could be a recording of the titration curve, or its first derivative.

Whatever the titration, Metrohm Titrators have the versatility and sensitivity to perform it automatically right to the final calculation at the touch of a switch.

In fact, there is hardly a titration procedure which Metrohm equipment, using appropriate accessories, cannot do more efficiently and conveniently. (A standard convenience feature of all Metrohm Titrators are the interchangeable 'snap-in' buret units, which permit repeated, non-stop change of titrants).

For a new 16-page brochure describing the complete line of Metrohm Recording Titrators and accessories, just write: Metrohm Division, Brinkmann Instruments, Cantiague Road, Westbury, N.Y. 11590. In Canada: 50 Galaxy Boulevard, Rexdale (Toronto), Ont.

A DIVISION OF BRINKMANN

Metrohm Titrators

CIRCLE 28 ON READER SERVICE CARD